University of Nottingham
UK | CHINA | MALAYSIA

New Bioinspired Polymer Consolidants for the Oseberg Artefacts and Other Archaeological Wood

Michelle Cutajar BSc (Hons), MPharm, MSc

Thesis submitted to the University of Nottingham for the degree of Doctor of Philosophy

September 2022

Acknowledgements

I would like to thank all my supervisors for their incredible depth of knowledge and for being my mentors these past four years. Prof. Stephen Harding for his persistent help and inspirational enthusiasm, Prof. Robert Stockman for his constant flow of ideas and support, Prof. Steven Howdle for his all his valuable advice and Dr Susan Braovac for all the encouraging support and for making me feel so welcome during my stay in Oslo. Thank you also to the EPSRC research council and the University of Oslo for providing funding for my PhD.

I would like to express my gratitude to all the people who helped me with this work, especially all my colleagues at the NCMH and the School of Chemistry at the University of Nottingham. I am also deeply grateful to all the members of the Saving Oseberg team at the Museum of Cultural History in Oslo for the all the help that they have given me over the years.

To my family for being a constant pillar of support and without whom I would have never been able to complete my PhD; my parents Liliana Cutajar and Vincent Cutajar and my sister Simone Cutajar. Thank you for your endless love, patience and support. My non-human family – Whiskers, Binx, Tigerlily, Remy – thank you for all the joy that you have brought me, I miss you every day; Haru and Yuki – thank you for never failing to put a smile on my face.

Abstract

The Oseberg Viking ship burial is one of the most extensive collections of Viking wooden artefacts discovered in the world. In the early 20th century, many of these artefacts were treated with alum. Today, it is known that this alum treatment was very damaging to the wood, as a significant number of the artefacts demonstrate a high degree of deterioration. The Saving Oseberg project was set up in 2014 by the Museum of Cultural History at the University of Oslo to work towards gaining understanding of the chemical composition of the alum-treated wood and establishing novel conservation treatments. Current studies on the state of the Oseberg collection prove that the artefacts are undergoing continuous degradation.

Alum-treated wood is a highly complex substance and no truly effective treatment has yet been developed for the most degraded objects. It is therefore crucial to develop new polymers which could be used to conserve these artefacts and prevent their disintegration. Consolidants which are soluble in organic solvents are particularly needed, as these could be used to treat some of the most degraded pieces in the Oseberg collection. Additionally, bioinspired polymers represent a more sustainable alternative to some of the consolidants currently in use. To this end, the research aim was to develop novel, organic solvent-soluble, bioinspired polymers which would be suitable to use for the retreatment of the Oseberg artefacts, as well as other archaeological wood.

Terpenes were identified as a suitable feedstock for the synthesis of such compounds, as they are derived from biomass and are easily functionalised. Two monomers were subsequently synthesised, derived from α-pinene, each modified with an acrylate group. An additional, non-terpene monomer was also prepared using oleic acid. These were then used to synthesise three hydroxylated polymers named TPA5, TPA6 and TPA7. TPA5 and TPA6 were homopolymers which were entirely terpene-derived, while TPA7 was a copolymer with α-pinene and oleic acid components. The polymerisation reactions of all three molecules were optimised so that each had a small molecular weight which enables wood penetration (~ <5 kDa). All the polymers were soluble in isopropanol, a solvent which was deemed acceptable to use in archaeological wood treatment.

These polymers were extensively characterised, primarily using analytical ultracentrifugation, viscometry and other hydrodynamic techniques, in order to investigate whether they would be suitable for wood consolidation purposes. These characterisation studies confirmed that TPA5, TPA6 and TPA7 were excellent candidates for use as potential consolidants. Due to time constraints it was decided to not continue developing TPA5 beyond this point and instead focus on TPA6 and TPA7. This was because the synthesis routes of these two polymers were more efficient and less laborious than that of TPA5. The synthesis of TPA6 and TPA7 was then scaled up to be able to make enough material for the subsequent wood testing.

These preliminary wood studies were carried out using archaeological pine. The polymers were dissolved in isopropanol at an appropriate concentration and the wood specimens were immersed in the solutions. Subsequent analyses involved weight and dimensional measurements, colour and pH measurements, Fourier-transform infrared spectroscopy, scanning electron microscopy and hardness tests. These studies confirmed that both TPA6 and TPA7 successfully penetrated the wood, with the highest concentration of polymer being found on the specimen surfaces. The hardness tests showed that treatment with these polymers caused the wood surface to become more resistant to indentation.

Other research that was carried out involved characterising two existing consolidants, Butvar® B-98 and PDMS-OH, with the use of analytical ultracentrifugation. This was used to confirm their molecular weight and heterogeneity. The tests that were carried out indicated that the samples showed considerable conformational asymmetry from measurements of intrinsic viscosity, which would facilitate networking interactions as consolidants. It is anticipated that the accumulated data on these two consolidants will enable conservators to make a more informed decision when it comes to choosing which treatment to administer to archaeological artefacts.

Table of Contents

List of Figures

List of Tables

List of Schemes

Abbreviations

a/b	axial ratio
AIBN	azobisisobutyronitrile
ATR-FTIR	attenuated total reflection-Fourier transform infrared
ATRP	atom transfer radical polymerisation
AUC	analytical ultracentrifugation
β	Scheraga-Mandelkern shape parameter
BH_3.THF	borane tetrahydrofuran complex
BHT	butylated hydroxytoluene
$CDCl_2$	deuterated chloroform
CD_3OD	deuterated methanol
$(CD_3)_2SO$	deuterated DMSO
c(r)	concentration at radial position
c(s)	continuous distribution of sedimentation coefficients
Đ	dispersity
DBTDA	dibutyltin-diacetate
DCM	dichloromethane
DSC	differential scanning calorimetry
$[\eta]$	intrinsic viscosity
η_{inh}	inherent viscosity
η_{red}	reduced viscosty
η_{rel}	relative viscosity
η_{sp}	specific viscosity
EDS	energy dispersive X-ray spectroscopy
Et_3N	triethylamine
EtoAc	ethyl acetate
eq.	equivalents
F_b	buoyancy force
F_f	frictional force
F_s	sedimentation force
FRP	free radical polymerisation
FTIR	Fourier-transform infrared
GC/MS	gas chromatography coupled with mass spectrometry

GPC	gel permeation chromatography
h	hours
^{1}H NMR	^{1}H nuclear magnetic resonance
H/L	ratio of holocellulose over lignin volume
HPLC-ESI-Q-ToF	electrospray ionisation and quadrupole time-of-flight mass spectrometry
HRMS	high resolution mass spectrometry
ICP-AES	plasma-atomic emission spectroscopy
IR	infrared
ls-g(s)*	least square Gaussian fit for sedimentation
M(r)*	point average molecular weight/molar mass (Da, g/mol)
M_n	number average molecular weight/molar mass (Da, g/mol)
M_w	weight average molecular weight/molar mass (Da, g/mol)
$M_{w,app}$	apparent weight average molecular weight/molar mass (Da, g/mol)
*m*CPBA	*meta*-chloroperoxybenzoic acid
MeCN	acetone
MeOH	methanol
MHKS	Mark–Houwink–Kuhn–Sakurada
MMC	maximum moisture content
mol%	mole percentage
MTES	methyltriethoxysilane
MTMOS	methyltrimethoxysilane
MWCO	molecular weight cut-off
NMR	nuclear magnetic resonance
P	Perrin shape parameter
PDMS-OH	hydroxy terminated polydimethylsiloxane
PEG	polyethylene glycol
PGMS	propylene glycol modified silane
PyGC/MS	analytical pyrolysis-gas chromatography/mass spectroscopy
TI	time invariant
ρ	density
RAFT	reversible addition−fragmentation chain-transfer
RH	relative humidity
RI	radial invariant
r. t.	room temperature

s	sedimentation coefficient
$s_{20,w}$	sedimentation coefficient corrected to standard solvent conditions (density and viscosity of water at 20 °C)
S	Svedberg units
SE	sedimentation equilibrium
SEM	scanning electron microscopy
SV	sedimentation velocity
T3P®	propyl phosphonic anhydride
T_g	glass transition temperature
TBDMS	*tert*-butyldimethylsilyl
TEOS	tetraethyl orthosilicate
THF	tetrahydrofuran
TLC	thin-layer chromatography
TPA5	triol acrylate polymer
TPA6	*trans*-sobrerol acrylate polymer
TPA7	*trans*-sobrerol acrylate/oleic acid acrylate copolymer
UV	ultraviolet
vs	versus
$\bar{v}$	partial specific volume
V	hydrated volume
ν	viscosity increment shape parameter
v_s	swollen specific volume
$(v_s/\bar{v})$	degree of solvent association
wt	weight
wt%	weight percentage
XRD	x-ray diffraction

Chapter 1. The Oseberg Artefacts – Past Conservation Efforts, Current Condition and Future Retreatment

This first chapter will offer a comprehensive literature review covering the discovery of the Oseberg artefacts, their initial alum treatment upon excavation and the chemical analyses carried out on these objects to understand their current state of degradation. Additionally, existing polymers which may be used to treat these artefacts will be detailed and future possibilities regarding new consolidants will be explored.

1.1 The Oseberg find

The Oseberg Viking ship burial is one of the most important and comprehensive collections of Viking artefacts ever found in the world. The burial mound itself was discovered in 1903 near Tønsberg in Norway and its excavation took place in 1904. The ship was the burial place of two high-ranking women and was dated back to 834 CE (Bonde and Christensen, 1993). It contained a variety of wooden artefacts, from kitchen utensils to ceremonial sledges (Figure 1), as well as textiles, animals and food (Rosenqvist, 1959). This array of objects provides a fascinating insight into the everyday life of the Norse people, as well as their ceremonial rituals and mastery of woodworking (Braovac *et al.*, 2016). A portion of this discovery is exhibited at the Viking Ship Museum in Oslo, which is currently closed for renovation.

Figure 1. One of the ceremonial sledges found in the Oseberg collection, exhibited at the Viking Ship Museum, Norway (Museum of Cultural History, University of Oslo).

The burial mound in which the ship and artefacts were found was lined with blue clay, which kept the water level underground relatively stable. This resulted in a low oxygen environment which protected the wood from rapid fungal decay (Rosenqvist, 1959; Braovac *et al.*, 2018). All the objects were found in a waterlogged and fragmented state (Rosenqvist, 1959; Braovac and Kutzke, 2012; Andriulo *et al.*, 2016; McQueen *et al.*, 2017). The conservation treatment used at the time of excavation was described by Rosenqvist (1959). The oak (*Quercus* L.) ship was relatively well-preserved and therefore could withstand a surface treatment with creosote and linseed oil, and again later with linseed oil and white spirit. The wooden artefacts, made from wood like maple (*Acer* L.) and birch (*Betula* L.) (Łucejko *et al.*, 2018), were much more degraded. Simple air-drying would cause these artefacts to irreversibly shrink at an alarming rate, as can be seen in Figure 2. This meant that they needed to be treated with a consolidant before they were allowed to dry from their waterlogged state. Most of the artefacts were treated with alum ($KAl(SO_4)_2 \cdot 12H_2O$ and $NH_4Al(SO_4)_2 \cdot 12H_2O$) between 1905 and ~ 1912 (Braovac *et al.*, 2018).

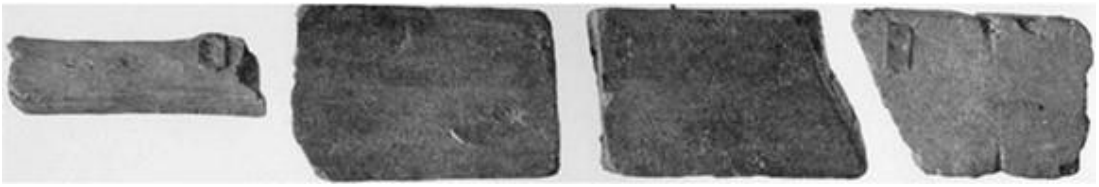

Figure 2. A comparison of the Oseberg wood during the alum treatment: the two centre pieces were still in a waterlogged state, the right piece was treated with alum and then dried, while the left piece was air-dried (Braovac *et al.*, 2018).

1.1.1 The alum treatment

Treating archaeological wood with alum was a popular method for almost a hundred years, especially in Scandinavia, with the earliest report of its usage being in Denmark in the 1850s (Braovac and Kutzke, 2012). Professor Gabriel Gustafson, who was in charge of the Oseberg excavations, learnt of the alum treatment during a visit to the National Museum of Denmark in 1904 (Braovac *et al.*, 2018). Since it was one of the only proven methods to treat highly degraded waterlogged archaeological wood, it became very widespread and was in use till the late 1950s (Braovac and Kutzke, 2012). Glycerol seemed to have become a common addition to the alum treatment after ~ 1910 (Braovac *et al.*, 2018), although it was not applied to the Oseberg artefacts. This was fortunate as glycerol's high hygroscopicity would have caused the wood to become even more sensitive to the ambient relative humidity, leading to its destruction (Braovac *et al.*, 2018).

The alum treatment primarily involved immersing the artefacts in a highly concentrated alum solution at approximately 90 °C, which would then replace the water in the cellular structure of the wood (Rosenqvist, 1959; Andriulo *et al.*, 2016; McQueen, Tamburini and Braovac, 2018). Rosenqvist (1959) documents that only potassium alum was utilised, but it has recently been reported that the salt solutions used were instead comprised of both potassium and ammonium alum (McQueen *et al.*, 2019). Once it recrystallised, the alum acted as a supportive framework for the wooden objects by preventing their shrinkage upon drying (Braovac and Kutzke, 2012). The dried wood was subsequently impregnated with linseed oil and varnish (Rosenqvist, 1959; Braovac and Kutzke, 2012). The artefacts were then

reconstructed using a variety of tools such as metal pins and screws, adhesives and fill material (Figure 3) (Braovac and Kutzke, 2012).

Figure 3. Conservator Paul Johannessen in the early 1900s during the alum treatment of the Oseberg artefacts (Museum of Cultural History, University of Oslo).

The alum did not undergo complete penetration into the wood, thus creating two areas of differing alum concentrations: a surface which was hard and alum-rich and a fragile core with a low level of alum (McQueen *et al.*, 2017). This arrangement of salt concentration has had important consequences on the mechanical properties of the wood. During the drying phase, the consolidated surface remained intact while the structurally weak core shrank, resulting in the formation of cracks inside the wood. New cracks that are currently being seen to develop on the surface of the Oseberg artefacts are likely to be extensions of these innermost cracks as a result of inadequate support (Braovac *et al.*, 2018).

Today, most of the alum-treated artefacts have become severely deteriorated and the wood itself is brittle and very acidic (pH ≤2) (McQueen *et al.*, 2017). The source of this deterioration was difficult to pinpoint, however it was hypothesised that the cause

was the sulfuric acid generated as a result of the alum treatment (Braovac and Kutzke, 2012). The correlation between sulfuric acid and wood deterioration was later confirmed through the use of analytical pyrolysis-gas chromatography/mass spectroscopy (PyGC/MS) and plasma-atomic emission spectroscopy (ICP-AES) (Braovac *et al.*, 2016). These studies have also shown that the lignin in the wood is highly oxidised and that it is lacking in carbohydrate content (Braovac and Kutzke, 2012; Braovac *et al.*, 2016).

1.1.2 Other aspects of the past treatment

Since many different materials such as metal bolts and various glues were used for their initial conservation, the artefacts nowadays are not composed entirely of just wood. Instead, in addition to alum, they contain a number of other non-wood inorganic components (McQueen, Tamburini and Braovac, 2018). These metal ions found in the Oseberg objects may have contributed to the deterioration of the wood and it has been postulated that there is a correlation between the level of wood degradation and the iron and calcium concentrations (Braovac *et al.*, 2016; McQueen *et al.*, 2017). There are many other studies which report on the problems posed by both sulfuric acid and metal ions in archaeological waterlogged wood (Fors and Sandström, 2006; Preston *et al.*, 2014; Zoia, Salanti and Orlandi, 2015; McQueen *et al.*, 2017).

The Oseberg findings present us with a particularly unique task. Other famous archaeological findings such as the Vasa have many documented issues with sulfuric acid and metal ions (Fors and Sandström, 2006). However, there are some important differences between these two cases. The Vasa was treated with polyethylene glycol (PEG) as opposed to alum (Braovac *et al.*, 2016; McQueen *et al.*, 2017). Additionally, it was found in a marine environment and as such, the sulfuric acid which exists in its wood is a product of iron sulfide oxidation which itself is a result of the action of sulfate-reducing bacteria and corroding iron during burial (McQueen, Tamburini and Braovac, 2018). It was postulated that post-conservation this oxidation process has been catalysed by iron ions found in some of the ship components, such as metal rods and screws (Sandström *et al.*, 2002; Braovac and Kutzke, 2012; Braovac *et al.*, 2016; McQueen, Tamburini and Braovac, 2018). Conversely, the Oseberg find was discovered in a waterlogged, terrestrial environment as opposed to a marine one and

therefore the presence of the sulfates and sulfuric acid is entirely due to the alum treatment (Braovac *et al.*, 2016; McQueen *et al.*, 2017; McQueen, Tamburini and Braovac, 2018).

Alum-treated wood is a highly complex substance and no truly effective treatment method has been discovered yet. Moreover, the polymers which are commonly used in conservation nowadays are mostly derived from fossil fuels (Wakefield *et al.*, 2018), therefore the sustainability of any new consolidants should be given careful consideration. Current studies on the state of the Oseberg collection confirm that the artefacts are undergoing continuous degradation (Braovac *et al.*, 2016). This deterioration could also be partly due to other as of yet undiscovered mechanisms, as it is particularly severe when compared to other archaeological findings like the Vasa (Braovac *et al.*, 2016; McQueen *et al.*, 2017). This makes the discovery of a novel conservation treatment even more vital.

The Saving Oseberg project (2014-2019) was set up by the Museum of Cultural History at the University of Oslo with the aim of safeguarding these artefacts. The research carried out by the Saving Oseberg team has focussed on understanding the processes of degradation of the alum-treated wood, as well as studying the viability of novel and existing consolidants. The two research areas go hand in hand since it is necessary to fully comprehend the degradation mechanism of the wood and its current state of preservation before planning a treatment strategy (Florian, 1989; Crisci *et al.*, 2010; Broda *et al.*, 2015). This review aims to provide an overview of the most recent research to date which has been published by the Saving Oseberg team. It will also cover the promising leads and methodologies which may lead to a new generation of green consolidants, not just for the Oseberg collection, but also for archaeological wood found in museum collections worldwide.

1.2 Chemical analyses of the alum-treated wood

The chemical analyses studies that have been carried out on the archaeological, alum-treated wood can be loosely broken down into those seeking to understand the

repercussions of the alum treatment, and those focussing on the effect of other inorganic materials on the wood.

1.2.1 The effect of alum on archaeological wood

One of the first papers published by the Alum Research project (which preceded the Saving Oseberg project) established a link between alum and wood degradation. Braovac and Kutzke recreated the original alum treatment using both archaeological and fresh wood (Braovac and Kutzke, 2012). Results showed that the alum treatment led to cell wall degradation in both kinds of samples, with infrared (IR) spectroscopy indicating a decrease in hemicellulose content. Similar patterns were observed when comparing the IR spectra of wood treated with heated alum vs wood treated with sulfuric acid alone. This suggested that the acidic condition of the alum-treated wood played a role in its degradation. This led to the discovery that the sulfuric acid in the artefacts originated from the thermal alum treatment undergone by the wood, which produced alum hydroxides and sulfuric acid (Braovac and Kutzke, 2012):

$$3KAl(SO_4)_2 + 6H_2O \rightarrow KAl_3(SO_4)_2(OH)_6 + K_2SO_{4(aq)} + 3H_2SO_{4(aq)}$$

This connection between the alum treatment and wood degradation was confirmed by later studies (Braovac *et al.*, 2016; McQueen *et al.*, 2017; Zoia *et al.*, 2017).

As mentioned previously, it was also demonstrated that the alum-treated archaeological wood was polysaccharide-depleted and had highly degraded lignin (Braovac *et al.*, 2016). This was surmised from the results which showed a dramatic decrease in the holocellulose content of the cell wall, as well as a high level of oxidised lignin. It was also the first time that *p*-hydroxy benzoic acid, an acid pyrolysis product which is related to lignin oxidation, was detected in archaeological wood. A correlation between the concentrations of potassium, sodium and aluminium and the level of acid lignin pyrolysis products was established in a separate study (McQueen, Tamburini and Braovac, 2018).

These findings were supported through a combination of techniques (nuclear magnetic resonance (NMR) spectroscopy, gel permeation chromatography (GPC) and PyGC/MS) to chemically characterise the whole cell wall of the archaeological wood (Zoia *et al.*, 2017). This study confirmed that the actual Oseberg ship (which was not treated with alum) was in a good preservative condition. By contrast, the alum-treated artefacts showed a large depletion of carbohydrates and a high level of oxidised lignin as was already reported (Braovac *et al.*, 2016).

More recently, McQueen *et al*. carried out chemical analyses to characterise both the surface and core of selected wood fragments (McQueen *et al.*, 2017; McQueen, Tamburini and Braovac, 2018). One study used samples which were not reconstructed, meaning they were treated with alum but not with any other material (McQueen *et al.*, 2017). PyGC/MS and Fourier-transform infrared (FTIR) spectroscopy detected oxidised lignin, as well as widespread deterioration of the holocellulose in the cell wall. The group confirmed that different alum concentrations exist in the surface and core of the wood. A higher level of degradation was found in the alum-rich wood surface when compared to the centre.

Alum products like mercallite ($KHSO_4$) have also been observed in the wood. This product was detected in all the tested samples using X-ray diffraction (XRD) and FTIR spectroscopy (McQueen *et al.*, 2017). A high level of sulfates which were not bound to alum or $KHSO_4$, corresponding to the sulfuric acid that is produced by alum hydrolysis, was also reported.

In a follow-up investigation, McQueen *et al*. chose alum-treated samples which were more chemically complex as they incorporated other materials such as corroding iron rods (McQueen, Tamburini and Braovac, 2018). Some of these rods were found in the original buried objects while others were used to rebuild the artefacts after excavation in the early 1900s. In contrast to the previous study (McQueen *et al.*, 2017), $KHSO_4$ was not detected to a large degree. There is currently no explanation as to why there is a discrepancy between these two studies regarding the $KHSO_4$ content but it is likely related to the general variability in the extent of preservation observed in the Oseberg collection, which is not yet fully understood.

The degree of the degradation caused by the alum was shown to be somewhat dependent on time, with the damage becoming worse the more time elapsed (Łucejko *et al.*, 2021). Other factors which are also known to affect the degradation are the wood's original condition before treatment, the type of alum solutions used and

impregnation times, the wood genus and the storage environment (Łucejko *et al.*, 2021).

1.2.2 Inorganic chemical analyses of the alum-treated wood

There are various inorganic compounds apart from alum which are present in the wood of the Oseberg artefacts. These compounds have many possible sources: metal decomposition, migration from outside elements and the conservation treatment itself (McQueen, Tamburini and Braovac, 2018). The link between iron ions and archaeological wood degradation has already been investigated in previous studies (Wetherall *et al.*, 2008; Almkvist and Persson, 2011; Pelé *et al.*, 2015; McQueen, Tamburini and Braovac, 2018; Monachon *et al.*, 2020). It should be noted that most of these studies were carried out on archaeological wood which was excavated from a marine environment, unlike the Oseberg artefacts. There are currently limited studies which focus on analysing the inorganic components of the Oseberg alum-treated wood.

One such study specifically aimed to carry out this task (McQueen, Tamburini and Braovac, 2018). Scanning electron microscopy (SEM)-energy dispersive X-ray spectroscopy (EDS), XRD, FTIR and Raman spectroscopy were utilised to analyse the chosen samples. The results proved that the Oseberg wood possesses a high degree of inhomogeneity. Even local environments within one sample had different compositions of inorganic compounds. Iron(II) sulfates were found to be present on the wooden surfaces. The production of these sulfates is presumably due to the corrosion of the iron rods in the wood which were inserted during the post-conservation reconstruction, which is further catalysed by the acidic nature of the artefacts. The resultant ferrous ions could cause more problems in the future since they have also reacted with the alum in the wood, producing sulfates with different cations like aluminium, iron(II) and iron(III). By contrast, iron sulfates were not detected to a large extent near the original nails which were still in place in the wood before treatment with alum and linseed oil. There was no clear explanation as to why

this is and whether this difference is down to the linseed oil or due to the original nails having a different composition than the rods used in the 1900s.

This uncertainty was investigated by Łucejko *et al*., who aimed to discover if the linseed oil provided any protective effects to the wood (Łucejko *et al.*, 2018). The original objective for using the oil was to improve the robustness of the artefacts, as the alum treatment resulted in the wood being very brittle. Samples were taken from various depths of the same fragment. Techniques such as PyGC/MS coupled to electrospray ionisation and quadrupole time-of-flight mass spectrometry (HPLC-ESI-Q-ToF) and gas chromatography coupled with mass spectrometry (GC/MS) were utilised. The results provided by HPLC-ESI-Q-ToF and GC/MS showed that the linseed oil had a higher level of oxidation near the surface of the fragment, as compared to that in the centre (that is, after over a hundred years, the linseed oil below the wood surface had not yet fully oxidised). There was a higher concentration of alum in the fragment surface as opposed to the core, as was similarly reported in a previous study (McQueen *et al.*, 2017). However, through Py-GC/MS it was concluded that there were more degraded lignocellulosic polymers in the alum-depleted core than the alum-rich surface of the linseed oil-coated object. This goes against the usual behaviour of archaeological wood and the previously drawn correlations between alum and the lignin oxidation level (Braovac and Kutzke, 2012). It could mean that the oil is preferentially oxidised, thus preventing wood degradation to some degree.

Other inorganic substances which exist in the alum-treated wood include alunite (a side product of alum breakdown), zinc compounds and reduced sulfur (McQueen, Tamburini and Braovac, 2018). The alunite originates from when the alum was heated during the initial treatment, while the zinc compounds may be due to the zinc tanks which were used for storage after excavation (McQueen, Tamburini and Braovac, 2018). The reduced sulfur forms could be from the sulfate-reducing bacteria which may have existed in the environment that the artefacts were buried in (McQueen, Tamburini and Braovac, 2018).

Presently, a procedure has not been developed to directly estimate the rate of degradation of the Oseberg artefacts. However, it was surmised that this could be partly measured through the use of oxygen consumption studies since the degradation is linked to lignin oxidation and holocellulose depletion (Braovac *et al.*, 2016; McQueen *et al.*, 2017). Consequently, oxygen consumption studies were carried out on wood specimens treated with alum in order to measure the rate of

oxidative degradation occurring in the Oseberg artefacts (McQueen *et al.*, 2020). It was shown that even low concentrations of iron salts in the wood increased the oxidation rate, although the alum treatment itself could have also affected this. This study proved that such oxygen consumption tests are a useful tool to measure the chemical stability of alum-treated test specimens, both before and after retreatment.

Overall, the studies demonstrated that alum-treated wood is a highly complex and heterogenous material and that it is essential to understand how each individual component affects the mechanism of wood degradation and any future retreatment.

1.3 The retreatment of the Oseberg artefacts

Why are new consolidants needed? Although alum-treated wooden artefacts exist in other museums, these represent vastly different scenarios when compared to the Oseberg collection. Two such institutions which have previously investigated alum-treated wood include The Swedish National Heritage Board and the National Museum of Denmark, whose artefacts were mostly treated with alum before the 1910s, and then a combination of alum and glycerol after this period (Braovac, 2015). The most common retreatment method practiced in these institutions involved using water to completely remove the alum salts and acid, and then putting the artefacts through PEG treatment and freeze-drying. Although this might work for some of the more simple and smaller objects in the Oseberg collection, it would not be suitable for others. The objects previously retreated with this method were not reconstructed from many pieces and did not have detailed carvings like the majority of the Oseberg artefacts. As such, a treatment like this may prove to cause more damage than good if applied to certain pieces.

The wide heterogeneity of the wood condition in the Oseberg collection instead requires a diverse toolkit for its retreatment. Some of the more well-preserved objects may well be retreated with aqueous consolidants like PEG since they would be able to withstand immersion in water. Others however are far too fragile to survive this kind of procedure, as it may result in the dissolution of the alum inside the wood and lead to total collapse. Additionally, some of the artefacts contain non-wood components which were added in past restorations such as metal rods, glue and plaster (Braovac

et al., 2018). For these objects, there is increased risk of damage if they are immersed in water. As a result, it is deemed preferable to retreat the most deteriorated and reconstructed artefacts with consolidants in non-aqueous solvents. Since this would not involve immersion in water, it therefore means that an alternative way has to be devised to deacidify the objects before the application of the consolidants.

Currently there is an active hunt for novel consolidants which may potentially be used to retreat the alum-treated Oseberg artefacts. Due to their ongoing degradation, this search is becoming increasingly urgent the more time passes. This section of the review will detail a number of potential candidates for retreating the Oseberg wood. These include materials which are already in circulation and in use in the conservation field. Others are in the investigatory phase and are therefore still being refined and evaluated.

1.3.1 Nanoparticles for deacidification

The use of nanomaterials has become increasingly relevant in the conservation of cultural heritage (Antonelli *et al*., 2020). A novel way of tackling the issue of acidic wood is through the use of alkaline nanoparticles such as calcium hydroxide $Ca(OH)_2$ (Andriulo *et al.*, 2016). Studies on deacidification using nanoparticles have previously been carried out on other archaeological finds such as the Vasa and the Mary Rose (Giorgi, Chelazzi and Baglioni, 2005; Schofield *et al.*, 2011; Poggi *et al.*, 2014, 2016). When applied to archaeological wood from the Oseberg collection, the addition of $Ca(OH)_2$ nanoparticles resulted in an increase in pH of 2 or 3 units (Andriulo *et al.*, 2016). Unfortunately, it was found that the nanoparticles did not show adequate penetration in the wood, which could be due to their interactions with the wood surface and the alum salts. Further investigation into their delivery should therefore be carried out in order to fully understand their mechanism of penetration.

More recently, hybrid systems which are programmed to simultaneously tackle the deacidification and consolidation of the alum-treated wood were examined. Building on the previous study (Andriulo *et al.*, 2016), a hybrid system of propylene glycol modified silane (PGMS) monomers, $Ca(OH)_2$ nanoparticles and hydroxy terminated polydimethylsiloxane (PDMS-OH) was tested on the archaeological samples

(Andriulo *et al.*, 2017). This system was found to not only deacidify the wood, but also to prevent its fragmentation upon handling. Another system which was reported on was made up of the $Ca(OH)_2$ nanoparticles, PDMS-OH, along with tetraethyl orthosilicate (TEOS) or methyltriethoxysilane (MTES) (Andriulo *et al.*, 2022). The system made up with MTES appeared to be particularly promising, as it showed good wood penetration as well as minimal colour change. The nanoparticles were shown to be very effective in increasing the pH of both fresh and archaeological wood and were able to re-adjust the pH of the alum-treated wood back to that of fresh wood (pH = 4 – 6).

1.3.2 Existing consolidants

Two consolidants which will not be included in this section are Butvar® B-98 and PDMS-OH. These polymers will instead be reviewed in Chapter 5, where their characterisation is described.

1.3.2.1 PEG

PEG is a polymer with ethylene oxide as its monomer (OCH_2CH_2) (Figure 4). Presently it is the most widely used consolidant in archaeological wood conservation (McHale *et al.*, 2017). The chain length of PEG may greatly affect its efficiency as a preservation treatment. Short chains are not effective at treating the wood surface, while long chains do not sufficiently penetrate the wood (Christensen, Kutzke and Hansen, 2012). Examples of its use include the conservation of the Vasa in Sweden (Hocker, Almkvist and Sahlstedt, 2012) and the Mary Rose in the UK (Walsh *et al.*, 2014, 2017).

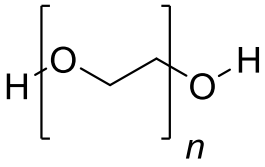

Figure 4. The chemical structure of PEG

A major concern regarding the use of PEG is the possibility that it may gradually degrade in archaeological wood (Christensen, Kutzke and Hansen, 2012), as may be presently happening with the Vasa (Glastrup *et al.*, 2006). This may occur through cleavage at the terminal hydroxyl end groups or through random severing of the polymer chains (Hocker, Almkvist and Sahlstedt, 2012). This degradation, which is accelerated by the iron ions found in the Vasa wood, may lead to the release of formic acid which further complicates conservation efforts and could lead to further wood degradation (Glastrup *et al.*, 2006). PEGs with lower molecular weight are especially problematic since they tend to be hygroscopic, which may further induce the formation of acid with any sulfates present in the wood (Kennedy and Pennington, 2014). Fortunately, the extent of PEG degradation appears to be minimal since even years after application, only a low concentration of formic acid has been found in PEG-treated objects such as the Vasa, the Bremen Cog and the Skuldelev Viking ships (Hunt *et al.*, 2021).

PEG also presents conservators with other issues. Walsh *et al*. list some of these concerns, using the conservation of the Mary Rose as a case study (Walsh *et al.*, 2014). These include the long treatment duration and the associated cost (Mortensen *et al.*, 2007), Another issue with PEG is that it may actually have a detrimental effect on the mechanical strength of the object it is used to treat (Tahira *et al.*, 2017). In fact, the PEG treatment of the Vasa was noted to have negatively affected the stiffness of the wood, causing it to deform over time (Bjurhager *et al.*, 2010; Lechner, Bjurhager and Kliger, 2013). Additionally, PEG is vulnerable to degeneration by microbes (Kawai, 2002; Hocker, Almkvist and Sahlstedt, 2012) and is prone to photochemical degeneration, a factor that may affect the lighting in museums (Hocker, Almkvist and Sahlstedt, 2012).

Despite these shortcomings, PEG is still the most popular treatment for archaeological wood, particularly since the above-mentioned problems are mostly

incited by the presence of metal ions and the use of high temperatures (Tahira *et al.*, 2017). It comes in a wide range of sizes with lower molecular weight preparations ranging from 200 to 600 Da, to higher molecular weight ones being over 1500 Da. A conservator can choose which type of PEG to use depending on the object that they are treating. The lower molecular weights can easily penetrate waterlogged wood to replace the water found in the cell wall in well-preserved wood cores. On the other hand, the larger PEGs are better at filling the spaces within the cell walls which have been consumed by bacteria during burial, thus giving better structural support (Jones *et al.*, 2009).

Due to its history of long use and the existing knowledge base that is available, the treatment of the more well-preserved Oseberg artefacts could be conceivably carried out with PEG, if the conditions are well-controlled. PEG however cannot be used to treat the artefacts which contain metal components, or those that are in a very fragile state. Such objects require treatment with a consolidant in a non-aqueous solvent, as this would remove the need for water immersion.

1.3.2.2 Kauramin®

Kauramin® is the trade name for a melamine urea formaldehyde resin (Figure 5) (Hoffmann and Wittköpper, 1999). Impregnation with Kauramin® results in it replacing the water in the cell walls, which leads to the degraded wood developing a strong, non-hygroscopic surface (Gregory, Jensen and Strætkvern, 2012; Collis, 2016). Once the Kauramin® resin is in the wood, the melamine and formaldehyde undergo *in situ* polymerisation when the pH reaches 6 – 7. This induces the formation of a three-dimensional, solidified resin network that provides structural strength (Gregory, Jensen and Strætkvern, 2012; Braovac *et al.*, 2018).

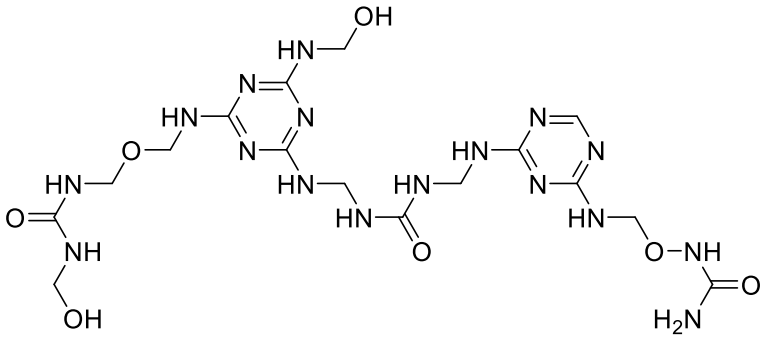

Figure 5. The chemical structure of Kauramin®

It has a low molecular weight and is water soluble, therefore it can easily penetrate wood (Hoffmann and Wittköpper, 1999). Other advantages include the short treatment period, its ability to stabilise wood containing inorganic substances like iron and the inhibition of microbial growth (Gregory, Jensen and Strætkvern, 2012).

One of the drawbacks to Kauramin® is that it is an irreversible treatment and any attempt to retreat the artefact may cause permanent damage to the wood (Collis, 2016). It is also reported to alter the physical properties of the wood, such as changing the colour to a lighter tone (Collis, 2016). Furthermore, treatment with Kauramin® generates toxic chemicals like formaldehyde when it is heated during the polycondensation step (Gregory, Jensen and Strætkvern, 2012).

An example of a successful large-scale conservation project which used Kauramin® as part of the treatment plan is the Yenikapi shipwreck project (Kocabaş, 2015; Collis, 2016; Kiliç and Asst, 2016). This project involved the conservation of a series of medieval shipwrecks excavated in Istanbul. The Kauramin® treatment was preferred due to its low cost and short treatment duration, however the authors point out that it is an irreversible procedure (Kiliç and Asst, 2016).

Along with PEG, Kauramin® is being tested as an aqueous-based treatment for the Oseberg artefacts which would be able to withstand such a procedure (Braovac *et al.*, 2018).

1.3.2.3 Sugars

Sugars are considered to be possible alternative aqueous treatments which can circumvent some of the problems that PEG causes (Parrent, 1985; Pennington *et al.*, 2016; Tahira *et al.*, 2017; Han *et al.*, 2022). Having such an option would be especially useful in order to avoid treating wood with low molecular weight PEG preparations (200 – 400 Da) which are highly hygroscopic (Babiński, 2015).

Sucrose was initially investigated as an alternative to PEG for the treatment of waterlogged wood (Parrent, 1985). Although it successfully prevented wood shrinkage, this sugar invariably undergoes hydrolysis as time passes and starts adsorbing moisture (Kennedy and Pennington, 2014). One way to counteract this is to use non-reducing sugars which are unable to undergo hydrolysis such as sucralose, trehalose, mannitol and sorbitol (Figure 6) (Kennedy and Pennington, 2014).

Sorbitol was found to have a high anti-shrink efficiency, higher than mannitol and trehalose (Jones *et al.*, 2009). These sugars can also be used in combination with PEG, as exemplified by Giachi *et al.* who showed that trehalose increased the efficacy of PEG when used together as a blend (Giachi *et al.*, 2010). Mixtures of different sugars can also be used. Combinations of lactitol and trehalose, as well as mannitol with trehalose were both found to perform successfully as pre-treatments for waterlogged, archaeological wood prior to freeze-drying (Babiński, 2015).

Tahira *et al.* have evaluated the mechanical strength of wood treated with sucrose, trehalose and sucralose (Tahira *et al.*, 2017). The three-point bend test was used to measure the longitudinal modulus of elasticity of both fresh wood and degraded wood treated with these sugars. The treated wood was found to have a significantly higher modulus of elasticity than fresh wood, indicating that such a treatment could be a viable alternative to PEG for conserving archaeological wood. In particular, trehalose had the highest modulus of elasticity, with sucralose having a greater resistance to breakages. Moreover, a recent study by Han *et al.* found that both sucralose and trehalose are better than PEG at improving the mechanical properties of waterlogged, archaeological wood (Han *et al.*, 2022).

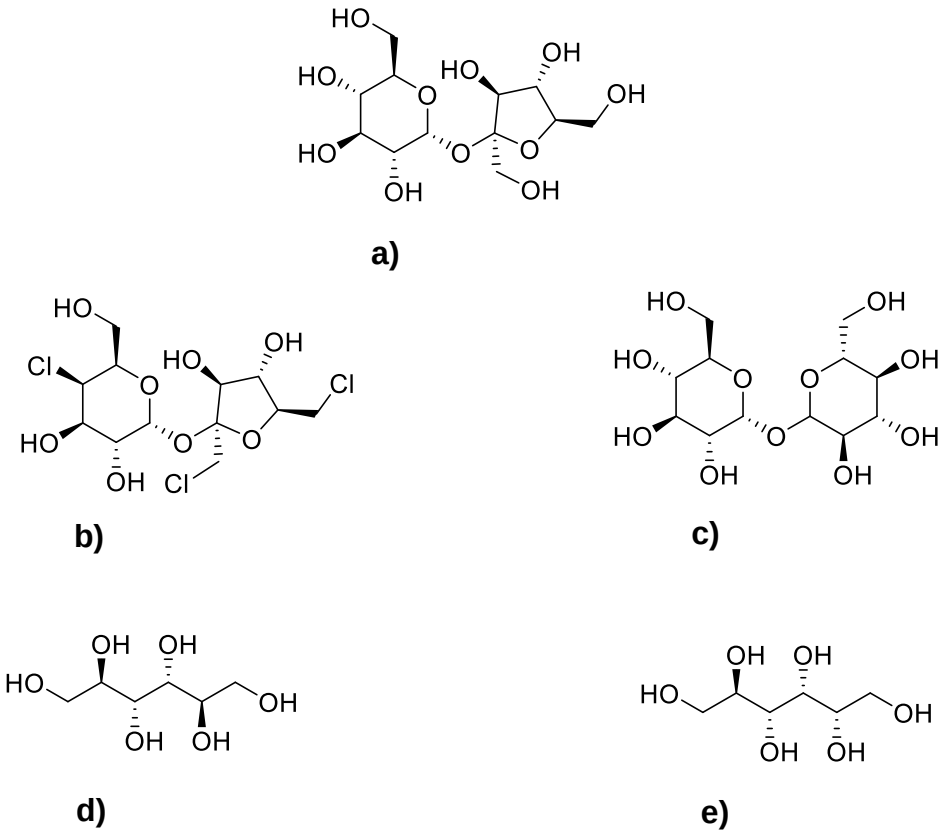

Figure 6. The chemical structures of some of the sugars investigated for conservation purposes: a) sucrose, b) sucralose, c) trehalose, d) mannitol and e) sorbitol.

Unfortunately, sugars can act as a source of nutrients for microorganisms (Han *et al.*, 2022) and therefore such consolidants require the use of biocides (Parrent, 1985). This is not ideal since it prompts both environmental and health concerns (Florian, 1989; McHale *et al.*, 2017). Moreover, sugars may cause the surface of a treated object to become sticky (Han *et al.*, 2022).

It is noted by Tahira *et al.* that more in-depth studies are needed on sugar consolidants, particularly regarding their reactivity and long-term stability, before they can be accepted as alternatives to PEG (Tahira *et al.*, 2017).

1.3.2.4 Paraloid™ B-72

Acrylic co-polymers are frequently used in the conservation field (Podany *et al.*, 2001). Paraloid™ B-72 is a thermoplastic acrylic resin (Figure 7) (Chapman and Mason, 2003; Vaz, Pires and Carvalho, 2008; Crisci *et al.*, 2010) currently used for the conservation of ceramics (Koob, 1986; Schmidt, Shugar and Ploeger, 2017) and wooden art (Crisci *et al.*, 2010). The material itself is made up of two different monomers: methyl acrylate and ethyl acrylate (Crisci *et al.*, 2010). Koob lists the advantageous properties provided by Paraloid™ B-72 namely high stability, reversibility and mechanical robustness (Koob, 1986). Additionally, Paraloid™ B-72 has a glass transition temperature (T_g) of 40 °C, which makes it less susceptible to deformation (Koob, 1986). Schmidt *et al*. however argue that its T_g is not high enough for it to be used in places with hot climates unless they are equipped with temperature-controlled facilities (Schmidt, Shugar and Ploeger, 2017).

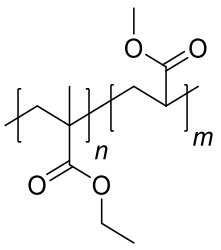

Figure 7. The chemical structure of Paraloid™ B-72

Crisci *et al*. carried out a study with the aim of characterising the behaviour of Paraloid™ B-72 once it was applied to wood samples from two species (broadleaf white poplar and conifer Norway spruce) (Crisci *et al.*, 2010). The effect of Paraloid™ B-72 on the samples was compared to that of a hydrocarbon resin, Regalrez® 1126. It was found that Paraloid™ B-72 caused a greater reduction in wood porosity, as it had more of a direct effect on the cell lumina. Regalrez® 1126 altered the surface colour of the wood to a lesser extent. Paraloid™ B-72 showed greater adherence to

the wood fibres, which translated to a higher resistance to mechanical damage caused by thermal stress. The study also showed that treating the wood with both consolidants carried various advantages, such as a decrease in mechanical damage. However, the combination also resulted in less protection against colour changes and oxidative mechanisms.

1.3.3 The need for new, bioinspired consolidants

PEG, although presently the most popular treatment for waterlogged wood, is not a sustainable material since it is manufactured from fossil fuels. PEG itself is water-soluble and non-hazardous however its monomer, ethylene oxide, is both toxic and flammable. Additionally, when used for conservation purposes it generates a large volume of waste, since a significant amount of polymer does not end up penetrating the wood at all (McHale *et al.*, 2017). As with many other industries, the entire conservation field requires a shift in mentality and should start focussing more on research concerning bioinspired, sustainable consolidants (Walsh-Korb, 2022)

Nature has long been a source of inspiration for the creation of new materials (Chen, McKittrick and Meyers, 2012; Fu *et al.*, 2013; Lintz and Scheibel, 2013; Studart, 2013; Iturri *et al.*, 2015; Cabane *et al.*, 2016). Cabane *et al*. (2016) provide some examples of the areas where scientists have found success when it comes to bioinspired materials including surface wettability, photonics, self-healing and composite mechanical reinforcing (Milwich *et al.*, 2006; Chen, McKittrick and Meyers, 2012; Yu *et al.*, 2013; Darmanin and Guittard, 2015; Diesendruck *et al.*, 2015). Polymers derived from nature represent a more sustainable alternative to some of the consolidants currently in use (Walsh *et al.*, 2014). Over the years there have been numerous studies surrounding the use of green and natural materials as consolidants in conservation treatments (Parrent, 1985; Cipriani *et al.*, 2010, 2013; Kennedy and Pennington, 2014; Babiński, 2015; Cavallaro *et al.*, 2015; Christensen *et al.*, 2015; Walsh *et al.*, 2017; McHale *et al.*, 2017; Wakefield, Hampe, *et al.*, 2020; Wakefield, Braovac, *et al.*, 2020; Łucejko *et al.*, 2021).

Ideally, a consolidant which is to be used for wood conservation should be compatible and interact with the cellular structure of the wood, providing additional support

without causing structural distortion (Christensen, Kutzke and Hansen, 2012; McHale *et al.*, 2017). After application it should preferably be distributed evenly throughout the wooden structure (Schniewind and Eastman, 1994). The consolidant should not alter the outer appearance of the artefacts and should also be sustainable and non-hazardous to conservators (Walsh *et al.*, 2014).

Christensen *et al*. argue that the possibility of a future retreatment is more important than the consolidant's treatment being reversible (Christensen, Kutzke and Hansen, 2012). Re-conservation is possible when the treatment leaves openings in the wood structure whereby new consolidants can pass through. This means that potential consolidants must ideally penetrate the wood to the appropriate depth whilst leaving room in the pores for future retreatment. Ideally, a consolidant will have a molecular weight of ~ <5 kDa in order to successfully penetrate the wood (Wakefield *et al.*, 2018) although there are some larger polymers which are still able to penetrate, possibly due to their surface interactions (see Butvar® B-98 and PDMS-OH in Chapter 5). As a point of reference, PEG usually has a molecular weight ranging from 0.2 to 4 kDa when used for conservation (Wakefield *et al.*, 2018). This is potentially problematic when it comes to seeking consolidants derived from natural sources as most of these materials have a higher molecular weight when compared to PEG (Wakefield *et al.*, 2018).

It is important to give sustainability due consideration when investigating new consolidants. Not only are non-renewable materials harmful to the environment, but they are also finite and will be nearing depletion within the next century (Wilbon, Chu and Tang, 2013). Naturally, there has been increased interest in the synthesis of green, biodegradable polymers from renewable resources (Wilbon, Chu and Tang, 2013; Sainz *et al.*, 2016; Thomsett *et al.*, 2016). This section of the review will cover a number of naturally derived polymers that could potentially act as consolidants for the alum-treated wood.

1.3.3.1 Lignin

Consolidants which are compatible with lignin are highly attractive since lignin is the one major constituent remaining in degraded archaeological wood (Kaye, 1995;

McHale *et al.*, 2017). Moreover, lignin is a waste product from the paper and pulp industry, thus making it a very sustainable option for consolidation (Łucejko *et al.*, 2021). Lignin-based oligomers derived from monomers like isoeugenol (Figure 8) have been investigated by McHale *et al*. (McHale *et al.*, 2016, 2017).

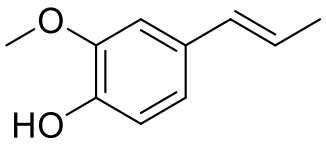

Figure 8. The chemical structure of isoeugenol

Isoeugenol is derived from the essential oil of the Ylang-Ylang tree (*Cananga odorata*) and is inexpensive when compared to other oligomers (McHale *et al.*, 2017). The *in situ* polymerisation of isoeugenol was investigated in order to avoid using organic solvents to impregnate it into wood (McHale *et al.*, 2017). This was accomplished by immersing samples in isoeugenol, water and ethanol to allow the impregnation of the wood with the monomer. Polymerisation of the isoeugenol was then carried out by adding hydrogen peroxide and horse radish peroxidase as a catalyst. While it was confirmed that the *in situ* polymerisation did take place, the consolidant properties of the material were not looked into, therefore it remains to be seen if poly-isoeugenol is a viable option for conservation.

A study evaluating soda lignin, derived from straw and Sarkanda grass, as a potential consolidant has been recently published (Łucejko *et al.*, 2021). The authors desired to test the degree of penetration of two lignins with different molecular weights (1 kDa and 3 kDa) in archaeological wood, using ethyl acetate as the solvent. The study showed that both types of lignin successfully penetrated the wood, with the 1 kDa preparation showing the better performance. This lignin treatment induced a large colour change however, causing the wood to become darker. Nevertheless it was argued that, if the archaeological wood is dark to begin with (as with the Oseberg artefacts), then such a colour change may not be noticeable. While this report

presented promising results, there have been no studies looking into the consolidative behaviour of these lignin treatments up till the present time.

1.3.3.2 Aminocellulose

Aminocelluloses are a class of synthetic water-soluble molecules derived from modified cellulose. They seem to possess properties which would prove valuable for the consolidation of archaeological wood (Harding, 2018).

The weight-average molecular weight M_w of aminocellulose monomers appear to be small enough for successful wood penetration (Harding, 2018). Additionally, these monomers have proven to be capable of forming larger molecules *via* self-assembly (Harding, 2018). This was demonstrated by two separate studies (Heinze *et al.*, 2011; Nikolajski *et al.*, 2014), both of which utilised analytical ultracentrifugation to establish this fact. Initially, it was reported that this self-assembling ability appeared to be partly reversible (Heinze *et al.*, 2011). In a follow-up study, it was observed that aminocelluloses can undergo fully reversible self-association (Nikolajski *et al.*, 2014). This was demonstrated *via* the reversible assembly of an aminocellulose monomer of M_w ~ 3.5 kDa to a larger, tetrameric structure with a final M_w of 13 kDa (Figure 9). These tetramers consequently further assembled into higher-order, supra-molecular oligomeric structures. This is highly unusual as until now fully reversible oligomerisation has never been observed in carbohydrates (Nikolajski *et al.*, 2014). A more recent study described the synthesis of a new aminocellulose which reversibly self-associates, a property which could be useful in conservation since it may potentially mean that it could be removed from the wood should the need arise (Wakefield, Hampe, *et al.*, 2020).

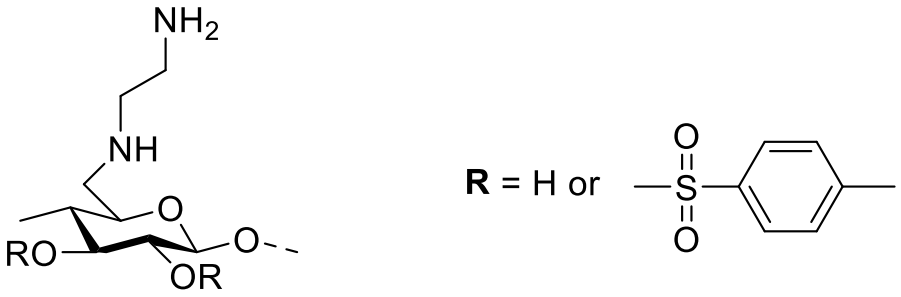

Figure 9. The chemical structure of the repeating unit of 6-deoxy-6-(2-aminoethyl) aminocellulose which was shown to undergo fully reversible tetramerisation (Nikolajski *et al.*, 2014).

1.3.3.4 Chitosan

Other bioinspired consolidants which have been studied include those based on chitosan, a polysaccharide obtained *via* the alkaline deacetylation of chitin (Figure 10) (Christensen, Kutzke and Hansen, 2012; Christensen *et al.*, 2015). Chitin has an identical structure to cellulose except for a hydroxyl group that is replaced by an acetamido group (Christensen, Kutzke and Hansen, 2012).

Chitosan has already been examined for use in a drug delivery context (Lalatsa *et al.*, 2015; Shitrit and Bianco-Peled, 2017). Its biodegradability, adhesive ability and safety make it attractive not only to the pharmaceutical field, but also for conservation applications (Christensen, Kutzke and Hansen, 2012). It does not degrade to acidic by-products, is highly compatible and is inexpensive since it is sourced from waste (Walsh *et al.*, 2014). It also possesses antifungal activity, may reduce the effects of acid and can be easily functionalised (Wakefield *et al.*, 2018).

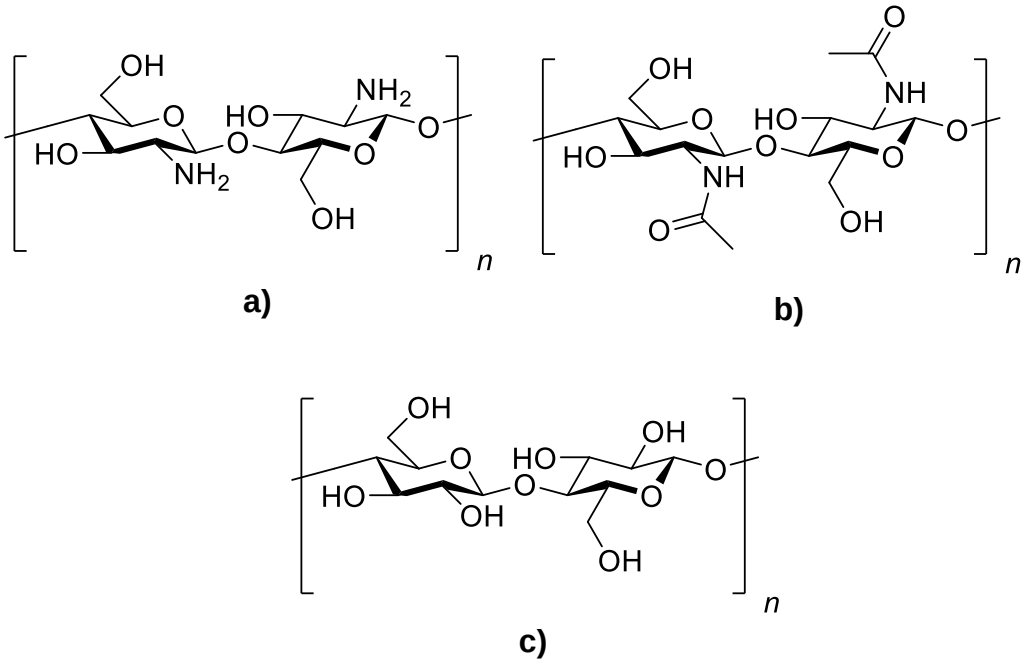

Figure 10. Comparison of the chemical structures of a) deacetylated chitosan, b) acetylated chitosan and c) cellulose. The degree of chitosan acetylation depends on the level of alkaline treatment.

It has already been reported that chitosan penetrates small wooden samples (Christensen *et al.*, 2015). These treated samples were shown to be more robust than untreated pieces. Chitosan not only provides physical support, but it also potentially stops reactive metal ions from acting as catalysts (Christensen, Kutzke and Hansen, 2012; Christensen *et al.*, 2015). Even though its chelating effect increases with high pH, it has shown activity at pH levels as low as 2 (Burke *et al.*, 2002). This makes it especially promising for treating acidic wooden artefacts like the Oseberg objects.

The ability of chitosan to penetrate wood increases as its molecular weight is reduced (Christensen *et al.*, 2015). Wakefield *et al*. achieved controlled depolymerisation of chitosan with hydrogen peroxide and ultraviolet (UV) radiation (Wakefield *et al.*, 2018). This process reduced the M_w of chitosan to 4.9 kDa from an M_w of ~ 14.1 kDa. The successful depolymerisation of chitosan increases its feasibility for use as a consolidant, although reproducibility during scale-up may prove challenging (Wakefield *et al.*, 2018). More recently, it was reported that *tert*-butyldimethylsilyl

(TBDMS) chitosan successfully penetrated several small, degraded birch samples, without blocking the cell lumina (Wakefield, Braovac, *et al.*, 2020).

A potential issue highlighted by Christensen *et al*. is the use of acetic acid as a solvent for chitosan (Christensen *et al.*, 2015). While it is not damaging to the archaeological wood, the group reported that the samples smelled of the acetic acid and "off-gassing" could potentially harm other objects in the museum. This was successfully circumvented by Wakefield *et al*., who instead used a mixture of toluene and ethyl acetate as a solvent for TBDMS chitosan (Wakefield, Braovac, *et al.*, 2020).

1.3.3.5 Terpene-based polymers

The word 'terpene' originates from 'turpentine', a pine tree extract and a major source of monoterpenes such as the pinenes (Ninkuu *et al.*, 2021). Terpenes are cycloaliphatic materials which may or may not be aromatic (Belgacem and Gandini, 2008; Wilbon, Chu and Tang, 2013). They have at least one carbon-carbon double bond and possess an isoprene group as a common component. Monoterpenes, the most common group that is used for polymerisation, contain two isoprene groups and have a general formula of $C_{10}H_{16.}$ They are derived from a number of natural resources, such as coniferous trees like pines (Wilbon, Chu and Tang, 2013; Sainz *et al.*, 2016; Thomsett *et al.*, 2016). They are considered to be the largest and the most diverse plant secondary metabolites that exist in nature and are mediators in plant interactions, both for defensive and informative purposes (Ninkuu *et al.*, 2021). They are therefore a potential source of renewable monomers and polymers, as their raw ingredient can be derived from biomass like wood waste (Sainz *et al.*, 2016). This makes them very promising as building blocks in chemical synthesis and they have been receiving increasing amounts of attention (Wilbon, Chu and Tang, 2013; Thomsett *et al.*, 2016). α-Pinene, β-pinene, limonene and myrcene (Figure 11) are some of the monoterpenes which may make excellent monomers due to their low cost, high abundance and the fact that they do not compete with food supplies (Vilela *et al.*, 2014; Sainz *et al.*, 2016; Schmidt, Shugar and Ploeger, 2017).

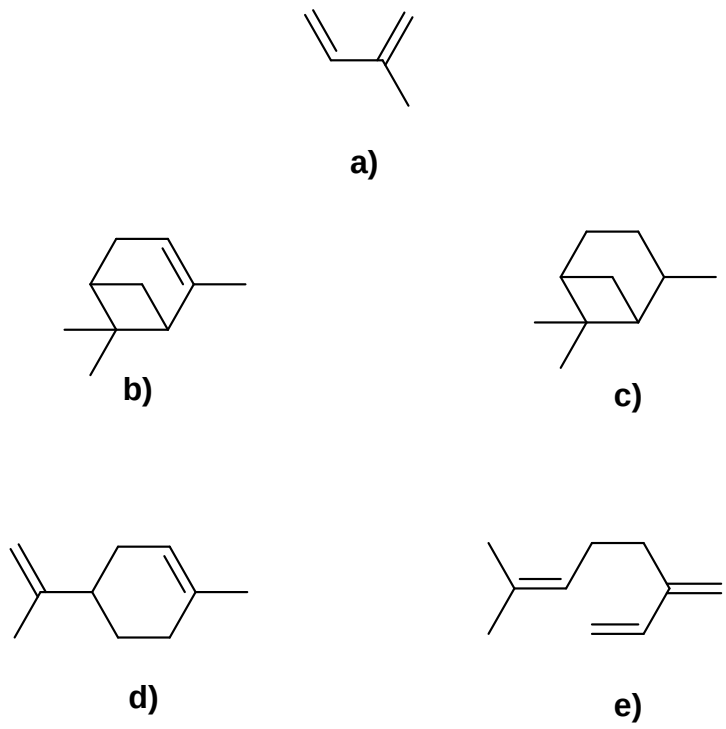

Figure 11. The chemical structures of the a) common isoprene group, b) α-pinene, c) β-pinene, d) limonene and e) myrcene

Sustainable polymers have several shortcomings which prevent their entry into the commercial market. Compared to fossil fuel-derived plastics, they are expensive and do not offer adequate properties which can compensate for their price (Anastas and Eghbali, 2010; Yao and Tang, 2013; Vilela *et al.*, 2014; Thomsett *et al.*, 2016). Terpenes themselves, without any prior modification, do not polymerise easily even with other monomers like acrylates (Sainz *et al.*, 2016). Moreover, some monoterpenes like limonene are known to behave as chain transfer agents in radical polymerisation processes, leading to low molecular weight polymers (Mathers *et al.*, 2006; Ren, Zhang and Dubé, 2015; Thomsett *et al.*, 2016). Nevertheless, while this is not ideal in many fields of study, it may potentially prove beneficial when applied to conservation, since consolidants are required to have low molecular weights to successfully penetrate wood.

Apart from their sustainable nature, a major advantage of terpenes is the fact that they can be modified with specific chemical groups to fine-tune their properties

(Thomsett *et al.*, 2016). This is exemplified with the research carried out by Sainz *et al*., who have found success in the development of new processes using conventional free radical and controlled polymerisation to efficiently produce polymers from terpene monomers functionalised with (meth)acrylates (Sainz *et al.*, 2016)**.**

Such functionalisation increases the chance of success for synthesising effective consolidants from terpenes. Not only can terpenes be transformed into monomers *via* (meth)acrylation, but they can also be modified with other functionalities. An example is the addition of hydroxyl groups to terpene monomers (Stamm *et al.*, 2019; Montanari *et al.*, 2020), to form hydroxylated polymers. Once impregnated in the wood, these materials would have an increased potential for hydrogen bonding with the cell wall. Wood contains a large amount of hydroxyl groups particularly along the cellulose chains, which accounts for its high hygroscopicity. The degradation of wood results in a higher availability of hydroxyl groups which are able to interact with atmospheric oxygen. Having a consolidant which can preferentially hydrogen bond with these exposed hydroxyl groups would therefore decrease the number of free hydroxyl groups which are able to interact with the moisture in the atmosphere, resulting in an overall decrease in the hygroscopicity of the wood (Parrent, 1985).

Although currently it is not possible to carry out commodity-scale production of terpene-based polymers, their modification with polymerisable functional groups may enable scientists to start synthesising specialty products from renewable resources. (Thomsett *et al.*, 2016). The production of functionalised polymers is therefore a compelling route to investigate as these compounds may potentially be used as consolidants for archaeological objects like the Oseberg artefacts.

1.3.3.5.1 Existing terpene applications

Terpenes have a multitude of beneficial properties which makes them useful for several applications. For example, pinenes are appealing to the pharmaceutical field due to their antifungal, antiviral and antioxidant activity (Nikitina *et al.*, 2009; Rivas da Silva *et al.*, 2012; Salehi *et al.*, 2019; Zielińska-Błajet and Feder-Kubis, 2020). This makes them a popular subject of biomedical research. A recent example is the testing of several terpenes extracted from the Red Sea ecosystem as inhibitors for severe acute respiratory syndrome coronavirus 2, the virus which caused the COVID-19

pandemic (Ibrahim *et al.*, 2021). Erylosides B, a terpene glycoside, was found to have a greater binding affinity for the main protease of the virus than lopinavir, an antiviral drug.

They could also potentially prove to be useful in pest management, particularly due to their low toxicity with regards to the environment and human health (Ninkuu *et al.*, 2021). It has recently been reported that a blend of terpenes (α-pinene, 3-carene, α-phellandrene and α-ocimene) was able to attract the insect *Nesidiocoris tenuis*, which preys on tomato plant pests *Tuta absoluta* and *Trialeurodes vaporariorum* (Ayelo *et al.*, 2021).

Additionally, terpenes have been garnering a lot of interest in the petrochemical industry as renewable alternatives to energy production so as to lessen the need for fossil fuels (Ninkuu *et al.*, 2021). A number of terpenes have been identified as speciality biofuels since they have all the requirements needed by industry, such as appropriate viscosities, flash points and freezing points (Mewalal *et al.*, 2017). Speciality biofuels are compounds which have the potential to become biofuels, either used on their own or in a mixture with petroleum-derived fuels (Hellier *et al.*, 2013; Mewalal *et al.*, 2017). Examples include β-pinene which has been used to synthesise a biofuel (Tracy *et al.*, 2009), while limonene and myrcene can be used in a blend with diesel (Harvey *et al.*, 2014).

Other applications of terpenes include their use in perfumes and sweeteners, as well as industrial solvents (Lima, Koester and Veiga-Junior, 2021).

1.3.3.5.2 Terpenes as a sustainable biomass

As is now common knowledge, the enormous amount of plastic waste that is currently being generated is extremely damaging to the environment (Geyer, Jambeck and Law, 2017). Despite this, the petrochemical industry still dominates global energy production. Fortunately, environmental awareness has become more prevalent worldwide and as a result, research into renewable energy is now widespread (Chu, Cui and Liu, 2016; Upton and Kasko, 2016; Della Monica and Kleij, 2020), with the European Union pledging to become carbon neutral by 2050 (Potrč *et al.*, 2021).

The chemical modification of natural molecules to create bioinspired, sustainable polymers is a popular line of research (Papageorgiou, 2018). Materials such as lignin, cellulose, chitosan, vegetable oils and starch are all the targets of continuous work in this regard (Rose and Palkovits, 2011; Chooi *et al.*, 2014; Llevot *et al.*, 2016; Upton and Kasko, 2016; Sarder *et al.*, 2022). Terpenes are also becoming a very popular sustainable feedstock (Thomsett *et al.*, 2016; Winnacker, 2018; O'Brien *et al.*, 2019; Mosquera *et al.*, 2021; Elsmore *et al.*, 2022).

Terpenes, especially pinene and limonene, are cheap and easily accessible (Wilbon, Chu and Tang, 2013). Nowadays, the recovery of terpenes from trees or plants such as pine, mints, eucalypts and citrus can be done on a commercial scale, with approximately 3 million tonnes of terpenes being recovered globally every year (Mewalal *et al.*, 2017), making them easily available. Their ubiquitous presence in certain trees and plants means that they are often by-products of large-scale, industrial processes. Turpentine is considered to be a waste product of the pulp and paper industry and is rich in various terpenes namely pinene, limonene and 3-carene (Sagorin *et al.*, 2021). Being derived from waste biomass, terpenes do not directly compete with food resources which also eliminates the ethical dilemma of food vs fuel (Thomsett *et al.*, 2016). This makes terpenes ideal building blocks for the synthesis of bioinspired, sustainable polymers.

1.3.3.5.3 Rationale for choosing terpenes for the synthesis of wood consolidants

Use of terpenes in the conservation field has not been reported on according to the available literature, except for where menthol was used as a temporary consolidant for Qin Shihuang's 2200-year-old Terracotta Army in China (Han *et al.*, 2014). The authors chose menthol over other materials due to its low toxicity, local availability and inexpensive cost. This had promising results, with menthol being able to offer temporary consolidation until the artefacts were transported from the excavation site to the laboratory.

The decision to use terpenes as the primary starting materials for novel, bioinspired consolidants was due to their characteristic properties that have been discussed in

the chapter. The extensive research that has already been carried out on terpene-derived monomers and polymers (Wilbon, Chu and Tang, 2013; Sainz *et al.*, 2016; Stamm *et al.*, 2019; Thomsett *et al.*, 2020; Atkinson *et al.*, 2021) confirmed that the synthesis of such materials was feasible, thus increasing the chances of the work carried out in this project being successful.

To properly evaluate the rationale for choosing terpenes, it would be useful to first consider some of the ideal properties that any wood consolidant should have:

1. A wood consolidant, for the Oseberg artefacts or otherwise, must first be able to penetrate the objects. One way to increase the chances of this happening is by ensuring that the consolidant has a small enough molecular weight. This is exemplified through the use of PEG, where higher molecular weights (~ 6000 Da) are less able to penetrate than lower molecular weight ones (300 – 600 Da) (Broda and Hill, 2021). There are various ways of controlling the molecular weight during polymerisation reactions, such as using a chain transfer agent or through controlled reactions like reversible addition−fragmentation chain-transfer (RAFT) or atom transfer radical polymerisation (ATRP). Since the polymerisation of terpene derivatives is well-documented, it was anticipated that synthesising a polymer with a controlled molecular weight would not be problematic.

2. A consolidant must also, by definition, provide consolidation. This means that it should increase the structural stability of the archaeological artefact and prevent its collapse both during transport, handling and display (Broda and Hill, 2021). Terpenes could be ideal for this purpose, considering their naturally protective function in plants and trees (Walsh-Korb, 2022). Another important consideration is their ability to be modified with specific functional groups which could alter their behaviour. It was anticipated that through such modification, for example by the addition of hydroxyl groups, the consolidative behaviour of such polymers could be enhanced through the formation of hydrogen bonds with the wood. This could improve the wood's dimensional stability through the increased interactions between the polymer and the wood. Additionally, such interactions would lead to a decrease in the number of hydroxyl groups in the cell wall which would result in heightened hydrophobicity, improved mechanical strength and slower decay (Li *et al.*, 2011; Jiang *et al.*, 2020). Being tree or plant extracts, it was anticipated that

terpenes would be compatible with wood, further aiding in the formation of a polymer network.

3. Another important aspect to consider is the toxicity of consolidants. Conservators have to be in close contact with these materials for prolonged periods of time, therefore they should be able to be handle them safely. Terpenes are generally considered to have low toxicity, although this of course depends on their concentration. In studies where they were tested as skin penetration enhancers, they were noted to have low systemic toxicity and low skin irritation effects (Paduch *et al.*, 2007; Mendanha *et al.*, 2013).

4. Another advantageous property that would make terpene derivatives promising candidates for wood consolidation is their antimicrobial activity (Nikitina *et al.*, 2009; Rivas da Silva *et al.*, 2012; Salehi *et al.*, 2019; Zielińska-Błajet and Feder-Kubis, 2020). Although museum conditions usually prevent the development of microbial complications in artefacts, a consolidant which can protect from biological degradation would still be useful since waterlogged wood can be subject to microbial attack post-excavation during storage and treatment (Antonelli *et al.*, 2020). Having antimicrobial activity would especially be useful if the consolidant is used for treating other types of old wood, such as timber found in historical buildings (Henriques *et al.*, 2014). The use of a biocide is generally required to stop bacterial and fungal growth, and a number of natural materials have been tested for this purpose (Henriques *et al.*, 2014; El-Gamal *et al.*, 2016; Veneranda *et al.*, 2018; Antonelli *et al.*, 2020; Cappitelli, Cattò and Villa, 2020). In fact, some of the most researched materials are essential oils, which are constituted of a large quantity of terpenes (Veneranda *et al.*, 2018; Antonelli *et al.*, 2020). Polymers derived from terpenes, such as the ones made from carvone reported on by O'Brien *et al.*, have been shown to retain their antifungal activity (O'Brien *et al.*, 2019). This could mean that the terpene-derived consolidants that have been investigated in this project could be multifunctional, providing both consolidation as well as biocidal activity.

Finally, it was important that any compounds that were to be used as building blocks for polymers should be sustainably sourced, otherwise this research would only contribute to the environmental damage that is building up day by day. The use of

waste products such as terpenes perfectly aligns with the concepts of waste valorisation and the circular economy.

1.4 General aim and organisation of thesis

The overall aim of this thesis was to develop novel, bioinspired polymers for use as consolidants for the Oseberg artefacts which could also be used for other archaeological wood. This was carried out through the synthesis of naturally derived monomers and polymers, followed by their characterisation and finally their testing on archaeological wood. This research was supplemented by additional work concerning the characterisation of other existing consolidants which were being investigated by the Saving Oseberg group at the time, in an effort to further aid in the progress towards finding suitable consolidants for these artefacts.

As such, the experimental work and results concerning the synthesis of the monomers and polymers is detailed in the Chapter 2. Chapter 3 concerns the characterisation of these materials, with the aim of determining whether they would be promising leads for wood consolidation. Chapter 4 is a report of the pilot wood studies that were carried out with the chosen polymers. Chapter 5 delves into the characterisation work that was performed on Butvar® B-98 and PDMS-OH, two consolidants that are being considered for the treatment of the Oseberg artefacts. Chapter 6 gives an overview of the research that has been carried out for this thesis and serves as a general conclusion, as well as giving insights into possible future work.

1.5 Conclusion

It is clear from the literature that there is a definite need for the development of new materials which can be used in the consolidation of alum-treated wood, especially those which are soluble in non-aqueous solvents. The Oseberg artefacts are very

particular, both in their physical and chemical composition, therefore any future consolidants which are to be used for their retreatment must be carefully chosen. The Saving Oseberg project was specifically set up in order to fulfil these requirements. Its objectives were primarily to fully characterise the archaeological alum-treated wood, to investigate how metal ions and other inorganic compounds affect the wood and to carry out research on potential consolidants and the deacidification of the wood.

This review has covered the research that has been carried out so far within the Saving Oseberg project, focussing on the studies concerning the characterisation of the wood as well as those on novel consolidants. It has also given a broad overview of other existing materials that may possibly be employed for consolidation. Table 1 lists the various advantages and disadvantages of the potential consolidants that have been discussed in this review.

Table 1. Overview of the properties of potential consolidants that may be used for treating archaeological wood

Consolidants	Advantages	Disadvantages
PEG	Has already been used for consolidation of archaeological wood (Hocker, Almkvist and Sahlstedt, 2012; Walsh *et al.*, 2014, 2017) Most widely used wood consolidant (McHale *et al.*, 2017) therefore there is an abundance of knowledge available regarding its use (as well as underlying its disadvantages)	Enables migration of iron and acidic salts (Walsh *et al.*, 2014) Low molecular weight PEGs are vulnerable to environmental conditions (Hocker, Almkvist and Sahlstedt, 2012) Long treatment duration (Mortensen *et al.*, 2007) Aqueous treatment therefore cannot be used for fragile or reconstructed objects
Kauramin®	Has already been used for consolidation of archaeological wood (Kocabaş, 2015; Collis, 2016; Kiliç and Asst, 2016) Can easily penetrate wood (Hoffmann and Wittköpper, 1999)	Irreversible (Kiliç and Asst, 2016) Causes colour change (Collis, 2016) Involves the use of hazardous materials and produces toxic chemicals (Gregory, Jensen and Strætkvern, 2012)

	Short treatment period, can stabilise wood containing inorganic compounds and inhibit microbial growth (Gregory, Jensen and Strætkvern, 2012)	Aqueous treatment therefore cannot be used for fragile or reconstructed objects
Sugars	Increase mechanical strength of archaeological wood (Tahira *et al.*, 2017) Could be viable alternatives to PEG (Han *et al.*, 2022)	May require use of biocides (Parrent, 1985; McHale *et al.*, 2017) Cause surface to become sticky (Han *et al.*, 2022) Reactivity and long-term stability studies are required (Tahira *et al.*, 2017) Aqueous treatment therefore cannot be used for fragile or reconstructed objects
Paraloid™ B-72	Already in use as a consolidant (Koob, 1986; Crisci *et al.*, 2010; Schmidt, Shugar and Ploeger, 2017) Highly stable, reversible and mechanically robust (Koob, 1986)	Its T_g makes it unsuitable for use in hot climates (Schmidt, Shugar and Ploeger, 2017) May cause colour change (Schmidt, Shugar and Ploeger, 2017)
Isoeugenol	Sustainable (McHale *et al.*, 2017) Lignin-based (McHale *et al.*, 2017) Can undergo *in situ* polymerisation (McHale *et al.*, 2017)	Its consolidative abilities still need to be investigated (McHale *et al.*, 2017)
Soda lignin	Sustainable (Łucejko *et al.*, 2021) Successfully penetrates wood (Łucejko *et al.*, 2021)	Induces large colour change (Łucejko *et al.*, 2021) Its consolidative abilities still need to be investigated
Aminocelluloses	Sustainable (Wakefield, Hampe, *et al.*, 2020)	

	Structurally similar to cellulose (Harding, 2018) Monomers are small enough to penetrate wood (Harding, 2018) Monomers can form larger molecules *via* self-assembly (Heinze *et al.*, 2011; Nikolajski *et al.*, 2014)	Further studies must be carried out in order to evaluate their effectiveness Aqueous treatment therefore cannot be used for fragile or reconstructed objects
Chitosan	Sustainable (Walsh *et al.*, 2014) Structurally similar to cellulose (Christensen, Kutzke and Hansen, 2012; Christensen *et al.*, 2015) Does not degrade to acidic by-products (Walsh *et al.*, 2014) Compatible and inexpensive (Walsh *et al.*, 2014) Has antifungal properties and can be easily functionalised (Wakefield *et al.*, 2018) May prevent metal ions from acting as catalysts (Christensen, Kutzke and Hansen, 2012; Christensen *et al.*, 2015) Can undergo depolymerisation in wood (Wakefield *et al.*, 2018)	Carrying out its depolymerisation on a large scale may be challenging (Wakefield *et al.*, 2018)
Terpene-based polymers	Sustainable (Sainz *et al.*, 2016; Thomsett *et al.*, 2016) Highly abundant, inexpensive and do not compete with food resources (Thomsett *et al.*, 2016) Can be functionalised (Sainz *et al.*, 2016; Thomsett *et al.*, 2016)	Have never been tested as consolidants Currently not produced on a large scale (Thomsett *et al.*, 2016)

	Antimicrobial activity (Nikitina *et al.*, 2009; Rivas da Silva *et al.*, 2012; Salehi *et al.*, 2019; Zielińska-Błajet and Feder-Kubis, 2020)	

There has been growing interest these past few years in the sustainability of compounds and it is important to give this due consideration when investigating novel materials. The consolidants which are currently favoured in the field of conservation, such as PEG, are primarily sourced from fossil fuels. This has led to a number of publications reporting on investigations of sustainable, naturally derived consolidants (Christensen *et al.*, 2015; McHale *et al.*, 2016, 2017; Wakefield *et al.*, 2018; Wakefield, Braovac, *et al.*, 2020; Wakefield, Hampe, *et al.*, 2020; Łucejko *et al.*, 2021).

Any future consolidant must ideally fulfil several requirements. It should not be derived from fossil fuels and must be non-hazardous to conservators. It needs to form a supportive network in the wood to provide structural stability and the network that is formed should also maintain an open structure in the wood in order to allow future retreatment. For the Oseberg artefacts, it is particularly important to have consolidants which are soluble in non-aqueous solvents, as these could be used to treat some of the more fragile pieces which would not be able to withstand immersion in water. It is clear from the literature that the Oseberg collection presents a complex challenge and finding materials which adhere to these conditions has proven difficult so far. Further research must therefore be carried out to investigate substances which may be used for the consolidation of alum-treated wood, as well as other archaeological wood that is found in museums worldwide. Terpenes were chosen as the starting point for this research as their advantageous properties make them a particular interesting avenue to explore and they have the potential to be transformed into effective consolidants.

Chapter 2. The Synthesis of Bioinspired Polymers from Nature-Derived Monomers

2.1 Introduction

This chapter will detail the studies that were carried out on the synthesis of hydroxylated, functionalised monomers and their subsequent polymerisation. The aim for these bioinspired polymers was to eventually use them as archaeological wood consolidants. The majority of these experiments were carried out using the terpene α-pinene as the primary starting material. An additional non-terpene, oleic acid-based monomer was also synthesised. The research detailed in this chapter has been published as two separate papers in a peer-reviewed journal (Cutajar *et al.*, 2021; Cutajar, Machado, *et al*., 2022) (refer to Appendix for more details).

2.1.1 α-Pinene

Amongst monoterpenes there has been extensive research done particularly on α-pinene and β-pinene. These molecules are the major components of turpentine, which is mainly derived from pine trees (Miyaji, Satoh and Kamigaito, 2016). It has been reported that the production of turpentine oil is approximately 350,000 tonnes per year (Winnacker, 2018), however this is likely to increase in the future (Yermakova *et al.*, 2009; Colonna *et al.*, 2011; Knuuttila, 2013; Nie *et al.*, 2014; Golets, Ajaikumar and Mikkola, 2015; Winnacker, 2018), making it a highly sustainable resource.

Of the two pinene isomers, α-pinene is the most abundant (Miyaji, Satoh and Kamigaito, 2016) and accordingly, research efforts into polymerisation have focussed

on this particular terpene (Thomsett *et al.*, 2016). It exists as two enantiomers (Figure 12) and possesses a four-membered and six-membered ring, the latter having a trisubstituted carbon-carbon double bond (Miyaji, Satoh and Kamigaito, 2016).

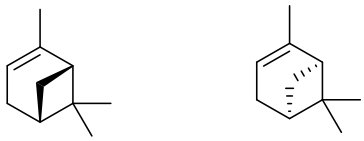

(1*R*)-(+)-α-pinene (1*S*)-(-)-α-pinene

Figure 12. The two enantiomers of α-pinene

Other than its abundance, α-pinene is also intriguing since it is known to possess certain pharmacological properties that might be useful when applied to wood preservation, such as antimicrobial and antifungal activity (Nikitina *et al.*, 2009; Salehi *et al.*, 2019; Zielińska-Błajet and Feder-Kubis, 2020). As with other terpenes, α-pinene can be functionalised to generate molecules that are subsequently converted to products which can then be used on an industrial scale. Examples of such chemical transformations of α-pinene currently being deployed include isomerisation, which converts it to materials like camphene (Corma Canos, Iborra and Velty, 2007; Firdaus, Espinosa and Meier, 2011) and camphor (Della Monica and Kleij, 2020), both heavily used by the fragrance industry. Similarly, α-pinene can be hydrated using aqueous mineral acids in order to produce *cis*-terpin hydrate that can thereafter be converted into α-terpineol, a monocyclic alcohol which is one of the key materials used in the manufacture of cosmetics and soaps (Firdaus, Espinosa and Meier, 2011).

Pinenes are unconjugated alkenes which do not possess aromatic or carbonyl groups, making radical homopolymerisation efforts difficult (Nishida, Satoh and Kamigaito, 2020). The direct polymerisation of α-pinene in particular has not been shown to be as favourable as that of β-pinene, mainly because it is missing a reactive exocyclic double bond (Miyaji, Satoh and Kamigaito, 2016; Thomsett *et al.*, 2016). The first reported cationic polymerisation of α-pinene was carried out in the 1950s using a Lewis acid (Roberts and Day, 1950), however it did not prove entirely successful as it only produced oligomers. It has been reported that some research groups have found success in producing homopolymers by adding antimony trichloride ($SbCl_3$) to

the Lewis acids as an activator (Thomsett *et al.*, 2016). However, most research found in the literature makes it clear that α-pinene is not a useful monomer for homopolymerisation.

2.1.1.1 Polymerisation of functionalised α-pinene

A more promising route is to modify terpenes like α-pinene with specific functionalities which transform them into more effective monomers. Structural elements of the monomer such as side-chains can consequently be transferred to the resultant polymer, offering the possibility to fine-tune its properties (Winnacker, 2018). Examples of functionalisation include that performed by Miyaji *et al*., who used visible-light irradiation to convert α-pinene to pinocarvone (Miyaji, Satoh and Kamigaito, 2016). This compound possesses an *exo* double bond, akin to that found in β-pinene. Meanwhile, Sainz *et al*. have reported on the modification of commercially available terpenes, such as α-pinene, through the use of a hydroboration/oxidation protocol (Scheme 1) (Sainz *et al.*, 2016). The resulting alcohols were then esterified with meth/acrylic acid to form monomers. These were successfully polymerised using conventional free radical and controlled polymerisation to efficiently produce polymers with different properties.

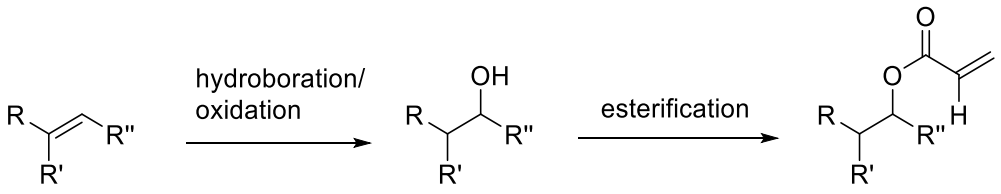

Scheme 1. A general route to synthesise terpene-derived acrylate monomers. The terpene undergoes hydroboration/oxidation and then esterification to form a monomer (Sainz *et al.*, 2016).

One of the most promising derivatives of α-pinene is sobrerol, a cyclic diol. Sobrerol is a particularly interesting starting point for polymers since it is adaptable to different polymerisation techniques and post-polymerisation chemical modifications (Stamm *et al.*, 2019). It has also been shown to have antifungal properties, which would be a useful feature for a wood consolidant to possess (Yuta and Baraniuk, 2005; Stamm *et al.*, 2019). The synthesis of sobrerol (meth)acrylate has been previously described by Lima *et al*., who then used these materials to replace styrene in polyester resins (Lima *et al.*, 2018). The polymerisation of sobrerol methacrylate using both enzymatic conversion and different radical polymerisation methods has also recently been reported (Scheme 2) (Stamm *et al.*, 2019). This involved converting α-pinene to sobrerol with the use of a Cytochrome P450 mutant. The sobrerol was then functionalised with a methacrylate group either *via* standard esterification, or through lipase catalysis. The monomer was then polymerised using several methods: free radical polymerisation (FRP), RAFT, ATRP and enzyme catalysis.

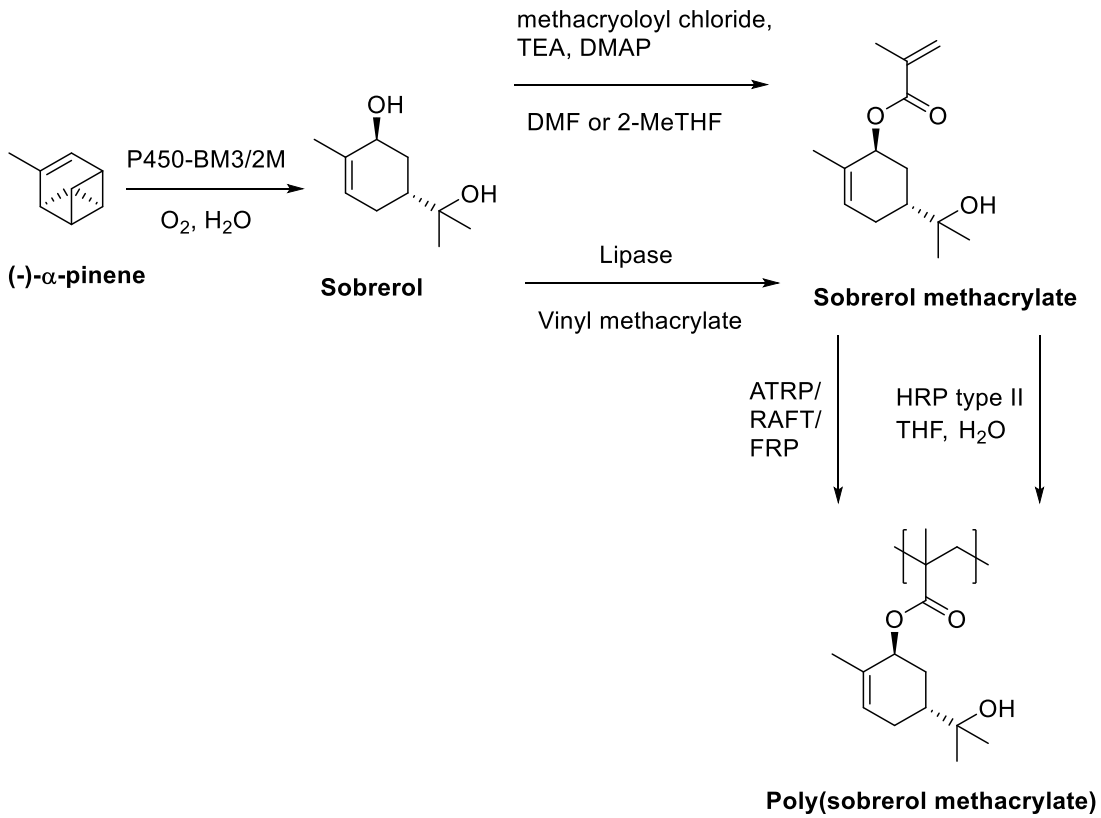

Scheme 2. The chemoenzymatic pathways for the synthesis of sobrerol methacrylate and poly(sobrerol methacrylate) (Stamm *et al.*, 2019).

2.1.2 Oleic acid

Fatty acids such as oleic acid (Figure 13) are considered to be one of the most accessible and affordable resources available (Lligadas *et al.*, 2010; Xia and Larock, 2010), so they are highly popular feedstocks for the synthesis of biobased polymers (Seniha Güner, Yağci and Tuncer Erciyes, 2006; Sharma and Kundu, 2006, 2008; Meier, Metzger and Schubert, 2007; Lligadas *et al.*, 2010; Xia and Larock, 2010). Additionally they generally have low toxicity (Baumann *et al.*, 1988; Biermann *et al.*, 2008; Lligadas *et al.*, 2010; Xia and Larock, 2010), making them very attractive to work with in conservation.

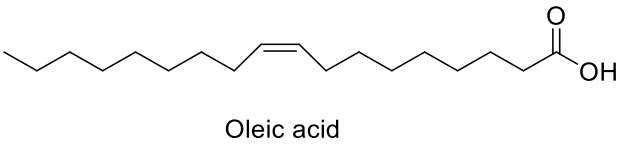

Oleic acid

Figure 13. The chemical structure of oleic acid

Oleic acid in particular is known for its non-toxicity and biocompatibility, moreover it is readily available on the market (Omolo *et al.*, 2017). It has been shown to have anti-bacterial activity (Omolo *et al.*, 2017) and has been used to prepare an antimicrobial and anticorrosive coating material along with an epoxy-acrylic copolymer and butylated melamine formaldehyde (Zafar *et al.*, 2009). It can form strong carboxylic bonds with iron and iron oxide nanoparticles (Zhang, He and Gu, 2006) and has recently been used to coat struvite-K, obtained from pumpkin pulp, in order to produce a mineral fertiliser along with chitosan (Atalay, Sargin and Arslan, 2022). Due to its biocompatibility oleic acid is also a popular material to use in drug delivery, an example is its combination with monomethoxy PEG to form an amphiphilic polymer which could potentially be used to deliver the antibiotic vancomycin (Omolo *et al.*, 2017).

Oleic acid has also been previously combined with wood components such as lignin and cellulose, mainly through esterification. Fatty acid-esterified lignins are known to have increased hydrophobicity and show potential as protective coatings for fibre-based packaging and wood products (An *et al.*, 2020). Cellulose nanofibers obtained from softwoods esterified with oleic acid demonstrated potential as a reinforcing filler in polymeric composites (Almasi *et al.*, 2015).

Oleic acid has recently been successfully functionalised *via* its epoxidation, followed by an acrylation process (Scheme 3) (Neto *et al.*, 2017). The acrylated oleic acid was used to coat magnetite nanoparticles which were thereafter encapsulated into polymer matrices. Its chemical modification provided higher encapsulation efficiency, due to the interaction between the acrylate chain and the polymer phase.

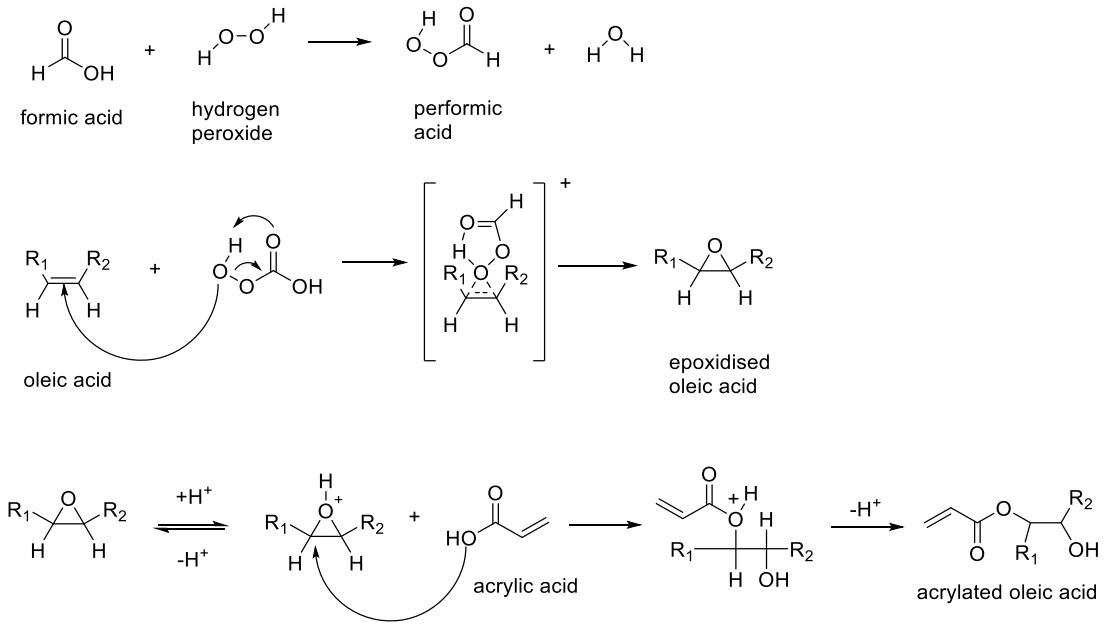

Scheme 3. The epoxidation and acrylation of oleic acid (Neto *et al.*, 2017)

With regards to this project, it was anticipated that the acrylated oleic acid described by Neto *et al.* (2017) would be easily polymerised by FRP, and thus could be combined with a terpene-derived monomer to produce a new co-polymer.

2.1.3 Free radical polymerisation

FRP is a type of chain polymerisation, where a monomer reacts to gradually form a long chain. It consists of three distinctive steps: initiation, propagation and termination. Initiation involves the creation of free radicals and the association of these radicals with a monomer. Propagation refers to the sequential addition of monomers to the growing polymer chain. Termination is the halting of the active centre, thus stopping the polymer chain from growing further. Initiation can be induced through multiple ways like thermal initiators, UV light, photochemical initiators, ionising light, redox reagents or electrochemical initiators (Carraher, 2013).

In this section, thermal initiators will be focussed on since these particular ones were used in the research described in this chapter. These types of initiators, like azobisisobutyronitrile (AIBN), are decomposed through the application of heat to form a pair of free radicals, which is essential for FRP. The rate of decomposition typically follows first-order kinetics and is dependent on the temperature and the solvent used in the polymerisation reaction (Carraher, 2013). Scheme 4 shows a typical route of decomposition for AIBN. The initiator efficiency is rarely 100%, partly due to the created free radical's side reactions.

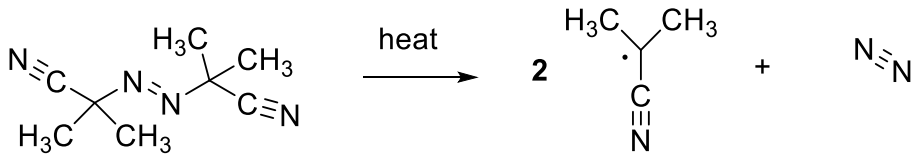

AIBN **free radical**

Scheme 4. A typical route of decomposition for AIBN, forming a pair of free radicals (Carraher, 2013).

Once the free radical is formed (Scheme 5), it adds to one of the monomer's π electrons. The remaining, unreacted electron becomes the new free radical (called the chain radical). This results in the rapid addition of other monomer molecules and thus the growth of the polymer chain, that is, propagation (Scheme 6).

$$I \rightarrow 2\ R\cdot$$

$$R\cdot + M \rightarrow RM\cdot$$

Scheme 5. The process of initiation in FRP. The initiator (I) decomposes to form two free radicals, after which it associates with the monomer (M).

$$RM_1\cdot + M \rightarrow RM_2\cdot$$

$$RM_2\cdot + M \rightarrow RM_3\cdot$$

Scheme 6. The process of propagation in FRP. Monomer molecules (M_1, M_2 and M_3) add on to the formed chain radical, rapidly forming a polymer chain.

In the case of AIBN, termination can be brought about by removing the heat source. It can also take place through 'combination' as a result of the radical pairs reacting with each other, leading to their destruction. This can happen through the reaction of a growing polymer chain with another, resulting in a non-reactive polymer chain which effectively stops growth (Scheme 7). Another type of termination process is called 'disproportionation', where a hydrogen atom is transferred from one radical to another. This results in the formation of two non-reactive polymer chains each with an initiator fragment, one with a saturated terminal group and another with an unsaturated end (Scheme 8).

$$M_x\cdot + M_y\cdot \rightarrow M_{x+y}$$

Scheme 7. Termination of FRP through 'combination'. Two polymer chains ($M_x\cdot$ and $M_y\cdot$) associate with each other, forming an unreactive polymer chain (M_{x+y}).

$$M_x\cdot + M_y\cdot \rightarrow M_x + M_y$$

Scheme 8. Termination of FRP through ‘disproportionation’. Two unreactive polymer chains (M_x and M_y) are produced through the transfer of a hydrogen atom from a radical to another.

2.2 Aims and objectives

Consolidants which are currently used in conservation are not appropriate for the requirements of the decaying Oseberg artefacts. The overall aim of the project was therefore to investigate and develop bioinspired consolidant materials with the goal of ultimately treating said artefacts.

It was decided to focus on terpene-based polymers because of the numerous advantages that they may offer. As previously mentioned in Chapter 1, they are derived from biomass and do not compete directly with food resources. Furthermore, functionalisation makes terpene monomers highly tuneable and gives them useful properties. Such properties include the ability to possibly form hydrogen bonds in the wood structure, as well as anti-microbial characteristics.

It was decided to incorporate an oleic acid-based monomer in one of the polymers, to exploit its advantageous properties and determine whether these would have an overarching effect on the consolidative effect of the resulting copolymer. Oleic acid is a plant-based, sustainable, biocompatible material with antibacterial effects. The branching and hydroxylated nature of its polymers would potentially enhance the interactivity of the consolidant with the wood.

An important requirement which had to be borne in mind was the molecular weight of the synthesised polymers. As discussed in Chapter 1, a small molecular weight is expected to enhance the penetration of a polymer in the wood. A target molecular weight of 5 kDa or below was therefore decided upon. Moreover, it was estimated that approximately 50 g of each polymer would be needed to run the pilot wood studies. The number of synthesis steps therefore had to be kept in balance with the

efficiency of the polymer production, whilst also considering the time limitations of this project.

Another aspect which was considered when planning the synthesis of these polymers was their potential solubility in organic solvents. The severe decay of the Oseberg artefacts is such that most of them are only held together by the alum found in their wooden structure. It is therefore preferable to treat the most fragile artefacts, such as those which have been reconstructed, with polymers in organic solvents as these would not dissolve the alum. Examples of such solvents which may be used in conservation include isopropanol, acetone, ethyl acetate (EtOAc) and mixtures of toluene in ethanol.

Having identified terpenes as being a suitable renewable feedstock for the synthesis of bio-based polymeric consolidants, with oleic acid as an adjunct, the overall aim of the work described in this chapter was therefore to synthesise three specific polymers (named TPA5, TPA6 and TPA7) using α-pinene (and oleic acid) as the base starting material (Schemes 9 – 11).

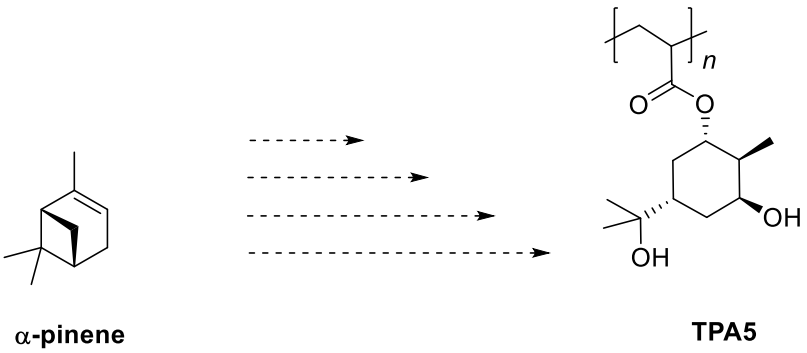

Scheme 9. The targeted formation of polymer TPA5 from α-pinene

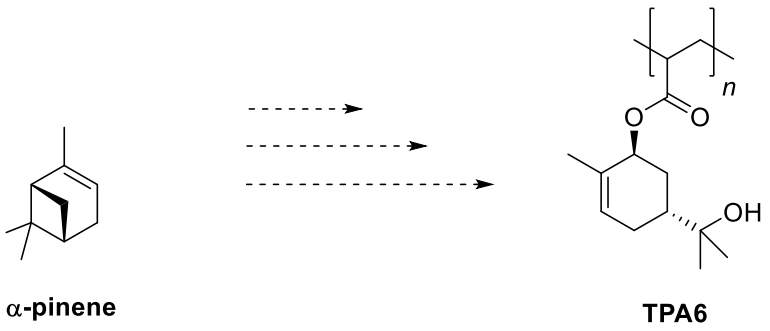

Scheme 10. The targeted formation of polymer TPA6 from α-pinene

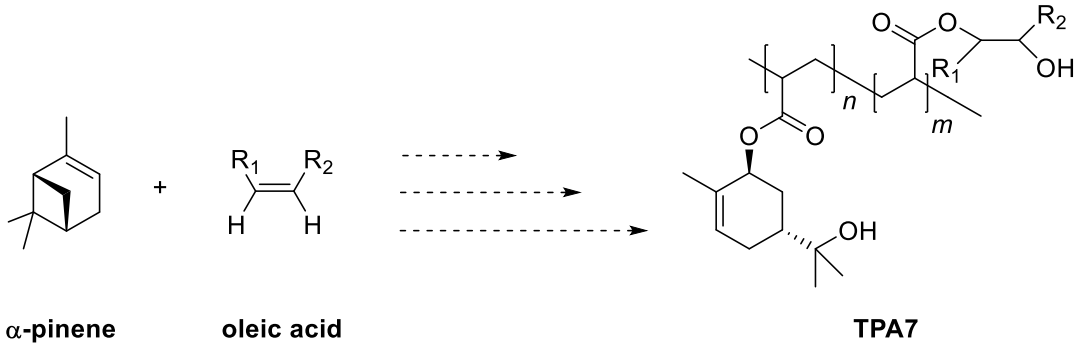

Scheme 11. The targeted formation of copolymer TPA7 from α-pinene and oleic acid

A divergent, terpene-based synthetic route was designed to arrive at potential monomers for this purpose. The planned route (Scheme 12) involved the synthesis of *trans*-sobrerol, which can be used to form a polyhydroxylated 'triol' terpenoid. The acrylation of the *trans*-sobrerol and the triol was then planned *via* an esterification reaction resulting in the potential monomers *trans*-sobrerol acrylate and triol acrylate. The hydroxylated nature of these monomers was designed to impart hydrogen bonding potential to the polymers TPA5, TPA6 and TPA7.

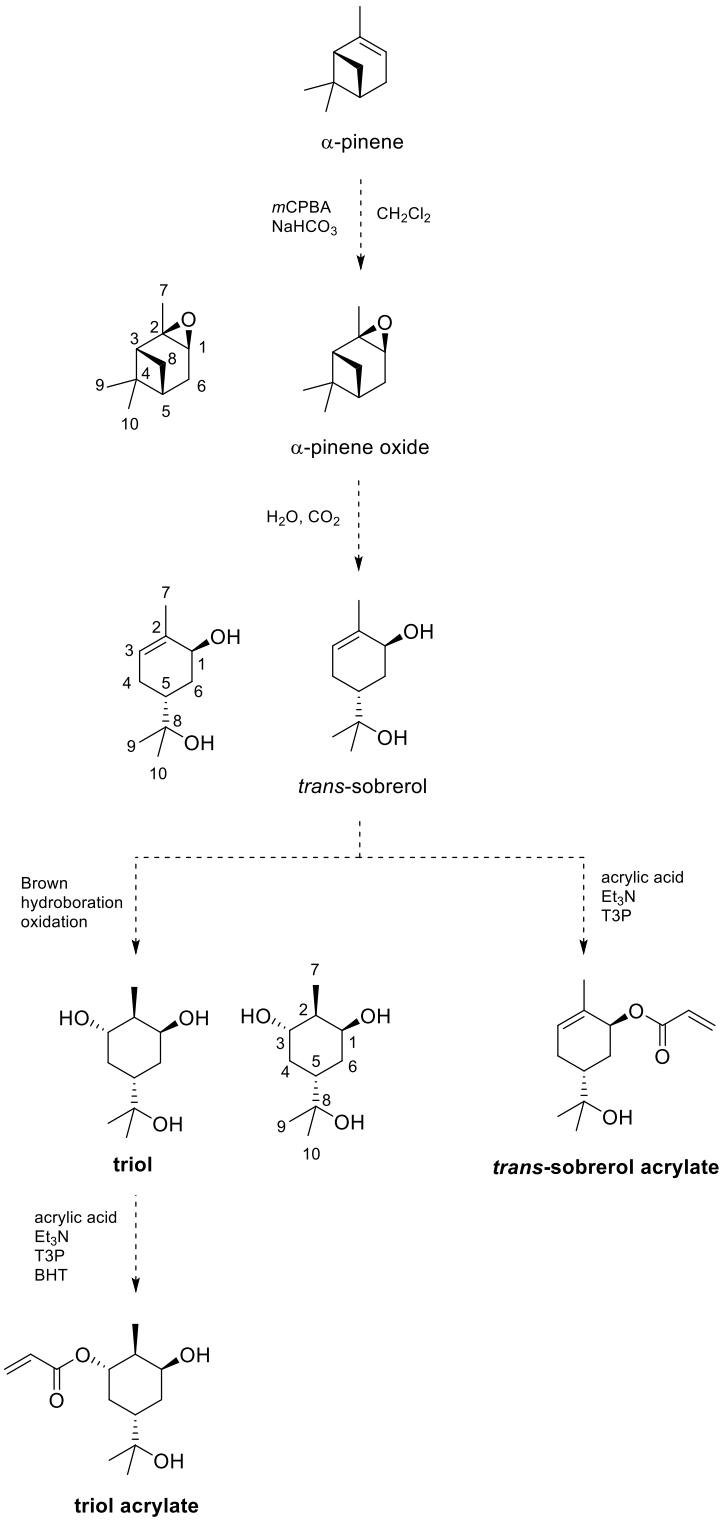

Scheme 12. Planned route for the formation of the desired terpene-derived monomers (*trans*-sobrerol acrylate and triol acrylate). Only major diastereomers are shown in this scheme.

Additionally, it was decided to synthesise an acrylated oleic acid monomer, using robust conditions that had been previously published (Scheme 13) (Neto *et al.*, 2017).

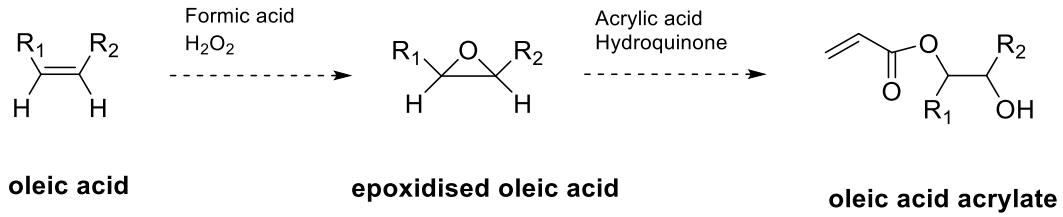

Scheme 13. The synthetic route for the production of an acrylated monomer from oleic acid (Neto *et al.*, 2017).

Monomers with acrylate moieties have been shown to easily undergo conventional FRP (Sainz *et al.*, 2016). After their synthesis, the polymerisation of monomers triol acrylate and *trans*-sobrerol acrylate was to be attempted in order to form TPA5 and TPA6 respectively (Schemes 14 and 15). Additionally, the oleic acid acrylate monomer could be combined with the *trans*-sobrerol acrylate monomer to form the copolymer TPA7 (Scheme 16). After synthesis, these polymers could then be investigated to determine whether they would be worth pursuing further.

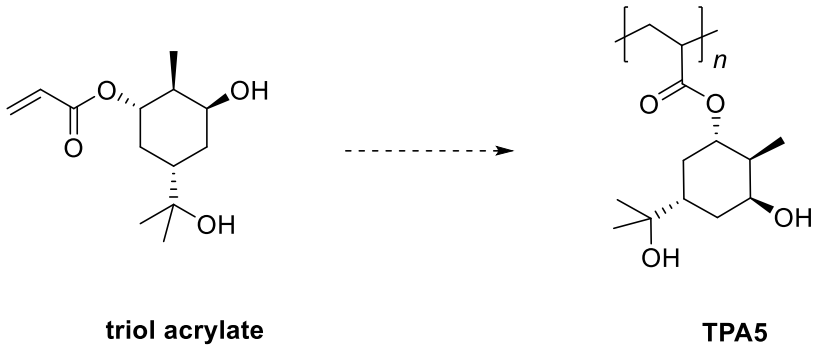

Scheme 14. Planned formation of polymer TPA5 from the triol acrylate monomer

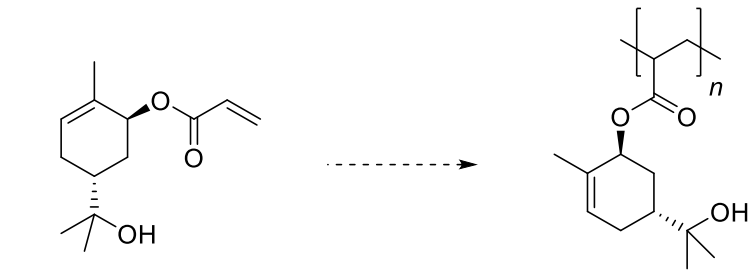

***trans*-sobrerol acrylate** **TPA6**

Scheme 15. Planned formation of polymer TPA6 from the *trans*-sobrerol acrylate monomer

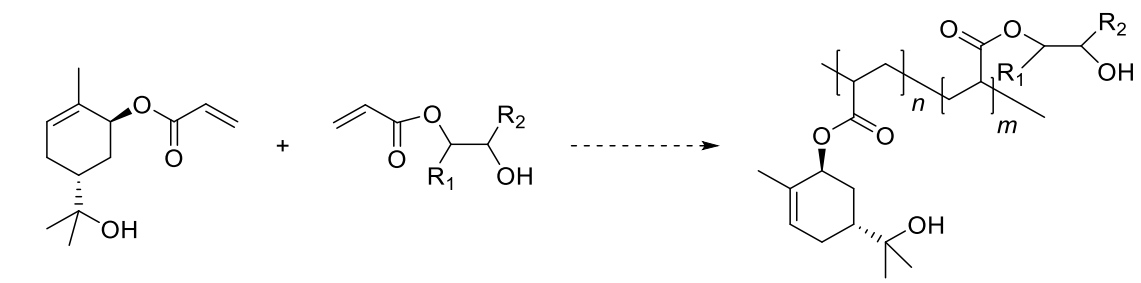

***trans*-sobrerol acrylate** **oleic acid acrylate** **TPA7**

Scheme 16. Planned formation of copolymer TPA7 from the *trans*-sobrerol acrylate and oleic acid acrylate monomers

2.3 Results and discussion

2.3.1 Synthesis of α-pinene-derived monomers

The formation of monomers triol acrylate and *trans*-sobrerol acrylate (Figure 14) has already been investigated in previous unpublished work carried out by the Stockman group at the University of Nottingham, and for this project it was decided to follow similar protocols.

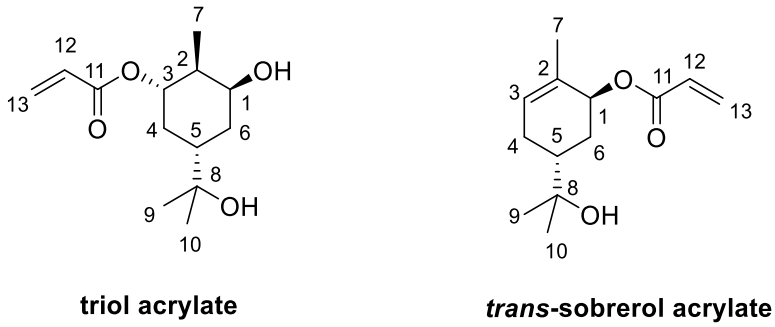

Figure 14. Monomers triol acrylate and *trans*-sobrerol acrylate derived from α-pinene

The triol is derived from the *trans*-sobrerol, and thus they share some fundamental structural characteristics. Both the *trans*-sobrerol and the triol possess a tertiary alcohol at C-8 and a hydroxyl group at C-1 (as seen in Scheme 12). The triol has a *p*-menthane core, with an additional hydroxyl group at C-3. In contrast, the C-3 in *trans*-sobrerol is bonded to a hydrogen atom. It was anticipated that both of these molecules could be functionalised with an acrylic moiety resulting in a pair of functionalised, terpene-derived monomers (Figure 14) which would theoretically be able to easily undergo FRP.

2.3.1.1 Synthesis of α-pinene oxide

α-Pinene oxide shows great promise as a starting material for synthesising functionalised monomers due to its reactivity as a result of the strained 4-membered ring. The epoxidation of α-pinene has in fact been the focus of extensive research (Corma Canos, Iborra and Velty, 2007) and it is currently synthesised on an industrial scale, as well as being widely available commercially.

This oxide was formed by carrying out an epoxidation reaction on α-pinene using *meta*-chloroperoxybenzoic acid (*m*CPBA) as an oxidant (Scheme 17). The terpene was first added to a solution of $NaHCO_3$ in dichloromethane (DCM), after which the mixture was cooled to 0 °C. 1.02 eq. of *m*CPBA was added and the reaction mixture stirred for 1 hour. After quenching with Na_2SO_3, the reaction was allowed to reach room temperature (r. t.) and stirred for another 30 minutes. The organic phases of the mixture were afterwards separated with $NaHCO_3$ and washed with brine. These were then dried over $MgSO_4$ and concentrated under reduced pressure, producing α-pinene oxide in a high yield of 86%. Only a single diastereomer forms due to the dimethyl group on C-4, which sterically blocks the oxygen molecule from attacking in that direction. The formation of the oxide was confirmed with ^1H nuclear magnetic resonance (^1H NMR) (Figure 15).

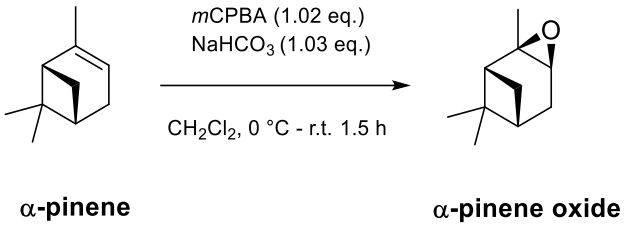

Scheme 17. Epoxidation of α-pinene to give α-pinene oxide

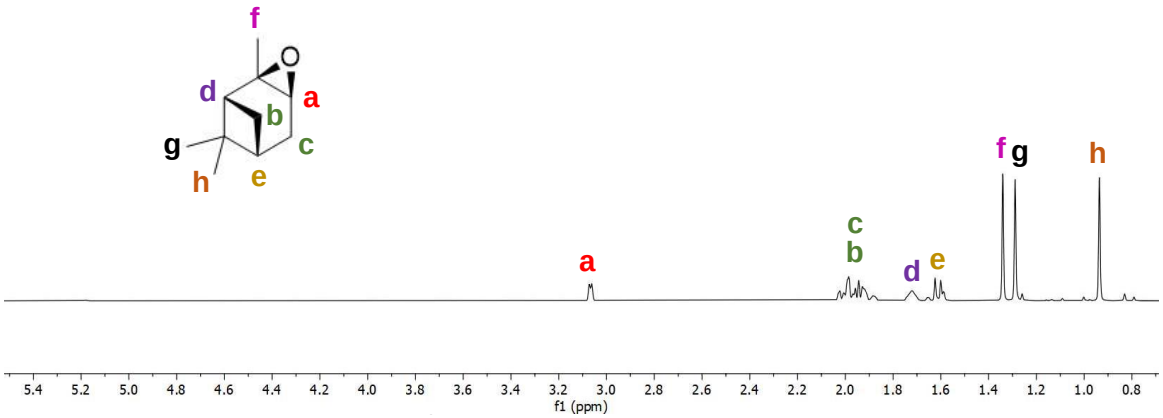

Figure 15. The ^{1}H NMR spectra obtained from α-pinene oxide in deuterated chloroform ($CDCl_2$)

2.3.1.2 Synthesis of *trans*-sobrerol

Trans-sobrerol is a common hydrolysis product of α-pinene oxide. It is achieved through the ring opening of the oxide. This compound was previously synthesised by the Stockman group using conditions adapted from the literature (Scheme 18) (Xu and Qu, 2013).

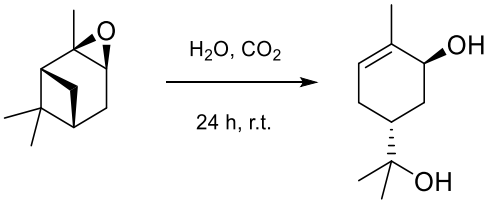

α-pinene oxide **trans-sobrerol**

Scheme 18. Synthesis of *trans*-sobrerol from α-pinene oxide as was carried out in this project

Carbonic acid, produced by generating gaseous CO_2 from dry ice and passing it through water at r. t., was used as a catalyst (Thomsett, 2018; O'Brien, 2020). As such, this reaction is relatively 'green' since apart from water it only makes use of CO_2, which is a common waste steam. α-Pinene oxide was added to the water and carbonic acid and left to stir for 24 hours. This protocol forgoes the organic extraction previously mentioned in the literature (Xu and Qu, 2013) in favour of evaporating the aqueous solvent under reduced pressure, which leaves behind the solid *trans*-sobrerol along with some side-products. A sample of the product which was deemed pure enough to use was thereafter obtained by washing the solid precipitate with cold EtOAc, resulting in a yield of 73% (Figure 16). This is a higher yield than the 68% yield previously reported (Thomsett, 2018).

The proposed mechanism for the formation of *trans*-sobrerol from α-pinene oxide is depicted in Scheme 19. Through acid catalysis the epoxide ring opens to give the carbocation, followed up by a rearrangement that occurs to break the strained 4-membered ring, resulting in the exocyclic cation. This then reacts with water, forming *trans*-sobrerol.

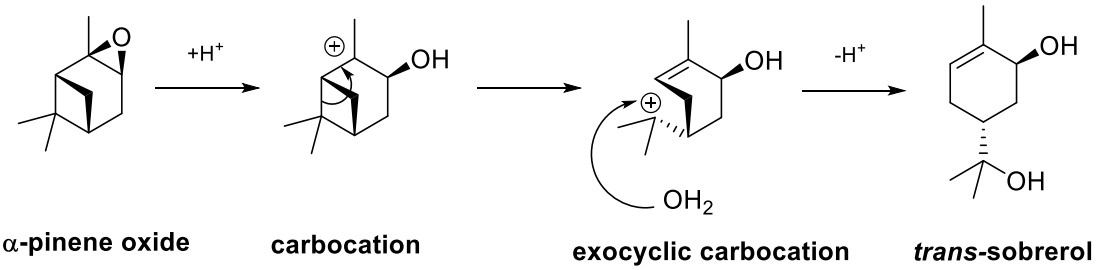

Scheme 19. Proposed mechanism for the acid catalysed transformation of α-pinene oxide to *trans*-sobrerol

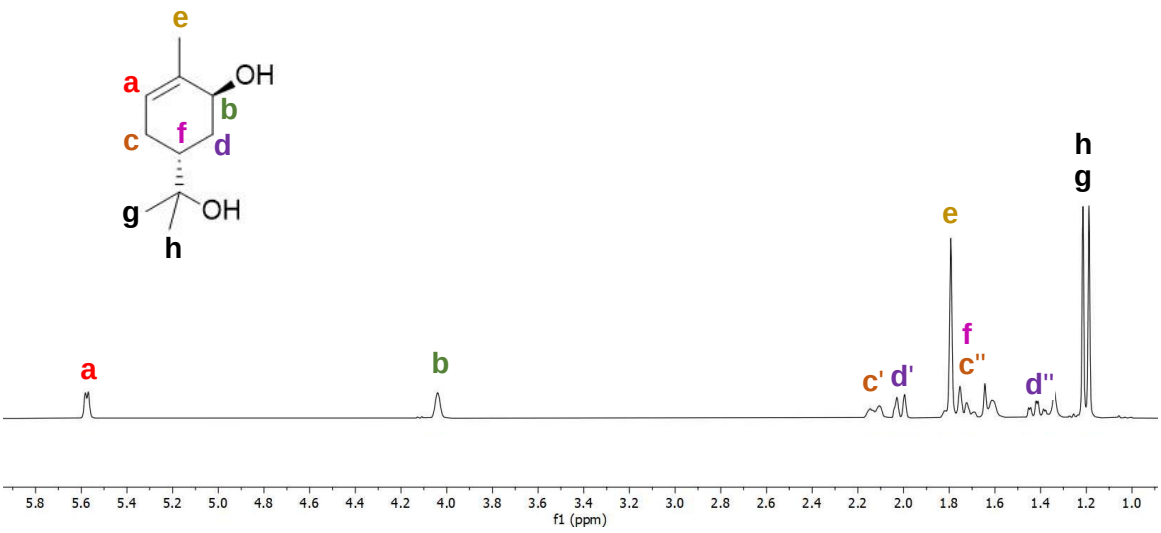

Figure 16. ^{1}H NMR analysis of *trans*-sobrerol in $CDCl_2$

2.3.1.3 Synthesis of the triol

It was decided to initially focus on the synthesis of the monomer derived from the triol, using a Brown hydroboration/oxidation sequence (Scheme 20) (Brown, 1961). The synthesis of this triol has been previously reported by Thomsett and O'Brien (Thomsett, 2018; O'Brien, 2020). Polyhydroxylated compounds such as the triol molecule have a lot of untapped potential, not only for wood consolidation purposes but also for other applications such as drug delivery (Valenti and Wagener, 1998).

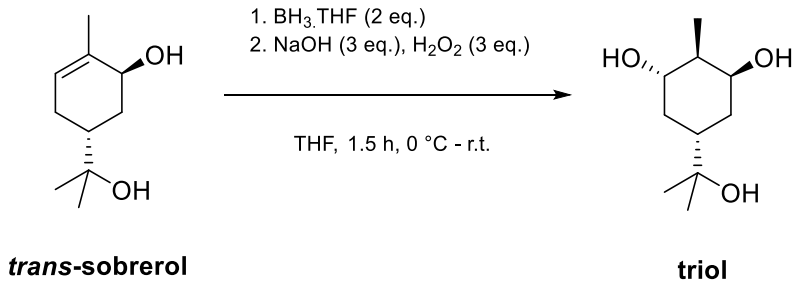

Scheme 20. Brown hydroboration/oxidation of *trans*-sobrerol to give the triol

A solution of *trans*-sobrerol and 2 eq. of borane tetrahydrofuran complex (BH_3.THF) solution in 1 M solution of dry tetrahydrofuran (THF) was cooled to 0 °C under an argon atmosphere. After stirring for 90 minutes, 3 eq. of saturated solution of NaOH and 3 eq. of H_2O_2 were added. The mixture was stirred for 16 hours, after which it was quenched with Na_2SO_3. This hydroboration/oxidation process successfully produced a mixture of two diastereomers (Figure 17). The mechanism dictates that the borane complex is added across the double bond in an anti-Markovnikov process, which means that the alcohol group is added to the least hindered carbon in the double bond, resulting in a *trans* relationship between the two alcohols C-1 and C-3 in the major diastereomer.

The mixture was concentrated under reduced pressure, with the final product being filtered and afterwards purified *via* recrystallisation in hot acetonitrile (MeCN). This recrystallisation isolates the major diastereomer as a solid, while the minor diastereomer is washed away with the hot MeCN. After recrystallisation, a pure sample of the major diastereomer was isolated with an overall yield of 50% (Figure 18). The NMR spectra matched those previously reported (Thomsett, 2018; O'Brien, 2020). This reaction proved to be relatively robust, giving good yields on a multi-gram scale.

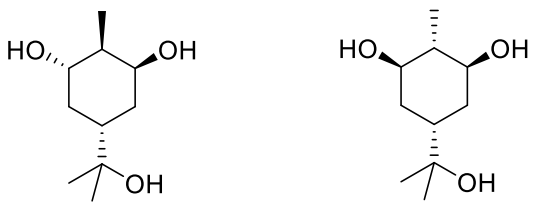

Figure 17. The major and minor diastereomers produced from the Brown hydroboration/oxidation of *trans*-sobrerol

While the minor diastereomer might possibly be isolated using silica gel chromatography, it is theorised that for wood consolidation it would not be needed and therefore this was not investigated further.

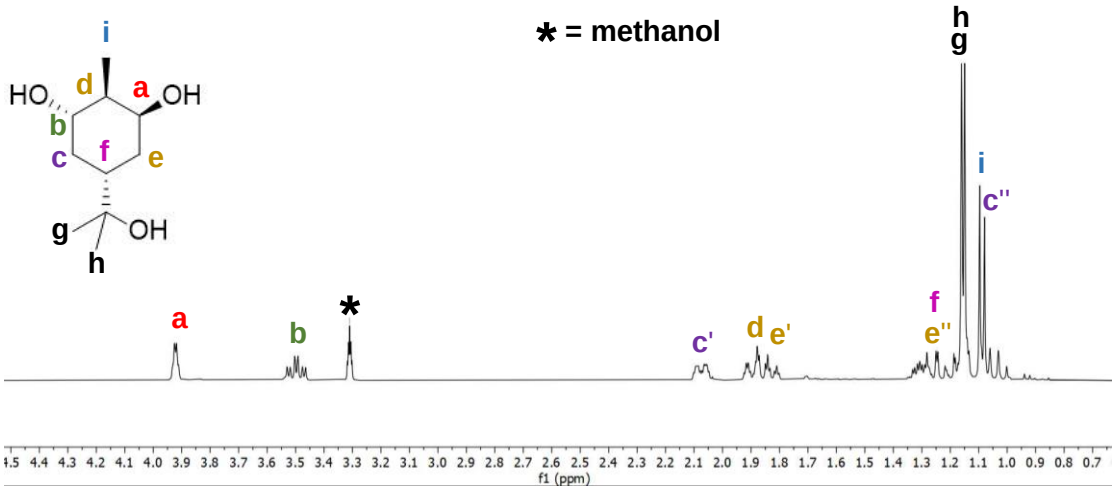

Figure 18. ^{1}H NMR analysis of the triol major diastereomer in deuterated methanol (CD_3OD)

2.3.1.4 Triol acrylate monomer synthesis by functionalisation with an acrylate moiety

Previous work in the Stockman and Howdle groups (Sainz *et al.*, 2016) has demonstrated the (meth)acrylation of a number of alcohols derived from several terpenes like (+)-α -pinene, (−)-β-pinene and (*R*)-(+)-limonene. The groups used a hydroboration/oxidation protocol to directly modify the terpenes to alcohols, in a similar method to that employed in section 2.3.1.3.

The addition of a (meth)acrylate functional group is a well-known process widely employed to enable a variety of monomers to undergo FRP. In one such example, Sainz *et al*. initially esterified hydroxyl-functionalised terpenes with (meth)acryloyl chloride using triethylamine (Et_3N) as a base. This route was further optimised by substituting the (meth)acryloyl chloride with (meth)acrylic acid. Although these acids are not currently renewable, it is likely they will both become commercially available from a sustainable source in the future (Sainz *et al.*, 2016). In fact, there have been recent studies on the sustainable production of acrylic acid and these involve deriving it from lactic acid (Yan *et al.*, 2014), lignocellulosic biomass (Bhagwat *et al.*, 2021) and glycerol (Dimian and Bildea, 2021). Additionally, the use of (meth)acrylic acid

generates ‘green’ and less toxic waste as opposed to chlorinated waste. This makes the reaction more sustainable and scalable.

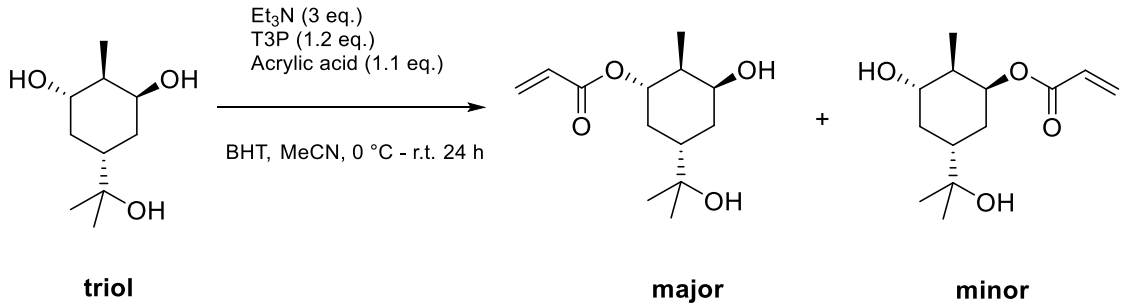

Scheme 21. Functionalisation of the triol with an acrylic group to give the triol acrylate monomer as two diastereomers

The triol and 3 eq. of Et_3N were added to butylated hydroxytoluene (BHT) and MeCN under an inert atmosphere. 1.2 Eq. of propyl phosphonic anhydride (T3P®) and 1.1 eq. of acrylic acid were added, and the reaction mixture was then cooled to 0 °C (Scheme 21). The T3P® was used to promote the ester coupling between acrylic acid and the triol. This reagent is particularly attractive since its by-product is a relatively harmless and water-soluble triphosphate, a preferable alternative to chloride waste generated when using acryloyl chloride (Lima *et al.*, 2018). With regards to the acrylic acid, a grade with low H_2O content (99.5% stab. with ca. 200 ppm methoxyphenol) was utilised.

The reaction mixture was left stirring for 24 hours at r. t. and then concentrated. In the protocol previously followed by the Stockman group (Thomsett, 2018; O’Brien, 2020), the concentration of the mixture was carried out under a flow of air. In this instance, concentration under reduced pressured was attempted instead and this did not appear to negatively affect the monomer in any way. The crude product was subsequently purified by column chromatography. A variety of solvents were screened with thin-layer chromatography (TLC) ahead of purification. The optimal solvent system that resulted in the best product elution proved to be 50% EtOAc in petroleum ether.

The reaction resulted in a mixture of diastereomers (Figure 19). The final product was successfully isolated in two separate fractions: one enriched in the major diastereomer (Figure 20) and another enriched in the minor diastereomer. The fraction enriched in the major diastereomer was isolated in a yield of 19% with a ratio of major:minor = 22.8:1. The fraction enriched in the minor diastereomer had a yield of 23% with a ratio of major:minor = 1:4.6. The total yield of the combined diastereomers was therefore 43% in total, with a ratio of major:minor = 1.3:1. This indicated an optimisation of the synthesis with respect to the previously utilised conditions of the Stockman group, who reported a yield of 37%.

The diastereomers were used together as a mixture for the subsequent polymerisation attempts. It should be noted that for the rest of this thesis the structure of the major diastereomer will be used when referring to the triol acrylate monomer.

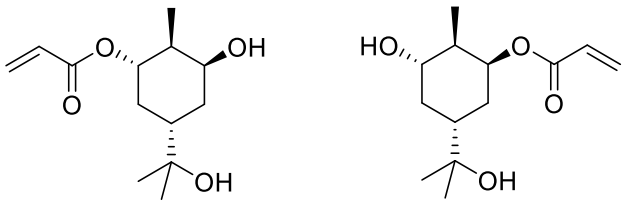

Figure 19. The triol acrylate major diastereomer and minor diastereomer produced from the esterification of the triol

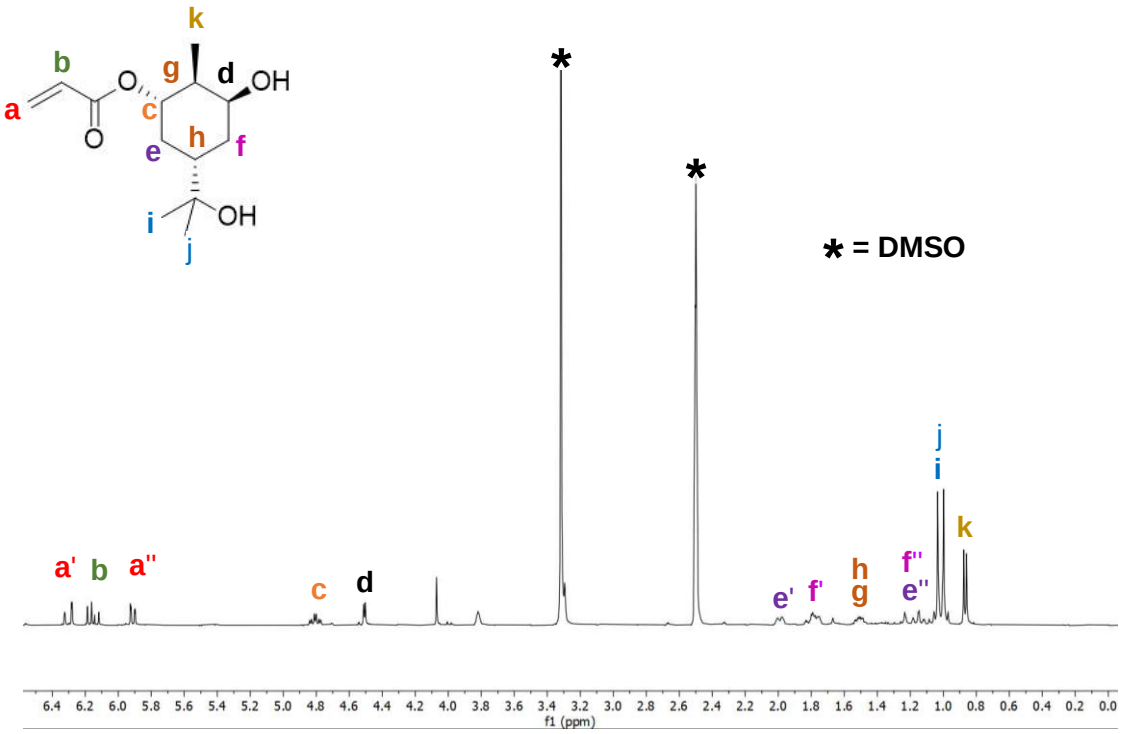

Figure 20. ^{1}H NMR analysis of the triol major diastereomer in deuterated DMSO ($(CD_3)_2SO$)

2.3.1.4.1 Isolation of the triol diacrylate

The isolation of the diacrylate molecule (Figure 21) was also achieved whilst purifying the products of the esterification reaction. This was identified through ^{1}H NMR analysis (Figure 22). It was isolated from the monoacrylated products by column chromatography using a solvent system of 50% EtOAc in petroleum ether, resulting in a yield of 13%.

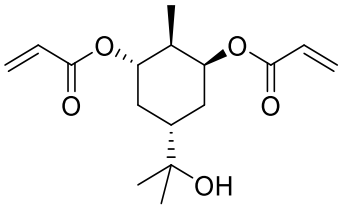

triol diacrylate

Figure 21. The proposed structure of the triol diacrylate isolated from the crude mixture of the triol acrylate diastereomers

It has been hypothesised that this diacrylate molecule may also be used as a monomer for polymerisation. If successful, the eventual polymer would theoretically be very promising as a wood consolidant due to the two acrylate chains that it possesses. These may enhance the crosslinking ability of the polymer, as it would potentially be able to have greater interaction with the wood as compared to polymers derived from the monoacrylate products. However, it was anticipated that a polymerisation such as this would prove difficult to control due to the two reactive acrylate groups and this was therefore not investigated further.

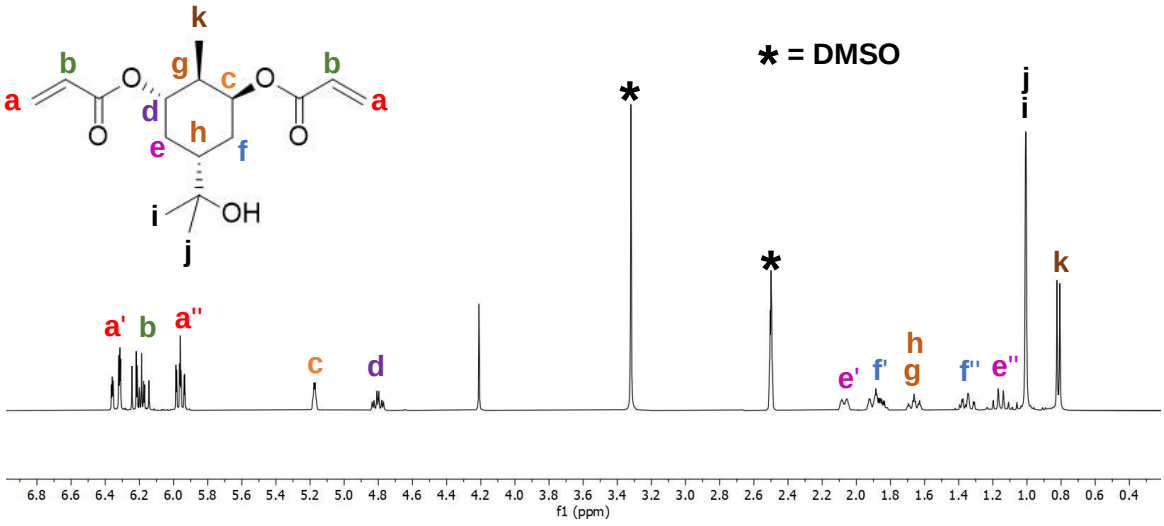

Figure 22. ^{1}H NMR analysis of the triol diacrylate in $(CD_3)_2SO$

2.3.1.5 *Trans*-sobrerol acrylate monomer synthesis by functionalisation with an acrylate moiety

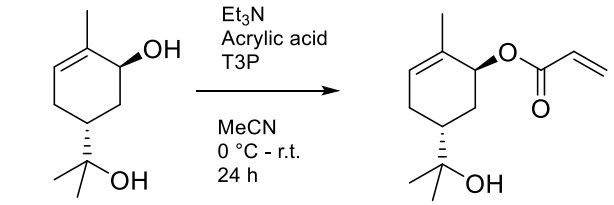

***trans*-sobrerol** ***trans*-sobrerol acrylate**

Scheme 22. The synthesis of the *trans*-sobrerol acrylate monomer from *trans*-sobrerol

The synthesis of the second terpene-derived monomer will now be described. As with the triol acrylate molecule, this protocol made use of the *trans*-sobrerol which was produced from α-pinene oxide. The *trans*-sobrerol then underwent direct acrylation. Although this provides a monomer having one less hydroxyl group than the triol acrylate, it makes the process quicker and more scalable. Apart from having one less synthesis step, it also requires a much simpler purification process, with column chromatography being replaced with solvent extraction. This was an important factor to consider in this work, as the synthesis needed to be efficient enough to be able to make sufficient material for eventual testing on wood, with approximately 50 g of each polymer needed to run a pilot study on wood samples.

Like the acrylation of the triol acrylate, this reaction made use of acrylic acid and T3P®. as a promoter of the ester coupling (Scheme 22). The *trans*-sobrerol was dissolved in MeCN and 3 eq. of Et_3N were added. 1.2 Eq. of T3P® and 1.1 eq. of acrylic acid (99.5% stab. with ca. 200 ppm methoxyphenol) were afterwards added, and the reaction mixture was then cooled to 0 °C. The reaction mixture was left stirring for 18 hours at r. t. and thereafter separated with diethyl ether followed up by 1M HCl, saturated $NaHCO_3$ and brine. The solution was then dried using $MgSO_4$ and concentrated to yield the monomer with a yield of 65%. With regards to the final drying (concentration), it was initially anticipated that air drying was required due to the

absence of BHT. BHT is usually added to monomers to prevent their polymerisation and enable safe storage. It was therefore thought that concentrating under reduced pressure would trigger the polymerisation of the monomer. In order to ascertain this, both drying methods were tested (air drying and drying under reduced pressure). The ^{1}H NMR analyses (Figure 23) demonstrated that drying with a rotary evaporator did not induce polymerisation, thus confirming that this method could be used for future studies.

In the previously established conditions that were utilised in the Stockman group, DCM was used as the primary solvent for this reaction. It was decided to substitute this for MeCN since this also allowed for the full dissolution of *trans*-sobrerol, whilst having a better safety profile. Less toxic solvents are always preferable especially when large quantities are required as with scale-up scenarios. Another change to the established protocol included substituting DCM with diethyl ether in the extraction process, again due to its lower toxicity.

Unlike the acrylation of the triol, it was decided to forgo using BHT in this reaction. When BHT is used, it first has to be removed before carrying out any polymerisation reactions. Not adding it in the first place removed the need for this purification step, thus making the polymer synthesis speedier. To prevent polymerisation in the absence of BHT, any resulting monomers would need to be stored under 0 °C.

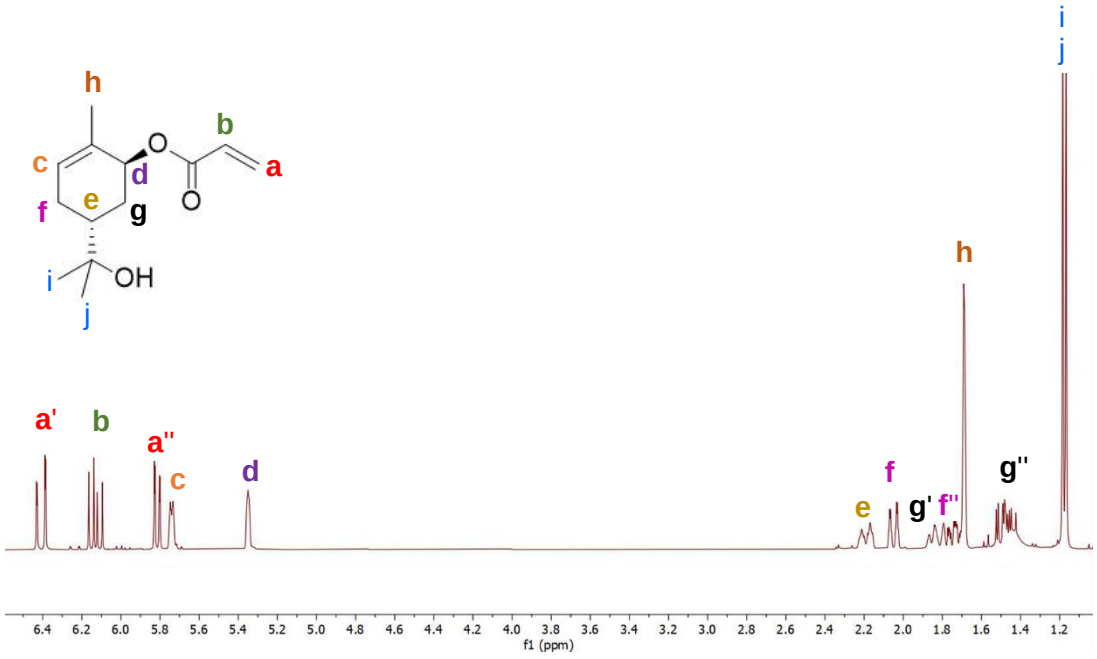

Figure 23. ^{1}H NMR analysis of the *trans*-sobrerol acrylate monomer in $CDCl_2$

2.3.2 Synthesis of an oleic acid-derived monomer

In addition to the terpene-based monomers that have been described, triol acrylate and *trans*-sobrerol acrylate, it was decided to synthesise another monomer in order to create opportunities for the production of copolymers. Oleic acid presented an interesting option as it possesses some attractive properties such as its hydroxylated nature, chain flexibility and ability to create a branched polymeric structure, all of which may potentially improve the ability of its polymer to interact with the wood. Like terpenes, it is a sustainable material and readily available on the market. Moreover it is derived from plants, which may also potentially contribute to it being compatible with wood.

2.3.2.1 Epoxidation of oleic acid

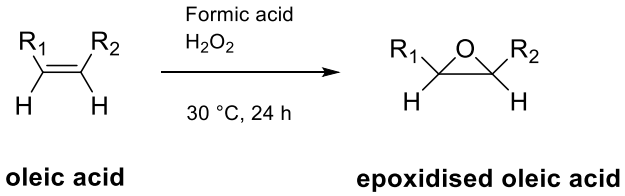

Scheme 23. The epoxidation of oleic acid (Neto *et al.*, 2017)

The synthesis of this monomer (Scheme 23) was carried out by following the procedure described by Neto *et al.* (2017), with modifications. This protocol consisted of two steps, first epoxidising oleic acid and then using acrylic acid to form the monomer (see Scheme 3 in section 2.1.3).

Oleic acid was dissolved in toluene and 3 eq. of formic acid were added. The solution was stirred under reflux at 30 °C. 22.1 Eq. of H_2O_2 were then added and the mixture was stirred for 24 hours. This solution was purified using $NaHCO_3$ and water, and

finally dried with $MgSO_4$ and filtered. It was then concentrated under reduced pressure to yield the epoxidised oleic acid with a good yield of 84% (Figure 24).

The unsaturation of oleic acid makes it highly reactive, allowing the introduction of functional groups like the epoxide ring (Neto *et al.*, 2017). The epoxidation mechanism involves a reaction between a peracid and the unsaturated carbons of the oleic acid. The peracid is formed *in situ* through the reaction of a carboxylic acid (formic acid) and H_2O_2.

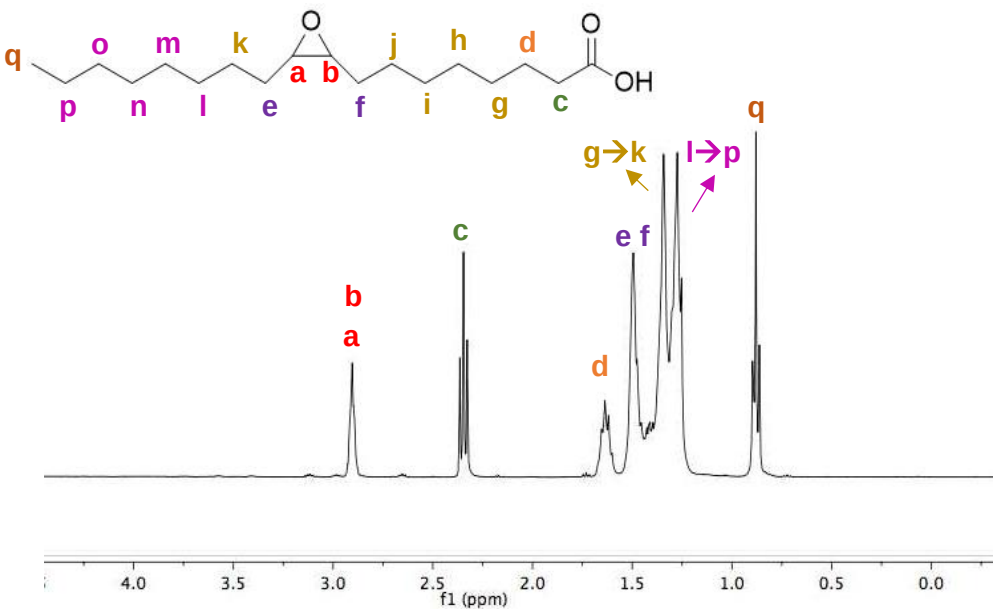

Figure 24. ^1H NMR analysis of the epoxidised oleic acid in $CDCl_2$

2.3.2.2 Synthesis of an oleic acid acrylate monomer by functionalisation with an acrylate moiety

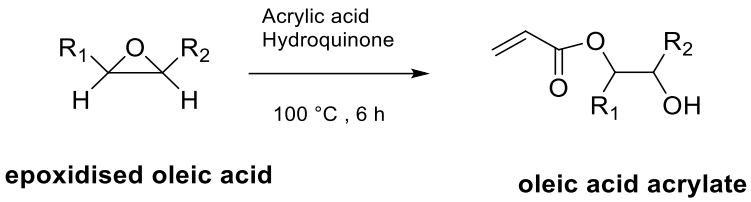

Scheme 24. The functionalisation of epoxidised oleic acid with acrylic acid (Neto *et al.*, 2017)

The epoxide ring of the modified oleic acid was opened with acrylic acid in the presence of hydroquinone. Hydroquinone is a polymerisation inhibitor and is therefore useful in reducing unwanted side reactions, such as acrylic acid homopolymerisation (Neto *et al.*, 2017). Acrylic acid (acid with low H_2O content, 99.5% stab. with ca. 200 ppm methoxyphenol) and hydroquinone were added to the epoxidised oleic acid and stirred for 6 hours at 100 °C. The reaction mixture was then purified with diethyl ether and $NaHCO_3$, dried with $MgSO_4$ and filtered. Concentration under reduced pressure yielded the acrylated oleic acid with an excellent yield of 97% (Figure 25).

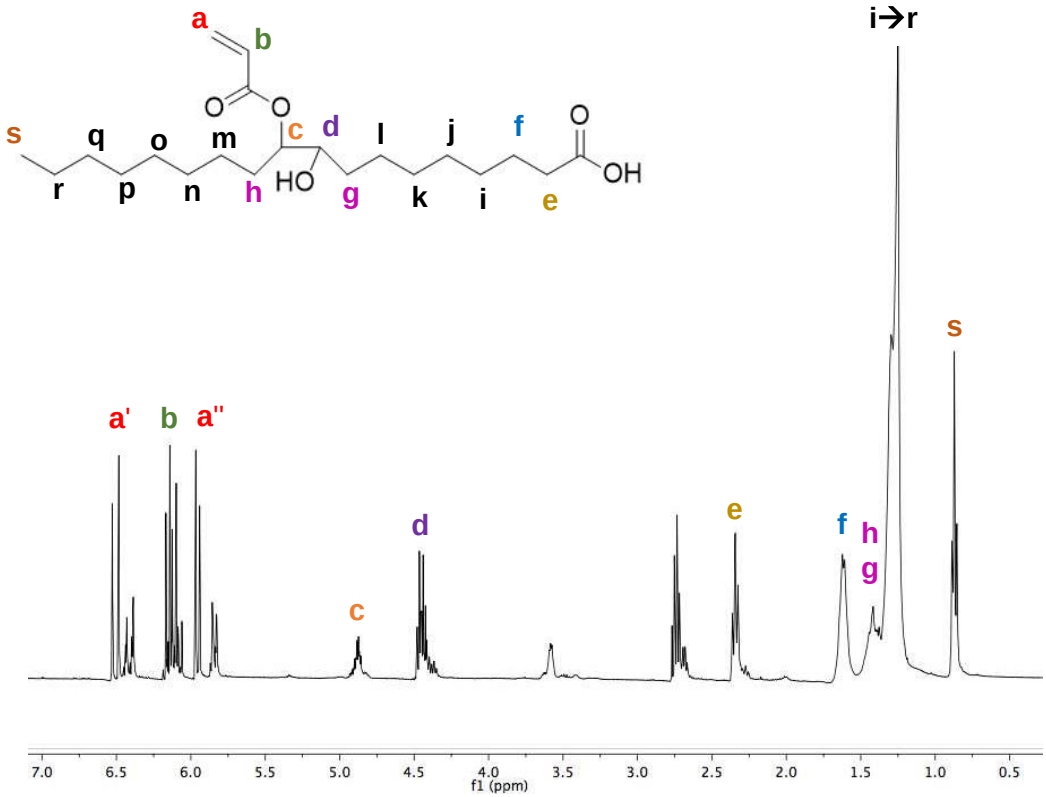

Figure 25. ^{1}H NMR analysis of the oleic acid acrylate monomer in $CDCl_2$

2.3.3 Polymerisations of the synthesised monomers

2.3.3.1 FRP of the triol acrylate, TPA5

As mentioned in section 2.3.1.4, a mixture of the two triol acrylate diastereomers was used for the polymerisation attempts. This diastereomer mixture will be simply referred to as ‘triol acrylate’ for the rest of this thesis.

It was decided to use conventional FRP to produce polymer TPA5, employing AIBN as an initiator. Initially, toluene was considered as a suitable solvent with which to investigate the polymerisation of the triol acrylate. It was chosen over other solvents like THF because it requires shorter reactions times when using AIBN as an initiator, due to its higher boiling point (110.6 °C). It is a common solvent used in FRP and RAFT polymerisations. Unfortunately, it was found that the monomer was insoluble in toluene therefore this protocol could not be followed through.

It was decided to instead attempt using 1,4-dioxane instead. 1,4-Dioxane’s boiling point is 101 °C which, like toluene’s, is higher than that of THF. It was also decided to bypass the freeze-pump-thaw method typically used in polymerisation studies in favour of simply degassing the solution in a constant stream of argon using a Schlenk pump line. After this procedure, the mixture was left to stir for 18 hours in an oil bath at 70 °C (Scheme 25).

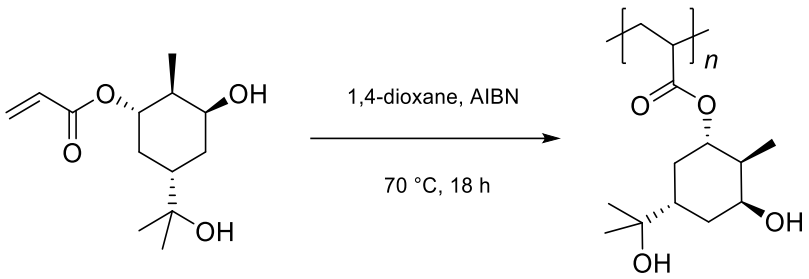

triol acrylate **TPA5**

Scheme 25. The polymerisation of the triol acrylate using 1,4-dioxane as a solvent to give polymer TPA5

After this time, it was planned to use a 1:1 mixture of petroleum ether and hexane to precipitate the polymer. The reaction mixture was mixed with these two solvents and left in the freezer overnight. After this time, it was observed that this mixture had formed long clear crystals. It was further noted that these crystals appeared to be unstable as they were seen to dissolve once taken out of the freezer and exposed to air. This presented a problem as the polymer could not be isolated from the remaining solvent. It was therefore concluded that the precipitation into petroleum ether and hexane could not be used to purify the polymer.

It was decided instead to perform dialysis to purify the polymer, using deionised water as the dialysate. Dialysis is a common diffusion-based separation technique used widely in polymer chemistry and biochemistry. It works *via* a concentration gradient over a semi-permeable membrane to isolate larger molecules from smaller ones. In this case, it was used to isolate the polymer from any remaining monomers and reaction elements.

A semi-permeable membrane with a 3.5 kDa molecular weight cut-off (MWCO) was used to isolate the polymer after stirring for 24 hours. After the dialysis was complete, the sample was concentrated under reduced pressure to isolate a white solid. Subsequent ^{1}H NMR analysis (Figure 26) and GPC analysis (Figure 27) indicated that this was a polymer, meaning that the polymerisation reaction had successfully taken place. The ^{1}H NMR analysis showed that the acrylate peaks had disappeared and that the remaining spectra were broad, all indications that the solid was indeed a polymer. GPC analysis thereafter confirmed a weight average molecular weight (M_w)

of 2.3 kDa and a dispersity (*Đ*) of 1.34. This value was within the targeted range of molecular weights (<5 kDa) and therefore no further modification regarding its size was needed.

Isolation of this polymer with dialysis was carried out on two separate occasions (denoted as Entries 1 and 2 in Table 2), each time producing polymers with a similar M_w and *Đ*, thus proving the replicability of the method. A concern was raised that the polymers may be diffusing through the semi-permeable membrane during the dialysis since according to the GPC results their M_ws were smaller than 3.5 kDa. A third run was therefore planned and carried out, this time using a membrane of 2 kDa MWCO. The results for this polymer (Entry 3 in Table 2) indicated that it had a M_w of 3.4 kDa and a *Đ* of 1.33, making it comparable to the polymers that were previously generated. The polymer in Entry 3 was thereafter named TPA5.

Table 2 shows the data obtained from the GPC analysis namely the M_w, number average molecular weight (M_n), and *Đ*. The results were promising as the polymer appeared to have molecular weights which were small enough to penetrate wood. The *Đ* values were larger than 1, meaning that the polymer chains were not the same length. This was expected however, since FRP polymerisations tend to lead to broader distributions (*Đ* >1.4) when compared to controlled reactions like RAFT or ATRP (*Đ* ~ 1.01 – 1.20) (Whitfield *et al.*, 2019).

Table 2. The results obtained from the GPC analyses of three batches of polymer TPA5

Entry	M_w (kDa)	M_n (kDa)	*Đ*
1	2.3	1.7	1.3
2	2.9	2.3	1.3
3	3.4	2.6	1.5

This last polymerisation attempt reached 46% monomer conversion after 24 hours under these reaction conditions, as determined by ^{1}H NMR. The calculation of the monomer conversion was carried out by Dr Benoit Couturaud (Institut de Chimie et des Matériaux Paris-Est). Higher conversion and narrower *Đ* values can potentially be envisaged by using controlled polymerisation techniques such as RAFT and ATRP. A possible reason for this low conversion was the presence of BHT in the monomer

which was not removed prior to polymerisation. It could have also been due to starting with a low monomer concentration, since this can lead to slower kinetics or lower conversions (Aksakal *et al.*, 2019). This could also explain why the polymer had such a small molecular weight without the use of any controlling agent.

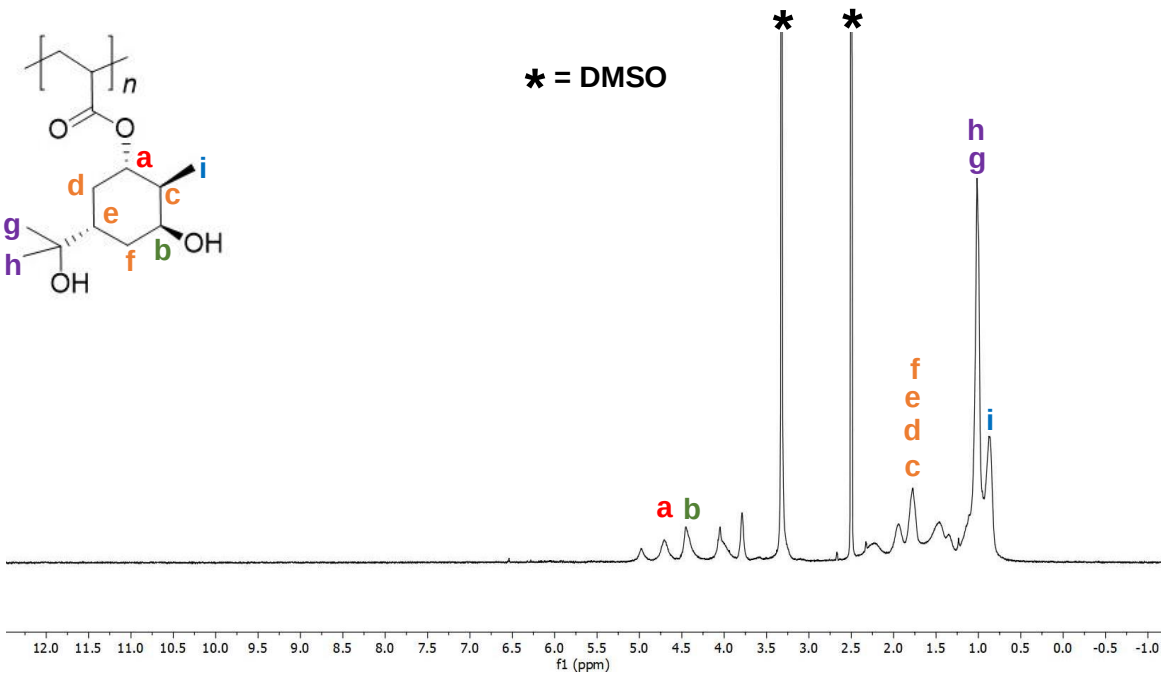

Figure 26. ^{1}H NMR analysis of polymer TPA5 in $(CD_3)_2SO$. The acrylate peaks at 6.30-5.91 ppm no longer appear, indicating that it was successfully purified.

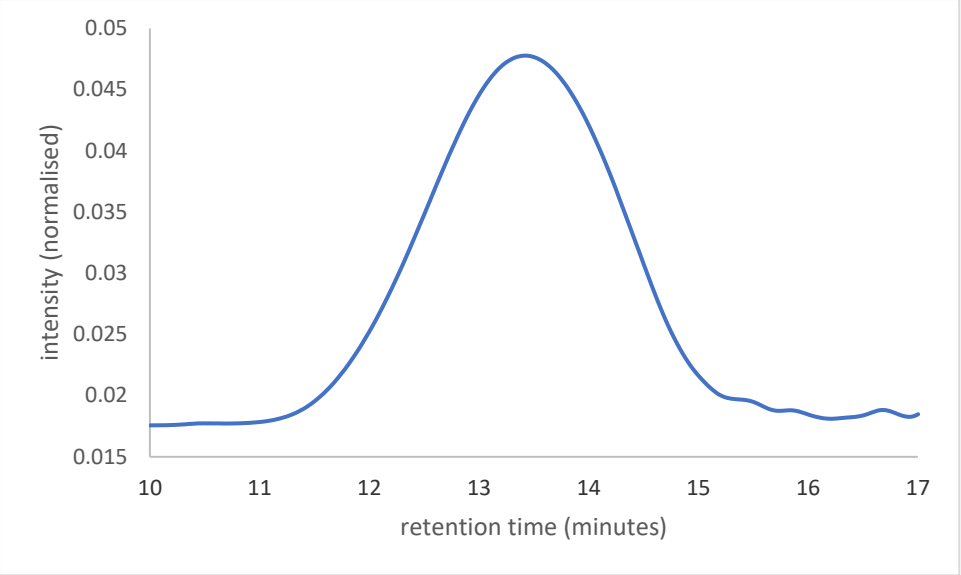

Figure 27. GPC analysis of polymer TPA5 showing the polymer peak. The chromatogram depicts a peak at approximately 13.5 minutes, corresponding to a M_w of 3.4 kDa and a $Đ$ of 1.5.

2.3.3.2 Thiol-mediated FRP of *trans*-sobrerol acrylate, TPA6

As with the polymerisation of the triol acrylate, it was decided to utilise FRP for the *trans*-sobrerol acrylate monomer. A molecular weight of 5 kDa or below was again being targeted. The method previously described for the FRP of sobrerol methacrylate made use of dimethylformamide as the polymerisation solvent and 4,4′-azobis(4-cyanovaleric acid) as the initiator (Stamm *et al.*, 2019). For this work, the homopolymerisation of *trans*-sobrerol acrylate was first attempted using cyclohexanone as the solvent and AIBN as the thermal initiator (Scheme 26). Cyclohexanone is known to be a good solvent for polymerisation reactions as it has a high boiling point of 155.6 °C which enables it to reach high reaction temperatures (Zhen *et al.*, 2005). Moreover it has a better safety profile than 1,4-dioxane, making it the preferred solvent to use.

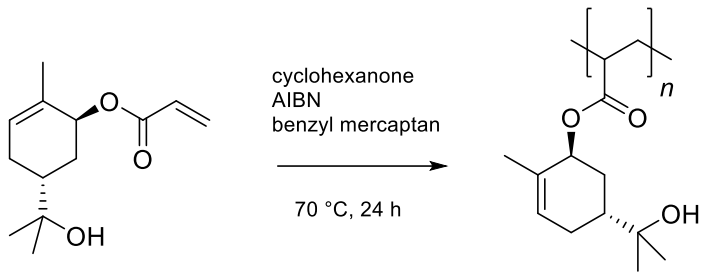

***trans*-sobrerol acrylate** **TPA6**

Scheme 26. The polymerisation of the *trans*-sobrerol acrylate to give polymer TPA6

The *trans*-sobrerol acrylate monomer and AIBN were dissolved in cyclohexanone and purged with argon. This reaction mixture was then left stirring for 24 hours at 70 °C. The polymer was afterwards precipitated in cold hexane and dried in a vacuum oven to yield the homopolymer. Unlike TPA5, this polymer did not require purification with dialysis since precipitation in cold hexane appeared to be adequate.

^{1}H NMR analysis indicated that the polymerisation was successful, with the signals representing the acrylate double bond of the monomer no longer appearing in the spectra after purification. The GPC analysis of this trial FRP reaction indicated that the M_w of this polymer was far too large at 24.3 kDa. It was therefore decided to employ benzyl mercaptan as a chain transfer agent to better control its weight. Thiols have been employed as efficient, nearly ideal, chain transfer agents thanks to the high efficiency in the control of the chain length attributed to a combination of the weakness of the S–H bond, and the high reactivity of the thiyl radicals (RS·) towards the double bonds (Heuts, Muratore and Davis, 2000; Henríquez *et al.*, 2003). A screening was subsequently run on this reaction to identify the optimal conditions (Table 3).

The first reactions that were carried out with the thiol involved the use of very small amounts of monomer (Entries 2 – 4 in Table 3). The thiol mol% was varied slightly with each reaction and the molecular weight change that it caused was monitored by GPC. A thiol mol% of 2%, 5% and 8% were all tested, all of which produced a polymer with a M_w ranging from 3.2 to 5.1 kDa. Another vital aspect which had to be considered at this point was the reproducibility of the reaction on scale-up. To investigate this, a set of reactions with gradually increasing monomer weight were carried out and the

resultant polymers' properties were monitored with GPC. The monomer weight was initially increased to 2.0 g (Entries 7 and 6) and then to 4.0 g (Entry 8). Table 3 demonstrates that the polymers retained similar M_w, M_n and $Đ$ values when the starting monomer weight was increased from 0.5 g to 4.0 g. This suggested that the reaction could be scaled-up further while still retaining the polymer's characteristics. The $Đ$ value is a measure of the different distributions of molecular weight in the system and so can have an effect on the polymer's physical properties (Whitfield *et al.*, 2020). It was therefore important that it remained consistent on scaling-up.

Table 3. The screen that was run for the homopolymerisation of *trans*-sobrerol acrylate, showing the different conditions that were used for each reaction and the results obtained with the GPC analyses.

Polymer ID	Thiol (mol%)	Starting monomer weight (g)	M_w (kDa)	M_n (kDa)	$Đ$
1	0	0.5	24.3	12.3	2.0
2	2	0.5	5.1	3.8	1.4
3	8	0.5	3.2	2.3	1.4
4	5	0.5	5.0	3.4	1.5
5	2	0.5	6.2	4.3	1.5
6	5	2.0	3.7	2.8	1.3
7	8	2.0	8.7	6.7	1.3
8	5	4.0	4.4	3.1	1.4

A final thiol amount of 5 mol% was decided upon since it appeared to produce consistent M_w results (Entry 8). The conditions used for Entry 8 were therefore selected as the optimal conditions to use for the synthesis of the polymer TPA6. Figures 28 and 29 show the ^{1}H NMR and GPC analyses for TPA6 respectively. The GPC chromatogram indicated a peak at approximately 16 minutes, corresponding to a M_w of 4.4 kDa. The $Đ$ of this polymer was 1.4 and the GPC chromatogram confirmed the quality of this reaction since it only depicted a single peak. The conversion of the polymer from the monomer using these conditions was found to be 82%, a much higher value than the one previously reported for TPA5. This was calculated from the ^{1}H NMR spectra of the polymer sample before hexane purification, using the integrals of the resonances corresponding to a proton at the monomer acrylate moiety and the proton at the cyclic alkene moiety in the polymer (signal a in Figure 28).

The T_g of Entry 8 was thereafter measured with differential scanning calorimetry (DSC). The T_g values of the previous entries were not measured since these reactions were not considered optimised. The T_g is the point at which a polymer changes from a tough or glassy material to a rubbery solid (Schilling, 1989). Having data on the T_g of a polymer makes it easier for conservators to select consolidants for specific applications (Schilling, 1989; Davis, Roberts and Poli, 2021). The T_g of TPA6, at the polymerisation conditions selected, was found to be 31.1 °C. This was comparable to that of Paraloid™ B-72 (40.0 °C), a consolidant frequently used in the conservation field (Koob, 1986; Davis, Roberts and Poli, 2021).

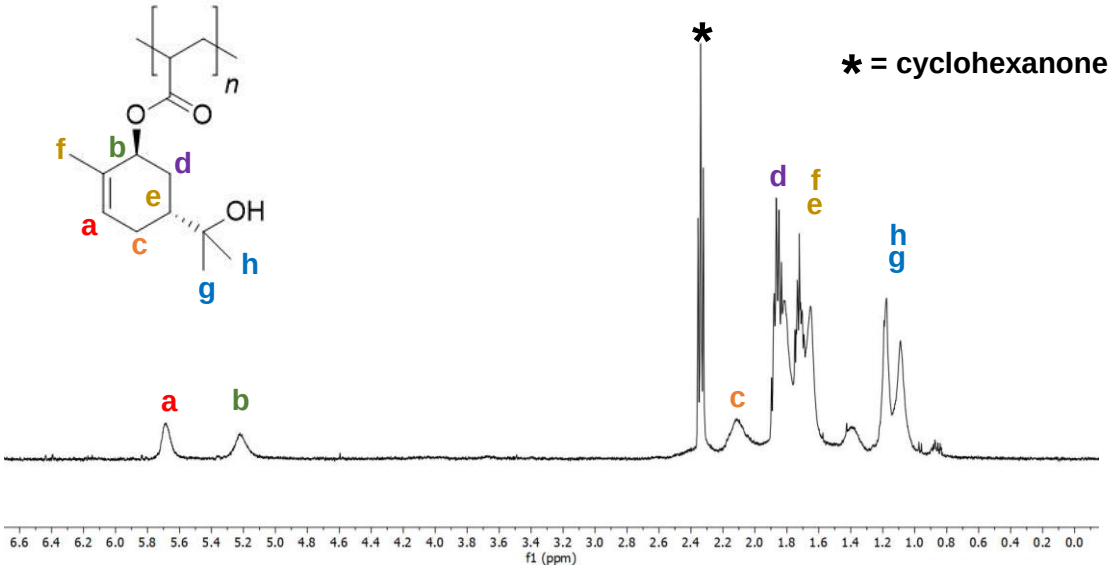

Figure 28. ^{1}H NMR analysis of polymer TPA6 in $CDCl_2$

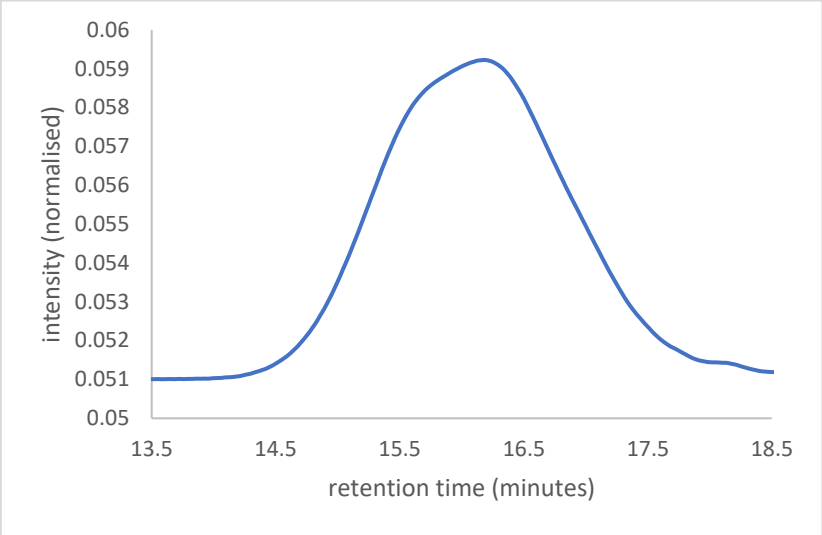

Figure 29. GPC analysis of polymer TPA6 showing the polymer peak. The chromatogram depicts a peak at approximately 16 minutes, corresponding to a M_w of 4.4 kDa and a $Đ$ of 1.4. Like TPA5, the chromatogram indicated that there was a single molecular weight distribution since only an individual peak was observed.

2.3.3.3 Thiol-mediated copolymerisation of *trans*-sobrerol acrylate and oleic acid acrylate, TPA7

Having successfully synthesised the *trans*-sobrerol acrylate monomer, the next step was to attempt to copolymerise it with the acrylated oleic acid. This would form a copolymer having both terpene- and oleic acid-derived properties. A protocol identical to the one that was used for the homopolymerisation of *trans*-sobrerol acrylate was carried out (Scheme 27). For the first trial reaction, equal amounts of both monomers were dissolved in cyclohexanone along with AIBN. This mixture was then purged in argon and afterwards left to stir for 24 hours at 70 °C. Again, polymer precipitation in cold hexane proved to be successful and the resulting solid was confirmed to be polymer according to ^{1}H NMR and GPC analyses.

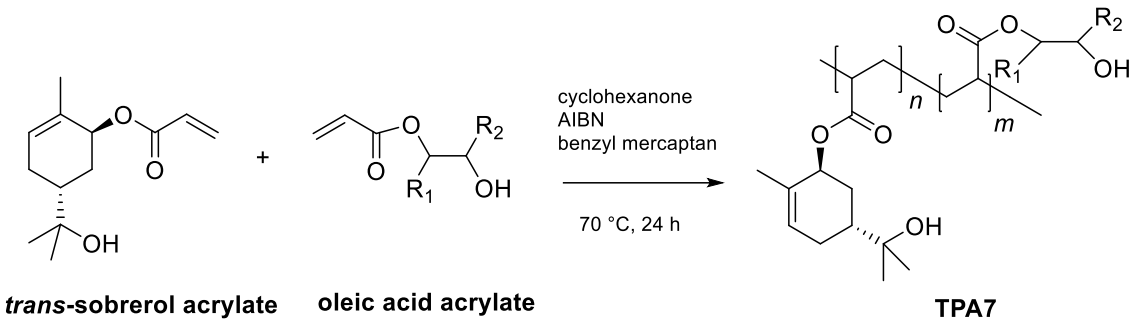

Scheme 27. The copolymerisation of the *trans*-sobrerol acrylate and oleic acid acrylate to give copolymer TPA7

As previously, the reaction was screened in order to decide on the conditions that would be best to produce a polymer with the desired physical properties (Table 4). This involved running several reactions whilst varying the weight (wt) ratios of monomers, along with the amounts of initiator and benzyl mercaptan.

Table 4. The screen that was run for the copolymerisation of *trans*-sobrerol acrylate and oleic acid acrylate, showing the different conditions that were used for each reaction and the results obtained with the GPC and DSC analyses. The monomer ratios shown are the ones that were targeted out at the start of each reaction.

Polymer ID	*Trans*-sobrerol acrylate monomer (wt%)	Oleic acid acrylate monomer (wt%)	Thiol (mol %)	AIBN (wt%)	M_w (kDa)	M_n (kDa)	$Đ$	T_g (°C)
1	70	30	0	0.5	16.8	8.2	2.0	-
2	70	30	0	1.0	17.4	7.3	2.4	-
3	30	70	0	1.0	16.4	7.6	2.2	-
4	70	30	0	2.0	17.0	6.9	2.4	-
5	30	70	0	2.0	13.9	5.5	2.5	-
6	70	30	5	1.0	4.2	2.3	1.8	4.6
7	50	50	5	1.0	4.6	2.3	2.0	-19.0
8	30	70	5	1.0	4.5	2.1	2.1	-28.0
9	70	30	5	1.0	5.0	2.9	1.8	-
10	80	20	5	1.0	4.0	2.3	1.7	18.9

A series of reactions (Entry 1 – 5 in Table 4) was first run without benzyl mercaptan and instead the AIBN concentration was increased from 0.5 wt% to 2.0 wt%. This resulted in the copolymers having a M_w between 13.9 and 17.4 kDa and a M_n between 8.2 and 6.9 kDa. In standard FRP, increasing the thermal initiator concentration would result in more polymer chains likely being initiated, leading to a reduction in molecular weight. This is because the degree of polymerisation is inversely proportional to the square root of the initiator concentration (Yasuda, 1985). This can be seen from the M_n results in Table 4, with the values decreasing with increasing concentration of thermal initiator.

The addition of 5 mol% of benzyl mercaptan had an immediate effect on all the polymers, with the M_w dropping to between 4.0 and 5.0 kDa. As a result of the work that had already been done on TPA6, it was known that the *trans*-sobrerol acrylate monomer behaves well in larger scale reactions. The monomer weights used for the last batch of these reactions (Entries 6 – 10 in Table 4) were therefore on the same scale as Entry 8 in Table 3 (4.0 g).

From the DSC analyses of the copolymers it was observed that the T_g decreased with increasing modified oleic acid molar content in the copolymer. This was expected since the T_g is closely associated with the final chemical structure of the random copolymer chains. It is reasonable to expect that the plasticising effect of the oleic acid acrylate comonomer influences the molecular mobility of the active species, leading to a reduction in the T_g of copolymers (Sander *et al.*, 2012; Lim and Hoag, 2013; Hazer *et al.*, 2019). Although the use of plasticisers is generally avoided in polymers used in conservation, this property may potentially prove to be beneficial for a wood consolidant as these materials are known to increase the free volume of polymer chains, enabling them to be more flexible and move more easily (Aharoni, 1998; Lim and Hoag, 2013). This could potentially translate to the copolymer having more opportunities for interactions with the wood structure once it penetrates, although its plasticity should not be too high as to deform the wood. Ideally, the T_g of a consolidant should be higher than the maximum temperature that a treated artefact will be subjected to (Schmidt, Shugar and Ploeger, 2017). A T_g which is too low may result in slumping of the object, as has been reported happening with the use of Paraloid™ B-72 in hot climates (Strahan *et al.*, 2002; Pohoriljakova and Moy, 2013; Davis, Roberts and Poli, 2021). On the other hand, a consolidant which is too stiff may cause artefacts to become brittle, which can result in cracking if put under stress (Horie, 2010).

Keeping this in mind, it was decided that the best conditions to use for TPA7 would be those utilised for Entry 10 in Table 4, as the copolymer had a small enough M_w (4.0 kDa) as well as the most appropriate T_g (18.9 °C). Figures 30 and 31 show the ^{1}H NMR and GPC analyses for TPA7 respectively. As with TPA5 and TPA6, the GPC chromatogram indicated a polymer with a narrow molecular weight distribution.

The monomer conversions under these reaction conditions were calculated, again by using the monomer and polymer resonances of the ^{1}H NMR spectra. These were found to be 85% for the *trans*-sobrerol acrylate monomer and 68% for the oleic acid acrylate monomer, comparable to the conversion calculated previously with TPA6. The comonomer ratios making up the copolymer were also obtained from the ^{1}H NMR spectra by comparing the integrals of a resonance corresponding to each of comonomers. This was found to be 5:1 = *trans*-sobrerol acrylate:oleic acid acrylate.

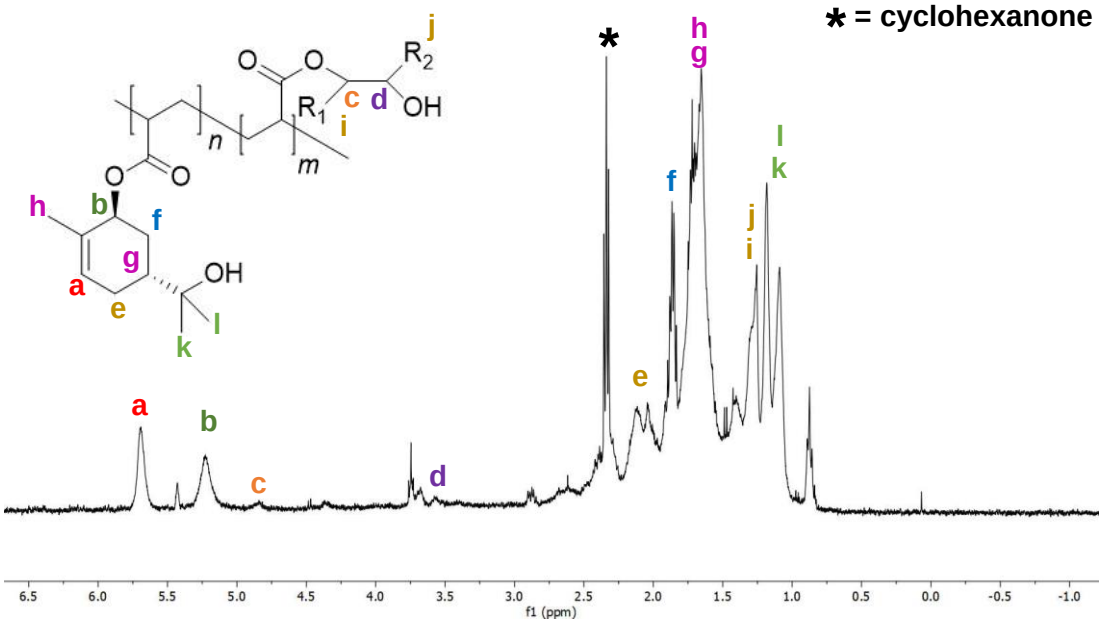

Figure 30. ^{1}H NMR analysis of copolymer TPA7 in $CDCl_2$

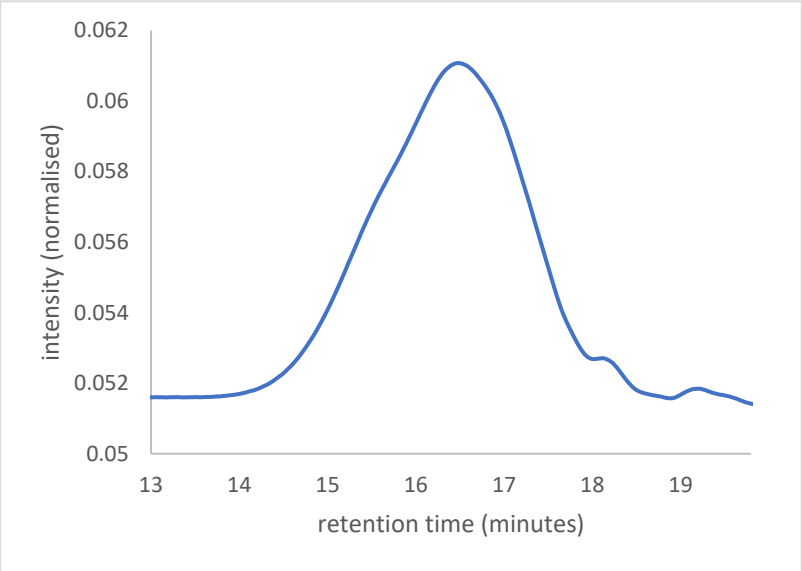

Figure 31. GPC analysis of TPA7. The chromatogram depicts a peak at approximately 16.5 minutes, corresponding to a M_w of 4.0 kDa and a $Đ$ of 1.7.

2.3.4 Polymer solubility testing

As has been mentioned previously, the aim for these synthesised polymers was to use them in organic solvents. This is due to the high degradation status of some of the Oseberg artefacts, which results in them not being able to withstand aqueous treatments.

Before carrying out any further characterisation studies, it was therefore essential to determine which organic solvents polymers TPA5, TPA6 and TPA7 were soluble in. Solvents which were tested included isopropanol, mixtures of toluene in ethanol, EtOAc and acetone. These solvents were selected as the most appropriate ones to be used in re-conservation after discussions with wood conservators Dr Susan Braovac and Dr Angeliki Zisi (Museum of Cultural History, University of Oslo). All of these solvents had previously already been used in non-aqueous retreatment tests, as described in internal reports of the Saving Oseberg group (Zisi and de Lamotte, 2020; Zisi *et al*, 2021; Braovac *et al*, 2021). TPA5 was tested first (Table 5). It was found to be soluble in isopropanol and the ethanol/toluene mixture. It was insoluble in both EtAOc and acetone. Out of isopropanol and the ethanol/toluene mixture, it

appeared to have the highest solvation rate in the former. Because of this, TPA6 and TPA7 were tested in isopropanol and they were both found to be soluble.

Table 5. The solubility of TPA5 in different organic solvents

Solvent	Solubility
isopropanol	✓
1:1 ethanol:toluene	✓
EtOAc	×
acetone	×

For all polymers, it was decided to carry out all further characterisation studies using isopropanol. This solvent was ideal since it has an acceptable safety profile and had been previously used in conservation experiments with degraded alum-treated wood (Andriulo *et al.*, 2017). Moreover, volatile solvents like isopropanol are particularly useful for wood impregnation since they can efficiently transport the consolidant polymers and then evaporate rapidly after treatment (Cavallaro *et al.*, 2017).

2.4 Conclusion

The successful synthesis of three monomers, triol acrylate; *trans*-sobrerol acrylate and oleic acid acrylate, has been described. All the monomers were derived from natural feedstocks: α-pinene and oleic acid. The monomers were all chemically functionalised with an acrylate moiety to enable them to undergo FRP. The synthesis of the triol acrylate consisted of four stages, with the final step having a relatively low yield of 43%. The *trans*-sobrerol acrylate had three synthesis steps and the last functionalisation reaction had a much better yield of 65%. The oleic acid acrylate was

synthesised based on a published methodology (Neto *et al.*, 2017) and consisted of two steps, with a final high yield of 97%.

These monomers were thereafter used to generate three bioinspired polymers. New protocols for the radical polymerisation of acrylated terpene monomers like triol acrylate and *trans*-sobrerol acrylate were designed and implemented, successfully yielding polymers TPA5 and TPA6. A new copolymer (TPA7) composed of *trans*-sobrerol acrylate and oleic acid acrylate was also successfully synthesised. TPA6 and TPA7 both showed much more favourable monomer conversions than TPA5. Additionally, their purification was much less laborious as they did not require dialysing like TPA5. The conditions for the TPA6 and TPA7 polymerisations appeared to behave well on larger scales, which would be very beneficial for their potential testing on wood and for their practical use as conservation materials.

After optimisation, all the polymers had M_w values below 5 kDa, making them very promising as wood consolidants. All polymers possessed hydroxyl groups which were anticipated to aid in the hydrogen bonding taking place between the consolidants and the wood. Additionally, all the polymers were soluble in isopropanol which was deemed an appropriate solvent to use both in further characterisation studies and in the ensuing wood tests.

This initial testing confirmed that all the polymers were worthy of further investigation. However, it was decided that further characterisation studies would be needed prior to scale-up to establish whether they would be good candidates to be brought forward for wood testing. These were to include testing to confirm the molecular weights of these polymers as well as their weight distributions. These studies would also provide information about their conformation and viscosity.

2.5 Experimental

2.5.1 Materials

All reagents were purchased from a chemical supplier (Acros Organics, Alfa Aesar, Merck, Sigma Aldrich and Fischer Scientific UK) and used without further purification. Water was deionised before use. Brine is a saturated aqueous solution of sodium chloride. TLCs were performed on silica gel mounted on aluminium and were visualised using a potassium permanganate dip with gentle heating. Dry solvents were obtained from solvent drying towers and contained <17 parts per million (ppm) of water. Experiments carried out under an inert atmosphere employed argon by means of a Schlenk line or a balloon.

2.5.2 General methods and instrumentation

^{1}H NMR spectra were recorded in deuterated chloroform ($CDCl_3$), deuterated DMSO ($(CD_3)_2SO$) and deuterated MeOH (CD_3OD) at ambient temperature using Bruker 400 MHz spectrometers. ^{13}C NMR spectra were recorded in $CDCl_3$, $(CD_3)_2SO$ and CD_3OD at ambient temperature using 100 MHz spectrometers. Data is expressed as chemical shifts (δ) in ppm relative to residual solvent signals ($CHCl_3$, ^{1}H NMR 7.26), ($CDCl_3$ ^{13}C NMR 77.16), ($(CH_3)_2SO$, ^{1}H NMR 2.50), ($(CD_3)_2SO$, ^{13}C NMR 39.52), (CH_3OH, ^{1}H NMR 3.31) or (CD_3OD, ^{13}C NMR 49.0) as the internal standard. MestReNova 6.0.2 copyright 2009 (Mestrelab Research S. L.) was used for analysing the spectra. The following abbreviations are used to designate the multiplicity of each signal: s, singlet; d, doublet; dd, doublet of doublets; ddd, doublet of doublet of doublets; td, triplet of doublets; ttd, triplet of triplet of doublets; t, triplet; dt, doublet of triplets; ddt, doublet of doublet of triplets; dtt, doublet of triplet of triplets; q, quartet; m, multiplet; br, broad. Couplings (*J*) are given in Hertz (Hz).

High resolution mass spectrometry (HRMS)

A Bruker MicroTOF spectrometer operating in electrospray ionisation (ESI) mode was used (Bruker Corporation, Germany).

Fourier-transform infra-red spectroscopy (FTIR)

A Bruker Tensor 27 FT-IR spectrophotometer with an ATR attachment was employed. The measurements were performed in the range of 4000–650 cm^{-1} and spectra were analysed using OPUS software (Bruker Corporation, Germany).

Gel permeation chromatography (GPC)

An Agilent 1260 Infinity Series HPLC (Agilent Technologies, USA) fitted with a differential refractive index detector (DRI) was used. THF (HPLC grade, Fisher Scientific) was used as the eluent at room temperature with two Agilent PL-gel mixed-D columns in series at a flow rate of 1 mL min^{-1}. A calibration curve was made using poly(methyl methacrylate) standards with ASTRA software (Wyatt Technology, USA) This was used for determination of the M_n, M_w and molecular weight distribution and dispersity (***Đ***, M_w/M_n).

Differential scanning calorimetry (DSC)

A TA-Q2000 (TA instruments) calibrated with an indium standard under an N_2 flow was used to measure T_g. A The sample (~ 5 mg) was weighed in a T-zero sample pan (TA instruments), leaving another T-zero pan empty as a reference. Both pans were heated at a rate of 10 °C min^{-1}, using a heat/cool/heat method.

2.5.3 Monomer synthesis

Synthesis of α-pinene oxide

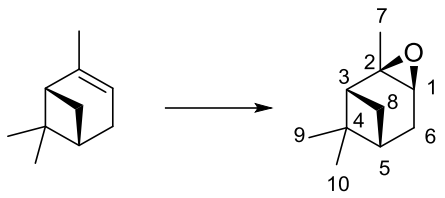

α-pinene **α-pinene oxide**

1S-(-)-α-pinene (5.82 mL, 36.7 mmol) was added to a solution of $NaHCO_3$ (3.92 g, 46.6 mmol) in CH_2Cl_2 (7.5 mL) and then cooled to 0 °C. *m*CPBA (~ 70%, 9.22 g, 37.4 mmol) was gradually added to the solution. The reaction was stirred (1 h) and saturated aqueous solution of Na_2SO_3 (27 mL) was added to the reaction mixture. The reaction was allowed to settle to r. t. and stirred for a further 30 minutes. The reaction mixture was diluted with saturated aqueous solution of $NaHCO_3$ (30 mL) and CH_2Cl_2 (60 mL). The aqueous washings were extracted with CH_2Cl_2 (75 mL). The organic phase was separated with saturated aqueous solution of $NaHCO_3$ (3 x 100 mL). The organic extracts were then combined, washed with brine (3 x 100 mL), dried over $MgSO_4$, filtered and concentrated under reduced pressure to yield the title compound (4.78 g, 31.4 mmol, 86% yield).

FTIR (ATR) ν_{max} /cm^{-1}: 2977, 2914, 2834, 1229, 1084, 943, 818; **^{1}H NMR** (400 MHz, $CDCl_3$) δ_H 3.07 (d, *J* = 4.1 Hz, 1H, H-1), 2.01 – 1.83 (m, 4H, H-8 and H-6), 1.72 (s, 1H, H-3 or H-5), 1.61 (d, *J* = 9.4, 1H, H-3 or H-5), 1.34 (s, 3H, H-7), 1.29 (s, 3H, H-9), 0.94 (s, 3H, H-10); **^{13}C NMR** (100 MHz, $CDCl_3$) δ_C 60.3, 56.9, 45.1, 40.5, 39.7, 27.6, 26.7, 25.9, 22.4, 20.2.

Synthesis of *trans*-sobrerol (Thomsett, 2018; O'Brien, 2020)

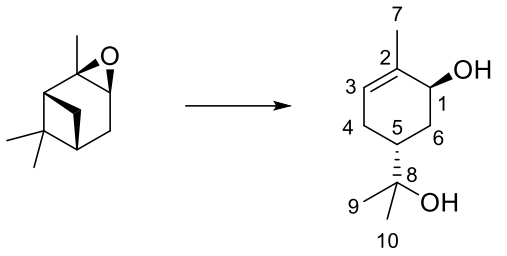

α-pinene oxide ***trans*-sobrerol**

CO_2 was continuously flowed through H_2O (52 mL) until the pH was approximately 4.5 – 5. α-Pinene oxide (4 g, 26.3 mmol) was then added and the mixture stirred at r. t. for 24 h. The solution was concentrated under reduced pressure and a white solid precipitated. The crude solid was washed with cold EtOAc (2 x 5 mL) to give the title compound as a white, crystalline solid (2.44 g, 14.4 mmol, 54% yield).

FTIR (ATR) ν_{max}/cm^{-1}: 3321, 2973, 2887, 1376, 1052, 919; **^{1}H NMR** (400 MHz, $CDCl_3$) δ_H 5.58 (d, *J* = 5.4 Hz, 1H, H-3), 4.04 (s, 1H, H-1), 2.17 – 2.08 (m, 1H, H-4), 2.05 – 1.97 (m, 1H, H-6), 1.84 – 1.67 (m, 5H, H-4, H-5, H-7), 1.42 (td, *J* = 13.1, 3.9 Hz, 1H, H-6), 1.22 (s, 3H, H-9 or H-10), 1.19 (s, 3H, H-9 or H-10); **^{13}C NMR** (100 MHz, $CDCl_3$) δ_C 133.2, 126.6, 71.3, 68.8, 38.9, 33.8, 27.8, 27.3, 26.5, 21.0; **HRMS** (ESI) m/z calculated for $[C_{10}H_{18}NaO_2]^+$ 193.1204 found 193.1210 (M^+ Na^+).

Synthesis of the triol (Thomsett, 2018; O'Brien, 2020)

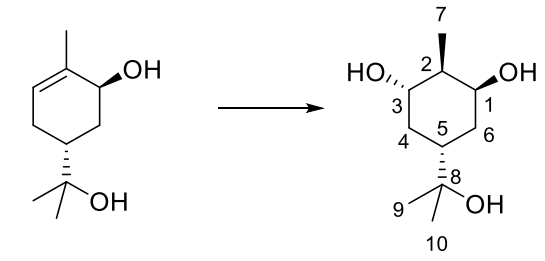

***trans*-sobrerol** **triol**

A solution of *trans*-sobrerol (2.17 g, 12.8 mmol) and BH_3.THF (1M in THF) (26 mL, 25.5 mmol) in dry THF (13 mL) was cooled to 0 °C under an argon atmosphere. The reaction mixture was stirred for 90 minutes, after which NaOH (2 M, 19 mL) and H_2O_2 (30%, 3.9 mL) were added dropwise. The mixture was allowed to warm to r. t. and left to stir (16 h). Afterwards, saturated aqueous solution of Na_2SO_3 (50 mL) was added and stirred (15 minutes). The mixture was concentrated under reduced pressure and the resulting solid was dissolved in hot MeCN (85 °C). The solid was filtered off while the solution was hot. The filtrate was concentrated under reduced pressure and recrystallised from MeCN to yield the title compound (1.21 g, 6.43 mmol, 50% yield).

FTIR (ATR) ν_{max} /cm^{-1}: 3298, 2975, 2886, 1276, 1082, 911; **^{1}H NMR** (400 MHz, CD_3OD) δ_H 3.92 (q, *J* = 3.0 Hz, 1H, H-1), 3.50 (td, *J* = 4.3 Hz, 1H, H-3), 2.11 – 2.04 (m, 1H, H-4), 1.94 – 1.86 (m, 1H, H-6), 1.87 – 1.79 (m, 1H, H-2), 1.35 – 1.26 (m, 1H, H-5), 1.25 (d, *J* = 2.6 Hz, 1H, H-6), 1.16 (s, 3H, H-9 or H-10), 1.15 (s, 3H, H-9 or H-10), 1.09 (m, 3H, H-7), 1.07 (m, 1H, H-4); **^{13}C NMR** (100 MHz, CD_3OD) δ_C 72.7 (C-8), 72.7 (C-1), 72.2 (C-3), 45.1 (C-5), 42.5 (C-2), 37.7 (C-4), 35.6 (C-6), 27.4 (C-9 or C-10), 26.8 (C-9 or C-10), 14.9 (C-7); **HRMS** (ESI) m/z calculated for $[C_{10}H_{18}NaO_2]^+$ 193.1204, found 193.1198 ($M + Na^+$).

Synthesis of the triol acrylate monomer

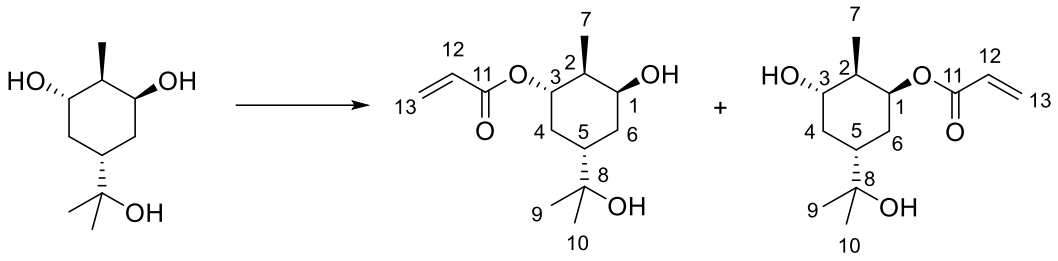

The triol (2 g, 10.6 mmol) and BHT (ca. 19 mg) were added to MeCN (13 mL) and put under an argon atmosphere. Et_3N (4.5 mL, 32 mmol) was added to the reaction mixture. The solution was cooled to 0 °C, after which T3P (50 wt. % in EtOAc, 7.6 mL, 12.8 mmol) and acrylic acid (acid with low H_2O content, 99.5% stab. with ca. 200 ppm methoxyphenol, 0.8 mL, 11.7 mmol) were added. The mixture was left to stir (10 minutes) and then allowed to warm to r t.. The mixture was left stirring (24 h) and then concentrated under reduced pressure. The crude product was purified by column chromatography (using 50% EtOAc in petroleum ether as a solvent system) to yield the title compounds as a white solid (1.10 g, major:minor = 1.3:1, 4.54 mmol, 43% yield). The mixture of diastereomers was partially separated by column chromatography to obtain a sample of the major diastereomer (0.50 g, 2.1 mmol, 19% yield).

The following reported data applies only to the major diastereomer:

FTIR (ATR) ν_{max}/cm^{-1}: 3340, 2975, 2934, 2874, 1720 (C=O), 1625, 1404, 1295, 1271, 1190; **^{1}H NMR** (400 MHz, $(CD_3)_2SO$) δ_H 6.30 (dd, *J* = 17.3, 1.7 Hz, 1H, H-13), 6.15 (dd, *J* = 17.3, 10.2 Hz, 1H, H-12), 5.91 (dd, *J* = 10.3 Hz, 1H, H-13), 4.81 (td, *J* = 11.1, 4.4 Hz, 1H, H-3), 4.51 (d, *J* = 4.1 Hz, 1H, H-1), 4.07 (s, 1H), 3.82 (m, 1H), 1.99 (dt, *J* = 11.8, 4.8 Hz, 1H), 1.79 (m, 2H), 1.51 (dtt, *J* = 13.3, 6.5, 3.6 Hz, 1H, H-2), 1.02 (d, *J* = 14.4 Hz, 6H, H-9 and H-10), 0.87 (d, *J* = 6.7 Hz, 3H, H-7); **^{13}C NMR** (100 MHz, $(CD_3)_2SO$) δ_C 165.0 (C-11), 131.1 (C-13), 127.8 (C-12), 75.6 (C-3), 69.9, 66.3, 42.8, 41.7, 36.7, 29.8, 27.2 (C-9), 26.2 (C-10),14.9 (C-7); **HRMS** (ESI) m/z calculated for $C_{13}H_{22}NaO_4$ $[M+Na]^+$ 265.1416 found 265.1427.

Synthesis of the triol diacrylate

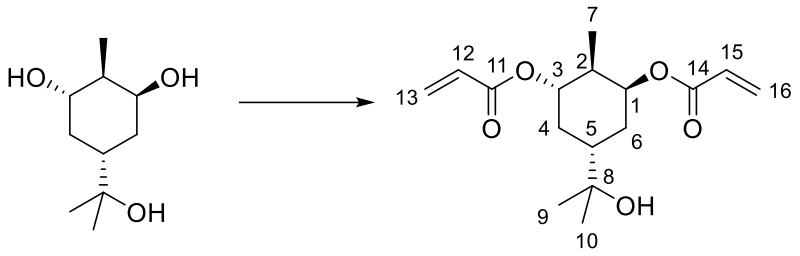

triol **triol diacrylate**

The triol (2 g, 10.6 mmol) and BHT (ca. 19 mg) were added to MeCN (13 mL) and put under an argon atmosphere. Et_3N (4.5 mL, 32 mmol) was added to the reaction mixture. The solution was cooled to 0 °C, after which T3P® (50 wt% EtOAc, 7.6 mL, 12.8 mmol) and acrylic acid (acid with low H_2O content, 99.5% stab. with ca. 200 ppm methoxyphenol, 0.8 mL, 11.7 mmol) were added. The mixture was left to stir (10 minutes) then allowed to warm to r. t.. The mixture was left stirring (24 h) and then concentrated under reduced pressure. The crude product was purified by column chromatography (using 50% EtOAc in petroleum ether as a solvent system) to yield the title compound as a slightly brown, oily liquid (0.42 g, 1.42 mmol, 13% yield).

FTIR (ATR) ν_{max}/cm^{-1}: 2970, 2882, 1717 (C=O), 1635, 1618, 1458, 1405, 1369, 1295, 1268, 1186 1122, 1046, 981, 956, 913, 875, 809, 670; **^{1}H NMR** (400 MHz, $(CD_3)_2SO$) δ_H 6.34 (ddd, *J* = 17.2, 2.5, 1.6 Hz, 2H, H-13 and H-16), 6.19 (ddd, *J* = 17.2, 12.3, 10.2 Hz, 2H, H-12 and H-15), 5.96 (ddd, *J* = 10.2, 8.5, 1.7 Hz, 2H, H-13 and H-16), 5.17 (q, *J* = 2.9 Hz, 1H, H-1), 4.80 (td, *J* = 11.1, 4.4 Hz, 1H, H-3), 4.21 (s, 1H), 2.07 (ddt, *J* = 11.8, 4.8, 2.3 Hz, 1H, H-4), 1.88 (ttd, *J* = 17.7, 6.7, 6.0, 3.0 Hz, 2H, H-6), 1.66 (tt, *J* = 12.8, 3.2 Hz, 1H, H-3, H-5), 1.39 – 1.08 (m, 1H, H-6, H-4), 1.01 (d, *J* = 1.6 Hz, 6H, H-9 and H-10), 0.82 (d, *J* = 6.7 Hz, 3H, H-7); **^{13}C NMR** (100 MHz, $(CD_3)_2SO$) δ_C 165.20 (C-11 or C-14), 164.93 (C-11 or C-14), 131.54 (C-13 and C-16), 128.52 (C-12 or C-15), 128.50 (C-12 or C-15), 74.36 (C-3), 73.98 (C-1), 69.81 (C-8), 41.25 (C-5), 39.05 (C-2), 32.27 (C-4 or C-6), 30.54 (C-4 or C-6), 26.94 (C-9 or C-10), 26.77 (C-9 or C-10), 13.63 (C-7); **HRMS** (ESI) m/z calculated for $C_{16}H_{24}NaO_5$ $[M+Na]^+$ 319.1521 found 319.1527.

Synthesis of the *trans*-sobrerol acrylate monomer

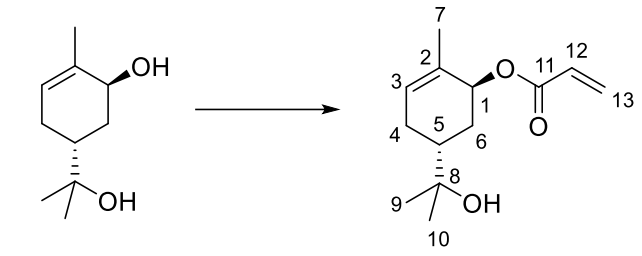

***trans*-sobrerol** ***trans*-sobrerol acrylate**

To a solution of *trans*-sobrerol (7.08 g, 41.6 mmol) in MeCN (200 mL) were added Et_3N (17.5 mL, 125.6 mmol) and acrylic acid (acid with low H_2O content, 99.5% stab. with ca. 200 ppm methoxyphenol, 3.14 mL, 45.8 mmol). The solution was cooled to 0 °C and T3P® (50 wt% in ethyl acetate, 29.7 mL, 99.8 mmol) was then added dropwise. The reaction mixture was stirred for 24 hours, after which H_2O (200 mL) was added and the reaction mixture separated. The aqueous layer was separated with diethyl ether (100 mL x 3) and the combined organic layers were washed with HCl (1M aqueous, 200 mL x 3), $NaHCO_3$ (sat. aq., 200 mL x 3) and brine (100 mL x 2). The reaction mixture was then dried with $MgSO_4$, filtered and concentrated to yield the title compound as a brownish orange viscous liquid (6.05 g, 27.0 mmol, 65% yield).

FTIR (ATR) ν_{max}/cm^{-1}: 3421, 2969, 2935, 1717, 1704, 1404, 1294, 1267, 1192, 1162, 1038. **^{1}H NMR** (400 MHz, CD_3OD) δ_H 6.42 (dd, *J* = 17.3, 1.5, 1H, H-13), 6.14 (dd, *J* = 17.3, 10.4, 1H, H-12), 5.82 (dd, *J* = 10.4, 1.5, 1H, H-13), 5.75 (dt, *J* = 5.6, 1.8, 1H, H-3), 5.36 (dt, *J* = 3.5, 1H, H-1), 2.19 (dddt, *J* = 17.0, 5.7, 4.3, 1.6, 1H, H-5), 2.05 (dq, *J* = 14.0, 2.2, 1H, H-4), 1.90–1.82 (m, 1H, H-6), 1.74 (tdd, *J* = 2.4, 4.0, 12.5, 1H, H-4), 1.71 (dt, *J* = 2.8, 1.5, 3H, H-7), 1.49 (ddd, *J* = 14.1, 12.9, 4.0, 2H, H-6), 1.18 (*J* = 6.9, 6H, H-9 and H-10); **^{13}C NMR** (101 MHz, CD_3OD) δ_C 166.1, 131.0, 130.6, 128.1, 125.3, 72.2, 71.0, 39.5, 30.0, 27.6, 27.4, 26.8, 20.9; **HRMS** (ESI): Calculated for $[C_{13}H_{20}NaO_3]^+$ 247.3000 obtained 247.1309 (M^+ Na^+).

Synthesis of epoxidised oleic acid (Neto *et al.*, 2017)

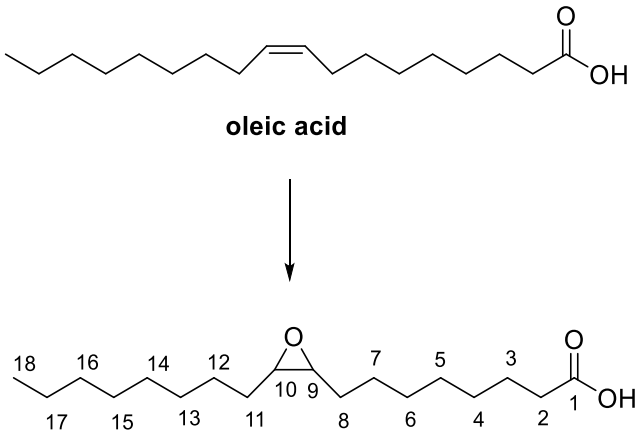

oleic acid

epoxidised oleic acid

To oleic acid (33.8 mL, 106.4 mmol) in toluene (180 mL) were added formic acid (12.3 mL, 326.0 mmol). The solution was stirred under reflux at 30 °C. H_2O_2 (72.1 mL, 2352.8 mmol) was added dropwise (over 1 h) and the mixture left to stir for 24 h. This was then transferred to a separation funnel and the organic phase was purified using $NaHCO_3$ (sat. aq., 50 mL x 3), deionised water (50 mL x 3) and dried with $MgSO_4$ and filtered. The solution was then concentrated under reduced pressure to yield the product as a white solid (26.5 g, 88.8 mmol, 84% yield).

FTIR (ATR) ν_{max} /cm^{-1}: 2958, 2849, 1696, 1473, 1431, 1276, 1031, 1012, 846. **^{1}H NMR** (400 MHz, CD_3OD) δ_H 2.92 (m, 2H, H-9 and H-10), 2.35 (t, *J* = 7.5, 2H, H-2), 1.65 (d, *J* = 6.9, 2H, H-3), 1.49 (dt, *J* = 6.9, 3.9, 4H, H-8, H-11), 1.35 (m, 10H, H-4, H-5, H-6, H-7, H-12), 1.29 – 1.27 (10H, m, 10H, H-13, H-14, H-15, H-16, H-17), 0.92 – 0.84 (m, 3H, H-18); **^{13}C NMR** (101 MHz, CD_3OD) δ_C 57.44, 57.39, 34.01, 32.00, 29,70, 29.68, 29.46, 29.32, 29.31, 29.09, 27.96, 27.92, 26.74, 26.70, 24.79, 22.81, 14.25; **HRMS** (ESI): Calculated for $[C_{13}H_{20}NaO_3]^+$ 320.47 obtained 321.24 (M^+ Na^+).

Synthesis of oleic acid acrylate (Neto *et al.*, 2017)

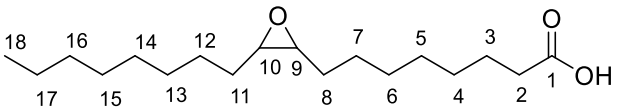

epoxidised oleic acid

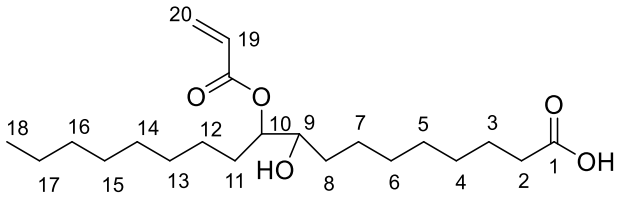

oleic acid acrylate

Acrylic acid (acid with low H_2O content, 99.5% stab. with ca. 200 ppm methoxyphenol, 76.12 mL, 1109.2 mmol) and hydroquinone (24 mg, 0.2 mmol) were added to epoxidised oleic acid (40 g, 0.1 mmol). The reaction mixture was maintained at a mass ratio of 2:1 acrylic acid:epoxidized oleic acid and left to stir for 6 h at 100 °C. The aqueous layer was separated with diethyl ether (100 mL x 3) and the organic layer was washed with $NaHCO_3$ (sat. aq., 50 mL x 3). The reaction mixture was then dried with $MgSO_4$, filtered and concentrated to yield the title compound as a whitish viscous liquid (48.2 g, 130.1 mmol, 97% yield).

FTIR (ATR) ν_{max}/cm^{-1}: 3461, 2959, 2873, 1697, 1431, 1261, 1193, 771. **^{1}H NMR** (400 MHz, CD_3OD) δ_H 6.56 – 6.36 (m, 1H, H-20), 6.11 (ddd, *J* = 17.3, 15.2, 10.4, 1H, H-19), 5.96 (dd, *J* = 10.4, 1,4, 1H, H-20), 4.87 (m, 1H, H-10), 4.44 (tt, *J* = 10.1, 6.3, 1H, H-9), 3.58 (m, 1H, H-9), 2.39 – 2.23 (m, 1H, H-2), 1.61 (m, 4H, H-8. H-11), 1.43 (m, 2H, H-3), 1.30 (m, 10H, H-4, H-5, H-6, H-7, H-12), 1.26 (m, 10H, H-13, H-14, H-15, H-16, H-17), 0.91 – 0.80 (m, 3H, H-18); **^{13}C NMR** (101 MHz, CD_3OD) δ_C 171.10, 133.14, 131.53, 128.12, 128.07, 60.19, 34.08, 33.71, 31.99, 29.64, 29.39, 29.05, 25.50, 24.74, 22.80, 14.24; **HRMS** (ESI): Calculated for $[C_{13}H_{20}NaO_3]^+$ 392.57 obtained 393.26 (M^+ Na^+).

2.5.4 Polymer synthesis

Synthesis of polymer TPA5

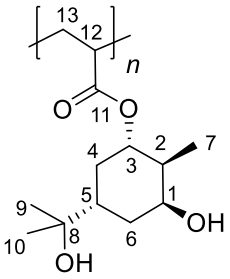

TPA5

1,4-Dioxane (18 mL) was added to triol acrylate (307 mg, 1.3 mmol) and AIBN (1.5 mg, 0.0091 mmol). The mixture was degassed under argon for 45 minutes after which it was stirred (18 h) at 70 °C under argon. The mixture was left to cool to r. t. and then concentrated under reduced pressure to approximately 5 mL. Deionised H_2O (5 mL) was added. This mixture was then dialysed in deionised H_2O (1000 mL) for 24 h using a membrane of 2 kDa MWCO. The dialysate was changed every 2 h. The solution was then concentrated under reduced pressure to yield the title compound as a white solid (67.4 mg).

FTIR (ATR) ν_{max}/cm^{-1}: 3370, 2967, 2928, 2880, 2114, 1717 (C=O), 1454, 1368, 1368, 1256, 1168, 1122, 1098, 916, 683; **^{1}H NMR** (400 MHz, $(CD_3)_2SO$) δ_H 4.98 (br, 1H), 4.70 (br, 1H, H-3), 4.44 (br, 1H, H-1), 4.05 (s, 1H), 3.79 (br, 1H), 2.23 (br, 1H, H-2 or H-4 or H-5 or H-6), 1.94 (br, 1H, H-2 or H-4 or H-5 or H-6), 1.78 (br, 2H, H-2 or H-4 or H-5 or H-6), 1.41 (br, 3H, H-2 or H-4 or H-5 or H-6), 1.02 (br, 10H, H-9 and H-10), 0.87 (br, 4H, H-7).

Synthesis of polymer TPA6

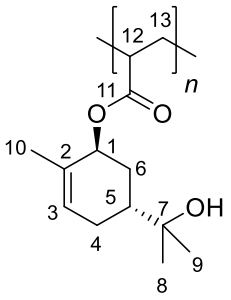

TPA6

Cyclohexanone (24 mL), AIBN (0.5 wt%, 20 mg, 0.1 mmol) and benzyl mercaptan (5 mol%, 112 µL, 1 mmol) were added to the *trans*-sobrerol acrylate monomer (4 g, 17.8 mmol). The mixture was purged with argon for 1 h 45 min, after which it was stirred for 24 h at 70.0 °C. The mixture was left to cool to r.t. and then purified with excess of hexane (4:1 v/v). The product was dried in a r.t. vacuum oven to yield the title compound (2.6 g).

FTIR (ATR) ν_{max}/cm^{-1}: 3434 (-OH), 2931 (C-H), 1725 (C=O), 1448 (C-H), 1378 (-OH), 1245 (-OH), 1154 (C-O), 1025 (C-O), 943 (C=C), 914 (C=C), 840 (C=C), 814 (C=C); **^{1}H NMR** (400 MHz, (CD_3OD) δ_H 5.69 (br, H-3), 5.24 (br, H-1), 2.09 (br, H-4), 1.87 (br, H-6), 1.73 – 1.67 (br, H-5, H-10), 1.21 – 1.07 (br, H-8, H-9).

Synthesis of copolymer TPA7

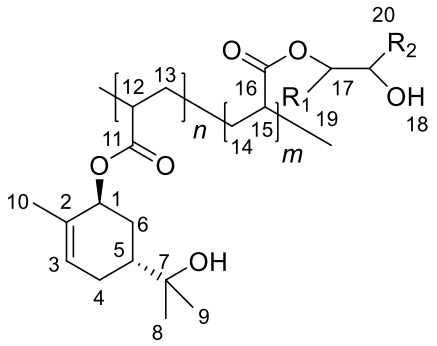

TPA7

To a mixture of the *trans*-sobrerol acrylate monomer (3.2 g, 14.3 mmol) and the oleic acid acrylate monomer (0.8 g, 2.2 mmol) were added cyclohexanone (24 mL), AIBN (1 wt%, 40 mg, 0.3 mmol) and benzyl mercaptan (5 mol%, 112 µL, 1 mmol). The mixture was purged with argon for 1 h 45 min, after which it was stirred for 24 h at 70.0 °C. The mixture was left to cool to r.t. and then purified with excess of hexane (4:1 v/v). The product was dried in a r.t. vacuum oven to yield the title compound (3.2 g).

FTIR (ATR) ν_{max}/cm^{-1}: 3434 (-OH), 2931 (C-H), 2856 (C-H), 1725 (C=O), 1448 (C-H), 1378 (-OH), 1245 (-OH), 1154 (C-O), 1025 (C-O), 943 (C=C), 914 (C=C), 840 (C=C), 814 (C=C); **^{1}H NMR** (400 MHz, (CD_3OD) δ_H 5.69 (br, H-3), 5.24 (br, H-1), 4.85 (br, H-17), 3.56 (br, H-18), 2.09 (br, H-4), 1.87 (br, H-6), 1.73 – 1.67 (br, H-5, H-10), 1.34 – 1.25 (br, H-19 and H-20), 1.21 – 1.07 (br, H-8, H-9).

Chapter 3: Characterisation of Polymers TPA5, TPA6 and TPA7

3.1 Introduction

It is important to fully characterise any future consolidant before putting it to use. The characterisation of polymers is much more challenging to achieve when compared to that of lower molecular weight molecules. This is because macromolecular materials are polydisperse, meaning that they are composed of molecules of various sizes. Up till now, it has not been possible to synthesise macromolecules of uniform molecular weight and structure, therefore any analysis can only produce average values (Braun *et al.*, 2013).

The work described in this chapter has been used to publish two peer-reviewed papers (Cutajar *et al.*, 2021; Cutajar, Machado *et al*., 2022) (refer to Appendix for more details).

3.1.1 Analytical ultracentrifugation

Analytical ultracentrifugation (AUC) is considered to be one of the most functional and adaptable techniques used in the study of macromolecules (Scott, Harding and Rowe, 2005; Harding, 2018). It is utilised for the characterisation of particles' sizes and shapes, as well as the quantitative analysis of their interactions in solutions (Scott, Harding and Rowe, 2005; Cole *et al.*, 2008; Harding, 2018). This instrument is particularly exceptional since it functions without the need of a separation matrix, determines particle sizes without calibration standards (Harding, 2018) and also does not require molecular modification or labelling (Scott, Harding and Rowe, 2005).

Being non-destructive, sample recovery and reuse is possible (Cole *et al.*, 2008). Moreover, it can be combined with other techniques like NMR, light scattering and viscometry to analyse the overall conformation and flexibility of macromolecules in solution (García de la Torre and Harding, 2013; Harding *et al.*, 2015; Harding, 2018). The technique is able to determine a wide range of molecular weights, from small molecules such as peptides to larger ones like organelles (Cole *et al.*, 2008).

AUC has already been employed in numerous studies focussing on different materials. It has been utilised in research concerning antibacterial resistance (Harding, 2018), as illustrated by Phillips-Jones *et al*. (Phillips-Jones, Channell, *et al.*, 2017; Phillips-Jones, Lithgo, *et al.*, 2017) who made use of the SEDFIT-MSTAR and the MultiSig algorithms to characterise VanS, a membrane kinase which is important in the resistance mechanism to vancomycin. The tetanus toxoid protein, an important component in the production of carbohydrate-based vaccines protecting against pathogens such as *Haemophilus influenzae* type b was also characterised with AUC (Astronomo and Burton, 2010; Harding, 2018).

3.1.1.1 AUC for wood conservation

AUC has been used extensively for the characterisation of wood components and possible consolidants, such as the determination of the distribution of molecular weights of lignin sourced from different wood (Alzahrani *et al.*, 2016a; Harding, 2018). McHale *et al*. worked on the development of lignin-based materials with a low enough molecular weight to penetrate the wood and polymerise *in situ* (McHale *et al.*, 2016, 2017). Using the SEDFIT-MSTAR algorithm, the team was able to determine the molecular weight range of the *in situ* polymerised oligomers (McHale *et al.*, 2016, 2017). Additionally, AUC has been utilised in studies of aminocelluloses (Heinze *et al.*, 2011; Nikolajski *et al.*, 2014; Harding, 2018; Wakefield, Hampe, *et al.*, 2020) and chitosans (Wakefield *et al.*, 2018; Wakefield, Braovac, *et al.*, 2020). Heinze *et al.* carried out sedimentation velocity studies while Nikolajski *et al.* performed both sedimentation velocity and sedimentation equilibrium experiments in order to establish the self-associative behaviour of aminocelluloses (Heinze *et al.*, 2011; Nikolajski *et al.*, 2014).

It was anticipated that analysis with AUC would prove very useful for this work. As described in Chapter 2, it was decided that at least 50 g of each polymer would be needed for initial wood testing. Having a thorough understanding of the physical properties of TPA5, TPA6 and TPA7 would help in deciding whether they would truly be suitable as wood consolidants. This is very important since it was essential to have as much certainty as possible since any scale-up of the polymers would entail a considerable amount of work and time. Moreover, archaeological wood which can be used for any subsequent testing is scarce and thus, extensive characterisation of the polymers would help in preventing any material wastage.

As mentioned, AUC works without calibration standards and is an absolute method of estimating molecular weight. This is in contrast to GPC, which compares the tested polymers to built-in standards such as poly(methyl methacrylate) standards. As a result, AUC is considered to be a more reliable method and the molecular weight values that are obtained from it are more accurate than the ones measured by GPC. Because of this, once the polymerisation reactions of TPA5, TPA6 and TPA7 were optimised (as described in Chapter 2), it was decided to re-measure their molecular weight with AUC in order to obtain a 'truer' value.

AUC also helps in the determination of molecular weight distribution and conformation of polymers. This is useful for wood consolidation purposes, since it would help predict how much of the polymers would be able to penetrate wood. If a large distribution of the particles in the system are deemed too large (approximately >10 kDa), it would not be scientifically sound to continue with their scale-up and testing (Wakefield, 2020). Likewise, having an idea of the shape of the polymers though conformation analyses could also help in understanding their behaviour. An example is PEG, whose long and flexible shape is thought to improve its penetration into wood (Wakefield, 2020).

3.1.1.2 AUC methodologies

The underlying principle of AUC is the administration of a centrifugal force to the macromolecules and then examining in real-time how they are re-distributed (Scott, Harding and Rowe, 2005). The purpose of the spinning motion is to provide a gravitational field which enables particles to sediment (Figure 32) (Cole *et al.*, 2008). Larger and more compact particles sediment first. Rod-shaped and coiled molecules take longer to sediment due to the high friction between them.

The polymer solution being investigated is inserted into one of the channels of a dual sector AUC cell. The other channel is filled with a reference solvent, usually the solvent that is used to dissolve the polymer. The cell is equipped with transparent windows which allow the passage of light and thus the optical detection of the sedimenting profile of the polymer solution. The two primary optical systems used for this purpose are Rayleigh interference and UV absorbance. In this work, the former optical system was used.

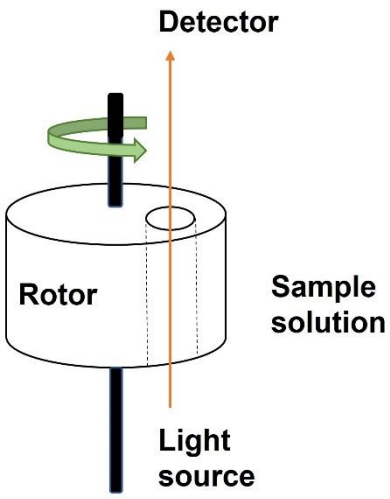

Figure 32. The underlying principle of AUC is the administration of a centrifugal force to the macromolecules. This provides a gravitational force, allowing the particles to sediment.

AUC can be used to either conduct a sedimentation velocity study or a sedimentation equilibrium experiment. A sedimentation velocity study measures the rate at which the particles move during redistribution while during a sedimentation equilibrium experiment, the particle concentration is measured at equilibrium (Cole *et al.*, 2008). There are various programmes which are used in these experiments. SEDFIT (Schuck, 2000; Dam and Schuck, 2004) is largely used to analyse sedimentation velocity. The SEDFIT-MSTAR algorithm (Schuck *et al.*, 2014) can be used to analyse the sedimentation equilibrium of polymers with a wide range of molecular weights. The MultiSig algorithm (Gillis *et al.*, 2013) makes it possible to obtain estimates for molecular weight distributions. More detail will be given on these systems in the next sections of this chapter.

3.1.1.2.1 Sedimentation velocity

Sedimentation velocity (SV) works at high rotor speeds, resulting in a centrifugal speed with minimal back diffusion effects. The sedimentation coefficient (*s*) distribution provides information on the distribution and interactions of macromolecules.

The sedimentation coefficient determined by SV is calculated using the Svedberg equation (Equation 1):

$$s = \frac{v}{\omega^2 r} = \frac{M\,(1-\bar{v}\rho)}{N_A f} \qquad \textbf{(1)}$$

M = molecular weight (Da) or molar mass (g/mol)

$\bar{v}$ = partial specific volume of the particle (mL/g)

ρ = density of the solvent (g/mL)

ω = rotor speed in radians per second

r = distance from the centre of the rotor

v = velocity (cm/sec)

s = sedimentation coefficient (Svedberg units S)

f = frictional coefficient (dvn.sec/cm)

N_A = Avogadro's number (6.02214 x 10^{23} mol^{-1})

In SV there are three primary forces at play: the sedimentation force (F_s), the frictional force (F_f) and the buoyancy force (F_b) (Figure 33). The F_s is produced from the high centrifugal force and leads away from the rotational centre towards the AUC cell base. The F_f and F_b are both back diffusion forces and lead towards the rotational centre, thus counteracting the F_s. Both the F_f and F_b are specific to the particle that is being studied. The F_f is dependent on the size and shape of the particle. Meanwhile, the F_b depends on properties like hydrophobicity and solubility. For example, higher hydrophobicity leads to a stronger F_b.

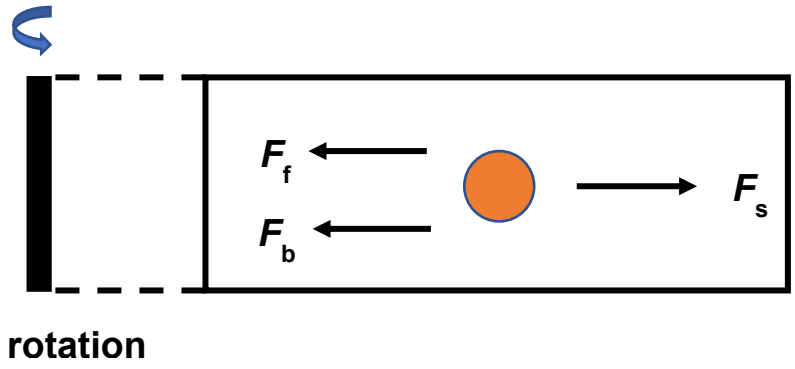

Figure 33. A depiction of the three primary forces affecting an SV experiment. Adapted from (González-Rubio *et al.*, 2021).

The sedimentation of the particle in SV depends on whether F_s is larger than the two back diffusion forces. To ensure this, high centrifugal speeds are usually used in SV experiments. The sedimentation rate is also highly dependent on the F_f, since both size and shape greatly affect how fast a particle sediments.

Hydrodynamic non-ideality is an important consideration to keep in mind when calculating the sedimentation coefficient and molecular weight. This phenomenon

particularly affects polydisperse particles larger than water molecules. Major contributors to non-ideality include asymmetry, size and hydration which affect the size exclusion volume of a molecule. Non-ideality is also affected by the viscosity and charge of a particle. Additionally, higher macromolecular concentration increases non-ideality. To minimise these non-ideality effects on experimental results, sedimentation coefficient values are usually extrapolated to zero concentration. The sedimentation coefficient *s* is then converted to $s_{20,w}$. This is the sedimentation coefficient value corrected to standard solvent conditions, that is, the density and viscosity of water at 20.0 °C (hence $_{20,w}$).

The sedimentation coefficient of monodisperse polymer systems can be simply calculated from the rate of movement of the concentration boundary and the rotor speed. In reality however, most polymer systems are polydisperse and this necessitates further calculations. In these cases, the shape of the boundary at a given concentration also becomes important and the Lamm equation is used to calculate the sedimentation coefficient. This equation describes the change of concentration distribution along the radius of the AUC cell relative to time (Equation 2).

$$\frac{\partial c}{\partial t} = D\left[\left(\frac{\partial^2 c}{\partial r^2} + \frac{1}{r}\left(\frac{\partial c}{\partial r}\right)\right)\right] - s\omega^2\left[r\frac{\partial c}{\partial r} + 2c\right] \quad \textbf{(2)}$$

c = concentration (mg/mL)

t = time (seconds)

D = diffusion constant

s = sedimentation coefficient (Svedberg units S)

ω = rotor speed in radians per second

r = distance from the centre of the rotor

Analysis packages such as SEDFIT (Schuck, 2000; Dam and Schuck, 2004) automatically fit the Lamm equation. SEDFIT uses the host computer to find solutions for the Lamm equation using two procedures: *ls-g*(s)* (least square Gaussian fit for sedimentation) vs *s* and *c(s)* (continuous distribution of sedimentation coefficients) vs *s* (Schuck, 2000). Both of these methods work by superimposing a fit of the raw data. During this fitting, noise such as TI (time invariant) and RI (radial invariant) is removed. The purpose of removing TI noise is to annul any patterns which do not change during

the course of an AUC run, while RI noise represents artefacts of the Fourier Transform.

It should be noted that *ls-g*(s)* is an apparent sedimentation coefficient value since it is obtained from a time derivative $\partial c/\partial t$. As such, plots derived from *ls-g*(s)* vs *s* have a tendency to be affected by diffusion broadening, since this method does not distinguish between sedimentation and diffusion (Dam and Schuck, 2004). On the other hand, *c(s)* vs *s* is a direct model for the raw data from the SV experiment, and can therefore be used to account for diffusion (Dam and Schuck, 2004). This is possible through the determination of the average frictional ratio $\frac{f}{f_0}$ (Equation 3)

$$\frac{f}{f_0} = \frac{M(1-\bar{\nu}\rho_0)N_A}{N_A 6\pi\eta_0}\left(\frac{4\pi N_A}{3\bar{\nu}M}\right)^{\frac{1}{3}}\frac{1}{s} \quad \textbf{(3)}$$

f = frictional coefficient of a macromolecule

f_0 = frictional coefficient of an anhydrous sphere of the same mass

M = molecular weight (Da) or molar mass (g/mol)

$\bar{\nu}$ = partial specific volume of the particle (mL/g)

ρ_0 = density of water at 293.15 K (0.99823 g/ml)

N_A = Avogadro's number (6.02214 x 10^{23} mol^{-1})

η_0 = viscosity of water at 293.15 K (0.010 Poise)

s = sedimentation coefficient (Svedberg units S)

The frictional ratio $\frac{f}{f_0}$ is a comparison of the molecular drag of a macromolecule compared to that of a sphere of the same mass and anhydrous volume. The *c(s)* process assumes that macromolecules with the same molecular weight have identical frictional coefficients. This does not always hold true, such as the case with polysaccharides (Wakefield, 2020). Nevertheless, the *c(s)* method has been successfully shown to be capable of distinguishing different components in polysaccharides (Heinze *et al.*, 2011). Due to this, it therefore may be safe to assume that it would also give reasonable results for synthetic polymers like TPA5, TPA6 and

TPA7. As such, the *c(s)* process was the one used for the work described in this chapter.

3.1.1.2.2 Sedimentation equilibrium

Sedimentation equilibrium (SE) is used for the direct estimation of the molecular weight (kDa) or molar mass (g/mol) of a macromolecule. Whereas with SV it is possible to run experiments with concentrations as low as 0.01 mg/mL, the minimum concentration that should be used for SE is ~ 0.4 – 0.5 mg/mL (Harding *et al.*, 2015).

SE works at lower rotational speeds when compared to SV, which results in the formation of a balance between the opposing sedimentation and diffusion forces (Cole *et al.*, 2008; Harding, 2012). This creates an equilibrium concentration distribution of particles in the AUC cell (Cole *et al.*, 2008). The concentration of the particles increases in the direction of the cell base. Unlike SV, this means that the particles in solution do not produce a sedimentation boundary. Instead, it results in the formation of a concentration curve which can be analysed at different points in order to determine the molecular weight of the macromolecule. The steady-state pattern achieved by SE is a function of the macromolecular molecular weight and is independent of shape. This is because net transport or frictional effects do not exist at equilibrium. This makes SE an absolute method of estimating molecular weight (Harding, 2005).

The polydispersity of polymer systems has to be taken into account when calculating M_w values. An analysis package called SEDFIT-MSTAR was designed for this purpose (Schuck *et al.*, 2014). The MSTAR algorithm was developed to calculate the M_w for the entire solute distribution of a given sample (Creeth and Harding, 1982). For monodisperse systems, the M_w can be determined by extrapolation of the particle concentration to the cell base. In polydisperse systems, there is usually a steep rise of the *c(r)* vs *r* plot at the cell base. *c(r)* stands for concentration at radial position *r* and *r* is the radial displacement. The MSTAR algorithm accounts for this by extrapolating a point average molecular weight *M*(r)* instead of *c(r)*. This is possible because *M*(r)* rises less steeply than *c(r)* in the cell base. The molecular weight derived from such an extrapolation is an apparent value $M_{w,app}$. This means that it is not corrected for thermodynamic non-ideality such as co-exclusion (Harding *et al.*,

2015). This MSTAR algorithm is fully integrated into the SEDFIT programme, allowing for easy data analysis (Schuck *et al.*, 2014).

SEDFIT-MSTAR also provides the hinge point $M_{w,app}$. The hinge point is defined as the radial position where the concentration *c(r)* is equal to the initial cell loading concentration *c* prior to redistribution (Harding *et al.*, 2015). Having a second measure for $M_{w,app}$ is useful since it can help provide confidence in the *M** results.

Another analysis package which can be used to process SE data is MultiSig (Gillis *et al.*, 2013). This gives the user a broader resolution of the aforementioned MSTAR data and thus provides information on the molecular weight distribution of the polymer system. It uses a 17-component system with 20 iterations and assumes that the polymer system is thermodynamically ideal. Although in comparison SV experiments offer better resolution, the MultiSig results are absolute and are independent of shape.

3.1.2 Other hydrodynamic parameters

3.1.2.1 Partial specific volume $\bar{\nu}$

The partial specific volume $\bar{\nu}$ can be described as the change of the solution volume when the solute is dissolved in the solvent at constant temperature and pressure (Murphy *et al.*, 1998). This is an essential value to determine as it is used in the analyses of the raw data derived from SV experiments. It can be obtained from composition data or by carrying out density measurements on different polymer solution concentrations with a density meter and subsequently through the use of Equation 4.

$$\bar{\nu} = \frac{1}{\rho_o}\left(1 - \frac{\partial \rho}{\partial c}\right) \quad \textbf{(4)}$$

ρ_o = the density of the reference solvent (g/mL)

$\frac{\partial \rho}{\partial c}$ = the slope of the ρ vs concentration plot

3.1.2.2 Intrinsic viscosity $[\eta]$

The viscosity of a solution can be defined as a measurement of its resistance to flow, which is affected by the intermolecular forces found in the sample (Harding, 1997). The intrinsic viscosity $[\eta]$ is a measurement of the solute's contribution to the viscosity of a solution, that is, it is the viscosity increment that a solute produces when dissolved in a solvent (Pamies *et al.*, 2008). It is an intrinsic property of a macromolecule in solution and can give information on its shape and flexibility (Harding, 1997).

The relative viscosity η_{rel} is a measure of the effect of the dissolved solute on the solution (Harding, 1997). It is a function of the specific viscosity η_{sp} (Equations 5a and 5b).

$$\eta_{rel} = \eta/\eta_0 \quad \textbf{(5a)}$$

$$\eta_{sp} = \eta_{rel} - 1 \quad \textbf{(5b)}$$

η = viscosity of the solution (mL/g)
η_0 = viscosity of the solvent (mL/g)

The reduced viscosity η_{red} can be used to determine the intrinsic viscosity, *via* an extrapolation to zero concentration. η_{red} is defined in Equation 6.

$$\eta_{red} = {}^{\eta_{sp}}/_{c} = {}^{(\eta_{rel} - 1)}/_{c} \quad \textbf{(6)}$$

c = weight concentration (mg/mL)

The inherent viscosity η_{inh} is a related parameter, as described in Equation 7.

$$\eta_{inh} = (In\eta_{rel})/c \quad \textbf{(7)}$$

$In\eta_{rel}$ = natural logarithm of η_{rel}

c = concentration (mg/mL)

Both η_{red} and η_{inh} are concentration dependent, as a result of non-ideality effects. The relationship between η_{red} and concentration is described by the Huggins equation (Equation 8) (Huggins, 1942).

$$\eta_{red} = [\eta](1 + K_H[\eta].c) \quad \textbf{(8)}$$

K_H = Huggins constant

c = concentration (mg/mL)

The concentration dependence of η_{inh} is related to the Kraemer constant as seen in Equation 9 (Kraemer, 1938).

$$\eta_{inh} = [\eta](1 - K_K[\eta].c) \quad \textbf{(9)}$$

K_K = Kraemer constant

c = concentration (mg/mL)

The K_H and K_K constants are useful when predicting the shape of macromolecules. For example, a K_H of 0.7 – 0.8 in globular particles indicates a spherical shape while a value of 0.4 – 0.7 is usually associated with a rod-like conformation (Pamies *et al.*, 2008).

These aforementioned equations all require multiple viscosity measurements at different concentrations. Other equations have been developed however which only need readings at a single macromolecular concentration. Among these is the Solomon-Ciuta equation (Solomon and Ciută, 1962), obtained by combining the Huggins and Kraemer relations (Equation 10). This is the equation that has been used in this work.

$$[\eta] = \frac{1}{c}\left(2\left(\eta_{sp}\right) - 2ln(\eta_{rel})\right)^{\frac{1}{2}} \quad \textbf{(10)}$$

c = concentration (mg/mL)

η = solution viscosity (mL/g)

η_0 = viscosity of solvent (mL/g)

η_{rel}= relative viscosity ($\frac{\eta}{\eta_0}$)

η_{sp}= specific viscosity ($\eta_{rel} - 1$)

3.1.2.3 Macromolecular conformational analysis

The 'ellipsoid' or 'whole-body' approach is used to determine the shape of macromolecules in solution through the use of hydrodynamic parameters (Harding, Horton and Cölfen, 1997). This approximates the whole macromolecule as a singular, regular ellipsoid with three perpendicular semi-axes *a* ≥ *b* ≥ *c* (Figure 34).

The ellipsoid approach is divided into two types: the 'ellipsoid of revolution' and the 'general triaxial ellipsoid' (Harding, Horton and Cölfen, 1997). The ellipsoid of revolution, which was the type used in this work, assumes that two of the three semi-axes are equal (*b* = *c*). Ellipsoids of revolution can either be prolate or oblate. A prolate ellipsoid (semi-axes *a, b, b*) is created when an ellipse of semi-axes *a* and *b* is rotated on the major axes (*a*) (Figure 35). Conversely, an oblate ellipsoid (semi axes *a, a, b*) comes about if it is rotated on its minor axes (*b*) (Figure 36). Both prolate and oblate ellipsoids can be defined by the axial ratio (a/b).

The general triaxial ellipsoid is a more sophisticated approach, in that it does not assume that two semi-axes are equal (*b*=c) (Harding, Horton and Cölfen, 1997). It is therefore not restricted to prolate or oblate ellipsoids, but instead allows for other conformations like rods and spheres.

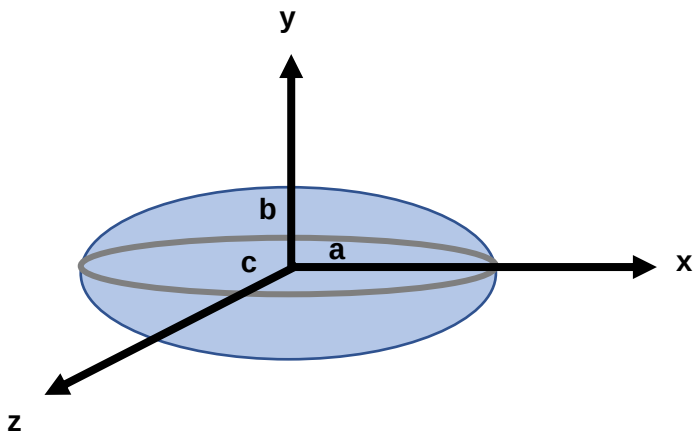

Figure 34. The general ellipsoid with three semi-axes *a* ≥ *b* ≥ *c*. Its shape is represented by the frictional ratios *(a/b)* and *(b/c)*. Adapted from (Harding, Horton and Cölfen, 1997).

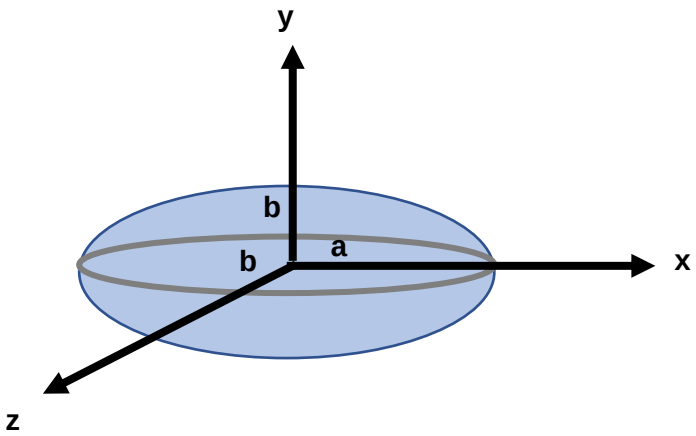

Figure 35. A prolate ellipsoid with semi-axes *(a, b, b)*. The shape is represented by the frictional ratio *(a/b)*. Adapted from (Harding, Horton and Cölfen, 1997).

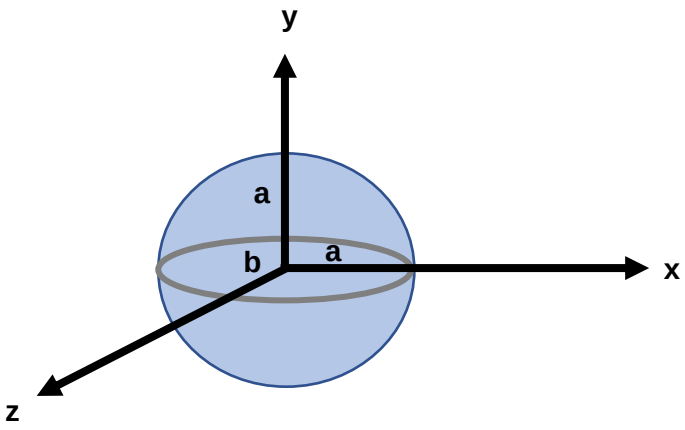

Figure 36. An oblate ellipsoid with semi-axes *(a, a, b)*. The shape is represented by the frictional ratio *(a/b)*. Adapted from (Harding, Horton and Cölfen, 1997).

The axial ratio (*a/b*) can be determined using a variety of hydrodynamic shape parameters, so-called as universal shape functions. This is because they are only dependent on the shape of the macromolecule, whereas the volume or size of said macromolecule does not have an effect (Harding, Horton and Cölfen, 1997). Some of these universal shape functions require information on the hydrated volume (V) of a macromolecule. V can be described by Equation 11.

$$V = \frac{\nu_S \,.M}{N_A} \qquad \textbf{(11)}$$

ν_S = specific volume of the hydrated macromolecule (mL/g)

M = molecular weight (Da) or molar mass (g/mol)

N_A = Avogadro's number (6.02214 x 10^{23} mol^{-1})

The hydration dependent universal shape functions that are made use of in this chapter are the viscosity increment ν (Equation 12) (Simha, 1940; Saito, 1951) and the Perrin function *P* (Equation 13a) (Perrin, 1936).

$$\nu = [\eta]M/(N_A V) \quad \textbf{(12)}$$

$[\eta]$ = intrinsic viscosity of the macromolecule (mL/g)

M = molecular weight (Da) or molar mass (g/mol)

N_A = Avogadro's number (6.02214 x 10^{23} mol^{-1})

V = hydrated volume of the macromolecule (mL)

$$P = (f/f_o)\,(\bar{v}/v_s)^{\frac{1}{3}} \quad \textbf{(13a)}$$

(f/f_o) = frictional ratio

$\bar{v}$ = partial specific volume of the particle (mL/g)

v_s = specific volume of the hydrated macromolecule (mL/g)

The frictional ratio $\frac{f}{f_o}$ is related to $s_{20,w}$ (Tanford, 1961) as described in Equation 13b.

$$\frac{f}{f_o} = \frac{M(1-\bar{v}\rho_0)}{N_A 6\pi\eta_o s^0 20,w}\left(\frac{4\pi N_A}{3\bar{v}M}\right)^{\frac{1}{3}} \quad \textbf{(13b)}$$

M = molecular weight (Da) or molar mass (g/mol)

$\bar{v}$ = partial specific volume of the particle (mL/g)

ρ_0 = density of water at 293.15 K (0.99823 g/ml)

N_A = Avogadro's number (6.02214 x 10^{23} mol^{-1})

η_0 = viscosity of water at 293.15 K (0.010 Poise)

Conversely, hydration independent universal shape functions are those that are not affected by V. An example is the Scheraga-Mandelkern parameter β (Equation 14)

(Scheraga and Mandelkern, 1953). Unlike the previously mentioned functions, β is very insensitive to shape. Because of this, it is usually used more as a check to confirm consistency of results rather than as a way to obtain new data (Harding, Horton and Cölfen, 1997).

$$\beta = N_A s[\eta]^{\frac{1}{3}}\eta_o \Big/ \left[M^{\frac{2}{3}}(1-\bar{v}\rho_o)100^{\frac{1}{3}}\right] \quad \textbf{(14)}$$

N_A = Avogadro's number (6.02214 x 10^{23} mol^{-1})

s = sedimentation coefficient (in Svedberg units S)

$[\eta]$ = intrinsic viscosity of the macromolecule (mL/g)

η_0 = viscosity of water at 293.15 K (0.010 Poise)

M = molecular weight (Da) or molar mass (g/mol)

$\bar{v}$ = partial specific volume of the particle (mL/g)

ρ_0 = density of water at 293.15 K (0.99823 g/ml)

The values derived from these shape factors are then used in specific software programmes which are capable of estimating the axial ratios of the molecules based on the input. An example is the ELLIPS1 algorithm which is part of a four-algorithm package and uses the ellipsoid of revolution approach to analyse polymer shapes (Harding, Horton and Cölfen, 1997). It predicts the axial ratio (a/b) according to hydrodynamic values inputted by the researcher.

3.2 Aims and objectives

The overall aim for the work described in this chapter was to carry out an extensive characterisation of the polymers TPA5, TPA6 and TPA7. The results would then be used to confirm whether these polymers would be good leads for further research as wood consolidants.

Several experiments were planned in order to carry this out, primarily through the use of SV and SE experiments to characterise the polymers. The SV studies would provide information on whether the polymer systems have a high degree of heterogeneity, whilst the SE experiments would confirm the molecular weights that were previously obtained by GPC. The target for these polymers was for them to have low heterogeneity and a small molecular weight (<5 kDa). Other tests which were to be carried out involved the determination of the partial specific volume $\bar{v}$ and intrinsic viscosity $[\eta]$ of the polymers, as well as analysing their conformation.

3.3 Results and Discussion

All the studies described in this chapter were carried out using isopropanol as the primary solvent.

3.3.1 TPA5

3.3.1.1 The partial specific volume $\bar{v}$

The method of Kratky *et al.* was followed (Kratky, Leopold and Stabinger, 1973). TPA5 was left to dissolve in isopropanol overnight to form a stock solution which was thereafter used to make up the required concentrations. The density of each concentration was then measured. The $\bar{v}$ was obtained by plotting all the density measurements against concentration (Figure 37) and consequently making use of Equation 4.

$$\bar{v} = \frac{1}{\rho_o}\left(1 - \frac{\partial \rho}{\partial c}\right) \quad \textbf{(4)}$$

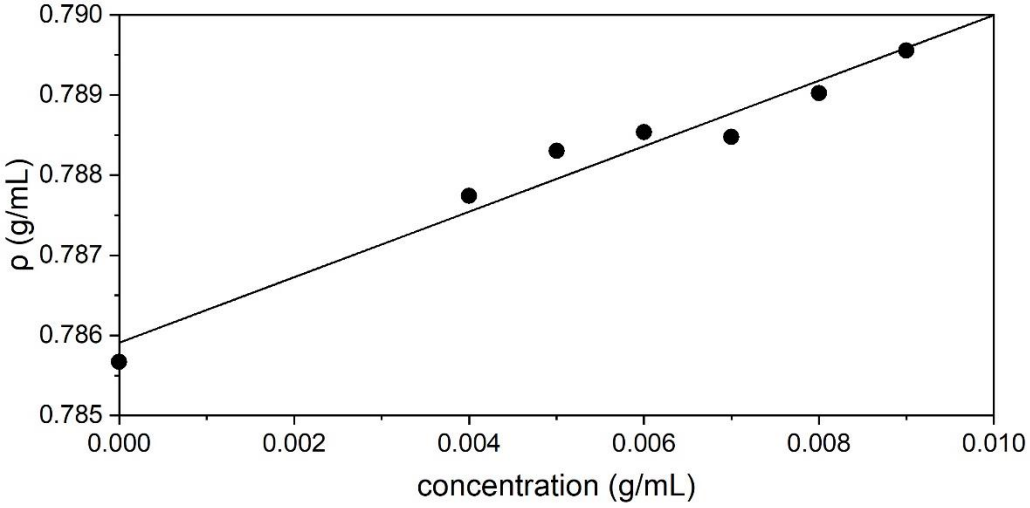

Figure 37. Dependence of solution density of TPA5 in isopropanol on concentration

This was calculated to be (0.753 ± 0.040) mL/g. This value appeared to be consistent with other $\bar{v}$ values previously reported for synthetic polymers, such as poly(methyl methacrylate) (Gill and Kunz, 1968). The $\bar{v}$ is an important value to calculate since it is used in the analysis of any subsequent SV studies.

3.3.1.2 SV

Figure 38 shows the sedimentation coefficient range *c(s)* vs *s* of TPA5 in isopropanol, run on SEDFIT (Schuck, 2000; Dam and Schuck, 2004). It revealed the presence of a high concentration of a very low molecular weight species at 0.8 S, with a smaller population of two larger sedimentation coefficient *s* value species (~ 1.4 and 2.05 S). This trend was observed in all the concentrations that were used in this study.

Since the largest peak had the smallest sedimentation coefficient, this meant that the majority of particles in the TPA5 polymer system had a small molecular weight. This was promising since it meant that most of the particles would theoretically be capable of penetrating wood.

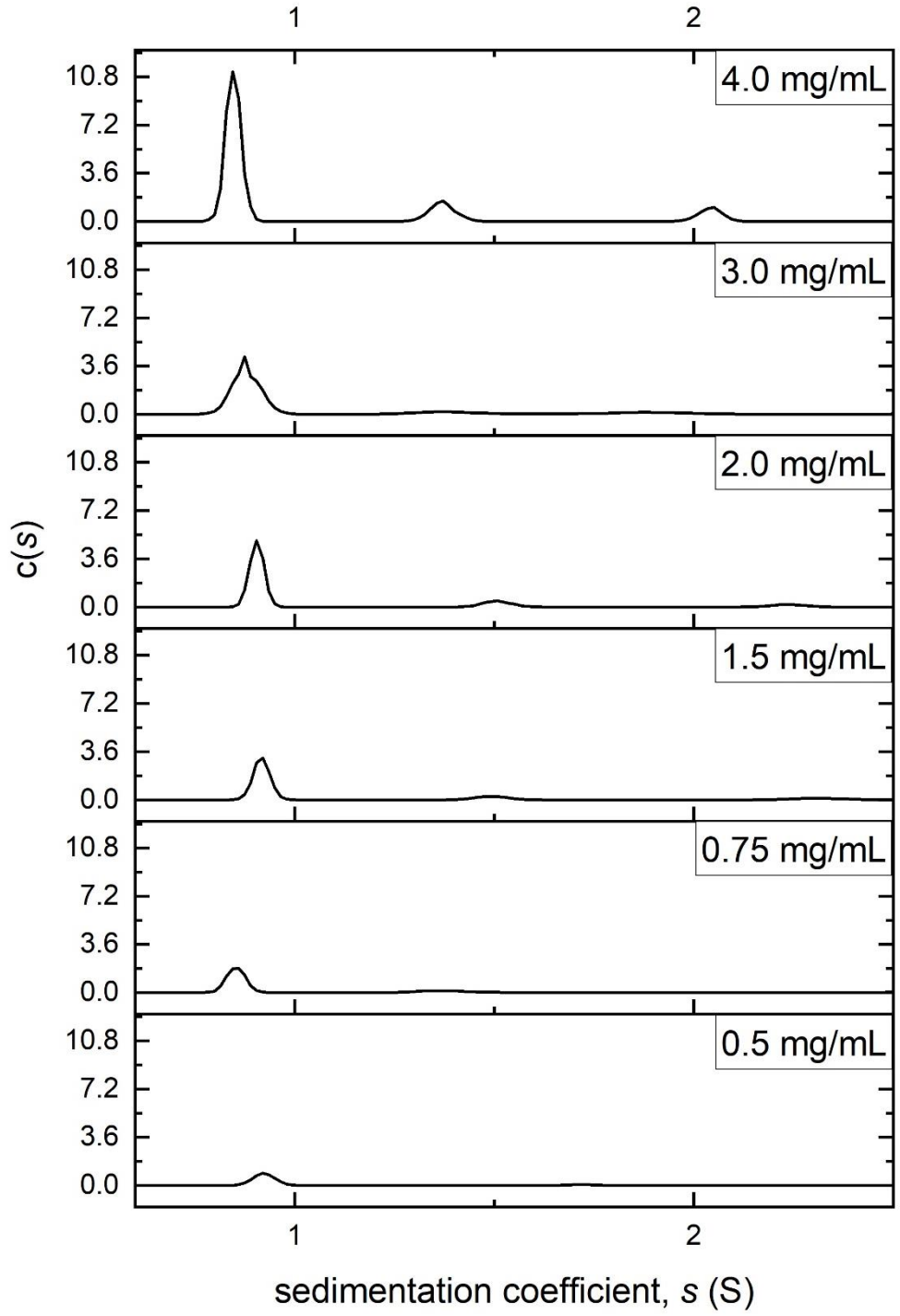

Figure 38. Sedimentation coefficient distributions *c(s)* vs sedimentation coefficient (S) for TPA5 in isopropanol. Rotor speed = 49,000 rpm.

After analysis, the sedimentation coefficient of the major peak was normalised to standard solvent conditions, that is, the viscosity and density of water at 20.0 °C ($s_{20,w}$) (Figure 39) (Tanford, 1961). This was found to be (0.696 ± 0.007) S.

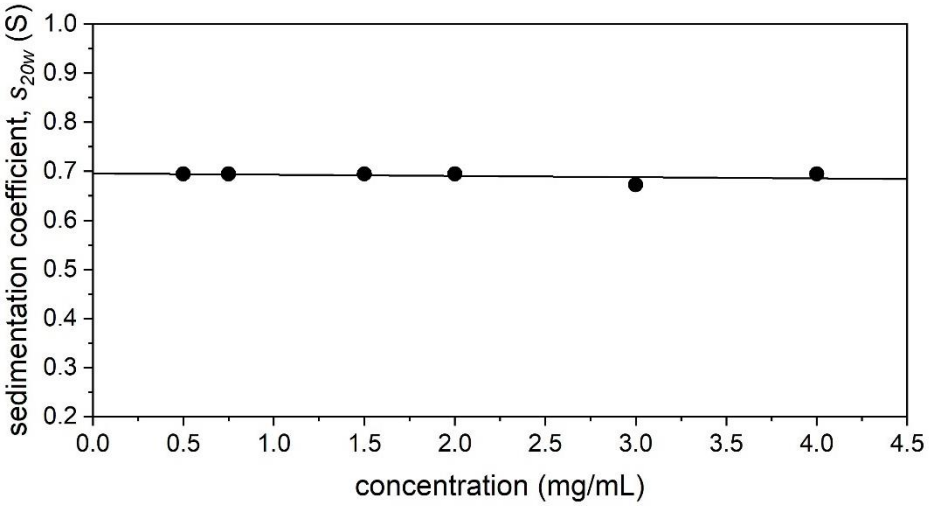

Figure 39. Sedimentation coefficient $s_{20,w}$ corrected to standard conditions (the density and viscosity of water at 20.0 °C) against sedimenting concentration for TPA5 in isopropanol. $s_{20,w}$ = (0.696 ± 0.007) S.

3.3.1.3 SE

An SE experiment was run on the TPA5 polymer, using a concentration series ranging from 0.5 mg/mL to 4.0 mg/mL, to estimate the absolute molecular weight. Although not dependent on poly(methyl methacrylate) standards like GPC, nonetheless sedimentation equilibrium yields apparent molecular weights M_{app} (that is, affected by non-ideality through polymer co-exclusion). Using different concentrations of polymer permits the determination of the extent of a polymer's non-ideal behaviour, and either a simple extrapolation to zero concentration or operating at a low concentration eliminates these effects.

For SE, it is important to have an idea of the molecular weight range of the analysed polymer so as to be able to select the appropriate centrifugal speed. A speed which

is too high puts the higher molecular weight molecules at risk of sedimentation to the cell base. If it is too slow, then this would result in the molecules diffusing back to the meniscus. Fortunately, the approximate molecular weight values of TPA5, TPA6 and TPA7 were already known due to their previous GPC analyses.

The data obtained from the various loading concentrations was analysed with SEDFIT-MSTAR (Schuck *et al.*, 2014), resulting in a plot of $M_{w,app}$ vs concentration for each sample. The $M_{w,app}$ was obtained by extrapolating the M^* function (Creeth and Harding, 1982) to the cell base, as well as by using the hinge point method (Schuck *et al.*, 2014). Table 6 shows a comparison of the $M_{w,app}$ values obtained from the SE study for all the tested concentrations. The results from the M^* analysis were all slightly lower than the hinge point values, however they could still be considered to be in accordance with one another. These results demonstrated that there was no significant change in $M_{w,app}$ with concentration, indicating that it was not concentration dependent and unaffected by non-ideality. It may therefore be assumed that the $M_{w,app}$ determined by this experiment was in fact the ideal molecular weight of the polymer at each given concentration ($M_{w,app} \sim M_w$). The overall average M_w was calculated by plotting the values obtained in the SE experiment against concentration and extrapolating to zero (Figure 40). This was determined to be (4.3 ± 0.2) kDa.

Table 6. $M_{w,app}$ values derived from the M^* function and the hinge point method, obtained from the SE of TPA5.

Concentration (mg/mL)	$M_{w,app}$ (M^*) (kDa)	$M_{w,app}$ (hinge point) (kDa)
0.5	4.0	3.5
0.75	4.3	3.8
1	4.5	4.2
2	4.2	3.8
3	4.6	4.4
4	4.3	4.0

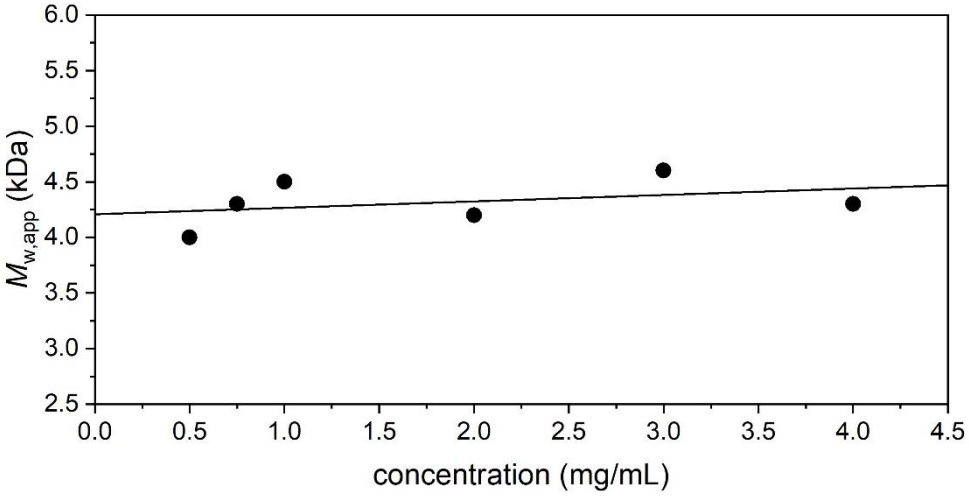

Figure 40. Dependence of apparent $M_{w,app}$ on concentration for TPA5 in isopropanol, with an extrapolation to obtain the thermodynamically ideal $M_{w,app}$. Analysed with SEDFIT-MSTAR using the *M** derived method to obtain the shown $M_{w,app}$ values. Rotor speed = 45,000 rpm. M_w = (4.3 ± 0.2) kDa.

The M_w values obtained by SE and the GPC analysis that was previously carried out (as described in Chapter 2) were compared. The M_w obtained by SE proved to be slightly larger, however it was expected that the values obtained from AUC would have a higher degree of accuracy as a result of it being an absolute method.

The SE data for the 4.0 mg/mL concentration was additionally analysed with the MultiSig algorithm (Gillis *et al.*, 2013). This was used to give a broader resolution of the *M** data, while also providing information about the M_w distribution of the polymer system. Figure 41 reveals a M_w distribution ranging from 2.3 to 9.3 kDa, with components peaking at 2.6 and 6.1 kDa. This was consistent with the SEDFIT-MSTAR analysis, confirming that the polymer had a low M_w and thus adding credibility to the results previously obtained by GPC. This further reinforced the status of this polymer as a very promising lead for the purpose of consolidation, since a low weight average M_w of ~ 4.3 kDa would increase the probability of it successfully penetrating archaeological wood.

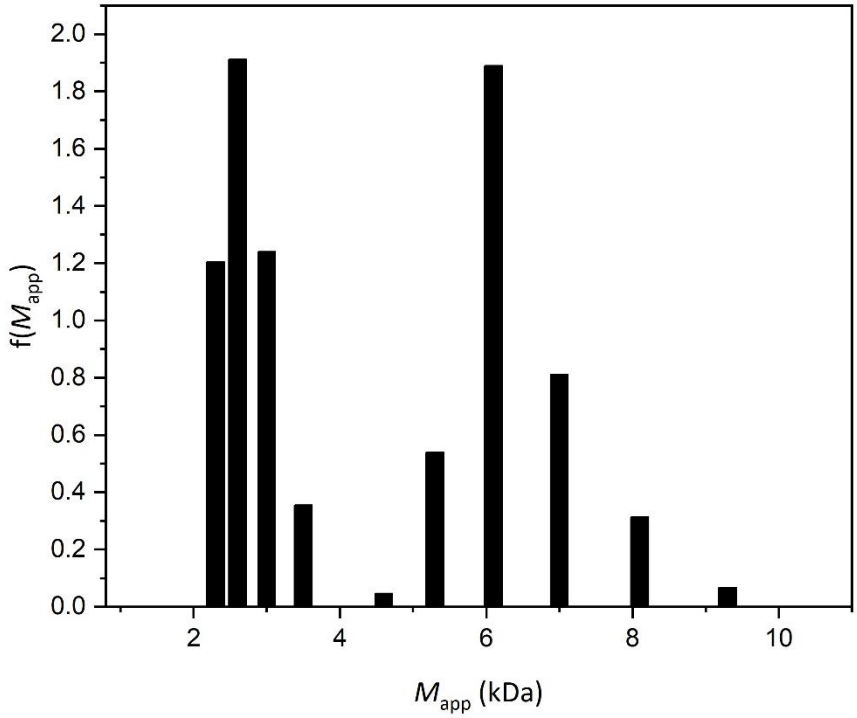

Figure 41. MultiSig analysis of the molecular weight distribution f(M_{app}) vs M_{app} of TPA5 in isopropanol at a concentration of 4.0 mg/mL. Rotor speed = 45,000 rpm.

3.3.1.4 The intrinsic viscosity $[\eta]$

It was initially planned to carry out the viscosity measurements with a conventional Ostwald U-tube capillary viscometer. This however did not prove ideal due to the high volatility of isopropanol. It was therefore decided to use a rolling ball viscometer at low temperatures in order to counteract this issue.

After measuring the viscosity of the polymer solution at 6.0 mg/mL, the $[\eta]$ of TPA5 was calculated to be (5.3 ± 0.1) mL/g with the Solomon-Ciuta equation (Equation 10) (Solomon and Ciută, 1962).

$$[\eta] = \frac{1}{c}\left(2\left(\eta_{sp}\right) - 2In(\eta_r)\right)^{\frac{1}{2}} \quad \textbf{(10)}$$

3.3.1.5 Conformational analyses

With the use of the $[\eta]$, along with the values for the M_w, $\bar{\nu}$ and $s_{20,w}$ values obtained from previous experiments, the conformation of TPA5 could then be investigated. These analyses were particularly important as a polymer's shape may determine whether it penetrates wood and the subsequent effect it would have.

The programme ELLIPS1 was used to estimate the conformation of the polymer using the viscosity increment (ν) (Equation 12) (Simha, 1940; Saito, 1951) and the Perrin function (*P*) (Equation 13a) (Perrin, 1936) shape factors.

$$\nu = [\eta]M/(N_A \mathrm{V}) \quad \textbf{(12)}$$

$$P = (f/f_o)\,(\bar{\nu}/v_s)^{\frac{1}{3}} \quad \textbf{(13a)}$$

ELLIPS1 is based on a simple ellipsoid of revolution model, where two of the three ellipsoid axes are of equal value (Harding, Horton and Cölfen, 1997). Both *P* and ν are universal shape parameters, meaning that they are described by a function of shape and not size (García de la Torre and Harding, 2013). *P* and ν are obtained respectively from the sedimentation coefficient and $[\eta]$ (Carrasco *et al.*, 1999).

Once calculated, ELLIPS1 was then used to report these shape functions in terms of their axial ratios (a/b) for ellipsoids of revolution (García de la Torre and Harding, 2013). Tables 7 and 8 show the values for the ν and *P* parameters and the corresponding axial ratios for TPA5 at different degrees of solvent association. The degree of solvent association describes the extent of interaction between a polymer in solution and a solvent. It is defined as $v_s/\bar{\nu}$, where v_s is the swollen specific volume and $\bar{\nu}$ is the partial specific volume. If the polymers did not bind with isopropanol, then the solvent association would be equal to their $\bar{\nu}$. In Tables 7 and 8, solvent association values of 1.0 – 1.4 were used for the shape analyses in order to determine whether these would drastically affect the results.

Along with the axial ratios, ELLIPS1 also provides a visual representation of the approximate shape of the macromolecule. Both *P* and ν gave consistent results,

indicating that the polymer had an elongated shape, as shown by Figures 42 and 43. Their axial ratios did not vary greatly with the different degrees of solvent association. This type of shape may prove to be advantageous for consolidants, as it could potentially increase the surface area available for possible interactions between the wood and the polymers.

Table 7. The TPA5 calculated values for the shape parameter ν and the axial ratios (prolate ellipsoid model) determined by ELLIPS1

	Degree of solvent association $(v_s/\bar{v})$		
	1.0	**1.2**	**1.4**
shape factor ν	7.0 ± 0.2	5.9 ± 0.2	5.0 ± 0.2
axial ratio (a/b)	5.9	5.1	4.3

Table 8. The TPA5 calculated values for the shape parameter *P* and the axial ratios (prolate ellipsoid model) determined by ELLIPS1

	Degree of solvent association $(v_s/\bar{v})$		
	1.0	**1.2**	**1.4**
shape factor *P*	1.2 ± 0.2	1.2 ± 0.2	1.1 ± 0.2
axial ratio (a/b)	4.6	3.8	2.9

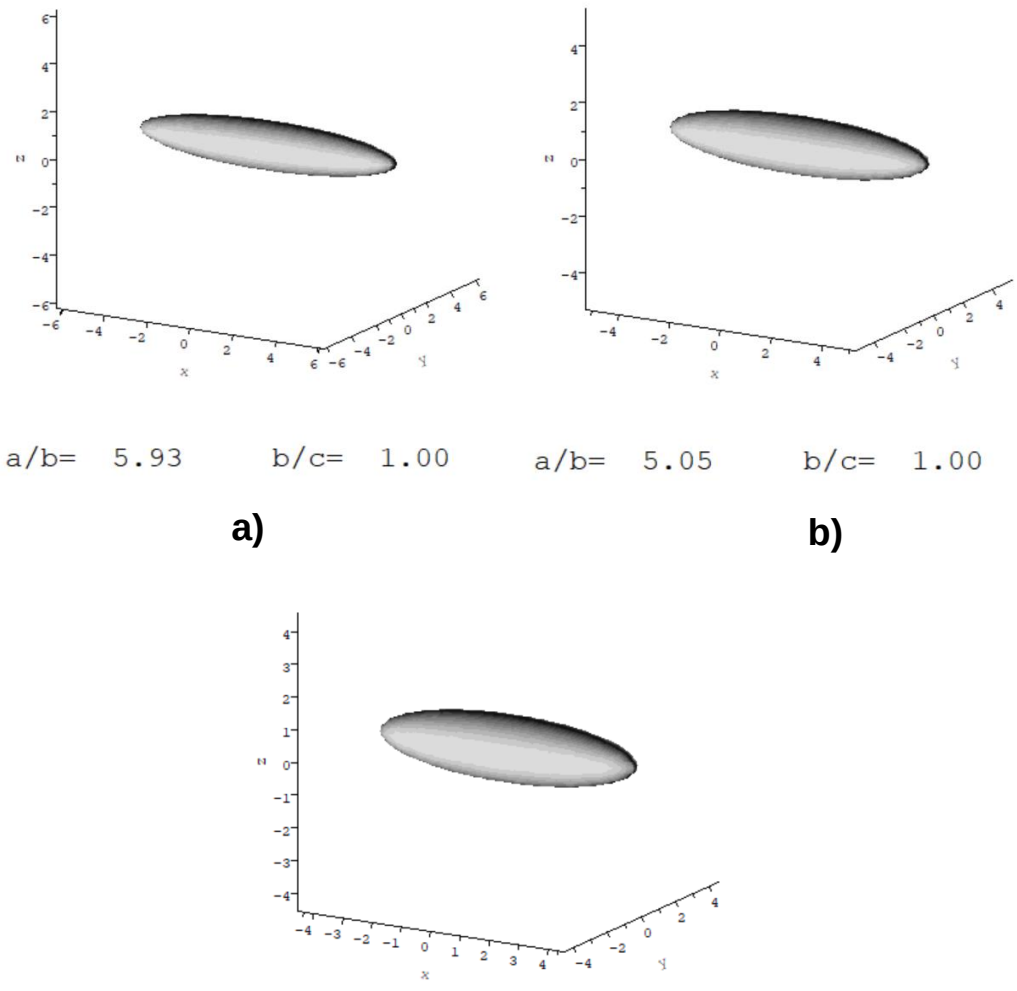

Figure 42. Ellipsoidal representations from the conformation analysis of TPA5 in isopropanol at different degrees of solvent association, using the programme ELLIPS1 with the shape parameter ν. a) $(v_s/\bar{v})$ = 1.0; b) $(v_s/\bar{v})$ = 1.2; c) $(v_s/\bar{v})$ = 1.4.

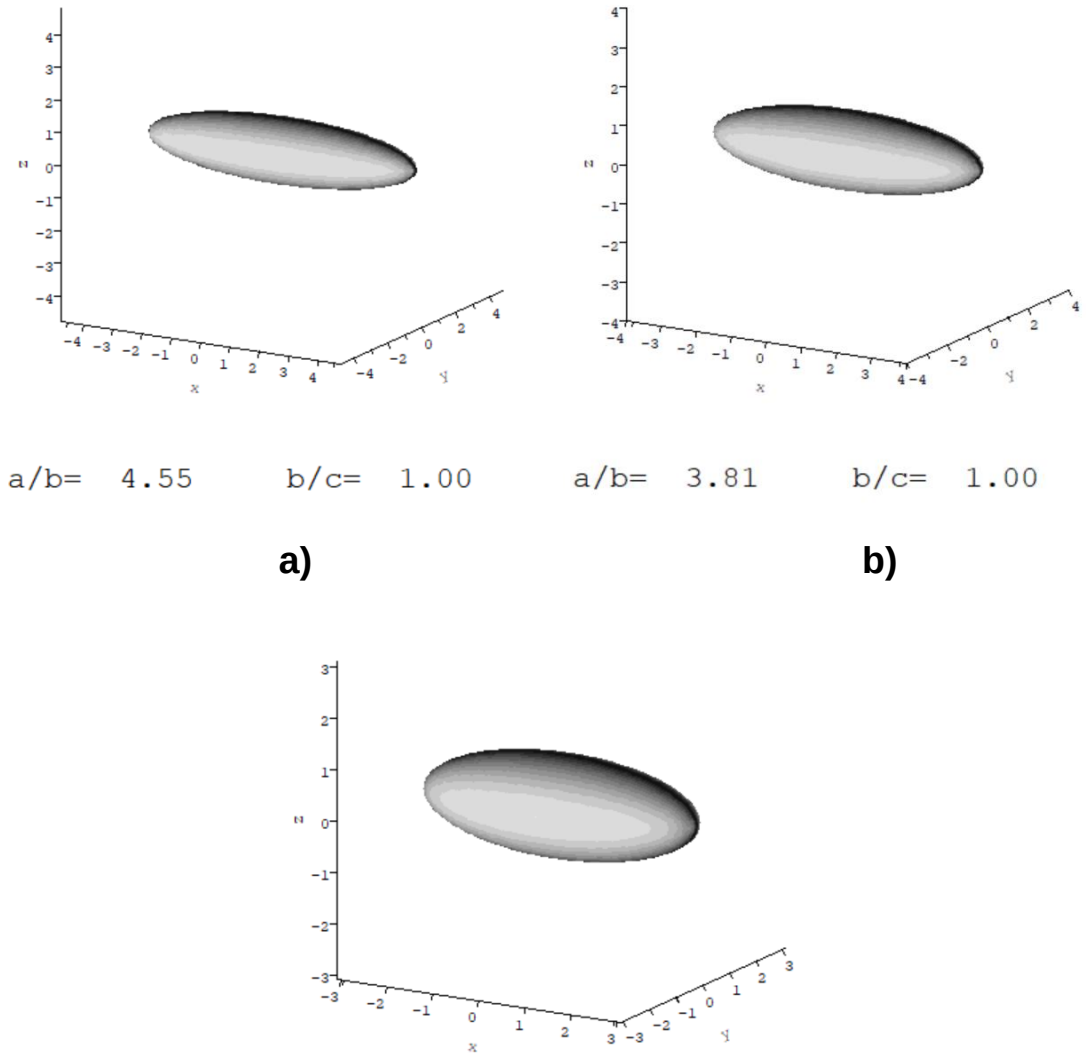

Figure 43. Ellipsoidal representations from the conformation analysis of TPA5 in isopropanol at different degrees of solvent association, using the programme ELLIPS1 with the shape parameter *P*. a) $(v_s/\bar{v})$ = 1.0; b) $(v_s/\bar{v})$ = 1.2; c) $(v_s/\bar{v})$ = 1.4.

An additional shape factor, the Scheraga-Mandelkern (β) parameter (Scheraga and Mandelkern, 1953), was used as a consistency check. This is a hydration-independent function, but it is very insensitive to shape (Equation 14) (Scheraga and Mandelkern, 1953).

$$\beta = N_A s[\eta]^{\frac{1}{3}}\eta_o \Big/ \left[M^{\frac{2}{3}}(1-\bar{v}\rho_o)100^{\frac{1}{3}}\right] \quad \textbf{(14)}$$

A value of $\beta = (2.4 \pm 0.2 \times 10^6)$ was calculated. This corresponded to a large axial ratio range, but it was nonetheless consistent with the value for the *a*/*b* found for the ν and *P* functions. Additionally, this value is only compatible with an elongated, prolate ellipsoid molecule, as opposed to a flat disc or oblate model like lignin (Figure 44) This therefore added further confidence to the shape analyses that were previously carried out.

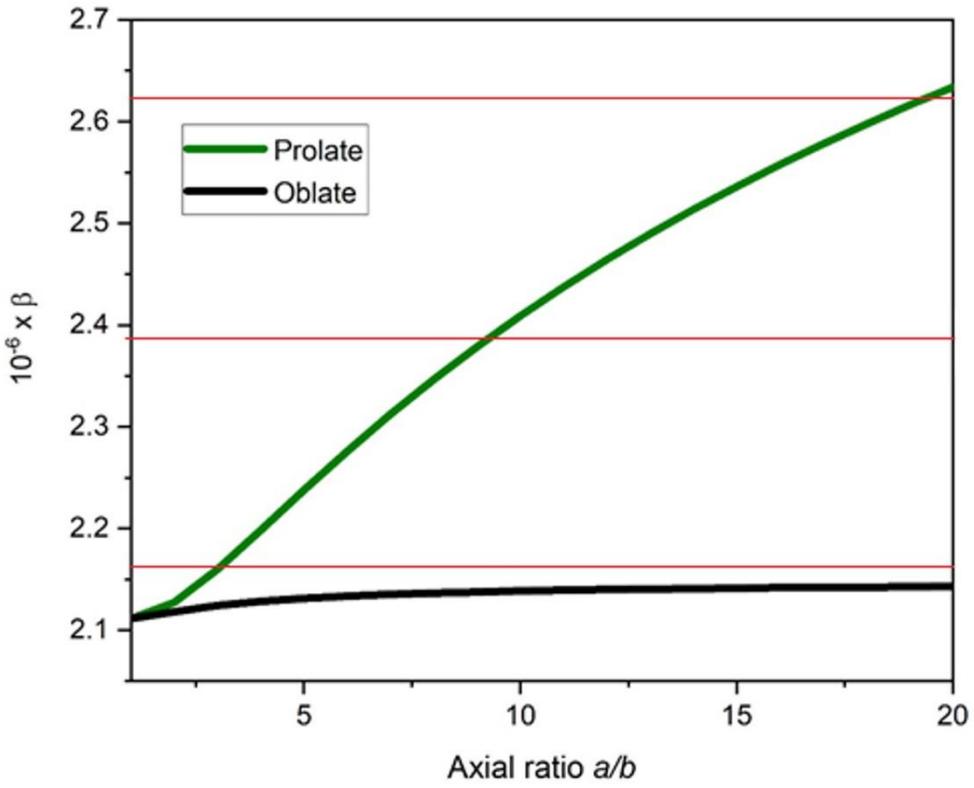

Figure 44. A plot of Scheraga-Mandelkern *β* function vs axial ratio with the green and black lines representing prolate and oblate shapes respectively. Red lines correspond to the experimental value of β = (2.4 ± 0.2 x 10^6) which excludes an oblate (disc) shape

3.3.1.6 Interaction study with soda lignin

It is anticipated that terpene-derived polymers such as TPA5 will eventually be used with lignin-based consolidants as a combination treatment for degraded wood. In such cases, knowing how they behave when they are in the same solution will be essential. Accordingly, it was decided to carry out a preliminary study using a combined solution of TPA5 with soda lignin, in order to discover whether these two materials interact with each other. The lignin samples were prepared using a protocol adapted from the literature (Alzahrani *et al.*, 2016b), with isopropanol as the solvent. The prepared lignin solution was then mixed with the polymer solution in isopropanol to achieve several different concentrations and combinations. These are summarised in Table 9.

An SV study was carried out with the prepared solutions. Figure 45 shows the results obtained by this experiment. The data does not indicate that there was any significant interaction between TPA5 and lignin. In the future it may be possible to repeat this experiment using sulfuric acid to catalyse the crosslinking of TPA5 and lignin, to see if this induces any kind of interactive behaviour between the two polymers. Carrying out such an experiment with sulfuric acid would be useful as this would help mirror the real-life conditions that the Oseberg artefacts are in. As such, this experiment could provide interesting initial observations on whether the acidic condition of the wood would change the behaviour of TPA5. Nevertheless, the non-interactive behaviour observed with this experiment could still be advantageous, as it may result in the absence of any aggregation phenomena between the lignin and the polymer should they be used together.

Table 9. The different combinations of TPA5 and soda lignin used for the interaction study. Cells 1 and 2 were used as controls.

Cell number	Content of sample	Overall concentration (mg/mL)
1	Polymer TPA5	0.2
2	Soda lignin	0.2
3	1:1 lignin : polymer (0.2 mg/mL)	0.4
4	1:2 lignin : polymer (0.2 mg/mL)	0.6
5	1:1 lignin : polymer (0.4 mg/mL)	0.4
6	1:2 lignin : polymer (0.4 mg/mL)	0.6
7	2:1 lignin : polymer (0.2 mg/mL)	0.6

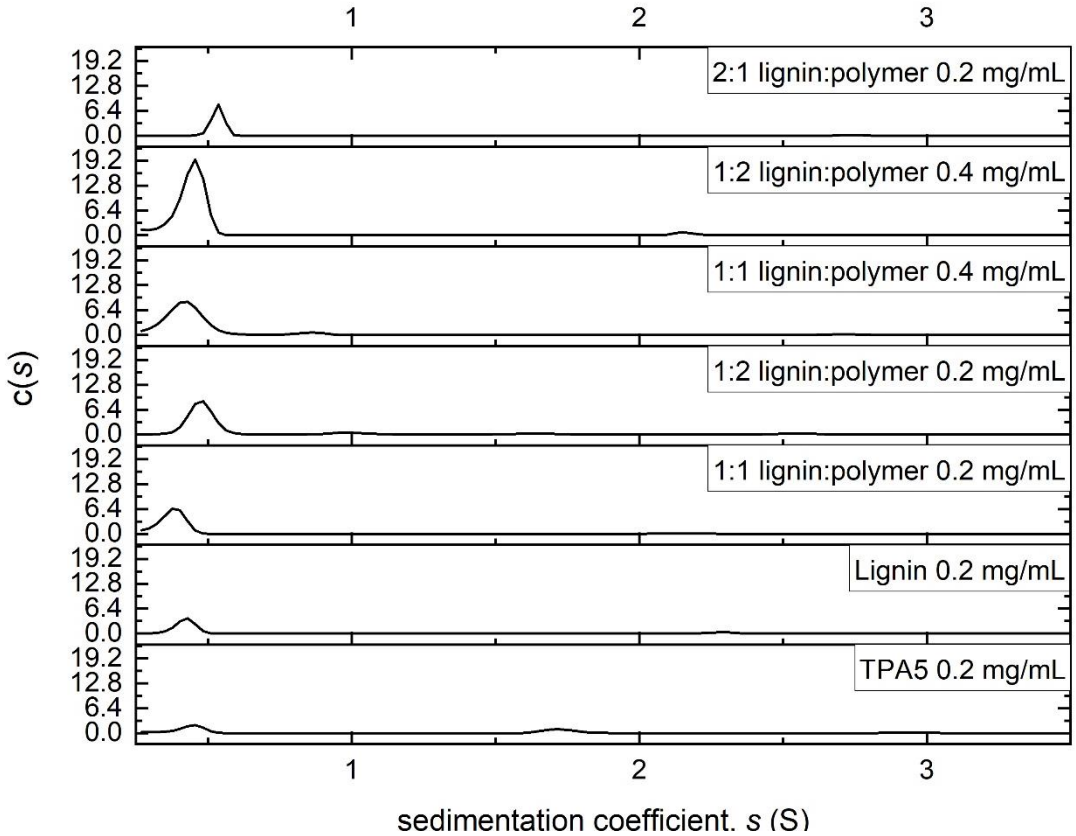

Figure 45. The results obtained by the SEDFIT analysis for all the different combinations of TPA5 and lignin. No major peaks were observed at higher S values, indicating that there were not any significant interactions between the polymer and soda lignin.

3.3.2 TPA6

3.3.2.1 The partial specific volume $\bar{v}$

The partial specific volume $\bar{v}$ of TPA6 was measured in the same manner as was done for TPA5 (Kratky, Leopold and Stabinger, 1973). Again, isopropanol was the solvent of choice. Density measurements were carried out using a concentration series of TPA6 in isopropanol and these were thereafter plotted against concentration (Figure 46).

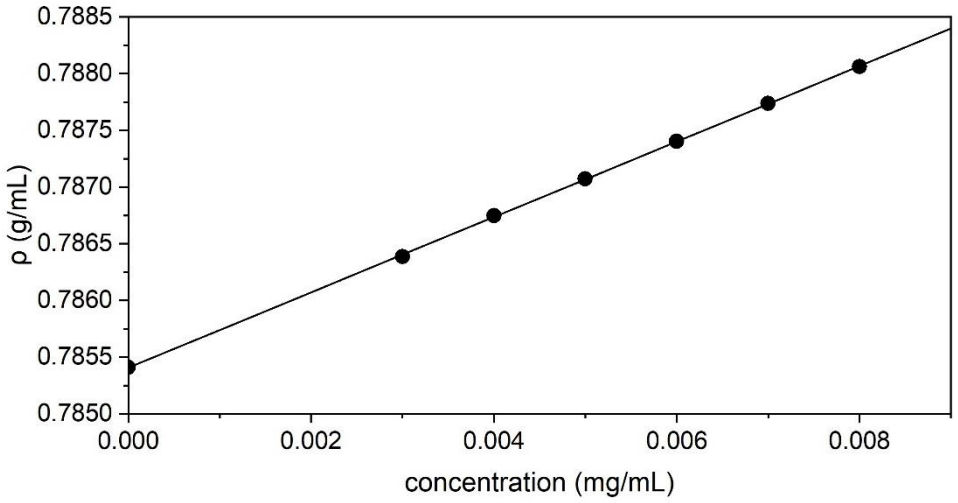

Figure 46. Dependence of solution density of TPA6 in isopropanol on concentration

Using Equation 4, the $\bar{v}$ of TPA6 was found to be (0.850 ± 0.002) mL/g. This was similar to the value that had previously been measured for TPA5.

3.3.2.2 SV

Like with TPA5, an SV study was carried out in isopropanol in order to get an indication of TPA6's degree of heterogeneity. Again, SEDFIT analyses provided the sedimentation coefficient range *c(s)* vs *s* of the polymer (Schuck, 2000; Dam and Schuck, 2004) (Figure 47).

The TPA6 polymer system appeared to possess a major peak with a low sedimentation coefficient value (~ 0.6 S), which corresponded to a small M_w value. Some minor peaks were observed at ~ 1.5 S, indicating that the polymer system was also composed of some larger M_w particles. As with TPA5, this heterogenous behaviour was more pronounced in the higher concentrations (2.0 – 4.0 mg/mL).

The $s_{20,w}$ for the major peak was calculated to be (0.646 ± 0.007) S (Figure 48).

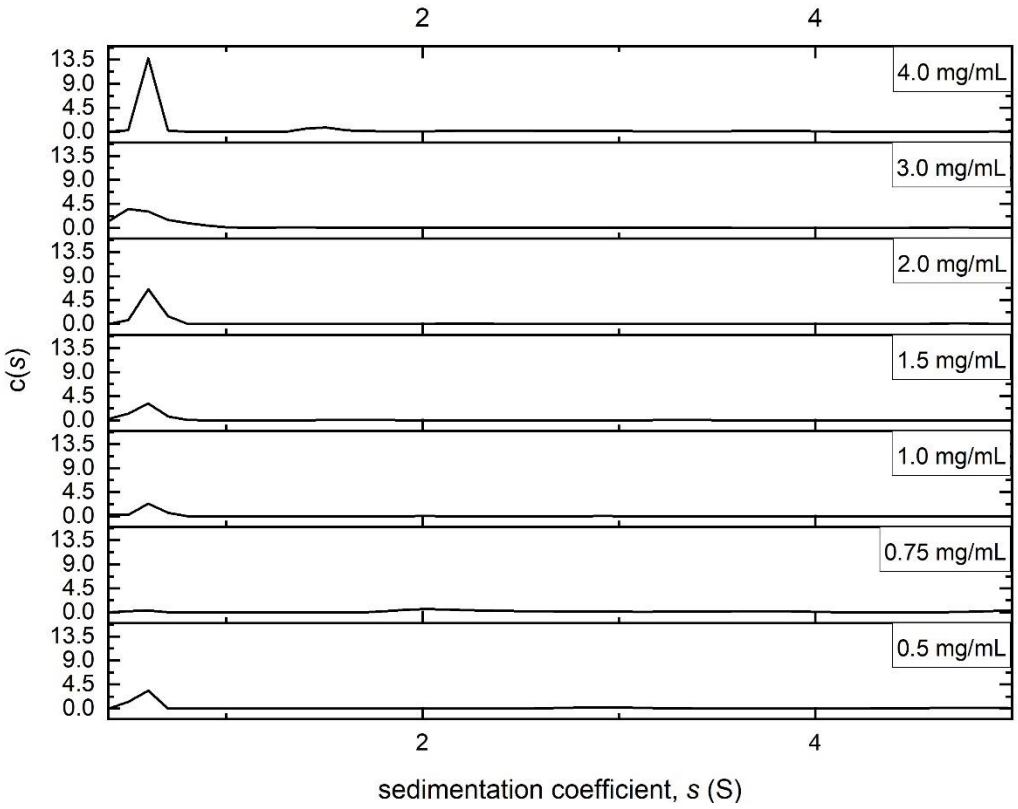

Figure 47. Sedimentation coefficient distributions *c(s)* vs sedimentation coefficient (S) for TPA6 in isopropanol. Rotor speed = 49,000 rpm.

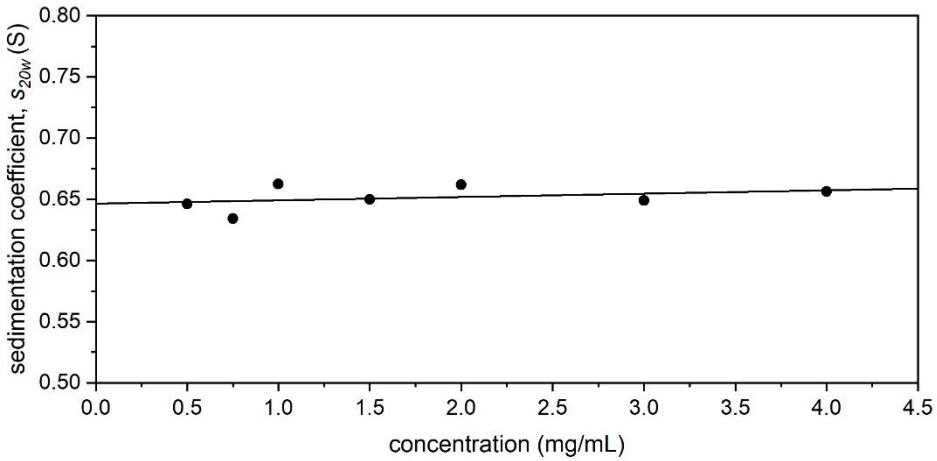

Figure 48. Sedimentation coefficient $s_{20,w}$ corrected to standard conditions (the density and viscosity of water at 20.0 °C) against sedimenting concentration for TPA6 in isopropanol. $s_{20,w}$ = (0.646 ± 0.007) S.

3.3.2.3 SE

SEDFIT-MSTAR (Schuck *et al.*, 2014) was used to obtain the $M_{w,app}$ *via* the M^* function (Creeth and Harding, 1982) and the hinge point method (Schuck *et al.*, 2014). Table 10 shows these values. From this data one could see that there was relatively low non-ideality especially in the lower concentrations, as the $M_{w,app}$ did not appear to be affected by the concentration. It was noted however that the both the M^* and the hinge point M_w values appeared to vary at higher concentrations, especially above 1.5 mg/mL. This could be due to the heterogeneity that was observed during the previous SV experiment. Another possible explanation for this could be aggregation or association activity at higher concentrations. This type of behaviour has been previously observed by Nikolajski *et al.* with a type of aminocellulose, where self-association was more prominent at higher concentrations (Figure 49) (Nikolajski *et al.*, 2014). This could be potentially problematic for a wood consolidant, since it could mean that it would be more difficult to penetrate at higher concentrations due to the higher M_w. While it is not possible given the current data to determine whether this actually takes place with TPA6, it is something that should be considered in the future. Further work may involve investigating this using higher concentrations (> 5.0 mg/mL) of TPA6 to confirm the existence of such behaviour.

Because of this, it was decided not to use the TPA6 concentrations above 1.5 mg/mL for the calculation of the M_w. The average M_w value was therefore determined by plotting the remaining $M_{w,app}$ values against concentration (Figure 50). This was found to be (3.9 ± 0.8) kDa.

Table 10. $M_{w,app}$ values derived from the M^* function and the hinge point method, obtained from the SE of TPA6.

Concentration (mg/mL)	$M_{w,app}$ (M^*) (kDa)	$M_{w,app}$ (hinge point) (kDa)
0.5	3.3	2.3
0.75	3.8	1.7
1.0	4.1	3.6
1.5	3.0	3.2
2.0	5.7	4.8
3.0	2.8	2.3
4.0	5.1	4.7

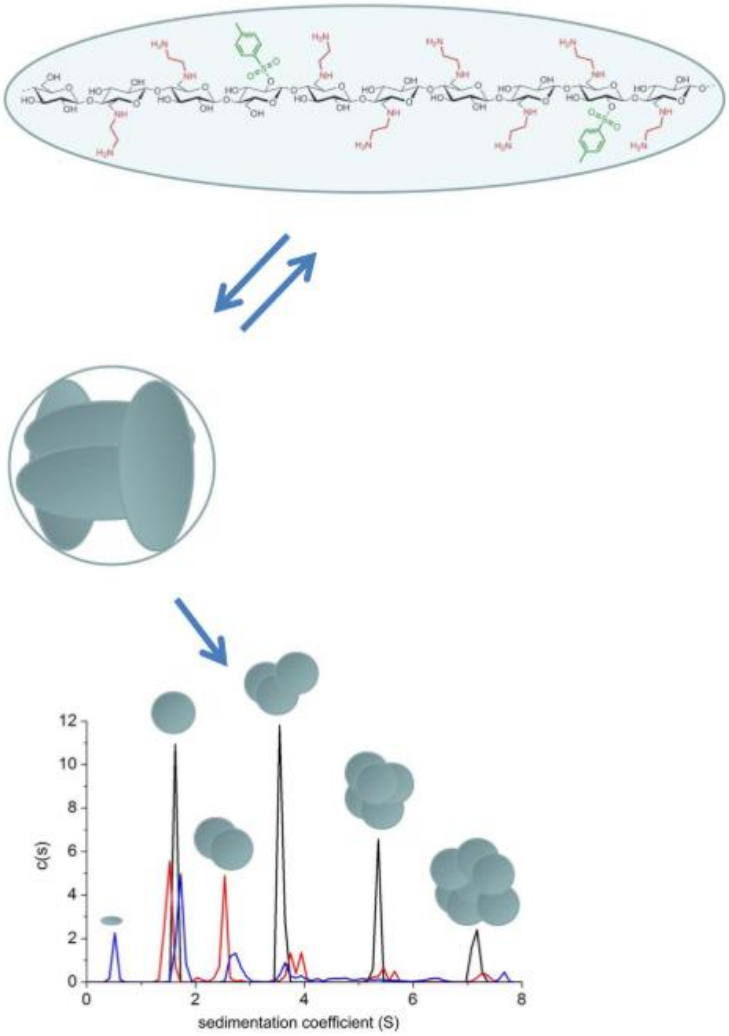

Figure 49. Depiction of the self-associative activity of polysaccharide 6-deoxy-6-(ω-aminoethyl)aminocellulose; blue = 0.75 mg/mL, red = 1.0 mg/mL and black = 2.0 mg/mL (Nikolajski *et al.*, 2014).

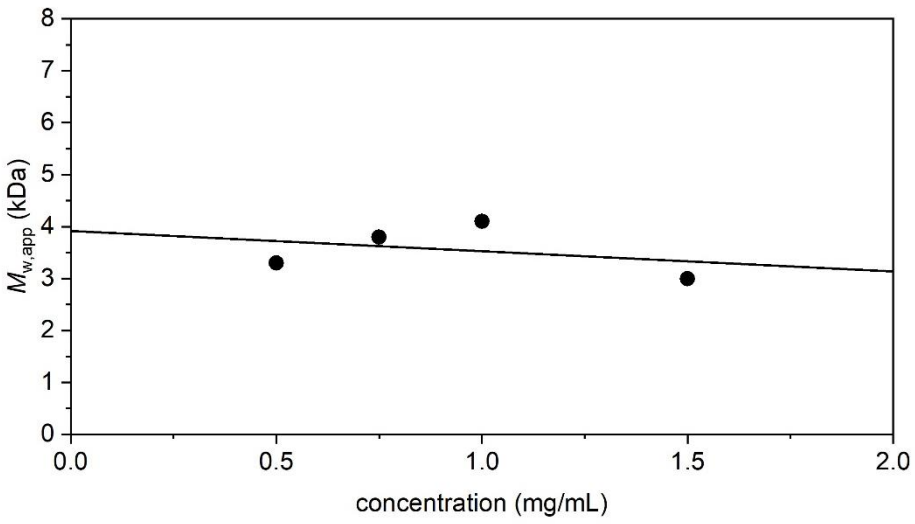

Figure 50. Dependence of apparent $M_{w,app}$ on concentration for TPA6 in isopropanol, with an extrapolation to obtain the thermodynamically ideal $M_{w,app}$. Analysed with SEDFIT-MSTAR using the M^* derived method to obtain the shown $M_{w,app}$ values. Rotor speed = 45,000 rpm. M_w = (3.9 ± 0.8) kDa.

The SE data from the 4.0 mg/mL concentration was also run through the MultiSig programme (Gillis *et al.*, 2013). Figure 51 shows the results, indicating that it had an M_w range from 1.8 to 16.4 kDa, with a peak at 4.7 kDa. These results appeared to correlate with the ones that were obtained from the SV study, showing that the highest population of molecules in the polymer systems had a small M_w. However, it also depicts other relatively high peaks at around 12.4 kDa, which could possibly correspond with the aggregation activity described previously.

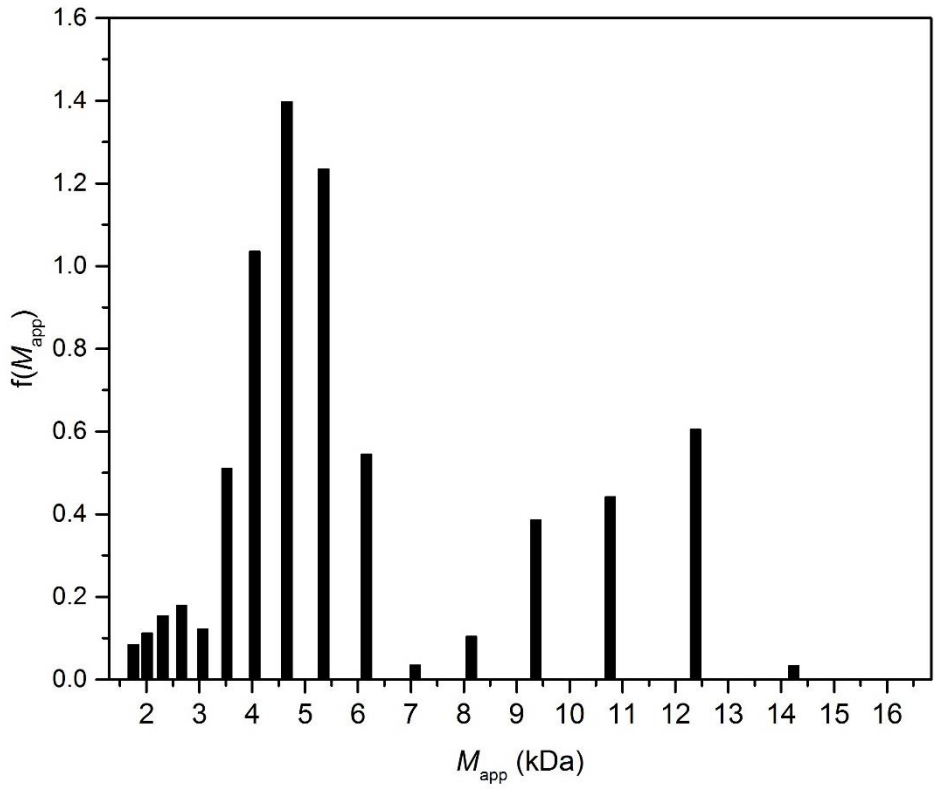

Figure 51. MultiSig analysis of the molecular weight distribution f(M_{app}) vs M_{app} of TPA6 in isopropanol at a concentration of 4.0 mg/mL. Rotor speed = 45,000 rpm.

3.3.2.4 The intrinsic viscosity $[\eta]$

The same method that was utilised for TPA5 was used to calculate the $[\eta]$. With the Solomon-Ciuta equation (Equation 10) (Solomon and Ciută, 1962), this was found to be (4.8 ± 0.2) mL/g.

3.3.2.5 Conformational analyses

The ν and *P* shape factors (Equations 12 and 13a) (Perrin, 1936; Simha, 1940; Saito, 1951) were used to predict the axial ratio of TPA6 with the programme ELLIPS1 (Harding, Horton and Cölfen, 1997).

Tables 11 and 12 depict the calculated values of these shape factors at different degrees of solvent association, along with the corresponding axial ratios. With regards to the *P* factor, the values were unfortunately too small to be inputted into ELLIPS1 and therefore the axial ratios were not possible to estimate. Figure 52 shows the visual representation of the shapes (prolate ellipsoid model) of TPA6 estimated from the ν values, As with TPA5, it appeared to have an elongated shape with the different degrees of solvent association having a minimal effect on the axial ratio.

Table 11. The TPA6 calculated values for the shape parameter ν and the axial ratios (prolate ellipsoid model) determined by ELLIPS1

	Degree of solvent association $(v_s/\tilde{v})$		
	1.0	**1.2**	**1.4**
shape factor ν	5.7 ± 0.6	4.8 ± 0.6	4.1 ± 0.6
axial ratio (a/b)	5.0	4.1	3.4

Table 12. The TPA6 calculated values for the shape parameter *P*

	Degree of solvent association $(v_s/\tilde{v})$		
	1.0	**1.2**	**1.4**
shape factor *P*	0.7 ± 0.8	0.7 ± 0.8	0.7 ± 0.8

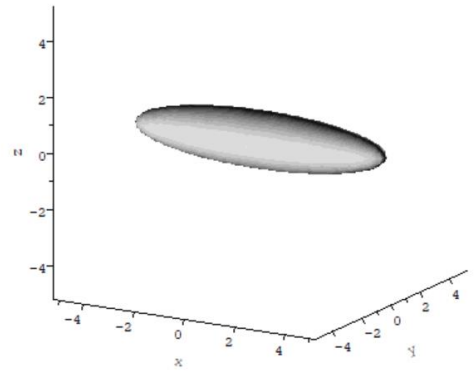

a/b= 4.96 b/c= 1.00

a)

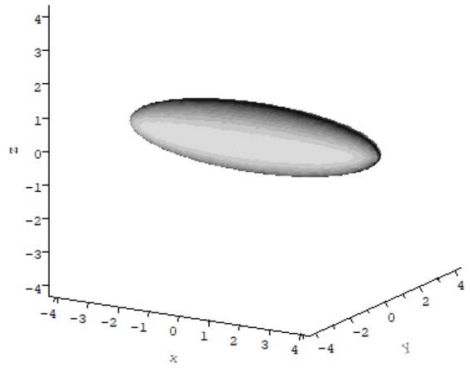

a/b= 4.11 b/c= 1.00

b)

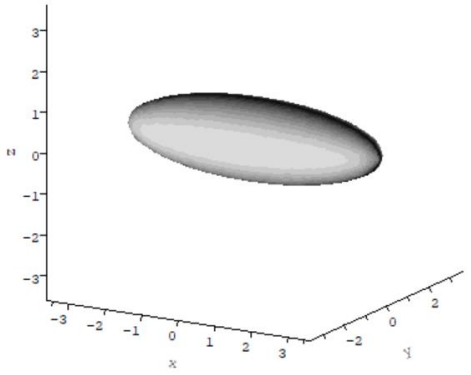

a/b= 3.44 b/c= 1.00

c)

Figure 52. Ellipsoidal representations from the conformation analysis of TPA6 in isopropanol at different degrees of solvent association, using the programme ELLIPS1 with the shape parameter ν. a) $(v_s/\bar{v})$ = 1.0; b) $(v_s/\bar{v})$ = 1.2; c) $(v_s/\bar{v})$ = 1.4.

3.3.3 TPA7

3.3.3.1 The partial specific volume $\bar{\nu}$

As with TPA5 and TPA6, Equation 4 was used for the calculation of $\bar{\nu}$. Figure 53 shows the solution densities of different TPA7 solutions in isopropanol plotted against concentration. The $\bar{\nu}$ of TPA7 was found to be (0.824 ± 0.013) mL/g. This was close in value to the previous $\bar{\nu}$ numbers that were calculated for TPA5 and TPA6. This was not surprising, as all the polymers shared similar fundamental structures.

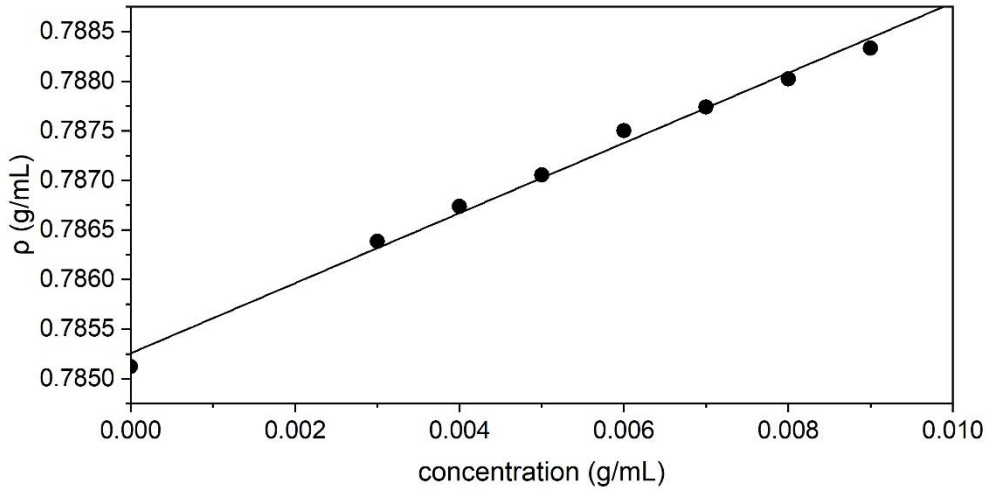

Figure 53. Dependence of solution density of TPA7 in isopropanol on concentration

3.3.3.2 SV

Results obtained by SEDFIT (Schuck, 2000; Dam and Schuck, 2004) showed that the primary peak had a slightly lower sedimentation coefficient value compared to TPA6 (~ 0.4 S) (Figure 54). A few smaller peaks were seen, approximately at 1.5 S,

meaning that the polymer system was not completely homogenous. This observation was anticipated as it was noted both with TPA5 and TPA6.

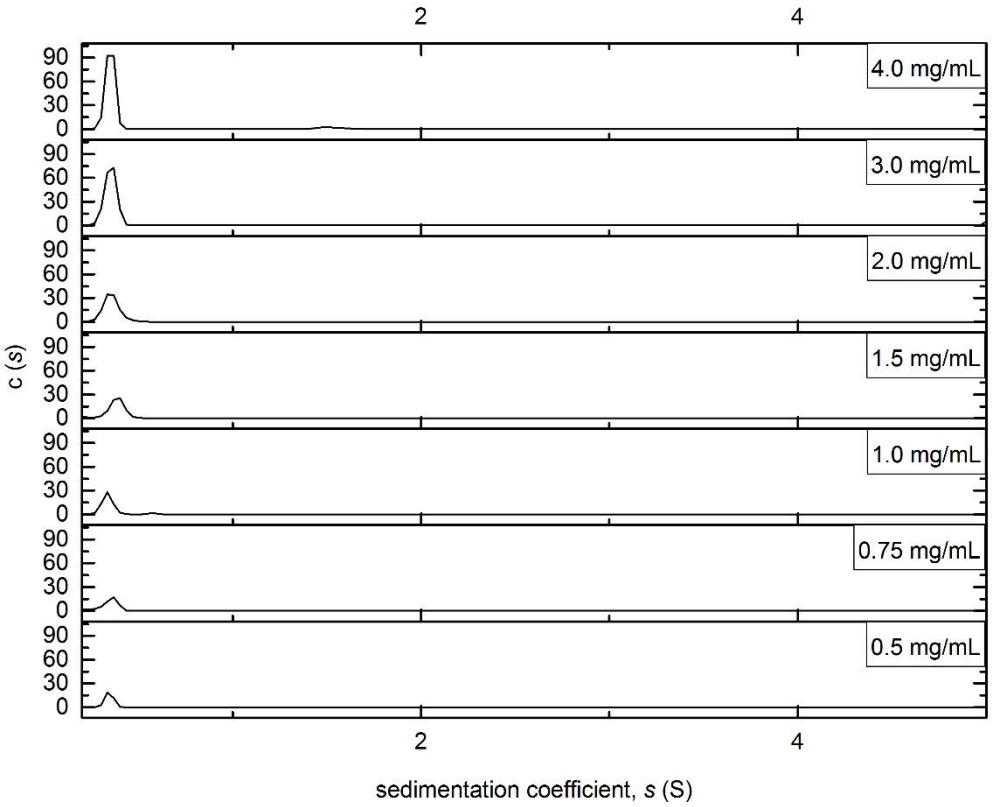

Figure 54. Sedimentation coefficient distributions *c(s)* vs sedimentation coefficient (S) for TPA7 in isopropanol. Rotor speed = 49,000 rpm.

The $s_{20,w}$ of the major peak observed in SEDFIT was calculated to be (0.423 ± 0.014) S (Figure 55).

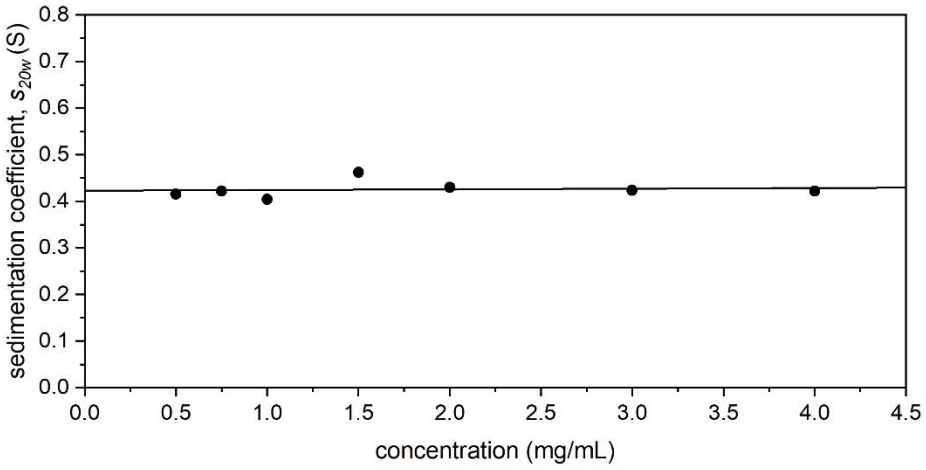

Figure 55. Sedimentation coefficient $s_{20,w}$ corrected to standard conditions (the density and viscosity of water at 20.0 °C) against sedimenting concentration for TPA7 in isopropanol. $s_{20,w}$ = (0.423 ± 0.014) S.

3.3.3.3 SE

Table 13 shows all the $M_{w,app}$ values obtained for TPA7 *via* the *M** function (Creeth and Harding, 1982) and the hinge point method (Schuck *et al.*, 2014). Figure 56 depicts the extrapolation of the absolute M_w value, using the *M** results. This was found to be (4.2 ± 0.2) kDa.

Table 13. $M_{w,app}$ values derived from the *M** function and the hinge point method, obtained from the SE of TPA7.

Concentration (mg/mL)	$M_{w,app}$ (*M**) (kDa)	$M_{w,app}$ (hinge point) (kDa)
0.5	4.4	3.8
0.75	4.0	3.9
1.0	4.2	3.8
1.5	4.7	4.3
2.0	4.7	4.2
3.0	4.6	4.1
4.0	4.6	4.1

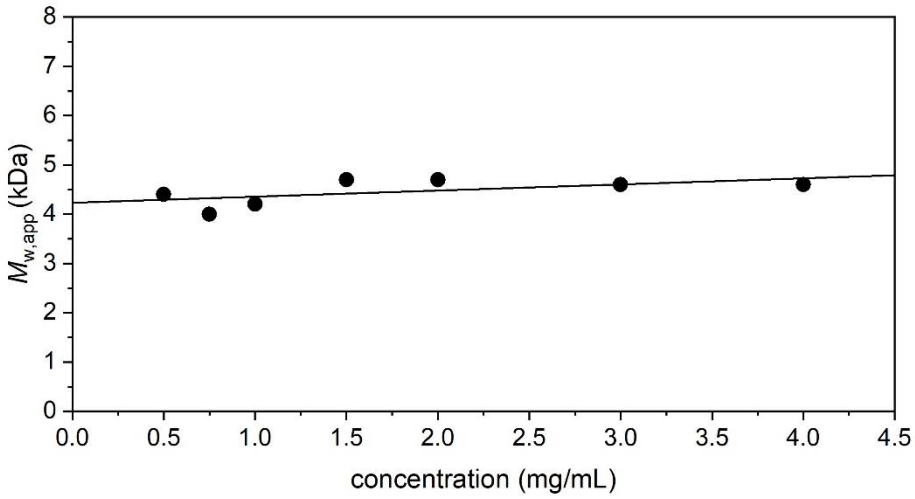

Figure 56. Dependence of apparent $M_{w,app}$ on concentration for TPA7 in isopropanol, with an extrapolation to obtain the thermodynamically ideal $M_{w,app}$. Analysed with SEDFIT-MSTAR using the M^* derived method to obtain the shown $M_{w,app}$ values. Rotor speed = 45,000 rpm. M_w = (4.2 ± 0.2) kDa.

From Table 13, one could see that there seemed to be relatively low non-ideality in the polymer system, as the $M_{w,app}$ did not appear to be affected by the concentration. This was not surprising for a polymer with such a low molecular weight. The concentration dependence appeared to be even lower than that observed with TPA5 and TPA6. Additionally, there did not appear to be any evidence of aggregation as was noted with TPA6.

This observation was reinforced by the ensuing MultiSig analysis (Figure 57), which was carried out on the 4.0 mg/mL concentration. The results revealed that TPA7 appeared to have a M_w distribution ranging from 1.9 to 17.5 kDa, with a major component peaking at 2.1 kDa. Another prominent peak was observed at 7.5 kDa, possibly alluding to the heterogeneity that was observed with the SV study. However, when these results were compared to the MultiSig analysis of TPA6 (Figure 51), it could clearly be seen that the TPA7 polymer system appeared to have a lower population of higher molecular weight particles.

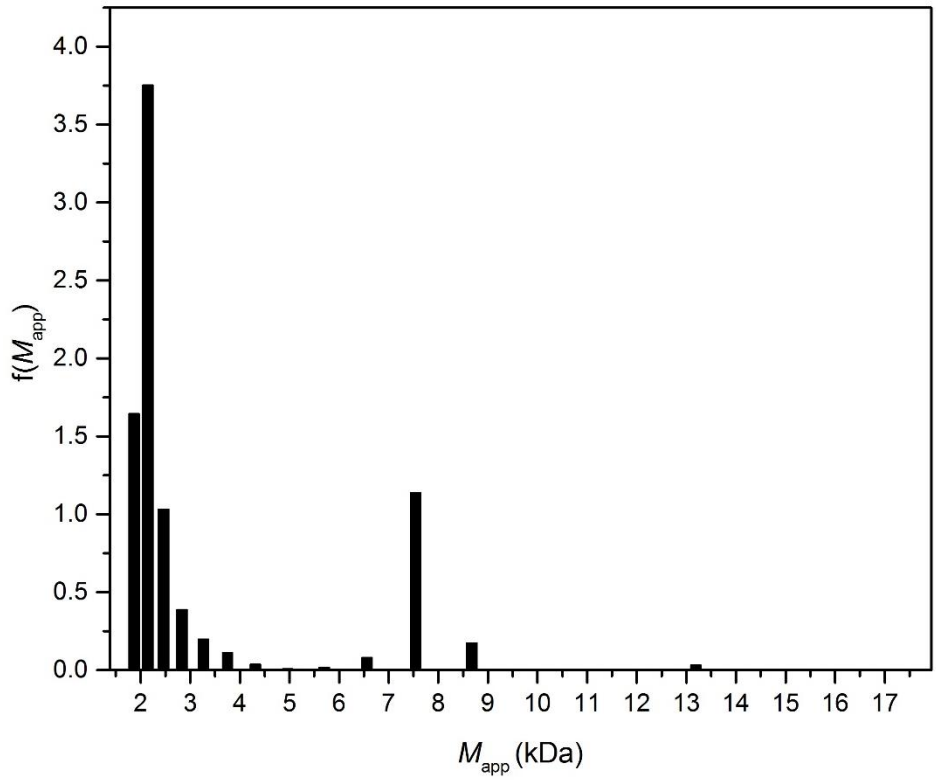

Figure 57. MultiSig analyses of the molar mass distribution f(M_{app}) vs M_{app} of TPA7 in isopropanol at a concentration of 4.0 mg/mL. Rotor speed = 45,000 rpm.

3.3.3.4 The intrinsic viscosity $[\eta]$

A 6.0 mg/mL concentration of TPA7 in isopropanol was used to take viscosity measurements with a rolling ball viscometer. The Solomon-Ciuta equation (Equation 10) (Solomon and Ciută, 1962) indicated that TPA7 had an $[\eta]$ value of (4.8 ± 0.2) mL/g, almost identical to that of TPA6.

3.3.3.5 Conformational analyses

As with the previous two polymers, the ν and *P* shape factors (Equations 12 and 13a) (Perrin, 1936; Simha, 1940; Saito, 1951) were used to predict the axial ratio of TPA7 with the programme ELLIPS1 (Harding, Horton and Cölfen, 1997).

Tables 14 and 15 show the results for the shape factors at different degrees of solvent association, with their corresponding axial ratios. Figures 58 and 59 show the prolate ellipsoid models estimated by ELLIPS1. As expected, TPA7 had a very similar shape to TPA5 and TPA6.

Table 14. The TPA7 calculated values for the shape parameter ν and the axial ratios (prolate ellipsoid model) determined by ELLIPS1

	Degree of solvent association $(v_s/\tilde{v})$		
	1.0	**1.2**	**1.4**
shape factor ν	5.7 ± 0.3	4.9 ± 0.3	4.2 ± 0.3
axial ratio (a/b)	4.9	4.2	3.6

Table 15. The TPA7 calculated values for the shape parameter *P* and the axial ratios (prolate ellipsoid model) determined by ELLIPS1

	Degree of solvent association $(v_s/\tilde{v})$		
	1.0	**1.2**	**1.4**
shape factor *P*	1.4 ± 0.6	1.3 ± 0.6	1.3 ± 0.6
axial ratio (a/b)	7.4	6.0	5.0

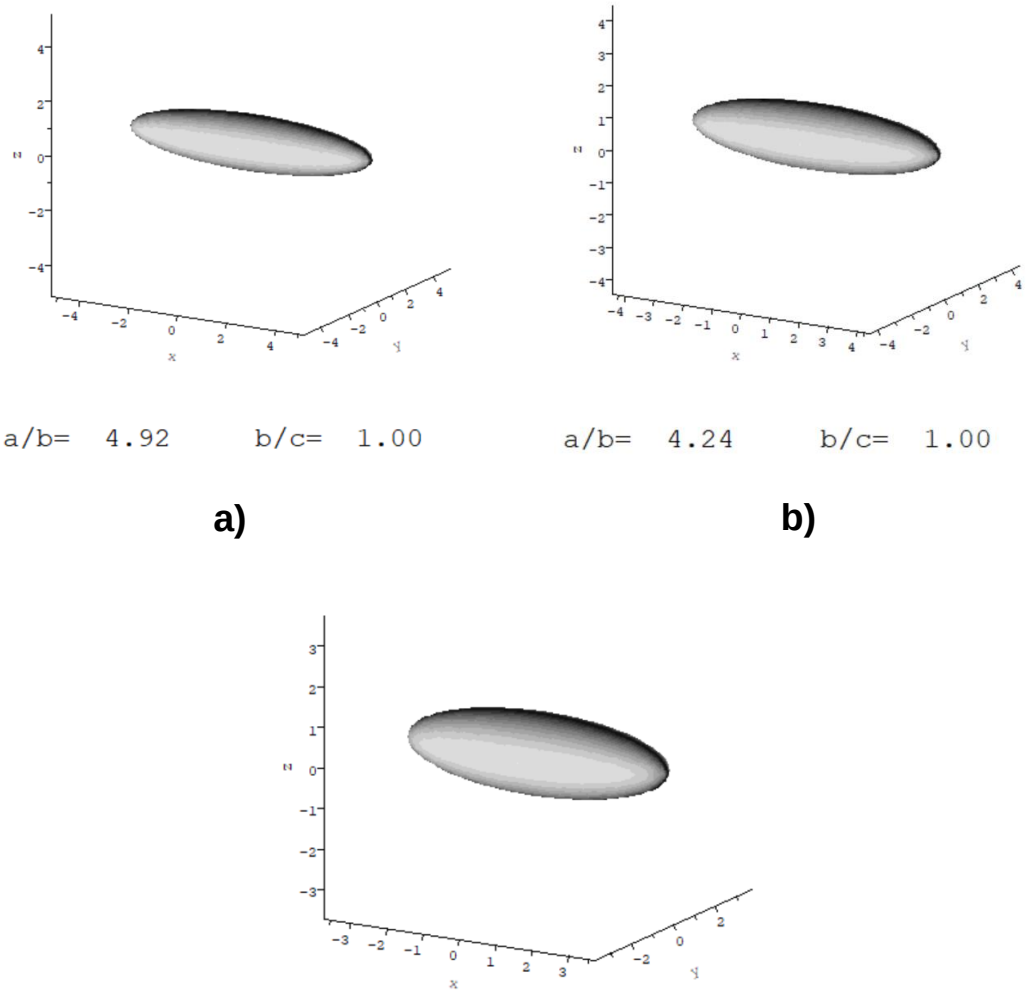

Figure 58. Ellipsoidal representations from the conformation analysis of TPA7 in isopropanol at different degrees of solvent association, using the programme ELLIPS1 with the shape parameter ν. a) $(v_s/\bar{v})$ = 1.0; b) $(v_s/\bar{v})$ = 1.2; c) $(v_s/\bar{v})$ = 1.4.

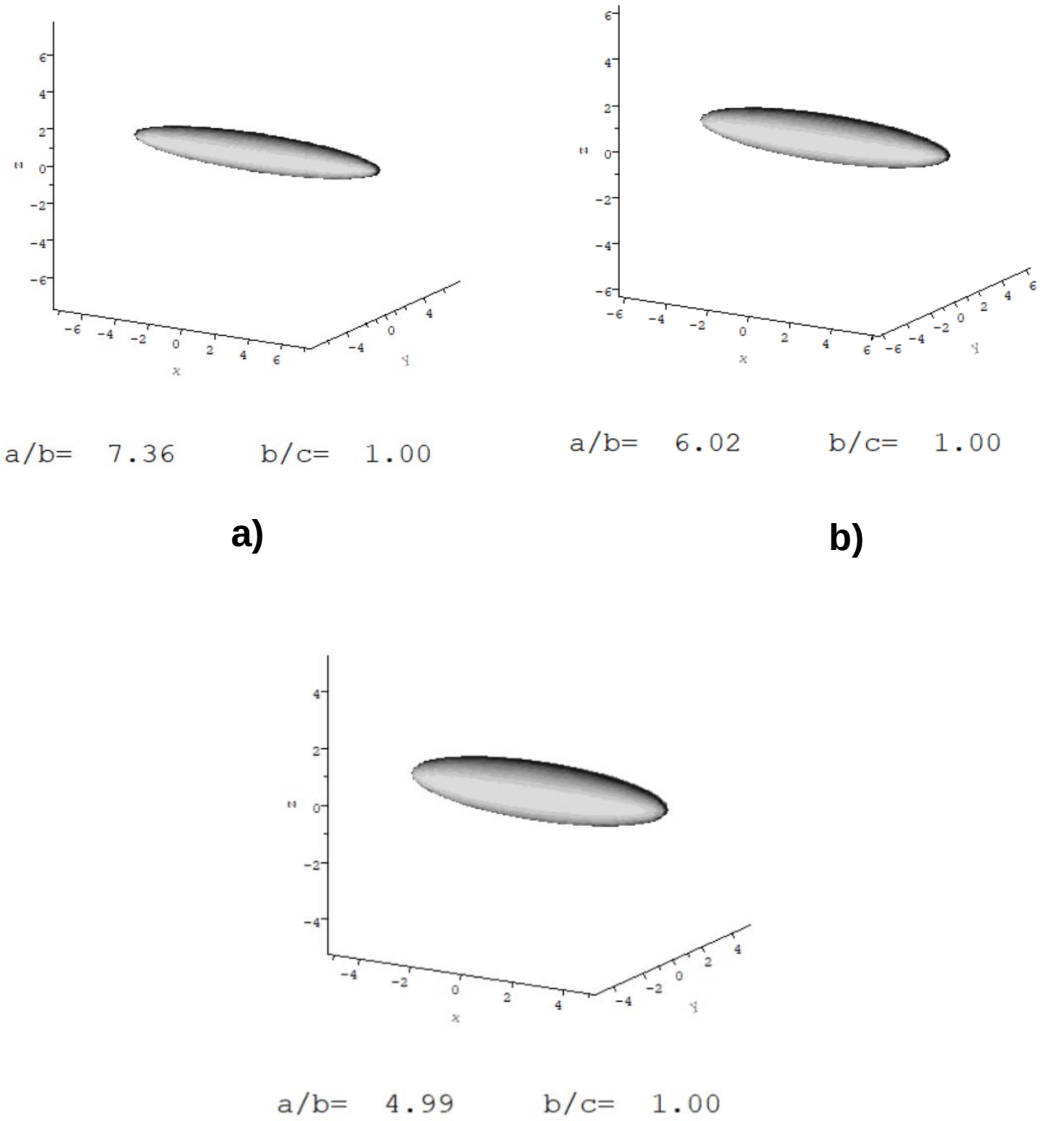

Figure 59. Ellipsoidal representations from the conformation analysis of TPA7 in isopropanol at different degrees of solvent association, using the programme ELLIPS1 with the shape parameter *P*. a) $(v_s/\bar{v})$ = 1.0; b) $(v_s/\bar{v})$ = 1.2; c) $(v_s/\bar{v})$ = 1.4.

3.3.4 Comparison between polymers TPA5, TPA6 and TPA7

The polymers all had a shared structure derived from α-pinene (with TPA7 having an additional oleic acid component), so it was anticipated that they would have similar properties. Their $\bar{v}$ results were very close in value, especially for TPA6 and TPA7, both of which were derived from *trans*-sobrerol acrylate. Likewise, their $[\eta]$ values were similar. Conformation analyses revealed that the three polymers had an elongated oval shape, as confirmed by all the shape factors that were used.

The SV experiments indicated that the polymers possessed some degree of heterogeneity. Their sedimentation coefficients were all small, due to their low molecular weight. This molecular weight was confirmed with SE. Due to their small size there were minimal non-ideality effects, as observed through the low concentration dependence on molecular weight. TPA6 appeared to diverge slightly from this trend with the higher polymer concentrations (2.0 – 4.0 mg/mL), possibly indicating a tendency to aggregate or associate.

The absolute molecular weights of the three polymers derived from SE were all comparable. Table 16 shows the M_w values obtained from both AUC and GPC (previously described in Chapter 2). The M_w of TPA7 was the most consistent, with there being only 0.2 kDa of difference between the AUC and GPC values. Next was TPA6, with a difference of 0.5 kDa. The largest discrepancy was with TPA5, as there was 0.9 kDa of difference. Both TPA5 and TPA7 had a larger M_w value when measured with AUC, whilst TPA6 had a smaller one. Nonetheless, the results obtained from AUC and GPC show consistency, as the discrepancies noted were not large. The values derived from AUC should be considered the more accurate ones, since the instrument does not make use of calibration standards like GPC.

Table 16. A comparison of the M_w results obtained from AUC and GPC (described in Chapter 2) for all the three polymers

Polymer	AUC M_w (kDa)	GPC M_w (kDa)
TPA5	4.3	3.4
TPA6	3.9	4.4
TPA7	4.2	4.0

3.3.5 Scale-up of TPA6 and TPA7

The next step after carrying out these characterisation studies was to decide on which polymers to focus on for scale-up. As mentioned previously, it was estimated that approximately 50 g of each polymer would be needed for pilot studies on wood.

Through the studies described in this chapter, all three polymers appeared to have promising characteristics which would make them good leads for further investigation in wood. It was however decided to only move forward with TPA6 and TPA7. This was primarily due to their better synthesis efficiency as time limitations had to be considered. Although theoretically TPA5 could possibly prove to be a better consolidant than TPA6 due to its extra hydroxyl group, its synthesis was considered too laborious and slow to be able to make enough polymer for wood testing.

As reported previously, the syntheses for both TPA6 and TPA7 had been carried out on a 4.0 g scale. This was successfully increased to an 8.0 g scale. It was decided not to increase it further since the monomer synthesis also had to be taken into consideration. The synthesis procedures for the monomers and polymers were described in detail in Chapter 2. Each polymerisation reaction that was carried out was checked with GPC to ascertain that it had the right molecular weight. It took approximately two months per polymer to make 50 g of material.

3.4 Conclusion

The three polymers that were synthesised, TPA5; TPA6 and TPA7, were extensively characterised and thus a thorough understanding of their physical properties was achieved.

AUC confirmed that all three polymers had a suitable M_w for wood consolidation. It also determined that the majority of the molecules in the polymer systems had a small M_w,which would ensure better penetration in wood. All three polymers appeared to have a linear shape, potentially similar to PEG, which could possibly also aid in their

penetration. A preliminary interaction study between TPA5 and soda lignin was carried out but there did not appear to be any significant interactions between the two materials.

Due to time limitations and practicality, it was decided to not scale-up TPA5 and instead focus on the other two polymers. These were successfully scaled up and 50 g of each was synthesised in preparation for archaeological wood testing.

With regards to future work, it would be useful to run further characterisation studies using higher polymer concentrations, in order to determine whether they behave differently. This would be especially relevant since concentrations of 5.0 mg/mL and upwards are usually used in wood testing. The possible aggregation or association behaviour that was noted for TPA6 could also be explored further.

Additionally, more interactions studies should be carried out, either with wood components such as cellulose or lignin, or with other materials that could be used for wood treatments. This is important as it is likely that the analysed polymers may be combined with other materials in real-life practice. Examples include lignin-derived materials (McHale *et al.*, 2016; Łucejko *et al.*, 2021) and aminocelluloses (Wakefield, Hampe, *et al.*, 2020). Others include $Ca(OH)_2$ nanoparticles (Andriulo *et al.*, 2016) which are currently being investigated by Saving Oseberg as a deacidifying treatment and are being tested in conjunction with other non-aqueous consolidants.

3.5 Experimental

3.5.1 Materials

All reagents and solvents were purchased from a chemical supplier (Acros Organics, Alfa Aesar, Merck, Sigma Aldrich and Fischer Scientific UK) and used without further purification. Water was deionised before use. Soda lignin was obtained from Dr Richard Gosselink and Dr Ted Slaghek (Wageningen University, Netherlands).

3.5.2 General methods and instrumentation

3.5.2.1 Density measurements – calculation of the partial specific volume $\bar{v}$

An Anton Paar DMA 5000 V5.003 was used at 20.0 °C. A 9.0 mg/mL stock solution of each polymer in isopropanol was prepared and then diluted to 8.0, 7.0, 6.0, 5.0 and 4.0 mg/mL. These concentrations were thereafter used for the density measurements. The results were evaluated following the procedure of Kratky *et al*. (Kratky, Leopold and Stabinger, 1973) and with the use of Equation 4.

$$\bar{v} = \frac{1}{\rho_o}\left(1 - \frac{\partial \rho}{\partial c}\right) \quad \textbf{(4)}$$

3.5.2.2 AUC studies

A Beckman Optima XL-I analytical ultracentrifuge with Rayleigh interference optics was used at 20.0 °C. 12 mm optical path length double sector cells with titanium centrepieces were employed. TPA5, TPA6 and TPA7 were all studied using identical procedures and conditions.

3.5.3.1 SV methodology

Loading concentrations of 0.5 to 4.0 mg/mL of the polymers in isopropanol were used. 405 µL of each concentration were injected in the sample solution channel of each AUC cell. Isopropanol was used as the reference solution. A rotational speed of 49,000 rpm was used and the samples centrifuged overnight. The weight average sedimentation coefficient (s) and the distributions of sedimentation coefficient *c(s)* vs *s* were obtained by analysis with the SEDFIT procedure (Schuck, 2000; Dam and Schuck, 2004). This analysis was carried out to determine the size distribution and heterogeneity of the polymer systems.

3.5.3.2 SE methodology

100 µL of the previous loading concentrations (0.5 to 4.0 mg/mL) of the polymers in isopropanol were added to each of the AUC cells. Isopropanol was used as the reference solution. The experiment was carried out at a rotational speed of 45,000 rpm over 2 days. The results were analysed with SEDFIT-MSTAR (Schuck *et al.*, 2014) in order to obtain the $M_{w,app}$, making use of the M^* extrapolation (Creeth and Harding, 1982) and the hinge point method. The data obtained from the highest concentration (4.0 mg/mL) of all polymers was additionally analysed with the MultiSig algorithm (Gillis *et al.*, 2013) to evaluate the molecular weight distribution.

3.5.3.3 Interaction study with TPA5 and soda lignin

A 2.0 mg/ml solution of soda lignin in isopropanol was prepared and placed on a roller mixer overnight. Any debris was afterwards removed by centrifugation (6000 g/15 minutes/ r. t.) (Alzahrani *et al.*, 2016b). This mixture was then used to prepare the different solutions that are described in section 3.3.1.6. 405 µL of each solution were injected in the sample solution channel of each AUC cell. Two cells were filled with pure solutions of TPA5 and lignin in isopropanol to be used as controls. Isopropanol was used as the reference solution. A rotational speed of 49,000 rpm was used and the samples centrifuged overnight. The weight average sedimentation coefficient (s) and the distributions of sedimentation coefficient *c(s)* vs *s* were obtained by analysis with the SEDFIT procedure (Dam and Schuck, 2004).

3.5.2.3 Viscosity measurements – calculation of the intrinsic viscosity $[\eta]$

An Anton-Paar AMVn (Graz, Austria) rolling ball viscometer was used at temperatures of 8.0 – 10.0 °C. Its closed capillary system was more suitable for working with volatile solvent systems compared to conventional Ostwald viscometers. The low temperatures were chosen so as to prevent the solvent (isopropanol) from evaporating due to its high volatility.

The viscosity measurement was carried out using solutions of 6.0 mg/mL concentration of each polymer in isopropanol. The $[\eta]$ values were then calculated with the Solomon-Ciuta equation (Equation 10) (Solomon and Ciută, 1962).

$$[\eta] = \frac{1}{c}\left(2\left(\eta_{sp}\right) - 2ln(\eta_r)\right)^{\frac{1}{2}} \quad \textbf{(10)}$$

3.5.4 Conformational analyses

The ELLIPS1 (Harding, Horton and Cölfen, 1997) algorithm was used to carry out analyses with the viscosity increment (ν) (Equation 12) (Simha, 1940; Saito, 1951), Perrin (*P*) (Equation 13a) (Perrin, 1936) and Scheraga-Mandelkern (*β*) (Equation 14) (Scheraga and Mandelkern, 1953) shape factors.

$$\nu = [\eta]M/(N_A \mathrm{V}) \quad \textbf{(12)}$$

$$P = (f/f_o)\,(\bar{v}/v_s)^{\frac{1}{3}} \quad \textbf{(13a)}$$

$$\beta = N_A s[\eta]^{\frac{1}{3}}\eta_o \Big/ \left[M^{\frac{2}{3}}(1-\bar{v}\rho_o)100^{\frac{1}{3}}\right] \quad \textbf{(14)}$$

Chapter 4. Polymer Testing on Archaeological Wood

4.1 Introduction

This chapter will detail all the experiments that were carried out on archaeological wood with TPA6 and TPA7. These tests (except the solvent retention studies) were carried out at the Museum of Cultural History in Oslo, Norway. A general overview on wood's composition and components will first be given. The research described in this chapter has been used to prepare a paper entitled 'Evaluation of two terpene-derived polymers as consolidants for archaeological wood' which has been accepted for publishing in a peer-reviewed journal (see Appendix for more details).

4.1.1 Wood structure and composition

A thorough understanding of the basic properties of wood is needed before exploring approaches of how to conserve it. The natural purpose of wood is to provide strength and transport nutrients across the tree (Cabane *et al.*, 2016). It has some unique characteristics which make it very useful as a construction material, namely its global abundance; processability and high mechanical strength as compared to its light weight (Ermeydan *et al.*, 2014; Keplinger *et al.*, 2015). Despite this, its dimensional instability is a significant shortcoming. Wood cells have a tendency to uptake and release moisture with changes in relative humidity due to their hydrophilic nature. The alterations in the moisture content of the cell wall make it subject to repeated dimensional changes, increasing the probability of cracking and fungal attack (Ermeydan *et al.*, 2014; Keplinger *et al.*, 2015).

As defined by Rowell, wood is a “three-dimensional polymeric composite comprised primarily of cellulose, hemicellulose, and lignin” (Rowell, 1983) and is made up of the elements carbon, hydrogen and oxygen, with minor quantities of various metal ions (Pettersen, 1984). The vast majority of its cells are carbohydrates (65 – 75%) combined with lignin (18 – 35%) (Rowell, Pettersen and Tshabalala, 2005). It also contains extraneous materials which do not make part of the cell wall, such as inorganic materials (ash) and a number of organic substances like fats, proteins and sugars (Pettersen, 1984). Many of these organic materials contribute to the metabolism and defence mechanisms of trees (Pettersen, 1984). Wood is generally divided into softwoods and hardwoods, with the former having a higher content of lignin (26 – 34%) as opposed to the latter (23 – 30%) (Rowell, Pettersen and Tshabalala, 2005). The cellulose and the hemicellulose components are collectively known as holocellulose.

Cellulose is made up of *D*-glucopyranose units linked together with *β*-(1,4)-glycosidic bonds (Figure 60) (Rowell, Pettersen and Tshabalala, 2005). These units form long chains which make up the cellulose polymer. Each unit has three hydroxyl groups which characterise the behaviour, structure and properties of cellulose, such as its tendency to form hydrogen bonds both intra- and intermolecularly (Unger, Schniewind and Unger, 2001). Most cellulose derived from wood is densely packed and is therefore crystalline. The rest of the cellulose is amorphous with lower packing density (Rowell, Pettersen and Tshabalala, 2005). These molecules then come together to form elementary fibrils, which then aggregate to form microfibrils (Unger, Schniewind and Unger, 2001).

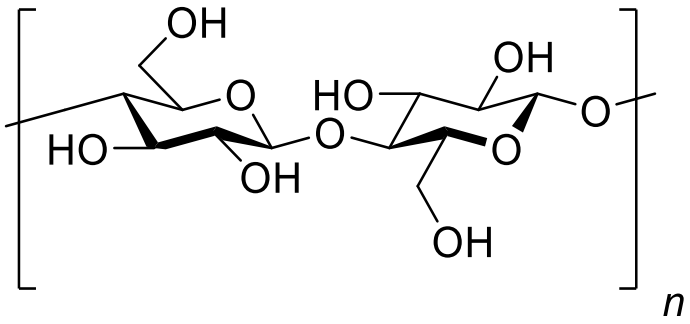

Figure 60. The chemical structure of cellulose

Hemicellulose is composed of various polysaccharides, with their backbones either being composed of identical or different sugar units (Unger, Schniewind and Unger, 2001). These chains make up fibrillar subunits which in turn serve as the main constituents of hemicellulose microfibrils (Unger, Schniewind and Unger, 2001). Its structural function is not clear but it may contribute to the fibre stiffness in the cell wall, as well as acting as a coupling agent between cellulose and lignin (Neagu *et al.*, 2006).

Unlike holocellulose, lignin is an aromatic compound derived from three precursors: *p*-coumaryl alcohol, coniferyl alcohol and sinapyl alcohol (Figure 61). It forms a three-dimensional network with the hemicellulose components in the cell wall (Unger, Schniewind and Unger, 2001), thus imparting rigidity and preventing buckling following longitudinal stress (Neagu *et al.*, 2006). The type of lignins varies between softwood and hardwoods. Those found in softwoods are derived from coniferyl alcohol and are called guaiacyl. In hardwoods, the lignins are copolymers composed of coniferyl and sinapyl alcohols, and are thus termed syringyl-guaiacyl (Rowell, Pettersen and Tshabalala, 2005).

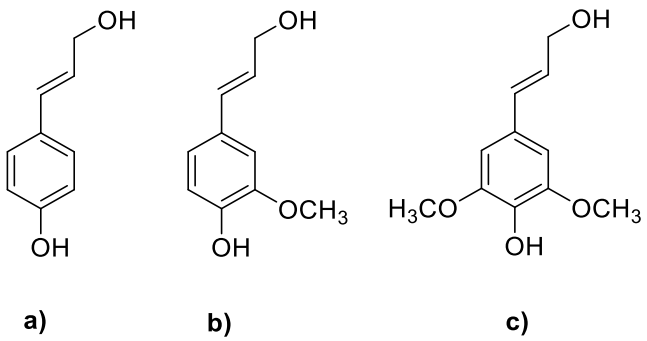

Figure 61. The three precursors of lignin: a) *p*-coumaryl alcohol; b) coniferyl alcohol; c) sinapyl alcohol.

The main structural components found in wood are packed together in a non-uniform but highly arranged manner to form the cell wall, which is a composite of parallel-oriented cellulose nanofibrils embedded in an amorphous network of hemicellulose and lignin (Rowell, Pettersen and Tshabalala, 2005). This structure arises from the

fibrillar units which are formed by cellulose and hemicellulose through hydrogen bonding. The hemicellulose fibrillar units can then associate with the cellulose microfibrils, forming an encompassing layer. Additionally, these hemicellulose units bond to the lignin, which is itself surrounding the polysaccharide components (Figure 62) (Unger, Schniewind and Unger, 2001).

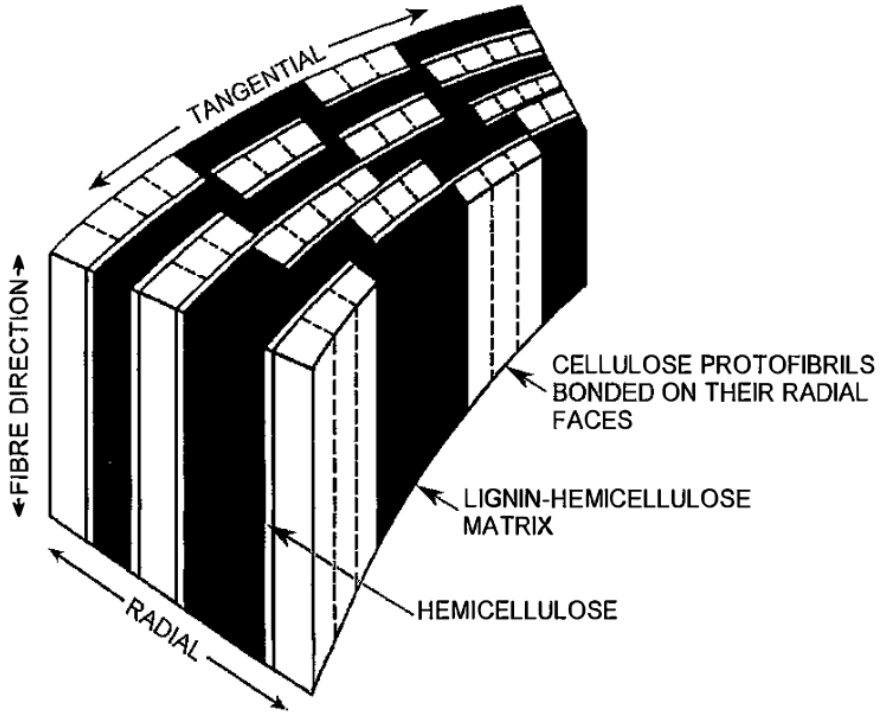

Figure 62. A structural arrangement model of the cell wall, showing the placement of the three main polymer components: cellulose, hemicellulose and lignin (Kerr and Goring, 1975).

Wood has three main orientations, depending on how the cells are aligned: transverse, radial and tangential (Figures 63 and 64). The transverse orientation is the cross-section of the tree, while the radial and tangential directions are found longitudinally (along the tree axis) (Nairn, 2007). This highly arranged nature of the cells in wood gives rise to its anisotropy. This means that the behaviour of wood upon the application of stress depends on the orientation in which the stress has been directed.

This is important to remember when measuring physical properties such as dimensional change and degree of hardness, as these will vary depending on which orientation is used in the measurements.

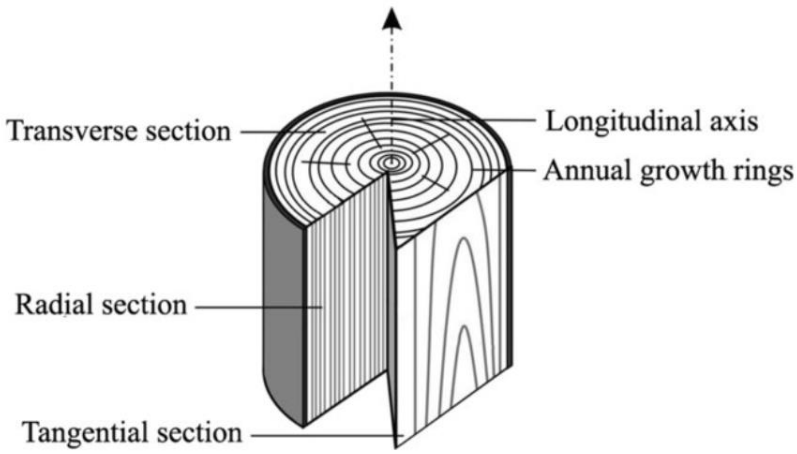

Figure 63. The three orientations of wood (from de Geus *et al.*, 2020)

Transverse face | **Radial longitudinal face** | **Tangential longitudinal face**

Figure 64. The three orientations as seen on a wood cube

4.1.2 The conservation of waterlogged archaeological wood

Wooden archaeological findings are relatively rare as a result of their biodegradability (Creangă, 2009; Nilsson and Rowell, 2012; McHale *et al.*, 2017). The degradation state of the archaeological wood depends on its age, the species and most importantly, its burial environment (Kaye, 1995; McHale *et al.*, 2017).

Some of the most common locations to make archaeological wood discoveries are wet environments like bogs or the seabed (Florian, 1989; McHale *et al.*, 2017). Wood that is not in contact with oxygen has a very slow degradation rate and thus can survive for thousands of years (Nilsson and Rowell, 2012; Broda *et al.*, 2015). This explains why the Oseberg collection was able to last as it was buried in blue clay which provided a highly anaerobic environment (Nilsson and Rowell, 2012; Harding, 2018). Such an environment is still hazardous, as there is a risk of attack by anaerobic bacteria causing wood erosion and loss of structure (Broda *et al.*, 2015).

The most stable biopolymer in wood is lignin while the least is hemicellulose, with pectin and cellulose having mid-stability (Florian, 1989). Accordingly, the first point of microbial attack is usually the hemicellulose component of the cell wall, which adversely affects its mechanical strength (Nilsson and Rowell, 2012; McHale *et al.*, 2017). This can be seen from the chemical analysis studies carried out on the Oseberg artefacts which show a high level of holocellulose degradation (Braovac *et al.*, 2016; McQueen *et al.*, 2017). The cell wall matrix becomes increasingly weaker as the hemicellulose is degraded, finally leading to collapse. There are different mechanisms that can lead to degradation, namely oxidation; reduction; hydrolysis; dehydration and free radical reactions. These processes convert wood back to its basic building blocks, that is, water and carbon dioxide (Nilsson and Rowell, 2012).

A particular concern for waterlogged archaeological wood is the dehydration that takes place when it is removed from its wet environment, causing the wood to become much more fragile (Creangă, 2009). Upon excavation, the drying process can result in the cracking of the wood surface as a direct result of cell wall shrinkage (Bugani *et al.*, 2009; Broda *et al.*, 2015; McHale *et al.*, 2017). This may lead to the collapse of the cell wall as a consequence of capillary drying tension which occurs above the fibre saturation point (Florian, 1989; Creangă, 2009; McHale *et al.*, 2017). It is therefore of paramount importance to keep the wood damp when initially excavated.

Quoting Creangă, once removed from their wet environment, objects can “lose 90% of their weight and 80% of their volume” (Creangă, 2009) after just a few hours if no precautions are taken. Consequently, consolidation of waterlogged archaeological wood is essential because of this tendency to crack and shrink (Kaye, 1995; Creangă, 2009; McHale *et al.*, 2017). Due to this instability, in most cases the archaeological wood must be treated with a consolidant before it is dried, in order to limit fragmentation and supply mechanical strength to the cell wall (McHale *et al.*, 2017).

The alum-treated Oseberg wood is radically different from both normal wood and other cases of archaeological wood (Zoia, Salanti and Orlandi, 2015; Braovac *et al.*, 2016; McQueen *et al.*, 2017; Łucejko *et al.*, 2018). This was illustrated by utilising the pyrolytic H/L index, which represents the ratio of holocellulose over lignin relative abundance. In healthy wood, the H/L index is usually between 1.7 to 3.7 (Łucejko *et al.*, 2018). The index value for Oseberg wood not treated with alum ranges from 0.2 to 0.5, as a direct consequence of the polysaccharide content being lost during burial and the natural process of aging (Braovac *et al.*, 2016). By contrast, alum-treated Oseberg wood can have a H/L index lower than 0.1 due to an almost complete loss of the holocellulose (Braovac *et al.*, 2016). It should be noted however the both the holocellulose and the lignin in the alum-treated wood have suffered degradation, so the H/L index measurement cannot be considered to be completely reliable.

As mentioned in previous chapters, retreating the Oseberg artefacts is not a simple matter due to the large variation of the wood’s preservation state. Some of the most highly degraded artefacts cannot withstand conventional aqueous treatments like PEG, as it may result in the dissolution of the alum inside the wood, leading to total collapse. Additionally, some of the artefacts contain non-wood components which were added in past restorations such as metal rods, glue and plaster (Braovac *et al.*, 2018). For these objects, there is increased risk of damage if they are immersed in water. Non-aqueous treatment options, such as TPA6 and TPA7, may therefore present a valuable addition to the Oseberg artefact treatment toolkit.

4.2 Aims and objectives

The aim for the work described in this chapter was to determine the extent to which these polymers penetrate archaeological wood after immersion and to investigate if they provided any consolidative effect. This was carried out by:

1. First investigating the solvent retention of wood powder/polymer films
2. Getting a general picture of the extent of degradation of the archaeological wood which was to be used for the main investigation
3. Treating said archaeological wood specimens with solutions of TPA6 and TPA7. The polymer penetration was estimated by measuring weight and dimensional changes, as well as colour change. The degree of polymer distribution in the wood was investigated with attenuated total reflection-Fourier transform infrared (ATR-FTIR) spectroscopy and SEM. The effect of the polymers on the wood was observed by carrying out pH measurements and hardness tests with a fruit penetrometer.

4.3 Materials and methods

4.3.1 Solvent retention studies with wood powder

The issue of solvent retention was first investigated. It is known that any solvent which is retained by the wood after treatment may potentially decrease the T_g of a consolidant, resulting in it being less effective (Schniewind, 1990). These preliminary studies also served to give an indication of the polymer concentration to be used in the subsequent wood penetration studies. The protocol which was followed was based on previous methodologies described in an internal report of the Saving Oseberg group (Zisi and de Lamotte, 2020).

Three different concentrations of TPA6 and TPA7 in isopropanol were prepared: 15% w/w, 10% w/w and 5% w/w (Figure 65). Using these stock solutions, mixtures made up of 7:1 polymer to ground modern wood powder were assembled. The wood powder was provided by Dr Susan Braovac (Museum of Cultural History, University of Oslo) and was made up of modern birch put through a two-step grinding process; first using a woodchipper and then followed with an analytical grinding mill. Approximately 0.5 mL of each mixture was poured onto pre-prepared strips cut out of a commercially available antistick baking sheet. This material was deemed to be light enough to allow the observation of differences in weight during the experiment. The wood films were put in boxes, partially covered and left in a fume-hood to dry at room temperature. Their weight was monitored periodically for 15 days. The solvent retention value was calculated based on the solid weight expected on the baking sheet strip after total evaporation of isopropanol, taking into consideration the concentration of the original polymer solution, as previously described by Zisi and de Lamotte (2020).

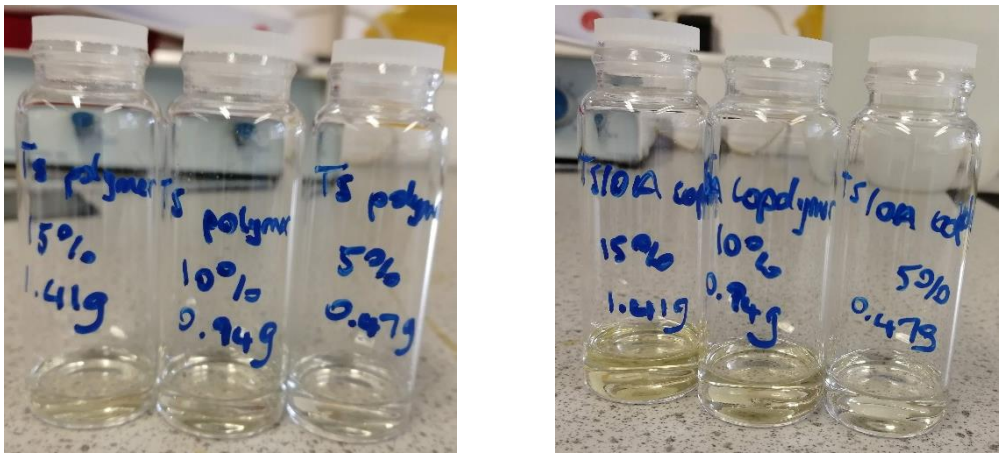

Figure 65. The polymer solutions prepared for the solvent retention studies (TPA6: left; TPA7: right). The solutions became more yellow with increasing polymer concentration.

4.3.2 Experiments with archaeological wood

4.3.2.1 Archaeological wood specimens

Discarded archaeological waterlogged wood was used for the wood penetration immersion experiments. The wood was initially in the form of a branch and this was sawn into six slices, with each slice then being cut into 2 x 2 x 2 cm^3 cubes (Figure 66). The cubes were afterwards either oven-dried or freeze-dried, depending on their assigned groups. The freeze-dried cubes were acclimatised to 20 °C and 50% RH. A total of 38 cubes of archaeological wood were used for these experiments: 20 for immersion tests with the polymer solutions and the remaining 18 for the various control groups. In addition, the leftover pieces of wood that remained after the cutting of the cubes were used for density and maximum moisture content measurements.

4.3.2.1.1 Naming system

The wood specimens were named in a way so that one could identify which slice they were cut from, and whether they were a surface or a core sample. Generally, the ID for each specimen was comprised of three characters: the first indicated their slice number (1 – 6), the second denoted whether they were cut from the surface or core (S = surface; C = core) and the last was a nominal specimen number. For each slice, eight cubes originated from the surface and two cubes from the core (Figure 66, bottom).

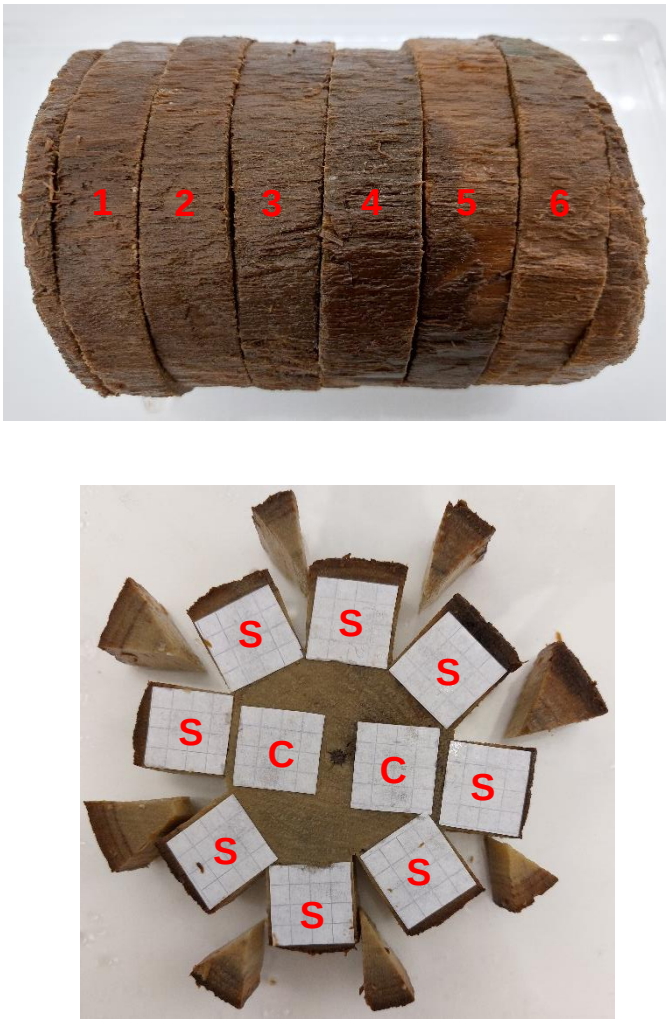

Figure 66. The original wood log which was used to cut the slices, numbered 1 to 6 (top) and the process of sawing off the specimens from one of said slices (bottom). The graph paper shows squares which are 2 x 2 cm^2. Each specimen is labelled S or C, indicating if it was cut from the surface (S) or the core (C) of each slice.

4.3.2.1.2 Wood identification

Wood identification was carried out using light microscopy. Thin slices were taken from the waterlogged wood from the main orientations: transverse, radial and tangential. Anatomical features were noted and compared with reference woods.

4.3.2.2 Density and maximum moisture content measurements

For density and maximum moisture content (MMC) measurements, 6 wedges from each of the six wood slices were used: 4 sawn from the surface from each slice, and 2 from the core (refer to Figure 66, bottom). This was done to determine whether the wood slices were degraded to different degrees and to observe whether there was any difference between the surface and the core of the wood. The density was determined by dividing the oven-dried weight by waterlogged volume. The waterlogged volume was determined from the weight of water displaced by the waterlogged samples. The MMC percentage was also calculated at the same time and is expressed as the weight of water contained in the sample relative to the oven-dried weight.

4.3.2.3 Experimental set-up

The wood cubes were divided into 4 control groups and two treatment groups. The conditions of the control and treatment groups are summarised in Tables 17 and 18. The cubes in treatment groups 1 and 2 were immersed in polymer solutions of TPA6 and TPA7 respectively.

All wood specimens (except those in control group 1) were freeze-dried from a waterlogged state. Those in control group 1 were instead oven-dried. After freeze-drying for six days, the specimens were stored in a desiccator in order to condition them to 20 °C and 50% RH before treatment.

After conditioning, the wood specimens in control group 3 were immersed in isopropanol after freeze-drying (Figure 69). The wood specimens in treatment groups 1 and 2 were immersed in solutions of TPA6 and TPA7 respectively. 50 g of each polymer was available for these experiments (Figure 67). The polymer solutions were prepared by dissolving TPA6 and TPA7 in isopropanol, keeping a 15% w/w concentration (Figure 68). Both polymers appeared to dissolve completely, therefore full dissolution was assumed. The specimens were left immersed for two weeks (Figure 69), based on previous reports of wood testing with non-aqueous treatments (Łucejko *et al.*, 2021). After two weeks, the specimens were partially covered and left

in the fume-hood for seven days to slowly dry (Figure 70). They were afterwards conditioned to 20 °C and 50% RH.

Table 17. The conditions of the various wood control groups used in the study

Control groups	Sample ID	Oven-drying	Freeze-drying	Reference pin insertion	Treatment with isopropanol
1	3.C.1.1 5.S.2.1 6.S.3.1 4.S.4.1	✓	×	Before oven-drying	×
2	1.S.6 2.S.4 4.C.1 5.S.5 6.S.5	×	✓	After freeze-drying	×
3	2.S.7 3.S.5 4.C.2 5.S.3 6.S.6	×	✓	After freeze-drying	✓
4	3.C.1.4 5.S.2.4 6.S.3.4 4.S.4.4	×	✓	Before freeze-drying	×

Table 18. The sample IDs of the wood specimens used in both wood treatment groups. The polymers used to treat the wood were both dissolved in isopropanol, using a 15% w/w concentration.

Treatment group 1 – TPA6	Treatment group 2 – TPA7
4.S.3	4.S.6
1.S.4	1.C.2
2.S.1	2.S.2
2.C.2	2.S.3
3.S.1	3.S.2
3.S.4	3.S.7
4.S.2	4.S.5
4.S.4	4.S.1
5.S.1	5.S.2
6.S.1	6.S.4

Figure 67. Undissolved polymers TPA6 (right) and TPA7 (left)

Figure 68. The polymer solutions made up with isopropanol

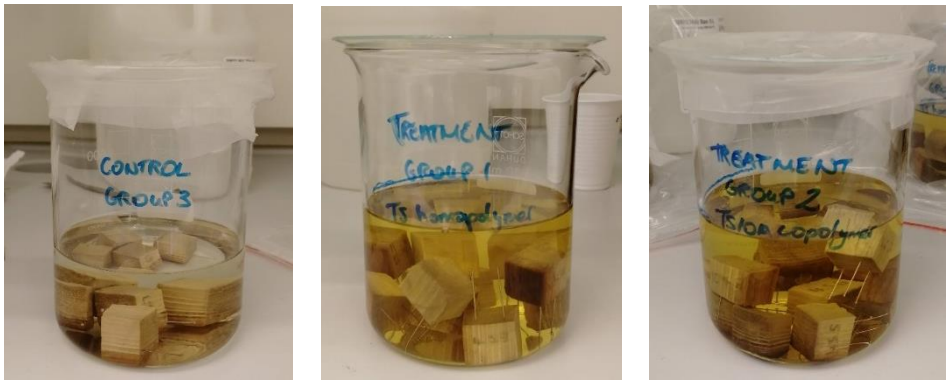

Figure 69. The immersion set-up for control group 3 (isopropanol; left), treatment group 1 (TPA6; middle) and treatment group 2 (TPA7; right).

Figure 70. The treated cubes drying in the fume-hood after two weeks of immersion

4.3.2.4 Change in weight and dimensions

Weight was measured using a four decimal balance. The weight of the treated cubes was reported before (after freeze-drying and conditioning to 20 °C and 50% RH) and after treatment (after drying and conditioning to 20 °C and 50% RH – refer to Figure 71 for conditioning set-up).

Dimensions were measured with electronic callipers, using reference pins inserted into the cross-section of the cubes (Figure 72). Both the radial and the tangential directions were measured. The point at which the pins were inserted differed according to the sample group (Table 19). Measurements were taken after freeze-drying and acclimatisation to 20 °C and 50% RH and after the relevant treatment steps. With regards to control groups 1 (oven-dried) and 4 (pins inserted before freeze-drying), the weight and dimensions were measured first in the wet state and then after drying.

% weight change and % linear dimensional change were calculated for the treated groups using Equations 15 and 16:

$$\%\ \text{weight change} = \frac{(\text{weight after} - \text{weight before})}{\text{weight before}} \times 100\% \quad \textbf{(15)}$$

$$\%\ \text{linear dimensional change} = \frac{(\text{dimension after} - \text{dimension before})}{\text{dimension before}} \times 100\% \quad \textbf{(16)}$$

Table 19. Indication of the time of insertion of the reference pins according to the sample group

Sample group	Pin insertion
Control group 1	Before oven-drying
Control group 2	After freeze-drying
Control group 3	After freeze-drying
Control group 4	Before freeze-drying
Treatment group 1	After freeze-drying
Treatment group 2	After freeze-drying

Figure 71. A photo depicting the conditioning set-up in a desiccator.

Figure 72. A photo depicting the method of measuring dimensional change with reference pins and electronic callipers.

4.3.2.5 Colour change

Colour measurements were taken for both treatment groups, as well as control groups 2 (freeze-dried only) and 3 (isopropanol-treated). This was carried out with a Konica Minolta CM-700d handheld spectrophotometer, making use of the CIELAB (L*a*b*) colour space (Figure 73). The change in colour caused by TPA6 and TPA7 was

calculated from the difference of the measurements between the treatment groups and control group 3. Additionally, the colour change caused by isopropanol was also estimated, using the measurements of control group 3 and control group 2. The absolute change, ΔE*, was finally calculated for all groups from the coordinate measurements using Equation 17:

$$\Delta E^* = (\Delta L^{*2} + \Delta a^{*2} + \Delta b^{*2})^{\frac{1}{2}} \quad \textbf{(17)}$$

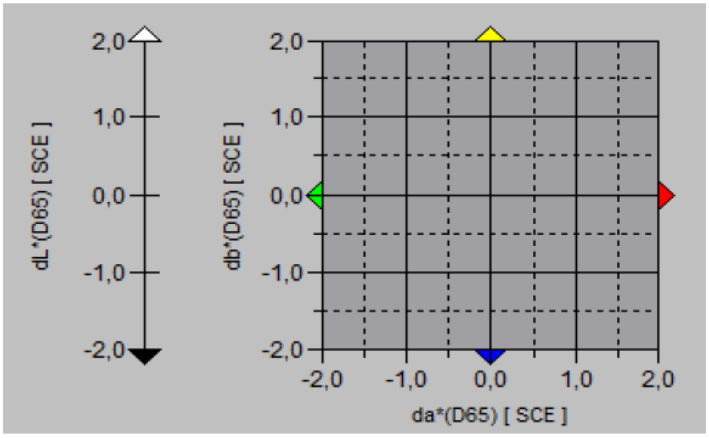

Figure 73. The CIELAB (L*a*b*) colour space.

4.3.2.6 pH measurements

The surface pH of three specimens from control group 2 (freeze-dried only), control group 3 (isopropanol-treated), treatment group 1 (TPA6) and treatment group 2 (TPA7) were measured. Additionally, the pH of the core of the specimens in the treatment groups was also tested. pH strips from Sigma (pH range 0 – 6) and VWR (pH range 0 – 14) were used.

4.3.2.7 ATR-FTIR spectroscopy

Fourier transform infrared spectroscopy was carried out using an attenuated total reflection mode on a Thermo Fischer FTIR spectrometer (Nicolet iS50), with a range of 4000 – 400 cm^{-1}. The specimens used included those from control groups 2 and 3, the treatment groups, as well as the pure polymers. Sound pine was also measured. A resolution of 4 cm^{-1} was used and each spectrum was derived from 32 scans. Three spectra from each sampling site were taken and averaged. The wood specimens were analysed at four points: the surface (Figure 74), the core and between the surface and core both along and across the grain (Figure 75). Thermo Scientific OMNIC FTIR software was used to analyse the data. Spectra were baseline corrected and normalised to 1508 cm^{-1} (wood spectra) or 1725 cm^{-1} (pure polymer spectra).

Figure 74. A treated specimen that was analysed with ATR-FTIR (top left). The specimen was split in half (top right). Samples were shaved off the specimen surface for analysis (bottom).

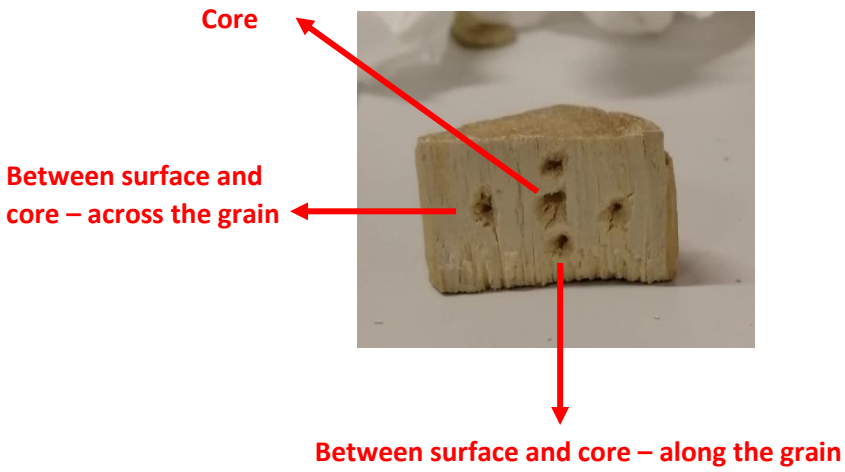

Figure 75. A photo showing a cross-section of a split specimen and the samples that were taken from it.

4.3.2.8 SEM analyses

A FEI Quanta 450 scanning electron microscope with a voltage of 8 kV on low vacuum was used. Spot size was 4.5, chamber pressure was 50 – 80 Pa with working distances of 7.0 – 10.0 mm.

4.3.2.9 Resistance to indentation (hardness test)

A fruit penetrometer (Lutron FR-5120) motorised with a TRINAMIC Motion control engine (Model TMCS-40.6.35-10000-AT-01) with 10000 P/R resolution was utilised (Figure 76). The penetrometer was fitted with a 3 mm radius tip which was used to apply a force on the tangential face of the wood specimens. The motor was operated through a hardwired controller. It was ensured that the wood specimens were lying

on a flat surface and that the penetrometer's tip touched the wood's testing face perpendicularly. The testing faces of the wood specimens were shaved with a razor to ensure that they were flat and parallel. This was not always possible however, as a balance had to be struck between how much material was shaved off and the flatness of the testing faces. A specimen of sound pine was first measured. The wood specimens in control group 2 (freeze-dried) and control group 3 (isopropanol-immersed) were all measured. Eight specimens were measured from each treatment group. Each wood specimen was measured five times on its tangential surface and the values were then averaged. Additionally, the wood specimens from the treatment groups were split in two and the core was measured once on each half and averaged (Figure 77). Prior to each measurement, a preload was applied by lowering the penetrometer tip on the testing face of the wood specimen until the force read by the sensor was between 6 – 10 N. For the actual measurement, the tip was lowered down 1 mm and the force in N was recorded. The net force was calculated by subtracting the preload force from the measured force. IBM® SPSS® software was used to analyse the data.

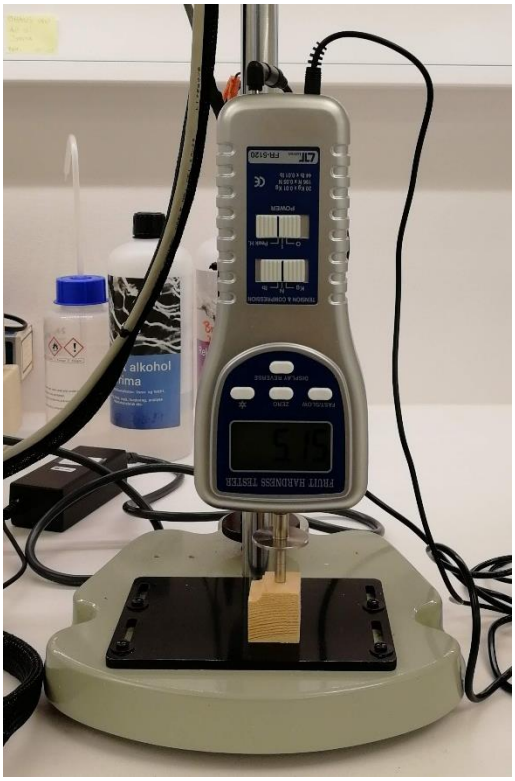

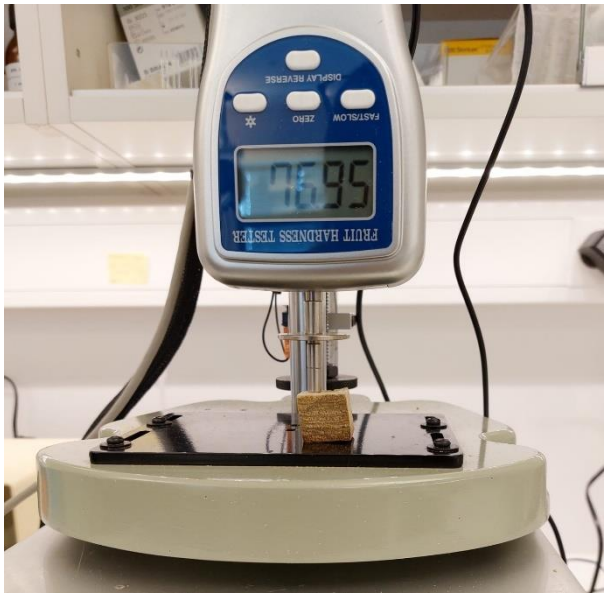

Figure 76. Photos showing the fruit penetrometer set-up, with a sound wood specimen (top) and an archaeological wood specimen (bottom).

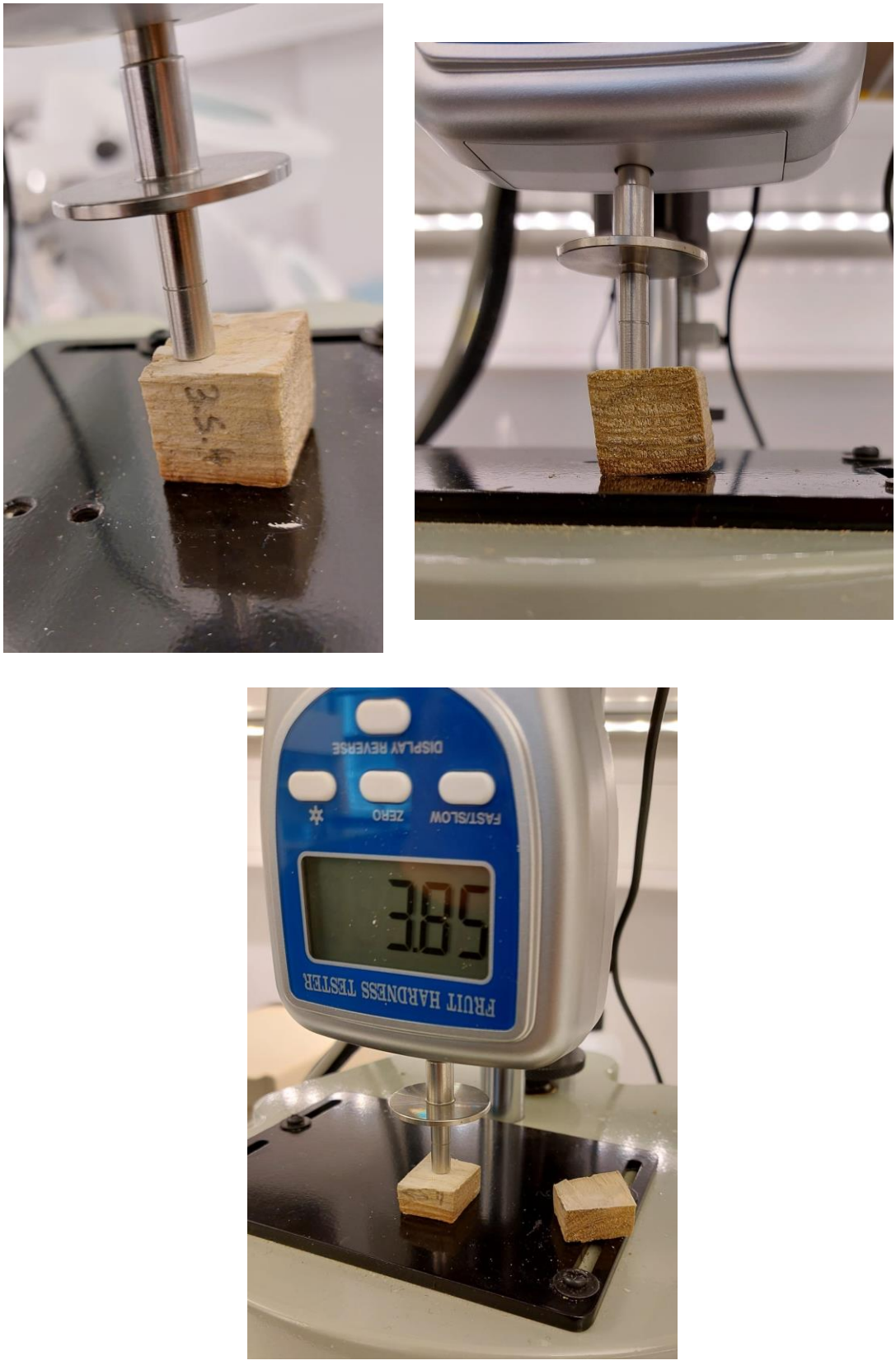

Figure 77. The tangential surface of a treated archaeological wood specimen being analysed with the fruit penetrometer (top left and right). The core of a treated specimen being analysed (bottom).

Table 20. A table indicating the wood specimens used for each of the tests that were carried out

	Sample ID	Colour change measurements	pH measurements	IR	SEM	Hardness test
Control group 2 (freeze-dried)	**1.S.6**	✓	✓	✓		✓
	2.S.4	✓				✓
	4.C.1	✓		✓	✓	✓
	5.S.5	✓	✓			✓
	6.S.5	✓	✓			✓
Control group 3 (IPA)	**2.S.7**	✓	✓			✓
	3.S.5	✓				✓
	4.C.2	✓	✓	✓		✓
	5.S.3	✓	✓			✓
	6.S.6	✓		✓	✓	✓
Treatment group 1 (TPA6)	**1.S.4**	✓	✓			✓
	2.S.1	✓	✓	✓		✓
	2.C.2	✓		✓		
	3.S.1	✓				✓
	3.S.4	✓	✓	✓		✓
	4.S.2	✓		✓	✓	
	4.S.3	✓				✓
	4.S.4	✓				✓
	5.S.1	✓				✓
	6.S.1	✓				✓
Treatment group 2 (TPA7)	**1.C.2**	✓		✓	✓	
	2.S.2	✓		✓		
	2.S.3	✓				✓
	3.S.2	✓				✓
	3.S.7	✓				✓
	4.S.1	✓				✓
	4.S.5	✓				✓
	4.S.6	✓	✓	✓		✓
	5.S.2	✓	✓	✓		✓
	6.S.4	✓	✓			✓

4.4 Results and discussion

4.4.1 Solvent retention tests

Table 21. The average solvent retention of the wood films made with the two polymers calculated after 15 days at room temperature

Polymer-wood films	Average solvent retention after 15 days (%)	Standard deviation	Number of replicates
TPA6 15%	10.7	2.0	4
TPA6 10%	13.1	1.0	4
TPA6 5%	17.2	1.4	4
TPA7 15%	12.1	0.5	4
TPA7 10%	14.2	2.0	3
TPA7 5%	14.8	1.7	4

Figure 78. The wood films made with TPA6 after slowly drying in the fume-hood for two weeks. a) 15% w/w, b) 10% w/w, c) 5% w/w.

Figure 79. The wood films made with TPA6 after handling. a) 15% w/w, b) 10% w/w c) 5% w/w. The film appeared to be sturdier with increasing polymer concentration, with the 15% one being the most robust and the 5% being the most powdery. The 15% wood film still broke upon handling, but whole chunks of film could be lifted off the sheet.

Figure 80. The wood films made with TPA7 after slowly drying in the fume-hood for two weeks. a) 15% w/w, b) 10% w/w, c) 5% w/w.

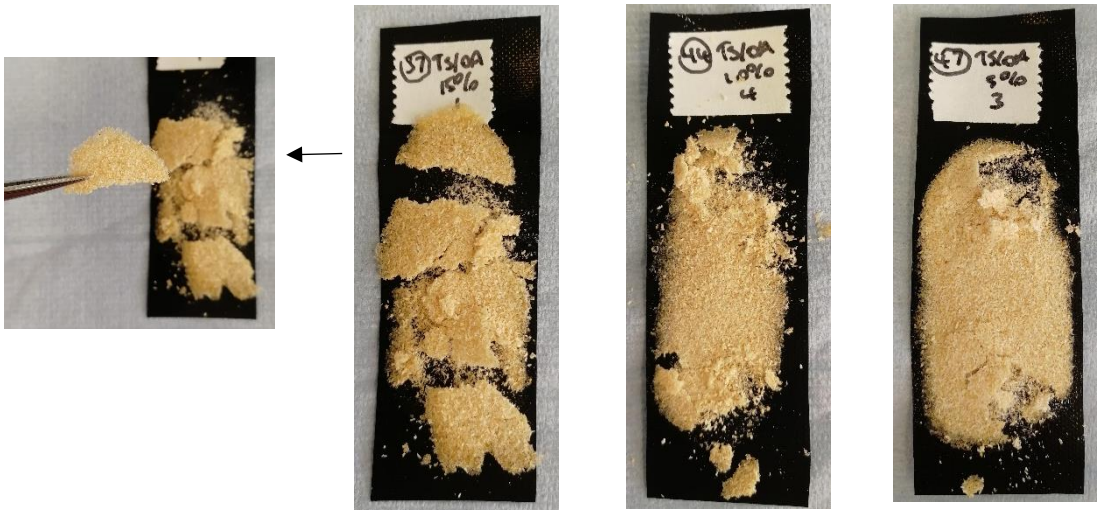

a) b) c)

Figure 81. The wood films made with TPA7 after handling. a) 15% w/w, b) 10% w/w c) 5% w/w. As with the TPA6 experiments, the sturdiness of the wood films increased with increasing polymer concentration.

The results (Table 21 and Figures 78 – 81) were compared with similar study which had previously been carried out with the polymer Butvar® B-98. They indicated that solvent retention for TPA6 and TPA7 appeared to be much lower than previously observed for Butvar® B-98 at a 15% w/w by by Zisi and de Lamotte, who reported a solvent retention value of 31% after 30 days of drying (Zisi and de Lamotte, 2020). Note that the solvent used in that instance was different: isopropanol was used in this study while Zisi and de Lamotte used a mixture of toluene and ethanol.

TPA6 appeared to show slightly less solvent retention than TPA7. For both polymers, the trend was for the solvent retention percentage to increase with decreasing concentration. The wood-polymer films may have partly prevented the isopropanol from diffusing freely, thus resulting in solvent retention (Carlson and Schniewind, 1990). Even for a volatile solvent like isopropanol, it is difficult to achieve full evaporation as a small percentage will be indefinitely retained (Horie, 2010).

4.4.2 Archaeological wood identification

The archaeological wood was identified as *Pinus* (pine) due to the observation of several characteristic features. The archaeological wood was compared to fresh pine to confirm this identification. Ray tracheids with dentate walls and fenestriform ray pits, two characteristics of pine, were both observed (Figure 82) (Hather, 2016). Resin canals were also present (Figures 83 and 84). There was a loss of birefringence under crossed polars when compared to the fresh wood, indicating the degradation of cellulose (Figure 85) (Schwarze, 2007). Birefringence separates plane-polarised light into two perpendicular rays, resulting in cellulose microfibrils appearing luminous (Ruzin, 1999). A loss of this luminance therefore means that there is a deficit in cellulose, and is usually the first sign of decay (Wilcox, 1993).

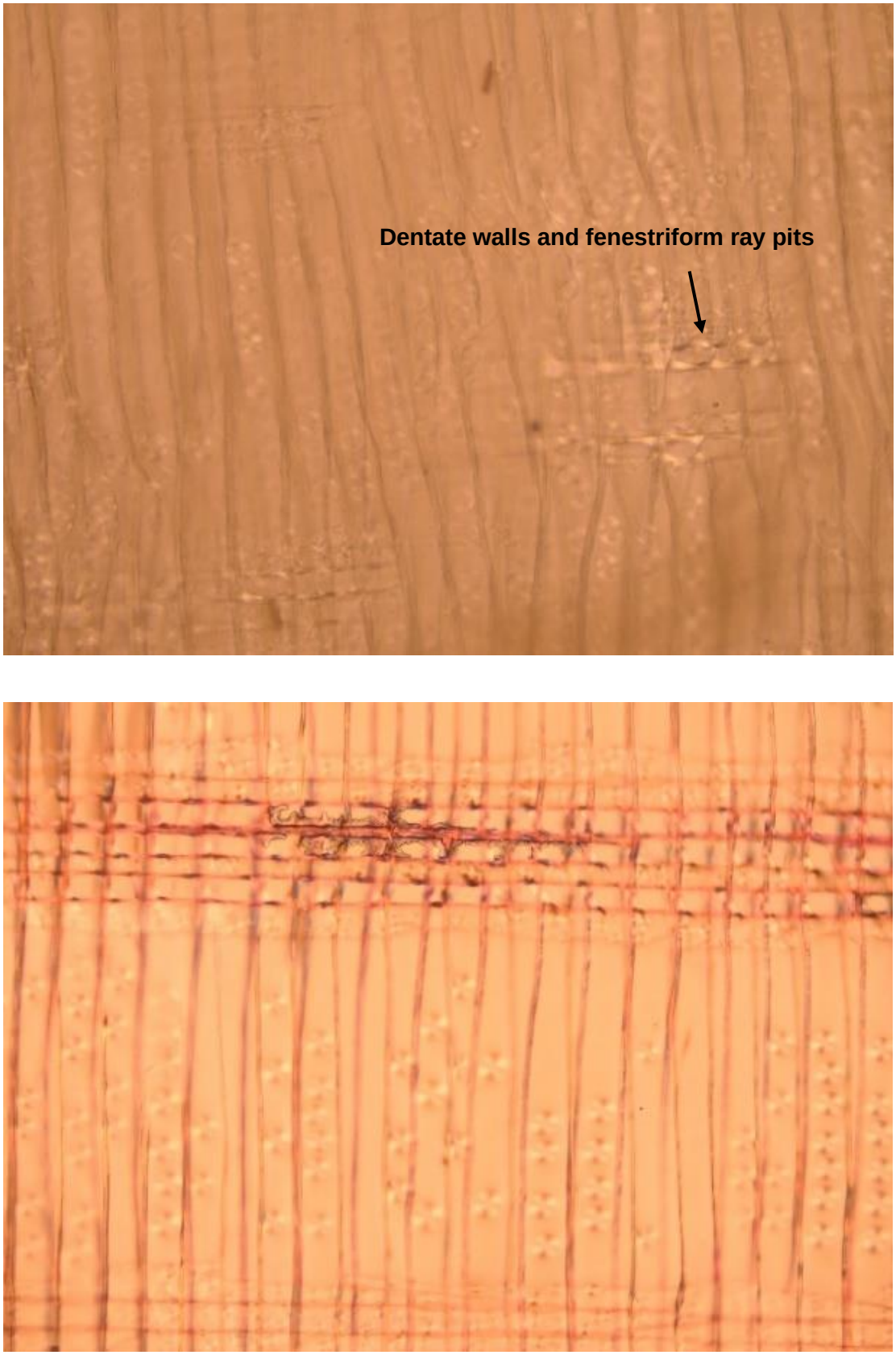

Figure 82. Radial face of archaeological pine (top) and sound pine (bottom), as seen under the light microscope with a magnification of 200x. Ray tracheids with dentate walls and fenestriform ray pits could be seen.

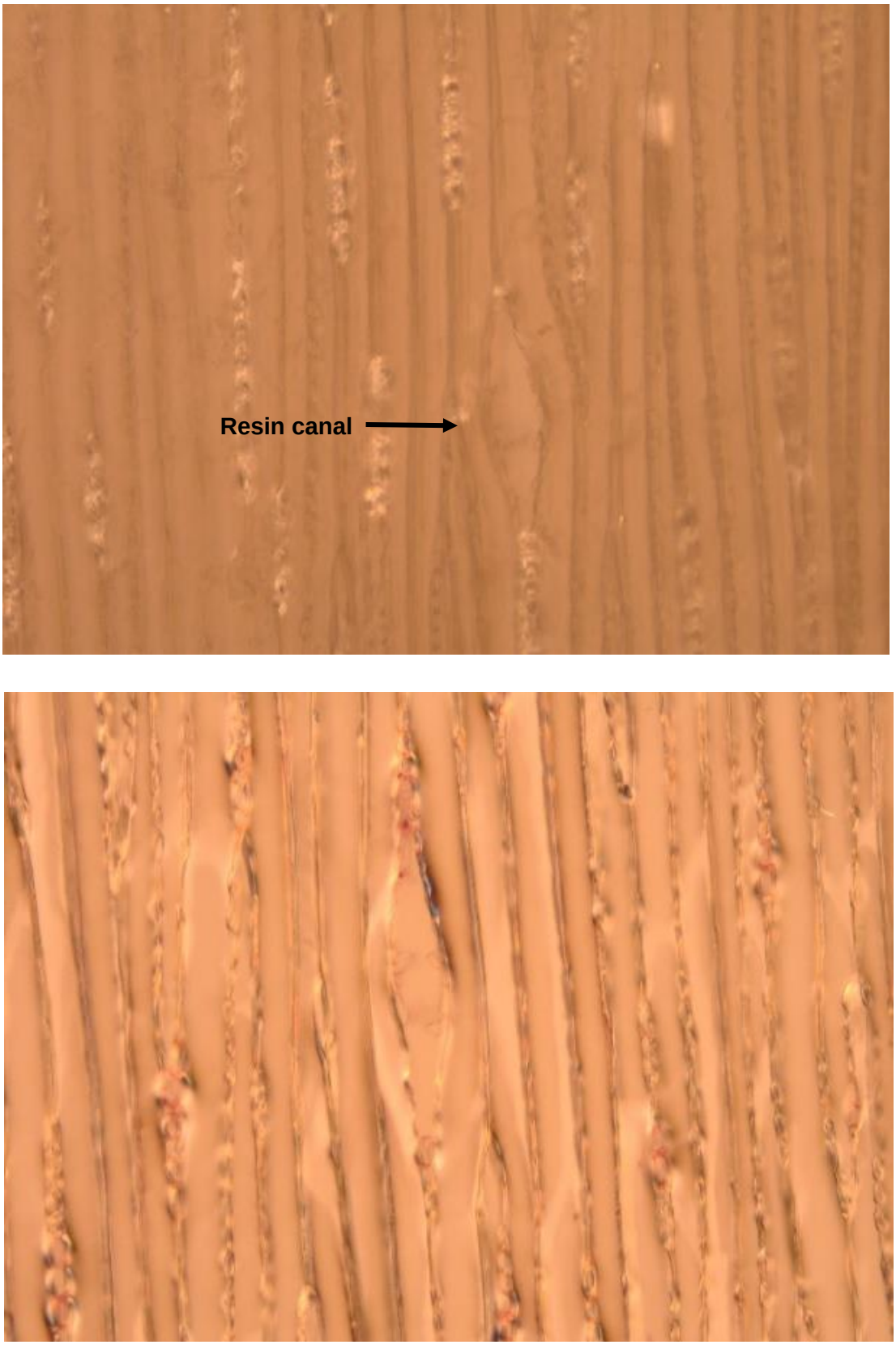

Figure 83. Tangential longitudinal face of archaeological pine (top) and sound pine (bottom), as seen under the light microscope with a magnification of 200x. A resin canal can be seen.

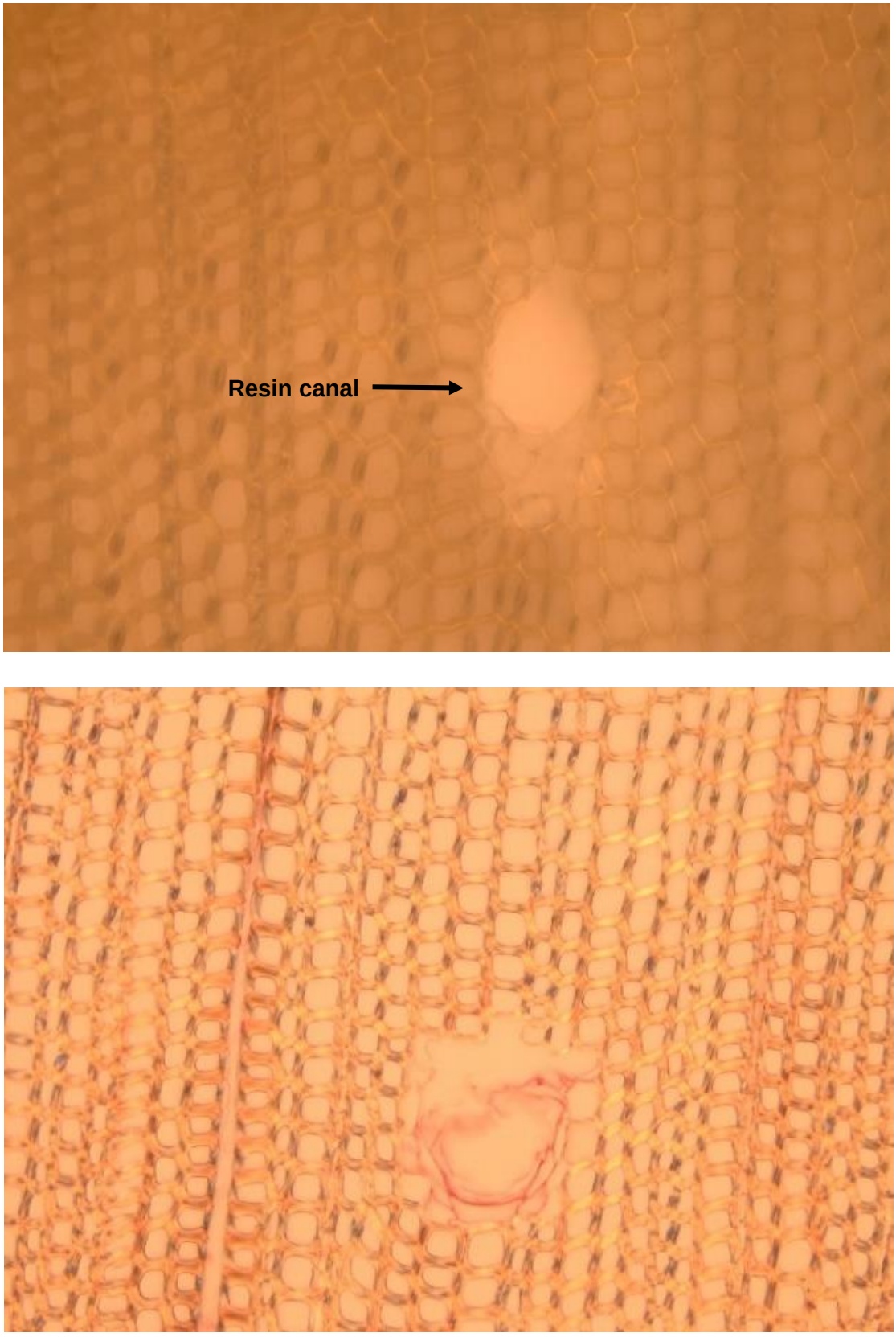

Figure 84. Transverse face of archaeological pine (top) and sound pine (bottom), as seen under the light microscope with a magnification of 200x. A resin canal can be seen.

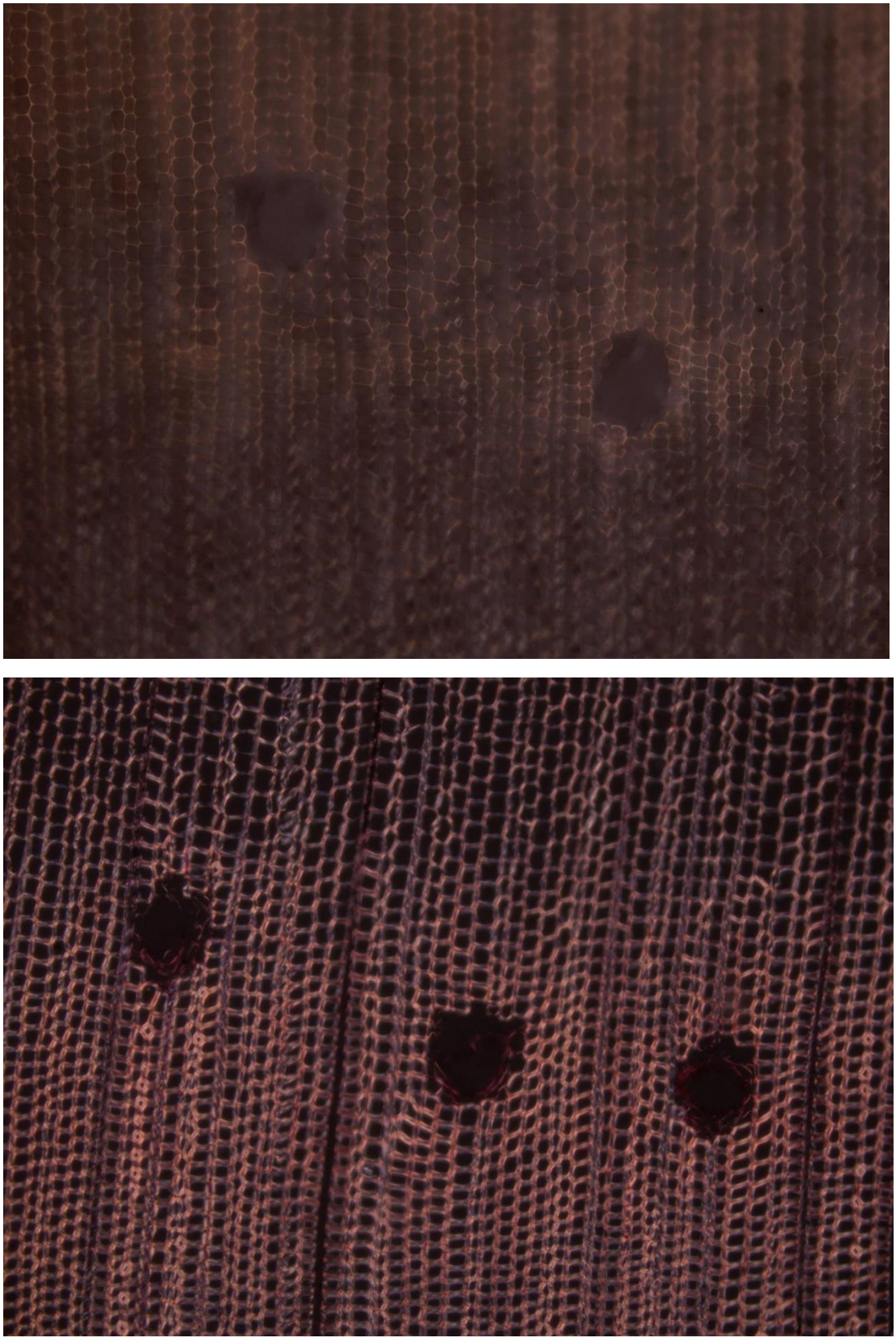

Figure 85. Transverse face of archaeological pine (top) and sound pine (bottom), as seen under the light microscope using a magnification of 200x. A loss of birefringence was observed under crossed polars when compared to the fresh wood, indicating the degradation of cellulose.

4.4.3 Density and MMC measurements

The density and MMC of wood are both important indicators of its extent of degradation. Knowing the density of the wood can give us an idea of the amount of consolidant required to conserve it (Jensen and Gregory, 2006). The MMC increases and the basic density decreases with increasing wood degradation, which results from the loss of mass and volume of cell wall material due to the bacterial degradation taking place during burial (Babiński, Izdebska-Mucha and Waliszewska, 2014). The moisture content of waterlogged wood is referred to as MMC since it is assumed that wood which has been preserved in such conditions would possess the highest possible volume of water in its pores (Macchioni, Pecoraro and Pizzo, 2018).

From the density and MMC measurements, it appeared that the state of preservation of the wood branch was approximately even throughout. All the samples showed similar results, except for one outlier (sample 24) (Figure 86). The density measurements ranged from 0.132 to 0.179 g/mL and the MMC from 492 to 653%. Wood with a high degree of degradation has a density of ~ 0.1 g/mL while sound wood usually has a density of ~ 0.4 - 0.5 g/mL (Jensen and Gregory, 2006). Well-preserved pine specifically is reported to have a density of around 0.5 g/mL (Łucejko *et al.*, 2021). With regards to MMC, a value of above 400% indicates that the wood is highly degraded (Jingran *et al.*, 2014). Based on this, the wood samples seemed to have a high degree of degradation, with the means of the density and MMC being 0.146 g/mL and 610% respectively (Figure 86). The core of a piece of wood is generally expected to be more well preserved than the surface, since the process of degradation affects the outer area first (Łucejko *et al.*, 2021). In this case, the samples taken from the surface and the core of the wood log appeared to show little difference in both density and MMC, meaning that they had similar preservation states.

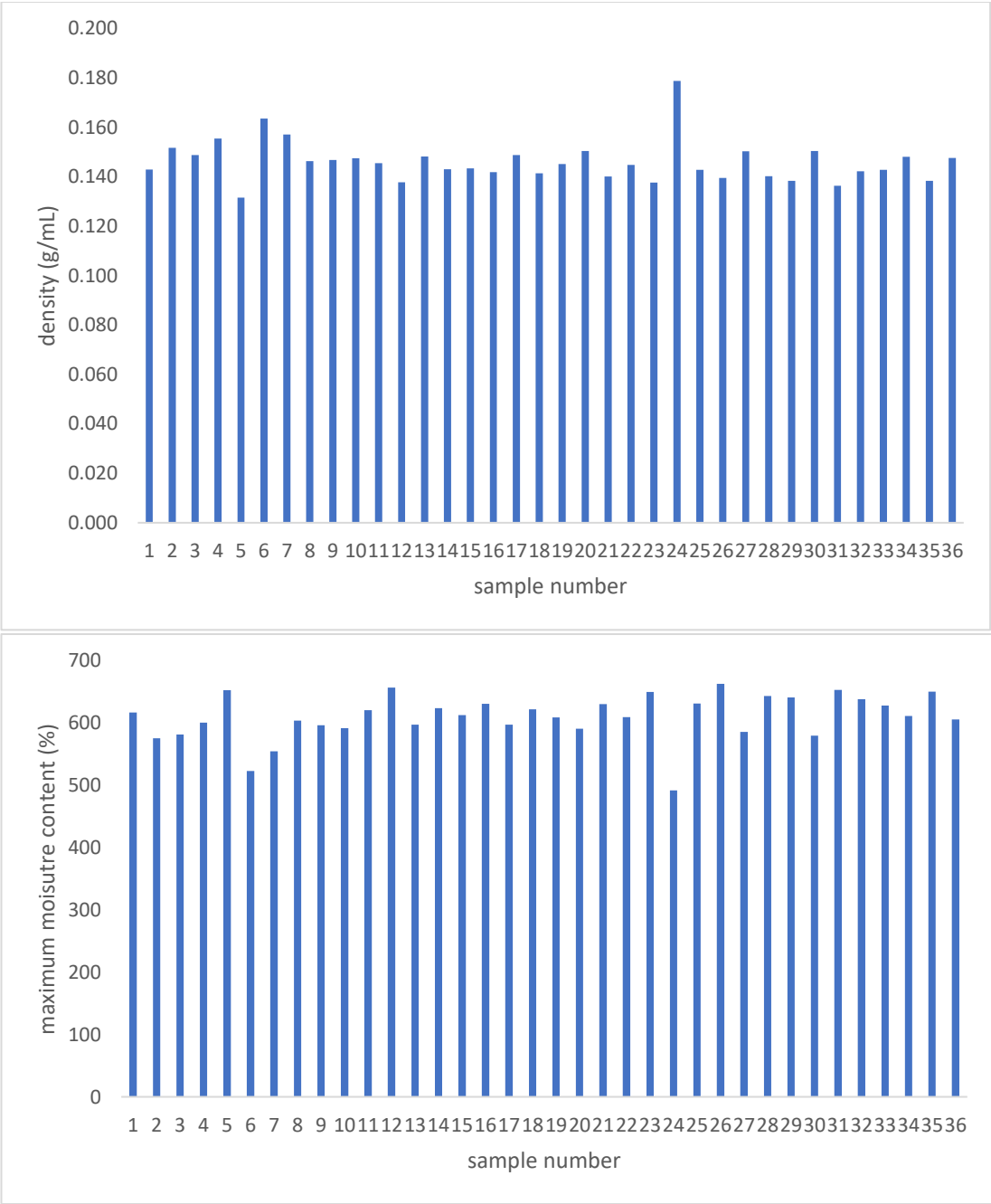

Figure 86. The density (top) and the MMC (bottom) measurements for the wood samples (made up of both surface and core pieces), showing the almost uniform preservation state of the wood log. The samples used for these measurements were the wedges that were left over from the cutting up of the specimen cubes, therefore they were nominally numbered 1 – 36.

These measurements were also carried out on control groups 1 and 4. Again, these samples showed very similar levels of preservation (Table 22).

Table 22. The density and MMC values calculated for control group 1 and 4

Control group	Sample number	Area	Density (g/mL)	MMC (%)
1	3.C.1.1	Core	0.151	594
	5.S.2.1	Surface	0.157	573
	6.S.3.1	Surface	0.155	579
	4.S.4.1	Surface	0.158	566
4	3.C.1.4	Core	0.156	572
	5.S.2.4	Surface	0.159	559
	6.S.3.4	Surface	0.155	561
	4.S.4.4	Surface	0.162	547

4.4.4 Observational changes

After treatment, the specimens treated with both polymers seemed darker, with a yellowish tinge. They felt denser when handled. When tapped on a surface, they sounded less muted/hollow than the untreated specimens. There did not appear to be any new cracks that developed on the wood after treatment and they kept their original shape. This was ascertained by looking at photos taken before and after treatment (see Figures 95 and 96 as examples).

4.4.5 Weight change

The groups treated with both TPA6 and TPA7 increased significantly in weight (Table 23). The control group treated with isopropanol (referred to as IPA in Table 23) was expected to decrease in weight due to the potential dissolution of some pine resin in the solvent. During immersion, the solvent was observed to turn from transparent to a pale yellow, possibly indicating that some resin had exited the wood. This was not found to be the case however since the specimens actually increased in weight, albeit very slightly. It is possible that these cubes were not conditioned to the same extent before and after isopropanol immersion, thus leading to a slight irregularity in the weight measurements.

Weight gain appeared to be uniform for both TPA6 and TPA7 (Figure 87). TPA6 had a % weight change ranging from 40.5 – 45.9% while TPA7 ranged from 39.5 – 50.4%. The specimen with the most weight gain overall (50.41%) was a core sample from the TPA7 group (1.C.2). The specimen showing the least weight gain (39.46%) was also from the TPA7 group (3.S.2). It is unclear why the polymer deviated in uptake for these two particular specimens. Taking this into consideration, TPA6's uptake in the wood appeared to be slightly more regular with no extremes. It is uncertain whether this is due to the polymer's properties, or if it is an effect of the wood's inherent variability.

Table 23. The weight measurements taken before and after treatment for control group 3, treatment group 1 and 2. The % weight change for all specimens was calculated.

WEIGHT CHANGE

		BEFORE TREATMENT	AFTER TREATMENT	
	Sample ID	**Weight (g)**	**Weight (g)**	**% weight change**
Control group 3 (IPA)	**2.S.7**	1.4229	1.4309	0.56
	3.S.5	1.6437	1.6529	0.56
	4.C.2	1.487	1.4932	0.42
	5.S.3	1.4215	1.4282	0.47
	6.S.6	1.5167	1.5248	0.53
Treatment group 1 (TPA6)	**1.S.4**	1.6562	2.4171	45.94
	2.S.1	1.5575	2.2479	44.33
	2.C.2	1.5216	2.2109	45.30
	3.S.1	1.6279	2.3632	45.17
	3.S.4	1.6375	2.3475	43.36
	4.S.2	1.6358	2.3609	44.33
	4.S.3	1.756	2.4672	40.50
	4.S.4	1.6762	2.4363	45.35
	5.S.1	1.5247	2.2184	45.50
	6.S.1	1.7729	2.5467	43.65
Treatment group 2 (TPA7)	**1.C.2**	1.5708	2.3626	50.41
	2.S.2	1.3471	1.9708	46.30
	2.S.3	1.86	2.6758	43.86
	3.S.2	1.7573	2.4507	39.46
	3.S.7	1.3352	1.9554	46.45
	4.S.1	1.6243	2.3669	45.72
	4.S.5	1.5288	2.2391	46.46
	4.S.6	1.681	2.3953	42.49
	5.S.2	1.2876	1.8828	46.23
	6.S.4	1.4271	2.073	45.26

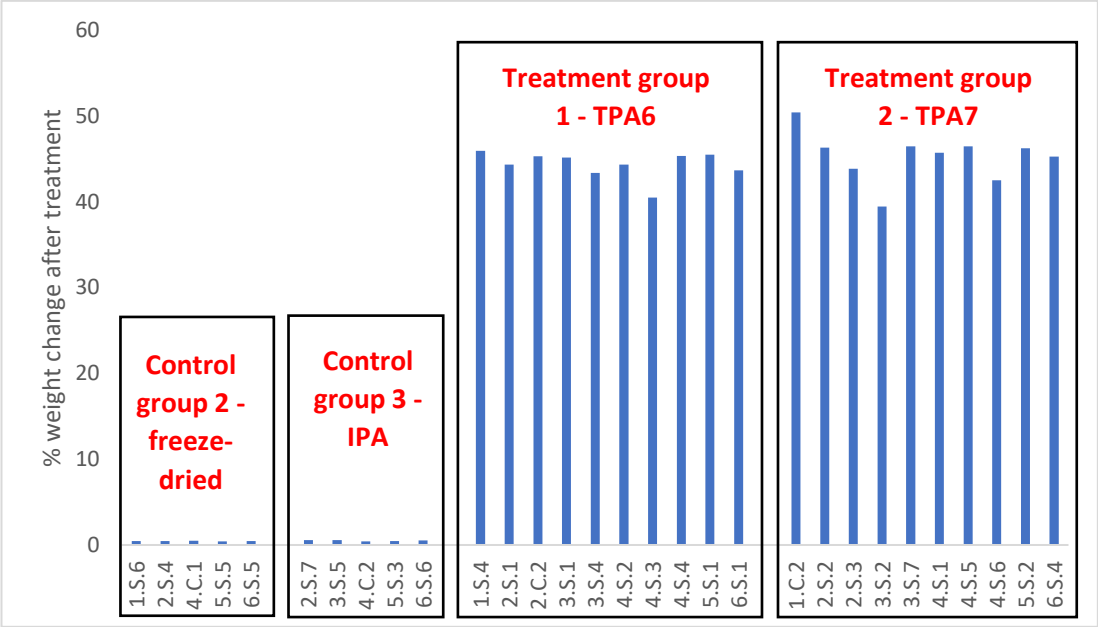

Figure 87. The % weight change for all the measured groups. Control group 2 was freeze-dried and kept in a desiccator at ~ 20 °C and 50% RH during the immersion of control group 3 (isopropanol-immersed) and treatment groups 1 and 2 (TPA6- and TPA7-immersed respectively).

4.4.6 Dimensional change

Control groups 1 (pins inserted before oven-drying) and 4 (pins inserted before freeze-drying) were compared to observe the effect that the different drying methods have on the wood. As expected, it was very clear that oven-drying causes more significant shrinkage, both in the radial and the tangential face (Figures 88 and 89).

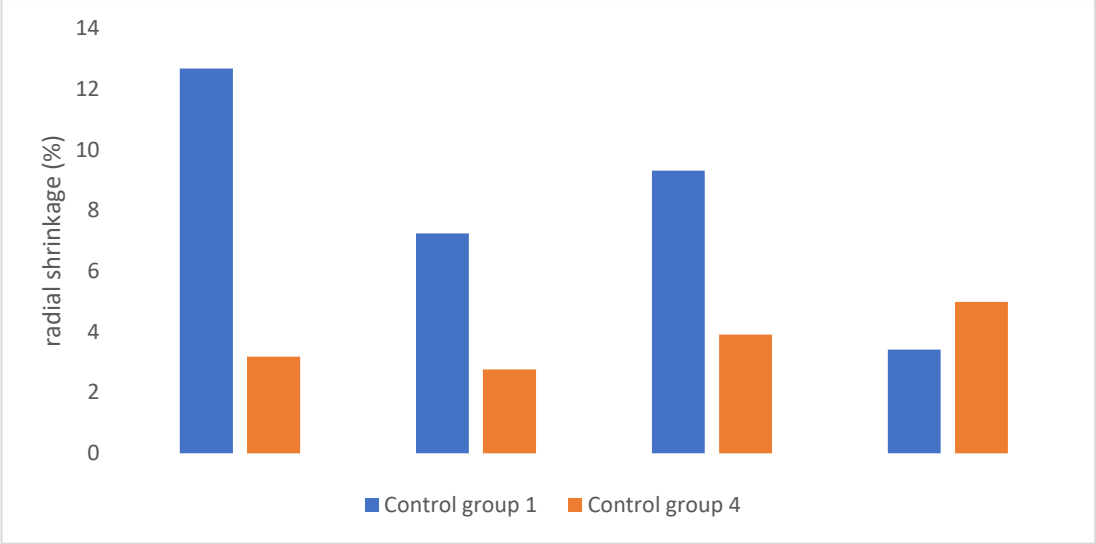

Figure 88. The % radial shrinkage for control group 1 (oven-dried) and control group 4 (freeze-dried).

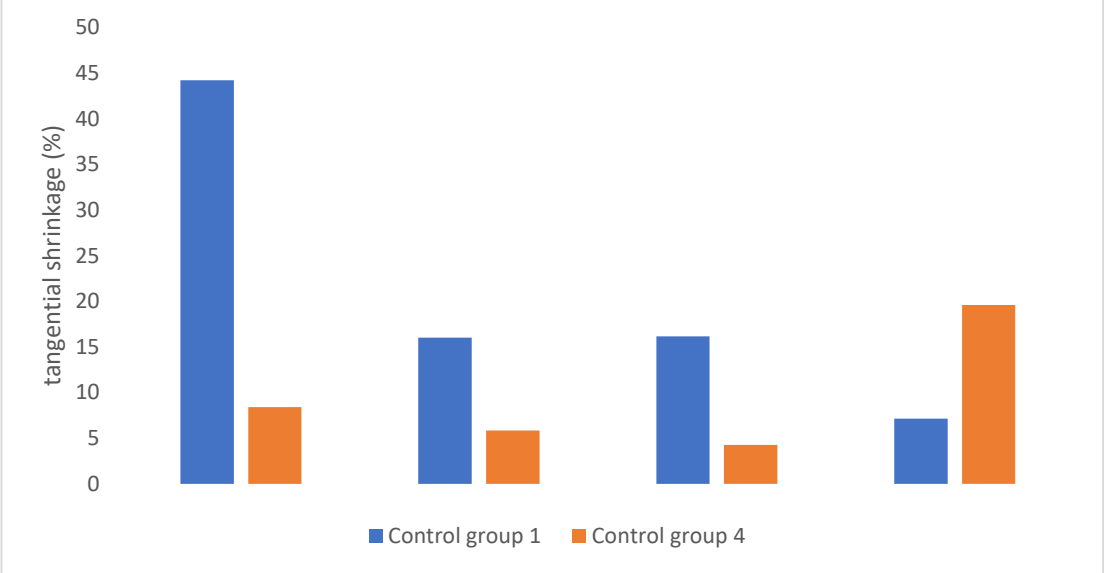

Figure 89. The % tangential shrinkage for control group 1 (oven-dried) and control group 4 (freeze-dried).

Table 24 shows the dimensional measurements of control group 3 (isopropanol-immersed) and both treatment groups, along with the % linear dimensional change (relative to their measurements before treatment). For all groups, the dimensional change for both radial and tangential faces primarily ranged at ± 2%, except for a few outliers (Figure 90). Both radial and tangential faces seemed to change to the same degree, that is, one face did not predominate over the other. Control group 3

appeared to shrink slightly after the isopropanol treatment. The polymer treatment groups had more varied results, showing both shrinkage (negative values) and swelling (positive values). TPA6 seemed to mainly cause shrinkage. TPA7 seemed to have a more variable effect, with swelling slightly predominating over shrinkage.

As mentioned, there were a few outliers in these measurements. The most extreme was 2.S.7 (control group 3), which showed a radial dimensional change of -8.69%. Other outliers included 4.C.2 (control group 3; tangential change of 3.09%), 6.S.1 (treatment group 1; tangential change of -3.21%) and 1.C.2 (treatment group 2; radial change of 4.21%). These measurements may potentially be attributed to the high variability of the wood or they may also be due to experimental error. The 'pin method' of measuring dimensional changes has limitations when it comes to the accuracy of the measurements. This is because the measurement values are highly dependent on the angle of the callipers relative to the pins. Therefore, if this angle is not exactly replicated during the 'before' and 'after' measurements, it will be difficult to get results that truly represent the dimensional change that has taken place.

With regards to control group 2 (freeze-dried only), the reference pins were inserted and measured directly after freeze-drying and then kept in a desiccator at ~ 20 °C and 50% RH during the soaking of the other groups. Its measurements were then repeated after the treatment of the other specimens was completed. This means that theoretically the specimens in control group 2 should have exhibited no dimensional changes since they were not subjected to any treatment after freeze-drying. Nevertheless, slight dimensional changes were still recorded. This demonstrates the inherent inaccuracy of this measuring method. The dimensional changes recorded in control group 2 may therefore be considered as the error range that can be expected in the other measurements (~ ± 2%). If this is taken into consideration, then this means that most of wood specimens did not exhibit significant dimensional changes after treatment.

Figure 91 compares the % dimensional change to the % weight change in all groups and confirms the observations that were made previously. The treatment groups gained weight after treatment due to polymer uptake. Conversely, the % dimensional measurements did not appear to have varied greatly after treatment. Since isopropanol has a low surface tension, it was not surprising that only minimal shrinkage was observed during drying after the treatment steps.

Table 24. The dimensional measurements (rad = radial, tan = tangential) taken before and after treatment for control group 3, treatment group 1 and 2. The % dimensional changes for both the radial and tangential faces for all specimens were calculated.

DIMENSIONAL MEASUREMENTS

		BEFORE TREATMENT		AFTER TREATMENT			
	Sample ID	Rad (mm)	Tan (mm)	Rad (mm)	Tan (mm)	% linear dimensional (rad) change	% linear dimensional (tan) change
Control group 3 (IPA)	2.S.7	11.85	10.7	10.82	10.45	-8.69	-2.34
	3.S.5	9.15	10.38	9.2	10.42	0.55	0.39
	4.C.2	11	10.37	10.89	10.69	-1.00	3.09
	5.S.3	12.06	11.94	11.92	11.72	-1.16	-1.84
	6.S.6	12.31	12.87	12.11	12.55	-1.62	-2.49
Treatment group 1 (TPA6)	1.S.4	11.62	12.94	11.56	12.72	-0.52	-1.70
	2.S.1	12.77	11.56	12.7	11.8	-0.55	2.08
	2.C.2	12.55	11.22	12.69	11.29	1.12	0.62
	3.S.1	10.56	12.15	10.74	12.23	1.70	0.66
	3.S.4	11.72	11.94	11.59	11.88	-1.11	-0.50
	4.S.2	14.04	12.72	14.06	12.59	0.14	-1.02
	4.S.3	11.6	12.13	11.62	12.01	0.17	-0.99
	4.S.4	14.39	9.88	14.27	9.71	-0.83	-1.72
	5.S.1	14.2	12.04	14.17	12	-0.21	-0.33
	6.S.1	12.92	13.07	13.05	12.65	1.01	-3.21
Treatment group 2 (TPA7)	1.C.2	9.5	11.27	9.9	11.5	4.21	2.04
	2.S.2	9.95	9.92	9.93	10.09	-0.20	1.71
	2.S.3	10.3	11.52	10.5	11.63	1.94	0.95
	3.S.2	9.53	13.18	9.53	13.18	0.00	0.00
	3.S.7	8.39	11.71	8.59	11.78	2.38	0.60
	4.S.1	8.91	11.9	9.05	11.8	1.57	-0.84
	4.S.5	12.13	11.02	12.08	11.29	-0.41	2.45
	4.S.6	12.67	13.39	12.71	13.17	0.32	-1.64
	5.S.2	11.53	13.04	11.52	13.06	-0.09	0.15
	6.S.4	13.66	12.5	13.31	12.42	-2.56	-0.64

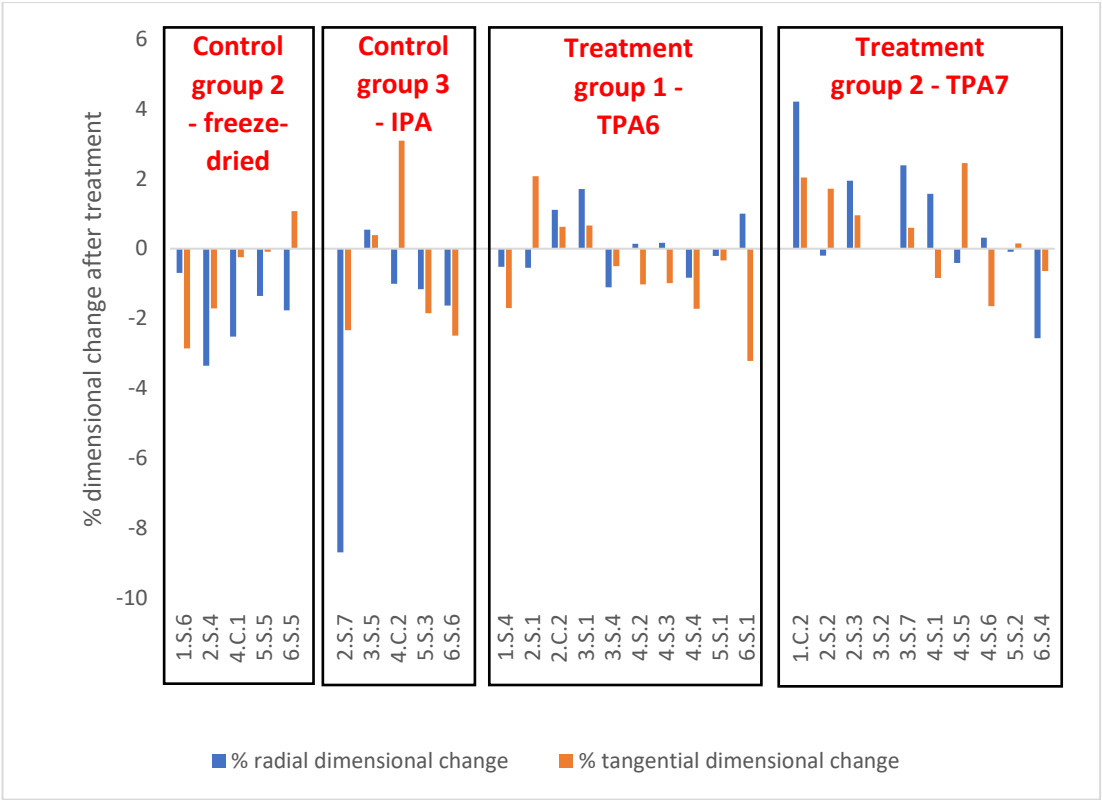

Figure 90. A comparison of the radial and tangential dimensional % changes for control groups 2 and 3 and treatment groups 1 and 2.

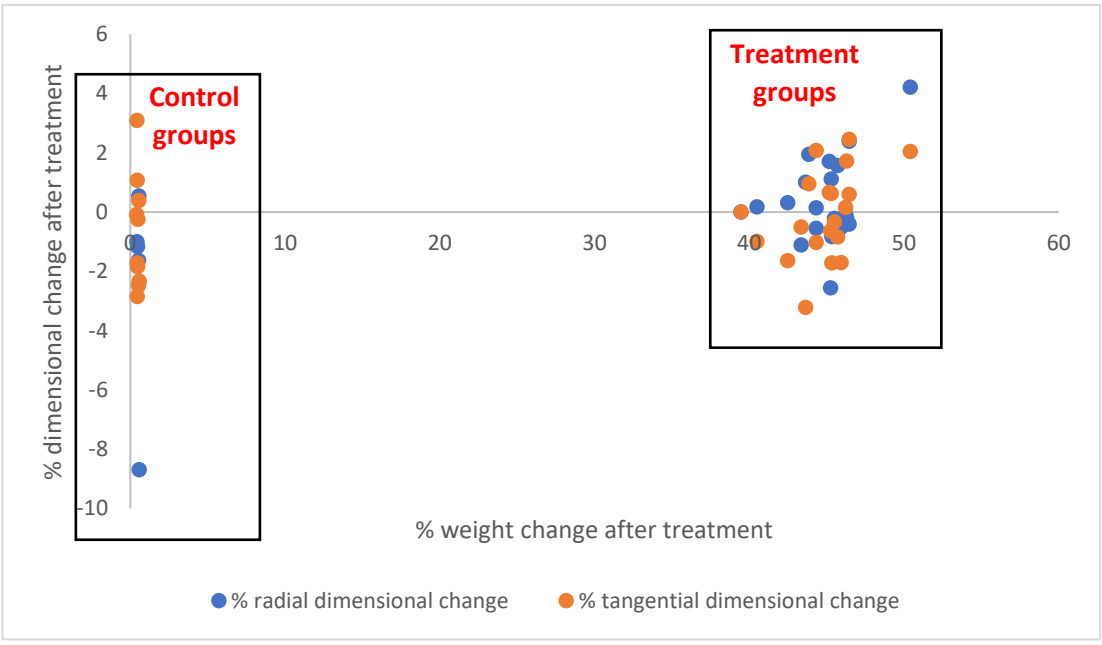

Figure 91. A comparison of the % dimensional changes of control groups 2 and 3 and treatment groups 1 and 2 with % weight change. The wood specimens gained weight after treatment due to polymer uptake. The % dimensional changes did not vary greatly after treatment.

4.4.7 Colour change

Based on visual inspection alone, it was obvious that the polymers had caused a colour change in the wood specimens, mostly darkening them and imparting a yellow hue (Figures 94 – 96). The colour measurements of both treatment groups were compared to control group 3, which was treated with isopropanol. As observed by the naked eye, both polymers seemed to change the colour to a similar degree.

The largest degree of change was observed in the L* coordinate which decreased after treatment, meaning that the specimens became darker. However, there was also a substantial difference in the b* axes, indicating a shift from blue to yellow. The measurements also showed a positive difference in the a* axes (green to red), although to a smaller degree. The spectrophotometer measurements show that TPA7 seemed to cause slightly less overall colour change than TPA6.

Figure 92 shows the colour change of the wood after it was solely treated with isopropanol, with a ΔE of 1.32. This correlates with what was seen visually, since there did not appear to be any colour change between control group 2 (freeze-dried) and 3 (isopropanol-immersed). Figure 93 shows the ΔE values for the treatment groups, in relation to control group 3. Treatment groups 1 (TPA6) and 2 (TPA7) had a ΔE value of 11.55 and 10.55 respectively. Again, this confirms what was observed since the treated wood was noticeably darker, with a yellowish tinge. Nevertheless, the polymers did not darken the wood to the same extent as other materials do. According to an internal report (Braovac, Łucejko and de Lamotte, 2020), lignin at a 10% concentration causes a colour change of ~ 23 – 29 when applied to archaeological wood, which would translate to a far greater colour change.

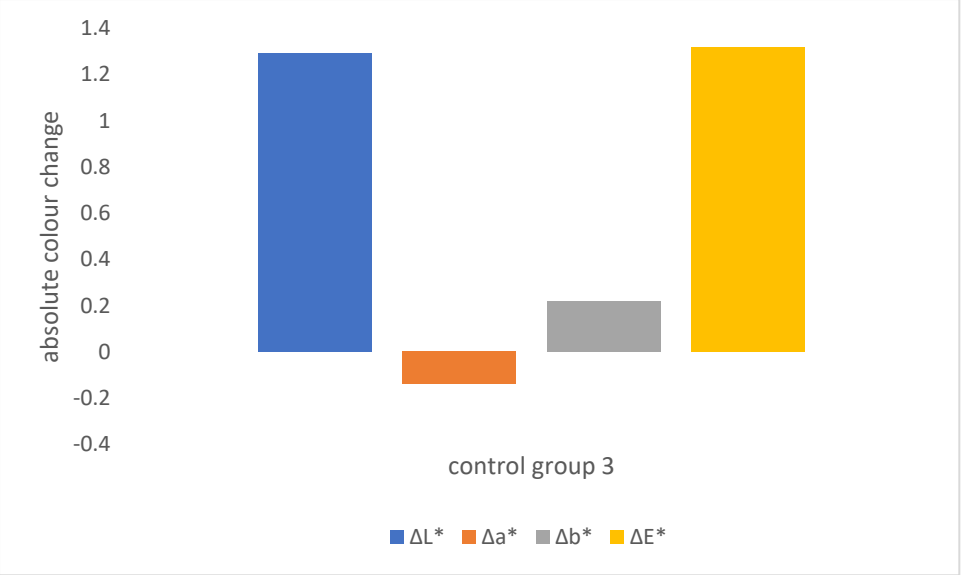

Figure 92. Colour change of control group 3 (isopropanol-immersed) relative to control group 2 (freeze-dried only). ΔE = 1.32.

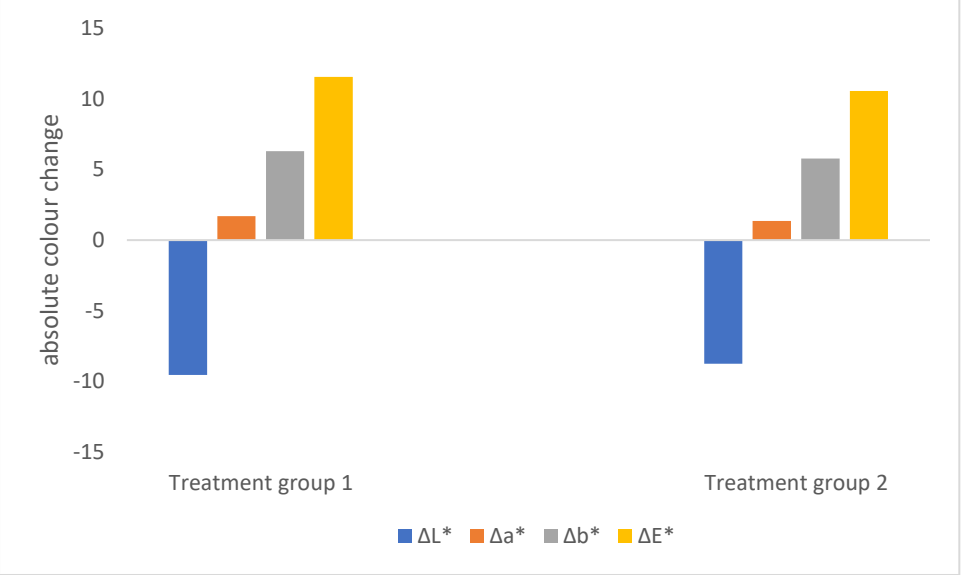

Figure 93. Colour change of treatment group 1 (TPA6) and treatment group 2 (TPA7) relative to control group 3 (isopropanol-immersed). Treatment group 1 ΔE = 11.55; treatment group 2 ΔE = 10.55.

An absolute colour change above 3 can be seen by the human eye (Hon and Shiraishi, 2021). Mokrzycki and Tatol (Mokrzycki and Tatol, 2011) also describe the following classification:

1. 0 < ΔE < 1: no colour change is detected
2. 1 < ΔE < 2: colour change is only detected by experienced observers
3. 2 < ΔE < 3.5: colour change is detected by inexperienced observers
4. 3.5 < ΔE < 5: clear colour change
5. 5 < ΔE: two different colours are detected

The colour change caused by TPA6 and TPA7 may possibly not be detected by the human eye if applied to the alum-treated Oseberg collection, since the artefacts are already dark (Łucejko *et al.*, 2021).

Figure 94. Photos of control group 3 (isopropanol-immersed) before (top) and after (bottom) immersion. Little or no colour change was detected by the naked eye.

Figure 95. Photos of treatment group 1 (TPA6) before (top) and after (bottom) treatment. Specimens became noticeably darker, with a yellow tinge.

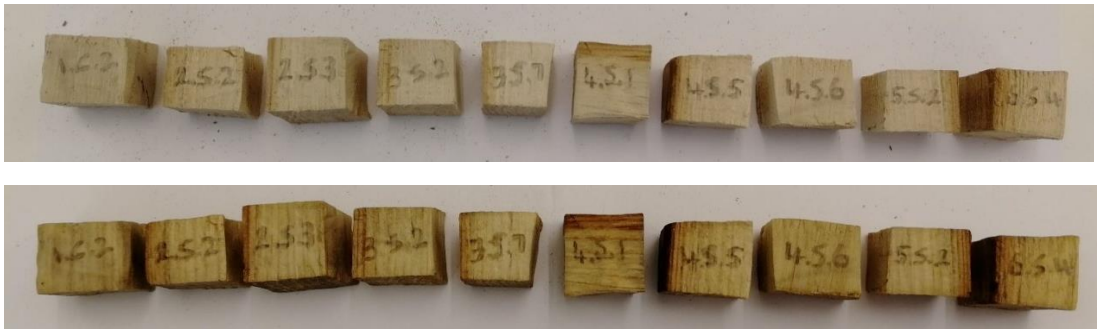

Figure 96. Photos of treatment group 2 (TPA7) before (top) and after (bottom) treatment. Specimens were similar to those treated with TPA6.

4.4.8 pH measurements

There were no discernible differences between the pH measurements of the control groups and treatment groups (both surfaces and cores) (Figure 97). The specimens from all groups had a pH of approximately 5 – 6. This indicated that the polymers did not seem to affect the wood's natural pH.

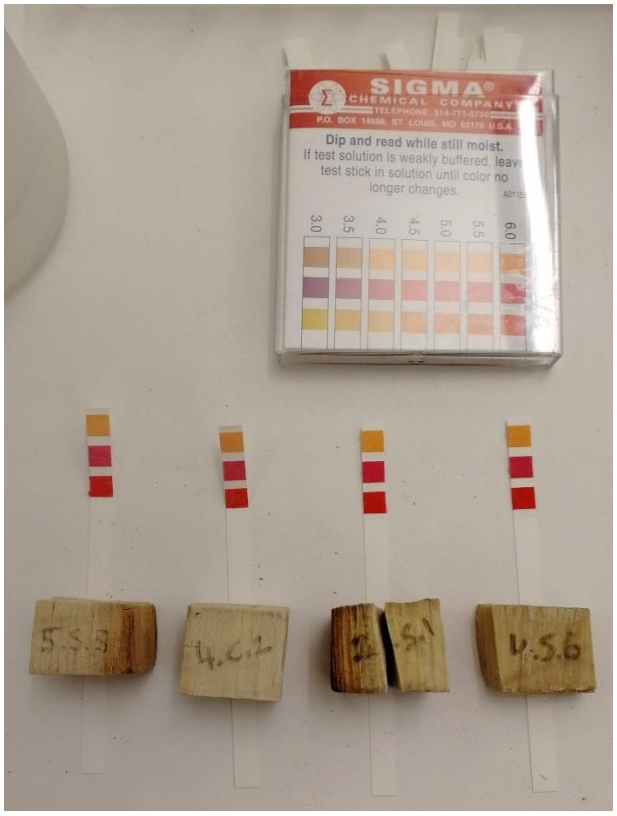

Figure 97. A photo depicting the pH measurements of four wood specimens: 5.S.5 (control group 2), 4.C.2 (control group 3), 2.S.1 (treatment group 1) and 4.S.6 (treatment group 2). Note that the pH paper is showing the same colours for all four specimens, indicating a pH of 5 – 6.

4.4.9 ATR-FTIR analyses

4.4.9.1 Sound pine vs archaeological pine

The archaeological wood controls were compared to sound wood, in order to better understand their state of degradation. Figure 98 shows such a comparison, with the use of sample 6.S.6 (isopropanol-immersed) as the archaeological wood. Normalisation was carried out at the lignin peak (1508 cm^{-1}). Table 25 is a detailed

description of the bands that are described here. One could see that the cellulose peaks (1369, 1159 and 896 cm^{-1}) were muted in the archaeological wood, indicating its state of degradation. Similarly, the hemicellulose peaks at 1731 and 1239 cm^{-1} were barely visible in the archaeological pine. Conversely, the lignin signals at 1595, 1263 and 1220 cm^{-1} are prominent in the archaeological pine, mainly due to their amplification as a result of the loss of cellulose and hemicellulose. The band at 1024 cm^{-1} was due to a combination of several wood components (cellulose, hemicellulose and lignin) and as such, it showed the greatest absorption in both sound and archaeological pine.

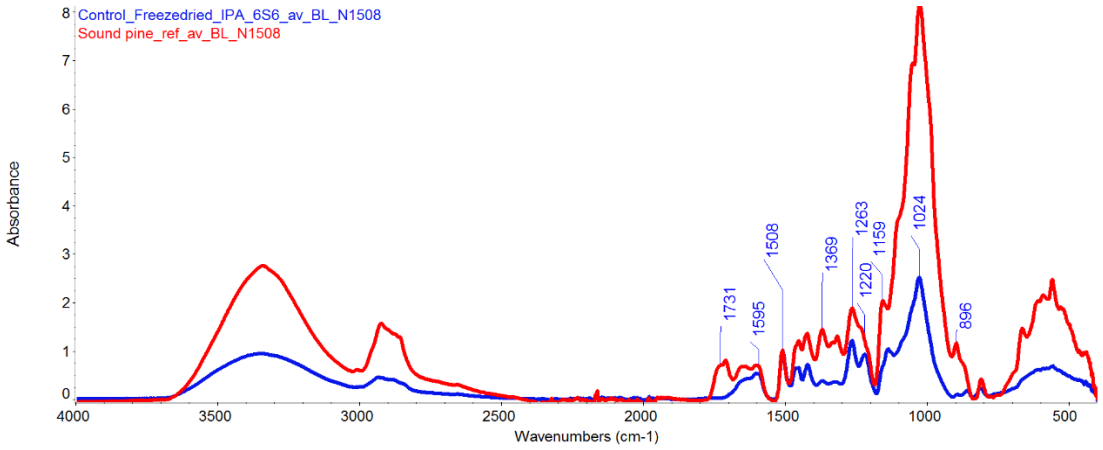

Figure 98. ATR-FTIR spectra of sound pine (red) and archaeological pine (blue; isopropanol immersed control 6.S.6). The major peaks of sound wood are annotated. The spectra were normalised at 1508 cm^{-1}.

Table 25. Major signals pertaining to wood as seen in ATR-FTIR

Band position (cm^{-1})	Assignment	Reference
1730 – 1725	C=O valence vibration of acetyl- or COOH- groups	(Schwanninger *et al.*, 2004)
1605 – 1593	aromatic skeletal vibrations plus C=O stretch	
1515 – 1505	aromatic skeletal vibrations	

1375 – 1374	C-H deformation vibration (cellulose)	
1270 – 1266	G ring plus C=O stretch	
1235 – 1225	-OH plane deformation plus COOH	
1230 – 1221	C-C plus C-O plus C=O stretch	
1162 – 1125	C-O-C asymmetric valence vibration (cellulose)	
1151	C-O-C asymmetric valence vibration in cellulose and hemicelluloses	(Mohebby, 2005)
1110 – 1107	ring asymmetric valence vibration	(Schwanninger *et al.*, 2004)
1024	C-O stretch in cellulose and hemicelluloses; C-O of primary alcohol	(Mohebby, 2005)
892	C-H deformation in cellulose; C1 group frequency in cellulose and hemicelluloses	

4.4.9.2 Extent of polymer penetration

Weight gain indicates the level of uptake of the polymer by the wood but it does not provide any information about the degree of distribution. IR spectra were therefore taken from four different depths of an individual wood specimen: the surface, core, between the surface and core along the grain and between the surface and core across the grain. This was done to be able to get an indication of how the polymer was distributed through the entire wood specimen. IR spectra of the two pure polymers were also compared (with each other and with a wood control).

4.4.9.2.1 TPA6 vs TPA7

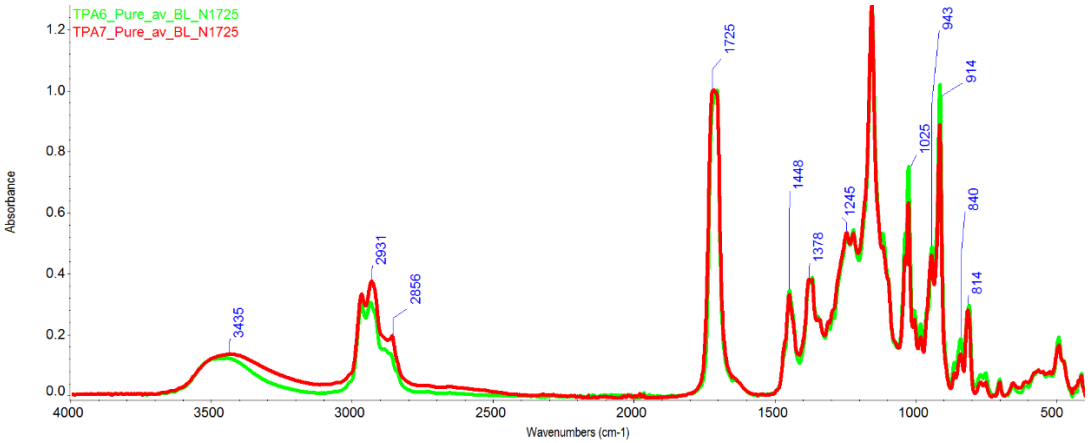

Figure 99. ATR-FTIR spectra of TPA6 (green) vs TPA7 (red). The spectra were normalised at 1725 cm^{-1}.

The spectra of the polymers were normalised at 1725 cm^{-1} (C=O bond). The spectra of the two polymers were almost identical to one another. This was expected as they are structurally very similar. The assignments of the annotated signals in Figure 99 are shown in Table 26. The major difference between the polymers was at 2856 cm^{-1}, where TPA7 had a more pronounced peak. This could be attributed to a C-H stretching vibration, possibly due to the oleic acid component of the copolymer.

Table 26. The FTIR peak assignments of the polymer TPA6 and TPA7

Band position (cm^{-1})	Assignment	Reference
3600 – 3200	-OH in H bond to sp^3 -O or -N	(Hesse, Meier and Zeeh, 1997)
2960 – 2850	C-H stretching vibration	
2890 – 2880	C-H bond	
1780 – 1710	C=O stretch	
1470 - 1430	C-H deformation vibration	
1410 – 1260	-OH deformation vibration	
1150 – 1040	C-O stretching vibration	
940 – 900	C=C bond	
840 – 790	C=C bond	

4.4.9.2.2 TPA6 and TPA7 vs archaeological wood

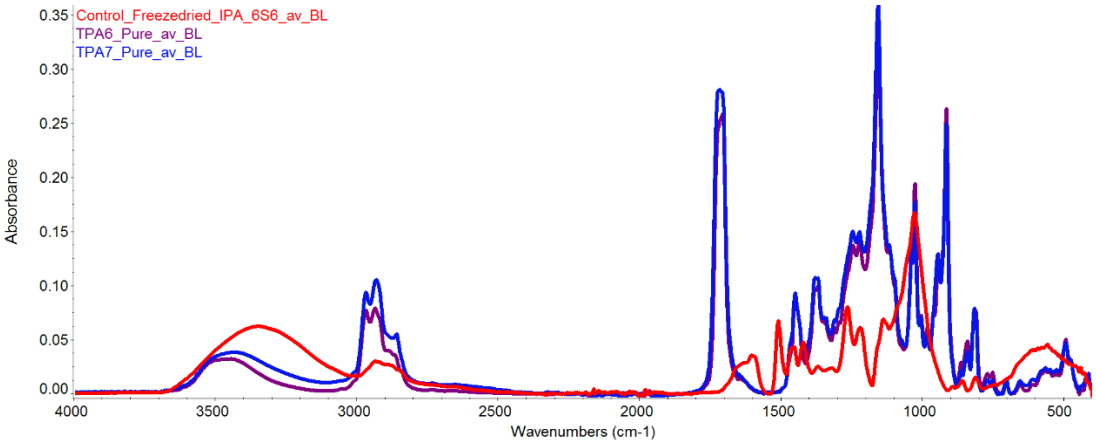

Figure 100. The spectra of the TPA6 (purple) and TPA7 (blue) vs archaeological wood (red; isopropanol immersed control 6.S.6). The spectra were not normalised.

The spectra of the two pure polymers were compared to those of a control specimen. This showed that both polymers were easily distinguishable from the wood, although some signals overlapped, such as at the 3500 – 3000 cm^{-1} region (Figure 100). The polymers had identifiable signals at 3000 – 2900 cm^{-1}, as well as at 1725 and 1154 cm^{-1} (assigned as C=O and C-O respectively). Due to these differences, it was expected that the polymers would be easily distinguished from the wood in the treated samples.

4.4.9.2.3 ATR-FTIR analyses of treated wood samples

The spectra of the different samples taken from each treated wood specimen were compared to those of an untreated, isopropanol-immersed control specimen to be able to distinguish the polymer signals. The spectra were normalised at the lignin peak at 1508 cm^{-1} as this was shared by all the samples.

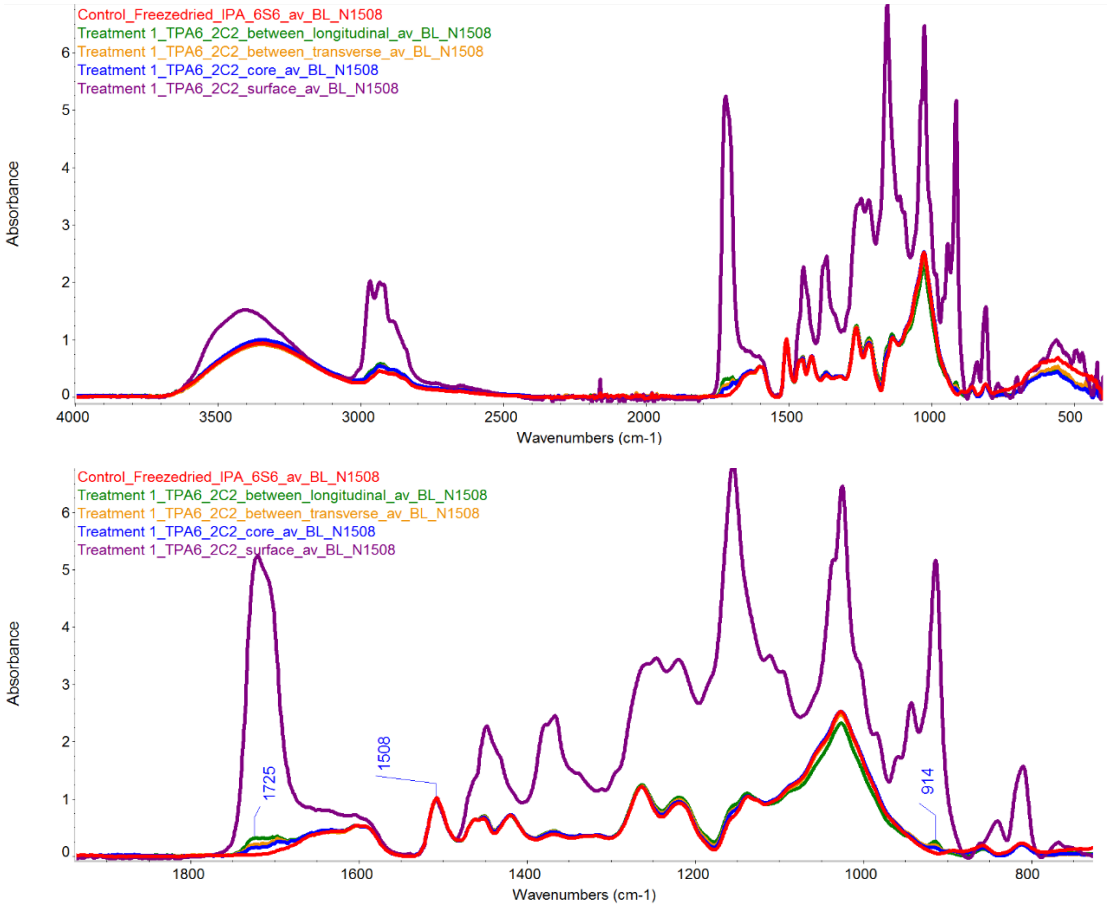

Figure 101. ATR-FTIR spectra comparison between the untreated, isopropanol-immersed control (red; 6.S.6) and a sample treated with TPA6 (2.C.2). The treated sample was measured at different depths: at the surface (purple), core (blue), between the surface and the core along the grain (green) and between the surface and the core across the grain (yellow). The top figure shows the overall spectra while the bottom focusses on the fingerprint region. The signals depicting polymer penetration are annotated. Spectra were normalised at 1508 cm^{-1}.

Figure 101 shows the spectra taken from a specimen treated with TPA6. The surface bands were very different from all the other samples, clearly showing a high concentration of polymer. The rest of the treated wood samples were more similar to the control sample, however they still showed a clear indication of polymer penetration. This was particularly seen at 1725 and 914 cm^{-1}. The spectra taken from the core of the treated specimen had the least absorbance. The samples taken from in between the surface and core absorbed less than the surface but more than the core. The sample taken along the grain had more absorbance than the one across the grain, as can be seen at both 1725 and 914 cm^{-1}. This was somehow expected

since it would be easier for the polymer to penetrate along the grain of the wood rather than across it.

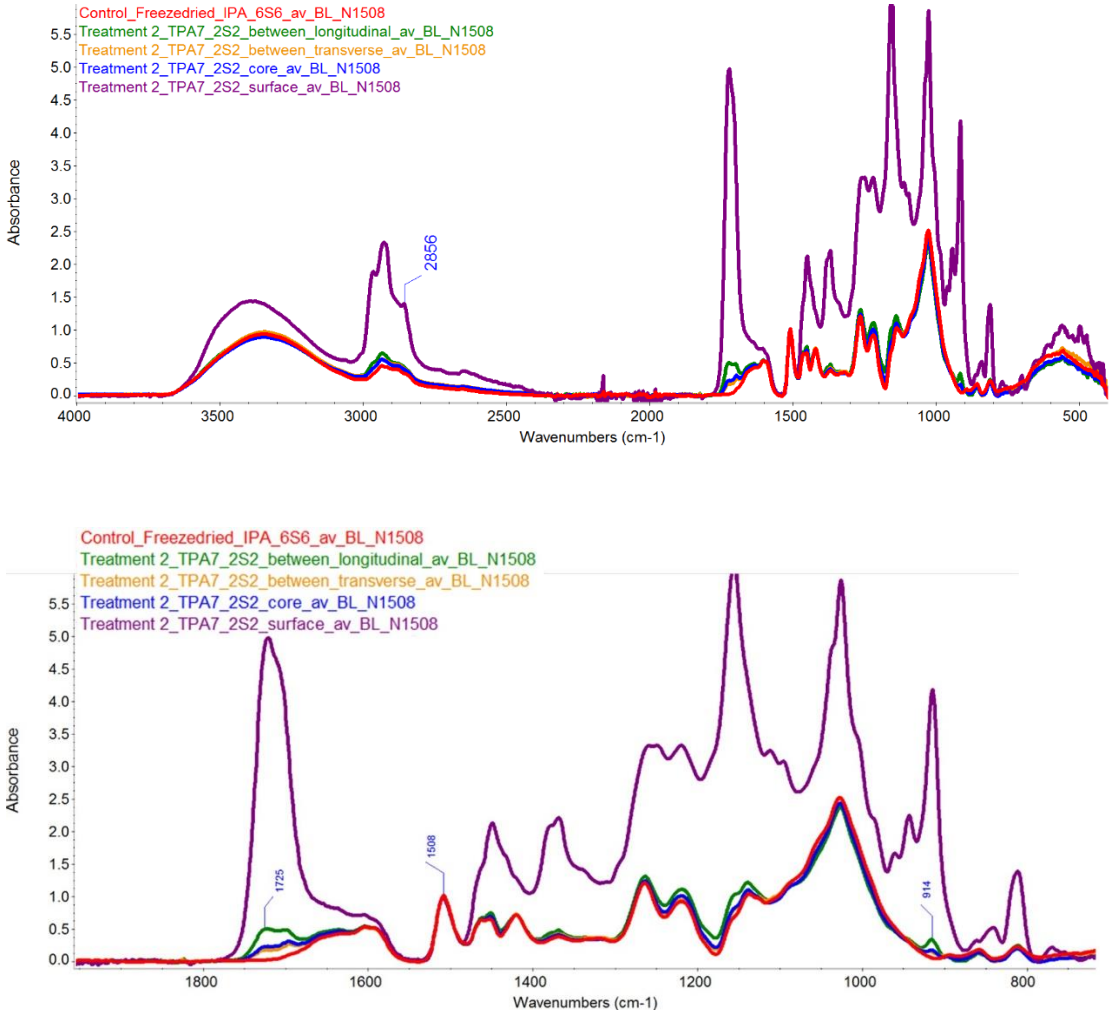

Figure 102. ATR-FTIR spectra comparison between the untreated, isopropanol-immersed control (red; 6.S.6) and a sample treated with TPA7 (2.S.2). The treated sample was measured at different depths: at the surface (purple), core (blue), between the surface and the core at the along the grain (green) and between the surface and the core at the across the grain (yellow). The top figure shows the overall spectra while the bottom focusses on the fingerprint region. The signals depicting polymer penetration are annotated. Spectra were normalised at 1508 cm^{-1}.

Figure 102 shows the spectra taken from a specimen treated with TPA7, compared to the untreated isopropanol-immersed wood. The level of distribution followed the same trend previously observed with the TPA6-treated samples, with the polymer

penetration increasing with increasing depth. As with the previous specimen, the in between samples showed a higher distribution of polymer along the grain than across it. In addition, the spectra of the TPA7-treated samples showed a signal at 2856 cm^{-1}. This was the peak which was previously used to distinguish between TPA6 and TPA7. This signal was seen to be the most intense with the surface sample, correlating with the observation that the polymer was deposited most abundantly at the surface of the wood specimen.

These observations confirmed that both polymers had the ability to penetrate to the cores of the wood samples. The highest concentration of polymer was found on the surface as was expected, with the spectra being almost indistinguishable from that of the pure polymer. Both TPA6 and TPA7 seemed to show preferential penetration along the grain of the wood. The decreasing degree of polymer penetration (both TPA6 and TPA7) could therefore be described as follows:

surface > between surface and core (along the grain) > between surface and core (across the grain) > core

4.4.10 SEM analyses

The SEM samples were carefully shaved with a razor in order to get a surface which was flat, enabling better visualisation of the wood cells. It was ensured that not too much material was shaved off from the surface, in order not to compromise the results. Latewood was primarily looked at, as opposed to earlywood. This is because generally, morphological changes appear more prominent in latewood due to its thicker cell walls. Sound wood was first compared to an archaeological wood control. The sound wood image showed that the cells clearly had a robust shape, with regular and thick cell walls. In contrast, the archaeological wood had cells which appeared ‘feathery’ and fragile, with very thin cell walls appearing to be mostly dislodged (Figures 103 and 104). This may be due to the loss of holocellulose which was previously demonstrated by the IR analyses.

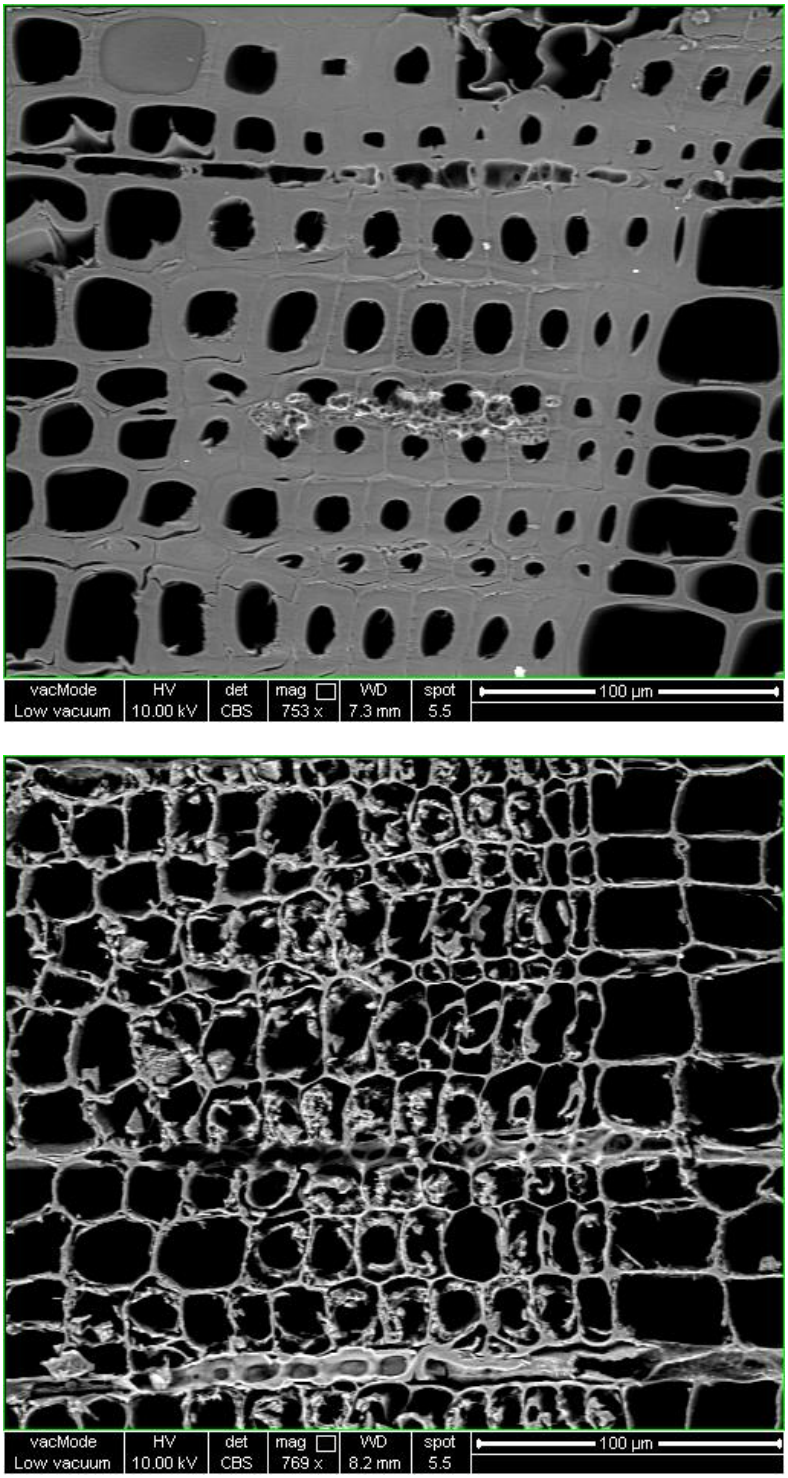

Figure 103. SEM images of sound pine (top) vs archaeological, isopropanol-immersed pine (bottom). The sound pine had regularly spaced cells with thick cell walls while the archaeological pine had lost most of its cellular structure.

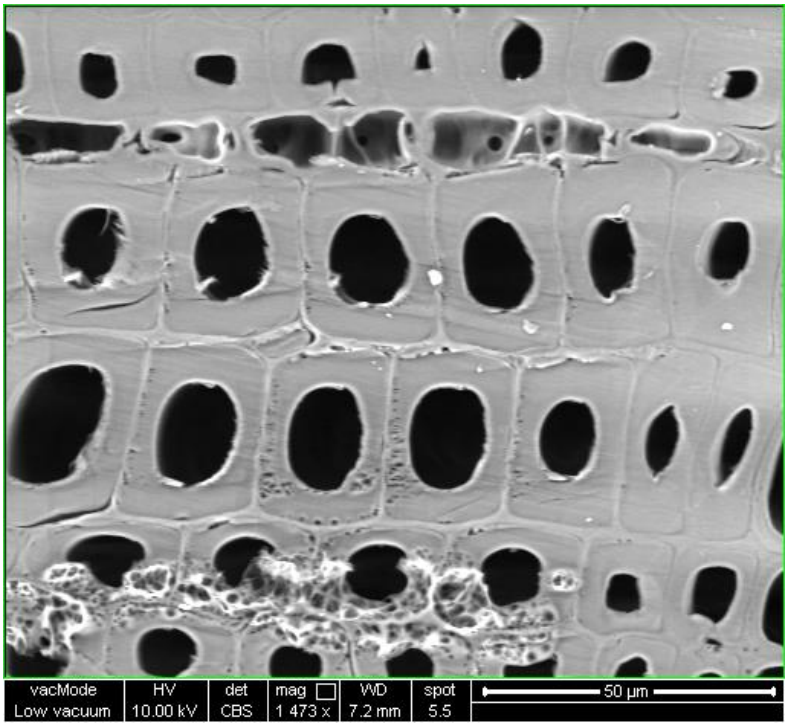

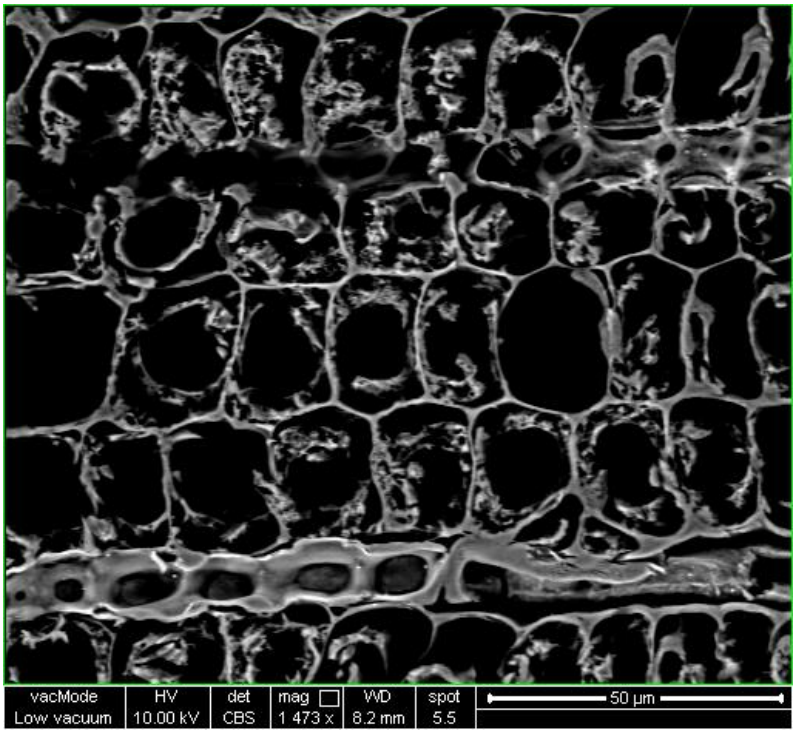

Figure 104. Higher magnification SEM images of sound pine (top) vs archaeological, isopropanol-immersed wood (bottom).

Samples from wood specimens treated with both TPA6 (Figures 105 and 106) and TPA7 (Figures 107 and 108) were taken. For each specimen, a sample was taken from the surface and the core. It should be noted that generally, it is difficult to identify organic polymers such as TPA6 and TPA7 from other organic materials such as wood with SEM. The specimens treated with both polymers showed similar results. The polymers were clearly visible in the surface samples, in some cases clogging the wood pores. The polymers were more difficult to discern in the samples taken from the cores. It could be noted however that the treated cores appeared to be less airy than the control sample, with some cells having slightly thicker cell walls. They also seemed to be less deformed and appeared to be able to withstand the shaving that was carried out on them more than the control, possibly indicating an increased resilience. It was however difficult to say for certain whether this was due to the presence of the polymer.

In general, the SEM analyses appeared to correlate with the IR results. The techniques showed that the highest concentration of both polymers was on the surface of the wood specimens. IR analyses indicated that the polymers managed to penetrate the cores of the specimens, albeit at a much lower concentration. This was difficult to observe with the SEM, but there were possible morphological changes that could perhaps indicate the presence of the polymers.

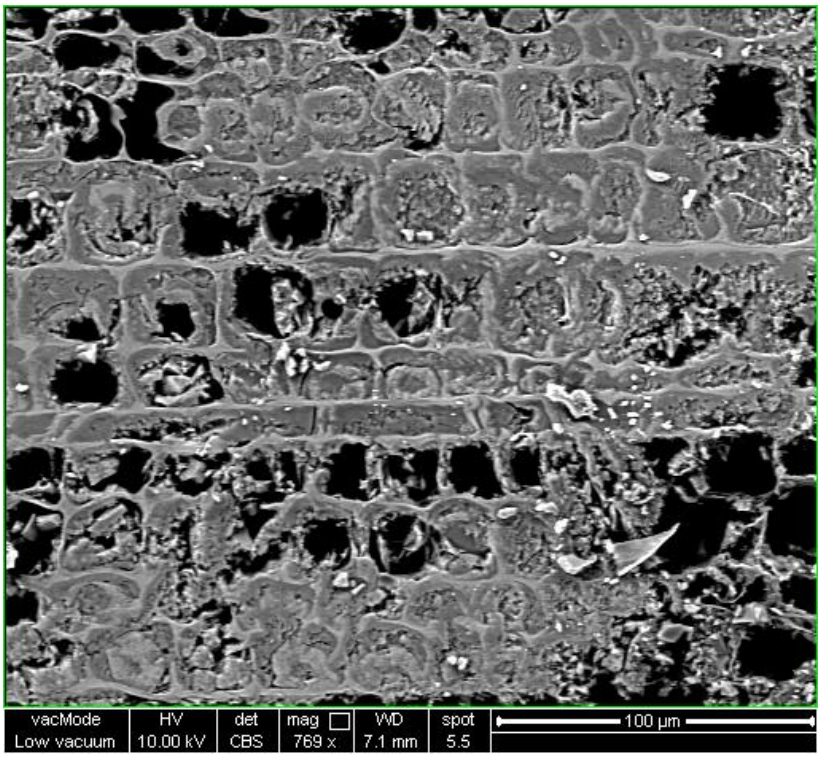

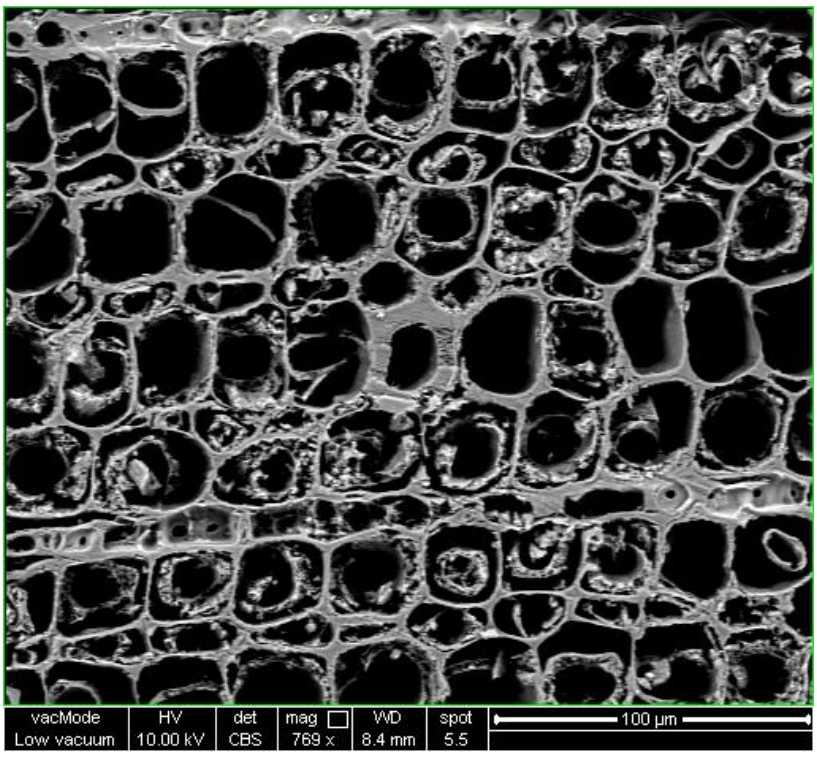

Figure 105. SEM images of samples treated with TPA6, taken from the surface (top) and core (bottom). The surface images show a high distribution of polymer, which filled many pores. The polymer was more difficult to observe in the core images, but the cells appeared to be more structurally sound than the untreated sample, indicating that it was present.

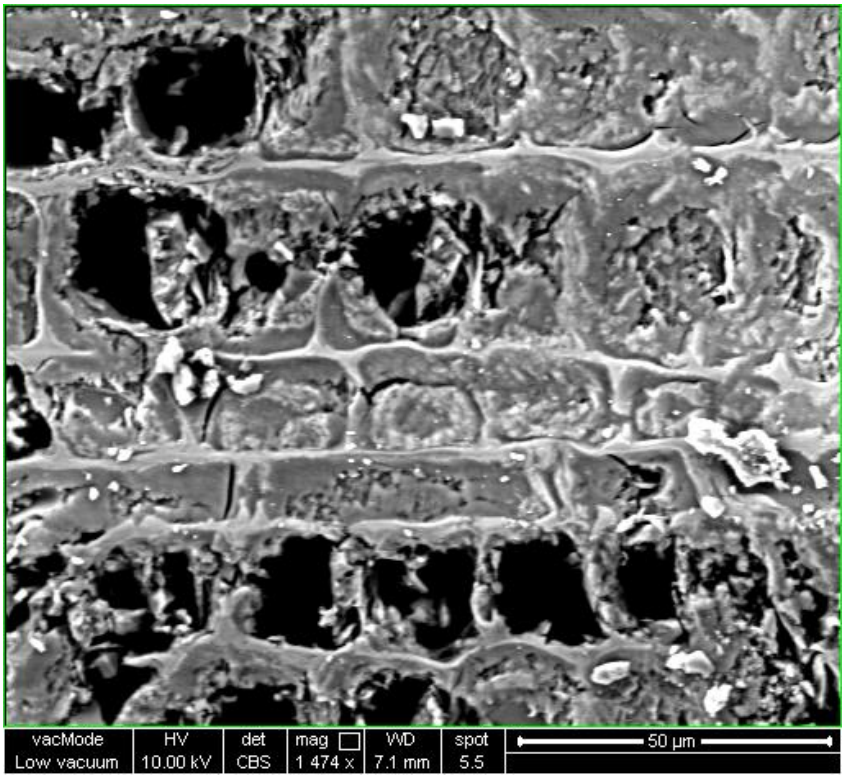

Figure 106. Higher magnification SEM images of samples treated with TPA6, taken from the surface (top) and core (bottom).

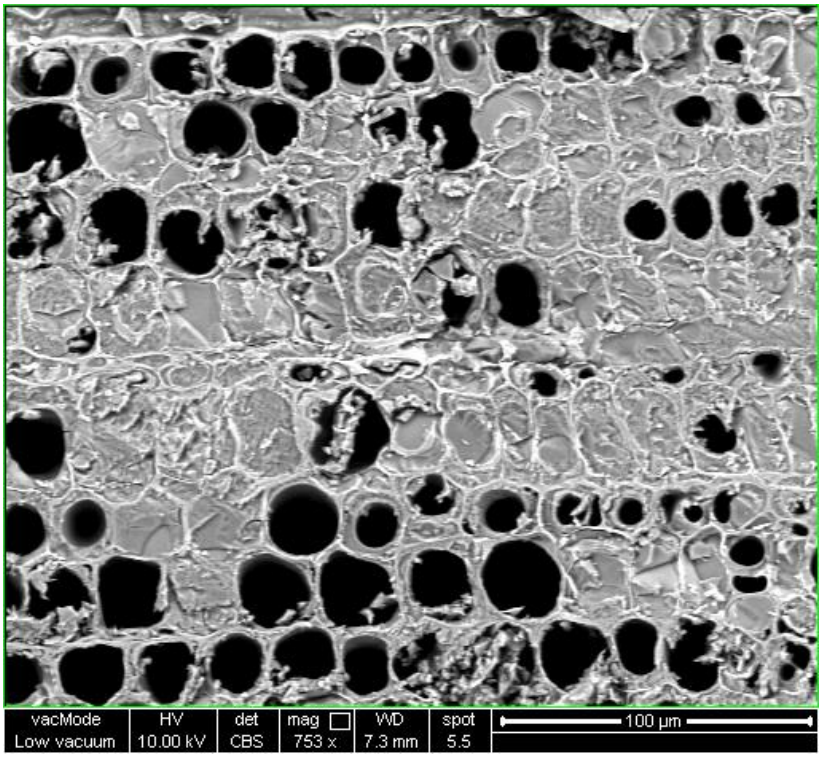

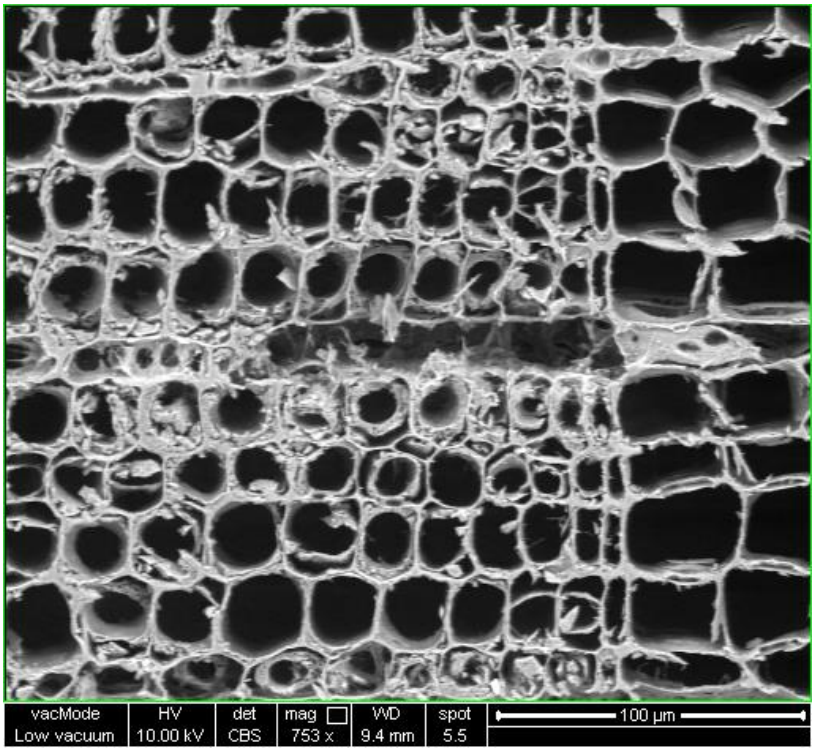

Figure 107. SEM images of samples treated with TPA7, taken from the surface (top) and core (bottom). The surface images showed a high distribution of polymer, filling many wood cells. Similarly with TPA6, the polymer was harder to distinguish in the core images, but it appeared that the remaining cell walls were better preserved than in the control, indicating polymer presence.

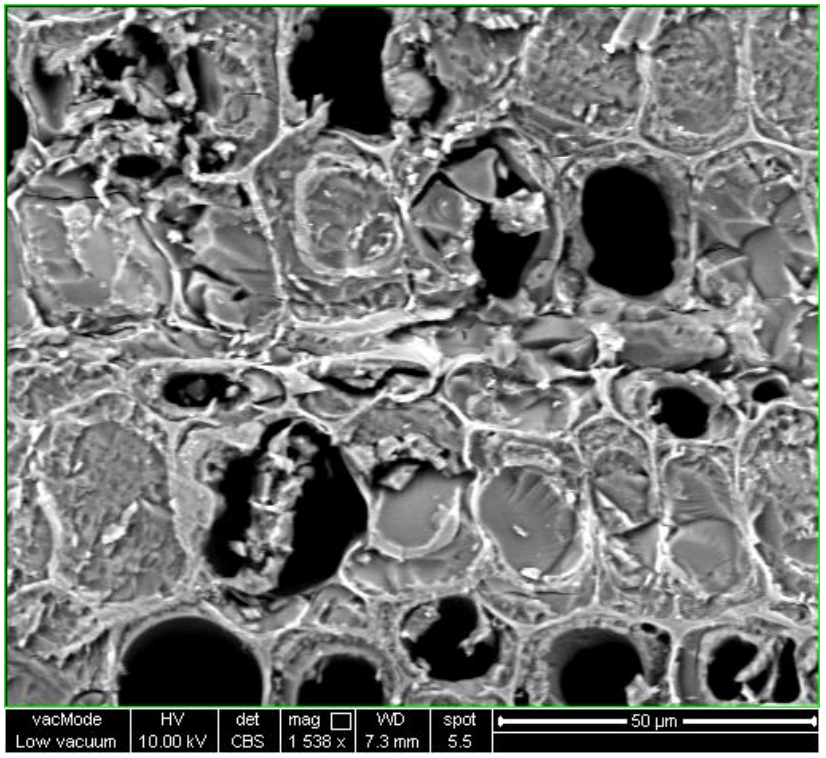

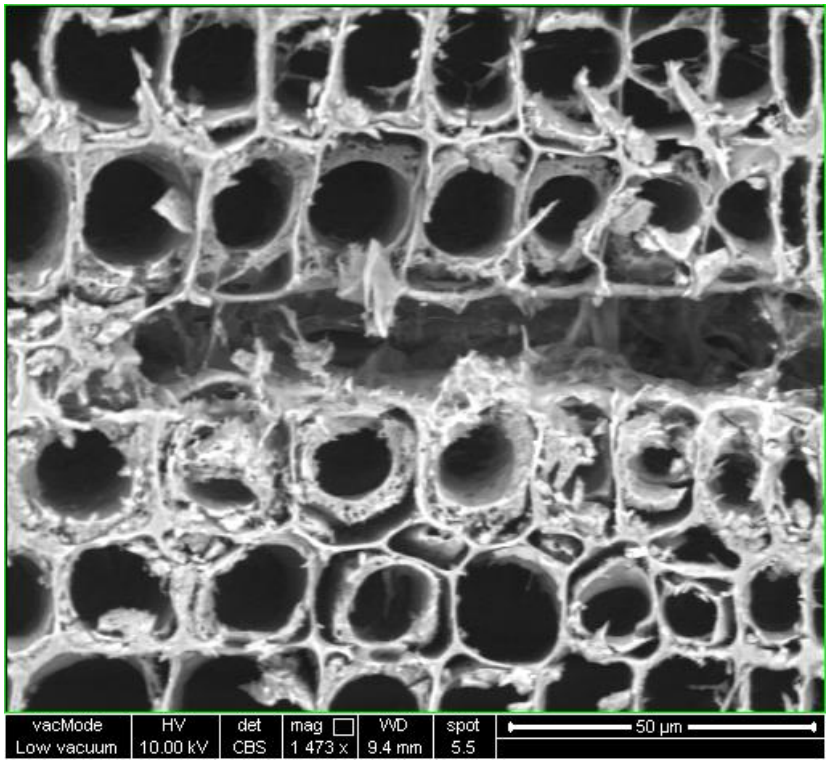

Figure 108. Higher magnification SEM images of samples treated with TPA7, taken from the surface (top) and core (bottom).

4.4.11 Resistance to indentation (hardness test)

A hardness test was undertaken using a fruit penetrometer in order to get an indication of the extent of consolidation that the polymers conferred. The fruit penetrometer measures the wood's resistance to indentation. A sample of sound pine was measured first. Specimens from control group 2 (freeze-dried only) and control group 3 (freeze-dried and immersed in isopropanol) were measured five times on the tangential surface. Specimens from both TPA6 and TPA7 treatment groups were measured five times on the tangential surface. In addition, each treated specimen was split in half and two measurements were taken from the core. The multiple measurements taken from every specimen were then averaged (Figures 109 and 110).

From the averaged values, one could see that there seemed to be an increase in the surface hardness of the treated specimens compared to the control. Conversely, the core hardness did not appear to change in the treated groups. Statistical analyses were carried out to determine whether any of the observed changes were significant. This was done using the individual measurements instead of the averaged values.

There were 25 measurements on freeze-dried controls and 25 measurements on isopropanol-treated controls. An independent-samples t-test was first run to determine if there were differences in hardness between the two control groups (Figure 111). One outlier was identified in the data, as assessed by inspection of a boxplot. This outlier was not removed as it was thought that it would not have an appreciable effect on the result. Hardness scores for the control groups were normally distributed, as assessed by Shapiro-Wilk's test ($p > 0.05$), and there was homogeneity of variances, as assessed by Levene's test for equality of variances ($p = 0.977$). Data is presented as mean ± standard deviation. The isopropanol-treated controls were harder (59.0 ± 7.8) than the freeze-dried only controls (55.3 ± 8.1), with a difference of 3.78 which was not statistically significant (95% CI, 0.00 to 8.32), $t(48) = 1.673$, $p = 0.101$.

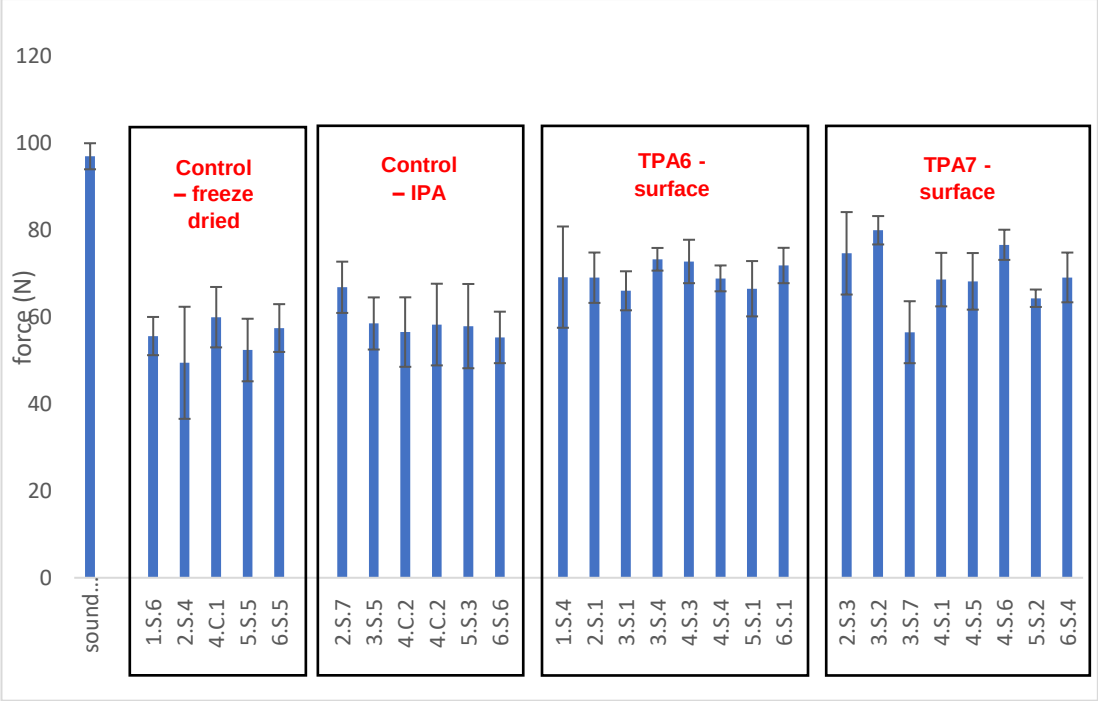

Figure 109. A comparison of the results from the hardness tests. For the treatment groups, only the values obtained from the surface measurements are depicted.

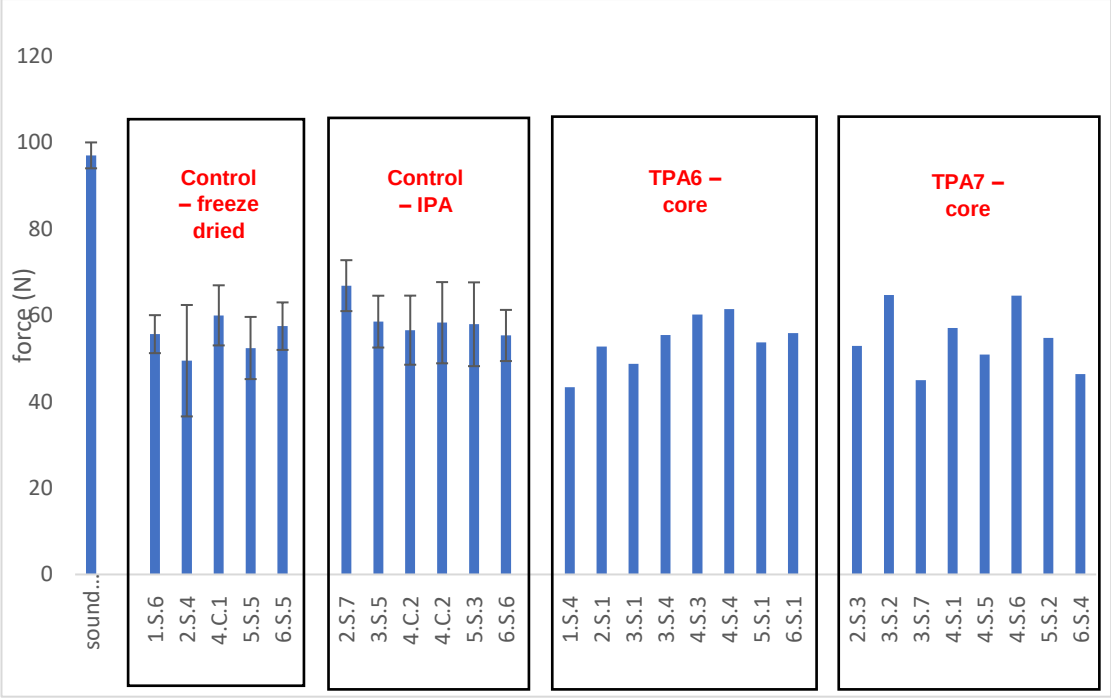

Figure 110. A comparison of the results from the hardness tests. For the treatment groups, only the values obtained from the core measurements are depicted.

The second round of analyses involved comparing the surface hardness of treatment groups with the control group, using a one-way ANOVA (Figure 112). The control group was made up of both the freeze-dried and isopropanol-treated controls. This was justified since the difference in means between the two groups was not significant. There were 40 values in the control, 40 values in the TPA6 treatment group and 40 values in the TPA7 treatment group. There were two outliers in the TPA6 treatment group, as assessed by a boxplot. It was decided to not remove these from the dataset. The data was normally distributed except for the TPA7 group, as assessed by the Shapiro-Wilk test ($p > 0.05$). However, the one-way ANOVA is known to be robust to deviations from normality, especially if the sample sizes are equal (as was the case here) (Lix, Keselman and Keselman, 1996). Homogeneity of variances was violated, as assessed by Levene's Test of Homogeneity of Variance ($p = 0.025$). The hardness score was statistically significantly different for the sample groups, Welch's $F(2, 1641.693) = 33.258$, $p < 0.001$. The hardness increased from the control (58.7 ± 6.8) to the TPA6 treatment group (69.8 ± 6.4), and the TPA7 treatment group (69.8 ± 8.9). Games-Howell *post hoc* analysis revealed that the increase from the control to the TPA6 treatment group (11.0875, 95% CI (7.561 to 14.614)) was statistically significant ($p < 0.001$), as well as the increase in hardness for the TPA7 treatment group (11.1050, 95% CI (6.855 to 15.355), $p < 0.001$). The difference between both treatment groups was not statistically significant (0.0175, 95% CI (0.0 to 4.174), $p = 1.00$).

The third round of analyses was carried out to compare the core hardness of the treatment groups with the control group (Figure 113), again with a one-way ANOVA. There were 16 values in the control, 16 values in the TPA6 treatment group and 16 values in the TPA7 treatment group. There were two outliers in the TPA6 treatment group, as assessed by a boxplot. It was decided to not remove these from the dataset. Hardness scores for the groups were normally distributed, as assessed by Shapiro-Wilk's test ($p > 0.05$), and there was homogeneity of variances, as assessed by Levene's test for equality of variances ($p = 0.471$. The hardness scores were as follows: the control was 57.9 ± 7.2, the TPA6 treatment group was 53.9 ± 6.9, and the TPA7 treatment group was 54.5 ± 7.6. The hardness score was not found to be statistically significantly different between the sample groups, $F(2, 45) = 1.374$, $p < 0.264$.

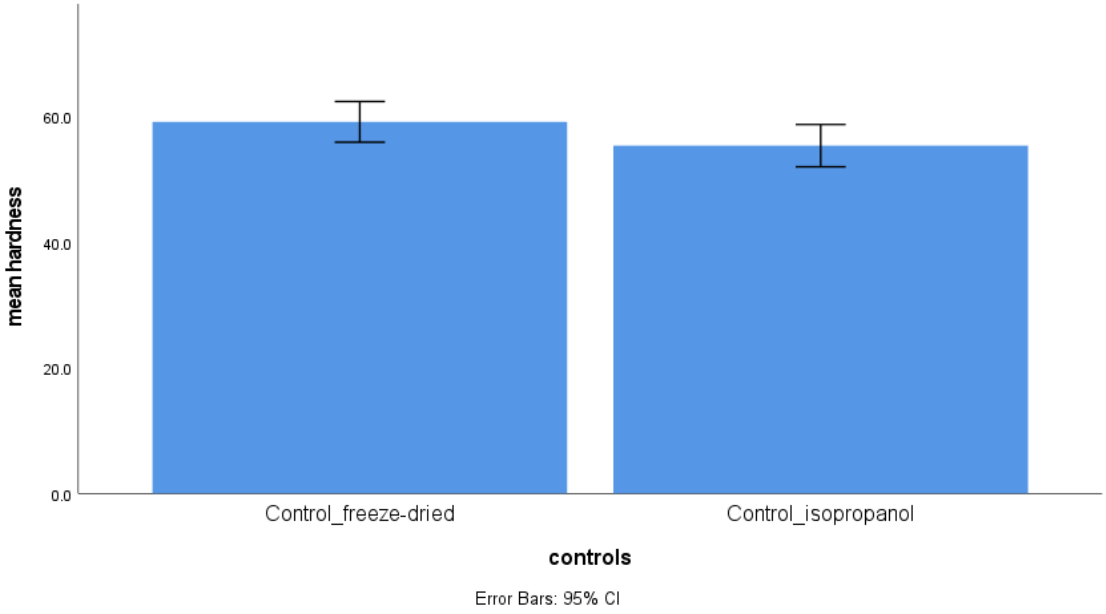

Figure 111. Results for the independent t-test run on the two control groups.

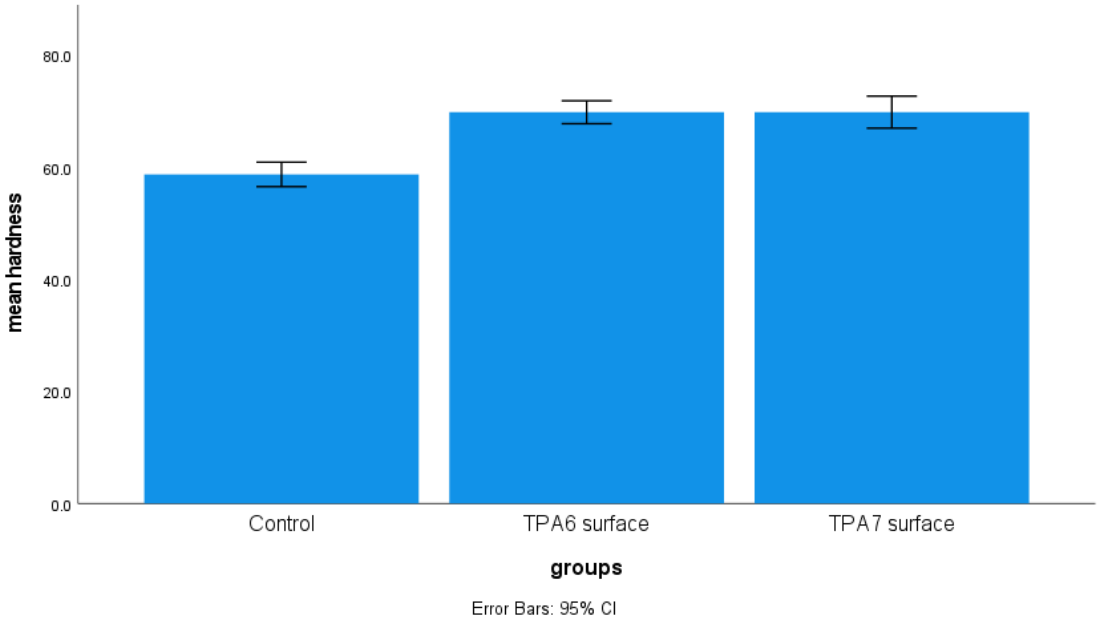

Figure 112. Results for the one-way ANOVA run on the treatment groups surface measurements.

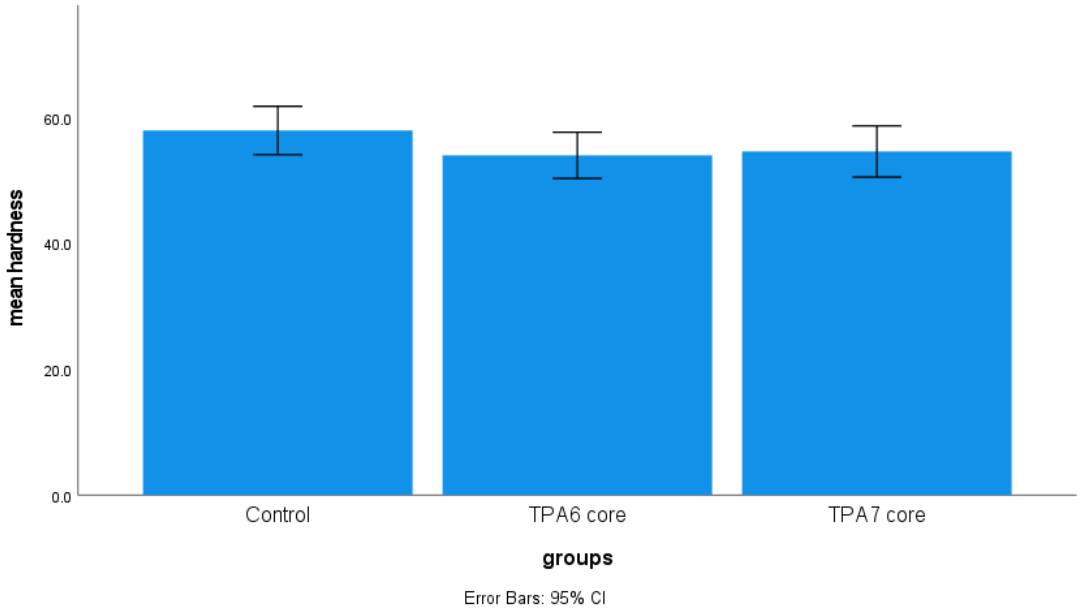

Figure 113. Results for the one-way ANOVA run on the treatment groups core measurements.

These analyses indicated that the polymers imparted a clear increase in surface hardness, possibly making the wood more resistant to stresses caused by handling or the environment. Both TPA6 and TPA7 seemed to increase the hardness to the same extent, as there was no statistical difference between them. Conversely, the core hardness of the treated samples did not significantly change after treatment but this was expected, as there was only a small amount of polymer present compared to the surfaces.

4.5 Conclusion

This study aimed to determine the extent of penetration of two terpene-derived polymers, TPA6 and TPA7. This was carried out by monitoring weight and dimensional change, as well as ATR-FTIR supplemented with SEM. Other tests were carried out in order to observe the effects that the polymers have on the wood. These

included colour change measurements, pH measurements and hardness tests. Archaeological pine wood was used for these studies and isopropanol served as the primary solvent.

Generally, all the treated specimens increased in weight, indicating polymer uptake. Dimensional changes were also recorded for all specimens, though these were not deemed significant. The colour of the wood treated with both polymers was slightly darker, with a yellowish tinge. pH measurements indicated that the treated wood did not become more acidic during treatment. ATR-FTIR showed that the polymers penetrated the wood, with the highest concentration observed on the surface of the cubes. This was confirmed by SEM. The polymers also successfully penetrated the core of the wood specimens, although to a much lesser extent. Hardness tests proved that the surfaces of the treated cubes were significantly harder than the controls. The differences between the two treatment groups were not significant and this was seen throughout all the tests that were carried out. Because of this, TPA6 should be favoured over TPA7 since its synthesis possesses fewer steps and is therefore less time-consuming to make.

The general scope of this study can be expanded in future work. A new, more accurate method of measuring dimensional change should be developed. A possible idea is to make markings on the wood with a pen before treatment, and then measure the dimensional changes with a technical ruler as opposed to callipers. Different concentrations of polymer can be used to determine whether this makes a difference in the extent of penetration to the core. The immersion time can also be prolonged as this may also potentially increase the amount of polymer that manages to penetrate. Other different methods of polymer administration can be explored, such as injection. Additionally, these tests would be run using higher sample numbers in order to increase the robustness of these studies.

Long-term stability studies on the polymers both in their pure form and after penetration in the wood should be carried out. The interactions between the polymers and the other components present in the wood should also be taken into consideration. These include the alum, inorganic ions (such as iron ions) and the $Ca(OH)_2$ nanoparticles. One way to do this is by monitoring a set number of parameters over time, such as pH and molecular weight.

Chapter 5. Characterisation of Butvar® B-98 and PDMS-OH

5.1 Introduction

In this chapter the characterisation of two commercially available polymers, Butvar® B-98 and hydroxy-terminated polydimethylsiloxane (PDMS-OH), is described. In addition to the work pertaining to terpene-derived polymers, part of this project also consisted of characterising consolidants which are already in use in the conservation field and currently being considered as candidates for the treatment of the Oseberg artefacts. These two materials are presently being appraised as non-aqueous options for the retreatment of part of the Oseberg collection.

The performance of a wood consolidant depends not only on its chemical composition but also on its physical properties notably molecular weight, molecular weight distribution, conformation and T_g, all of which affect its ability to penetrate through the wood and form stable networks with wood components. With this research, it was hoped that the information currently available for Butvar® B-98 and PDMS-OH would be extended or reinforced, thereby assisting an archaeological wood conservator in their choice of the appropriate material.

This level of characterisation of these two consolidants, in terms of size distribution, molecular weight and conformation, has never been carried out according to the available literature and it was anticipated that such data would prove to be very useful when it comes to deciding which consolidants to choose for the retreatment of the Oseberg artefacts. Moreover, it will also be helpful to other future conservation projects which have similar predicaments to the Saving Oseberg project.

The work described in this chapter has been published in a peer-reviewed journal (Cutajar, Stockman, *et al.*, 2022).

5.1.1 Butvar® B-98

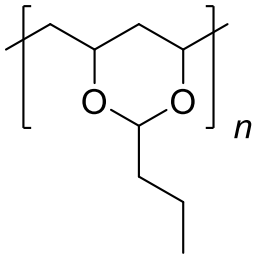

Figure 114. The chemical structure of Butvar® B-98

Butvar® B-98 is a polyvinyl butyral-based resin (Figure 114) produced by the reaction of polyvinyl alcohol with butyraldehyde (Spirydowicz *et al.*, 2001; Fernández, Fernández and Hoces, 2006). It has been widely investigated as a consolidant for archaeological wood and other materials and has already been used as a conservation treatment for archaeological artefacts.

Some of the earliest investigations into its consolidative properties involved wooden objects excavated from tombs dating back to the 8th century BCE in Gordion, Turkey (Spirydowicz *et al.*, 2001). In 1982, samples from these artefacts were consolidated with Butvar® B-98 in toluene and ethanol. After drying it was shown that the wood had undergone little or no shrinkage and minimal colour change. It should be noted that unlike the Oseberg findings, these artefacts were not found in a waterlogged environment. Spirydowicz *et al*. reported that treating samples with 10% Butvar® B-98 resulted in stabilisation without any significant micromorphological changes to the structure of the wood (Spirydowicz *et al.*, 2001). Using SEM, it was confirmed that while the Butvar® B-98 filled some of the cell lumina, it commonly only coated the surfaces.

It has also been tested as a treatment for wooden statues from Ancient Egypt (Davis *et al.*, 2021). The treated samples showed improved cohesion of the wood. Additionally, it also acted well as an adhesive for the topmost fragmented paint layer of the statues and for detached wood fragments, leaving a less glossy finish when compared to other materials which were tested.

Apart from wood, Butvar® B-98 has also been used to treat other materials, an example being a Minoan woven basket found in Crete (Paterakis, 1996). This consolidation was deemed to be successful, as it imparted sufficient strength and did not drastically alter the colour. It has also been used in the treatment of archaeological bone where several advantageous properties were noted such as a matte finish, short drying period and quick penetration (Kres and Lovell, 1995).

It has been suggested that Butvar® B-98 should be used as a supplement to other consolidants like Paraloid™ B-72 (Schmidt, Shugar and Ploeger, 2017) due to its T_g (72 – 78 °C), which enables it to be used in higher temperatures (Spirydowicz *et al.*, 2001; Schmidt, Shugar and Ploeger, 2017). However, although Butvar® B-98 appears to be stable with good aging properties (Johnson, 1994), there are no long-term studies regarding its reversibility (Davis, Roberts and Poli, 2021). Other combination treatments which have been investigated include those with carboxymethyl cellulose poly(ethyl) acrylate in the treatment of historical paper, as Butvar® B-98 is known to increase the mechanical strength of paper by promoting the inter fibre bonding between the cellulose chains (Noshy, Hassan and Mohammed, 2022).

With regards to the Oseberg wood, Butvar® B-98 is currently being investigated as a possible non-aqueous treatment by the Saving Oseberg group. It has been found to successfully decrease both radial and tangential shrinkage of the archaeological wood (Zisi *et al.*, 2021). Additionally, it did not appear to fill the wood pores when viewed with SEM and there was not as drastic colour change (Figure 115).

Before treatment **After treatment**

Figure 115. Wood fragment from the Oseberg collection before and after retreatment by immersion with Butvar® B-98 in a mixture of 60%/40% toluene/ethanol mixture and $Ca(OH)_2$ nanoparticles. The fragment had originally been treated with alum and linseed oil upon excavation (Museum of Cultural History, University of Oslo).

5.1.2 Silicone-based consolidants

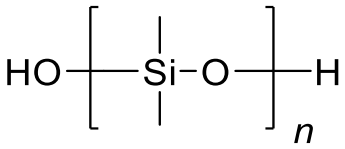

Figure 116. The chemical structure of PDMS-OH

Polymers based on silicon possess great potential for conservation as they have a number of desirable properties. These include hydrophobicity, high chemical and temperature resistance and minimal flammability (Kavvouras *et al.*, 2009). In order to access these properties, the polymers need to form a macromolecular network *via* crosslinking (Kavvouras *et al.*, 2009). To this end, silanol groups can be condensed to form siloxane bonds. These siloxane consolidants are often mixed with a solvent, either organic or aqueous, in order to form a hydrophobic resin (Cnudde *et al.*, 2007). After mixing, the solvent will evaporate and non-polar groups (such as methyl groups) will increase its hydrophobicity, which in turn prevents deterioration (Cnudde *et al.*, 2007).

The use of silicone-based compounds as consolidants has long been considered, with a patent in 1980 (von Hagens, 1980) describing the preservation of animal and vegetable tissue with a silanol-based synthetic resin. A much more recent patent (Klosowski, Smith and Hamilton, 2004) concerns the conservation of materials, especially ancient artefacts, using silanol-based polymers crosslinked with trialkoxysilanes. Kavvouras *et al*. investigated the use of silanol-terminated polydimethylsiloxane, together with a catalyst and a crosslinker, for conserving archaeological waterlogged wood from the Neolithic period (Kavvouras *et al.*, 2009). The process resulted in the formation of a three-dimensional polysiloxane network which effectively protected against shrinking of the wood cells, whilst retaining the appearance of natural wood. Some concerns remained involving the irreversibility of

the procedure and the safety of certain substances that were used, such as turpentine and MTES.

In addition to wood, silicone-based treatments have also been studied as a consolidative treatment for stone (Cnudde *et al.*, 2007; Ksinopoulou, Bakolas and Moropoulou, 2016; Briffa and Vella, 2019; Ershad-Langroudi, Fadaei and Ahmadi, 2019), concrete (Kapetanaki *et al.*, 2020) and terracotta (Han *et al.*, 2016).

The use of PDMS-OH (Figure 116) has been evaluated by the Saving Oseberg group as a possible retreatment option for the artefacts (Figure 117). PDMS-OH has been combined with $Ca(OH)_2$ nanoparticles and PGMS to create a hybrid system which was shown to increase the pH of alum-treated wood and also to decrease the amount of powdering upon handling (Andriulo *et al.*, 2017).

Figure 117. Wood fragment from the Oseberg collection before and after retreatment by injection with PDMS-OH (36,000 Da) in turpentine (5% concentration) and $Ca(OH)_2$ nanoparticles. The fragment had originally been treated with alum and linseed oil after excavation. The fragment was injected for a period of 11 days and then left to dry for 34 days (Museum of Cultural History, University of Oslo).

Another system that was tested was instead made up of PDMS-OH, methyltrimethoxysilane (MTMOS) (as a cross-linker) and dibutyltin-diacetate (DBTDA) (as a catalyst) (Zisi *et al.*, 2021). This involved impregnating the wood with the PDMS-OH and DBTDA, and then subjecting it to a two-stage curing process. MTMOS was added during the first stage in a dry environment, thus preventing its

self-polymerisation. During the second stage, the wood was exposed to a high RH environment, which promoted cross-linking. This treatment caused minimal colour change and it was also capable of bulking up the cell walls, improving its consolidative effect. In contrast to Butvar® B-98, SEM analyses indicated that it filled some of the wood lumina, which could prove problematic should it need to be removed in the future.

Recent research has been published reporting on the consolidative ability of a hybrid system made up of PDMS-OH and TEOS or MTES, combined with $Ca(OH)_2$ nanoparticles (Andriulo *et al.*, 2022). This system used a sol-gel process and was tested on both fresh and Oseberg wood. The sol-gel process involves the formation of silanols from alkoxysilanes, which then undergo condensation to produce gels made of silica colloidal particles (Andriulo *et al.*, 2017). It was anticipated that the elasticity introduced by the PDMS-OH could improve the gel's resistance towards strain produced by capillary pressure. PDMS-OH chains are postulated to be able to react to external pressure by curling or uncurling, thus leading to their elastic nature. This is due to the ability of the non-bridging groups CH_3-Si-CH_3 to rotate around the Si-O-Si bond.

The authors were hoping that the alum salts found in the Oseberg wood could act as catalysers for the hydrolysis and condensation reactions of TEOS and MTES (Andriulo *et al.*, 2022). IR analyses indicated that the Si-OH bond in PDMS-OH can copolymerise with the Si-OH bond of TEOS or MTES, increasing the robustness of the polymer network in the wood. Additionally, there could have been co-condensation between the TEOS or MTES monomers and PDMS-OH. Mechanical tests carried out with a fruit penetrometer showed that the treated wood retained its resistance level, but the treatments did not seem to increase its hardness. The hybrid system composed with MTES appeared to show the most promising results, with better wood penetration and the least colour change.

Table 27 shows an overview of the known advantageous and disadvantageous properties of Butvar® B-98 and PDMS-OH when used as consolidants, derived from a literature review.

Table 27. Overview of the advantageous and disadvantageous properties of Butvar® B-98 and PDMS-OH as consolidants

Consolidant	Advantages	Disadvantages
Butvar® B-98	Causes minimal colour change (Paterakis, 1996; Spirydowicz *et al.*, 2001) Only minimal filling of cell lumina (Spirydowicz *et al.*, 2001) Can be used in combination with other consolidants in hot climates (Schmidt, Shugar and Ploeger, 2017) Does not cause wood to undergo shrinkage (Spirydowicz *et al.*, 2001) Has a matte finish, a short drying period and quick penetration (Kres and Lovell, 1995)	Not derived from sustainable sources No long-term studies on reversibility (Davis *et al.*, 2021)
PDMS-OH	May cause minimal colour change (Zisi *et al.*, 2021) Hydrophobic and chemically resistant (Kavvouras *et al.*, 2009) Can react with monomers to form a polymer network in wood (Andriulo *et al.*, 2022) Can bulk up cell walls (Zisi *et al.*, 2021) May aid in decreasing powdering of archaeological wood (Andriulo *et al.*, 2017)	Not derived from sustainable sources Fills up some cell lumina (Zisi *et al.*, 2021) Preparations make use of toxic solvents (Kavvouras *et al.*, 2009)

5.2 Aims and objectives

The overall aim for the work described in this chapter was to perform an extensive characterisation of Butvar® B-98 and four different preparations of PDMS-OH. This was to be carried out primarily by AUC, supplemented with viscometry. Through these experiments, a more thorough understanding of these consolidants could be obtained which would aid in understanding any past and future studies involving these polymers in wood.

5.3 Results and discussion

5.3.1. Butvar® B-98

The experiments with Butvar® B-98 were all carried out using isopropanol as the primary solvent. As a result of the previous studies described in Chapter 3, it was already known that this solvent worked well in AUC experiments and provided reliable results. The Saving Oseberg group had carried out their investigations with Butvar® B-98 in a toluene/ethanol mixture, however this solvent system was not considered appropriate for use in the analytical ultracentrifuge due to risk of damaging the centrepieces. Isopropanol was deemed a good alternative.

5.3.1.1 SV

Figure 118 shows the sedimentation coefficient distribution *c(s)* vs *s* of Butvar® B-98 in isopropanol, analysed using the algorithm SEDFIT (Schuck, 2000; Dam and Schuck, 2004). The analysis revealed a material of low sedimentation coefficient (<1 S) and close to the lowest limit of the technique (~ 0.4 S). Low sedimentation coefficients are a feature of either low molecular weights, extended conformations or a combination of both. Two peaks were distinguishable at ~ 0.4 – 0.5 S and ~ 0.7 – 0.8 S.

SEDFIT enables normalisation of the sedimentation coefficient to standard conditions (density and viscosity of water at 20.0 °C) for comparative purposes (Tanford, 1961). The normalised sedimentation coefficients ($s_{20,w}$) for the two observed peaks were then plotted against concentration (Figure 119). The extrapolated $s_{20,w}$ values were (0.40 ± 0.02) S and (0.65 ± 0.02) S. These values are considered to be on the lowest limit of sedimentation coefficient measurement.

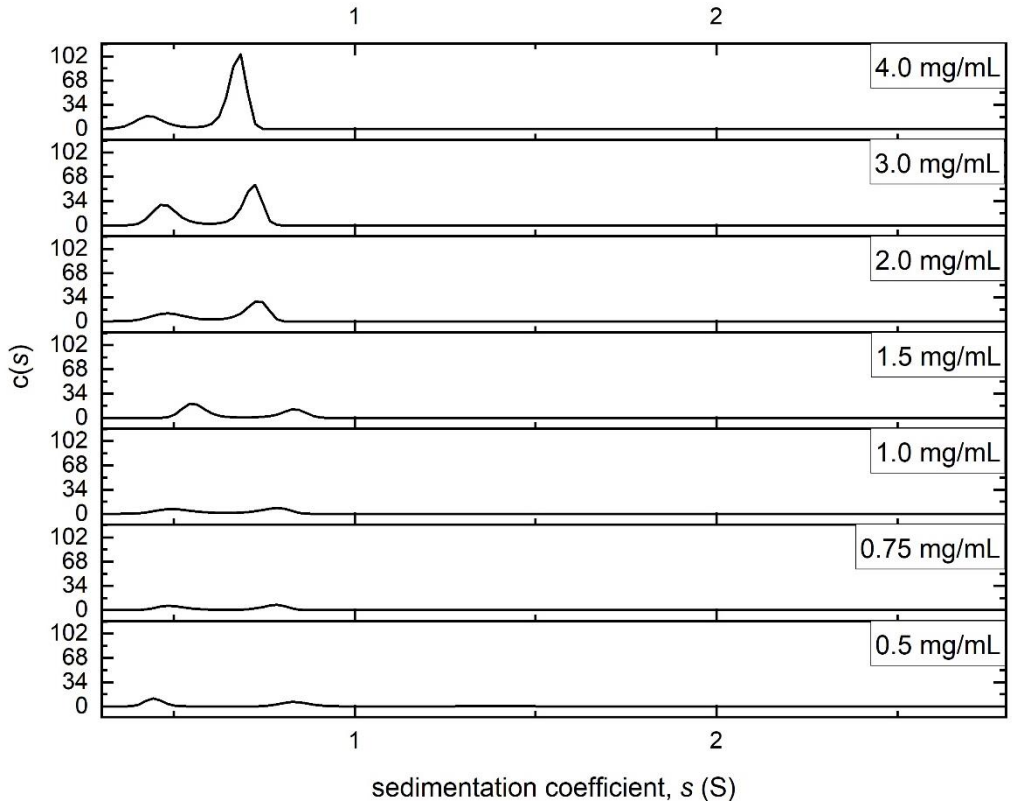

Figure 118. Sedimentation coefficient distributions of Butvar® B-98 at different loading concentrations in isopropanol. Rotor speed = 49,000 rpm, temperature = 20.0 °C.

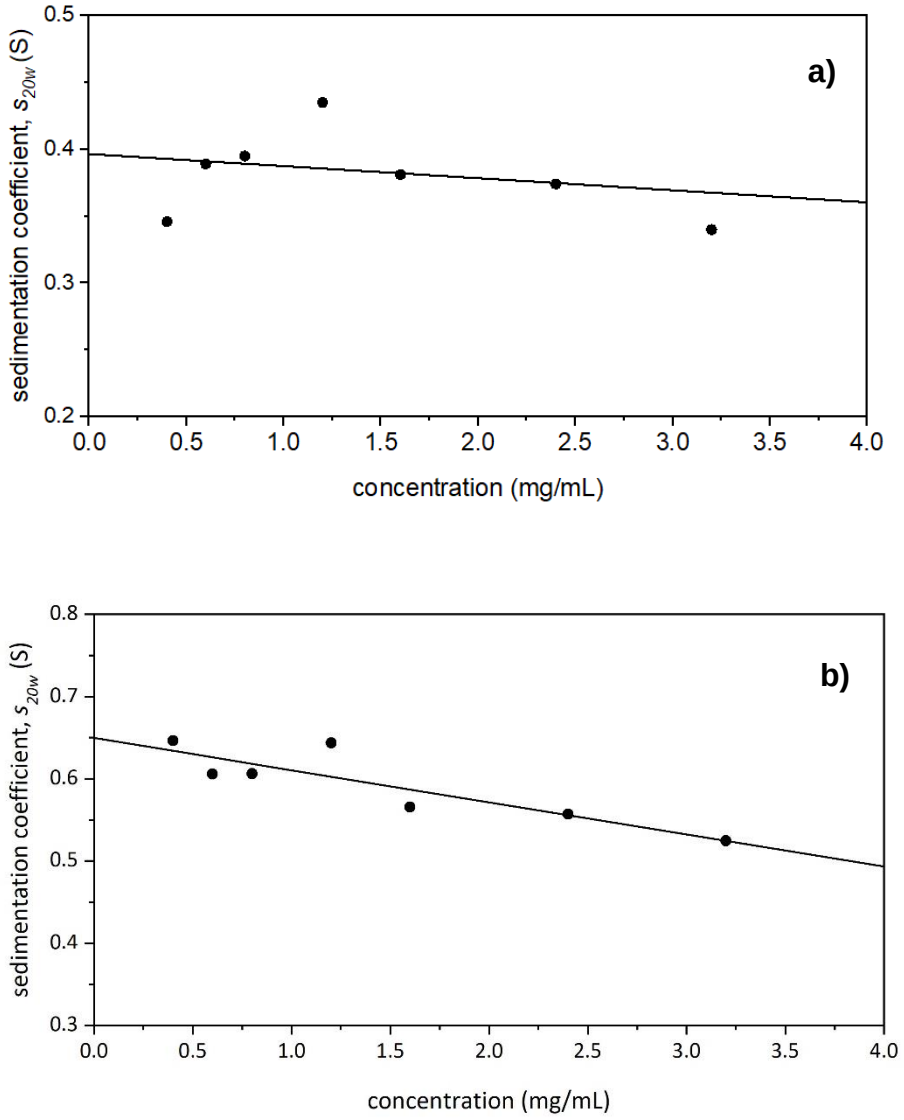

Figure 119. Dependence of $s_{20,w}$ on sedimenting concentration (corrected for radial dilution) for Butvar® B-98. a) Slower component $s_{20,w}$ = (0.40 ± 0.02) S; b) Faster component $s_{20,w}$ = (0.65 ± 0.02) S.

5.3.1.2 SE

SE experiments were then performed in order to determine the M_w. The algorithm SEDFIT-MSTAR (Schuck *et al.*, 2014) was used to evaluate the $M_{w,app}$ at cell loading concentrations ranging from 0.5 mg/mL (the minimum concentration required to give an adequate concentration distribution at SE) to 4.0 mg/mL (Table 28).

Values are apparent at finite concentration because of the effects of thermodynamic non-ideality through molecular excluded volume effects, which leads to an underestimate of the true M_w value. Depending on the size of the molecule, at sufficiently low concentrations $M_{w,app}$ can be considered to be approximately equal to M_w, the thermodynamically ideal value. Alternatively, measurements of $M_{w,app}$ can be made at a series of concentrations, c, and extrapolated back to c = 0 where non-ideality effects are eliminated and hence, $M_{w,app} = M_w$. The $M_{w,app}$ values themselves are obtained from SEDFIT-MSTAR using either the M^* function (Creeth and Harding, 1982) or the hinge method (Table 28) (Schuck *et al.*, 2014). Figure 120 shows an extrapolation to zero concentration to eliminate non-ideality effects to yield an 'ideal' M_w of (54.0 ± 1.5) kDa for Butvar® B-98.

The SE data for the 4.0 mg/mL loading concentration was additionally analysed with the MultiSig algorithm (Gillis *et al.*, 2013). Figure 121 revealed a broad distribution ranging from 17.5 to 163.4 kDa, with components peaking at 17.5 and 61.4 kDa . The was consistent with the results previously obtained with SV. Both the weighted average whole distribution value M_w = (54.0 ± 1.5) kDa and the f(M) vs M_{app} distribution are consistent with values previously quoted for Butvar® B-98, namely 40 – 70 kDa (Eastman Chemical Company, 2013).

Table 28. $M_{w,app}$ values derived from the M^* function and the hinge point method, obtained from the SE of Butvar® B-98.

Concentration (mg/mL)	$M_{w,app}$ (M^*) (kDa)	$M_{w,app}$ (hinge point) (kDa)
0.5	51.5	29.6
0.75	39.2	26.2
1.0	50.9	36.3
1.5	50.2	34.8
2.0	43.8	31.6
3.0	41.1	32.0
4.0	39.4	31.6

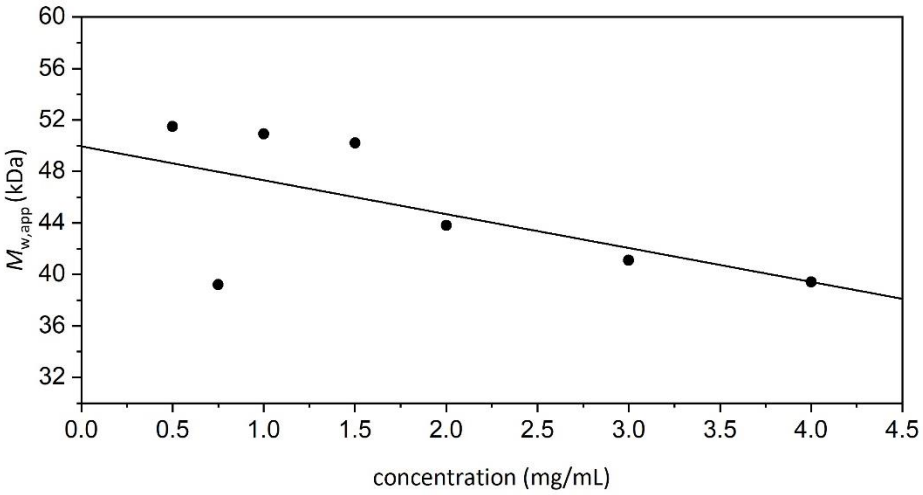

Figure 120. Dependence of apparent $M_{w,app}$ on concentration, with an extrapolation to obtain the thermodynamically ideal $M_{w,app}$ of Butvar® B-98 in isopropanol. Analysed with SEDFIT-MSTAR using the M^* extrapolation to obtain the shown $M_{w,app}$ values. Rotor speed = 22,000 rpm. Temperature = 20.0 °C. The value extrapolated to zero concentration was calculated to be M_w = (54.0 ± 1.5) kDa.

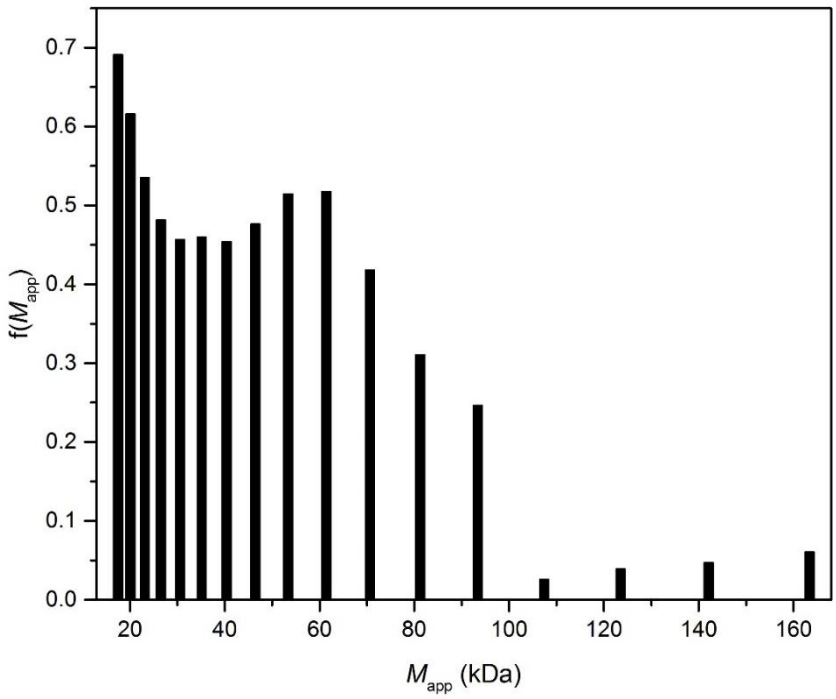

Figure 121. Estimation using MultiSig of the molecular weight distribution f(*M*) vs M_{app} at a loading concentration of 4.0 mg/mL for Butvar® B-98. Rotor speed = 22,000 rpm. A broad distribution is seen consistent with SV (see Figure 118).

5.3.1.3 The intrinsic viscosity $[\eta]$

Intrinsic viscosity (Tanford, 1961; Harding, 1997) measurements were carried out on Butvar® B-98 with a rolling ball viscometer at 10.0 °C in isopropanol. The concentration of the polymer solution that was used for these experiments was 6.0 mg/mL to give a sufficient flow time difference to that of the solvent. The $[\eta]$ value was evaluated using the Solomon–Ciuta equation (Equation 10), previously described in Chapter 3 (Solomon and Ciută, 1962).

$$[\eta] = \frac{1}{c}\left(2\left(\eta_{sp}\right) - 2ln(\eta_{rel})\right)^{\frac{1}{2}} \quad \textbf{(10)}$$

The $[\eta]$ of Butvar B-98 in isopropanol was found to be (57.7 ± 2.9) mL/g.

5.3.1.4 Conformational analyses

The programme ELLIPS1 (Harding, Horton and Cölfen, 1997) was used to provide an estimate of polymer conformation or asymmetry in terms of the axial ratio (a/b) of the equivalent hydrodynamic ellipsoid (prolate) of the polymers using the viscosity increment ν (Simha, 1940; Saito, 1951) and Perrin *P* (Perrin, 1936) shape factors. These models do not take into account flexibility effects, but nonetheless provide a useful relative comparison of asymmetry. ν is related to $[\eta]$ by the relation described in Equation 12 (Simha, 1940; Saito, 1951; Harding and Rowe, 1982) whereas *P* is defined by Equation 13a.

$$\nu = [\eta]M/(N_A \mathrm{V}) \quad \textbf{(12)}$$

$$P = (f/f_o)\,(\bar{v}/v_s)^{\frac{1}{3}} \quad \textbf{(13a)}$$

Tables 29 and 30 show these shape functions in terms of their aspect (axial) ratios (a/b) for ellipsoids of revolution (Harding, Horton and Cölfen, 1997) using a plausible range of solvent associations. Figures 122 and 123 show the visual representations of the axial ratios.

The axial ratios obtained by the ν shape factor proved to be smaller than those estimated for *P*. Nevertheless, they provided consistent results with all the conformations being very thin and elongated.

Table 29. The Butvar® B-98 calculated values for the shape parameter ν and the axial ratios (prolate ellipsoid model) determined by ELLIPS1

	Degree of solvent association $(\boldsymbol{v_s/\tilde{v}})$		
	1.0	**1.2**	**1.4**
shape factor ν	63.4 ± 3.3	52.8 ± 3.3	45.3 ± 3.2
axial ratio $(\boldsymbol{a/b})$	27.1	24.1	21.7

Table 30. The Butvar® B-98 calculated values for the shape parameter *P* and the axial ratios (prolate ellipsoid model) determined by ELLIPS1

	Degree of solvent association $(\boldsymbol{v_s/\tilde{v}})$		
	1.0	**1.2**	**1.4**
shape factor $\boldsymbol{P}$	3.1 ± 1.5	2.9 ± 1.5	2.8 ± 1.5
axial ratio $(\boldsymbol{a/b})$	55.0	48.1	42.9

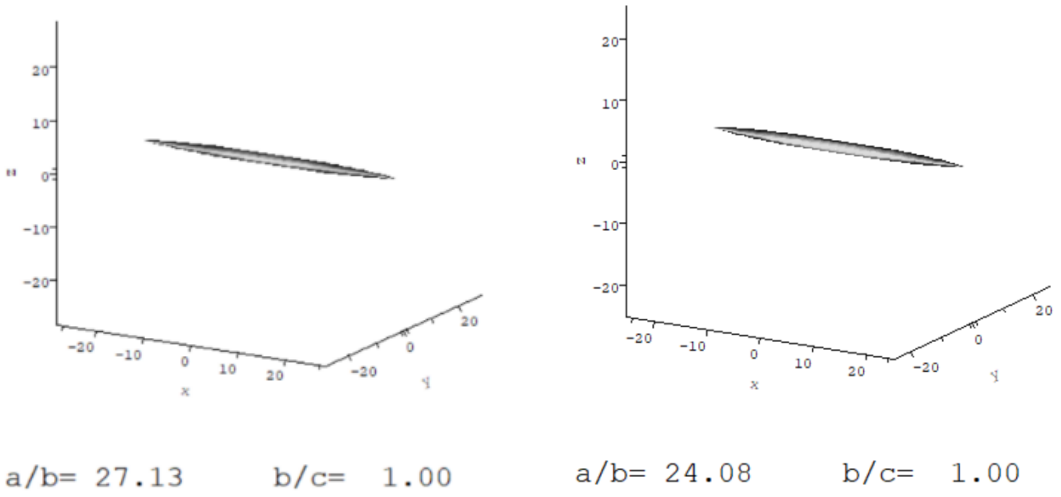

a) **b)**

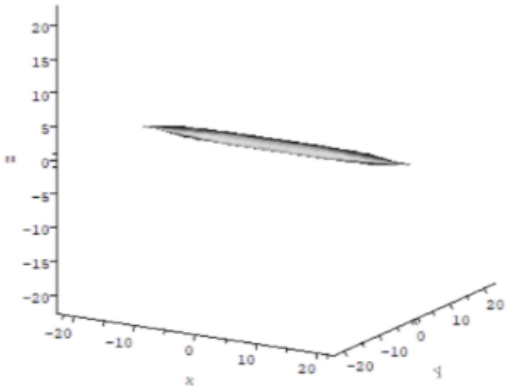

c)

Figure 122. Ellipsoidal representations from the conformation analysis of Butvar® B-98 in isopropanol at different degrees of solvent association, using the programme ELLIPS1 with the shape parameter ν. a) $(v_s/\bar{v})$ = 1.0; b) $(v_s/\bar{v})$ = 1.2; c) $(v_s/\bar{v})$ = 1.4.

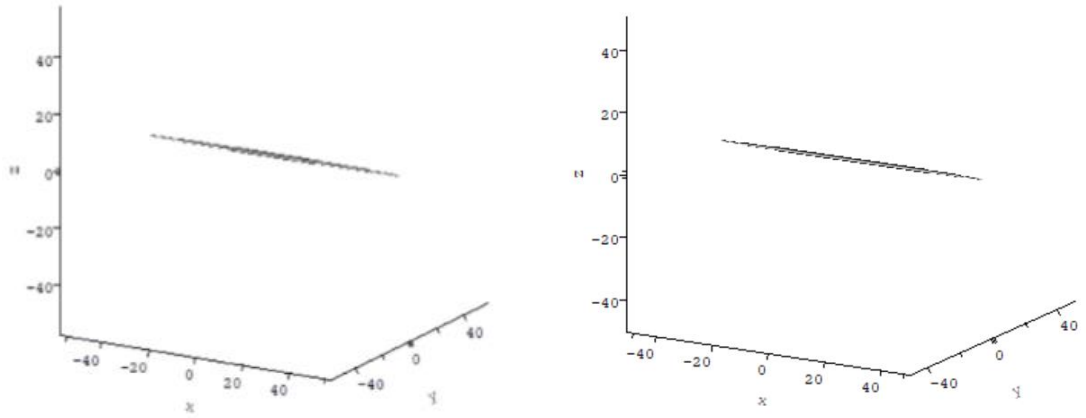

a) **b)**

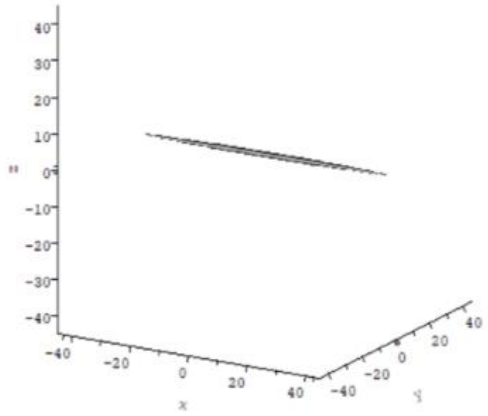

c)

Figure 123. Ellipsoidal representations from the conformation analysis of Butvar® B-98 in isopropanol at different degrees of solvent association, using the programme ELLIPS1 with the shape parameter *P*. a) $(v_s/\bar{v})$ = 1.0; b) $(v_s/\bar{v})$ = 1.2; c) $(v_s/\bar{v})$ = 1.4.

5.3.2 PDMS-OH

Four different preparations of PDMS-OH were studied across a range of molecular weights assigned by the manufacturer based on size exclusion chromatography as 36,000 Da and 18,000 Da (both relative to polystyrene standards), and 4200 Da and ~ 550 Da. These samples are hitherto named PS36000, PS18000, PS4200, and PS550.

The initial plan was to run these AUC studies using both isopropanol and turpentine as solvents. This is because these two solvents were the ones which were being investigated by the Saving Oseberg group. Unfortunately, it was found that there was not a sufficient density difference between turpentine and the PDMS-OH polymers and so these studies could not give reliable data. Consequently, only the results from the AUC experiments performed in isopropanol are reported in this chapter.

5.3.2.1 PS36000

5.3.2.1.1 SV

A rotational speed of 49,000 rpm at a temperature of 20.0 °C was used for the SV experiments of all the PDMS-OH samples. SEDFIT (Schuck, 2000; Dam and Schuck, 2004) was used for the analyses. Figure 124 shows the sedimentation coefficient distributions obtained for PS36000 across a range of concentrations. No evidence of high molecular weight aggregation products was evident. There was a single peak with a sedimentation coefficient value of ~ 0.7 S, possibly alluding to the fact that there was not a high degree of heterogeneity in the PS36000 polymer system.

When an attempt was made to calculate the $s_{20,w}$ of PS36000, it was discovered that all values came out negative. This indicated that, had these molecules been soluble in water, they would have moved in the opposite direction to the ultracentrifugal field – that is, *flotation velocity* – somewhat similar to what was previously observed for another polymer, ‘CoPo9′. This was a block copolymer made of poly(ethylene oxide)

and poly(isoprene), and is soluble as unimers in chloroform but forms micelles in water (Morgan, Harding and Petrak, 1990). This was found to be the case for all of the PDMS-OH samples (PS36000, PS18000, PS4200 and PS550). Such behaviour should not have a negative impact on the consolidative action of PDMS-OH.

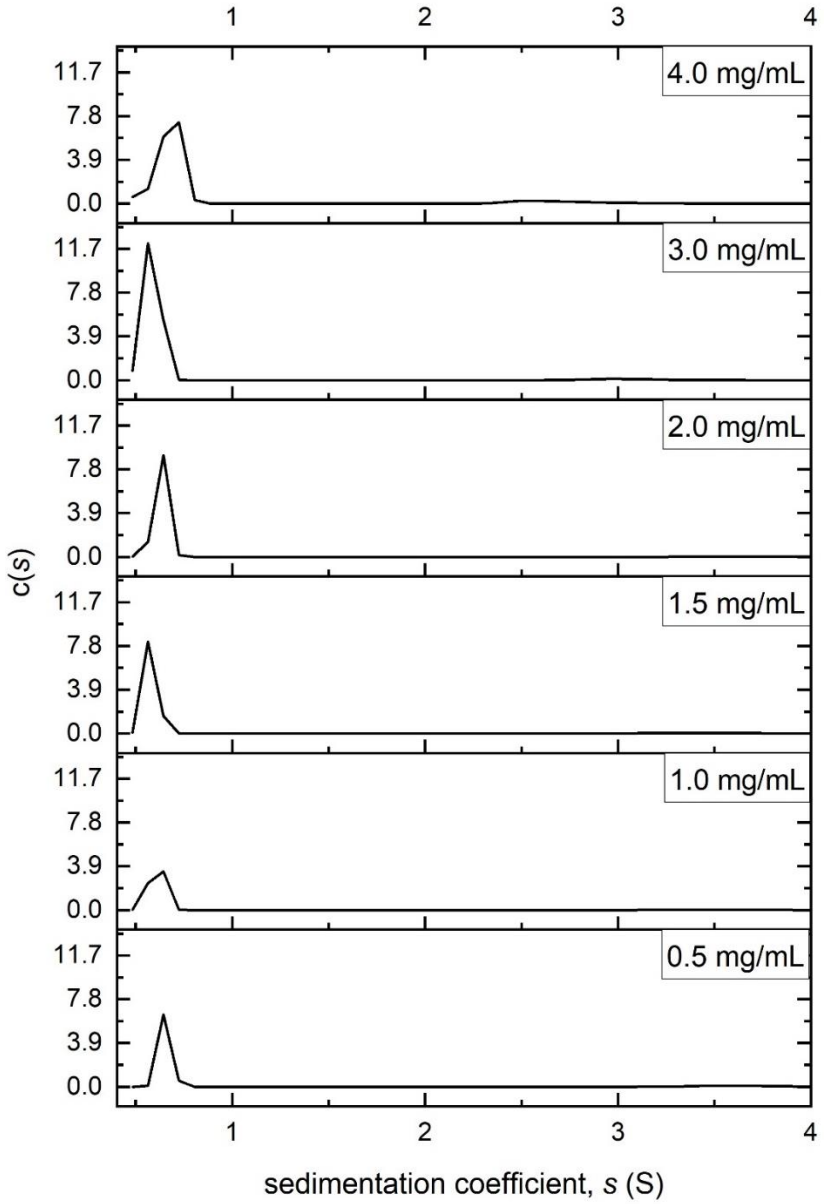

Figure 124. Sedimentation coefficient distributions of the PS3600 at different loading concentrations in isopropanol. Rotor speed = 49,000 rpm, temperature = 20.0 °C.

5.3.2.1.2 SE

SE experiments were performed on all PDMS-OH samples, using appropriate rotational speeds according to their approximate sizes. A rotor speed of 22,000 rpm was selected for PS36000. The *M** (Creeth and Harding, 1982) and hinge point values were obtained using SEDFIT-MSTAR (Schuck *et al.*, 2014) (Table 31). The thermodynamically ideal whole distribution weight average M_w value was afterwards calculated, as with Butvar® B-98, by plotting the $M_{w,app}$ values against concentration and extrapolating to zero concentration (Figure 125). The extrapolated M_w, (52.5 ± 3.0) kDa, proved to be higher than the relative molecular weight M_r (relative to polystyrene standards) provided by the manufacturer for PS36000.

Figure 126 shows the corresponding molecular weights at a loading concentration of 4.0 mg/mL from the MultiSig (Gillis *et al.*, 2013) analysis of the equilibrium data. Unlike what was seen with the SV experiment, PS36000 appeared to be to be fairly heterogeneous, having a wide range of molecular weights.

Table 31. $M_{w,app}$ values derived from the *M** function and the hinge point method, obtained the from SE of PS36000.

Concentration (mg/mL)	$M_{w,app}$ (*M**) (kDa)	$M_{w,app}$ (hinge point) (kDa)
0.5	48.7	44.4
1.0	49.0	38.2
2.0	35.6	34.4
3.0	29.1	28.9
4.0	27.7	26.8

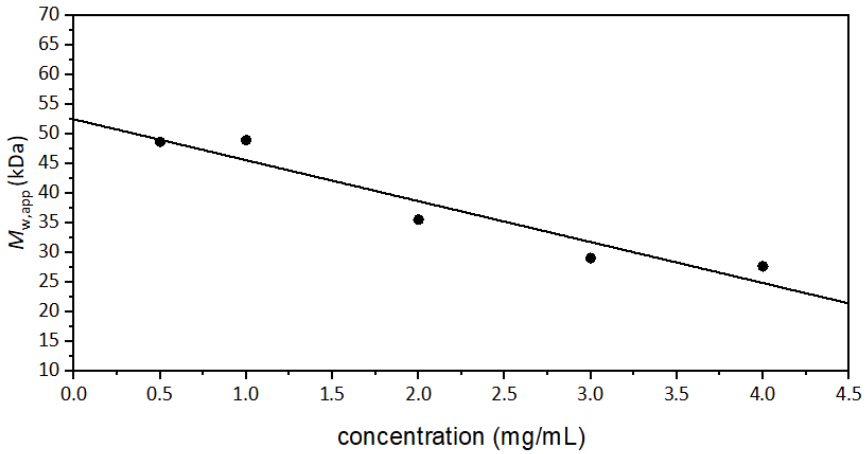

Figure 125. Dependence of apparent $M_{w,app}$ on concentration, with an extrapolation to obtain the thermodynamically ideal $M_{w,app}$ of PS36000 in isopropanol. Analysed with SEDFIT-MSTAR using the M^* extrapolation to obtain the shown $M_{w,app}$ values. Rotor speed = 22,000 rpm. Temperature = 20.0 °C. The value extrapolated to zero concentration was calculated to be M_w = (52.5 ± 3.0) kDa.

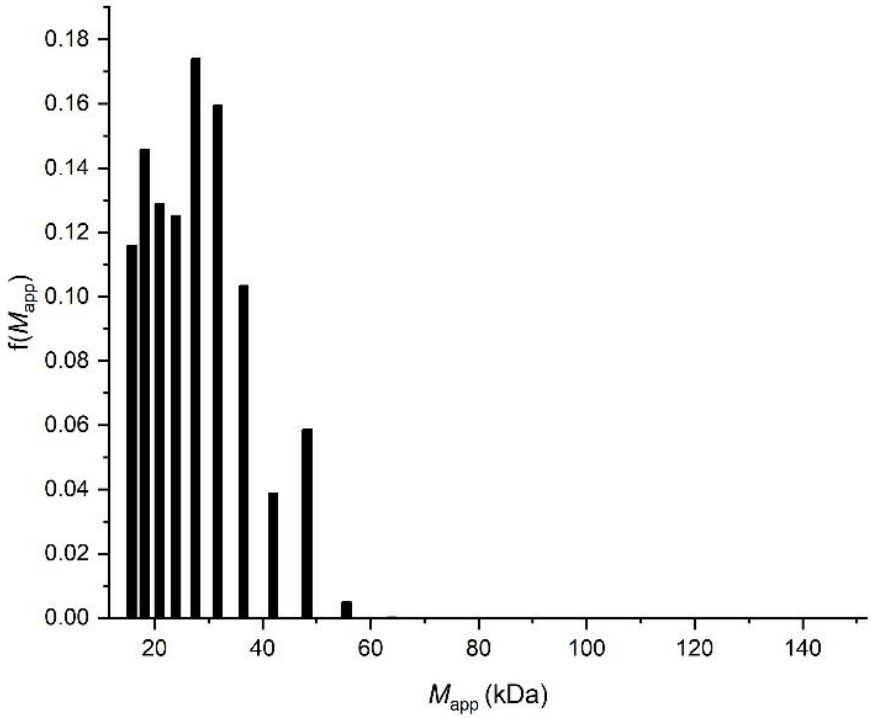

Figure 126. MultiSig analysis of the molecular weight distribution f(*M*) vs *M* of PS36000 in isopropanol at a concentration of 4.0 mg/mL. Rotor speed = 22,000 rpm.

5.3.2.1.3 The intrinsic viscosity $[\eta]$

Intrinsic viscosity (Tanford, 1961; Harding, 1997) measurements were carried out using the same method employed with Butvar® B-98. All the PDMS-OH samples were measured both in isopropanol and in turpentine. Using the Solomon-Ciuta equation (Solomon and Ciută, 1962), the $[\eta]$ values of PS36000 were calculated to be (6.0 ± 0.3) mL/g in isopropanol and (22.4 ± 1.1) mL/g in turpentine.

5.2.2.1.4 Conformational analyses

Tables 32 and 33 show the ν (Simha, 1940; Saito, 1951) and *P* (Perrin, 1936) shape function values and the axial ratios (a/b) for PS36000. Figures 127 – 129 show the estimated shapes for these axial ratios obtained from ELLIPS1 (Harding, Horton and Cölfen, 1997). It was also possible to calculate the ν shape function of the polymer in turpentine, as a result of the viscosity measurements previously performed in this solvent. The *P* shape function was not calculated for turpentine since the $s_{20,w}$ of the PDMS-OH samples could not be extrapolated from the SV experiments.

Table 32. The PS36000 calculated values for the shape parameter ν and the axial ratios (prolate ellipsoid model) determined by ELLIPS1

		Degree of solvent association $(\boldsymbol{\nu_s/\bar{\nu}})$		
		1.0	**1.2**	**1.4**
Isopropanol	**shape factor ν**	5.9 ± 2.0	4.9 ± 2.0	4.2 ± 2.0
	axial ratio $(\boldsymbol{a/b})$	5.1	4.2	3.6
Turpentine	**shape factor ν**	21.9	18.3	15.7
	axial ratio $(\boldsymbol{a/b})$	13.5	12.1	11.1

Table 33. The PS36000 calculated values for the shape parameter *P* in isopropanol and the axial ratios (prolate ellipsoid model) determined by ELLIPS1

	Degree of solvent association $(\boldsymbol{v_s/\bar{v}})$		
	1.0	**1.2**	**1.4**
shape factor $\boldsymbol{P}$	2.3 ± 0.2	2.1 ± 0.2	2.0 ± 0.2
axial ratio $(\boldsymbol{a/b})$	27.5	23.8	20.9

As previously with Butvar® B-98, the shapes estimated from the *P* values appeared to be 'thinner' than the ν ones. Moreover, the PS36000 dissolved in turpentine had a larger axial ratio than the one dissolved in isopropanol, possibly due to the different interactions between the solvent and the polymer.

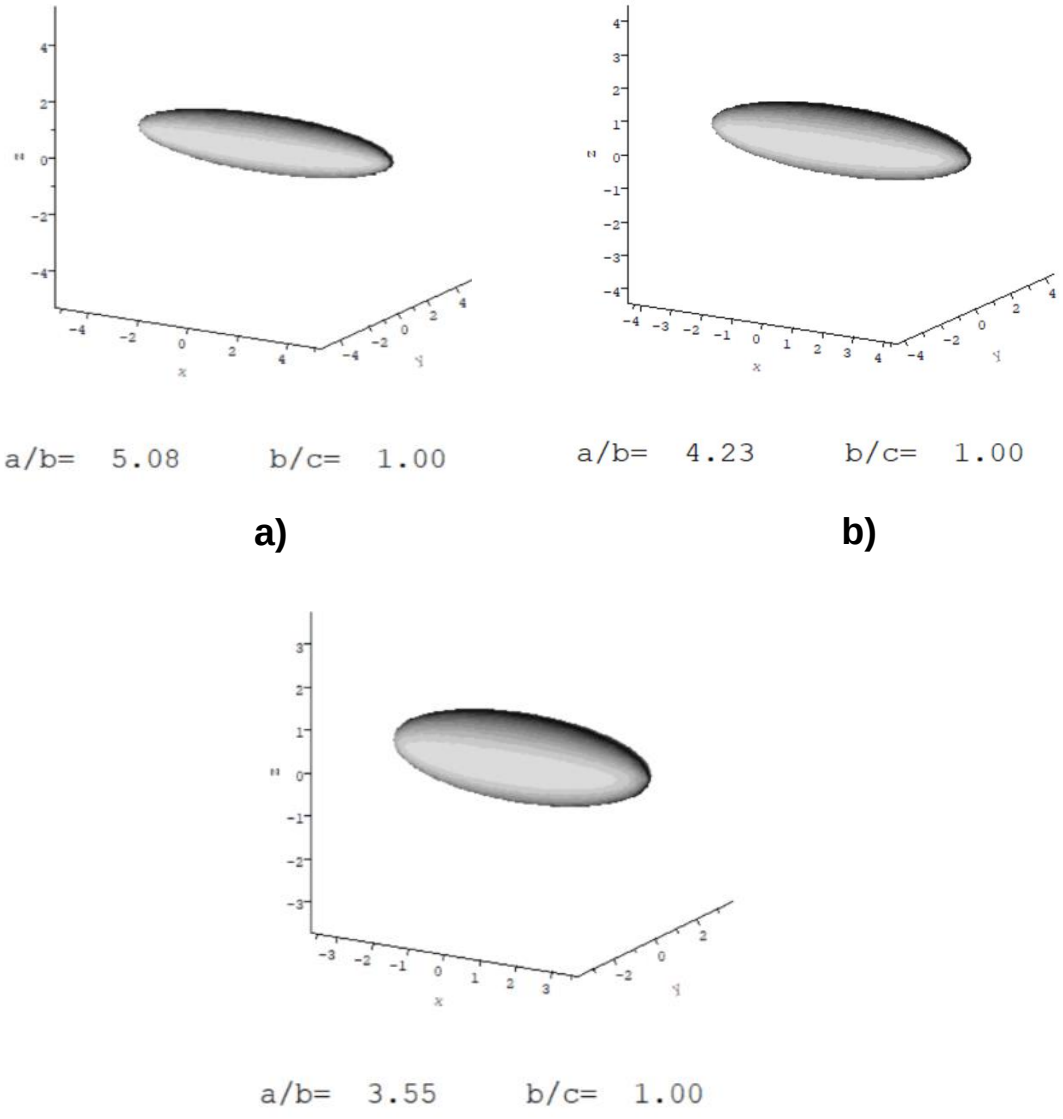

Figure 127. Ellipsoidal representations from the conformation analysis of PS36000 in isopropanol at different degrees of solvent association, using the programme ELLIPS1 with the shape parameter ν. a) $(v_s/\bar{v})$ = 1.0; b) $(v_s/\bar{v})$ = 1.2; c) $(v_s/\bar{v})$ = 1.4.

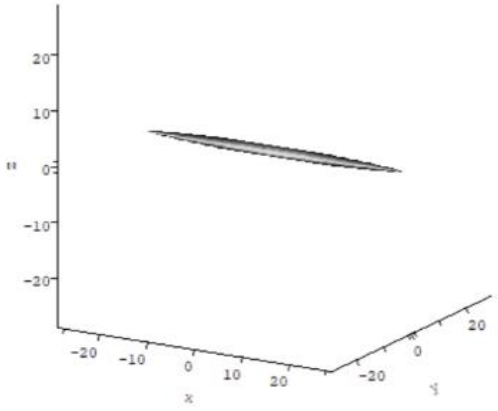

a/b= 27.50 b/c= 1.00

a)

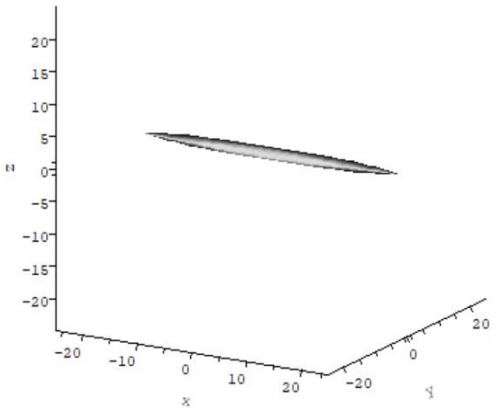

a/b= 23.76 b/c= 1.00

b)

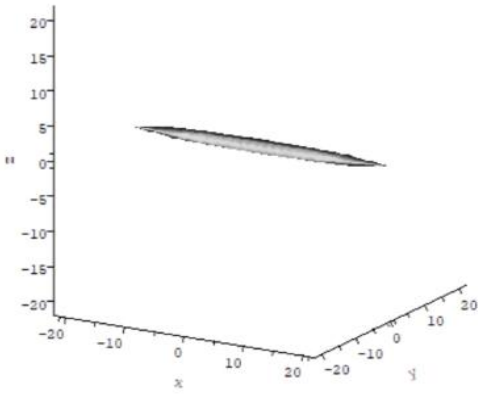

a/b= 20.93 b/c= 1.00

c)

Figure 128. Ellipsoidal representations from the conformation analysis of PS36000 in isopropanol at different degrees of solvent association, using the programme ELLIPS1 with the shape parameter *P*. a) $(v_s/\bar{v})$ = 1.0; b) $(v_s/\bar{v})$ = 1.2; c) $(v_s/\bar{v})$ = 1.4.

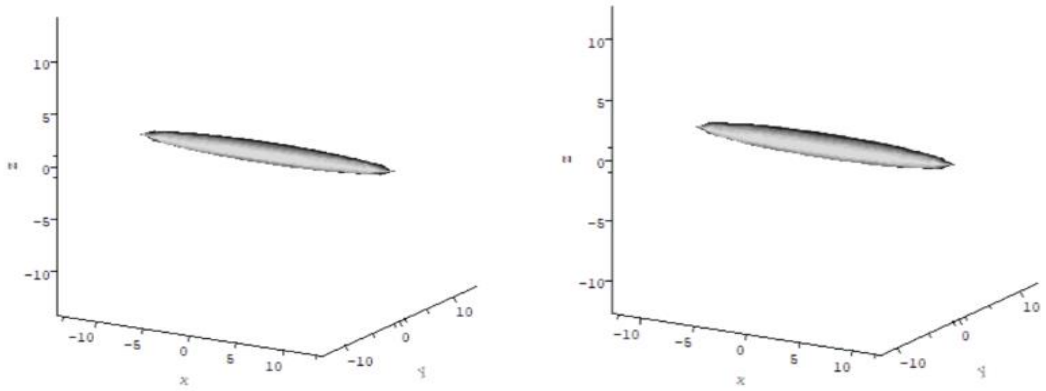

a) **b)**

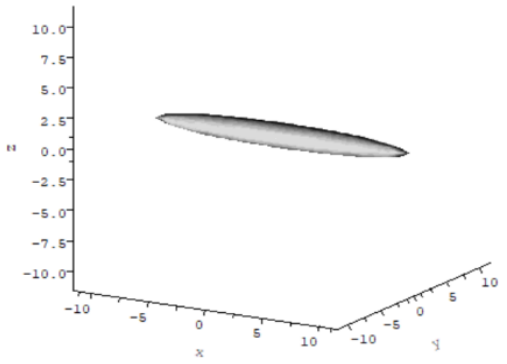

c)

Figure 129. Ellipsoidal representations from the conformation analysis of PS36000 in turpentine at different degrees of solvent association, using the programme ELLIPS1 with the shape parameter ν. a) $(v_s/\bar{v})$ = 1.0; b) $(v_s/\bar{v})$ = 1.2; c) $(v_s/\bar{v})$ = 1.4.

5.3.2.2 PS18000

5.3.2.2.1 SV

Figure 130 shows the SV results obtained from SEDFIT (Schuck, 2000; Dam and Schuck, 2004) for PS18000. In contrast to PS36000, PS18000 revealed two components. As the concentration increased, these two peaks showed a tendency to merge, possibly due to the Johnston-Ogston effect (Johnston and Ogston, 1946) where the faster moving component is slowed down by having to move through a solution of the slower moving component.

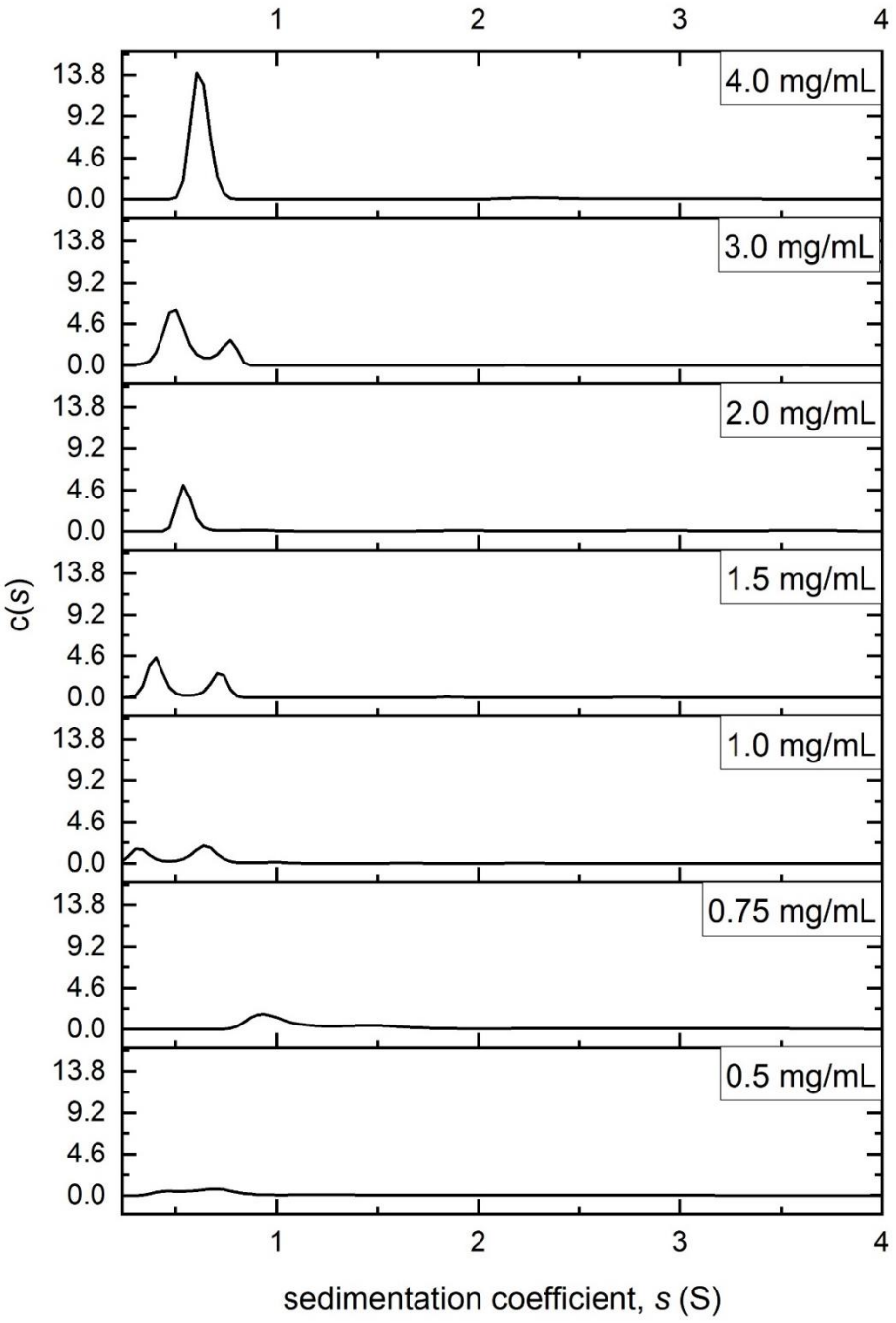

Figure 130. Sedimentation coefficient distributions of PS18000 series at different loading concentrations in isopropanol. Rotor speed = 49,000 rpm, temperature = 20.0 °C.

5.3.2.2.2 SE

A rotor speed of 30,000 rpm was used for PS18000. Table 34 shows the *M** (Creeth and Harding, 1982) and hinge point M_w values obtained by SEDFIT-MSTAR (Schuck *et al.*, 2014). The *M** weights were plotted against concentration (Figure 131). The extrapolated M_w was (37.4 ± 2.3) kDa. Like PS36000, this proved to higher than the M_r stipulated by the manufacturer.

The MultiSig algorithm (Gillis *et al.*, 2013) was run on the 4.0 mg/mL concentration to reveal a molecular weight distribution ranging from 6.5 to 60.8 kDa (Figure 132). Having such a dispersion of molecular weights corresponded with the multiple sedimentation coefficient values that were obtained previously with the SV experiment.

Table 34. $M_{w,app}$ values derived from the *M** function and the hinge point method, obtained from the SE of PS18000.

Concentration (mg/ml)	$M_{w,app}$ (*M**) (kDa)	$M_{w,app}$ (hinge point) (kDa)
1.0	33.6	31.0
2.0	29.8	25.2
3.0	22.9	18.5
4.0	22.3	19.9

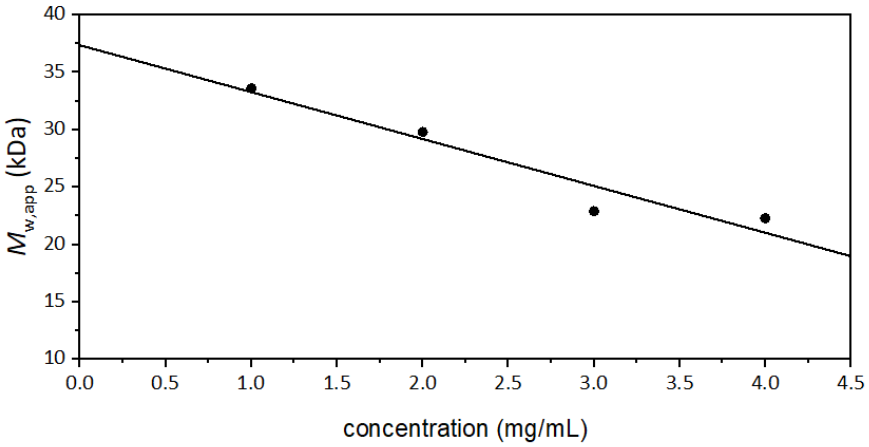

Figure 131. Dependence of apparent $M_{w,app}$ on concentration, with an extrapolation to obtain the thermodynamically ideal $M_{w,app}$ of PS18000 in isopropanol. Analysed with SEDFIT-MSTAR using the *M** extrapolation to obtain the shown $M_{w,app}$ values. Rotor speed = 30,000 rpm. Temperature = 20.0 °C. The value extrapolated to zero concentration was calculated to be M_w = (37.4 ± 2.3) kDa.

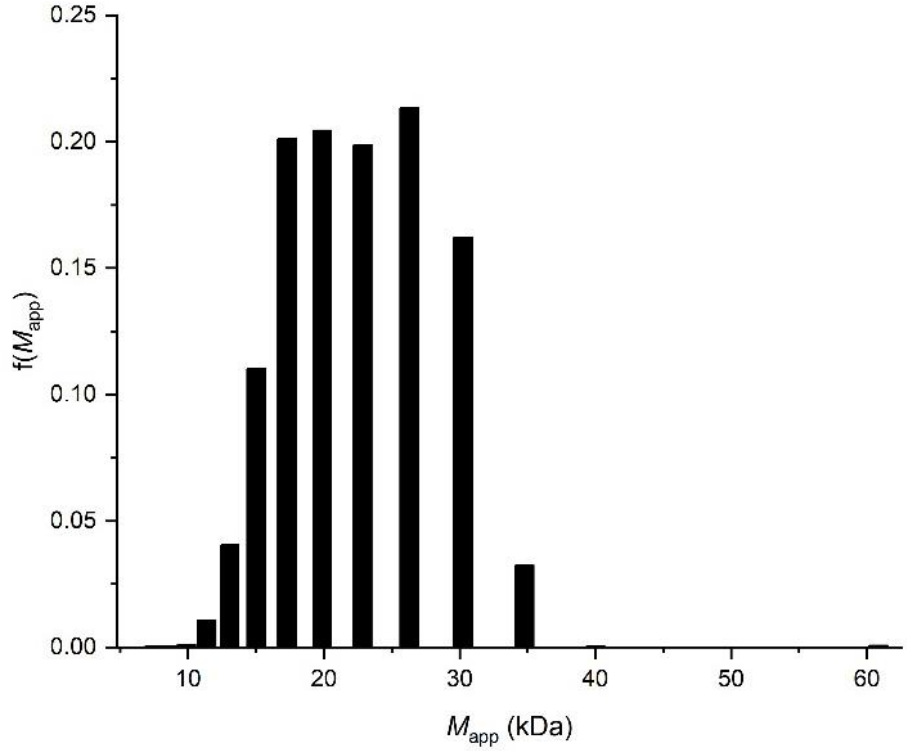

Figure 132. MultiSig analysis of the molecular weight distribution f(*M*) vs *M* of PS18000 in isopropanol at a concentration of 4.0 mg/mL. Rotor speed = 30,000 rpm.

5.3.2.2.3 The intrinsic viscosity $[\eta]$

With the rolling ball viscometer and the Solomon-Ciuta equation (Solomon and Ciută, 1962), the $[\eta]$ value of PS18000 was found to be (7.5 ± 0.4) mL/g in isopropanol and (15.8 ± 0.8) mL/g in turpentine.

5.3.2.2.4 Conformational analyses

Tables 35 and 36 show the ν (Simha, 1940; Saito, 1951) and *P* (Perrin, 1936) shape function values and their axial ratios (a/b) for PS18000. The ELLIPS1-estimated shapes are shown in Figures 133 – 135 for both shape factors (Harding, Horton and Cölfen, 1997).

Table 35. The PS18000 calculated values for the shape parameter ν and the axial ratios (prolate ellipsoid model) determined by ELLIPS1

		Degree of solvent association $(v_s/\bar{v})$		
		1.0	**1.2**	**1.4**
Isopropanol	**shape factor ν**	7.2 ± 2.3	6.0 ± 2.3	5.1 ± 2.3
	axial ratio (a/b)	6.1	5.2	4.5
Turpentine	**shape factor ν**	15.4	12.8	11.0
	axial ratio (a/b)	10.9	9.6	8.5

Table 36. The PS18000 calculated values for the shape parameter *P* in isopropanol and the axial ratios (prolate ellipsoid model) determined by ELLIPS1

	Degree of solvent association $(v_s/\bar{v})$		
	1.0	**1.2**	**1.4**
shape factor P	1.4 ± 0.1	1.3 ± 0.1	1.3 ± 0.1
axial ratio (a/b)	7.6	6.3	5.2

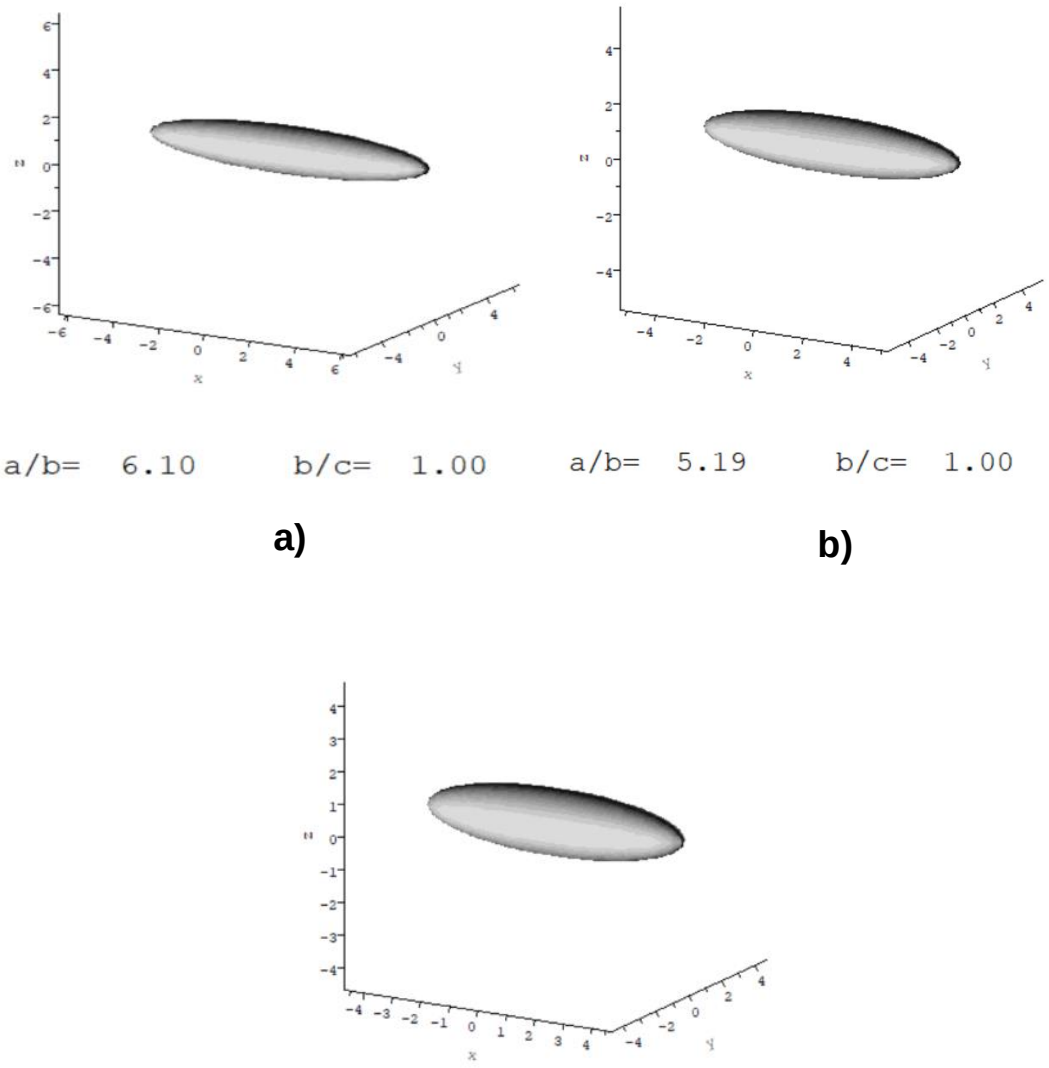

Figure 133. Ellipsoidal representations from the conformation analysis of PS18000 in isopropanol at different degrees of solvent association, using the programme ELLIPS1 with the shape parameter ν. a) $(v_s/\bar{v})$ = 1.0; b) $(v_s/\bar{v})$ = 1.2; c) $(v_s/\bar{v})$ = 1.4.

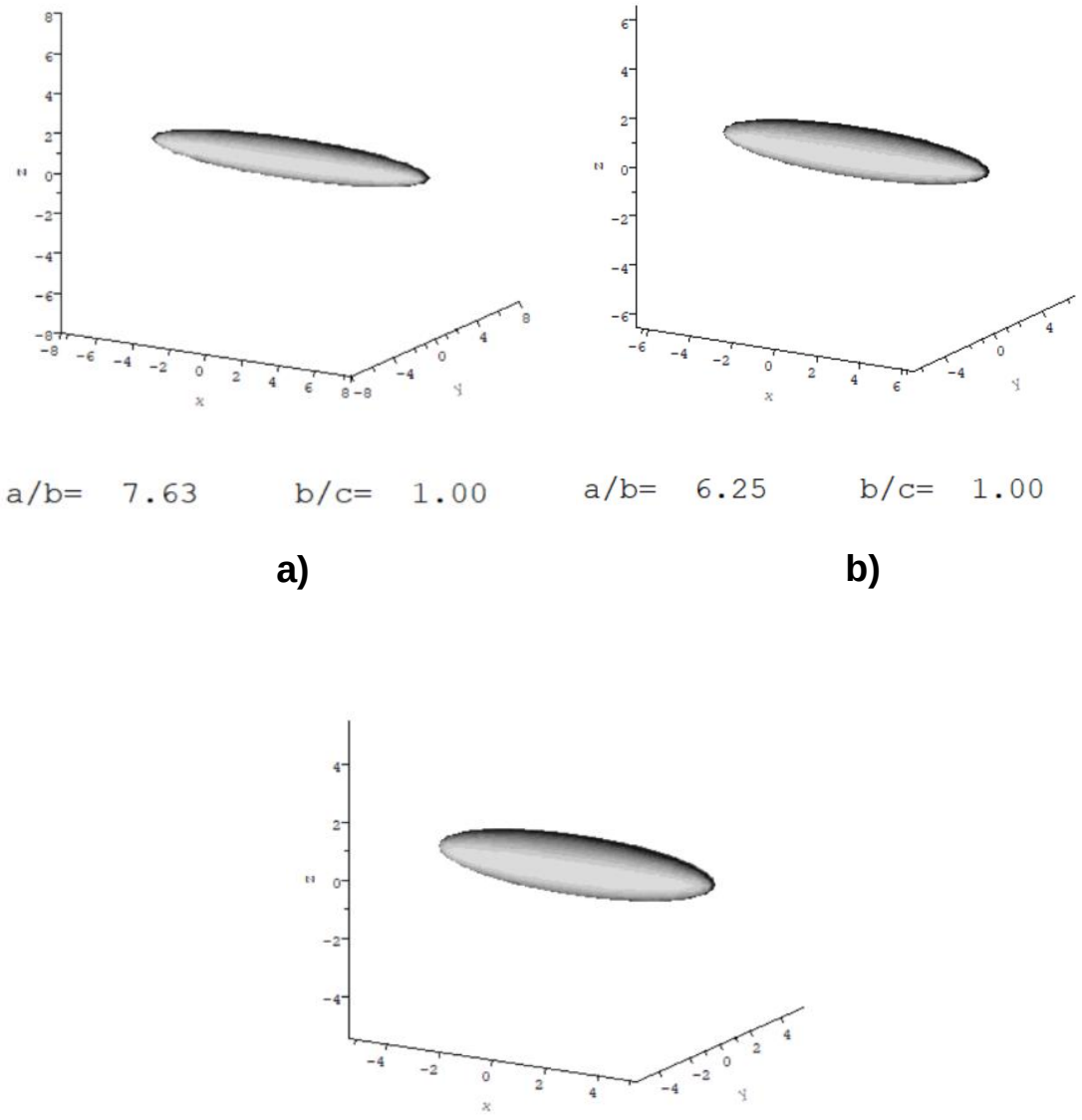

Figure 134. Ellipsoidal representations from the conformation analysis of PS18000 in isopropanol at different degrees of solvent association, using the programme ELLIPS1 with the shape parameter *P*. a) $(v_s/\bar{v})$ = 1.0; b) $(v_s/\bar{v})$ = 1.2; c) $(v_s/\bar{v})$ = 1.4.

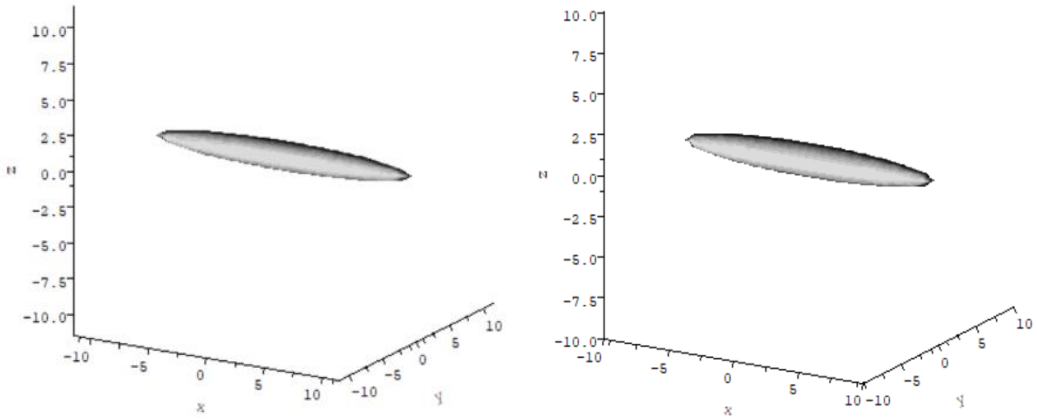

a) **b)**

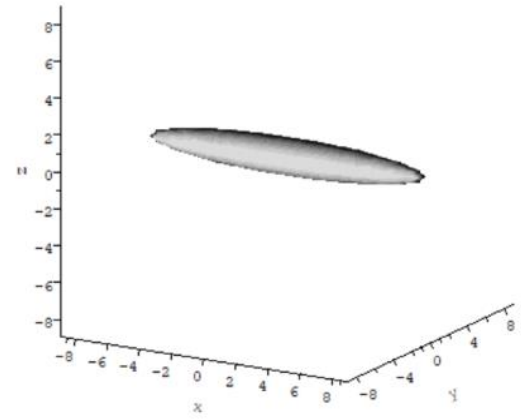

c)

Figure 135. Ellipsoidal representations from the conformation analysis of PS18000 in turpentine at different degrees of solvent association, using the programme ELLIPS1 with the shape parameter ν. a) $(v_s/\bar{v})$ = 1.0; b) $(v_s/\bar{v})$ = 1.2; c) $(v_s/\bar{v})$ = 1.4.

5.3.2.3 PS4200

5.3.2.3.1 SV

The SV results from SEDFIT (Schuck, 2000; Dam and Schuck, 2004) for PS4200 are shown in Figure 136. The results were very similar to those of PS18000, with the higher concentrations especially having two primary components. This is again possibly due to the Johnston-Ogston effect (Johnston and Ogston, 1946), with the faster moving component (that is, the heavier component) being slowed by having to pass through the slower moving one (that is, the lighter component).

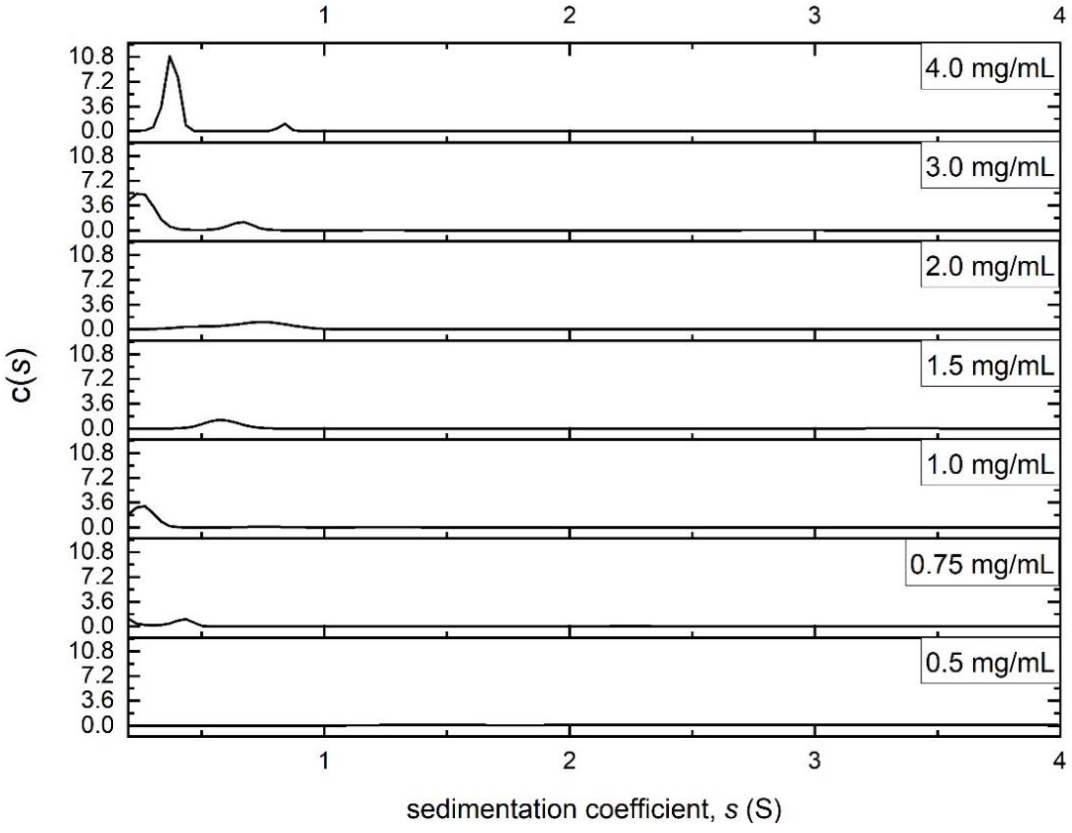

Figure 136. Sedimentation coefficient distributions of PS4200 series at different loading concentrations in isopropanol. Rotor speed = 49,000 rpm, temperature = 20.0 °C.

5.3.2.3.2 SE

Due to the small size of the polymer, a high rotor speed of 49,500 rpm was used for PS4200. The *M** (Creeth and Harding, 1982) and hinge point M_w values were obtained by SEDFIT-MSTAR (Schuck *et al.*, 2014), as displayed by Table 37. Figure 137 shows the plot of the *M** values against concentration. The 'ideal' M_w was found to be (6.2 ± 0.7) kDa.

The MultiSig analysis (Gillis *et al.*, 2013) that was carried out revealed a dispersion that was quite different to those previously seen with PS36000 and PS18000 (Figure 138). Although it was still comprised of multiple molecular weights, the level of heterogeneity appeared to be much lower. Most of the particles in the polymer system appeared to have a very similar molecular weight, as observed by the sharp peak at 4.8 kDa.

Table 37. $M_{w,app}$ values derived from the *M** function and the hinge point method, obtained from the SE of PS4200.

Concentration (mg/ml)	$M_{w,app}$ (*M**) (kDa)	$M_{w,app}$ (hinge point) (kDa)
1.0	5.9	5.2
1.5	4.6	3.8
2.0	5.7	5.1
3.0	5.1	4.5
4.0	3.9	3.4

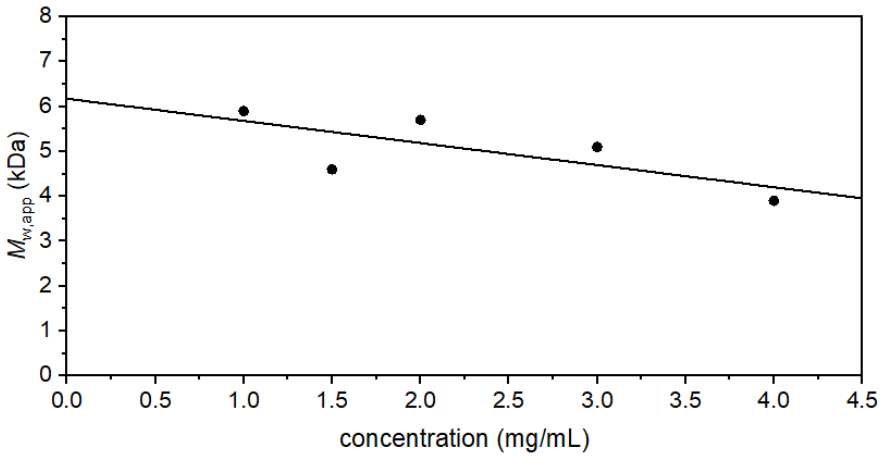

Figure 137. Dependence of apparent $M_{w,app}$ on concentration, with an extrapolation to obtain the thermodynamically ideal $M_{w,app}$ of PS4200 in isopropanol. Analysed with SEDFIT-MSTAR using the M^* extrapolation to obtain the shown $M_{w,app}$ values. Rotor speed = 49,500 rpm. Temperature = 20.0 °C. The value extrapolated to zero concentration was calculated to be M_w = (6.2 ± 0.7) kDa.

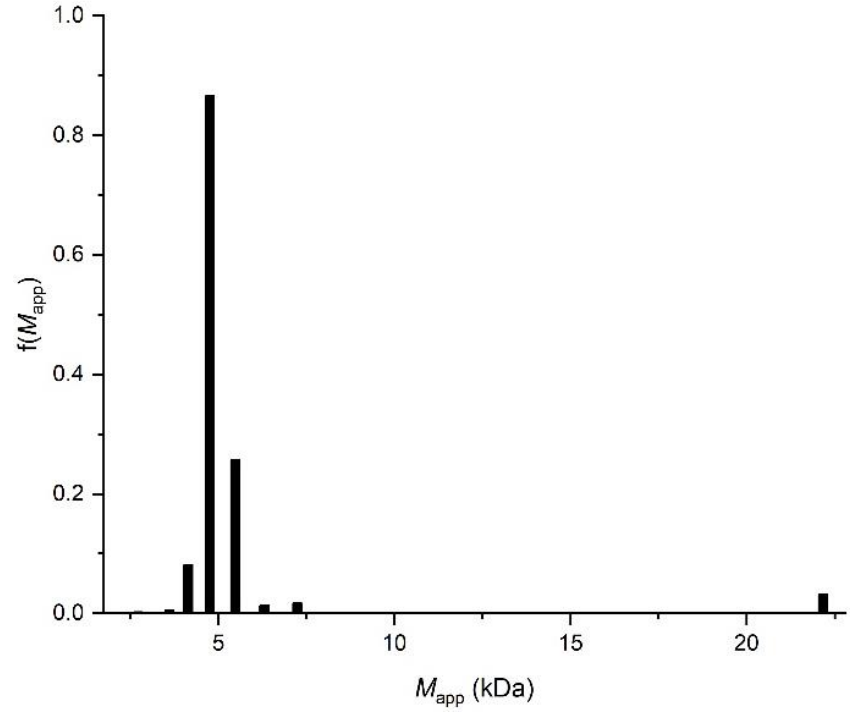

Figure 138. MultiSig analysis of the molecular weight distribution f(M) vs M of PS4200 in isopropanol at a concentration of 4.0 mg/mL. Rotor speed = 49,500 rpm.

5.3.2.3.3 The intrinsic viscosity $[\eta]$

Like with the previous siloxanes, the viscosity was measured in both isopropanol and turpentine, using a 6.0 mg/mL concentration. The $[\eta]$ values were calculated to be (4.1 ± 0.2) mL/g in isopropanol and (5.5 ± 0.3) mL/g in turpentine.

5.3.2.3.4 Conformational analyses

Tables 38 and 39 show the values calculated for the ν (Simha, 1940; Saito, 1951) and the *P* shape factors (Perrin, 1936) respectively. In the case of the *P* shape function, the values were found to be too small to be inputted into ELLIPS1 (Harding, Horton and Cölfen, 1997) and therefore their axial ratios (a/b) could not be calculated. Figures 139 and 140 show the estimated conformations based on the values obtained by the ν shape function.

Table 38. The PS4200 calculated values for the shape parameter ν and the axial ratios (prolate ellipsoid model) determined by ELLIPS1

		Degree of solvent association $(v_s/\bar{v})$		
		1.0	**1.2**	**1.4**
Isopropanol	**shape factor ν**	4.0 ± 0.7	3.3 ± 0.7	2.8 ± 0.7
	axial ratio (a/b)	3.3	2.5	1.9
Turpentine	**shape factor ν**	5.4	4.5	3.8
	axial ratio (a/b)	4.6	3.8	3.1

Table 39. The PS4200 calculated values for the shape parameter *P* in isopropanol

	Degree of solvent association $(v_s/\bar{v})$		
	1.0	**1.2**	**1.4**
shape factor *P*	0.68 ± 0.07	0.64 ± 0.07	0.61 ± 0.07

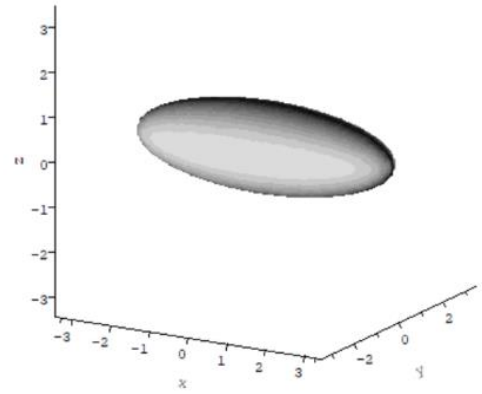

a/b= 3.29 b/c= 1.00

a)

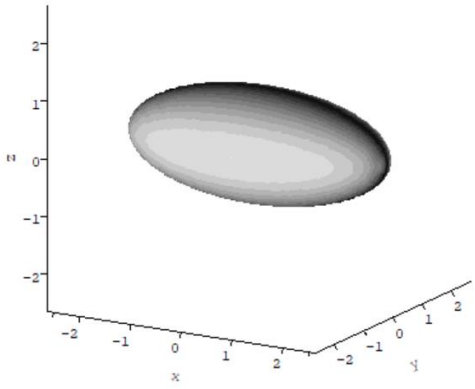

a/b= 2.52 b/c= 1.00

b)

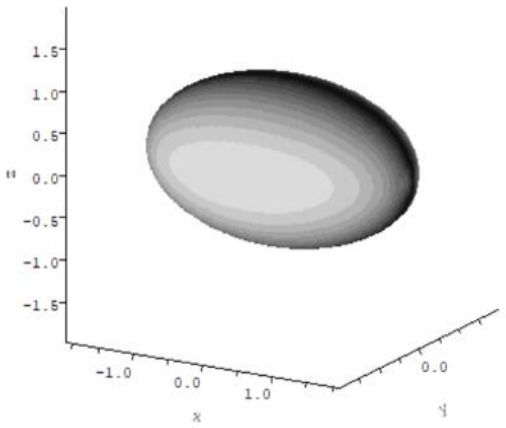

a/b= 1.89 b/c= 1.00

c)

Figure 139. Ellipsoidal representations from the conformation analysis of PS4200 in isopropanol at different degrees of solvent association, using the programme ELLIPS1 with the shape parameter ν. a) $(v_s/\bar{v})$ = 1.0; b) $(v_s/\bar{v})$ = 1.2; c) $(v_s/\bar{v})$ = 1.4.

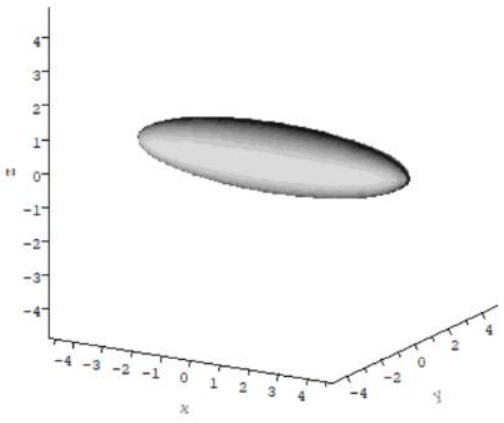

a/b= 4.63 b/c= 1.00

a)

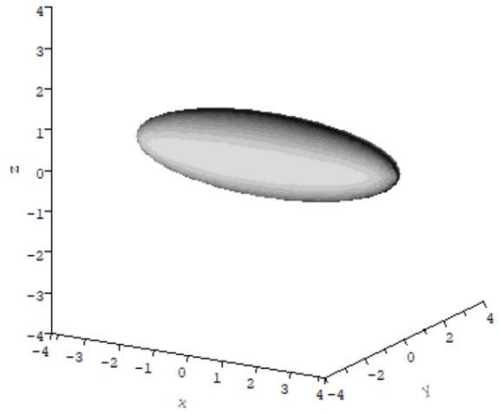

a/b= 3.81 b/c= 1.00

b)

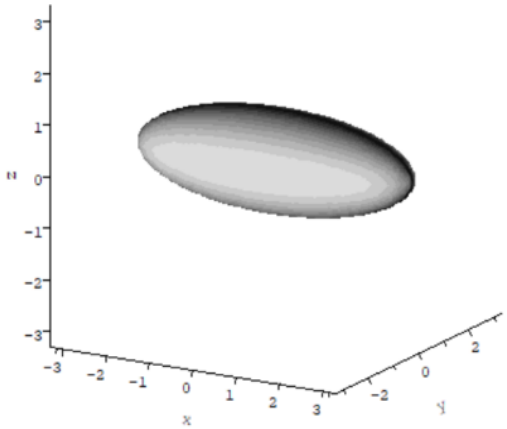

a/b= 3.14 b/c= 1.00

c)

Figure 140. Ellipsoidal representations from the conformation analysis of PS4200 in turpentine at different degrees of solvent association, using the programme ELLIPS1 with the shape parameter ν. a) $(v_s/\bar{v})$ = 1.0; b) $(v_s/\bar{v})$ = 1.2; c) $(v_s/\bar{v})$ = 1.4.

The shapes for the isopropanol-dissolved polymer were seen to be more spherical than those previously observed for PS36000 and PS18000, possibly due to its smaller molecular weight and hence lower $[\eta]$. The shapes for PS4200 dissolved in turpentine followed the same trend as the previous polymers, with the oval conformation having a higher axial ratio than the one dissolved in isopropanol.

5.3.2.4 PS550

5.3.2.4.1 SV

Figure 141 shows the SEDFIT (Schuck, 2000; Dam and Schuck, 2004) results for the SV experiment that was run for PS550. The distribution plot did not show the presence of higher molecular weight aggregates, however it should be kept in mind that the sedimentation coefficient of PS550 was probably too small to be reliably detected.

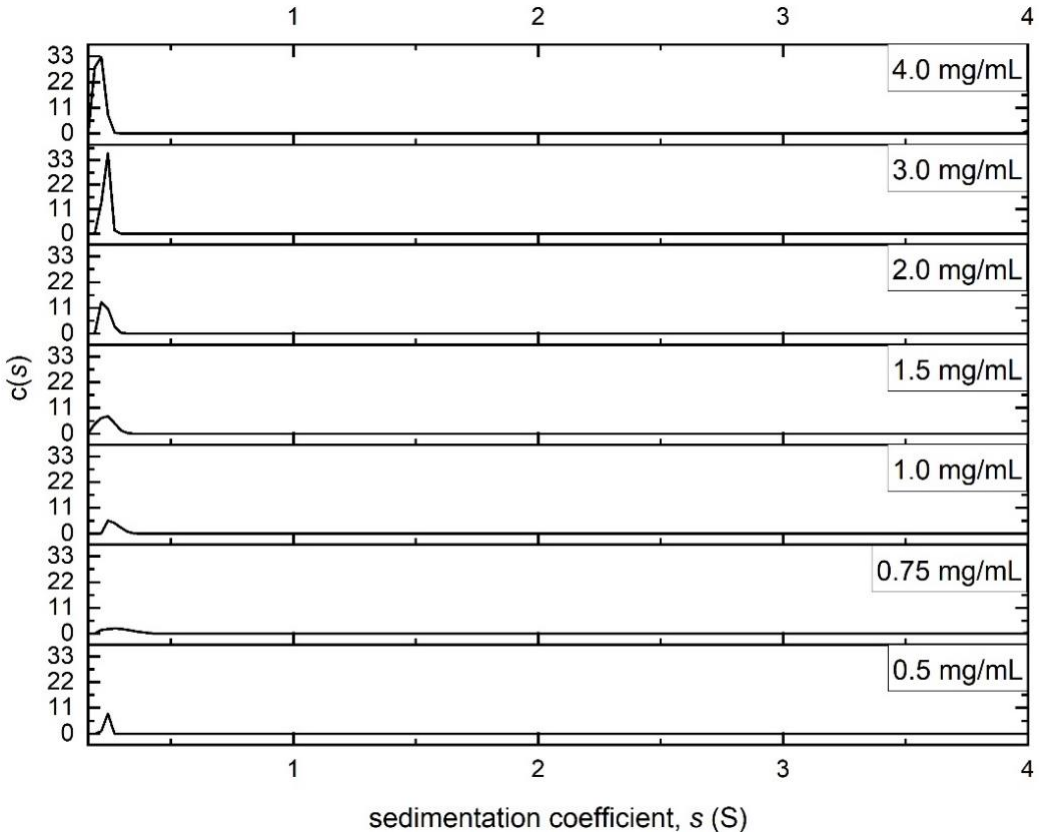

Figure 141. Sedimentation coefficient distributions of PS550 series at different loading concentrations in isopropanol. Rotor speed = 49,000 rpm, temperature = 20.0 °C.

5.3.2.4.2 SE

Due to the very small size of PS550, a high rotor speed of 49,500 rpm was used for SE. Again, as a result of its small size, measurable fringe increments were only possible at higher concentrations so the M_w was obtained simply by taking the average of the 3.0 mg/mL and 4.0 mg/mL measurements (Table 40). This was justified since its exclusion volume and non-ideality effects would be minimal (Tanford, 1961). The M_w was found to be (1.6 ± 0.5) kDa.

Table 40. $M_{w,app}$ values derived from the *M** function and the hinge point method, obtained from the SE of PS550.

Concentration (mg/ml)	$M_{w,app}$ (*M**) (kDa)	$M_{w,app}$ (hinge point) (kDa)
3.0	1.6	2.5
4.0	1.5	2.1

5.3.2.4.3 The intrinsic viscosity $[\eta]$

The $[\eta]$ was obtained using the same methodology that was described previously. Whilst taking the viscosity measurements with the rolling ball viscometer it was found that the flow time increment in turpentine was too small to reliably be able to calculate the $[\eta]$. Because of this, only the $[\eta]$ in isopropanol was calculated for PS550. This was found to be (3.4 ± 0.2) mL/g.

5.3.2.4.4 Conformational analyses

As with PS4200, it was only possible to estimate the axial ratios (a/b) of the ν shape factor (Simha, 1940; Saito, 1951), due to the small value obtained for *P* (Perrin, 1936). Tables 41 and 42 show these calculated values. Since the $[\eta]$ for PS550 in turpentine was not measured, the ν shape factor value could therefore not be calculated for that scenario.

In contrast to the other PDMS-OH preparations, especially the higher molecular weight ones, the axial ratios for the PS550 conformations were very small, corresponding with an almost globular shape (Figure 142).

Table 41. The PS550 calculated values for the shape parameter ν in isopropanol and the axial ratios (prolate ellipsoid model) determined by ELLIPS1

	Degree of solvent association $(v_s/\bar{v})$		
	1.0	**1.2**	**1.4**
shape factor ν	3.6 ± 0.2	3.0 ± 0.2	2.5 ± 0.2
axial ratio (a/b)	2.8	2.1	1.2

Table 42. The PS4200 calculated values for the shape parameter *P* in isopropanol

	Degree of solvent association $(v_s/\bar{v})$		
	1.0	**1.2**	**1.4**
shape factor P	0.42 ± 0.04	0.39 ± 0.07	0.37 ± 0.07

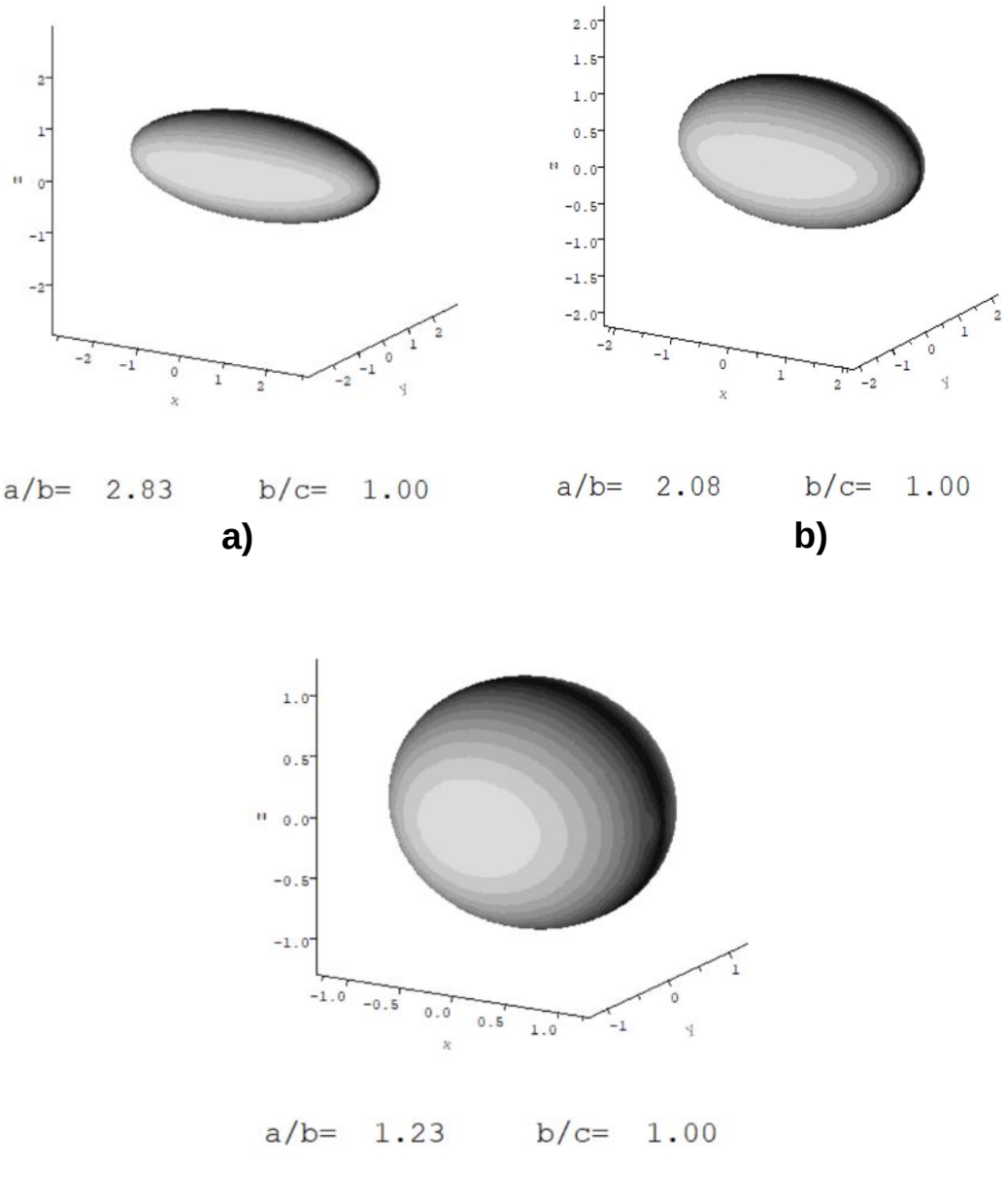

Figure 142. Ellipsoidal representations from the conformation analysis of PS550 in isopropanol at different degrees of solvent association, using the programme ELLIPS1 with the shape parameter ν. a) $(v_s/\bar{v})$ = 1.0; b) $(v_s/\bar{v})$ = 1.2; c) $(v_s/\bar{v})$ = 1.4.

5.3.2.5 Mark–Houwink–Kuhn–Sakurada plots

From the M_w and $[\eta]$ values calculated from these experiments, it was possible to construct Mark–Houwink–Kuhn–Sakurada (MHKS) plots of log $[\eta]$ vs log M_w (Figure 143) for the siloxanes to yield the MHKS *'a'* coefficient from the slope where

$$[\eta] = K_n {M_w}^a \quad \textbf{(18)}$$

and K_η is a constant. MHKS '*a'* values range from ~ 0 for a spherical/globular particle, 0.5 – 0.8 for a flexible-extended coil, and >1.2 for a rod (see for example Harding, 1997).

In isopropanol (Figure 143a), the slope '*a*' ~ (0.15 ± 0.07) was consistent with a spherical/globular approximation so the application of the ellipsoid models is justified. In turpentine '*a*' was ~ (0.66 ± 0.05), which was approaching an extended coil, again consistent with the aspect ratios obtained from the conformation analyses. It should be noted that for the turpentine plot (Figure 143b), the M_w values obtained from the previous SE experiments carried out in isopropanol were used. This was because, as previously discussed, it was not possible to carry out SE in turpentine.

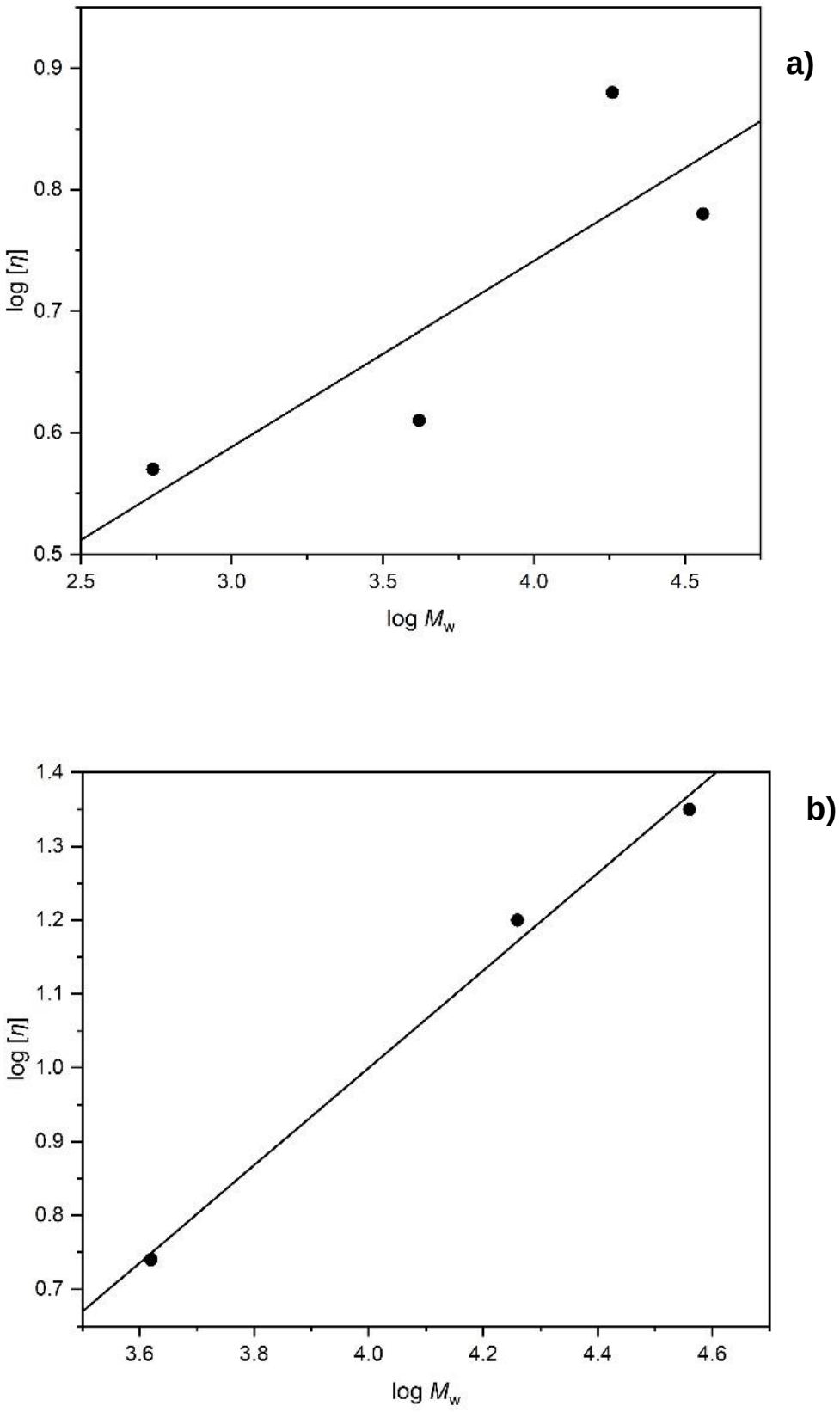

Figure 143. MHKS plots of the siloxanes in (a) isopropanol (a ~ 0.15) and (b) turpentine (a ~ 0.66).

5.3.3 Overall discussion

The characterisation of the consolidants Butvar® B-98 and four different PDMS-OH preparations (PS36000, PS18000, PS4200 and PS550) was successfully carried out, primarily with the use of AUC. The SE studies revealed that Butvar® B-98 had a M_w of ~ 54.0 kDa, while the different samples of siloxanes had an M_w of ~ 52.5 kDa, 38.8 kDa, 6.2 kDa, and 1.6 kDa.

Table 43 shows a comparison of the experimental M_w results and the data reported on the technical sheets of these materials. The experimental M_w value of Butvar® B-98 was shown to be consistent with the data provided by the manufacturer, which was based on size exclusion chromatography coupled to a low angle light scattering detector. Like SE, this is an absolute method not requiring assumptions concerning polymer conformation. The absolute values for the M_ws of the siloxanes obtained in this research may provide a more accurate measure of molecular weight compared to the previously available M_w values, which were relative to polystyrene standards. The differences were probably due to the different conformations of the siloxanes and the standards.

Table 43. A comparison of the molecular weight values provided by the manufacturer and the experimental M_w values obtained by the SE experiments

Polymer	M_w according to manufacturer (Da)	M_w value obtained by sedimentation equilibrium (Da)
Butvar® B-98	40,000 -70,000	54,000 ± 1,500
PS36000	36,000	52,500 ± 3,000
PS18000	18,000	38,800 ± 1,500
PS4200	4,200	6,200 ± 700
PS550	~ 550	1,550 ± 50

SV, reinforced by the MultiSig analysis of SE solute distributions, demonstrated that all polymers (Butvar® B-98 and PDMS-OH) were heterogeneous with a broad range of molecular weights. This may affect how efficiently these polymers can penetrate and consolidate archaeological wood.

Conformational analyses in isopropanol confirmed that the polymers, in general, possessed an elongated shape. This was especially true for Butvar® B-98, with the

viscosity increment ν indicating an axial ratio of ~ 25 (allowing for a plausible solvation range). Note that these Butvar® B-98 tests were carried out in isopropanol whilst the Saving Oseberg team had used a solvent system of a different non-aqueous solvent, namely toluene/ethanol. However, one can expect the Butvar® B-98 dissolved in both isopropanol and toluene/ethanol to have similar properties, assuming comparable solubilities. The different samples of PDMS-OH had much less extended conformations in isopropanol, with ν aspect ratios in the range of 2 – 6. In turpentine the two largest PDMS-OH samples appeared to be more extended, which was also reflected in their high $[\eta]$ (Table 44). This difference may relate to previous observations made by the Saving Oseberg group from the use of PS36000 in both turpentine and isopropanol to treat degraded archaeological wood (Zisi, 2020). Figure 144 shows separation between the PS36000 and solvent almost immediately after mixing with isopropanol. In contrast, such a separation is absent in the mix of the polymer with turpentine, even after one month. The more extended conformation of PS36000 in turpentine is most likely due to the greater solvent interaction with turpentine.

Table 44. A comparison of the $[\eta]$ values obtained for all the tested polymers

	$[\eta]$ in isopropanol (mL/g)	**$[\eta]$ in turpentine (mL/g)**
Butvar® B-98	57± 3	N/A
PS36000	6.0 ± 0.3	22.4 ± 1.1
PS18000	7.5 ± 0.4	15.8 ± 0.8
PS4200	4.1 ± 0.2	5.5 ± 0.3
PS550	3.7 ± 0.2	*

*flow time increment too small

The Saving Oseberg group has tested three different concentrations of PS36000 in the two solvents, 30%, 50%, and 70%. These were used to immerse a number of archaeological wood test specimens for a period of two weeks (Zisi, 2020). Due to the experimental set-up, test specimens were layered in an immersion bath. When the weight percentage gain of the wood test specimens was calculated for all concentrations and solution types, it was noted that the specimens stacked at the top of the isopropanol/polymer bath all had consistently gained the least weight. This was in contrast to the test specimens immersed in the turpentine/polymer bath. In this case, there was no relationship observed between the weight percentage gain and the positioning of a test specimen in the immersion bath. Essentially, the wood test

specimens sitting on the top part of the polymer/isopropanol bath were exposed to a lower polymer concentration than aimed for, due to the previously observed separation of the two components.

The practical meaning of this for a conservator is that, for instances involving application of the large molecular weight siloxanes such as PS36000 as a consolidant in wood *via* immersion, the preferable solvent to work with would be turpentine to ensure the desired amount of consolidant uptake by the wood. This is especially true considering the prolonged periods of immersion time. Moreover, this choice is reinforced by its natural or 'green' origins from pine wood. However, solutions of PS36000 in isopropanol could be recommended for applications on wood *via* injection, as long as the mixture is gently shaken before administration, since short application times are involved. Since a consolidant application *via* injection brings conservators in close contact with a wooden object, the choice of a solvent that is less harmful to human health, that is isopropanol, would be better than turpentine in this case. Lengthy evaporation rates (months to years) of turpentine may also be considered problematic.

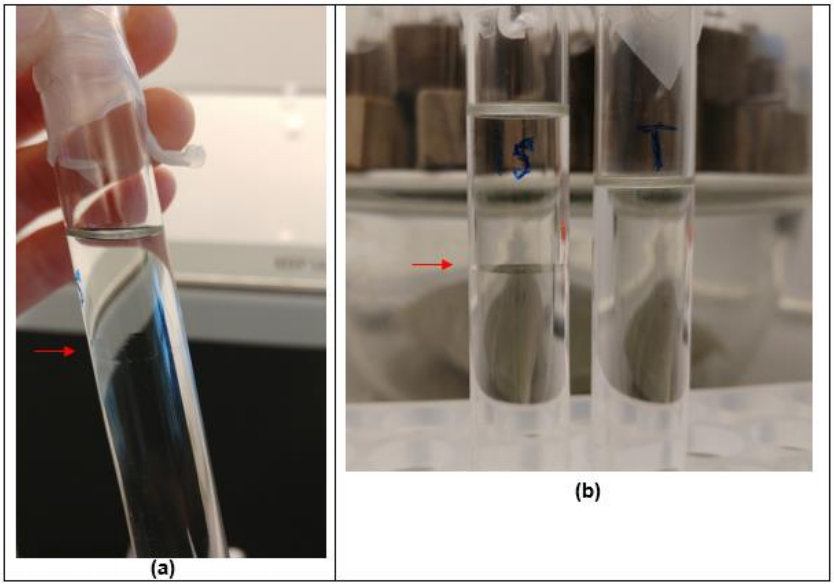

Figure 144. (a) PS36000 in isopropanol, showing phase separation of components as indicated by the red arrow (b) A comparison of PS36000 in isopropanol (left) and turpentine (right) after one month. Photos: Dr Angeliki Zisi, Museum of Cultural History, University of Oslo.

5.4 Conclusion

Butvar® B-98 and PDMS-OH possess the common advantage of being soluble in organic solvents. This is particularly important for some of the Oseberg artefacts, as avoiding aqueous treatment will help in preventing further possible damage during retreatment. Consequently, the Saving Oseberg group has already run some wood studies with these polymers in order to understand how they affect archaeological wood (Zisi, 2020; Zisi *et al.*, 2021). The work described here was performed with the aim of building up on these investigations.

Regarding future work, an area of curiosity regarding Butvar® B-98 and PDMS-OH which still has not been investigated is the fact that they manage to penetrate wood at all, given their large molecular weights. There is currently no clear answer why this is so. It could be somehow related to their shape or interactions with both the wood and the solvent, or maybe it is only the lower molecular weight components found in these polymer systems that actually manage to penetrate wood. Such an investigation could be carried out by testing the different molecular weights of PDMS-OH separately and then comparing their extent of penetration with IR or SEM. The differences in consolidation between the PDMS-OH samples could also be analysed using hardness tests, as was described for TPA6 and TPA7.

The work in this chapter has successfully expanded the knowledge base of Butvar® B-98 and PDMS-OH and has helped in understanding their behaviour. This will hopefully result in a higher confidence level when it comes to deciding which consolidants to use in the retreatment of the Oseberg finds, as it will certainly do for other archaeological artefacts.

5.5 Experimental

5.5.1 Materials

All reagents and solvents were purchased from a chemical supplier (Acros Organics Ltd, Alfa Aesar Ltd., Merck Ltd., or Fisher Scientific Ltd.) and used without further purification. Butvar® B-98 and PDMS-OH 36,000 (PS36000) and 18,000 (PS18000) were obtained from Acros Organics Ltd. and Fluorochem Ltd. respectively. PDMS-OH 4200 (PS4200) and ~ 550 (PS550) were obtained from VWR International Ltd. and Merck Ltd.

5.5.2 General methods and instrumentation

5.5.2.1 AUC studies

A Beckman Optima XL-I analytical ultracentrifuge with Rayleigh interference optics was used at 20.0 °C. 12 mm optical path length double sector cells with titanium centrepieces were employed.

5.5.2.1.1 SV methodology

The general procedure was the same for all polymers (Butvar® B-98 and PDMS-OH). An amount of 405 µL of different concentrations (0.5 to 4.0 mg/mL) of polymer in isopropanol was added to each of the cells. Isopropanol was used as the reference solvent. The experiments were carried out at a temperature of 20.0 °C. A rotational speed of 49,000 rpm was used, and the samples were centrifuged overnight. The

weighted average sedimentation coefficient and the distributions of sedimentation coefficient *c(s)* vs *s* were obtained by analysis with the SEDFIT procedure (Schuck, 2000; Dam and Schuck, 2004).

5.5.2.1.2 SE methodology

The same general procedure was used for all polymers. The rotational speed utilised in each experiment depended on the approximated weight of each polymer. Loading concentrations of 0.5 to 4.0 mg/mL of polymer in isopropanol were used. An amount of 100 µL of each concentration was injected into the sample solution channel of the cell. Isopropanol was used as the reference solvent. The experiments were carried out at a temperature of 20.0 °C. For Butvar® B-98, the experiment was carried out at a rotational speed of 22,000 rpm over 2 days. For PS36000 and PS18000, the experiments were carried out over 2 days using rotational speeds of 22,000 rpm and 30,000 rpm respectively. The experiments for PS4200 and PS550 were both carried out at a speed of 49,500 rpm and left overnight. The results were analysed with SEDFIT-MSTAR (Schuck *et al.*, 2014) in order to obtain the apparent weight-average molecular weight $M_{w,app}$, making use of the *M** extrapolation (Creeth and Harding, 1982) and the hinge point method (Schuck *et al.*, 2014). The data obtained from the highest concentration (4.0 mg/mL) was additionally analysed with the MultiSig algorithm (Gillis *et al.*, 2013) to evaluate the molecular weight distribution.

5.5.2.2 Viscosity measurements – calculation of the intrinsic viscosity $[\eta]$

An Anton-Paar AMVn (Graz, Austria) rolling ball viscometer was used at a temperature of 10.0 °C. Its closed capillary system was more suitable for working with volatile solvent systems compared to conventional Ostwald viscometers. The low temperatures were chosen to prevent the solvents (isopropanol and turpentine) from evaporating due to their high volatility.

The viscosity measurements were carried out using solutions of 6.0 mg/mL concentration of each polymer dissolved in solvent. The measurement for Butvar® B-98 was only carried out in isopropanol. The PDMS-OH polymers were all measured in both isopropanol and turpentine. The $[\eta]$ values were then calculated with the Solomon-Ciuta equation (Equation 10) (Solomon and Ciută, 1962).

$$[\eta] = \frac{1}{c}\left(2\left(\eta_{sp}\right) - 2ln(\eta_r)\right)^{\frac{1}{2}} \quad \textbf{(10)}$$

5.5.2.3 Conformational analyses

The ELLIPS1 (Harding, Horton and Cölfen, 1997) algorithm was used to carry out analyses with the viscosity increment (ν) (Equation 12) (Simha, 1940; Saito, 1951) and the Perrin (*P*) (Equation 13a) (Perrin, 1936) shape factors.

$$\nu = [\eta]M/(N_A \mathrm{V}) \quad \textbf{(12)}$$

$$P = (f/f_o)\,(\bar{v}/v_s)^{\frac{1}{3}} \quad \textbf{(13a)}$$

Additional analysis was also performed for the PDMS-OH series with Mark–Houwink–Kuhn–Sakurada (MHKS) plots. This was carried out by plotting log $[\eta]$ vs log M_w. The M_w values used were the ones calculated by SE. Two plots were prepared, one using the $[\eta]$ value calculated with isopropanol and the other using the $[\eta]$ value that was calculated with turpentine.

6. Overall Conclusions and Outlook

6.1 Overview

The Oseberg collection features some of the most precious Viking wooden artefacts in the world. The alum treatment that they were subjected to upon excavation in the early 20th century, while successfully providing support for the weakened structure of the waterlogged wood, also inadvertently led to the formation of a very acidic environment and the state of degradation that the artefacts find themselves in presently. Because of this, there is currently a race against time to develop new methodologies to reduce their active degradation and increase their structural strength.

The severe decay of the Oseberg artefacts is such that many are only held together by the alum present in their wooden structure. Additionally, many objects have been reconstructed in ways that are not possible to undo without causing further damage. The objects with the highest degree of degradation and those which have been heavily reconstructed cannot be retreated with polymers in aqueous solutions. This is because the alum remaining in the artefacts may dissolve in water and consequently diffuse from the wooden structure, leading to total disintegration. As a result, it is deemed preferable to treat the most deteriorated and reconstructed artefacts with non-aqueous methods.

The primary aim of the work described in this thesis was to develop novel, bioinspired consolidants which would potentially be able to form part of the treatment toolkit available to wood conservators. Terpenes were the chosen feedstock from which to produce these consolidants, taking into consideration their sustainable source and their ability to be functionalised. Two hydroxylated monomers were successfully synthesised from α-pinene, each modified with an acrylate moiety. To complement this work another monomer was also synthesised, this time derived from oleic acid. These monomers were used to produce three polymers which were named TPA5, TPA6 and TPA7. TPA5 and TPA6 were fully terpene-based whilst TPA7 was a

copolymer composed of both terpene and fatty acid components. These reactions were successfully optimised to achieve low molecular weight polymers which would be able to penetrate wood. All three polymers were soluble in isopropanol, a solvent which was deemed appropriate to use in the future retreatment of the most fragile Oseberg artefacts.

The characterisation of these compounds was carried out primarily using AUC and other hydrodynamic techniques. These studies provided extensive information on the nature of the polymer systems. They confirmed that the polymers had appropriate molecular weights, these being ~ 4.3 kDa, 3.9 kDa and 4.2 kDa for TPA5, TPA6 and TPA7 respectively. The size distribution studies carried out by AUC indicated that these polymer systems, whilst heterogeneous, were comprised primarily of these small molecular weight molecules. This meant that if used as consolidants, most of the polymer molecules would be easily able to penetrate wood, making the treatments more effective and less wasteful.

The syntheses of TPA6 and TPA7 was scaled up and 50 g of each polymer were successfully made. Due to time constraints and low reaction efficiency, it was decided to not scale up TPA5. TPA6 and TPA7 were subjected to studies using archaeological wood, with the main aim being to determine their extent of penetration. These studies showed that both polymers managed to penetrate, with the highest concentration being found on the surface of the wood specimens. This was confirmed by both ATR-FTIR and SEM. Moreover, as detected by ATR-FTIR, it could also be seen that the polymers were present in the core of the wood specimens. Both TPA6 and TPA7 induced a colour change in the wood, although this was not considered to be drastic. Hardness tests confirmed that both polymers increased the resistance of the wood surface to indentation, compared to untreated wood. These changes were found to be statistically significant, meaning that these polymers had a positive consolidative effect on the archaeological wood. With such promising results it can be envisaged that TPA6 and TPA7 could become viable treatment options not only for the Oseberg artefacts but also for other archaeological wood requiring non-aqueous conservation, since there is no reason why they should be restricted to treating only the Oseberg collection.

Other work that was carried out as part of this thesis involved the characterisation of two existing consolidants, Butvar® B-98 and PDMS-OH, which were being tested concurrently by the Saving Oseberg group. This was important since, along with the terpene-derived polymers, they are considered to be promising candidates for

treating the most highly degraded pieces of the Oseberg collection. This set of studies, carried out mainly by AUC and viscometry, widened the knowledge base of both consolidants. The results can now be used to help explain some of the behaviour that these polymers exhibit during treatment. For example, the different conformations that PDMS-OH assumes in isopropanol and turpentine could be the reason why it behaves differently in these solvents. As such, this work will help conservators to be able to make more confident choices about which consolidant to use between Butvar® B-98 and the different preparations of PDMS-OH, both for the retreatment of the Oseberg artefacts and for other conservation projects.

6.2 Future work

Suggestions for further investigations were given at the end of each chapter. This section will build upon and expand those ideas. There are several lines of research that could be picked up. TPA6 and TPA7 were found to have a relatively low T_g (~ 31 and 19 °C respectively), which would limit their use somewhat to colder climates. While this should not be a problem, seeing that most museums have a temperature control system, a higher T_g would still be preferable, especially for TPA7. As such, it would be useful to attempt synthesising the same monomers and functionalise them with methacrylate groups instead of acrylate moieties. This could lead to polymers having a higher T_g (Sainz *et al.*, 2016), which could thereafter be used in environments with hotter climates.

Additionally, one of the main issues regarding the synthesis of such monomers and polymers is the use of unsustainable solvents and reactants. Bioinspired polymers such as TPA5, TPA6 and TPA7 have reduced negative impact on the environment by virtue of being sourced from biomass, however their production cannot be considered to be truly sustainable (Walsh-Korb, 2022). Every effort has been made to make the chemical synthesis processes described in this thesis as ‘green’ as possible. These included using water and mild conditions (the synthesis of *trans*-sobrerol) and making reagent substitutions when appropriate (replacing acryloyl chloride with acrylic acid and T3P®). It should be recognised however that these processes and reagents are still far from being environmentally harmless. More

optimisation of the monomer and polymer synthesis protocols can therefore be carried out in the future to attempt to make them more sustainable. Moreover, it would also be worth looking into the optimisation of the synthesis of the TPA5 polymer so that it can become more scalable and thus transform it into a viable option for wood consolidation.

With regards to TPA6 and TPA7, more extensive testing would be required before they can be considered proper options for the treatment of wood. In particular, long-term stability studies will be essential as these would provide information on how these polymers fare in the wood after months or years. In order to be a viable consolidant, more information would also be needed on their toxicity and by-product formation (Walsh-Korb, 2022). Additionally, since TPA6 and TPA7 do not have any deacidifying properties, it is anticipated that they would be used as a combination treatment with $Ca(OH)_2$ nanoparticles. This can be done using a two-step process whereby the wood is first treated with the nanoparticles, followed by the consolidants. These polymers should therefore be tested with the alkaline nanoparticles to gain an understanding of any interactions that may take place between them.

In addition to terpene-derived polymers, other biobased consolidants should be investigated. A particularly interesting material that can be explored is sporopollenin. This is an inert biopolymer found in the cell walls of all pollen and spores (Li *et al.*, 2019). It is impervious to attacks from chemical, physical or biological sources (Brooks and Shaw, 1968; Mackenzie *et al.*, 2015; Jardine *et al.*, 2017), with Mackenzie *et al*. calling it “the toughest plant substance known” (Mackenzie *et al.*, 2015). It is so stable that it has been retrieved from rocks which are millions of years old (Wellman, Osterloff and Mohiuddin, 2003; Archibald *et al.*, 2014; Mackenzie *et al.*, 2015). Li *et al*. have managed to elucidate the chemical structure of pine sporopollenin using thioacidolysis and NMR (Figure 145) (Li *et al.*, 2019). This is the first time that the molecular structure of sporopollenin has been determined. It is composed of phenylpropanoid and polyhydroxylated aliphatic lipid monomers covalently bound by ether and ester linkages (Brooks and Shaw, 1968; Shi *et al.*, 2015). Sporopollenin acts as a protective outer layer for the exine (the coatings of pollen or spores) and aids in the terrestrial migration of the plant (Shi *et al.*, 2015; Li *et al.*, 2019). Sporopollenin exines protect the plant gamete from light (Rozema *et al.*, 2001; Atkin *et al.*, 2011; Mackenzie *et al.*, 2015) and have antioxidant properties (Mackenzie *et al.*, 2015). Its extreme robustness makes the sporopollenin microcapsules particularly attractive for many applications. There have been numerous studies concerning the possible uses of sporopollenin (Archibald *et al.*,

2014), from the use as microreactors in nanoscience (Paunov, Mackenzie and Stoyanov, 2007), delivery of drugs or other ligands (Ayar and Mercimek, 2006; Ayar *et al.*, 2008; Wakil *et al.*, 2010; Diego-Taboada *et al.*, 2013) to medical imaging (Lorch *et al.*, 2009). It has also been investigated for its potential use as a green support for lipases (De Souza *et al.*, 2015) and more recently, as an anchor for ionic liquids (Palazzo *et al.*, 2018). To date, there are not any reports which discuss the application of sporopollenin as a consolidant in conservation. Its viability should be investigated thoroughly in the future as it has several promising properties such as its sustainable source, compatibility and high resilience.

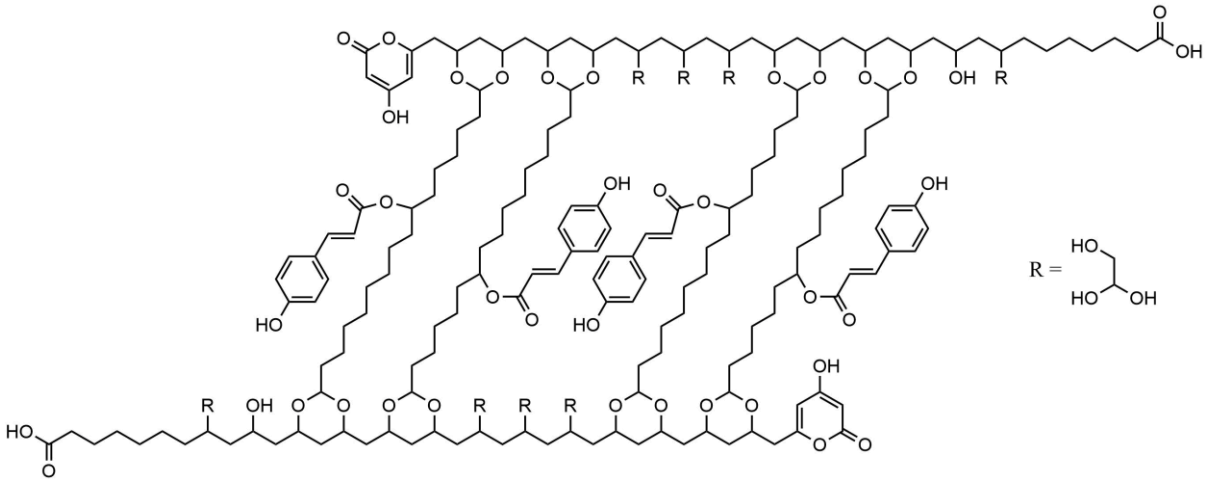

Figure 145. The average structure of pine sporopollenin elucidated by Li *et al*. using quantitative ^{13}C NMR (Li *et al.*, 2019)

The perfect consolidant – one that provides stability and strength, is non-toxic, compatible, reversible, inexpensive, stable and sustainable – has so far proved elusive (Broda and Hill, 2021). Indeed, the existence of such a perfect compound might not prove realistic. Nevertheless, the research carried out for this thesis has striven to develop polymers that are a step above the current crop of consolidants. TPA6 and TPA7, given further time and research, could potentially prove to be a valuable addition to the treatment toolkit that conservators have at hand, not only for the Oseberg collection but also for other archaeological wooden artefacts.

References

Aharoni, S. M. (1998) 'Increased glass transition temperature in motionally constrained semicrystalline polymers', *Polymers for Advanced Technologies*, 9(3), pp. 169–201. doi: 10.1002/(SICI)1099-1581(199803)9:3<169::AID-PAT740>3.0.CO;2-Z.

Aksakal, S. *et al.* (2019) 'Copper mediated RDRP of thioacrylates and their combination with acrylates and acrylamides', *Polymer Chemistry*. Royal Society of Chemistry, 10(48), pp. 6622–6629. doi: 10.1039/c9py01518c.

Almasi, H. *et al.* (2015) 'Heterogeneous modification of softwoods cellulose nanofibers with oleic acid: Effect of reaction time and oleic acid concentration', *Fibers and Polymers*, 16(8), pp. 1715–1722. doi: 10.1007/s12221-015-4294-1.

Almkvist, G. and Persson, I. (2011) 'Distribution of iron and sulfur and their speciation in relation to degradation processes in wood from the Swedish warship Vasa', *New Journal of Chemistry*, 35, pp. 1491–1502. doi: 10.1039/c1nj20056a.

Alzahrani, Q. E. *et al.* (2016a) 'Matrix-free hydrodynamic study on the size distribution and conformation of three technical lignins from wood and non-wood', *Holzforschung*, 70, pp. 117–125. doi: 10.1515/hf-2014-0318.

Alzahrani, Q. E. *et al.* (2016b) 'Matrix-free hydrodynamic study on the size distribution and conformation of three technical lignins from wood and non-wood', *Holzforschung*. Walter de Gruyter GmbH, 70(2), pp. 117–125. doi: 10.1515/hf-2014-0318.

An, L. *et al.* (2020) 'Efficient and green approach for the esterification of lignin with oleic acid using surfactant-combined microreactors in water', *BioResources*, 15(1), pp. 89–104. doi: 10.15376/biores.15.1.89-104.

Anastas, P. and Eghbali, N. (2010) 'Green chemistry: Principles and practice', *Chemical Society Reviews*, 39, pp. 301–312. doi: 10.1039/b918763b.

Andriulo, F. *et al.* (2016) 'Nanotechnologies for the restoration of alum-treated archaeological wood', *Applied Physics A: Materials Science and Processing*, 122, pp. 1–9. doi: 10.1007/s00339-016-9833-0.

Andriulo, F. *et al.* (2017) 'Hybrid nanocomposites made of diol-modified silanes and nanostructured calcium hydroxide. Applications to Alum-treated wood', *Pure Appl. Chem.*, 89, pp. 29–39. doi: 10.1515/pac-2016-1014.

Andriulo, F. *et al.* (2022) 'Evaluation of sol-gel hybrid nanocomposites for dry medieval wood', *Journal of Cultural Heritage*. Elsevier Masson SAS, 56, pp. 96–107. doi: 10.1016/j.culher.2022.06.004.

Antonelli, F. *et al.* (2020) 'Essential oils as alternative biocides for the preservation of waterlogged archaeological wood', *Microorganisms*, 8(12), pp. 1–25. doi: 10.3390/microorganisms8122015.

Antonelli, F. *et al.* (2020) 'Cellulose and Lignin Nano-Scale Consolidants for Waterlogged Archaeological Wood', *Front. Chem.*, 8, p. 32. doi: 10.3389/fchem.2020.00032.

Archibald, S. J. *et al.* (2014) 'How does iron interact with sporopollenin exine capsules? An X-ray absorption study including microfocus XANES and XRF imaging', *Journal of Materials Chemistry B*, 2, pp. 945–959. doi: 10.1039/c3tb21523g.

Astronomo, R. D. and Burton, D. R. (2010) 'Carbohydrate vaccines: Developing sweet solutions to sticky situations?', *Nature Reviews Drug Discovery*, 9, pp. 308–324. doi: 10.1038/nrd3012.

Atalay, S., Sargin, I. and Arslan, G. (2022) 'Slow-release mineral fertilizer system with chitosan and oleic acid-coated struvite-K derived from pumpkin pulp', *Cellulose*. Springer Netherlands, 29(4), pp. 2513–2523. doi: 10.1007/s10570-022-04453-5.

Atkin, S. L. *et al.* (2011) 'UV and visible light screening by individual sporopollenin exines derived from Lycopodium clavatum (club moss) and Ambrosia trifida (giant ragweed)', *Journal of Photochemistry and Photobiology B: Biology*, 102, pp. 209–217. doi: 10.1016/j.jphotobiol.2010.12.005.

Atkinson, R. L. *et al.* (2021) 'RAFT polymerisation of renewable terpene (meth)acrylates and the convergent synthesis of methacrylate-acrylate-methacrylate triblock copolymers', *Polymer Chemistry*. Royal Society of Chemistry, 12(21), pp. 3177–3189. doi: 10.1039/d1py00326g.

Ayar, A. *et al.* (2008) 'On the removal of some phenolic compounds from aqueous solutions by using a sporopollenin-based ligand-exchange fixed bed - Isotherm analysis', *Desalination*, 219, pp. 160–170. doi: 10.1016/j.desal.2007.05.012.

Ayar, A. and Mercimek, B. (2006) 'Interaction of nucleic acid bases and nucleosides with cobalt ions immobilized in a column system', *Process Biochemistry*, 41, pp. 1553–1559. doi: 10.1016/j.procbio.2006.02.016.

Ayelo, P. M. *et al.* (2021) 'Terpenes from herbivore-induced tomato plant volatiles attract Nesidiocoris tenuis (Hemiptera: Miridae), a predator of major tomato pests', *Pest Management Science*, 77(11), pp. 5255–5267. doi: 10.1002/ps.6568.

Babiński, L. (2015) 'Dimensional changes of waterlogged archaeological hardwoods pre-treated with aqueous mixtures of lactitol/trehalose and mannitol/trehalose before freeze-drying', *Journal of Cultural Heritage*, 16, pp. 876–882. doi: 10.1016/j.culher.2015.03.010.

Babiński, L., Izdebska-Mucha, D. and Waliszewska, B. (2014) 'Evaluation of the state of preservation of waterlogged archaeological wood based on its physical properties: Basic density vs. wood substance density', *Journal of Archaeological Science*, 46(1), pp. 372–383. doi: 10.1016/j.jas.2014.03.038.

Baumann, H. *et al.* (1988) 'Natural Fats and Oils-Renewable Raw Materials for the Chemical Industry', *Angewandte Chemie (International ed. in English)*, 27, pp. 41–62.

Belgacem, M. N. and Gandini, A. (2008) *Monomers, Polymers and Composites from Renewable Resources*. Oxford, UK: Elsevier. Available at: https://app.knovel.com/hotlink/toc/id:kpMPCRR002/monomers-polymers-composites/monomers-polymers-composites.

Bhagwat, S. S. *et al.* (2021) 'Sustainable Production of Acrylic Acid via 3-Hydroxypropionic Acid from Lignocellulosic Biomass', *ACS Sustainable Chemistry and Engineering*, 9(49), pp. 16659–16669. doi: 10.1021/acssuschemeng.1c05441.

Biermann, U. *et al.* (2008) 'New Syntheses with Oils and Fats as Renewable Raw Materials for the Chemical Industry', *Biorefineries-Industrial Processes and Products: Status Quo and Future Directions*, 2, pp. 253–289. doi:

10.1002/9783527619849.ch25.

Bjurhager, I. *et al.* (2010) 'Towards improved understanding of PEG-impregnated waterlogged archaeological wood: A model study on recent oak', *Holzforschung*, 64(2), pp. 243–250. doi: 10.1515/HF.2010.024.

Bonde, N. and Christensen, A. E. (1993) 'Dendrochronological dating of the Viking Age ship burials at Oseberg, Gokstad and Tune, Norway', *Antiquity*, 67, pp. 575–83.

Braovac, S. (2015) *Alum-treated wood Material characterization A case-study of the Oseberg finds*. The Royal Danish Academy of Fine Arts, Schools of Architecture, Design and Conservation.

Braovac, S. *et al.* (2016) 'Chemical analyses of extremely degraded wood using analytical pyrolysis and inductively coupled plasma atomic emission spectroscopy', *Microchem. J.*, 124, pp. 368–379. doi: 10.1016/j.microc.2015.09.016.

Braovac, S. *et al.* (2018) 'Navigating conservation strategies: linking material research on alum-treated wood from the Oseberg collection to conservation decisions', *Heritage Science*, 6, pp. 1–16. doi: 10.1186/s40494-018-0241-y.

Braovac, S. and Kutzke, H. (2012) 'The presence of sulfuric acid in alum-conserved wood - Origin and consequences', *Journal of Cultural Heritage*, 13(3 SUPPL.), pp. S203–S208. doi: 10.1016/j.culher.2012.02.002.

Braovac, S., Łucejko, J. and de Lamotte, A. (2020) *D.2.2.1 Penetration of soda lignin from straw in archaeological wood*.

Braovac, S. *et al.* (2021) *D.3.8.1 Retreatment of alum-treated wood from the Oseberg collection*.

Braun, D. *et al.* (2013) 'Methods and Techniques for Synthesis, Characterization, Processing, and Modification of Polymers', in *Polymer Synthesis: Theory and Practice*. 5th edn. Berlin, Heidelberg: Springer-Verlag, pp. 33–147.

Briffa, S. M. and Vella, D. A. (2019) 'The behaviour of as-applied and artificially weathered silica–epoxy consolidants on a typical Mediterranean porous limestone: a comparison with TEOS', *Heritage Science*. Springer, 7(30), pp. 1–13. doi: 10.1186/s40494-019-0270-1.

Broda, M. *et al.* (2015) 'The state of degradation of waterlogged wood from different environments', *Ann. WULS - SGGW, For. and Wood Technol.*, 91, pp. 23–27.

Broda, M. and Hill, C. A. S. (2021) 'Conservation of waterlogged wood—past, present and future perspectives', *Forests*, 12, pp. 1–57. doi: 10.3390/f12091193.

Brooks, J. and Shaw, G. (1968) 'Chemical structure of the exine of pollen walls and a new function for carotenoids in nature', *Nature*, 219, pp. 532–533. doi: 10.1038/219532a0.

Brown, H. C. (1961) 'Hydroboration—a powerful synthetic tool', *Tetrahedron*, 12, pp. 117–138.

Bugani, S. *et al.* (2009) 'Study on the impregnation of archaeological waterlogged wood with consolidation treatments using synchrotron radiation microtomography', *Analytical and Bioanalytical Chemistry*, 395, pp. 1977– 1985. doi: 10.1007/s00216-009-3101-5.

Burke, A. *et al.* (2002) 'Iron(III) ion removal from solution through adsorption on chitosan', *Journal of Applied Polymer Science*, 84, pp. 1185–1192. doi: 10.1002/app.10416.

Cabane, E. *et al.* (2016) 'Functional lignocellulosic materials prepared by ATRP from a wood scaffold', *Scientific Reports*, 6, pp. 1–10. doi: 10.1038/srep31287.

Cappitelli, F., Cattò, C. and Villa, F. (2020) 'The control of cultural heritage microbial deterioration', *Microorganisms*, 8(10), pp. 1–20. doi: 10.3390/microorganisms8101542.

Carlson, S. M. and Schniewind, A. P. (1990) 'Residual Solvents in Wood-Consolidant Composites', *Studies in Conservation*, 35(1), pp. 26–32.

Carraher, C. E. J. (2013) 'Free-Radical Chain Polymerization (Addition Polymerization)', in *Carraher's Polymer Chemistry*. CRC Press LLC, pp. 199–234.

Carrasco, B. *et al.* (1999) 'Novel size-independent modeling of the dilute solution conformation of the immunoglobulin IgG Fab' domain using SOLPRO and ELLIPS', *Biophysical Journal*. Biophysical Society, 77(6), pp. 2902–2910. doi: 10.1016/S0006-3495(99)77123-7.

Cavallaro, G. *et al.* (2015) 'Thermal and dynamic mechanical properties of beeswax-halloysite nanocomposites for consolidating waterlogged archaeological woods', *Polymer Degradation and Stability*, 120, pp. 220–225. doi: 10.1016/j.polymdegradstab.2015.07.007.

Cavallaro, G. *et al.* (2017) 'Nanocomposites based on esterified colophony and halloysite clay nanotubes as consolidants for waterlogged archaeological woods', *Cellulose*. Springer Netherlands, 24(8), pp. 3367–3376. doi: 10.1007/s10570-017-1369-8.

Chapman, S. and Mason, D. (2003) 'Literature review: the use of Paraloid B72 as a surface consolidant for stained glass', *Journal of the American Institute for Conservation*, 42, pp. 381–392.

Chen, P. Y., McKittrick, J. and Meyers, M. A. (2012) 'Biological materials: Functional adaptations and bioinspired designs', *Progress in Materials Science*, 57, pp. 1492–1704. doi: 10.1016/j.pmatsci.2012.03.001.

Chooi, K. W. *et al.* (2014) 'Physical characterisation and long-term stability studies on quaternary ammonium palmitoyl glycol chitosan (GCPQ) - A new drug delivery polymer', *Journal of Pharmaceutical Sciences*, 103(8), pp. 2296–2306. doi: 10.1002/jps.24026.

Christensen, M. *et al.* (2015) 'Treatment of waterlogged archaeological wood using chitosan- and modified chitosan solutions. Part 1: Chemical compatibility and microstructure', *Journal of the American Institute for Conservation*, 54, pp. 3–13. doi: 10.1179/1945233014Y.0000000034.

Christensen, M., Kutzke, H. and Hansen, F. K. (2012) 'New materials used for the consolidation of archaeological wood-past attempts, present struggles, and future requirements', *Journal of Cultural Heritage*, 13S, pp. S183–S190. doi: 10.1016/j.culher.2012.02.013.

Chu, S., Cui, Y. and Liu, N. (2016) 'The path towards sustainable energy', *Nature Materials*. Nature Publishing Group, 16(1), pp. 16–22. doi: 10.1038/nmat4834.

Cipriani, G. *et al.* (2010) 'Cellulose as a renewable resource for the synthesis of wood consolidants', *Journal of Applied Polymer Science*, 118, pp. 2939–2950. doi: 10.1002/app.32634.

Cipriani, G. *et al.* (2013) 'Synthesis of hydroxylated oligoamides for their use in wood conservation', *Journal of Applied Polymer Science*, 127, pp. 420–431. doi:

10.1002/app.37678.

Cnudde, V. *et al.* (2007) 'Determination of the impregnation depth of siloxanes and ethylsilicates in porous material by neutron radiography', *Journal of Cultural Heritage*. Elsevier Masson SAS, 8(4), pp. 331–338. doi: 10.1016/j.culher.2007.08.001.

Cole, J. L. *et al.* (2008) 'Analytical Ultracentrifugation: Sedimentation Velocity and Sedimentation Equilibrium', *Methods in Cell Biology*, 84, pp. 143–179. doi: 10.1016/S0091-679X(07)84006-4.

Collis, S. (2016) 'Revisiting conservation treatment methodologies for waterlogged archaeological wood: an Australian study', *AICCM*, 36, pp. 88–96. doi: 10.1080/10344233.2015.1111597.

Colonna, M. *et al.* (2011) 'Synthesis and radiocarbon evidence of terephthalate polyesters completely prepared from renewable resources', *Green Chemistry*, 13, pp. 2543–2548. doi: 10.1039/c1gc15400a.

Corma Canos, A., Iborra, S. and Velty, A. (2007) 'Chemical routes for the transformation of biomass into chemicals', *Chemical Reviews*, 107, pp. 2411–2502. doi: 10.1021/cr050989d.

Creangă, D. M. (2009) 'The conservation of archaeological wood', *European Journal of Science and Theology*, 5, pp. 57–68.

Creeth, J. and Harding, S. (1982) 'Some observations on a new type of point average molecular weight', *Journal of Biochemical and Biophysical Methods*, 7, pp. 25–34.

Crisci, G. M. *et al.* (2010) 'Consolidating properties of Regalrez 1126 and Paraloid B72 applied to wood', *Journal of Cultural Heritage*, 11, pp. 304–308. doi: 10.1016/j.culher.2009.12.001.

Cutajar, M. *et al.* (2021) 'Terpene polyacrylate TPA5 shows favorable molecular hydrodynamic properties as a potential bioinspired archaeological wood consolidant', *Scientific Reports*. Nature Publishing Group UK, 11(1), p. 7343. doi: 10.1038/s41598-021-86543-1.

Cutajar, M., Machado F., *et al*. (2022) 'Comparative hydrodynamic characterisation of two hydroxylated polymers based on α-pinene- or oleic acid-derived monomers for potential use as archaeological consolidants', *Scientific Reports*. Nature Publishing Group UK, 12(1), p. 18411. doi: 10.1038/s41598-022-21027-4

Cutajar, M., Stockman R., *et al.* (2022) 'Comparative Hydrodynamic Study on Non-Aqueous Soluble Archaeological Wood Consolidants: Butvar B-98 and PDMS-OH Siloxanes', *Molecules*, 27(7), p. 2133. doi: 10.3390/molecules27072133

Dam, J. and Schuck, P. (2004) 'Calculating Sedimentation Coefficient Distributions by Direct Modeling of Sedimentation Velocity Concentration Profiles', *Methods in Enzymology*, 384, pp. 185–212. doi: 10.1016/S0076-6879(04)84012-6.

Darmanin, T. and Guittard, F. (2015) 'Superhydrophobic and superoleophobic properties in nature', *Materials Today*, 18, pp. 273–285. doi: 10.1016/j.mattod.2015.01.001.

Davis, S. L. *et al.* (2021) 'Conservation of Severely Deteriorated, Dry Painted Wood: A Case Study From Abydos, Egypt', *Journal of the American Institute for Conservation*. Taylor & Francis, 0(0), pp. 1–21. doi: 10.1080/01971360.2021.1951551.

Davis, S. L., Roberts, C. and Poli, A. (2021) 'Paraloid® B-72/B-48N 1:1 as an

Adhesive for Use in Hot Climates: Literature Review, Laboratory Testing, and Observational Field Study', *Studies in Conservation*. Taylor & Francis, 0(0), pp. 1–9. doi: 10.1080/00393630.2021.1891810.

Diego-Taboada, A. *et al.* (2013) 'Protein free microcapsules obtained from plant spores as a model for drug delivery: Ibuprofen encapsulation, release and taste masking', *Journal of Materials Chemistry B*, 1, pp. 707–713. doi: 10.1039/c2tb00228k.

Diesendruck, C. E. *et al.* (2015) 'Biomimetic Self-Healing', *Angew. Chem., Int. Ed.*, 54, pp. 10428–10447. doi: 10.1002/ange.201500484.

Dimian, A. C. and Bildea, C. S. (2021) 'Sustainable process design for manufacturing acrylic acid from glycerol', *Chemical Engineering Research and Design*. Institution of Chemical Engineers, 166, pp. 121–134. doi: 10.1016/j.cherd.2020.12.002.

Eastman Chemical Company (2013) *Butvar. Polyvinyl butyral resin: Properties and uses*. Available at: http://www.butvar.com/pdfs/en/BVR-001.pdf.

El-Gamal, R. *et al.* (2016) 'The use of chitosan in protecting wooden artifacts from damage by mold fungi', *Electronic Journal of Biotechnology*. Elsevier B.V., 24, pp. 70–78. doi: 10.1016/j.ejbt.2016.10.006.

Elsmore, M. T. *et al.* (2022) 'Sustainable terpene triblock copolymers with tuneable properties for pressure sensitive adhesive applications', *Polymer Testing*. Elsevier Ltd, 109(February), p. 107530. doi: 10.1016/j.polymertesting.2022.107530.

Ermeydan, M. A. *et al.* (2014) 'Improvement of wood material properties via in situ polymerization of styrene into tosylated cell walls', *RSC Advances*, 4, pp. 12981–12988. doi: 10.1039/c4ra00741g.

Ershad-Langroudi, A., Fadaei, H. and Ahmadi, K. (2019) 'Application of polymer coatings and nanoparticles in consolidation and hydrophobic treatment of stone monuments', *Iranian Polymer Journal (English Edition)*. Springer London. doi: 10.1007/s13726-018-0673-y.

Fernández, M. D., Fernández, M. J. and Hoces, P. (2006) 'Synthesis of poly(vinyl butyral)s in homogeneous phase and their thermal properties', *Journal of Applied Polymer Science*, 102, pp. 5007–5017. doi: 10.1002/app.25004.

Firdaus, M., Espinosa, L. M. De and Meier, M. A. R. (2011) 'Terpene-Based Renewable Monomers and Polymers via Thiol-Ene Additions', *Macromolecules*, 44, pp. 7253–7262.

Florian, M.-L. E. (1989) 'Scope and History of Archaeological Wood', in Rowell, R. and Barbour, R. (eds) *Archaeological Wood*. American Chemical Society, pp. 3–32. doi: 10.1021/ba-1990-0225.ch001.

Fors, Y. and Sandström, M. (2006) 'Sulfur and iron in shipwrecks cause conservation concerns', *Chem. Soc. Rev.*, 35, pp. 399–415. doi: 10.1039/b507010b.

Fu, Q. *et al.* (2013) 'Toward strong and tough glass and ceramic scaffolds for bone repair', *Advanced Functional Materials*, 23, pp. 5461–5476. doi: 10.1002/adfm.201301121.

García de la Torre, J. and Harding, S. E. (2013) 'Hydrodynamic modelling of protein conformation in solution: ELLIPS and HYDRO', *Biophysical Reviews*, 5, pp. 195–206. doi: 10.1007/s12551-013-0102-6.

de Geus, A. R. *et al.* (2020) 'An analysis of timber sections and deep learning for wood species classification', *Multimedia Tools and Applications*, 79(45–46), pp.

34513–34529. doi: 10.1007/s11042-020-09212-x.

Geyer, R., Jambeck, J. R. and Law, K. L. (2017) 'Production, use, and fate of all plastics ever made', *Science Advances*, 3(7), pp. 3–8. doi: 10.1126/sciadv.1700782.

Giachi, G. *et al.* (2010) 'A methodological approach in the evaluation of the efficacy of treatments for the dimensional stabilisation of waterlogged archaeological wood', *Journal of Cultural Heritage*, 11, pp. 91–101. doi: 10.1016/j.culher.2009.04.003.

Gill, T. J. and Kunz, H. W. (1968) 'The Immunogenicity of Vinyl Polymers', *PNAS*, 61, pp. 490–496.

Gillis, R. B. *et al.* (2013) 'MultiSig: A new high-precision approach to the analysis of complex biomolecular systems', *European Biophysics Journal*, 42, pp. 777–786. doi: 10.1007/s00249-013-0924-y.

Giorgi, R., Chelazzi, D. and Baglioni, P. (2005) 'Nanoparticles of calcium hydroxide for wood conservation. The deacidification of the Vasa warship', *Langmuir*, 21, pp. 10743–10748. doi: 10.1021/la0506731.

Glastrup, J. *et al.* (2006) 'Degradation of PEG in the warship Vasa', *Macromolecular Symposia*, 238, pp. 22–29. doi: 10.1002/masy.200650604.

Golets, M., Ajaikumar, S. and Mikkola, J. P. (2015) 'Catalytic Upgrading of Extractives to Chemicals: Monoterpenes to "eXICALS"', *Chemical Reviews*. American Chemical Society, 115, pp. 3141–3169. doi: 10.1021/cr500407m.

González-Rubio, G. *et al.* (2021) 'Simple determination of gold nanocrystal dimensions by analytical ultracentrifugation via surface ligand-solvent density matching', *Nanomaterials*, 11(6). doi: 10.3390/nano11061427.

Gregory, D., Jensen, P. and Strætkvern, K. (2012) 'Conservation and in situ preservation of wooden shipwrecks from marine environments', *Journal of Cultural Heritage*, 13S, pp. S139–S148. doi: 10.1016/j.culher.2012.03.005.

von Hagens, G. (1980) 'Science and Technology of Advanced Materials 9(2) (2008) 1-6.Animal and Vegetal Tissues Permanently Preserved by Synthetic Resin Impregnation'.

Han, L. *et al.* (2022) 'Evaluation of PEG and sugars consolidated fragile waterlogged archaeological wood using nanoindentation and ATR-FTIR imaging', *International Biodeterioration and Biodegradation*. Elsevier Ltd, 170(February), p. 105390. doi: 10.1016/j.ibiod.2022.105390.

Han, X. *et al.* (2014) 'The use of menthol as temporary consolidant in the excavation of qin shihuang's terracotta army', *Archaeometry*, 56(6), pp. 1041–1053. doi: 10.1111/arcm.12069.

Han, X. *et al.* (2016) 'Bridged siloxanes as novel potential hybrid consolidants for ancient Qin terracotta', *Progress in Organic Coatings*. Elsevier B.V., 101, pp. 416–422. doi: 10.1016/j.porgcoat.2016.09.013.

Harding, S. E. (1997) 'The intrinsic viscosity of biological macromolecules. Progress in measurement, interpretation and application to structure in dilute solution', *Progress in Biophysics and Molecular Biology*, 68, pp. 207–262.

Harding, S. E. (2005) 'Challenges for the modern analytical ultracentrifuge analysis of polysaccharides', *Carbohydrate Research*. Elsevier BV, 340(5), pp. 811–826. doi: 10.1016/j.carres.2005.01.027.

Harding, S. E. (2012) 'Viscometry, analytical ultracentrifugation and light scattering

probes for carbohydrate stability', in Harding, S. E. (ed.) *Stability of Complex Carbohydrate Structures: Biofuels, Foods, Vaccines and Shipwrecks*. Cambridge, UK: Royal Society of Chemistry, pp. 80–98. Available at: https://www.researchgate.net/publication/300448683.

Harding, S. E. *et al.* (2015) 'Ultracentrifuge Methods for the Analysis of Polysaccharides, Glycoconjugates, and Lignins', *Methods in Enzymology*, 562, pp. 391–439. doi: 10.1016/bs.mie.2015.06.043.

Harding, S. E. (2018) 'The Svedberg Lecture 2017. From nano to micro: the huge dynamic range of the analytical ultracentrifuge for characterising the sizes, shapes and interactions of molecules and assemblies in Biochemistry and Polymer Science', *European Biophysics Journal*, 47, pp. 697–707. doi: 10.1007/s00249-018-1321-3.

Harding, S. E., Horton, J. C. and Cölfen, H. (1997) 'The ELLIPS suite of macromolecular conformation algorithms', *Eur. Biophys. J.*, 25, pp. 347–359.

Harding, S. E. and Rowe, A. J. (1982) 'Modelling biological macromolecules in solution: 3. The A-R intersection method for triaxial ellipsoids', *International Journal of Biological Macromolecules*, 4, pp. 357–361.

Harvey, B. G. *et al.* (2014) 'High-density biosynthetic fuels: The intersection of heterogeneous catalysis and metabolic engineering', *Physical Chemistry Chemical Physics*, 16(20), pp. 9448–9457. doi: 10.1039/c3cp55349c.

Hather, J. G. (2016) *The Identification of Northern European Woodso Title A Guide for Archaeologists and Conservators*. Abingdon and New York: Routledge.

Hazer, B. *et al.* (2019) 'Autoxidized Oleic Acid Bifunctional Macro Peroxide Initiators for Free Radical and Condensation Polymerization. Synthesis and Characterization of Multiblock Copolymers', *Journal of Polymers and the Environment*. Springer US, 27(11), pp. 2562–2576. doi: 10.1007/s10924-019-01536-6.

Heinze, T. *et al.* (2011) 'Protein-like oligomerization of carbohydrates', *Angewandte Chemie - International Edition*, 50, pp. 8602–8604. doi: 10.1002/anie.201103026.

Hellier, P. *et al.* (2013) 'Combustion and emissions characterization of terpenes with a view to their biological production in cyanobacteria', *Fuel*. Elsevier Ltd, 111, pp. 670–688. doi: 10.1016/j.fuel.2013.04.042.

Henriques, D. *et al.* (2014) 'Consolidating preservative-treated wood: Combined mechanical performance of boron and polymeric products in wood degraded by Coniophora puteana', *Journal of Cultural Heritage*. Elsevier Masson SAS, 15(1), pp. 10–17. doi: 10.1016/j.culher.2012.11.008.

Henríquez, C. *et al.* (2003) 'Thiols as chain transfer agents in free radical polymerization in aqueous solution', *Polymer*, 44(19), pp. 5559–5561. doi: 10.1016/S0032-3861(03)00581-0.

Hesse, M., Meier, H. and Zeeh, B. (1997) *Spectroscopic Methods in Organic Chemistry*. Stuttgart, New York: Thieme.

Heuts, J. P. A., Muratore, L. M. and Davis, T. P. (2000) 'Preparation and characterization of oligomeric terpolymers of styrene, methyl methacrylate and 2-hydroxyethyl methacrylate: A comparison of conventional and catalytic chain transfer', *Macromolecular Chemistry and Physics*, 201(18), pp. 2780–2788. doi: 10.1002/1521-3935(20001201)201:18<2780::AID-MACP2780>3.0.CO;2-Z.

Hocker, E., Almkvist, G. and Sahlstedt, M. (2012) 'The Vasa experience with polyethylene glycol: A conservator's perspective', *Journal of Cultural Heritage*, 13S,

pp. S175–S182. doi: 10.1016/j.culher.2012.01.017.

Hoffmann, P. and Wittköpper, M. (1999) 'The Kauramin method for stabilizing waterlogged wood', in Bonnot-Diconne, C. et al. (eds) *Proceedings of the 7th ICOM Group on Wet Organic Archaeological Materials Conference*. Grenoble - Arc-Nucléart, pp. 163–166.

Hon, D. N. S. and Shiraishi, N. (eds) (2021) *Wood and Cellulosic Chemistry*. New York and Basel: Marcel Dekker.

Horie, V. (2010) *Materials for Conservation: Organic consolidants, adhesives and coatings, Second Edition*. Elsevier.

Huggins, M. L. (1942) 'Thermodynamic Properties of Solutions of Long-Chain Compounds', *Annals of the New York Academy of Sciences*, XLIII, pp. 1–32.

Hunt, S. *et al.* (2021) 'Effect of polyethylene glycol treatment on acetic acid emissions from wood', *Forests*, 12(12), pp. 1–8. doi: 10.3390/f12121629.

Ibrahim, M. A. A. *et al.* (2021) 'In silico mining of terpenes from red-sea invertebrates for SARS-CoV-2 main protease (Mpro) inhibitors', *Molecules*, 26(7). doi: 10.3390/molecules26072082.

Iturri, J. *et al.* (2015) 'Torrent frog-inspired adhesives: Attachment to flooded surfaces', *Advanced Functional Materials*, 25, pp. 1499–1505. doi: 10.1002/adfm.201403751.

Jardine, P. E. *et al.* (2017) 'Shedding light on sporopollenin chemistry, with reference to UV reconstructions', *Review of Palaeobotany and Palynology*, 238, pp. 1–6. doi: 10.1016/j.revpalbo.2016.11.014.

Jensen, P. and Gregory, D. J. (2006) 'Selected physical parameters to characterize the state of preservation of waterlogged archaeological wood: A practical guide for their determination', *Journal of Archaeological Science*, 33(4), pp. 551–559. doi: 10.1016/j.jas.2005.09.007.

Jiang, J. *et al.* (2020) 'Improved hydrophobicity and dimensional stability of wood treated with paraffin/acrylate compound emulsion through response surface methodology optimization', *Polymers*, 12(1). doi: 10.3390/polym12010086.

Jingran, G. *et al.* (2014) 'Degradation assessment of waterlogged wood at Haimenkou site', *Frattura ed Integrita Strutturale*, 30, pp. 495–501. doi: 10.3221/IGF-ESIS.30.60.

Johnson, J. S. (1994) 'Consolidation of archaeological bone: A conservation perspective', *Journal of Field Archaeology*, 21(2), pp. 221–233. doi: 10.1179/009346994791547661.

Johnston, J. P. and Ogston, A. G. (1946) 'A boundary anomaly found in the ultracentrifugal sedimentation of mixtures', *Transactions of the Faraday Society*, 42, pp. 789–799. doi: 10.1039/TF9464200789.

Jones, S. P. P. *et al.* (2009) 'Investigating the processes necessary for satisfactory freeze-drying of waterlogged archaeological wood', *Journal of Archaeological Science*. Elsevier Ltd, 36(10), pp. 2177–2183. doi: 10.1016/j.jas.2009.05.028.

Kapetanaki, K. *et al.* (2020) 'TEOS Modified With Nano-Calcium Oxalate and PDMS to Protect Concrete Based Cultural Heritage Buildings', *Frontiers in Materials*. Frontiers Media S.A., 7, pp. 1–13. doi: 10.3389/fmats.2020.00016.

Kavvouras, P. K. *et al.* (2009) 'Use of Silanol-Terminated Polydimethylsiloxane in the Conservation of Waterlogged Archaeological Wood', *Studies in Conservation*, 54(2), pp. 65–76. Available at: https://www.jstor.org/stable/27867072?seq=1&cid=pdf-

reference#references_tab_contents.

Kawai, F. (2002) ‘Microbial degradation of polyethers’, *Applied Microbiology and Biotechnology*, 58, pp. 30–38. doi: 10.1007/s00253-001-0850-2.

Kaye, B. (1995) ‘Conservation of waterlogged archaeological wood’, *Chem. Soc. Rev*, 24, pp. 35–43. doi: 10.1039/CS9952400035.

Kennedy, A. and Pennington, E. R. (2014) ‘Conservation of chemically degraded waterlogged wood with sugars’, *Studies in Conservation*, 59, pp. 194–201. doi: 10.1179/2047058413Y.0000000109.

Keplinger, T. *et al.* (2015) ‘A versatile strategy for grafting polymers to wood cell walls’, *Acta Biomaterialia*, 11, pp. 256–263. doi: 10.1016/j.actbio.2014.09.016.

Kerr, A. J. and Goring, D. A. I. (1975) ‘The ultrastructural arrangement of the wood cell wall’, *Cellulose Chemistry and Technology*, 9, pp. 563–573.

Kiliç, N. and Asst, R. (2016) ‘Conservation of a group of frames from YK 16 shipwreck’, *Art-Sanat*, 6, pp. 85–97.

Klosowski, J. M., Smith, C. W. and Hamilton, D. L. (2004) ‘Conservation of organic and inorganic materials’.

Knuuttila, P. (2013) ‘Wood sulphate turpentine as a gasoline bio-component’, *Fuel*, 104, pp. 101–108. doi: 10.1016/j.fuel.2012.06.036.

Kocabaş, U. (2015) ‘The Yenikapi byzantine-era shipwrecks, Istanbul, Turkey: A preliminary report and inventory of the 27 wrecks studied by Istanbul University’, *International Journal of Nautical Archaeology*, 44, pp. 5–38. doi: 10.1111/1095-9270.12084.

Koob, S. P. (1986) ‘The use of Paraloid B-72 as an adhesive: its application for archaeological ceramics and other materials’, *Studies in Conservation*, 31, pp. 7–14. doi: 10.1179/sic.1986.31.1.7.

Kraemer, E. O. (1938) ‘Molecular Weights of Celluloses and Cellulose Derivatives’, *Industrial and Engineering Chemistry*, 30(10), pp. 1200–1203. doi: 10.1021/ie50346a023.

Kratky, O., Leopold, H. and Stabinger, H. (1973) ‘[5] The determination of the partial specific volume of proteins by the mechanical oscillator technique’, *Methods in Enzymology*, 27, pp. 98–110.

Kres, L. A. and Lovell, N. C. (1995) ‘A comparison of consolidants for archaeological bone’, *Journal of Field Archaeology*, 22(4), pp. 508–515. doi: 10.1179/009346995791974134.

Ksinopoulou, E., Bakolas, A. and Moropoulou, A. (2016) ‘Modifying Si-based consolidants through the addition of colloidal nano-particles’, *Applied Physics A: Materials Science and Processing*. Springer Verlag, 122(267), pp. 1–10. doi: 10.1007/s00339-016-9772-9.

Lalatsa, A. *et al.* (2015) ‘Chitosan amphiphile coating of peptide nanofibres reduces liver uptake and delivers the peptide to the brain on intravenous administration’, *Journal of Controlled Release*, 197, pp. 87–96. doi: 10.1016/j.jconrel.2014.10.028.

Lechner, T., Bjurhager, I. and Kliger, R. I. (2013) ‘Strategy for developing a future support system for the Vasa warship and evaluating its mechanical properties’, *Heritage Science*, 1(1), pp. 1–11. doi: 10.1186/2050-7445-1-35.

Li, F.-S. *et al.* (2019) 'The molecular structure of plant sporopollenin', *Nature Plants*, 5, pp. 41–46. Available at: http://dx.doi.org/10.1101/415612.

Li, Y. *et al.* (2011) 'Improvement of decay resistance of wood via combination treatment on wood cell wall: Swell-bonding with maleic anhydride and graft copolymerization with glycidyl methacrylate and methyl methacrylate', *International Biodeterioration and Biodegradation*. Elsevier Ltd, 65(7), pp. 1087–1094. doi: 10.1016/j.ibiod.2011.08.009.

Lim, H. and Hoag, S. W. (2013) 'Plasticizer effects on physical-mechanical properties of solvent cast Soluplus® films', *AAPS PharmSciTech*, 14(3), pp. 903–910. doi: 10.1208/s12249-013-9971-z.

Lima, Á. A. N., Koester, L. S. and Veiga-Junior, V. F. (2021) 'Formulating Bioactive Terpenes', *Biomolecules*, 11(12), pp. 9–12. doi: 10.3390/biom11121745.

Lima, M. S. *et al.* (2018) 'A simple strategy toward the substitution of styrene by sobrerol-based monomers in unsaturated polyester resins', *Green Chemistry*. Royal Society of Chemistry, 20(21), pp. 4880–4890. doi: 10.1039/c8gc01214h.

Lintz, E. S. and Scheibel, T. R. (2013) 'Dragline, egg stalk and byssus: A comparison of outstanding protein fibers and their potential for developing new materials', *Advanced Functional Materials*, 23, pp. 4467–4482. doi: 10.1002/adfm.201300589.

Lix, L. M., Keselman, J. C. and Keselman, H. . J. (1996) 'Consequences of Assumption Violations Revisited : A Quantitative Review of Alternatives to the One-Way Analysis of Variance "F" Test Author (s): Lisa M . Lix , Joanne C . Keselman and H . J . Keselman Published by : American Educational Research Assoc', *Review of Educational Research*, 66(4), pp. 579–619.

Llevot, A. *et al.* (2016) 'Renewability is not Enough: Recent Advances in the Sustainable Synthesis of Biomass-Derived Monomers and Polymers', *Chem. Eur. J.*, 22, pp. 11510–11521. Available at: www.chemeurj.org.

Lligadas, G. *et al.* (2010) 'Oleic and undecylenic acids as renewable feedstocks in the synthesis of polyols and polyurethanes', *Polymers*, 2(4), pp. 440–453. doi: 10.3390/polym2040440.

Lorch, M. *et al.* (2009) 'MRI contrast agent delivery using spore capsules: Controlled release in blood plasma', *Chemical Communications*, 0, pp. 6442–6444. doi: 10.1039/b909551a.

Łucejko, J. J. *et al.* (2018) 'Protective effect of linseed oil varnish on archaeological wood treated with alum', *Microchemical Journal*, 139, pp. 50–61. doi: 10.1016/j.microc.2018.02.011.

Łucejko, Jeannette Jacqueline *et al.* (2021) 'Comparative chemical investigations of alum treated archaeological wood from various museum collections', *Heritage Science*. Springer International Publishing, 9(1), pp. 1–18. doi: 10.1186/s40494-021-00517-0.

Łucejko, Jeannette J. *et al.* (2021) 'Evaluation of soda lignin from wheat straw/sarkanda grass as a potential future consolidant for archaeological wood', *Forests*, 12(7), pp. 1–28. doi: 10.3390/f12070911.

Macchioni, N., Pecoraro, E. and Pizzo, B. (2018) 'The measurement of maximum water content (MWC) on waterlogged archaeological wood: A comparison between three different methodologies', *Journal of Cultural Heritage*. Elsevier Masson SAS, 30, pp. 51–56. doi: 10.1016/j.culher.2017.10.005.

Mackenzie, G. *et al.* (2015) 'Sporopollenin, The Least Known Yet Toughest Natural Biopolymer', *Frontiers in Materials*, 2, pp. 1–5. doi: 10.3389/fmats.2015.00066.

Mathers, R. T. *et al.* (2006) 'Ring-opening metathesis polymerizations in D-limonene: A renewable polymerization solvent and chain transfer agent for the synthesis of alkene macromonomers', *Macromolecules*, 39, pp. 8982–8986. doi: 10.1021/ma061699h.

McHale, E. *et al.* (2016) 'Synthesis and characterisation of lignin-like oligomers as a bio-inspired consolidant for waterlogged archaeological wood', *Pure Appl. Chem.*, (88), pp. 969–977. doi: 10.1515/pac-2016-0814.

McHale, E. *et al.* (2017) 'In situ polymerisation of isoeugenol as a green consolidation method for waterlogged archaeological wood', *Scientific Reports*, 7, pp. 1–9. doi: 10.1038/srep46481.

McQueen, C. M. A. *et al.* (2017) 'New insights into the degradation processes and influence of the conservation treatment in alum-treated wood from the Oseberg collection', *Microchemical Journal*, 132, pp. 119–129. doi: 10.1016/j.microc.2017.01.010.

McQueen, C. M. A. *et al.* (2019) 'Ammonium alum in alum-treated wooden artefacts: discovery, origins and consequences', *Heritage Science*, 7(1), p. 78. doi: 10.1186/s40494-019-0321-7.

McQueen, C. M. A. *et al.* (2020) 'Oxidative degradation of archaeological wood and the effect of alum, iron and calcium salts', *Heritage Science*. Springer International Publishing, 8(1), pp. 1–11. doi: 10.1186/s40494-020-00377-0.

McQueen, C. M. A., Tamburini, D. and Braovac, S. (2018) 'Identification of inorganic compounds in composite alum-treated wooden artefacts from the Oseberg collection', *Scientific Reports*, 8, pp. 1–8. doi: 10.1038/s41598-018-21314-z.

Meier, M. A. R., Metzger, J. O. and Schubert, U. S. (2007) 'Plant oil renewable resources as green alternatives in polymer science', *Chemical Society Reviews*, 36(11), pp. 1788–1802. doi: 10.1039/b703294c.

Mendanha, S. A. *et al.* (2013) 'Toxicity of terpenes on fibroblast cells compared to their hemolytic potential and increase in erythrocyte membrane fluidity', *Toxicology in Vitro*, 27, pp. 323–329.

Mewalal, R. *et al.* (2017) 'Plant-Derived Terpenes: A Feedstock for Specialty Biofuels', *Trends in Biotechnology*. Elsevier Ltd, 35(3), pp. 227–240. doi: 10.1016/j.tibtech.2016.08.003.

Milwich, M. *et al.* (2006) 'Biomimetics and technical textiles: Solving engineering problems with the help of nature's wisdom', *American Journal of Botany*, 93, pp. 1455–1465. doi: 10.3732/ajb.93.10.1455.

Miyaji, H., Satoh, K. and Kamigaito, M. (2016) 'Bio-Based Polyketones by Selective Ring-Opening Radical Polymerization of α-Pinene-Derived Pinocarvone', *Angewandte Chemie - International Edition*. Wiley-VCH Verlag, 55, pp. 1372–1376. doi: 10.1002/anie.201509379.

Mohebby, B. (2005) 'Attenuated total reflection infrared spectroscopy of white-rot decayed beech wood', *International Biodeterioration and Biodegradation*, 55(4), pp. 247–251. doi: 10.1016/j.ibiod.2005.01.003.

Mokrzycki, W. S. and Tatol, M. (2011) 'Colour difference ∆E - A survey', *Machine Graphics and Vision*, 20(4), pp. 383–411.

Monachon, M. *et al.* (2020) 'Characterization of model samples simulating degradation processes induced by iron and sulfur species on waterlogged wood', *Microchemical Journal*. Elsevier, 155, pp. 1–11. doi: 10.1016/j.microc.2020.104756.

Della Monica, F. and Kleij, A. W. (2020) 'From terpenes to sustainable and functional polymers', *Polymer Chemistry*. Royal Society of Chemistry, 11(32), pp. 5109–5127. doi: 10.1039/d0py00817f.

Montanari, U. *et al.* (2020) 'Synthesis of novel carvone (meth)acrylate monomers for the production of hydrophilic polymers with high terpene content', *Polymer International*, 70, pp. 499–505. doi: 10.1002/pi.6096.

Morgan, P. J., Harding, S. E. and Petrak, K. (1990) 'Hydrodynamic Properties of a Polyisoprene/Poly(Oxyethylene) Block Copolymer', *Macromolecules*, 23(20), pp. 4461–4464. doi: 10.1021/ma00222a020.

Mortensen, M. N. *et al.* (2007) 'Characterisation of the polyethylene glycol impregnation of the Swedish warship Vasa and one of the Danish Skuldelev Viking ships', *Journal of Archaeological Science*, 34, pp. 1211–1218. doi: 10.1016/j.jas.2006.10.012.

Mosquera, M. E. G. *et al.* (2021) 'Terpenes and Terpenoids: Building Blocks to Produce Biopolymers', *Sustainable Chemistry*, 2(3), pp. 467–492. doi: 10.3390/suschem2030026.

Murphy, L. R. *et al.* (1998) 'Protein hydration and unfolding – insights from experimental partial specific volumes and unfolded protein models', *Folding and Design*, 3(2), pp. 105–118. doi: 10.1016/s1359-0278(98)00016-9.

Nairn, J. A. (2007) 'A numerical study of the transverse modulus of wood as a function of grain orientation and properties', *Holzforschung*, 61(4), pp. 406–413. doi: 10.1515/HF.2007.079.

Neagu, R. C. *et al.* (2006) 'Ultrastructural features affecting mechanical properties of wood fibres', *Wood Material Science and Engineering*, 1(3–4), pp. 146–170. doi: 10.1080/17480270701195374.

Neto, W. S. *et al.* (2017) 'Superparamagnetic nanoparticles stabilized with free-radical polymerizable oleic acid-based coating', *Journal of Alloys and Compounds*, 739, pp. 1025–1036. doi: 10.1016/j.jallcom.2017.12.338.

Nie, G. *et al.* (2014) 'HPW/MCM-41 catalyzed isomerization and dimerization of pure pinene and crude turpentine', *Catalysis Today*. Elsevier, 234, pp. 271–277. doi: 10.1016/j.cattod.2013.12.003.

Nikitina, L. E. *et al.* (2009) 'Synthesis and antifungal activity of compounds of the pinane series', *Pharmaceutical Chemistry Journal*, 43(5), pp. 251–254. doi: 10.1007/s11094-009-0282-3.

Nikolajski, M. *et al.* (2014) 'Protein-like fully reversible tetramerisation and super-association of an aminocellulose', *Scientific Reports*, 4, pp. 1–5. doi: 10.1038/srep03861.

Nilsson, T. and Rowell, R. (2012) 'Historical wood - structure and properties', *Journal of Cultural Heritage*, 13S, pp. S5–S9. doi: 10.1016/j.culher.2012.03.016.

Ninkuu, V. *et al.* (2021) 'Biochemistry of terpenes and recent advances in plant protection', *International Journal of Molecular Sciences*, 22(11). doi: 10.3390/ijms22115710.

Nishida, T., Satoh, K. and Kamigaito, M. (2020) 'Biobased Polymers via Radical Homopolymerization and Copolymerization of a Series of Terpenoid-Derived Conjugated Dienes with exo-Methylene and 6-Membered Ring', *Molecules (Basel, Switzerland)*, 25(24), pp. 1–17. doi: 10.3390/molecules25245890.

Noshy, W., Hassan, R. R. A. and Mohammed, N. (2022) 'Using biopolymers to strengthen the historical printed paper: mechanical and optical characters', *Pigment and Resin Technology*, 51(2), pp. 212–226. doi: 10.1108/PRT-01-2021-0008.

O'Brien, D. (2020) *The Functionalisation of Terpenes for Sustainable Polymerisations Towards Biomedical Applications*. University of Nottingham.

O'Brien, D. M. *et al.* (2019) 'Epoxy–amine oligomers from terpenes with applications in synergistic antifungal treatments', *Journal of Materials Chemistry B*. Royal Society of Chemistry (RSC), 7, pp. 5222–5229. doi: 10.1039/c9tb00878k.

Omolo, C. A. *et al.* (2017) 'Pegylated oleic acid: A promising amphiphilic polymer for nano-antibiotic delivery', *European Journal of Pharmaceutics and Biopharmaceutics*. Elsevier B.V., 112, pp. 96–108. doi: 10.1016/j.ejpb.2016.11.022.

Paduch, R. *et al.* (2007) 'Terpenes: Substances useful in human healthcare', *Archivum Immunologiae et Therapiae Experimentalis*, 55(5), pp. 315–327. doi: 10.1007/s00005-007-0039-1.

Palazzo, I. *et al.* (2018) 'Chiral ionic liquids supported on natural sporopollenin microcapsules', *RSC Advances*, 8, pp. 21174–21183. doi: 10.1039/c8ra03455a.

Pamies, R. *et al.* (2008) 'Determination of intrinsic viscosities of macromolecules and nanoparticles. Comparison of single-point and dilution procedures', *Colloid and Polymer Science*, 286(11), pp. 1223–1231. doi: 10.1007/s00396-008-1902-2.

Papageorgiou, G. Z. (2018) 'Thinking green: Sustainable polymers from renewable resources', *Polymers*, 10(9). doi: 10.3390/polym10090952.

Parrent, J. M. (1985) 'The Conservation of Waterlogged Wood Using Sucrose', *Studies in Conservation*, 30(2), pp. 63–72. Available at: https://www.jstor.org/stable/1506090?seq=1&cid=pdf-reference#references_tab_contents.

Paterakis, A. (1996) 'Conservation of a Late Minoan Basket from Crete', *Studies in Conservation*, 41, pp. 179–182.

Paunov, V. N., Mackenzie, G. and Stoyanov, S. D. (2007) 'Sporopollenin micro-reactors for in-situ preparation, encapsulation and targeted delivery of active components', *Journal of Materials Chemistry*, 17, pp. 609–612. doi: 10.20964/2018.04.41.

Pelé, C. *et al.* (2015) 'Iron removal from waterlogged wood: Extraction by electrophoresis and chemical treatments', *Studies in Conservation*, 60(3), pp. 155–171. doi: 10.1179/2047058413Y.0000000110.

Pennington, E. R. *et al.* (2016) 'Thermodynamics of interaction between carbohydrates and unilamellar dipalmitoyl phosphatidylcholine membranes: Evidence of dehydration and interdigitation', *Journal of Thermal Analysis and Calorimetry*. Springer Netherlands, 123(3), pp. 2611–2617. doi: 10.1007/s10973-016-5288-y.

Perrin, F. (1936) 'Mouvement Brownian d'un ellipsoide II. Rotation libre et dépolarisation des fluorescences. Translation et diffusion de molécules ellipsoidales.', *J Phys Radium*, 7, pp. 1–11.

Pettersen, R. C. (1984) ‘The Chemical Composition of Wood’, in Rowell, R. (ed.) *The Chemistry of Solid Wood*. American Chemical Society, pp. 57–126. doi: 10.1021/ba-1984-0207.ch002.

Phillips-Jones, M. K., Lithgo, R., *et al.* (2017) ‘Full hydrodynamic reversibility of the weak dimerization of vancomycin and elucidation of its interaction with VanS monomers at clinical concentration’, *Scientific Reports*, 7, pp. 1–10. doi: 10.1038/s41598-017-12620-z.

Phillips-Jones, M. K., Channell, G., *et al.* (2017) ‘Hydrodynamics of the VanA-Type VanS histidine kinase: An extended solution conformation and first evidence for interactions with vancomycin’, *Scientific Reports*, 7, pp. 1–12. doi: 10.1038/srep46180.

Podany, J. *et al.* (2001) ‘Paraloid B-72 as a Structural Adhesive and as a Barrier within Structural Adhesive Bonds: Evaluations of Strength and Reversibility’, *Journal of the American Institute for Conservation*, 40, pp. 15–33. doi: 10.1179/019713601806113120.

Poggi, G. *et al.* (2014) ‘Calcium hydroxide nanoparticles for the conservation of cultural heritage: New formulations for the deacidification of cellulose-based artifacts’, *Applied Physics A: Materials Science and Processing*, 114, pp. 685–693. doi: 10.1007/s00339-013-8172-7.

Poggi, G. *et al.* (2016) ‘Calcium hydroxide nanoparticles from solvothermal reaction for the deacidification of degraded waterlogged wood’, *Journal of Colloid and Interface Science*, 473, pp. 1–8. doi: 10.1016/j.jcis.2016.03.038.

Pohoriljakova, I. and Moy, S. A. (2013) ‘A re-evaluation of adhesives used for mending ceramics at Kaman-Kalehöyük: a Final Assessment’, *Anatolian archaeological studies*, 9, pp. 83–92.

Potrč, S. *et al.* (2021) ‘Sustainable renewable energy supply networks optimization – The gradual transition to a renewable energy system within the European Union by 2050’, *Renewable and Sustainable Energy Reviews*, 146. doi: 10.1016/j.rser.2021.111186.

Preston, J. *et al.* (2014) ‘The effects of Mary Rose conservation treatment on iron oxidation processes and microbial communities contributing to acid production in marine archaeological timbers’, *PLoS ONE*, 9, pp. 1–8. doi: 10.1371/journal.pone.0084169.

Ren, S., Zhang, L. and Dubé, M. A. (2015) ‘Free-radical terpolymerization of n-butyl acrylate/butyl methacrylate/ d -limonene’, *Journal of Applied Polymer Science*, 132, pp. 42821 (1–8). doi: 10.1002/app.42821.

Rivas da Silva, A. C. P. *et al.* (2012) ‘Biological Activities of α-Pinene and β-Pinene Enantiomers’, *Molecules*, 17, pp. 6305–6316.

Roberts, W. J. and Day, A. R. (1950) ‘A Study of the Polymerization of α- and β-Pinene with Friedel-Crafts Type Catalysts’, *Journal of the American Chemical Society*, 72, pp. 1226–1230. Available at: https://pubs.acs.org/sharingguidelines.

Rose, M. and Palkovits, R. (2011) ‘Cellulose-based sustainable polymers: State of the art and future trends’, *Macromolecular Rapid Communications*, 32(17), pp. 1299–1311. doi: 10.1002/marc.201100230.

Rosenqvist, A. M. (1959) ‘The Stabilizing of Wood Found in the Viking Ship of Oseberg: Part I’, *Studies in Conservation*, 4(1), pp. 13–22.

Rowell, R. M. (1983) *Bioactive Polymer-Wood Composites. In: Controlled Release Delivery Systems*. New York, New York and Basel: Marcel Dekker Inc.

Rowell, R. M., Pettersen, R. and Tshabalala, M. A. (2005) 'Cell Wall Chemistry', in Rowell, R. (ed.) *Handbook of Wood Chemistry and Wood Composites*. Boca Raton, FL: CRC Press, pp. 35–74. doi: 10.1016/j.jclepro.2015.07.070.

Rozema, J. *et al.* (2001) 'UV-B absorbance and UV-B absorbing compounds (para-coumaric acid) in pollen and sporopollenin: The perspective to track historic UV-B levels', *Journal of Photochemistry and Photobiology B: Biology*, 62, pp. 108–117. doi: 10.1016/S1011-1344(01)00155-5.

Ruzin, S. E. (1999) *Plant Microtechnique and Microscopy*. Oxford: Oxford University Press.

Sagorin, G. *et al.* (2021) 'From Pine to Perfume', *Chimia*, 75(9), pp. 780–787. doi: 10.2533/chimia.2021.780.

Sainz, M. F. *et al.* (2016) 'A facile and green route to terpene derived acrylate and methacrylate monomers and simple free radical polymerisation to yield new renewable polymers and coatings', *Polymer Chemistry*, 7, pp. 2882–2887. doi: 10.1039/c6py00357e.

Saito, N. (1951) 'The effect of Brownian motion on the viscosity of solutions of macromolecules, I. Ellipsoid of revolution', *J Phys Soc (Japan)*, 6, pp. 297–301.

Salehi, B. *et al.* (2019) 'Therapeutic potential of α-and β-pinene: A miracle gift of nature', *Biomolecules*, 9(11), pp. 1–34. doi: 10.3390/biom9110738.

Sander, M. M. *et al.* (2012) 'Plasticiser effect of oleic acid polyester on polyethylene and polypropylene', *Polymer Testing*. Elsevier Ltd, 31(8), pp. 1077–1082. doi: 10.1016/j.polymertesting.2012.08.006.

Sandström, M. *et al.* (2002) 'Deterioration of the seventeenth-century warship Vasa by internal formation of sulphuric acid', *Nature*, 415, pp. 895–897. doi: 10.1038/415893a.

Sarder, R. *et al.* (2022) 'Copolymers of starch, a sustainable template for biomedical applications: A review', *Carbohydrate Polymers*. Elsevier Ltd, 278(December 2021), p. 118973. doi: 10.1016/j.carbpol.2021.118973.

Scheraga, H. A. and Mandelkern, L. (1953) 'Consideration of the hydrodynamic properties of proteins', *J Am Chem Soc*, 75, pp. 179–184. Available at: https://pubs.acs.org/sharingguidelines.

Schilling, M. R. (1989) 'The Glass Transition of Materials Used in Conservation', *Studies in Conservation*. JSTOR, 34, pp. 110–116. doi: 10.2307/1506226.

Schmidt, P. L., Shugar, A. and Ploeger, R. (2017) 'Analytical Observations Regarding Butvar B-98 and Paraloid B-72 Blends as a Suitable Adhesive in Hot Climates', *MRS Advances*, 2, pp. 1927–1941. doi: 10.1557/adv.2017.229.

Schniewind, A. P. (1990) *Consolidation of dry archaeological wood by impregnation with thermoplastic resins*, *Archaeological Wood: Properties, Chemistry and Preservation. Advances in Chemistry Series, vol. 225*. Edited by R. M. Rowell and J. R. Barbour. Washington DC: American Chemical Society.

Schniewind, A. P. and Eastman, P. Y. (1994) 'Consolidant Distribution in Deteriorated Wood Treated with Soluble Resins', *Journal of the American Institute for Conservation*, 33(3), pp. 247–255.

Schofield, E. J. *et al.* (2011) 'Nanoparticle de-acidification of the Mary Rose', *Materials Today*, 14, pp. 354–358. doi: 10.1016/S1369-7021(11)70166-3.

Schuck, P. (2000) 'Size-distribution analysis of macromolecules by sedimentation velocity ultracentrifugation and Lamm equation modeling', *Biophysical Journal*. Biophysical Society, 78(3), pp. 1606–1619. doi: 10.1016/S0006-3495(00)76713-0.

Schuck, P. *et al.* (2014) 'SEDFIT-MSTAR: Molecular weight and molecular weight distribution analysis of polymers by sedimentation equilibrium in the ultracentrifuge', *Analyst*, 139, pp. 79–92. doi: 10.1039/c3an01507f.

Schwanninger, M. *et al.* (2004) 'Effects of short-time vibratory ball milling on the shape of FT-IR spectra of wood and cellulose', *Vibrational Spectroscopy*, 36(1), pp. 23–40. doi: 10.1016/j.vibspec.2004.02.003.

Schwarze, F. W. M. R. (2007) 'Wood decay under the microscope', *Fungal Biology Reviews*, 21, pp. 133–170. doi: 10.1016/j.fbr.2007.09.001.

Scott, D., Harding, S. and Rowe, A. (2005) *Analytical ultracentrifugation: techniques and methods*. Cambridge UK: Royal Society of Chemistry. Available at: https://app.knovel.com/hotlink/toc/id:kpAUTM0001/analytical-ultracentrifugation/analytical-ultracentrifugation.

Seniha Güner, F., Yağci, Y. and Tuncer Erciyes, A. (2006) 'Polymers from triglyceride oils', *Progress in Polymer Science (Oxford)*, 31(7), pp. 633–670. doi: 10.1016/j.progpolymsci.2006.07.001.

Sharma, V. and Kundu, P. P. (2006) 'Addition polymers from natural oils-A review', *Progress in Polymer Science (Oxford)*, 31(11), pp. 983–1008. doi: 10.1016/j.progpolymsci.2006.09.003.

Sharma, V. and Kundu, P. P. (2008) 'Condensation polymers from natural oils', *Progress in Polymer Science (Oxford)*, 33(12), pp. 1199–1215. doi: 10.1016/j.progpolymsci.2008.07.004.

Shi, J. *et al.* (2015) 'Genetic and Biochemical Mechanisms of Pollen Wall Development', *Trends in Plant Science*, 20, pp. 741–753. doi: 10.1016/j.tplants.2015.07.010.

Shitrit, Y. and Bianco-Peled, H. (2017) 'Acrylated chitosan for mucoadhesive drug delivery systems', *International Journal of Pharmaceutics*, 517, pp. 247–255. doi: 10.1016/j.ijpharm.2016.12.023.

Simha, R. (1940) 'The Influence of Brownian Movement on the Viscosity of Solutions', *J. Phys. Chem*, 44(25), p. 34. Available at: https://pubs.acs.org/sharingguidelines.

Solomon, O. and Ciută, I. Z. (1962) 'Détermination de la viscosité intrinsèque de solutions de polymères par une simple détermination de la viscosité', *Journal of Applied Polymer Science*, VI(24), pp. 683–686.

De Souza, S. P. *et al.* (2015) 'Sporopollenin as an efficient green support for covalent immobilization of a lipase', *Catalysis Science and Technology*, 5, pp. 3130–3136. doi: 10.1039/c4cy01682c.

Spirydowicz, K. E. *et al.* (2001) 'Alvar and Butvar: The Use of Polyvinyl Acetal Resins for the Treatment of the Wooden Artifacts from Gordion, Turkey', *Journal of the American Institute for Conservation*, 40(1), pp. 43–57.

Stamm, A. *et al.* (2019) 'Chemo-enzymatic pathways toward pinene-based renewable materials', *Green Chemistry*. Royal Society of Chemistry, 21(10), pp. 2720–2731. doi:

10.1039/c9gc00718k.

Strahan, D. *et al.* (2002) 'Conservation of Ceramic Artifacts on Archaeological Sites', *Field Notes: Practical Guides for Archaeological Conservation and Site Preservation*, 12, pp. 1–6.

Studart, A. R. (2013) 'Biological and bioinspired composites with spatially tunable heterogeneous architectures', *Advanced Functional Materials*, 23, pp. 4423–4436. doi: 10.1002/adfm.201300340.

Tahira, A. *et al.* (2017) 'Mechanical strength studies on degraded waterlogged wood treated with sugars', *Studies in Conservation*, 62, pp. 223–228. doi: 10.1080/00393630.2016.1169364.

Tanford, C. (1961) *Physical Chemistry of Macromolecules*. New York: Wiley.

Thomsett, M. R. *et al.* (2016) 'Progress in the synthesis of sustainable polymers from terpenes and terpenoids', *Green Materials*, 4, pp. 115–134. doi: 10.1680/jgrma.16.00009.

Thomsett, M. R. (2018) *Investigations into the Synthetic Modifications of Terpenes for the Synthesis of Renewable Polyesters*. University of Nottingham.

Thomsett, M. R. *et al.* (2020) 'Exploiting the chirality of sustainably-sourced polyesters: tuning thermal properties via stereocomplexation', *Submitted manuscript*.

Tracy, N. I. *et al.* (2009) 'Hydrogenated monoterpenes as diesel fuel additives', *Fuel*. Elsevier Ltd, 88(11), pp. 2238–2240. doi: 10.1016/j.fuel.2009.02.002.

Unger, A., Schniewind, A. P. and Unger, W. (2001) *Conservation of wood artifacts :a handbook*. Germany: Springer Science & Business Media.

Upton, B. M. and Kasko, A. M. (2016) 'Strategies for the conversion of lignin to high-value polymeric materials: Review and perspective', *Chemical Reviews*, 116(4), pp. 2275–2306. doi: 10.1021/acs.chemrev.5b00345.

Valenti, D. J. and Wagener, K. B. (1998) 'Direct synthesis of well-defined alcohol-functionalized polymers via acyclic diene metathesis (ADMET) polymerization', *Macromolecules*. American Chemical Society, 31, pp. 2764–2773. doi: 10.1021/ma9714833.

Vaz, M. F., Pires, J. and Carvalho, A. P. (2008) 'Effect of the impregnation treatment with Paraloid B-72 on the properties of old Portuguese ceramic tiles', *Journal of Cultural Heritage*, 9, pp. 269–276. doi: 10.1016/j.culher.2008.01.003.

Veneranda, M. *et al.* (2018) 'Evaluating the exploitability of several essential oils constituents as a novel biological treatment against cultural heritage biocolonization', *Microchemical Journal*. Elsevier B.V., 138, pp. 1–6. doi: 10.1016/j.microc.2017.12.019.

Vilela, C. *et al.* (2014) 'The quest for sustainable polyesters-insights into the future', *Polymer Chemistry*, 5, pp. 3119–3141. doi: 10.1039/c3py01213a.

Wakefield, J. (2020) *Natural polymers for consolidation of the Oseberg artefacts*. University of Nottingham.

Wakefield, J. M. K. *et al.* (2018) 'Controlled depolymerisation assessed by analytical ultracentrifugation of low molecular weight chitosan for use in archaeological conservation', *Eur. Biophys. J.*, 47, pp. 769–775. doi: 10.1007/s00249-018-1290-6.

Wakefield, J. M. K., Hampe, R., *et al.* (2020) 'Aminoethyl substitution enhances the

self-assembly properties of an aminocellulose as a potential archaeological wood consolidant', *European Biophysics Journal*. Springer International Publishing, 49(8), pp. 791–798. doi: 10.1007/s00249-020-01451-y.

Wakefield, J. M. K., Braovac, S., *et al.* (2020) 'Tert-butyldimethylsilyl chitosan synthesis and characterization by analytical ultracentrifugation, for archaeological wood conservation', *European Biophysics Journal*. Springer International Publishing, 49(8), pp. 781–789. doi: 10.1007/s00249-020-01450-z.

Wakil, A. *et al.* (2010) 'Enhanced bioavailability of eicosapentaenoic acid from fish oil after encapsulation within plant spore exines as microcapsules', *Lipids*, 45, pp. 645–649. doi: 10.1007/s11745-010-3427-y.

Walsh-Korb, Z. (2022) 'Sustainability in Heritage Wood Conservation: Challenges and Directions for Future Research', *Forests*, 13(1), pp. 1–35. doi: 10.3390/f13010018.

Walsh, Z. *et al.* (2014) 'Multifunctional supramolecular polymer networks as next-generation consolidants for archaeological wood conservation', *Proceedings of the National Academy of Sciences*, 111, pp. 17743–17748. doi: 10.1073/pnas.1406037111.

Walsh, Z. *et al.* (2017) 'Natural polymers as alternative consolidants for the preservation of waterlogged archaeological wood', *Studies in Conservation*, 62, pp. 173–183. doi: 10.1179/2047058414Y.0000000149.

Wellman, C. H., Osterloff, P. L. and Mohiuddin, U. (2003) 'Fragments of the earliest land plants', *Nature*, 425, pp. 282–284. doi: 10.1038/nature01884.

Wetherall, K. M. *et al.* (2008) 'Sulfur and iron speciation in recently recovered timbers of the Mary Rose revealed via X-ray absorption spectroscopy', *Journal of Archaeological Science*, 35, pp. 1317–1328. doi: 10.1016/j.jas.2007.09.007.

Whitfield, R. *et al.* (2019) 'Tailoring polymer dispersity and shape of molecular weight distributions: Methods and applications', *Chemical Science*, 10(38), pp. 8724–8734. doi: 10.1039/c9sc03546j.

Whitfield, R. *et al.* (2020) 'Tailoring Polymer Dispersity by RAFT Polymerization: A Versatile Approach', *Chem*. Elsevier Inc., 6(6), pp. 1340–1352. doi: 10.1016/j.chempr.2020.04.020.

Wilbon, P. A., Chu, F. and Tang, C. (2013) 'Progress in renewable polymers from natural terpenes, terpenoids, and rosin', *Macromolecular Rapid Communications*, 34, pp. 8–37. doi: 10.1002/marc.201200513.

Wilcox, W. W. (1993) 'Comparison of scanning electron microscopy and light microscopy for the diagnosis of early stages of brown rot wood decay', *IAWA*, 14(3), pp. 219–226.

Winnacker, M. (2018) 'Pinenes: Abundant and Renewable Building Blocks for a Variety of Sustainable Polymers', *Angewandte Chemie*. Wiley, 130, pp. 14560–14569. doi: 10.1002/ange.201804009.

Xia, Y. and Larock, R. C. (2010) 'Vegetable oil-based polymeric materials: Synthesis, properties, and applications', *Green Chemistry*, 12(11), pp. 1893–1909. doi: 10.1039/c0gc00264j.

Xu, Z. B. and Qu, J. (2013) 'Hot water-promoted SN1 solvolysis reactions of allylic and benzylic alcohols', *Chemistry - A European Journal*. Wiley-VCH Verlag, 19, pp. 314–323. doi: 10.1002/chem.201202886.

Yan, B. *et al.* (2014) 'Sustainable production of acrylic acid: Alkali-Ion exchanged beta zeolite for gas-phase dehydration of lactic acid', *ChemSusChem*, 7(6), pp. 1568–1578. doi: 10.1002/cssc.201400134.

Yao, K. and Tang, C. (2013) 'Controlled polymerization of next-generation renewable monomers and beyond', *Macromolecules*, 46, pp. 1689–1712. doi: 10.1021/ma3019574.

Yasuda, H. (1985) *Plasma Polymerization*. Orlando, Florida: Academic Press Inc.

Yermakova, A. *et al.* (2009) 'High-pressure thermolysis of sulfate turpentine', *Journal of Supercritical Fluids*, 48, pp. 139–145. doi: 10.1016/j.supflu.2008.10.013.

Yu, K. *et al.* (2013) 'Biomimetic optical materials: Integration of nature's design for manipulation of light', *Progress in Materials Science*, 58, pp. 825–873. doi: 10.1016/j.pmatsci.2013.03.003.

Yuta, A. and Baraniuk, J. N. (2005) 'Therapeutic Approaches to Mucus Hypersecretion'.

Zafar, S. *et al.* (2009) 'Synthesis, Characterization, and Anticorrosive Coating Properties of Waterborne Interpenetrating Polymer Network Based on Epoxy-Acrylic-Oleic Acid with Butylated Melamine Formaldehyde', *Journal of Applied Polymer Science*, 113, pp. 827–838. doi: 10.1002/app.

Zhang, L., He, R. and Gu, H. C. (2006) 'Oleic acid coating on the monodisperse magnetite nanoparticles', *Applied Surface Science*, 253(5), pp. 2611–2617. doi: 10.1016/j.apsusc.2006.05.023.

Zhen, Y. *et al.* (2005) 'Atom transfer radical polymerization of solketal acrylate using cyclohexanone as the solvent', *Macromolecular Chemistry and Physics*, 206(5), pp. 607–612. doi: 10.1002/macp.200400414.

Zielińska-Błajet, M. and Feder-Kubis, J. (2020) 'Monoterpenes and their derivatives—recent development in biological and medical applications', *International Journal of Molecular Sciences*, 21(19), pp. 1–38. doi: 10.3390/ijms21197078.

Zisi, A. (2020) *Saving Oseberg Phase II D2.4 Silanol-based consolidant for retreating Oseberg wood: Adjusting a method initially developed for conserving waterlogged archaeological wood*.

Zisi, A. *et al.* (2021) *Saving Oseberg Phase II D3.6.4 A comparative study of non-aqueous consolidants using modern and archaeological wood Test Specimens*.

Zisi, A. and de Lamotte, A. (2020) *Saving Oseberg Phase II D3.5.3 In vitro evaluation of non-aqueous consolidants, Paraloid B72 and Butvar B98*.

Zoia, L. *et al.* (2017) 'Chemical characterisation of the whole plant cell wall of archaeological wood: an integrated approach', *Analytical and Bioanalytical Chemistry*, 409, pp. 1–13. doi: 10.1007/s00216-017-0378-7.

Zoia, L., Salanti, A. and Orlandi, M. (2015) 'Chemical characterization of archaeological wood: Softwood Vasa and hardwood Riksapplet case studies', *Journal of Cultural Heritage*, 16, pp. 428–437. doi: 10.1016/j.culher.2014.09.015.

Appendix

The appendix contains copies of papers which have been published in or accepted by peer-reviewed journals as a result of the work described in this thesis:

1. ‘Terpene polyacrylate TPA5 shows favorable molecular hydrodynamic properties as a potential bioinspired archaeological wood consolidant’ – published in *Scientific Reports* in April 2021.
2. ‘Comparative Hydrodynamic Study on Non-Aqueous Soluble Archaeological Wood Consolidants: Butvar B-98 and PDMS-OH Siloxanes’ – published in *Molecules* in March 2022.
3. ‘Comparative hydrodynamic characterisation of two hydroxylated polymers based on α-pinene- or oleic acid-derived monomers for potential use as archaeological consolidants’ – published in *Scientific Reports* in November 2022.
4. ‘Evaluation of two terpene-derived polymers as consolidants for archaeological wood’ – accepted (still unpublished) by *Scientific Reports* in December 2022.

This section also contains a copy of a poster, prepared by Prof. Stephen Harding (University of Nottingham) and Mr Chas Jones (Fulford Battle Society), which was presented at the ‘Advances in Isotope Ratio and Related Analyses for Mapping Migrations’ conference held at the Royal Society of Chemistry in June 2022. This work was part of a collaborative side project and was outside the main scope of this thesis. It involved preparing samples for quadrupole inductively coupled plasma mass spectrometry to help analyse the chemical composition of iron artefacts found in ancient battlefields in the UK.

scientific reports

Check for updates

OPEN

Terpene polyacrylate TPA5 shows favorable molecular hydrodynamic properties as a potential bioinspired archaeological wood consolidant

Michelle Cutajar[1,2]✉, Fabrizio Andriulo[3], Megan R. Thomsett[2], Jonathan C. Moore[2], Benoit Couturaud[4], Steven M. Howdle[2], Robert A. Stockman[2]✉ & Stephen E. Harding[1,3]✉

There is currently a pressing need for the development of novel bioinspired consolidants for waterlogged, archaeological wood. Bioinspired materials possess many advantages, such as biocompatibility and sustainability, which makes them ideal to use in this capacity. Based on this, a polyhydroxylated monomer was synthesised from α-pinene, a sustainable terpene feedstock derived from pine trees, and used to prepare a low molar mass polymer TPA5 through free radical polymerisation. This polymer was extensively characterised by NMR spectroscopy (chemical composition) and molecular hydrodynamics, primarily using analytical ultracentrifugation reinforced by gel filtration chromatography and viscometry, in order to investigate whether it would be suitable for wood consolidation purposes. Sedimentation equilibrium indicated a weight average molar mass M_w of (4.3 ± 0.2) kDa, with minimal concentration dependence. Further analysis with MULTISIG revealed a broad distribution of molar masses and this heterogeneity was further confirmed by sedimentation velocity. Conformation analyses with the Perrin *P* and viscosity increment ν universal hydrodynamic parameters indicated that the polymer had an elongated shape, with both factors giving consistent results and a consensus axial ratio of ~ 4.5. These collective properties—hydrogen bonding potential enhanced by an elongated shape, together with a small injectable molar mass—suggest this polymer is worthy of further consideration as a potential consolidant.

Throughout history, people have been constructing artefacts and tools out of wood. Such archaeological discoveries provide us with a fascinating insight into the everyday life of that particular civilisation, as well as their ceremonial rituals and mastery of woodworking[1,2]. Unfortunately, wooden archaeological findings are relatively rare due to their biodegradability[3–5] and are therefore considered to be very precious, requiring carefully tailored treatment strategies in order to conserve them for future generations. The degradation state of the archaeological wood depends on multiple factors such as its age, species and most importantly, its environment[4,6]. Common locations where archaeological wood discoveries are usually made include wet environments like bogs or the seabed[4,7], as wood that is not in contact with oxygen has a slow degradation rate due to low microbial survival, as has been well reported[2,8]. An example is the Oseberg Viking Ship collection which was able to last thousands of years as it was buried in blue clay that provided a highly anaerobic environment[9]. Most of the artefacts found on the Oseberg ship were treated with alum (aluminium potassium sulfate dodecahydrate, $KAl(SO_4)_2{\cdot}12H_2O$) in the early twentieth century[10], which is now known to have directly contributed to the artefacts' current state of degradation[1,11].

[1]National Centre for Macromolecular Hydrodynamics (NCMH), School of Biosciences, University of Nottingham, Sutton Bonington LE12 5RD, UK. [2]School of Chemistry, University of Nottingham, University Park Nottingham NG7 2RD, UK. [3]Museum of Cultural History, University of Oslo, St. Olavs plass, Postboks 6762, 0130 Oslo, Norway. [4]Univ Paris Est Creteil, CNRS, Institut de Chimie et des Matériaux Paris-Est (ICMPE), UMR 7182, 2 rue Henri Dunant, 94320 Thiais, France. ✉email: michelle.cutajar@nottingham.ac.uk; robert.stockman@nottingham.ac.uk; steve.harding@nottingham.ac.uk

There is a pressing need for the development of new consolidant materials which may be used to treat archaeological waterlogged wood, especially unique cases like the Oseberg artefacts. Such consolidants should ideally be biocompatible and interact with the structure of the archaeological artefact, providing support without causing morphological distortion[12]. Potential consolidants must also penetrate the wood to an appropriate depth whilst leaving room in the pores for future re-treatment. Polymers which are to be used as consolidants are therefore required to have a low molar mass in order to be able to adequately penetrate the wood cells. As a point of reference, polyethylene glycol (PEG) usually has a molar mass ranging from 0.2 to 4.0 kDa when used for conservation[13].

PEG has long been popular for treating archaeological wood and has notably been used for the conservation of famous shipwrecks like the Mary Rose[14] and the Vasa[15]. Despite its popularity, there are several valid reasons why it is necessary to find an alternative. Not only is it petroleum-derived, but there is also the possibility that it may gradually degrade in wood, potentially leading to the release of formic acid[12,16]. Additionally, PEG is vulnerable to environmental factors such as high temperatures[15], as well microbial degeneration[17].

Walsh et al.[18] note that biological based polymers offer several advantages and that they represent a greener and more sustainable alternative to some of the consolidants currently in use, such as PEG. Such materials have already been implemented successfully in different areas of scientific research, with Cabane et al.[19] providing us with various examples including surface wettability; photonics; self-healing and composite mechanical reinforcing[20–24]. With regards to conservation, there have been numerous studies over the years surrounding the use of green materials as consolidants[25–31]. A consolidant should ideally have high hydrogen bonding and other interaction potential, through appropriate residues and enhanced by an elongated shape, together with a small injectable molar mass which after curing inside the wood makes a strong, slightly flexible polymer network which interacts with the remaining wood materials. Additionally, from an environmental perspective, it should ideally come from natural materials, i.e. be "bioinspired": inspired by or based on biological structures or processes.

Terpenes are an example of such compounds which have recently generated considerable interest due to their potential as feedstocks for renewable polymers[32]. They are derived from a number of natural resources, such as trees and other plants[33], and are especially interesting since they can be obtained from biomass like wood waste without competing with food production[34]. Apart from their sustainable nature, other advantages include the ability to lend unique structural features like functionalities and stereocentres to their resultant polymers[34–41]. Stereocentres provide three-dimensionality to the molecules which can improve their potential for interactions, possibly leading to an increase in strength. Such functionalisation makes these polymers highly tuneable and gives them useful characteristics, including the ability to form hydrogen bonding, networking with the wood structure and possible anti-microbial properties. The production of such materials - which must be small enough to penetrate the wood prior to interacting/ curing or networking with the wood structure - is a compelling route to investigate as these compounds may potentially be used as consolidants for archaeological objects like the Oseberg artefacts. It was therefore decided to focus on terpene-based polymers for this study, due to the numerous advantages that they offer. Up until the present, we have been unable to find any literature detailing research around the use of terpene-based compounds as consolidants in heritage conservation.

In this study, we describe the synthesis and polymerisation of a functionalised monomer derived from α-pinene. This is a particularly interesting monoterpene as it is highly abundant, being a major component of turpentine which is itself derived from pine resin[42]. As a result, it has already been the focus of numerous studies as detailed in a recent review by Thomsett et al.[34] It was decided to furnish the monomer with two hydroxyl groups which would increase the potential for hydrogen bonding with the wood structure and consequently, its consolidative ability[43]. Extensive characterisation studies were subsequently run on the polymer, primarily using analytical ultracentrifugation. This is considered to be one of the most functional and adaptable techniques used in the study of macromolecules[9,44]. It is used for the characterisation of particles' sizes and shapes, as well as the quantitative analysis of their interactions in solutions[9,44,45]. This instrument is particularly useful since it functions without the need of separation matrices and calibration standards[9]. Such a hydrodynamic study will allow us to evaluate the polymer's potential as a consolidant for waterlogged, archaeological wood: finding favorable molecular hydrodynamic properties is very much Phase 1 in the process of finding a successful consolidant.

Results and discussion

Monomer synthesis from α-pinene. We have recently reported the synthesis of the terpene-derived triol **3** (Fig. 1) and its co-polymerisation with succinic acid via step-growth polymerisation[46]. The resulting polyesters were shown to be stereoregular; a feature that was exploited through the formation of a polymer stereocomplex[46]. As hydrogen bonding potential is anticipated to be a valuable property in wood consolidants, we were keen to investigate the polyhydroxylated derivative **3** for this purpose. Nevertheless, it was anticipated that the aforementioned polyesters would be biodegradable, a feature which is of course undesirable in this context. Accordingly, we instead investigated the formation of an acrylate derivative.

The synthesis of the acrylated monomer **4** was achieved in four steps from the cheap and readily available residue material α-pinene (Fig. 1 and also Supplementary Information for full synthetic details of **1**, **2** and **3**). The first step is epoxidation to the corresponding oxirane α-pinene oxide (**1**). The epoxidation of α-pinene has been the focus of extensive research (as detailed by Corma Canos et al.[46]) and it is currently synthesised on an industrial scale, as well as being widely available commercially. The next step involved forming *trans*-sobrerol (**2**), which is a common hydrolysis product of **1** and is a known molecule from our in-house library[35,47].The triol **3** was synthesised from **2** using a Brown hydroboration/oxidation sequence[48] and subsequently isolated as a single diastereomer, the stereochemistry of which was confirmed by X-ray crystallography. It should be noted that a higher yield for **3** can be achieved via column chromatography, at the expense of the diastereomeric ratio[46].

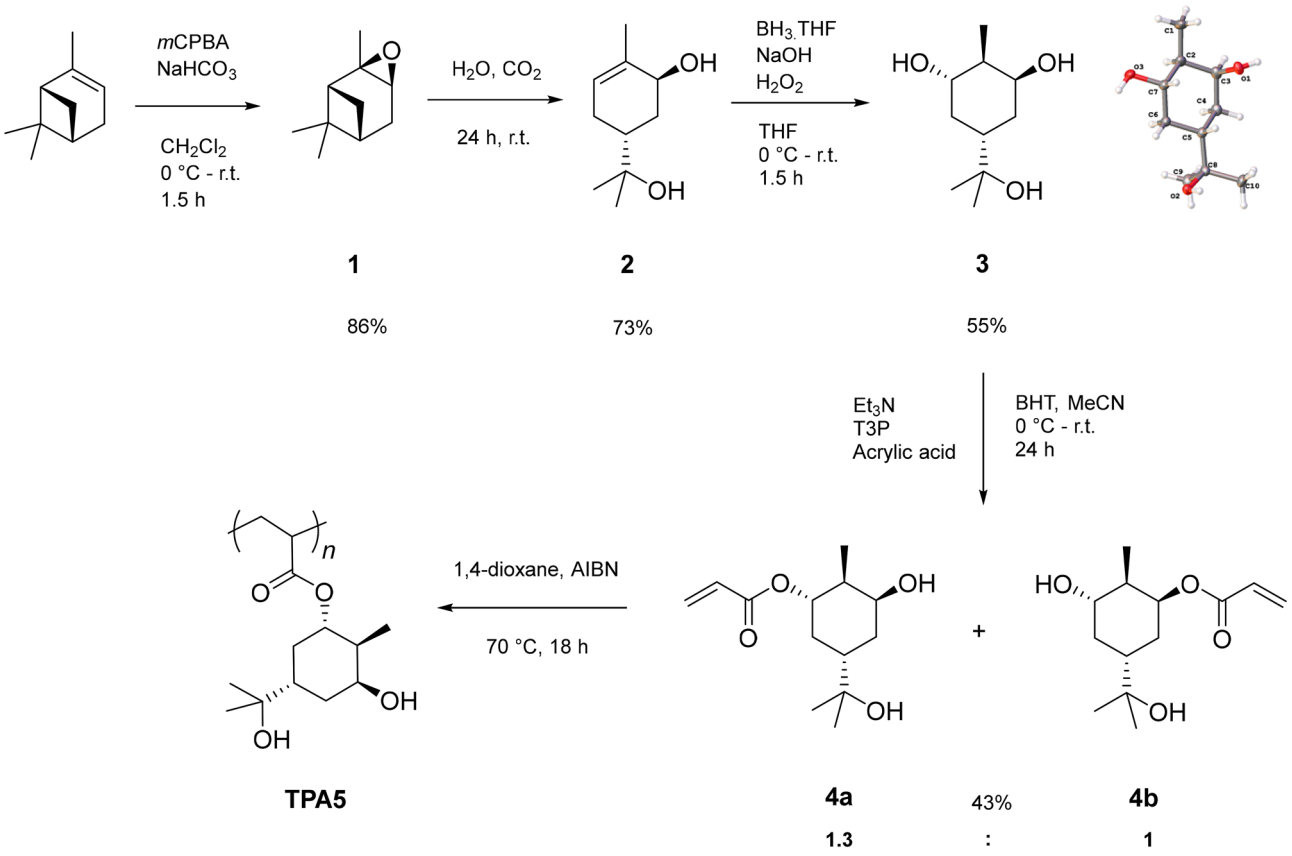

Figure 1. The synthesis route for the final monomer. An epoxidation of the starting terpene was carried out to form α-pinene oxide **1**, which was then hydrolysed to give *trans*-sobrerol **2**. This in turn was used to carry out a hydroboration/oxidation reaction to give the triol **3**, which was afterwards functionalised with an acrylate group to form the monomer as a mixture of two diastereomers **4a** and **4b**. These were then polymerised to form **TPA5**.

Polyhydroxylated compounds such as these have a lot of untapped potential, not only for wood consolidation purposes but also for other applications such as drug delivery[49].

The final step in the monomer synthesis involved functionalising **3** with an acrylate moiety. Previous work[35] has demonstrated the (meth)acrylation of a number of alcohols derived from several terpenes like (+)-α -pinene, (−)-β-pinene and (*R*)-(+)-limonene. The addition of a (meth)acrylate functional group is a well-known process widely employed to enable a variety of monomers to undergo free radical polymerisation (FRP). In one such example[35], hydroxyl-functionalised terpenes were initially esterified with (meth)acryloyl chloride using triethylamine as a base. This route was further optimised by substituting the (meth)acryloyl chloride with (meth)acrylic acid. Although these acids are not currently renewable, it is likely they will both become commercially available from a sustainable source in the future[35]. Additionally, the use of (meth)acrylic acid generates 'green' and less toxic waste as opposed to chlorinated waste, making the reaction more sustainable and scalable.

Propylphosphonic anhydride (T3P) was used to promote the ester coupling between the acrylic acid and **3**. This reagent is particularly attractive since its by-product is a relatively harmless and water-soluble triphosphate, again a preferable alternative to chloride waste generated when using acryloyl chloride. The reaction resulted in a mixture of diastereomers **4a** and **4b**. The final product was successfully isolated in two separate fractions: one enriched in the major diastereomer **4a** and another enriched in the minor diastereomer **4b**. The fraction enriched in the major diastereomer **4a** was isolated in a yield of 19% with a ratio of **4a**:**4b** = 22.8:1. The fraction enriched in the minor diastereomer **4b** had a yield of 23% with a ratio of **4a**:**4b** = 1:4.6. The total yield of diastereomers **4a** and **4b** was therefore 43%, in a ratio of **4a**:**4b** = 1.3:1. The diastereomers **4a** and **4b** were used together as a mixture for the subsequent polymerisation attempts. Diastereomer **4a** shows a large 11 Hz coupling on the proton adjacent to the acrylated oxygen (which is upshifted from 3.5 to 4.8 ppm by the electron-withdrawing carbonyl), consistent with a coupling between two axial protons.

Polymerisation of triol acrylate, TPA5. The triol acrylate monomer was then polymerised via conventional free radical polymerisation (FRP) to produce polymer **TPA5**, employing AIBN as an initiator and 1,4-dioxane as the solvent at 70 °C. The reaction was monitored using ^{1}H NMR and gel permeation chromatography (GPC) in THF (Supplementary Fig. S1). The investigated polymerisation reached 46% monomer conversion after 24 h under these reaction conditions as determined by ^{1}H NMR. **TPA5** was then isolated by precipitation in acetonitrile as a white solid, with subsequent analyses confirming that the desired polymer was obtained (Supplementary Fig. S2). GPC analysis confirmed a number average molar mass (M_n) of 2.6 kDa, a weight

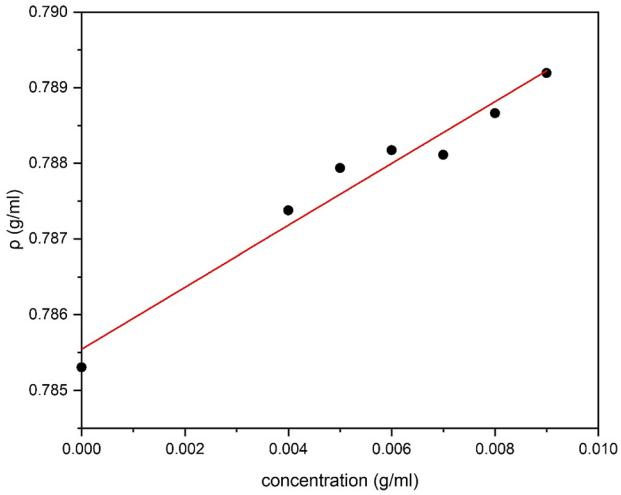

Figure 2. Solution density of **TPA5** in isopropanol plotted against concentration.

average molar mass of 3.8 kDa (relative to polymethylmethacrylate standards) and a broad polydispersity ($Đ$) of 1.5. These results were promising for our application as the polymer obtained appeared to have a low molar mass which was highly suitable for wood penetration. Nevertheless, higher conversion and narrower polydispersities can potentially be envisaged by using controlled polymerisation techniques such as reversible addition—fragmentation chain-transfer polymerisation (RAFT) or atom transfer radical polymerisation (ATRP).

Solubility testing. The severe decay of the Oseberg artefacts is such that most of them are only held together by the alum present in their wooden structure. The objects with the highest degree of degradation cannot be treated with polymers in aqueous solvents as has been done previously with the Mary Rose[50] and the Vasa[15]. This is because the alum remaining in the artefacts may dissolve in aqueous solvents and consequently exit the wooden structure, leading to total disintegration. As a result, it is deemed preferable to treat the most deteriorated artefacts with polymers in organic solvents.

Before continuing with the characterisation studies, it was therefore essential to determine which organic solvents the polymer was soluble in. Solvents which were tested included isopropanol, a 1:1 mixture of toluene in ethanol, ethyl acetate and acetone. The polymer was found to be soluble in isopropanol and the ethanol/toluene mixture, but insoluble in both ethyl acetate and acetone. It was therefore decided to carry out all further characterisation studies in isopropanol as this solvent has already been used in conservation studies and its high volatility ensures that it does not interact with the wood[51,52]. Furthermore, it has a low surface tension which allows for total permeability of the wood cells[52].

Calculation of the partial specific volume $\bar{\nu}$. We essentially followed the method of Kratky et al.[53] The density measurements were carried out using a concentration series of **TPA5** in isopropanol. The $\bar{\nu}$ was then obtained by plotting all the density measurements against concentration (Fig. 2) and consequently making use of Eq. 1. This was calculated to be (0.753 ± 0.040) cm^3/g. This value appeared to be consistent with other $\bar{\nu}$ values previously reported for synthetic polymers such as polymethacrylate[54], and was subsequently used for the sedimentation velocity and equilibrium analyses.

$$\bar{\nu} = \frac{1}{\rho_o}\left(1 - \frac{\partial \rho}{\partial c}\right) \tag{1}$$

Molar mass determination and distribution. Various loading concentrations were used to run the sedimentation equilibrium experiment in order to determine whether the measured or apparent molar mass $M_{w,app}$ was dependent on concentration. The data was analysed with SEDFIT-MSTAR[55,56], resulting in a plot of $M_{w,app}$ vs concentration for each sample. The $M_{w,app}$ was obtained by extrapolating the M^* function to the cell base, as well as by using the hinge point method (Table 1). The 'hinge point' is defined as the radial position where the local concentration is equal to the initial loading concentration[55,56]. This analysis also provided information on the apparent z-average molar mass $M_{z,app}$, which along with the $M_{w,app}$ could then be used to calculate $Đ$. Table 1 shows a comparison of the $M_{w,app}$, $M_{z,app}$ and $Đ$ values obtained from the sedimentation equilibrium study for all the tested concentrations. These results demonstrated that there was no significant change in $M_{w,app}$ with concentration, indicating that it was not concentration dependent and not affected by non-ideality. It may therefore be assumed that the $M_{w,app}$ determined by this experiment is in fact the ideal molar mass of the polymer at each given concentration ($M_{w,app} \sim M_w$). The overall average M_w was calculated by plotting the values obtained in the sedimentation equilibrium experiment against concentration (Fig. 3). This was determined to be (4.3 ± 0.2) kDa.

Concentration (mg/mL)	$M_{w,app}$ (from M^*) (kDa)	$M_{w,app}$ (hinge point) (kDa)	$M_{z,app}$ (kDa)	$Đ$ ($M_{z,app}/M_{w,app}$)
0.5	4.0	3.5	5.4	1.4
0.75	4.3	3.8	5.7	1.3
1	4.5	4.2	5.7	1.3
2	4.2	3.8	5.6	1.3
3	4.6	4.4	5.6	1.2
4	4.3	4.0	5.4	1.3

Table 1. The $M_{w,app}$ and $Đ$ values obtained from the sedimentation equilibrium experiment for all concentrations. The $M_{w,app}$ values obtained by the hinge point analysis were all slightly lower than the $M_{w,app}$ (M^*) values.

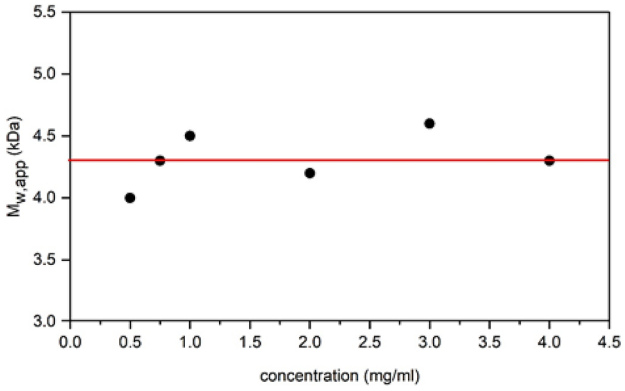

Figure 3. A plot of the apparent weight average molar mass, $M_{w,app}$ against concentration, from sedimentation equilibrium. The $M_{w,app}$ values were not significantly concentration-dependent, meaning that they were not affected by non-ideality. The ideal value was therefore taken as the average (red line), $M_w = (4.3 \pm 0.2)$ kDa. The data was analysed with SEDFIT-MSTAR using the M^* method to obtain the shown $M_{w,app}$ values. Rotor speed = 45,000 rpm.

The M_w values obtained by sedimentation equilibrium and the GPC analysis that was previously carried out were compared, with the M_w obtained by sedimentation equilibrium proving to be slightly larger. It was expected that the values obtained from AUC would have a higher degree of accuracy as a result of it being an absolute method, meaning that it is matrix-free and does not require calibration standards.

The sedimentation equilibrium data for the 4.0 mg/mL concentration was additionally analysed with the MULTISIG algorithm. This programme provides a distribution of the molar masses by making use of a 17-component system with 20 iterations, assuming thermodynamic ideality[57]. It was used to give a broader resolution of the M^* data, while also providing information about the M_w distribution of the polymer system. Figure 4 revealed a M_w distribution ranging from 2.3 to 9.3 kDa, with components peaking at 2.6 and 6.1 kDa. This was consistent with the SEDFIT-MSTAR analysis, confirming that the polymer has a low M_w and thus adding credibility to the results previously obtained by GPC. This further reinforced the status of this polymer as a very promising lead for the purpose of consolidation, since a low weight average M_w of ~ 4.3 kDa would increase the probability of it successfully penetrating archaeological wood.

Determining the heterogeneity of the polymer system. Figure 5 shows the sedimentation coefficient range $c(s)$[58] vs s of the polymer in isopropanol, run on SEDFIT. This algorithm normalises the sedimentation coefficient values to standard conditions (density and viscosity of water at 20.0 °C)[59]. The analysis confirmed that the polymer system is comprised of different components, as previously demonstrated by the MULTISIG analysis. It revealed the presence of a high concentration of a very low molar mass species, with a smaller population of two larger sedimentation coefficient, s value species. This trend was observed in all the concentrations that were used in this study.

Calculation of the intrinsic viscosity $[\eta]$. It was initially planned to carry out the viscosity measurements of **TPA5** with a conventional Ostwald U-tube capillary viscometer[60]. This however did not prove ideal due to the high volatility of isopropanol. It was therefore decided to use a rolling ball viscometer at 8.0 °C in order to counteract this issue. After measuring the viscosity of the polymer solution at 6.0 mg/mL, the $[\eta]$ was calculated to be (5.27 ± 0.11) mL/g with the Solomon-Ciuta equation (Eq. 2).

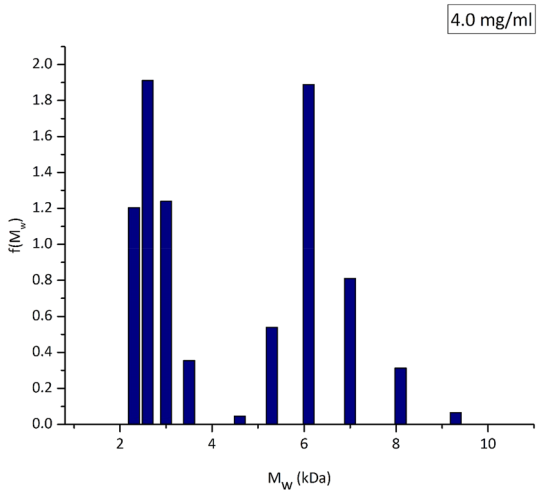

Figure 4. MULTISIG analysis of sedimentation equilibrium data to give the molar mass distribution f(M) vs M_w of **TPA5** at a concentration of 4.0 mg/mL. Rotational speed = 45,000 rpm.

$$[\eta] = \frac{1}{c}\left(2\left(\eta_{sp}\right) - 2ln(\eta_r)\right)^{\frac{1}{2}} \tag{2}$$

Conformation analyses. With the use of $[\eta]$, along with the values for the M_w, $\bar{\nu}$ and sedimentation coefficient obtained from previous experiments, the conformation of the polymer could then be investigated. This is particularly important as its shape may determine whether it penetrates wood and the subsequent effect it would have.

The programme ELLIPS1 was used to estimate the conformation of the polymer using the Perrin function (P) and the viscosity increment (ν) shape factors. ELLIPS1 is based on a simple ellipsoid of revolution model, where two of the three ellipsoid axes are of equal value[62]. Both P and ν are universal shape parameters, meaning that they are described by a function of shape not size[63], and are obtained respectively from the sedimentation coefficient and $[\eta]$[64].

P is related to the frictional ratio (f/f_o), which can be derived from the sedimentation coefficient $s_{20,w}$ (Eq. 3)[65]:

$$\frac{f}{f_o} = \frac{M\left(1-\bar{\nu}p\right)}{N_A 6\pi\eta_o}\left(\frac{4\pi N_A}{3\bar{\nu}M}\right)^{\frac{1}{3}}\frac{1}{s^o_{20,w}} \tag{3a}$$

$$P = (f/f_o)(\bar{\nu}/\nu_s)^{\frac{1}{3}} \tag{3b}$$

ν is described by Eq. 4:[66–68]

$$\nu = [\eta]M/(N_A \mathrm{V}) \tag{4}$$

Once calculated, ELLIPS1 was then used to report these shape functions in terms of their axial ratios (a/b) for ellipsoids of revolution[63]. Table 2 shows the values obtained for these parameters. A sedimentation coefficient ($s_{20,w}$) - normalised to the standard solvent conditions of the viscosity and density of water at 20.0°C - was used in these calculations (Fig. 6). Along with the axial ratios, ELLIPS1 also provides a visual representation of the approximate shape of the macromolecule. The shape factors were calculated using different degrees of 'solvation' or solvent association or "dynamic binding" ($\nu_s/\bar{\nu}$), in order to determine whether the final value estimate for the type and axial ratio was significantly affected. Both P and ν were seen to alter slightly to higher or lower values according to the ($\nu_s/\bar{\nu}$), however they both gave consistent results, indicating that the polymer had an elongated shape, as shown by Fig. 7.

A consensus value of ~ 4.5 was obtained from the mean of the all the determinations. An additional shape factor, the Scheraga-Mandelkern (β) parameter, was used as a consistency check. This is a hydration-independent function, but it is very insensitive to shape (Eq. 5):[69]

$$\beta = N_A s[\eta]^{\frac{1}{3}}\eta_o/\left[M_r^{\frac{2}{3}}(1-\bar{\nu}\rho_o)100^{\frac{1}{3}}\right] \tag{5}$$

A value of $\beta = (2.39 \pm 0.23) \times 10^6$ was calculated. This corresponded to a large axial ratio range, but it was nonetheless consistent with the value for the a/b found for the P and ν functions. Additionally, this value is only compatible with an elongated, prolate ellipsoid molecule, as opposed to a flat disc or oblate model like lignin (Fig. 8). This therefore adds further confidence to the shape analyses that were previously carried out.

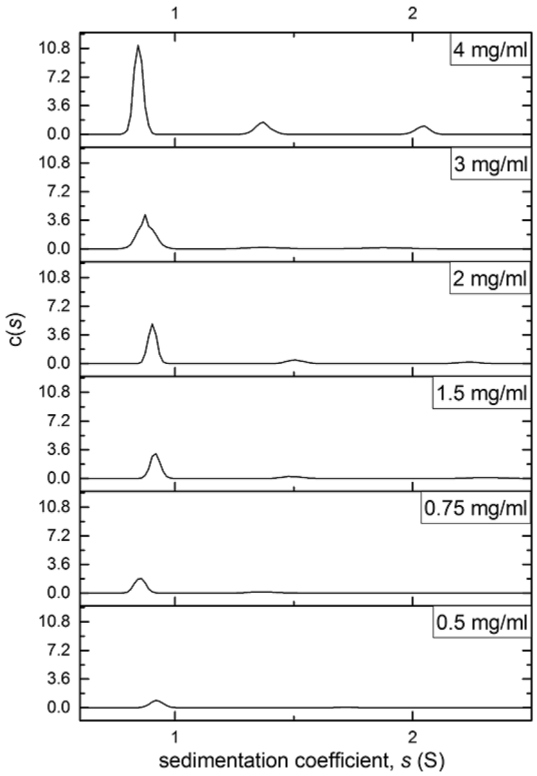

Figure 5. Sedimentation velocity sedimentation coefficient distributions c(*s*) vs *s* for **TPA5** in isopropanol. Distributions obtained by the SEDFIT approach of Dam and Schuck[61]. Rotor speed = 49,000 rpm.

Conclusion

In this study, the successful synthesis of an acrylated triol monomer **4** has been described. A new protocol for the radical polymerisation of such acrylated terpene monomers was designed and implemented, successfully yielding polymer **TPA5**. This methodology may potentially also be applied to other types of (meth)acrylated monomers derived from different terpenes. The polymer proved to be soluble in isopropanol, a common and relatively non-toxic solvent which can easily be used in conservation studies.

The hydrodynamic characterisation analyses from sedimentation equilibrium demonstrated that the polymer had a M_w of ~ 4.3 kDa, reinforced by the approximate value (relative to polymethylmethacrylate standards) obtained by GPC. Sedimentation velocity showed that the polymer system had a degree of heterogeneity, with a high population of a low molar mass species. Conformation analyses indicated that the polymer had an elongated shape, with both *P* and ν giving consistent results and the β-function confirming an elongated prolate rather than a flat oblate disc shape.

The collective properties of our synthesised bioinspired polymer **TPA5** appear to satisfy the essential molecular criteria as a consolidant: high hydrogen bonding potential enhanced by an elongated shape, together with a small injectable molar mass which can be cured into larger, stronger and stable structures once infused or injected into the wood, suggesting this polymer is worthy of further consideration as a potential consolidant.

In future papers in this series we will explore the wood penetration ability of this and related polymers and the ability, after curing, to form a strong stable hydrogen bonded network with porous, degraded wood structures. The interactions with other materials such as calcium hydroxide nanoparticles, used to lower the acid levels in archaeological wood[51], and their ability to interact in a compatible way with other consolidants, such as the sheet like lignin molecules[70] will be also be explored. In archaeological wood, lignin has a much slower degradation profile than cellulose, so consolidants should ideally be able to network or interact with the remaining lignin within the wood.

Materials and methods

Materials. All reagents and solvents were purchased from a chemical supplier (Acros Organics, Alfa Aesar, Merck, Sigma Aldrich or Fischer Scientific UK) and used without further purification. Water was deionised before use. Brine is a saturated aqueous solution of sodium chloride. Thin layer chromatography was performed on silica gel mounted on aluminium and was visualised using a potassium permanganate dip with gentle heating. Rotary evaporators under reduced pressure were used for solvent evaporation. Dry solvents were obtained from solvent drying towers and contained < 17 parts per million (ppm) of water. Experiments carried out under an inert atmosphere employed argon by means of a Schlenk line or a balloon.

Degree of solvent association ($v_s/\bar{v}$)	Shape factor	Calculated value	Axial ratio (a/b) (prolate)	Axial ratio (a/b) (prolate) + error	Axial ratio (a/b) (prolate)—error
1	*P*	(1.22 ± 0.20)	4.6	4.8	4.4
	ν	(7.00 ± 0.23)	5.9	6.1	5.7
1.2	*P*	(1.17 ± 0.20	3.8	4.0	3.6
	ν	(5.86 ± 0.23)	5.1	5.3	4.9
1.4	*P*	(1.11 ± 0.20)	3.0	3.2	2.8
	ν	(5.02 ± 0.23)	4.3	4.5	4.1

Table 2. The calculated values for the two different shape parameters *P* and ν at different degrees of solvent association (dynamic binding), along with the axial ratios determined by ELLIPS1. The axial ratios obtained by adding or subtracting the error from the calculated value (± 0.20 for *P* and ± 0.23 for ν) are also shown.

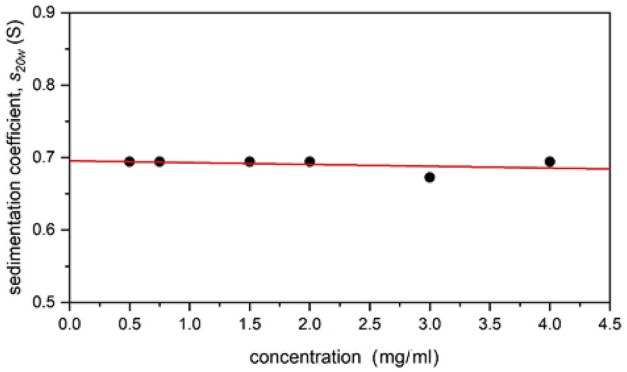

Figure 6. A plot of sedimentation coefficient $s_{20,w}$ (corrected to standard conditions—the density and viscosity of water at 20.0 °C) against sedimenting concentration. The ideal or "infinite dilution" value, $s^{o}_{20,w} = (0.696 \pm 0.007)$ S.

Nuclear magnetic resonance. ^{1}H NMR spectra were recorded in deuterated chloroform ($CDCl_3$), deuterated DMSO ($(CD_3)_2SO$) and deuterated methanol (CD_3OD) at ambient temperature using Bruker 400 MHz spectrometers (Bruker Corporation, Germany). ^{13}C NMR spectra were recorded in $CDCl_3$, $(CD_3)_2SO$ and CD_3OD at ambient temperature using 100 MHz spectrometers. Data is expressed as chemical shifts (δ) in ppm relative to solvent signals ($CHCl_3$, ^{1}H NMR 7.26), ($CDCl_3$ ^{13}C NMR 77.16), ($(CH_3)_2SO$, ^{1}H NMR 2.50), ($(CD_3)_2SO$, ^{13}C NMR 39.52), (CH_3OH, ^{1}H NMR 3.31) or (CD_3OD, ^{13}C NMR 49.0) as the internal standard. MestReNova 6.0.2 copyright 2009 (Mestrelab Research S. L.) was used for analysing the spectra.

High resolution mass spectrometry. Electrospray ionisation (ESI) high-resolution mass spectrometry (HRMS) analyses were performed on a Bruker micrOTOFII mass spectrometer (Bruker Daltonik, Bremen, Germany), interfaced to an Agilent 1200 HPLC (Agilent Technologies, Santa Clara, USA). Samples were presented in solution for analysis by Flow Injection, 1 µL of solution being injected into the ion source of the instrument along with a flow of 0.2 mL min^{-1} of 70% methanol/water eluent. The mass spectrometer was operated in electrospray ionisation (ESI) mode at a typical resolving power of 8000. Control of the analysis was performed through Bruker's Compass Open Access QC automated data acquisition and reporting software (v1.3; Bruker Daltonik, Bremen, Germany).

Fourier-transform infra-red spectroscopy.. A Bruker Tensor 27 FT-IR spectrophotometer with an ATR attachment was employed. The measurements were performed in the range of 4000–650 cm^{-1} and spectra were analysed using OPUS software (Bruker Corporation, Germany).

Monomer and polymer synthesis. The synthesis of α-pinene oxide (**1**), *trans*-sobrerol (**2**) and the triol (**3**) followed the methods described by Thomsett et al.[46] and are detailed in the Supplementary Information.

Synthesis of triol acrylate, 4. **3** (2 g, 10.6 mmol) and butylated hydroxytoluene (BHT) (ca. 19 mg) were added to acetonitrile (13 mL). Triethylamine (4.5 mL, 32 mmol) was added to the reaction mixture. The solution was cooled to 0 °C, after which propylphosphonic anhydride (T3P) (50 wt. % in ethyl acetate, 7.6 mL, 12.8 mmol) and acrylic acid (acid with low H_2O content, 99.5% stab. with ca. 200 ppm methoxyphenol, 0.8 mL, 11.7 mmol) were added. The mixture was left to stir for 10 min and then allowed to warm to room temperature. The mixture was left stirring for a further 24 h and then concentrated under reduced pressure. The crude product was purified by column chromatography to yield the title compounds as a white solid (**4a** and **4b**) (1.10 g, **4a**:**4b** = 1.3:1,

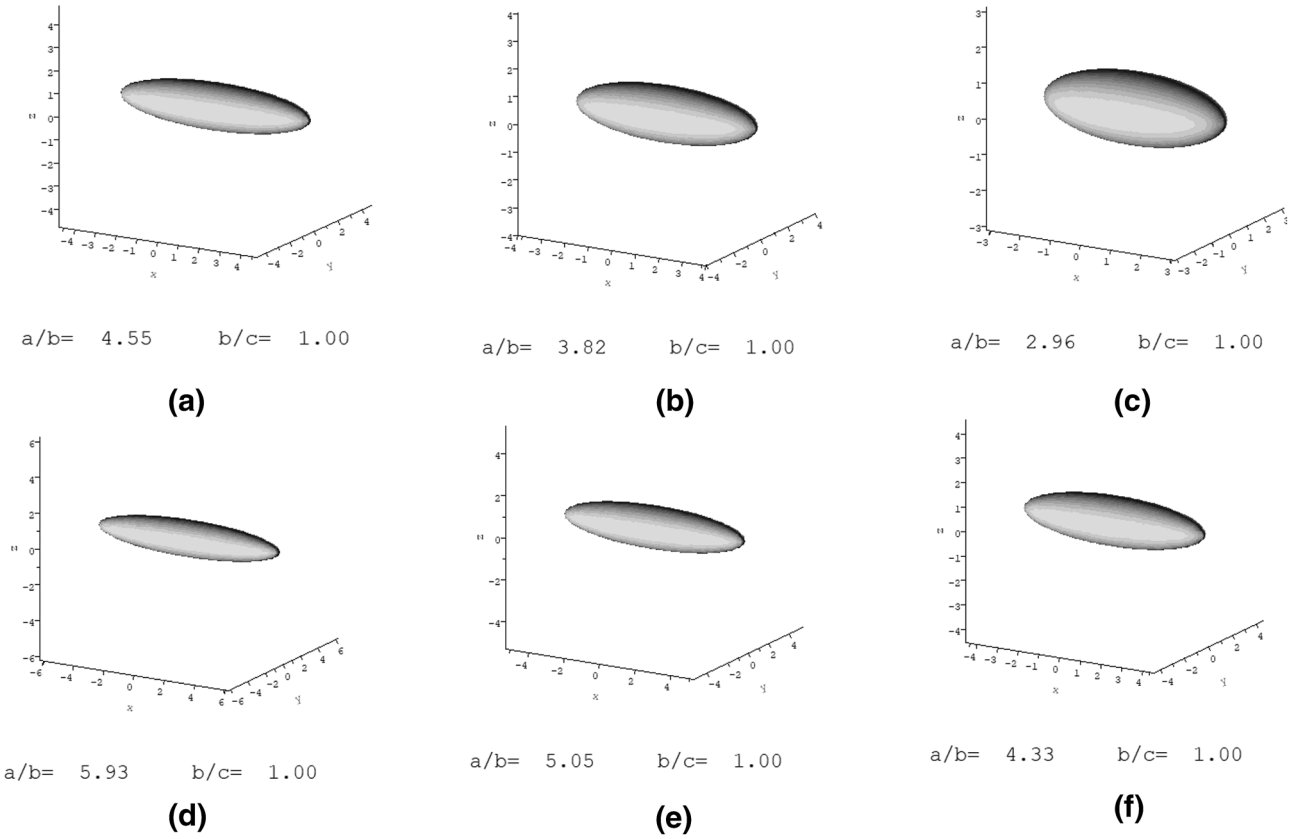

Figure 7. Ellipsoidal representations from the conformation analyses of **TPA5** in isopropanol, using ELLIPS1. (**a**) *P* for a $(v_s/\bar{v}) = 1.0$; (**b**) *P* for a $(v_s/\bar{v}) = 1.2$; (**c**) *P* for a $(v_s/\bar{v}) = 1.4$; (**d**) ν for a $(v_s/\bar{v}) = 1.0$; (**e**) ν for a $(v_s/\bar{v}) = 1.2$; (**f**) ν for a $(v_s/\bar{v}) = 1.4$. The data is consistent with an elongated shape in all the analyses.

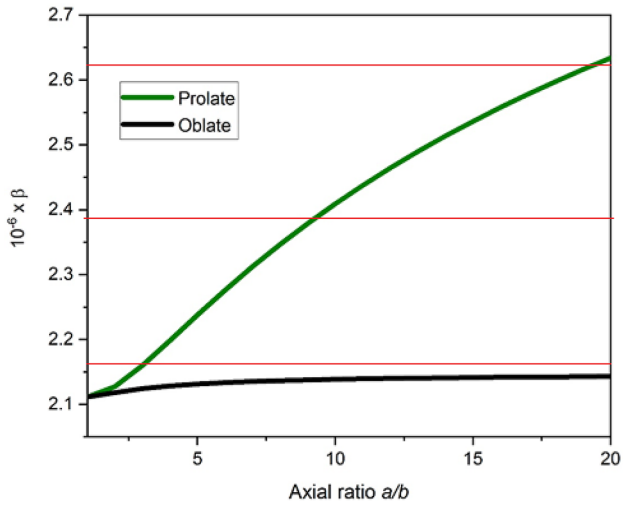

Figure 8. A plot of Scheraga-Mandelkern β function versus axial ratio with the green and black lines representing prolate and oblate shapes respectively. Red lines correspond to the experimental value of $\beta = (2.39 \pm 0.23) \times 10^6$ which excludes an oblate (disc) shape.

4.54 mmol, 43% yield). The mixture of diastereomers was partially separated by column chromatography to obtain a pure sample of the major diastereomer **4a** (0.50 g, 2.1 mmol, 19% yield).

General procedure for the polymerisation of triol acrylate, 4, to yield a terpene-derived acrylated polymer, TPA5. 1,4-dioxane (25 mL) was added to triol acrylate (with a diastereomeric ratio of **4a**:**4b** = 1.3:1) (515 mg,

2.2 mmol) and azobisisobutyronitrile (AIBN) (2.5 mg, 0.015 mmol). The mixture was purged with argon for 45 min, after which it was stirred for 18 h at 70.0 °C under argon. The mixture was left to cool to room temperature and then mixed with 80 mL of acetonitrile to precipitate a white solid. The solution was decanted and the solid dried in a high vacuum oven to yield the title compound (**TPA5**).

Hydrodynamic characterisation studies. *Gel permeation chromatography (GPC).* An Agilent 1260 Infinity Series HPLC (Agilent Technologies, USA) fitted with a differential refractive index detector (DRI) was used. THF (HPLC grade, Fisher Scientific) was used as the eluent at room temperature with two Agilent PL-gel mixed-E columns in series at a flow rate of 1 mL min^{-1}. A calibration curve was made using polymethylmethacrylate standards with ASTRA software (Wyatt Technology, USA). This was used for the determination of the M_n, M_w and molar mass distribution (dispersity, $Đ = M_w/M_n$).

Density measurements—calculation of the partial specific volume $\bar{\nu}$. An Anton Paar DMA 5000 V5.003 was used at 20.0 °C. A 9.0 mg/mL stock solution of TPA5 in isopropanol was prepared and then diluted to 8.0, 7.0, 6.0, 5.0 and 4.0 mg/mL. These concentrations were thereafter used for the density measurements. The partial specific volume—needed for the sedimentation velocity and equilibrium experiments—was evaluated following the procedure of Kratky et al.[53].

Analytical ultracentrifugation (AUC). Two Beckman Optima XL-I analytical ultracentrifuges with Rayleigh interference optics were used at 20.0 °C. 12 mm optical path length double sector cells with titanium centrepieces were employed.

Sedimentation equilibrium. Loading concentrations of 0.5 to 4 mg/mL of **TPA5** in isopropanol were used. 100 µL of each concentration were injected in the sample solution channel of the AUC cell. Isopropanol was used as the reference solution. The experiment was carried out at a rotational speed of 45,000 rpm over 2 days. The results were analysed with SEDFIT-MSTAR[55] in order to obtain the $M_{w,app}$, making use of the M^* function and extrapolation[56] and the hinge point method. No significant concentration dependence was observed suggesting that non-ideality was not significant. The data obtained from the highest concentration (4.0 mg/ml) was additionally analysed with the MULTISIG algorithm[57] to evaluate the molar mass distribution.

Sedimentation velocity. 405 µL of the previous loading concentrations (0.5 to 4.0 mg/mL) of **TPA5** in isopropanol were added to each of the cells. A rotational speed of 49,000 rpm was used and the samples centrifuged overnight. The weight average sedimentation coefficient and the distributions of sedimentation coefficient *c(s)* vs s were obtained by analysis with the SEDFIT procedure[61].

Viscosity measurements—calculation of the intrinsic viscosity. An Anton-Paar AMVn (Graz, Austria) rolling ball viscometer was used at a temperature of 8.0 °C. Its closed capillary system is more suitable for working with volatile solvent systems compared to conventional Ostwald viscometers.

The viscosity measurements were carried out using a 6.0 mg/mL concentration of **TPA5** in isopropanol. The intrinsic viscosity was then calculated with the Solomon-Ciuta equation:

$$[\eta] = \frac{1}{c}\left(2\left(\eta_{sp}\right) - 2ln(\eta_r)\right)^{\frac{1}{2}} \quad (6)$$

Conformation analyses. The ELLIPS1[62] algorithm was used to carry out analyses on the Perrin function (P), viscosity increment (ν) and the hydration independent Scheraga-Mandelkern (β) shape factors.

Received: 3 December 2020; Accepted: 25 February 2021
Published online: 01 April 2021

References

1. Braovac, S. *et al.* Chemical analyses of extremely degraded wood using analytical pyrolysis and inductively coupled plasma atomic emission spectroscopy. *Microchem. J.* **124**, 368–379 (2016).
2. Nilsson, T. & Rowell, R. Historical wood—structure and properties. *J. Cult. Herit.* **13S**, S5–S9 (2012).
3. Creangă, D. M. The conservation of archaeological wood. *Eur. J. Sci. Theol.* **5**, 57–68 (2009).
4. McHale, E., Steindal, C. C., Kutzke, H., Benneche, T. & Harding, S. E. In situ polymerisation of isoeugenol as a green consolidation method for waterlogged archaeological wood. *Sci. Rep.* **7**, 1–9 (2017).
5. Colombini, M. P. *et al.* A multi-analytical study of degradation of lignin in archaeological waterlogged wood. *Talanta* **80**, 61–70 (2009).
6. Kaye, B. Conservation of waterlogged archaeological wood. *Chem. Soc. Rev* **24**, 35–43 (1995).
7. Florian, M.-L.E. Scope and History of Archaeological Wood. In *Archaeological Wood* (eds Rowell, R. & Barbour, R.) 3–32 (American Chemical Society, 1989). https://doi.org/10.1021/ba-1990-0225.ch001.
8. Broda, M., Mazela, B., Królikowska-Pataraja, K. & Siuda, J. The state of degradation of waterlogged wood from different environments. *Ann. For. Wood Technol.* **91**, 23–27 (2015).
9. Harding, S. E. The Svedberg Lecture 2017. From nano to micro: the huge dynamic range of the analytical ultracentrifuge for characterising the sizes, shapes and interactions of molecules and assemblies in Biochemistry and Polymer Science. *Eur. Biophys. J.* **47**, 697–707 (2018).

10. Rosenqvist, A. M. The stabilizing of wood found in the viking ship of Oseberg: part I. *Stud. Conserv.* **4**, 13–22 (1959).
11. Braovac, S. & Kutzke, H. The presence of sulfuric acid in alum-conserved wood—Origin and consequences. *J. Cult. Herit.* **13**, S203–S208 (2012).
12. Christensen, M., Kutzke, H. & Hansen, F. K. New materials used for the consolidation of archaeological wood-past attempts, present struggles, and future requirements. *J. Cult. Herit.* **13S**, S183–S190 (2012).
13. Wakefield, J. M. K., Gillis, R. B., Adams, G. G., McQueen, C. M. A. & Harding, S. E. Controlled depolymerisation assessed by analytical ultracentrifugation of low molecular weight chitosan for use in archaeological conservation. *Eur. Biophys. J.* **47**, 769–775 (2018).
14. Walsh, Z. *et al.* Multifunctional supramolecular polymer networks as next-generation consolidants for archaeological wood conservation. *Proc. Natl. Acad. Sci.* **111**, 17743–17748 (2014).
15. Hocker, E., Almkvist, G. & Sahlstedt, M. The Vasa experience with polyethylene glycol: A conservator's perspective. *J. Cult. Herit.* **13S**, S175–S182 (2012).
16. Glastrup, J., Shashoua, Y., Egsgaard, H. & Mortensen, M. N. Degradation of PEG in the warship Vasa. *Macromol. Symp.* **238**, 22–29 (2006).
17. Kawai, F. Microbial degradation of polyethers. *Appl. Microbiol. Biotechnol.* **58**, 30–38 (2002).
18. Walsh, Z., Janeček, E.-R., Jones, M. & Scherman, O. A. Natural polymers as alternative consolidants for the preservation of waterlogged archaeological wood. *Stud. Conserv.* **62**, 173–183 (2017).
19. Cabane, E., Keplinger, T., Künniger, T., Merk, V. & Burgert, I. Functional lignocellulosic materials prepared by ATRP from a wood scaffold. *Sci. Rep.* **6**, 1–10 (2016).
20. Chen, P. Y., McKittrick, J. & Meyers, M. A. Biological materials: Functional adaptations and bioinspired designs. *Prog. Mater. Sci.* **57**, 1492–1704 (2012).
21. Yu, K., Fan, T., Lou, S. & Zhang, D. Biomimetic optical materials: Integration of nature's design for manipulation of light. *Prog. Mater. Sci.* **58**, 825–873 (2013).
22. Darmanin, T. & Guittard, F. Superhydrophobic and superoleophobic properties in nature. *Mater. Today* **18**, 273–285 (2015).
23. Diesendruck, C. E., Sottos, N. R., Effrey, J., Moore, S. & White, S. R. Biomimetic self-healing. *Angew. Chem. Int. Ed.* **54**, 10428–10447 (2015).
24. Milwich, M., Speck, T., Speck, O., Stegmaier, T. & Planck, H. Biomimetics and technical textiles: Solving engineering problems with the help of nature's wisdom. *Am. J. Bot.* **93**, 1455–1465 (2006).
25. Kennedy, A. & Pennington, E. R. Conservation of chemically degraded waterlogged wood with sugars. *Stud. Conserv.* **59**, 194–201 (2014).
26. Parrent, J. M. The conservation of waterlogged wood using sucrose. *Stud. Conserv.* **30**, 63–72 (1985).
27. Cipriani, G., Salvini, A., Fioravanti, M., Di Giulio, G. & Malavolti, M. Synthesis of hydroxylated oligoamides for their use in wood conservation. *J. Appl. Polym. Sci.* **127**, 420–431 (2013).
28. Cavallaro, G., Lazzara, G., Milioto, S., Parisi, F. & Sparacino, V. Thermal and dynamic mechanical properties of beeswax-halloysite nanocomposites for consolidating waterlogged archaeological woods. *Polym. Degrad. Stab.* **120**, 220–225 (2015).
29. Cipriani, G., Salvini, A., Baglioni, P. & Bucciarelli, E. Cellulose as a renewable resource for the synthesis of wood consolidants. *J. Appl. Polym. Sci.* **118**, 2939–2950 (2010).
30. Endo, R., Kamei, K., Iida, I., Yokoyama, M. & Kawahara, Y. Physical and mechanical properties of waterlogged wood treated with hydrolyzed feather keratin. *J. Archaeol. Sci.* **37**, 1311–1316 (2010).
31. Babiński, L. Dimensional changes of waterlogged archaeological hardwoods pre-treated with aqueous mixtures of lactitol/trehalose and mannitol/trehalose before freeze-drying. *J. Cult. Herit.* **16**, 876–882 (2015).
32. Wilbon, P. A., Chu, F. & Tang, C. Progress in renewable polymers from natural terpenes, terpenoids, and rosin. *Macromol. Rapid Commun.* **34**, 8–37 (2013).
33. Miyaji, H., Satoh, K. & Kamigaito, M. Bio-based polyketones by selective ring-opening radical polymerization of α-pinene-derived pinocarvone. *Angew. Chemie Int. Ed.* **55**, 1372–1376 (2016).
34. Thomsett, M. R., Storr, T. E., Monaghan, O. R., Stockman, R. A. & Howdle, S. M. Progress in the synthesis of sustainable polymers from terpenes and terpenoids. *Green Mater.* **4**, 115–134 (2016).
35. Sainz, M. F. *et al.* A facile and green route to terpene derived acrylate and methacrylate monomers and simple free radical polymerisation to yield new renewable polymers and coatings. *Polym. Chem.* **7**, 2882–2887 (2016).
36. Thomsett, M. R., Moore, J. C., Buchard, A., Stockman, R. A. & Howdle, S. M. New renewably-sourced polyesters from limonene-derived monomers. *Green Chem.* **21**, 149–156 (2019).
37. O'Brien, D. M. *et al.* Epoxy–amine oligomers from terpenes with applications in synergistic antifungal treatments. *J. Mater. Chem. B* **7**, 5222–5229 (2019).
38. Winnacker, M. Pinenes: Abundant and renewable building blocks for a variety of sustainable polymers. *Angew. Chemie* **130**, 14560–14569 (2018).
39. Llevot, A. *et al.* Renewability is not enough: Recent advances in the sustainable synthesis of biomass-derived monomers and polymers. *Chem. Eur. J.* **22**, 11510–11521 (2016).
40. Hillmyer, M. A. & Tolman, W. B. Aliphatic polyester block polymers: Renewable, degradable, and sustainable. *Acc. Chem. Res.* **47**, 2390–2396 (2014).
41. Vilela, C. *et al.* The quest for sustainable polyesters-insights into the future. *Polym. Chem.* **5**, 3119–3141 (2014).
42. Silvestre, A. J. D. & Gandini, A. Terpenes: major sources, properties and applications. In *Monomers, Polymers and Composites from Renewable Resources* (eds Belgacem, M. & Gandini, A.) 17–38 (Elsevier Science, 2008).
43. McHale, E. *et al.* Synthesis and characterisation of lignin-like oligomers as a bio-inspired consolidant for waterlogged archaeological wood. *Pure Appl. Chem.* https://doi.org/10.1515/pac-2016-0814 (2016).
44. Scott, D.J., Harding, S.E. & Rowe, A.J., eds. *Analytical Ultracentrifugation: Techniques and Methods* (Royal Society of Chemistry, 2005).
45. Cole, J. L., Lary, J. W., Moody, T. & Laue, T. M. Analytical ultracentrifugation: Sedimentation velocity and sedimentation equilibrium. *Methods Cell Biol.* **84**, 143–179 (2008).
46. Corma Canos, A., Iborra, S. & Velty, A. Chemical routes for the transformation of biomass into chemicals. *Chem. Rev.* **107**, 2411–2502 (2007).
47. Lima, M. S., Costa, C. S. M. F., Coelho, J. F. J., Fonseca, A. C. & Serra, A. C. A simple strategy toward the substitution of styrene by sobrerol-based monomers in unsaturated polyester resins. *Green Chem.* **20**, 4880–4890 (2018).
48. Brown, H. C. Hydroboration—a powerful synthetic tool. *Tetrahedron* **12**, 117–138 (1961).
49. Valenti, D. J. & Wagener, K. B. Direct synthesis of well-defined alcohol-functionalized polymers via acyclic diene metathesis (ADMET) polymerization. *Macromolecules* **31**, 2764–2773 (1998).
50. Schofield, E. J. *et al.* Nanoparticle de-acidification of the Mary Rose. *Mater. Today* **14**, 354–358 (2011).
51. Andriulo, F. *et al.* Hybrid nanocomposites made of diol-modified silanes and nanostructured calcium hydroxide. Applications to Alum-treated wood. *Pure Appl. Chem.* **89**, 29–39 (2017).
52. Chelazzi, D., Giorgi, R. & Baglioni, P. Nanotechnologies for the conservation of waterlogged wood: The Vasa case studies. In *Heritage, Weathering and Conservation Conference - HWC-2006* (eds Fort, R., Alvarez de Buergo, M., Gomez-Heras, M. & Vazquez-Calvo, C.) 797–802 (Taylor & Francis/A. A. Balkema Publishers, 2006).

53. Kratky, O., Leopold, H. & Stabinger, H. The determination of the partial specific volume of proteins by the mechanical oscillator technique. *Methods Enzymol.* **27**, 98–110 (1973).
54. Gill, T. J. & Kunz, H. W. The immunogenicity of vinyl polymers. *PNAS* **61**, 490–496 (1968).
55. Schuck, P. *et al.* SEDFIT-MSTAR: Molecular weight and molecular weight distribution analysis of polymers by sedimentation equilibrium in the ultracentrifuge. *Analyst* **139**, 79–92 (2014).
56. Creeth, J. M. & Harding, S. E. Some observations on a new type of point average molecular weight. *J. Biochem. Biophys. Meth.* **7**, 25–34 (1982).
57. Gillis, R. B. *et al.* MultiSig: A new high-precision approach to the analysis of complex biomolecular systems. *Eur. Biophys. J.* **42**, 777–786 (2013).
58. Schuck, P. Size-distribution analysis of macromolecules by sedimentation velocity ultracentrifugation and Lamm equation modeling. *Biophys. J.* **78**, 1606–1619 (2000).
59. Tanford, C. *Physical Chemistry of Macromolecules* (Wiley, 1961).
60. Harding, S. E. The intrinsic viscosity of biological macromolecules. Progress in measurement, interpretation and application to structure in dilute solution. *Prog. Biophys. Mol. Biol.* **68**, 207–262 (1997).
61. Dam, J. & Schuck, P. Calculating sedimentation coefficient distributions by direct modeling of sedimentation velocity concentration profiles. *Methods Enzymol.* **384**, 185–212 (2004).
62. Harding, S. E., Horton, J. C. & Cölfen, H. The ELLIPS suite of macromolecular conformation algorithms. *Eur. Biophys. J.* **25**, 347–359 (1997).
63. García de la Torre, J. & Harding, S. E. Hydrodynamic modelling of protein conformation in solution: ELLIPS and HYDRO. *Biophys. Rev.* **5**, 195–206 (2013).
64. Carrasco, B. *et al.* Novel size-independent modeling of the dilute solution conformation of the immunoglobulin IgG Fab' domain using SOLPRO and ELLIPS. *Biophys. J.* **77**, 2902–2910 (1999).
65. Perrin, F. Mouvement Brownian d'un ellipsoide. II Rotation libre et dépolarisation des fluorescences. Translation et diffusion de molécules ellipsoidales. *J. Phys. Radium* **7**, 1–11 (1936).
66. Simha, R. The influence of Brownian movement on the viscosity of solutions. *J. Phys. Chem.* **44**, 34 (1940).
67. Saito, N. The effect of Brownian motion on the viscosity of solutions of macromolecules, I. Ellipsoid of revolution. *J. Phys. Soc.* **6**, 297–301 (1951).
68. Harding, S. E. & Rowe, A. J. Modeling biological macromolecules in solution. II. The general tri-axial ellipsoid. *Biopolymers* **22**, 1813–1829 (1983).
69. Scheraga, H. A. & Mandelkern, L. Consideration of the hydrodynamic properties of proteins. *J. Am. Chem. Soc.* **75**, 179–184 (1953).
70. Alzahrani, Q. E. *et al.* Matrix-free hydrodynamic study on the size distribution and conformation of three technical lignins from wood and non-wood. *Holzforschung* **70**, 117–125 (2016).

Acknowledgements

This work was supported by the UK Engineering & Physical Sciences Research Council [grant number EP/L015633/1], the Norwegian Ministry of Education and Research, and the University of Oslo as part of the Saving Oseberg project. M.C. is a UK EPSRC Centre for Doctoral Training in Sustainable Chemistry student. Special thanks to Dr. Mary Phillips-Jones and Dr. Vincenzo Taresco for reviewing the article and contributing to scientific discussions.

Author contributions

The synthetic, analytical and characterisation work was carried out by M.C. S.E.H. and R.A.S. contributed to the planning of the experiments and provided supervision for the research work, along with S.M.H. and F.A. M.R.T. and J.C.M. carried out the exploratory work for the synthesis of α-pinene oxide, *trans*-sobrerol and triol molecule. B.C. carried out the polymerisation kinetics studies. The paper was written by M.C. and S.E.H. and all authors reviewed the article.

Competing interests

The authors declare no competing interests.

Additional information

Supplementary Information The online version contains supplementary material available at https://doi.org/10.1038/s41598-021-86543-1.

Correspondence and requests for materials should be addressed to M.C., R.A.S. or S.E.H.

Reprints and permissions information is available at www.nature.com/reprints.

Publisher's note Springer Nature remains neutral with regard to jurisdictional claims in published maps and institutional affiliations.

molecules

MDPI

Article

Comparative Hydrodynamic Study on Non-Aqueous Soluble Archaeological Wood Consolidants: Butvar B-98 and PDMS-OH Siloxanes

Michelle Cutajar [1,2,*], Robert A. Stockman [2], Susan Braovac [3], Calin Constantin Steindal [3], Angeliki Zisi [3] and Stephen E. Harding [1,3,*]

[1] National Centre for Macromolecular Hydrodynamics (NCMH), School of Biosciences, University of Nottingham, Sutton Bonington LE12 5RD, UK
[2] School of Chemistry, University Park Campus, University of Nottingham, Nottingham NG7 2RD, UK; robert.stockman@nottingham.ac.uk
[3] Museum of Cultural History, University of Oslo, Kabelgata 34, 0580 Oslo, Norway; s.d.braovac@khm.uio.no (S.B.); c.c.steindal@khm.uio.no (C.C.S.); angeliki.zisi@khm.uio.no (A.Z.)
* Correspondence: michelle.cutajar@nottingham.ac.uk (M.C.); steve.harding@nottingham.ac.uk (S.E.H.)

Abstract: Butvar B-98 and PDMS-OH both have a demonstrable ability as consolidants for archaeological wood. This makes them both potential treatment options for the Oseberg collection, which is one of the most important archaeological finds from the Viking era. Both Butvar B-98 and PDMS-OH are soluble in organic solvents, offering a useful alternative to aqueous-based consolidants. Extensive characterisation studies were carried out on both of these polymers, with the use of analytical ultracentrifugation and viscometry, for the benefit of conservators wanting to know more about the physical properties of these materials. Short column sedimentation equilibrium analysis using SEDFIT-MSTAR revealed a weight-average molar mass (weight-average molecular weight) M_w of (54.0 ± 1.5) kDa (kg · mol^{-1}) for Butvar B-98, while four samples of PDMS-OH siloxanes (each with a different molar mass) had an M_w of (52.5 ± 3.0) kDa, (38.8 ± 1.5) kDa, (6.2 ± 0.7) kDa and (1.6 ± 0.1) kDa. Sedimentation velocity confirmed that all polymers were heterogeneous, with a wide range of molar masses. All molecular species showed considerable conformational asymmetry from measurements of intrinsic viscosity, which would facilitate networking interactions as consolidants. It is anticipated that the accumulated data on these two consolidants will enable conservators to make a more informed decision when it comes to choosing which treatment to administer to archaeological artefacts.

Keywords: analytical ultracentrifugation; Butvar B-98; PDMS-OH; Oseberg artefacts

Citation: Cutajar, M.; Stockman, R.A.; Braovac, S.; Steindal, C.C.; Zisi, A.; Harding, S.E. Comparative Hydrodynamic Study on Non-Aqueous Soluble Archaeological Wood Consolidants: Butvar B-98 and PDMS-OH Siloxanes. *Molecules* **2022**, *27*, 2133. https://doi.org/10.3390/molecules27072133

Academic Editors: Maria Perla Colombini, Erika Ribechini and Jeannette Jacqueline Łucejko

Received: 20 February 2022
Accepted: 20 March 2022
Published: 25 March 2022

1. Introduction

Archaeological artefacts are unique time-travelling devices, transporting information from the past to the present. These artefacts not only provide us with a historical record but also with a source of cultural identity. It is therefore important that they are preserved for future generations. The Oseberg collection, discovered and excavated in 1903 and 1904 respectively [1], is comprised of highly valuable wooden artefacts and there is currently a race against time to develop new methodologies to reduce their active degradation and increase their strength. This unique assembly of archaeological artefacts was treated with hot alum salt solutions ($KAl(SO_4)_2 \cdot 12H_2O$ and $NH_4Al(SO_4)_2 \cdot 12H_2O$) between 1905 and ca. 1912 [2,3].

While this successfully provided support for the weakened structure of the waterlogged wood, it also inadvertently led to the formation of a very acidic environment in the wood (pH ca. 1–2.5) and the highly degraded state that the artefacts are presently in [4,5]. The severe decay of the Oseberg artefacts is such that many are only held together

by the alum present in their wooden structure. Additionally, many objects have been reconstructed in ways that are not possible to undo without causing further damage. The objects with the highest degree of degradation and those which have been highly reconstructed cannot be re-treated with polymers in aqueous solutions. This is because the alum remaining in the artefacts may dissolve in water and consequently diffuse from the wooden structure, leading to total disintegration. As a result, it is deemed preferable to treat the most deteriorated and highly reconstructed artefacts with non-aqueous methods.

In this study, we carried out the extensive characterisation of two commercially available polymers representing such non-aqueous treatments, Butvar B-98 and hydroxy-terminated polydimethylsiloxane (PDMS-OH). These are currently being considered as candidates for the retreatment of part of the Oseberg wooden collection of artefacts. The performance of a wood consolidant depends not only on its chemical composition but also on its physical properties, notably molecular weight and molecular weight distribution and conformation, both of which affect the property to penetrate through the wood and interact/form stable networks with wood components. In so doing, we will extend/reinforce the information already available for these materials, thereby assisting an archaeological wood conservator in his/her choice of the appropriate material.

This level of characterisation, in terms of size distribution, molar mass, and conformation of these two consolidants have never been carried out according to our knowledge, and we are anticipating that it will prove to be very useful when it comes to deciding which consolidants to choose for retreatment. Moreover, it will also be helpful to other future conservation projects.

Butvar B-98 is a polyvinyl butyral-based resin produced by the reaction of polyvinyl alcohol with butyraldehyde [6,7] (Figure 1a). It has already been used as a conservation treatment for archaeological artefacts, such as wooden objects excavated from tombs dating back to the 8th century BCE in Gordion, Turkey [6]: samples from these artefacts were consolidated with Butvar B-98 diluted in a solution of toluene and ethanol. After drying, it was shown that the wood had little or no shrinkage and minimal colour change. Spirydowicz et al. [6] reported that treating samples with 10% Butvar B-98 resulted in stabilisation without any significant micromorphological changes to the structure of the wood. Using scanning electron microscopy, it was confirmed that while the Butvar B-98 filled some of the cell lumina, it commonly coated their surfaces/cell walls.

Silicone-based polymers such as PDMS-OH (Figure 1b) possess a number of desirable properties such as hydrophobicity, high chemical, and temperature resistance, and minimal flammability [8]. These polymers form a macromolecular network in the wood via crosslinking, achieved by condensing the silanol groups to form siloxane bonds [8]. Kavvouras et al. [8] investigated the use of PDMS-OH together with a catalyst and a crosslinker, for conserving archaeological waterlogged wood from the Neolithic period in Greece. The process resulted in the formation of a three-dimensional polysiloxane network which effectively protected against the shrinking of the wood cells, whilst retaining the appearance of natural wood.

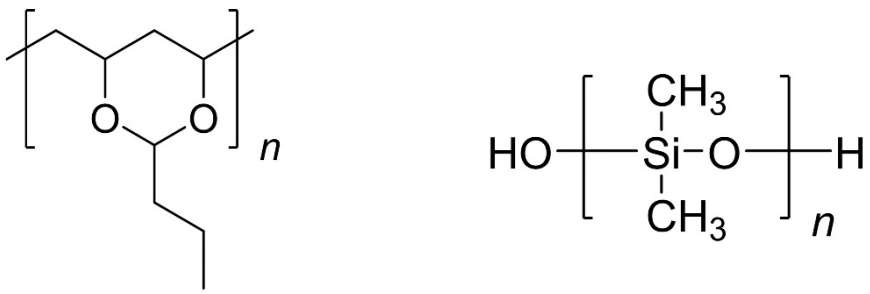

(**a**) (**b**)

Figure 1. Structures of (**a**) Butvar B-98 and (**b**) PDMS-OH siloxanes.

The characterisation described in the present study was primarily carried out by analytical ultracentrifugation, an absolute and matrix-free technique commonly used in the study of macromolecules [9]. This method has been recently described for the study of potential wood consolidants [10–14]. It is particularly attractive when compared to the more classical method of gel-permeation chromatography (GPC) since apart from the determination of particle sizes and shapes, it can also be used for the quantitative analysis of their interactions in solutions [9]. Moreover, unlike GPC, it can directly give molecular weights without the use of calibration standards of known molecular weight and a shape identical to that of the polymer being characterised. This eliminates the uncertainty that a method such as GPC generates when the polymer being tested does not have the same conformation as the standards employed.

There are two principle techniques that are carried out by analytical ultracentrifugation: a sedimentation velocity study and a sedimentation equilibrium experiment. Sedimentation velocity is a powerful matrix-free method that is used to gain information about the size distribution in terms of the sedimentation coefficient *s* (in Svedberg units, S), where s is the sedimentation rate per unit centrifugal field. It can also provide information on the shape of the macromolecule, as well as its interactions in solution. Since it generally works at relatively high rotor speeds, a high centrifugal force is developed which tend to dominate back diffusion effects. Although it is highly resolving, the *s* depends not only on the size but also on the shape of the molecule since extended molecules sediment slower. In contrast, sedimentation equilibrium is run at lower speeds; during such an experiment, the sedimentation and diffusion forces come to an equilibrium, and this provides direct information on the molar mass of the macromolecule, as there are no shape or friction effects, and without the need for standards. It also requires much shorter columns, minimising the effects of solvent compressibility issues. We also investigated the viscosity/conformational (shape) using a rolling ball viscometer [14] (with data analysed using the programme ELLIPS1) [15,16]. The primary solvent we used was isopropanol because the studied polymers are soluble in this; there is a sufficient density and viscosity difference between polymer and solvent, and it also has lower compressibility compared to many other organic solvents [17,18].

We also investigated the viscosity and shape behaviour of the siloxanes in turpentine as a second solvent. Turpentine (Figure 2) was chosen as an additional solvent for investigation as siloxanes are soluble in it and it is also a natural or "green" solvent consisting of terpenes obtained from the wood of pine trees by steam distillation. This was not possible for the ultracentrifuge studies due to the insufficient density difference of the siloxanes with the solvent, nor for Butvar B-98 due to its insolubility in turpentine.

Figure 2. Wood fragment from the Oseberg collection before and after retreatment by injection with siloxane PS36000 in turpentine at a concentration of ~5% (50 g/L). The fragment had been originally treated with alum and linseed oil shortly after excavation in 1904.

2. Results

2.1. Butvar B-98

2.1.1. Sedimentation Velocity in the Analytical Ultracentrifuge

Figure 3 shows the sedimentation coefficient distribution c(*s*) [19] vs. *s* of Butvar B-98 in isopropanol, analysed using the algorithm SEDFIT [20]. The analysis revealed material of a low sedimentation coefficient (<1 S) and close to the lowest limit of the technique (~0.4 S). No evidence of aggregation products was seen at higher sedimentation coefficient values. Low sedimentation coefficients are a feature of either low molar masses, extended conformations, or a combination of both. Two peaks are distinguishable at ~0.4–0.5 S and ~0.7–0.8 S. SEDFIT also enables the normalisation of the sedimentation coefficient to standard conditions (density and viscosity of water at 20.0 °C) for comparative purposes [21]. The normalised sedimentation coefficients ($s_{20,w}$) for the two peaks were then plotted against concentration (Figure 4). It has to be stressed that these are on the lowest limit of sedimentation coefficient measurement.

2.1.2. Sedimentation Equilibrium in the Analytical Ultracentrifuge

Sedimentation equilibrium experiments were then performed in order to determine weight-average molar masses. The algorithm SEDFIT-MSTAR [22] was used to evaluate the apparent weight-average molar mass $M_{w,app}$ at cell loading concentrations ranging from 0.5 mg/mL (the minimum concentration required to give an adequate concentration distribution at sedimentation equilibrium) to 5.0 mg/mL (Supplementary Table S1).

Values are apparent at finite concentration because of the effects of thermodynamic non-ideality through molecular excluded volume effects [21], which leads to an underestimate of the true molar mass value. Depending on the size of the molecule, at sufficiently low concentrations $M_{w,app}$ can be considered to be approximately equal to M_w, the thermodynamically ideal value. Alternatively, measurements of $M_{w,app}$ can be made at a series of concentrations, *c*, and extrapolated back to $c = 0$ where non-ideality effects are eliminated and hence, $M_{w,app} = M_w$. The $M_{w,app}$ values themselves are obtained from SEDFIT-MSTAR using either (i) the M^* function, or (ii) the hinge method (see Schuck et al. [22]).

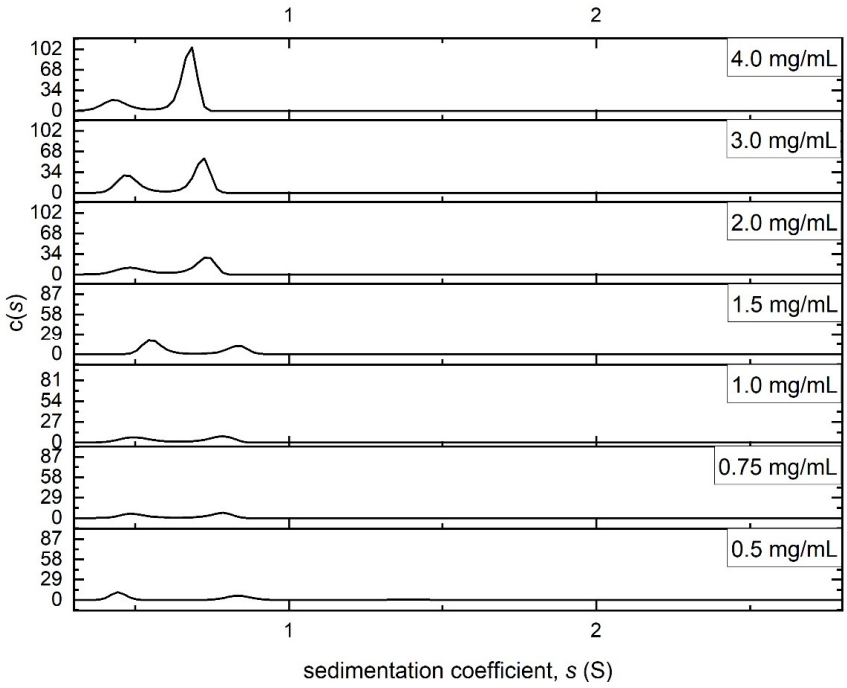

Figure 3. Sedimentation coefficient distributions of Butvar B-98 at different loading concentrations in isopropanol. Rotor speed = 49,000 rpm, temperature = 20.0 °C.

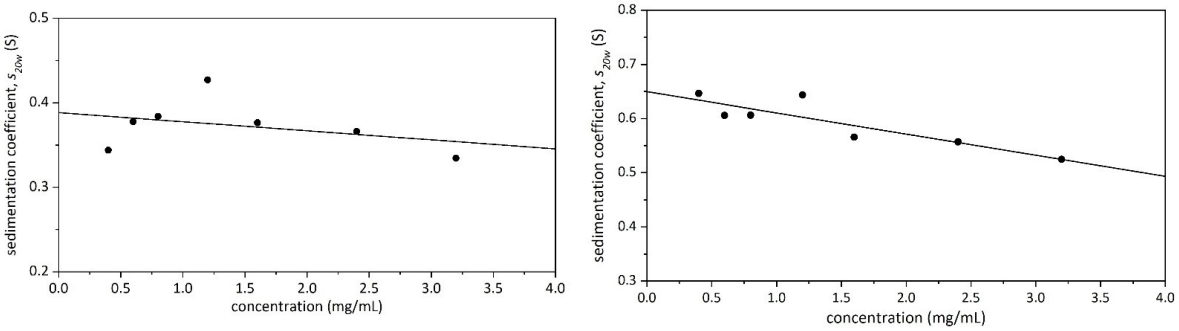

Figure 4. Dependence of $s_{20,w}$ on sedimenting concentration (corrected for radial dilution) for Butvar B-98. (**a**) Slower component $s^{o}_{20,w}$ = (0.40 ± 0.02) S; (**b**) Faster component $s^{o}_{20,w}$ (0.65 ± 0.02) S.

Figure 5a shows an extrapolation to zero concentration to eliminate non-ideality effects to yield an "ideal" weight-average molar mass M_w = (54.0 ± 1.5) kDa for Butvar B-98. SEDFIT-MSTAR also provides an estimate for the (apparent) z-average molar mass, $M_{z,app}$, and hence the apparent polydispersity $Đ = M_{z,app}/M_{w,app}$.

The sedimentation equilibrium data for the 4.0 mg/mL loading concentration were additionally analysed with the MULTISIG algorithm. This programme utilises a 17-component system with 20 iterations to provide a distribution of the (apparent) molar masses in a polymer system [23]. Figure 5b reveals a broad distribution ranging from 17.5 to 163.4 kDa, with components peaking at 17.5 and 61.4 kDa for Butvar B-98. Both the weighted average whole distribution value M_w = (54.0 ± 1.5) kDa and the f(M) vs. M_{app} distribution are consistent with values previously quoted for Butvar B-98, namely 40–70 kDa [24].

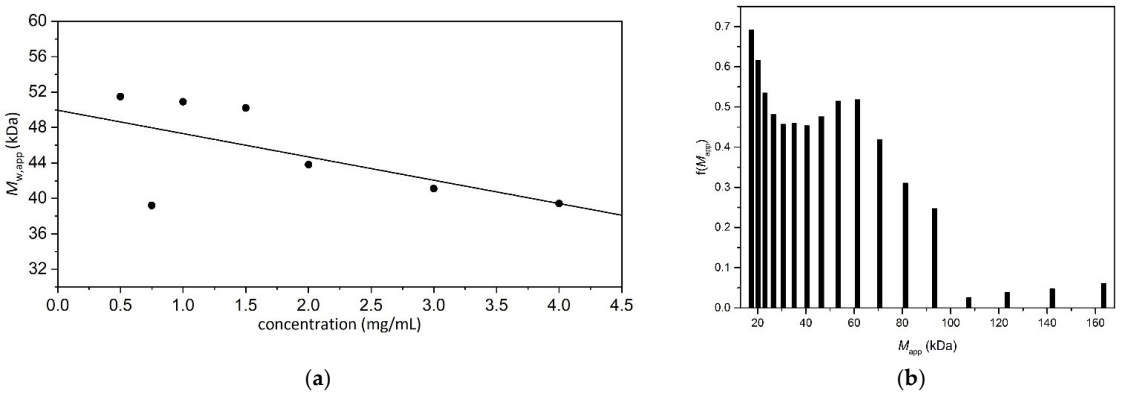

Figure 5. Sedimentation equilibrium of Butvar B-98 in isopropanol. Rotor speed 22,000 rpm. Temperature = 20.0 °C. (**a**) Dependence of the apparent $M_{w,app}$ on concentration, with an extrapolation to obtain the thermodynamically ideal M_w of Butvar B-98 = (54.0 ± 1.5) kDa. The data was analysed with SEDFIT-MSTAR using the M^* method. (**b**) Estimation using MULTISIG of the molar mass distribution f(M) vs. M_{app} at a loading concentration of 4.0 mg/mL. A broad distribution is seen consistent with sedimentation velocity (see Figure 3).

2.2. Siloxanes: PDMS-OH

Four different preparations of PDMS-OH were studied across a range of molar masses assigned by the manufacturer based on size exclusion chromatography as 36,000 Da and 18,000 Da (both relative to polystyrene standards), and 4200 Da and ~550 Da: these samples are hitherto named as PS36000, PS18000, PS4200, and PS550.

2.2.1. Sedimentation Velocity in the Analytical Ultracentrifuge

The PDMS-OH series was solubilised in isopropanol. A rotational speed of 49,000 rpm at a temperature of 20.0 °C was used for all samples: Figure 6a–d compares the sedimenta-

tion coefficient distributions obtained from these experiments for the four samples across the range of concentrations. No evidence of high molar mass aggregation products was evident across the range. PS36000 (Figure 6a) had a single peak with a sedimentation coefficient value *s* of ~0.7 S. In contrast, PS18000 (Figure 6b) revealed two components. As the concentration increased, these two peaks showed a tendency to merge, possibly due to the Johnston—Ogston [25] effect where the faster moving component was slowed down by having to move through a solution of the slower moving component. PS4200 (Figure 6c) had very similar results to PS18000, especially at higher concentrations, where two primary components were observed. For PS550 (Figure 6d) the sedimentation coefficient was too small to be reliably detected, but the distribution plot did not show the presence of higher molar mass aggregates. When an attempt was made to calculate the $s_{20,w}$ of the PDMS-OH samples, that is, the sedimentation coefficient normalised to the standard solvent conditions of the density and viscosity of water at 20.0 °C, it was discovered that all values came out negative. This would indicate that, had these molecules been soluble in water they would have moved in the opposite direction to the ultracentrifugal field—i.e., *flotation velocity*—somewhat similar to what we had previously observed for another polymer, 'CoPo9', a block copolymer made of poly(ethylene oxide), poly(isoprene) and poly(ethylene oxide)—which is soluble as unimers in chloroform but forms micelles in water [26].

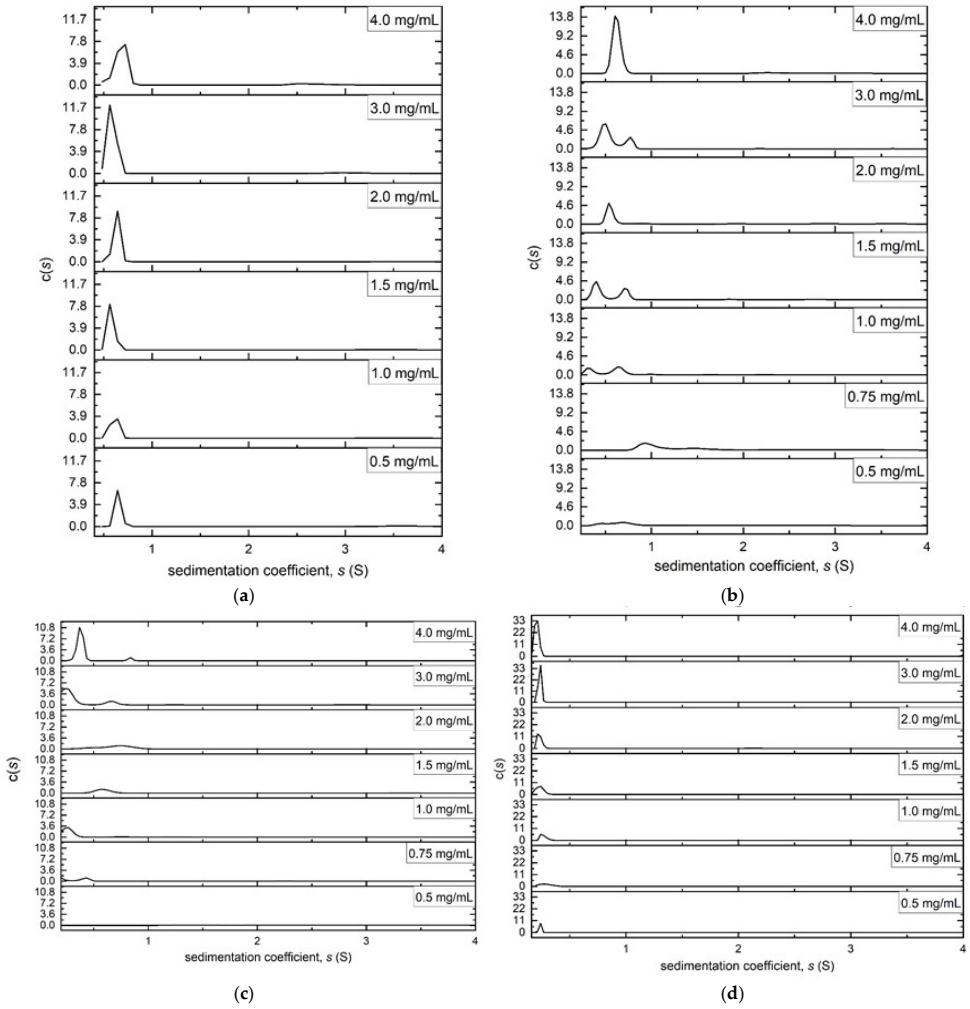

Figure 6. Sedimentation coefficient distributions of the PDMS-OH series at different loading concentrations in isopropanol. Rotor speed = 49,000 rpm, temperature = 20.0 °C (**a**) PS36000, (**b**) PS18000, (**c**) PS4200, (**d**) PS550.

2.2.2. Sedimentation Equilibrium in the Analytical Ultracentrifuge

Sedimentation equilibrium experiments were performed on all samples, using appropriate rotational speeds according to their approximate sizes. (Supplementary Tables S2–S5). The thermodynamically ideal whole distribution weight average M_w values were obtained, as with Butvar B-98, by plotting the apparent $M_{w,app}$ values against concentration and extrapolating to zero concentration (Figure 7). These weight-average molar mass values proved to be a little higher than the relative molar mass estimates M_r (relative to polystyrene standards) provided by the manufacturer (Table 1): this may be due to the different conformations of the siloxanes to the polystyrene standards in the solvent used. Because of the small size of PS550, measurable fringe increments were only possible at the higher concentrations, therefore M_w is obtained by taking the average of the 3.0 mg/mL and 4.0 mg/mL measurements (Table S5). Approximating $M_w \sim M_{w,app}$ is justified because its exclusion volume/ non-ideality effects will be minimal [21].

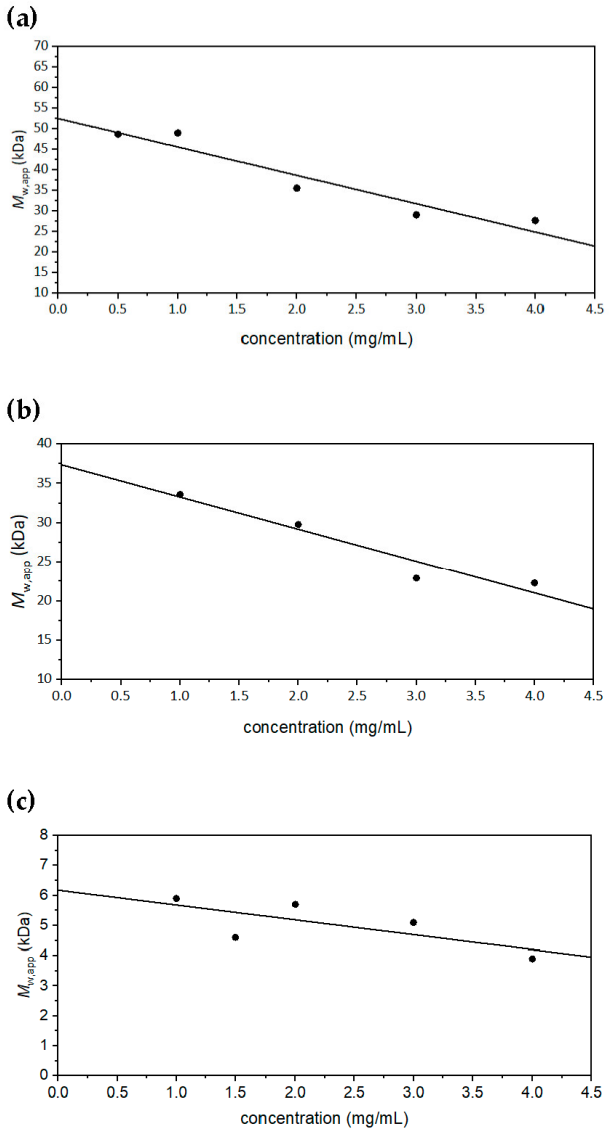

Figure 7. Dependence of apparent $M_{w,app}$ from sedimentation equilibrum using SEDFIT-MSTAR on concentration, with an extrapolation to obtain the thermodynamically ideal $M_{w,app}$ of the PDMS-OH siloxanes in isopropanol. (**a**) PS36000, rotor speed = 22,000 rpm, temperature = 20.0 °C. The value extrapolated to zero concentration was calculated to be M_w = (52.5 ± 3.0) kDa. (**b**) PS18000 in isopropanol, rotor speed = 30,000 rpm. M_w = (37.4 ± 2.3) kDa. (**c**) PS4200 in isopropanol, rotor speed = 49,500 rpm. M_w = (6.2 ± 0.7) kDa.

Table 1. Molar mass values for PDMS-OH siloxanes in isopropanol M_w: weight-average molar mass values in isopropanol from sedimentation equilibrium in the analytical ultracentrifuge. M_r: relative molar mass values relative to polystyrene standards.

Polymer	M_r (Da)	M_w (Da)
PS36000	36,000	52,500 ± 3000
PS18000	18,000	38,800 ± 1500
PS4200	4200	6200 ± 700
PS550	~550	1550 ± 50

Figure 8a–c shows the corresponding molar masses at a loading concentration of 4.0 mg/mL from the MULTISIG [23] analyses of the equilibrium data (the PS550 was not possible for this type of analysis due to its small size). The polymers appear to be fairly heterogeneous, with each having a wide range of molar mass.

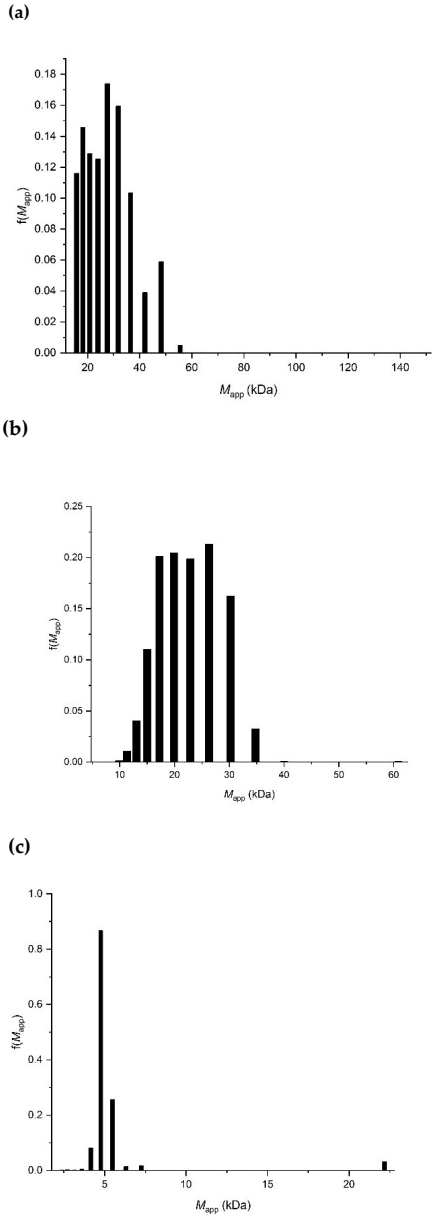

Figure 8. MULTISIG analysis of the molar mass distribution f(*M*) vs. *M* of PDMS-OH siloxanes in isopropanol at a concentration of 4.0 mg/mL and temperature = 20.0 °C. (**a**) PS36000; (**b**) PS18000; (**c**) PS4200.

2.3. Intrinsic Viscosity [η]

Intrinsic viscosity [21,27] measurements on Butvar B-98 and PDMS-OH were carried out with a rolling ball viscometer at 10.0 °C in isopropanol. The PDMS-OH samples were additionally measured in turpentine. The concentration of the polymer solutions that were used for these experiments was 6.0 mg/mL to give a sufficient flow time difference to that of the solvent. The [η] values (Table 2) were evaluated using the Solomon–Ciuta equation:

$$[\eta] = \frac{1}{c}\left(2\left(\eta_{sp}\right) - 2ln(\eta_r)\right)^{\frac{1}{2}} \quad (1)$$

where η_r is the relative viscosity (ratio of the viscosity of the solution to that of the solvent) and η_{sp}, the specific viscosity = $\eta_r - 1$.

Table 2. A comparison of the [η] values obtained for all the tested polymers.

	[η] in Isopropanol (mL/g)	[η] in Turpentine (mL/g)
Butvar B-98	57± 3	N/A
Siloxane PS36000	6.0 ± 0.3	22.4 ± 1.1
Siloxane PS18000	7.5 ± 0.4	15.8 ± 0.8
Siloxane PS4200	4.1 ± 0.2	5.5 ± 0.3
Siloxane PS550	3.7 ± 0.2	*

* flow time increment too small to record.

2.4. Conformation Analyses

The programme ELLIPS1 [15,16] was used to provide an estimate of polymer conformation or asymmetry in terms of the axial ratio of the equivalent hydrodynamic ellipsoid (prolate) of the polymers using the viscosity increment (ν) shape factor. These models do not take into account flexibility effects, but nonetheless provide a useful relative comparison of asymmetry. A similar exercise has been reported recently for a potential consolidant derived from terpenes [14]. ν is related to [η] by the relation [28–30]:

$$\nu = [\eta]/v_s \quad (2)$$

where v_s is the swollen specific volume. Tables 3 and 4 show these shape functions in terms of their aspect (axial) ratios (*a*/*b*) for ellipsoids of revolution [16] using a plausible range of solvent associations. Figure 9 (and Supplementary Materials) gives some examples.

Table 3. Viscosity increment ν for different degrees of solvent association (dynamic binding) and corresponding axial ratios (a/b) for Butvar B-98 and PDMS-OH polymers in isopropanol.

		Degree of Solvent Association ($v_s/\bar{v}$)		
		1	**1.2**	**1.4**
Butvar B-98	ν	64 ± 3	53 ± 3	45 ± 3
	(a/b)	27	24	22
PS36000	ν	5.9 ± 2.0	4.9 ± 2.0	4.2 ± 2.0
	(a/b)	5	4	4
PS18000	ν	7.2 ± 2.3	6.0 ± 2.3	5.2 ± 2.3
	(a/b)	6	5	5
PS4200	ν	4.0 ± 0.7	3.3 ± 0.7	2.8 ± 0.7
	(a/b)	3	3	3
PS550	ν	3.6 ± 0.2	3.0 ± 0.2	2.5 ± 0.2
	(a/b)	3	2	1

Table 4. Viscosity increment ν for PDMS-OH polymers in turpentine.

		Degree of Solvent Association $(v_s/\bar{v})$		
		1	**1.2**	**1.4**
PS36000	ν	22.0	18.3	15.7
	(a/b)	14	12	11
PS18000	ν	15	13	11
	(a/b)	11	10	9
PS4200	ν	5.4	4.5	3.8
	(a/b)	5	4	3

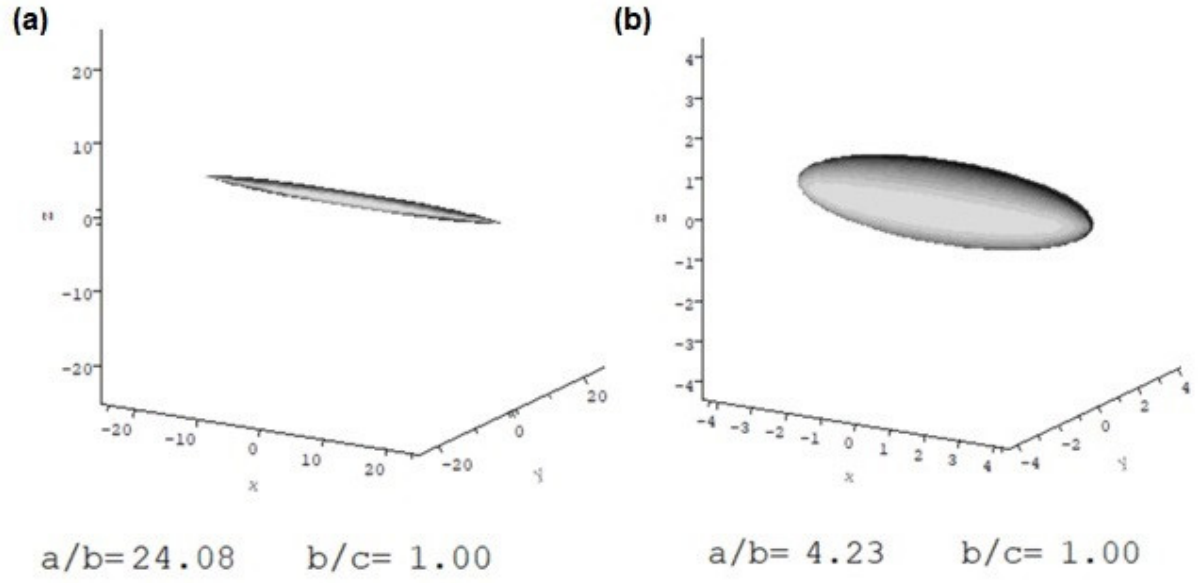

Figure 9. Conformation in isopropanol (equivalent hydrodynamic ellipsoids) for ν at $(v_s/\bar{v})$ = 1.2 using the programme ELLIPS1 of (**a**) Butvar B-98 in isopropanol; (**b**) PS36000 siloxane in isopropanol. ELLIPS1 representations of PS18000, PS4200, and PS550, as well as polymers in turpentine, are shown in Supplementary Figure S1.

Mark–Houwink–Kuhn–Sakurada (MHKS) Plots

From Tables 1 and 2 it is possible to construct Mark–Houwink–Kuhn–Saurada plots of log [η] vs. log M_w (Figure 10) for the siloxanes to yield the MHKS *'a'* coefficient from the slope where

$$[\eta] = K_\eta M_w{}^a \quad (3)$$

and K_η is a constant. MHKS a values range from ~0 for a spherical/globular particle, 0.5–0.8 for a flexible-extended coil, and >1.2 for a rod (see for example Harding [27]). In isopropanol, the slope "a"~(0.15 ± 0.07) is consistent with a spherical/globular approximation so the application of the ellipsoid models is justified. In turpentine "a" = ~(0.66 ± 0.05), which is approaching an extended coil, again consistent with the aspect ratios shown in Table 4.

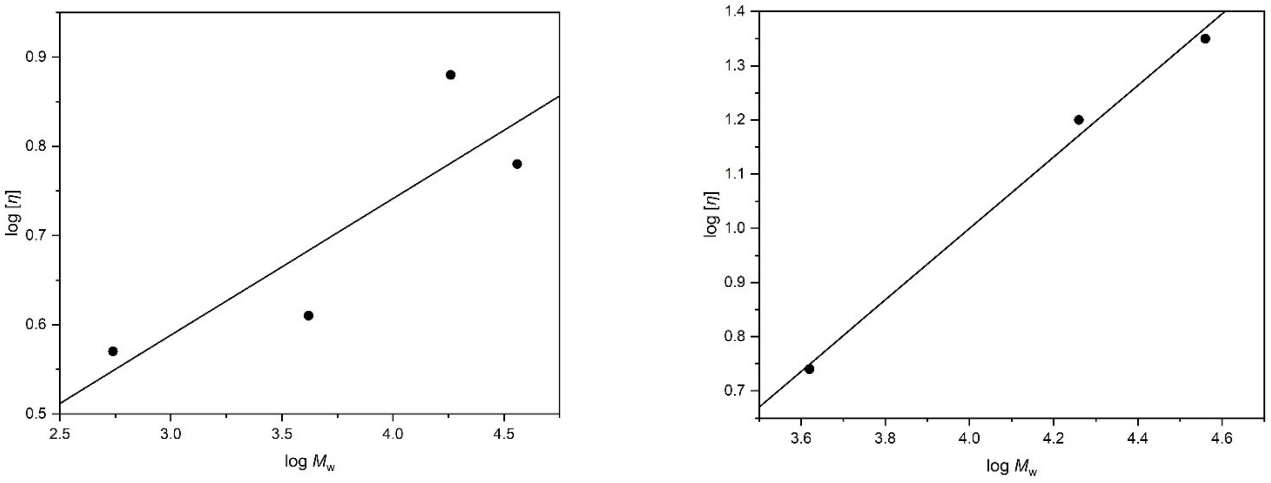

Figure 10. Mark–Houwink–Kuhn–Sakurada plots of the siloxanes in (**a**) isopropanol (a ~ 0.15) and (**b**) turpentine (a ~ 0.66).

3. Discussion

In this study, the characterisation of the consolidants Butvar B-98 and four different PDMS-OH series were successfully carried out, primarily with the use of analytical ultracentrifugation. The sedimentation equilibrium studies revealed that Butvar B-98 had a M_w of ~54.0 kDa, while the different samples of PDMS-OH had an M_w of ~52.5 kDa, 38.8 kDa, 6.2 kDa, and 1.6 kDa. The experimental M_w value of Butvar B-98 was shown to be consistent with the data provided by the manufacturer based on size exclusion chromatography coupled to a low angle light scattering detector, which like sedimentation equilibrium, is an absolute method not requiring assumptions concerning polymer conformation. Our absolute values for the weight-average molar masses for the siloxanes may provide a more accurate measure of molar mass to the previously available relative molar mass values, which were relative to polystyrene standards. The differences are probably due to the different conformations of the siloxanes and the standards. Sedimentation velocity, reinforced by the MULTISIG analysis of sedimentation equilibrium solute distributions, demonstrated that all polymers were heterogeneous with a broad range of molar masses. This may affect how efficiently these polymers can penetrate and consolidate archaeological wood.

Conformational analyses in isopropanol confirmed that the polymers, in general, possessed an elongated shape. This was especially true for Butvar B-98, with the viscosity increment ν indicating an axial ratio of ~25 (allowing for a plausible solvation range). The different samples of PDMS-OH had much less extended conformations, with aspect ratios in the range from 2–5. In turpentine the two largest samples appeared to be more extended, which is also reflected in their increase in intrinsic viscosity (Table 2). This difference may relate to observations on the use of PS36000 in both turpentine and isopropanol to treat degraded archaeological wood [31]. Figure 11a shows separation between the PS36000 and solvent almost immediately after mixing it with isopropanol. In contrast, such a separation is absent in the mix of the polymer with turpentine, even after one month (Figure 11b). The more extended conformation of PS36000 in turpentine is most likely due to a greater solvent interaction with turpentine.

Nonetheless, three different concentrations of the polymer in the two solvents, 30%, 50%, and 70%, were used to immerse a number of archaeological wood test specimens for a period of two weeks during experimental work in the framework of the Saving Oseberg project [31]. Due to the experimental set-up, test specimens were layered in the immersion bath. When the weight percentage gain of the wood test specimens was calculated for all concentrations and solution types, for those stacked at the top of the isopropanol/polymer bath, all had consistently gained the least weight. This was in

contrast to the test specimens immersed in the turpentine/polymer bath. In this case, there was no relationship observed between the weight percentage gain and the positioning of a test specimen in the immersion bath. Essentially, the wood test specimens sitting on the top part of the polymer/isopropanol bath were exposed to a lower polymer concentration than aimed for, due to the separation of the two components.

The practical meaning of this for a conservator is that, for instances involving application of the large molar mass siloxanes such as PDMS-OH PS36000 as a consolidant in wood via immersion, and considering the prolonged periods of immersion time, the preferable solvent to work with would be turpentine to ensure the desired amount of consolidant uptake by the wood—and this choice is reinforced by it's natural or "green" origins from pinewood. However, solutions of PS36000 in isopropanol could be recommended for applications on wood via injection—as long as the mixture is gently shaken before injection—since short application times are involved. Moreover, since a consolidant application via injection brings conservators in close contact with a wooden object, the choice of a solvent that is less harmful to human health, isopropanol, is better than turpentine in this case. Lengthy evaporation rates (months to years) of turpentine may also be considered problematic.

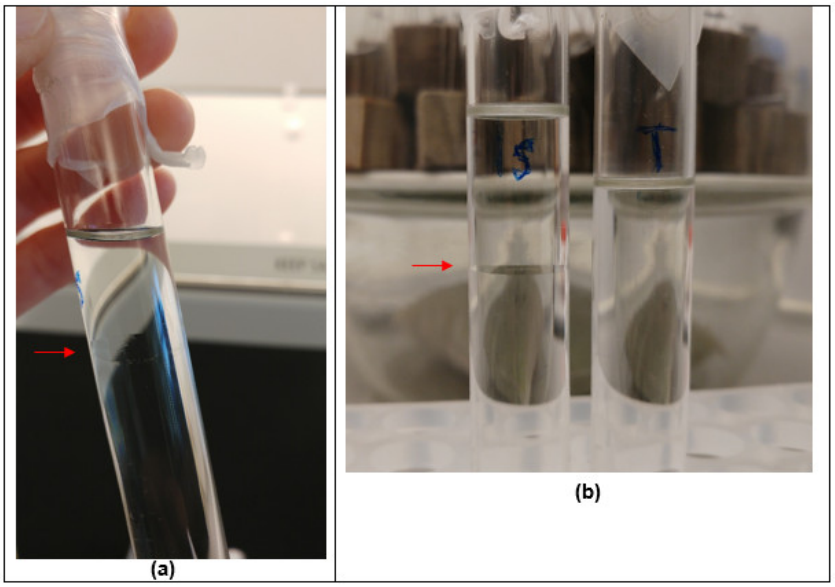

Figure 11. (**a**) PS36000 in isopropanol, showing phase separation of components as indicated by the red arrow. (**b**) = A comparison of PS36000 in isopropanol (**left**) and turpentine (**right**) after one month.

4. Concluding Remarks

Butvar B-98 and PDMS-OH both possess the common advantage of being soluble in organic solvents. This is particularly important for the Oseberg artefacts, as avoiding aqueous treatment will help in preventing further possible damage during reconservation. The work described here has successfully expanded the knowledge base of these two polymers, which will hopefully result in a higher confidence level when it comes to deciding which consolidants to use in the retreatment of the Oseberg finds, as it will certainly do for other archaeological artefacts.

5. Materials and Methods

5.1. Materials

All reagents and solvents were purchased from a chemical supplier (Acros Organics Ltd., Geel, Belgium; Alfa Aesar Ltd., Haverhill, MA, USA; Merck Ltd., Darmstadt, Germany; or Fisher Scientific Ltd., Loughborough, UK) and used without further purification. Butvar B-98 and PDMS-OH 36,000 and 18,000 were obtained from Acros Organics www.acros.com

(accessed on 10 November 2021) (part of Thermo Fisher Ltd., Scientific) Geel, Belgium, and Fluorochem, Glossop, UK, respectively. PDMS-OH 4200 and ~550 were obtained from VWR International, Lutterworth, UK, and Merck Ltd., Darmstadt, Germany.

5.2. Analytical Ultracentrifugation

A Beckman Optima XL-I analytical ultracentrifuge with Rayleigh interference optics was used at 20.0 °C. Furthermore, 12 mm optical path length double sector cells with titanium centrepieces were employed. A description of the sedimentation velocity and sedimentation equilibrium techniques are given in Harding et al. [32], Dam and Schuck, [20] Schuck et al. [22], and Harding et al. [33].

5.2.1. Sedimentation Velocity

An amount of 405 µL of the previous loading concentrations (0.5 to 4.0 mg/mL) of polymer (Butvar B-98 or PDMS-OH) in isopropanol were added to each of the cells. A rotational speed of 49,000 rpm was used, and the samples were centrifuged overnight. The weighted average sedimentation coefficient and the distributions of sedimentation coefficient c(s) vs. s were obtained by analysis with the SEDFIT procedure [20].

5.2.2. Sedimentation Equilibrium

Loading concentrations of 0.5 to 4.0 mg/mL of polymer in isopropanol were used. An amount of 100 µL of each concentration was injected into the sample solution channel of the cell. Isopropanol was used as the reference solvent. For Butvar B-98, the experiment was carried out at a rotational speed of 22,000 rpm over 2 days. For PS36000 and PS18000, the experiments were carried out over 2 days using rotational speeds of 22,000 rpm and 30,000 rpm, respectively. The experiments for PS4200 and PS550 were both carried out at a speed of 49,000 rpm and left overnight. The results were analysed with SEDFIT-MSTAR [22] in order to obtain the apparent weight-average molar mass $M_{w,app}$, making use of the M* extrapolation [34] and the hinge point method [21]. No significant concentration dependence was observed, suggesting that non-ideality was not significant. The data obtained from the highest concentration (4.0 mg/mL) was additionally analysed with the MULTISIG algorithm [23] to evaluate the molar mass distribution.

5.3. Viscosity Measurements

An Anton Paar AMVn (Graz, Austria) rolling ball viscometer was used at a temperature of 10.0 °C. Its closed capillary system is more suitable for working with volatile solvent systems compared to conventional Ostwald viscometers. The intrinsic viscosity measurements were carried out using a 6.0 mg/mL concentration of Butvar B-98 and PDMS-OH in isopropanol and turpentine. The intrinsic viscosity was then calculated with the Solomon–Ciuta Equation (1).

5.4. Infusion Experiment

The sample of Oseberg wood (Figure 2 was injected with a concentrated suspension (~5% or 50 g/L) of PS36000 solution in siloxane in turpentine. The fragment was injected for a period of 11 days and then left to dry for 34 days. The retreatment was conducted in a fume hood at room temperature.

Supplementary Materials: The following are available online at https://www.mdpi.com/article/10.3390/molecules27072133/s1, Table S1. Apparent weight-average molar masses $M_{w,app}$ and polydispersity Đ values obtained from sedimentation equilibrium of Butvar B-98; Table S2. Apparent weight-average molar masses $M_{w,app}$ and polydispersity Đ values for PS36000 in isopropanol at different concentrations; Table S3. Apparent weight-average molar masses $M_{w,app}$ and polydispersity Đ values for PS18000 in isopropanol at different concentrations; Table S4. Apparent weight-average molar masses $M_{w,app}$ and polydispersity Đ values for PS4200 in isopropanol at different concentrations; Table S5. Apparent weight-average molar masses $M_{w,app}$ and polydispersity Đ values for PS550 in isopropanol at different concentrations; Figure S1. Conformations (equivalent hydrodynamic

ellipsoids) for ν at $(v_s/\overline{v})$ = 1.2 of the polymers, using the programme ELLIPS1. (a) = PS18000 in isopropanol; (b) = PS4200 in isopropanol; (c) = PS550 in isopropanol; (d) P36000 in turpentine; (e) = PS18000 in turpentine; (f) = P4200 in turpentine.

Author Contributions: The analytical and characterisation work was carried out by M.C.; S.E.H. contributed to the planning of the experiments and provided supervision for the research work, along with R.A.S. and S.B.; C.C.S. and A.Z. sourced and provided the materials and contributed to the scientific discussion; M.C. wrote the paper with S.E.H. and all authors reviewed and edited the article. All authors have read and agreed to the published version of the manuscript.

Funding: This work was supported by the UK Engineering & Physical Sciences Research Council [grant number EP/L015633/1], the Norwegian Ministry of Education and Research, and the University of Oslo as part of the Saving Oseberg project. M.C. is supported by a UK EPSRC Centre for Doctoral Training award.

Acknowledgments: Special thanks to the Saving Oseberg group and the rest of the NCMH team at the University of Nottingham.

Conflicts of Interest: The authors declare no conflict of interest.

Sample Availability: Samples of the polymers are commercially available.

Abbreviations

GPC gel-permeation chromatography; M_n, M_w, M_z number, weight, z-average molar masses or molecular weights; M_{app} weight-average molar mass; PDMS-OH hydroxy-terminated polydimethylsiloxane; S Svedberg units; s sedimentation coefficient; $s_{20,w}$ sedimentation coefficient normalised to standard solvent conditions (density & viscosity of water at 20.0 °C); $\overline{v}$ partial specific volume; v_s swollen specific volume; [η] intrinsic viscosity; ν viscosity increment.

References

1. Braovac, S.; McQueen, C.M.A.; Sahlstedt, M.; Kutzke, H.; Łucejko, J.J.; Klokkernes, T. Navigating conservation strategies: Linking material research on alum-treated wood from the Oseberg collection to conservation decisions. *Herit. Sci.* **2018**, *6*, 1–16. [CrossRef]
2. Rosenqvist, A.M. The stabilizing of wood found in the Viking Ship of Oseberg: Part I. *Stud. Conserv.* **1959**, *4*, 13–22.
3. McQueen, C.M.A.; Łucejko, J.J.; Flåte, I.M.T.; Modugno, F.; Braovac, S. Ammonium alum in alum-treated wooden artefacts: Discovery, origins and consequences. *Herit. Sci.* **2019**, *7*, 78. [CrossRef]
4. Braovac, S.; Kutzke, H. The presence of sulfuric acid in alum-conserved wood—origin and consequences. *J. Cult. Herit.* **2012**, *13*, S203–S208. [CrossRef]
5. Braovac, S.; Tamburini, D.; Łucejko, J.J.; McQueen, C.; Kutzke, H.; Colombini, M.P. Chemical analyses of extremely degraded wood using analytical pyrolysis and inductively coupled plasma atomic emission spectroscopy. *Microchem. J.* **2016**, *124*, 368–379. [CrossRef]
6. Spirydowicz, K.E.; Simpson, E.; Blanchette, R.A.; Schniewind, A.P.; Toutloff, M.K.; Murray, A. Alvar and Butvar: The use of polyvinyl aqcetal resins for the treatment of the wooden artifacts from Gordion, Turkey. *J. Am. Inst. Conserv.* **2001**, *40*, 43–57. [CrossRef]
7. Fernández, M.D.; Fernández, M.J.; Hoces, P. Synthesis of poly(vinyl butyral)s in homogeneous phase and their thermal properties. *J. Appl. Polym. Sci.* **2006**, *102*, 5007–5017. [CrossRef]
8. Kavvouras, P.K.; Kostarelou, C.; Zisi, A.; Petrou, M.; Moraitou, G. Use of silanol-terminated polydimethylsiloxane in the conservation of waterlogged archaeological wood. *Stud. Conserv.* **2009**, *54*, 65–76. [CrossRef]
9. Harding, S.E. The Svedberg Lecture 2017. From nano to micro: The huge dynamic range of the analytical ultracentrifuge for characterising the sizes, shapes and interactions of molecules and assemblies in Biochemistry and Polymer Science. *Eur. Biophys. J.* **2018**, *47*, 697–707. [CrossRef]
10. McHale, E.; Braovac, S.; Steindal, C.C.; Gillis, R.B.; Adams, G.G.; Harding, S.E.; Benneche, T.; Kutzke, H. Synthesis and characterisation of lignin-like oligomers as a bio-inspired consolidant for waterlogged archaeological wood. *Pure Appl. Chem.* **2016**, *88*, 969–977. [CrossRef]
11. Wakefield, J.M.K.; Gillis, R.B.; Adams, G.G.; McQueen, C.M.A.; Harding, S.E. Controlled depolymerisation assessed by analytical ultracentrifugation of low molecular weight chitosan for use in archaeological conservation. *Eur. Biophys. J.* **2018**, *47*, 769–775. [CrossRef]

12. Wakefield, J.M.K.; Braovac, S.; Kutzke, H.; Stockman, R.A.; Harding, S.E. Tert-butyldimethylsilyl chitosan synthesis and characterization by analytical ultracentrifugation, for archaeological wood conservation. *Eur. Biophys. J.* **2020**, *49*, 781–789. [CrossRef]
13. Wakefield, J.M.K.; Hampe, R.; Gillis, R.B.; Sitterli, A.; Adams, G.G.; Kutzke, H.; Heinze, T.; Harding, S.E. Aminoethyl substitution enhances the self-assembly properties of an aminocellulose as a potential archaeological wood consolidant. *Eur. Biophys. J.* **2020**, *49*, 791–798. [CrossRef]
14. Cutajar, M.; Andriulo, F.; Thomsett, M.R.; Moore, J.C.; Couturaud, B.; Howdle, S.M.; Stockman, R.A.; Harding, S.E. Terpene polyacrylate TPA5 shows favorable molecular hydrodynamic properties as a potential bioinspired archaeological wood consolidant. *Sci. Rep.* **2021**, *11*, 7343. [CrossRef]
15. Harding, S.E.; Cölfen, H.; Aziz, Z. The ELLIPS suite of whole-body protein conformation algorithms for Microsoft WINDOWS. In *Analytical Ultracentrifugation—Techniques and Methods*; Scott, D.J., Harding, S.E., Rowe, A.J., Eds.; Royal Society of Chemistry: Cambridge UK, 2005; pp. 468–483.
16. García de la Torre, J.; Harding, S.E. Hydrodynamic modelling of protein conformation in solution: ELLIPS and HYDRO. *Biophys. Rev.* **2013**, *5*, 195–206. [CrossRef]
17. Fujita, H. *Mathematical Theory of Sedimentation Analysis*; Academic Press: Cambridge, MA, USA, 1962.
18. Schuck, P. A model for sedimentation in inhomogeneous media. II. Compressibility of aqueous and organic solvents. *Biophys. Chem.* **2004**, *108*, 201–214. [CrossRef]
19. Schuck, P. Size-distribution analysis of macromolecules by sedimentation velocity ultracentrifugation and Lamm equation modeling. *Biophys. J.* **2000**, *78*, 1606–1619. [CrossRef]
20. Dam, J.; Schuck, P. Calculating sedimentation coefficient distributions by direct modeling of sedimentation velocity concentration profiles. *Methods Enzymol.* **2004**, *384*, 185–212. [CrossRef]
21. Tanford, C. *Physical Chemistry of Macromolecules*; Wiley: New York, NY, USA, 1961.
22. Schuck, P.; Gillis, R.B.; Besong, T.M.D.; Almutairi, F.; Adams, G.G.; Rowe, A.J.; Harding, S.E. SEDFIT-MSTAR: Molecular weight and molecular weight distribution analysis of polymers by sedimentation equilibrium in the ultracentrifuge. *Analyst* **2014**, *139*, 79–92. [CrossRef]
23. Gillis, R.B.; Adams, G.G.; Heinze, T.; Nikolajski, M.; Harding, S.E.; Rowe, A.J. MultiSig: A new high-precision approach to the analysis of complex biomolecular systems. *Eur. Biophys. J.* **2013**, *42*, 777–786. [CrossRef]
24. Eastman Chemical Company: Butvar. Polyvinyl Butyral Resin: Properties and Uses. Available online: http://www.butvar.com/pdfs/en/BVR-001.pdf (accessed on 15 November 2021).
25. Johnston, J.P.; Ogston, A.G. A boundary anomaly found in the ultracentrifugal sedimentation of mixtures. *Trans. Faraday Soc.* **1946**, *42*, 789–799. [CrossRef]
26. Morgan, P.J.; Harding, S.E.; Petrak, K. Hydrodynamic properties of a polyisoprene/poly(oxyethylene) block copolymer. *Macromolecules* **1990**, *23*, 4461–4464. [CrossRef]
27. Harding, S.E. The intrinsic viscosity of biological macromolecules. Progress in measurement, interpretation and application to structure in dilute solution. *Prog. Biophys. Mol. Biol.* **1997**, *68*, 207–262. [CrossRef]
28. Simha, R. The influence of Brownian movement on the viscosity of solutions. *J. Phys. Chem* **1940**, *44*, 34. [CrossRef]
29. Saito, N. The effect of Brownian motion on the viscosity of solutions of macromolecules, I. Ellipsoid of revolution. *J. Phys. Soc.* **1951**, *6*, 297–301. [CrossRef]
30. Harding, S.E.; Rowe, A.J. Modeling biological macromolecules in solution. II. The general tri-axial ellipsoid. *Biopolymers* **1983**, *22*, 1813–1829. [CrossRef]
31. Zisi, A. *Saving Oseberg Phase II D2.4 Silanol-Based Consolidant for Retreating Oseberg Wood: Adjusting a Method Initially Developed for Conserving Waterlogged Archaeological Wood*; University of Oslo: Oslo, Norway, 2020.
32. Harding, S.E.; Rowe, A.J.; Horton, J.C. *Analytical Ultracentrifugation in Biochemistry and Polymer Science*; Royal Society of Chemistry: Cambridge, UK, 1992.
33. Harding, S.E.; Gillis, R.B.; Adams, G.G. Assessing sedimentation equilibrium profiles in analytical ultracentrifugation experiments on macromolecules: From simple average molecular weight analysis to molecular weight distribution and interaction analysis. *Biophys. Rev.* **2016**, *8*, 299–308. [CrossRef]
34. Creeth, J.M.; Harding, S.E. Some observations on a new type of point average molecular weight. *J. Biochem. Biophys. Methods* **1982**, *7*, 25–34. [CrossRef]

scientific reports

Check for updates

OPEN

Comparative hydrodynamic characterisation of two hydroxylated polymers based on α-pinene- or oleic acid-derived monomers for potential use as archaeological consolidants

Michelle Cutajar[1,2]✉, Fabricio Machado[2,3], Valentina Cuzzucoli Crucitti[4], Susan Braovac[5], Robert A. Stockman[2], Steven M. Howdle[2] & Stephen E. Harding[1,5]✉

The Oseberg Viking ship burial is one of the most extensive collections of Viking wooden artefacts ever excavated in Norway. In the early twentieth century, many of these artefacts were treated with alum in order to preserve them, inadvertently leading to their current degraded state. It is therefore crucial to develop new bioinspired polymers which could be used to conserve these artefacts and prevent further disintegration. Two hydroxylated polymers were synthesised (TPA6 and TPA7), using α-pinene- and oleic acid-derived monomers functionalised with an acrylate moiety. Characterisation using biomolecular hydrodynamics (analytical ultracentrifugation and high precision viscometry) has shown that these polymers have properties which would potentially make them good wood consolidants. Conformation analyses with the viscosity increment (ν) universal hydrodynamic parameter and ELLIPS1 software showed that both polymers had extended conformations, facilitating in situ networking when applied to wood. SEDFIT-MSTAR analyses of sedimentation equilibrium data indicates a weight average molar mass M_w of (3.9 ± 0.8) kDa and (4.2 ± 0.2) kDa for TPA6 and TPA7 respectively. Analyses with SEDFIT (sedimentation velocity) and MultiSig however revealed that TPA7 had a much greater homogeneity and a lower proportion of aggregation. These studies suggest that both these polymers—particularly TPA7—have characteristics suitable for wood consolidation, such as an optimal molar mass, conformation and a hydroxylated nature, making them interesting leads for further research.

The Oseberg Viking ship burial is one of the foremost discoveries of Viking artefacts in the world. The treatment that these artefacts underwent upon excavation in the early twentieth century[1] has unfortunately resulted in their current state of degradation. This treatment was applied to the wooden finds which had been most degraded during burial. It involved the use of hot alum ($KAl(SO_4)_2{\cdot}12H_2O$ and/or $NH_4Al(SO_4)_2{\cdot}12H_2O$) which we now know generated sulfuric acid during immersion which the wood absorbed. The acid has led to post-conservation deterioration of the remaining wood polymers resulting in the artefacts being almost destroyed[2,3]. Analyses of the alum-treated Oseberg artefacts with scanning electron microscopy (SEM) have confirmed that the secondary cell walls of the wood are more or less missing entirely[4]. Moreover, the alum did not completely penetrate the wood, resulting in a hard, alum-rich surface and a structurally weak, alum-poor core[5]. This has had a detrimental effect

[1]School of Biosciences, National Centre for Macromolecular Hydrodynamics (NCMH), University of Nottingham, Sutton Bonington LE12 5RD, UK. [2]School of Chemistry, University of Nottingham, University Park Nottingham NG7 2RD, UK. [3]Instituto de Química, Universidade de Brasília, Campus Universitário Darcy Ribeiro, Brasília, DF 70910-900, Brazil. [4]Centre for Additive Manufacturing, Department of Chemical and Environmental Engineering, Faculty of Engineering, University of Nottingham, Nottingham NG7 2RD, UK. [5]Museum of Cultural History, University of Oslo, Kabelgata 34, 0580 Oslo, Norway. ✉email: michelle.cutajar@nottingham.ac.uk; steve.harding@nottingham.ac.uk

on the mechanical properties of the artefacts, due to crack formations between alum-rich and alum-poor zones as well as in the alum-poor core caused by shrinkage during post-treatment drying[4]. Alum-treated wooden objects are in various states of preservation and reconstruction which makes current water-based methods inappropriate to reconserve them. Due to cases like those of the Oseberg artefacts, it is imperative that we expand the currently existing toolbox of materials for treating archaeological wood.

Compounds inspired by naturally occurring materials, that is bioinspired compounds, have long generated a considerable amount of interest for such purposes[6,7]. Any wood consolidant should ideally fulfil a number of requirements such as being derived from sustainable materials, being able to form interactions with the wood and having an appropriately small molar mass[8]. Reversible treatments are considered to be the ethical ideal for conservation of culturally significant objects. However, it has been argued that in the case of the Oseberg objects, future retreatability is more important than the actual reversibility of a treatment since the objects are unlikely to survive future attempts to remove consolidants before application of a new conservation treatment[9]. Retreatment is only possible if the openings in the wood structure are not clogged with polymer, leaving space for future consolidants to pass through. As a result, any new consolidants should ideally penetrate to a sufficient depth whilst leaving room in the cells for future retreatment. As a point of reference, the molar masses of polyethylene glycol (PEG) preparations which are used in the conservation field are usually between 0.2 and 4.0 kDa[10,11]. Wakefield et al.[10] stipulate that a molar mass of 5.0 kDa or below should be targeted for potential archaeological wood consolidants in order to maximise polymer penetration. For example, Christensen et al.[12] have demonstrated that the uptake of chitosan by wood was shown to increase when it was depolymerised to ~ 6.0 kDa. In addition, interactions between the consolidant and wood (such as through hydrogen bonding) improve its mechanical stability. Polymer-wood interactions may also result in a lower number of hydroxyl groups in the wood cell wall, leading to increased hydrophobicity (which increases dimensional stability) and slower decay[13,14].

The Oseberg collection is made up of highly heterogenous wood in various states of preservation and it therefore requires a diverse toolkit for its retreatment. Some of the pieces are far too fragile to be able to withstand treatment with PEG, which involves water immersion. This is because such a procedure would result in the dissolution of the remaining alum in the wood, leading to total disintegration. Other pieces have been re-constructed with various components such as metal rods, glue and plaster[4]. For these objects, there is also increased risk of damage if they are treated with an aqueous consolidant. Consequently, such artefacts should instead be preserved using consolidants in non-aqueous solvents, applied through injection, for example. Such organic-soluble consolidants which are in use in the conservation field include Paraloid™ B-72, a thermoplastic acrylic resin, and Butvar® B-98, a polyvinyl butyral-based resin. The aim for this work was to synthesise 'greener' alternatives to these consolidants, which can thereafter be used to treat both the highly degraded and highly reconstructed objects of the Oseberg collection.

We have recently reported on the synthesis and characterisation of an α-pinene-derived polymer which showed encouraging properties for a wood consolidant[15]. This polymer possessed hydroxyl moieties, which may enhance its hydrogen bonding potential[8]. Moreover, it had a small molar mass of 4.2 kDa and conformation analyses indicated that it had an elongated shape, both of which may increase its penetration in wood. Terpenes such as α-pinene appear to be an ideal basis for the development of such materials[16]. Not only are they abundantly available, but they can also be easily functionalised with specific chemical groups, such as hydroxyl groups, which may lead to interactions with the wood[17–20].

As an evolution of that work, in this paper we describe the synthesis and characterisation of two other α-pinene-derived materials: a homopolymer and a copolymer with an oleic acid-based monomer. For the terpene component of the polymers, α-pinene was first converted to *trans*-sobrerol and then acrylated before polymerisation. The synthesis of sobrerol methacrylate has been previously described by Lima et al.[21], who then used these materials to replace styrene in polyester resins. Stamm et al.[22] have recently reported on the polymerisation of sobrerol methacrylate using both enzymatic conversion and different radical polymerisation methods. Sobrerol is a particularly interesting starting point for polymers since it is adaptable to different polymerisation techniques and post-polymerisation chemical modifications[22].

Vegetable oils such as oleic acid are considered to be one of the most accessible and affordable resources available[23,24], making them highly popular feedstocks for the synthesis of biobased polymers[23–28]. Additionally they generally have low toxicity[23,24,29,30], making them very attractive to work with in conservation. In this work, oleic acid was acrylated in order to transform it into a monomer. To the best of our knowledge, a copolymer made up of these two monomers, α-pinene acrylate and oleic acid acrylate, has not yet been reported on.

Analytical ultracentrifugation (AUC) was used to characterise the size distribution and molar mass of both polymers, as it has proven to be a robust and highly accurate technique to study polymers[31,32]. Moreover, it has recently been used in the study and characterisation of existing and potential wood consolidants[10,15,33–36]. Being an absolute method it does not require a calibration standard[37]. Combining this with other techniques, such as viscometry and differential scanning calorimetry (DSC), has also allowed us to get an estimate of the shape and glass transition temperature (T_g) of the polymers. This will enable us to more accurately predict whether the synthesised polymers would make successful wood consolidants.

Results and discussion

Monomer synthesis from α-pinene. The synthesis of the terpene-derived monomer utilised in both polymerisations makes use of α-pinene as the primary starting material (Fig. 1). The first two synthesis steps for this monomer have already been described in previous publications[15,16,21,38], and consist of first oxidising the terpene (1), followed by its hydrolysation to form *trans*-sobrerol (2). In our previous work[15], the *trans*-sobrerol was put through a Brown hydroboration/oxidation sequence in order to yield a polyhydroxylated triol

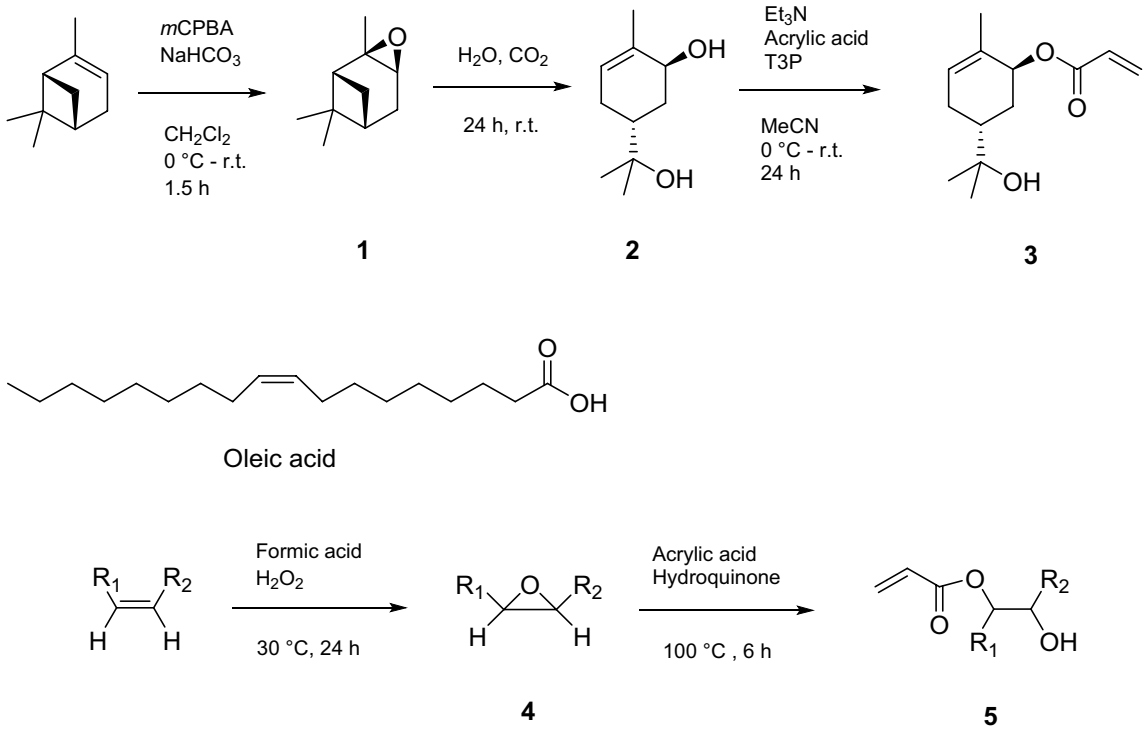

Figure 1. The synthesis routes for the *trans*-sobrerol acrylate monomer (3) and the acrylated oleic acid monomer (5).

molecule. This step was forgone this time, in favour of direct acrylation of *trans*-sobrerol. Although this provides a monomer having one less hydroxyl group, it also makes the process quicker and more scalable. This was an important factor to consider in our work, as the synthesis needed to be efficient enough to be able to make sufficient material for eventual testing on wood, with approximately 50 g of each polymer needed to run a pilot study on wood samples.

The acrylation of *trans*-sobrerol was carried out based on similar reactions previously described[15,16], with the use of acrylic acid and propanephosphonic acid anhydride (T3P®) as a promoter of the ester coupling. This was deemed preferable to the alternative method which makes use of acryloyl chloride[21]. Unlike the latter reagent, acrylic acid and T3P® produce non-chlorinated waste, making the reaction more environmentally sustainable.

Monomer synthesis from oleic acid. In addition to the *trans*-sobrerol acrylate monomer (3), we synthesised another monomer in order to create opportunities for the production of copolymers. Oleic acid presented an interesting option as it possesses some attractive properties such as a hydroxylated nature, chain flexibility and ability to create a branched polymeric structure, all of which may potentially improve the ability of its polymer to interact with the wood.

The synthesis of this monomer (Fig. 1) was carried out by following the procedure described by Neto et al.[39] with modifications, and consisted of first epoxidising oleic acid and then using acrylic acid to form the monomer. The epoxidised oleic acid was first obtained by reacting it with formic acid in the presence of hydrogen peroxide. This is possible due to the high reactivity of the unsaturation present in oleic acid, which allows the introduction of functional groups like the epoxide ring[39]. The epoxide ring was then ring-opened with acrylic acid in the presence of hydroquinone. Hydroquinone is a polymerisation inhibitor and is therefore useful in reducing unwanted side reactions, such as acrylic acid polymerisation[39].

Thiol-mediated free radical polymerisation of *trans*-sobrerol acrylate (3), TPA6. Free radical polymerisation (FRP) was used for all polymerisation attempts. A molar mass of 5 kDa or below was being targeted. The method previously described for the FRP of sobrerol methacrylate made use of dimethylformamide as the polymerisation solvent and 4,4′-azobis(4-cyanovaleric acid) as the initiator[22]. For our work, the homopolymerisation of *trans*-sobrerol acrylate was first attempted using cyclohexanone as the solvent and azobisisobutyronitrile (AIBN) as the thermal initiator (Fig. 2). Nuclear magnetic resonance (^{1}H NMR) analysis indicated that the polymerisation was successful, with the signals representing the acrylate double bond of the monomer no longer appearing in the spectra at the completion of the reaction after purification with hexane (Fig. S7). The gel permeation chromatography (GPC) analysis of this trial FRP reaction indicated that the relative weight average molar mass ($M_{r\,w}$) of this polymer was far too large at 24.3 kDa. It was therefore decided to employ benzyl mercaptan as a chain transfer agent in order to better control its molar mass. Thiols have been employed as efficient, nearly ideal, chain transfer agents thanks to the high efficiency in the control of the chain length attributed to a combination of the weakness of the S–H bond, and the high reactivity of the thiyl radicals

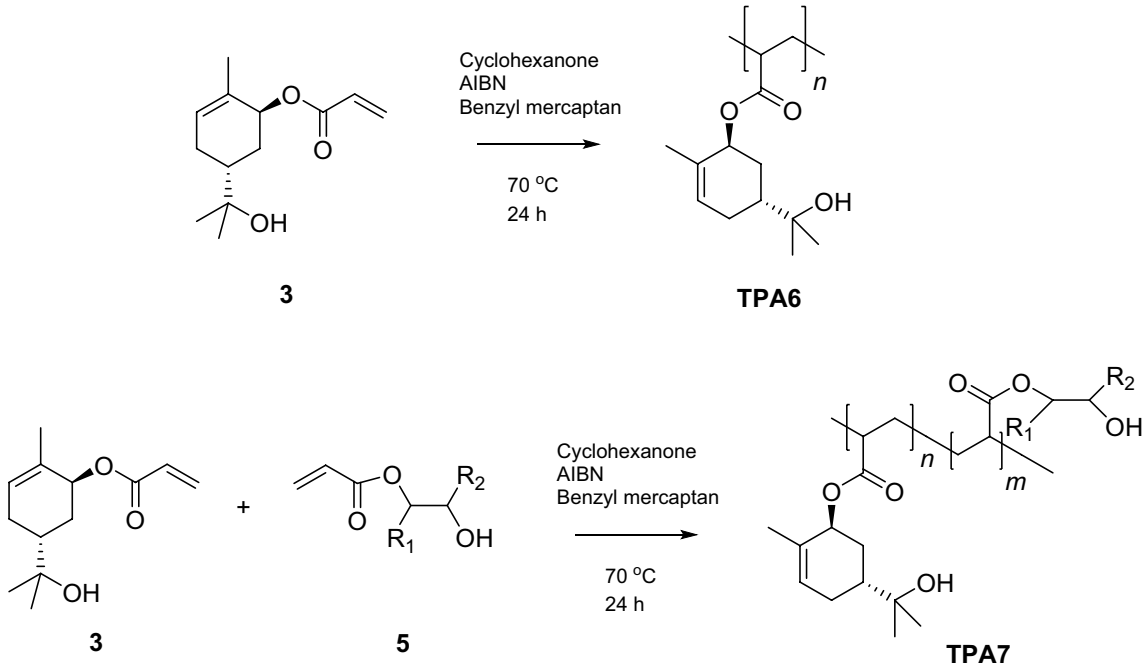

Figure 2. The formation of the *trans*-sobrerol acrylate homopolymer (TPA6) and the *trans*-sobrerol acrylate/acrylated oleic acid copolymer (TPA7).

Polymer ID	Thiol (mol%)	Starting monomer mass (g)	$M_{r,w}$ (kDa)	$M_{r,n}$ (kDa)	$Đ$	T_g (°C)
1	0	0.5	24.3	12.3	2.0	–
2	2	0.5	5.1	3.8	1.4	–
3	8	0.5	3.2	2.3	1.4	–
4	5	0.5	5.0	3.4	1.5	–
5	2	0.5	6.2	4.3	1.5	–
6	5	2.0	3.7	2.8	1.3	–
7	8	2.0	8.7	6.7	1.3	–
8	5	4.0	4.4	3.1	1.4	31.1

Table 1. Homopolymerisation screen of *trans*-sobrerol acrylate (3) as a function of thiol concentration. $M_{r,w}$, $M_{r,n}$—relative weight and number average molar masses (relative to poly(methyl methacrylate) standards) from gel permeation chromatography, $Đ = M_{r,w}/M_{r,n}$. T_g—glass transition temperature (from DSC).

(RS·) towards the double bonds[40,41]. A screening was subsequently run on this reaction to identify the optimal conditions (Table 1).

The first reactions that were carried out with the thiol involved the use of very small amounts of monomer (Entries 2–4 in Table 1). The thiol mol% was varied slightly with each reaction and the molar mass change that it caused was monitored by GPC. A thiol mol% of 2%, 5% and 8% were all tested, all of which produced a polymer with a relative weight average molar mass (relative to polystyrene standards) $M_{r,w}$ ranging from 3.2 to 5.1 kDa. Another vital aspect which had to be considered at this point was the reproducibility of the reaction on scale-up. In order to investigate this, a set of reactions with gradually increasing monomer weight were carried out and the resultant polymers' properties were monitored with GPC. The monomer weight was initially increased to 2.0 g (Entries 7 and 6) and then to 4.0 g (Entry 8). Table 1 demonstrates that the polymers retained similar relative $M_{r,w}$, also relative number-average molar mass ($M_{r,n}$) and relative dispersity ($Đ$) values when the starting monomer mass was increased from 0.5 to 4.0 g. This suggested that the reaction could be scaled-up further while still retaining the polymer's characteristics. The $Đ$ value is a measure of the different distributions of molecular weight in the system and can have an effect on the polymer's physical properties. It was therefore important that it remained consistent on scaling-up[42].

A final thiol amount of 5 mol% was decided upon since it appeared to produce consistent $M_{r,w}$ results (Entry 8). It was therefore decided that the conditions used for Entry 8 were the ones that should be utilised for the synthesis of our desired homopolymer, TPA6. The glass transition temperature (T_g) of Entry 8 was thereafter measured with differential scanning calorimetry (DSC). The T_g is the point at which a polymer changes from a tough or glassy material to a rubbery solid[43]. Having data on the T_g of a polymer makes it easier for conservators to select consolidants for specific applications[43,44]. The T_g of TPA6, at the polymerisation conditions selected,

Polymer ID	Monomer 3 (w%)	Monomer 5 (w%)	Thiol (mol %)	AIBN (w%)	$M_{r,w}$ (kDa)	$M_{r,n}$ (kDa)	$Đ$	T_g (°C)
1	70	30	0	0.5	16.8	8.2	2.0	–
2	70	30	0	1.0	17.4	7.3	2.4	–
3	30	70	0	1.0	16.4	7.6	2.2	–
4	70	30	0	2.0	17.0	6.9	2.4	–
5	30	70	0	2.0	13.9	5.5	2.5	–
6	70	30	5	1.0	4.2	2.3	1.8	4.6
7	50	50	5	1.0	4.6	2.3	2.0	− 19.0
8	30	70	5	1.0	4.5	2.1	2.1	− 28.0
9	70	30	5	1.0	5.0	2.9	1.8	–
10	80	20	5	1.0	4.0	2.3	1.7	18.9

Table 2. Copolymerisation screen of *trans*-sobrerol acrylate (3) and oleic acid acrylate (5). Monomer ratios shown are the ones that were measured out at the start of each reaction. $M_{r,w}$, $M_{r,n}$—relative weight and number average molar masses (relative to poly(methyl methacrylate) standards) from gel permetation chromatography. $Đ = M_{r,w}/M_{r,n}$. T_g glass transition temperature (from DSC); w% mass or "weight" %.

was found to be 31.1 °C, which is comparable to that of Paraloid™ B-72 (40.0 °C), a consolidant frequently used in the conservation field[44,45].

Copolymerisation of *trans*-sobrerol acrylate (3) and oleic acid acrylate (5), TPA7. Having successfully synthesised the *trans*-sobrerol acrylate monomer (3), the next step was to attempt to copolymerise it with the acrylated oleic acid (5). This would form a copolymer having both terpene- and oleic acid-derived properties. A protocol identical to the one that was used for the homopolymerisation of *trans*-sobrerol acrylate was carried out (Fig. 2). As previously, the reaction was screened in order to decide on the conditions that would be best to produce a polymer with the desired physical properties (Table 2). This involved running several reactions whilst varying the weight (wt) ratios of monomers, along with the amounts of initiator and benzyl mercaptan.

A series of reactions (Entry 1–5 in Table 2) was first run without benzyl mercaptan and instead the AIBN concentration was increased from 0.5 to 2.0 wt%. This resulted in the copolymers having a $M_{r,w}$ between 13.9 and 17.4 kDa and a $M_{r,n}$ between 8.2 and 6.9 kDa. In standard FRP, increasing the thermal initiator concentration would result in more polymer chains likely being initiated, leading to a reduction in molar mass. This is because the Degree of Polymerisation (DP) is inversely proportional to the square root of the initiator concentration[46]. This can be seen from the $M_{r,n}$ results in Table 2, with the values decreasing with increasing concentration of thermal initiator.

The addition of 5 mol% of benzyl mercaptan had an immediate effect on all the polymers, with the $M_{r,w}$ dropping to between 4.0 and 5.0 kDa. From the DSC analyses of the copolymers we saw that the T_g decreased with increasing modified oleic acid molar content in the copolymer, since this is closely associated with the final chemical structure of the random copolymer chains. It is reasonable to expect that the plasticising effect of the oleic acid acrylate comonomer influences the molecular mobility of the active species, leading to a reduction in the T_g of copolymers[47–49]. This property may potentially prove to be beneficial for a wood consolidant as plasticisers are known to increase the free volume of polymer chains, enabling them to be more flexible and move more easily[48,50]. This could possibly translate to the copolymer having more opportunities for interactions with the wood structure once it penetrates, although its plasticity should not be too high as to deform the wood. Ideally, the T_g of a consolidant should be higher than the maximum temperature that a treated artefact will be subjected to[51]. A T_g which is too low may result in slumping of the object, as has been reported happening with the use of Paraloid™ B-72 in hot climates[44,52,53]. On the other hand, a consolidant which is too stiff may cause artefacts to become brittle, which can result in cracking if put under stress[54]. Keeping this in mind, it was decided that the best conditions to use for TPA7 would be those utilised for Entry 10 in Table 2, as the copolymer had a small enough $M_{r,w}$ (4.0 kDa) as well as the most appropriate T_g (18.9 °C).

Hydrodynamic characterisation studies of TPA6 and TPA7. Having a thorough understanding of the physical properties of TPA6 and TPA7 is vital in order to help us in deciding whether they would truly be suitable as wood consolidants. It is essential to have as much certainty as possible since any scale-up of the polymers would entail a considerable amount of work and time. Moreover, archaeological wood which can be used for any subsequent testing is scarce and thus, extensive characterisation of the polymers would help in preventing material wastage.

As mentioned, analytical ultracentrifugation (AUC) is matrix-free—not requiring a separation matrix or membrane and works without the need of calibration standards i.e. it is an absolute method of estimating molecular weight[32]. This is in contrast to the relative method of gel permeation chromatography or GPC, which compares the tested polymers to built-in standards such as poly(methyl methacrylate) standards. As a result, AUC is considered to be a more reliable method and the molar mass values that are obtained from it are more accurate than the ones measured by GPC, as they are absolute and not dependent on standards, and without assumptions

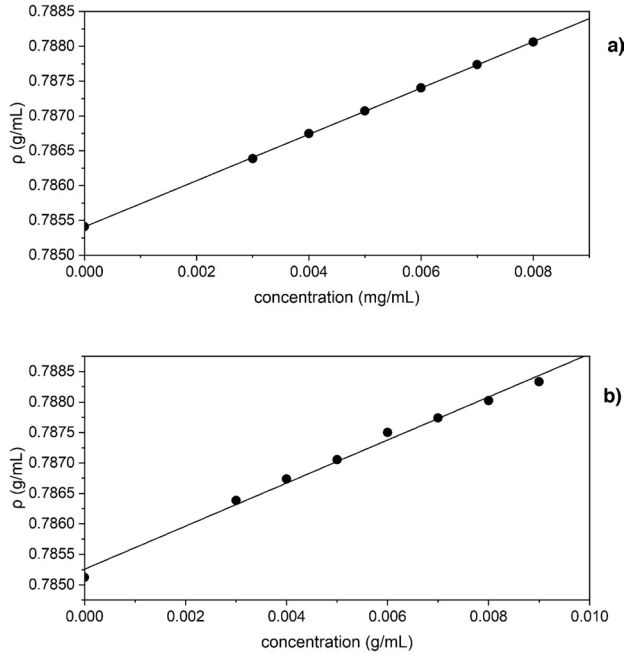

Figure 3. Dependence of solution density of TPA6 (**a**) and TPA7 (**b**) in isopropanol on concentration.

of column inertness. Because of this, once the polymerisation reactions of TPA6 and TPA7 were optimised, it was decided to re-measure their molecular weights with AUC in order to obtain more accurate or absolute values.

AUC also helps in the determination of molecular weight distribution and conformation of the polymers. This is useful for wood consolidation purposes, since it would help to predict how much of the polymer fraction would be able to penetrate wood. If a major polymer fraction is deemed too large (approximately > 10 kDa), it would not be scientifically sound to continue with their scale-up and testing[55]. Likewise, having an idea of the shape of the polymers though conformation analysis could also help in understanding their behaviour. An example is PEG, whose long and flexible shape might improve its penetration into wood[55].

Calculation of the partial specific volume $\overline{\nu}$. The partial specific volumes $\overline{\nu}$ of both polymers was measured since these values are essential for the analyses of the subsequent AUC studies. The method previously described by Kratky et al.[56] was followed. This involved measuring the density of different concentrations of polymer dissolved in an appropriate solvent. It was decided to carry out all characterisation studies in isopropanol since it has been previously used in experiments with degraded alum-treated wood[57]. These density values were then plotted against concentration (Fig. 3) and Eq. (1) was used to obtain the $\overline{\nu}$ values. These were found to be (0.850 ± 0.002) and (0.824 ± 0.013) cm^3/g for TPA6 and TPA7 respectively. These were similar to the value that had previously been measured for our other terpene-derived acrylated polymer[15].

$$\overline{\nu} = \frac{1}{\rho_o}\left(1 - \frac{\partial \rho}{\partial c}\right) \tag{1}$$

where ρ_o—the density of the reference solvent; $\frac{\partial \rho}{\partial c}$—the slope of the ρ versus concentration.

Sedimentation velocity in the analytical ultracentrifuge. Sedimentation velocity (SV) studies were carried out on both polymers in isopropanol in order to get an indication of their degree of heterogeneity. SEDFIT analyses provided us with the sedimentation coefficient range *c(s)*[58] vs sedimentation coefficient (S) of the polymers (Fig. 4). Both polymer systems appeared to be similar, with the major peak having a low sedimentation coefficient value (ca. 0.6 and 0.4 S for TPA6 and TPA7 respectively), which corresponds with the particle having a small M_w value. Some minor peaks were observed at ~1.5 S, indicating that the polymer systems were also composed of some larger M_w particles. These were more pronounced in TPA6, which could potentially mean that this polymer may have a tendency to aggregate at higher concentrations, especially above 1.5 mg/mL.

Sedimentation equilibrium in the analytical ultracentrifuge. Sedimentation equilibrium (SE) experiments were run on both polymers, using a concentration series ranging from 0.5 to 4.0 mg/mL, to estimate absolute molar masses. As stressed previously although not dependent on poly(methyl methacrylate) standards like GPC which are assumed to have the same conformation, nonetheless sedimentation equilibrium yields *apparent* molar masses (i.e. affected by non-ideality through polymer co-exclusion) M_{app}. Using different concentrations of polymer allowed us to determine the extent of the polymers' non-ideal behaviour, and either

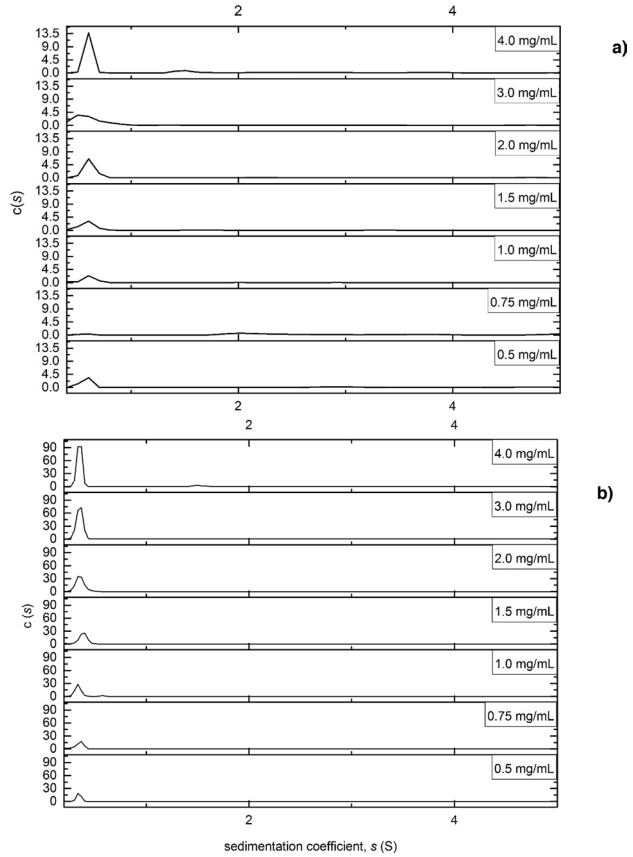

Figure 4. Sedimentation coefficient distributions c(*s*) vs sedimentation coefficient (S) for (**a**) TPA6 and (**b**) TPA7 in isopropanol. Rotor speed = 49,000 rpm.

a simple extrapolation to zero concentration (or operating at a low concentration) eliminates these effects. SEDFIT-MSTAR[59] was used to obtain the apparent weight average molar mass $M_{w,app}$ via the M^* function[60] and the hinge-point method[59]. Tables S1 and S2 (Supplementary Information) show these values. From this data we could see that there seems to be relatively low non-ideality in both polymer systems, as the $M_{w,app}$ did not appear to be significantly affected by the concentration. This was not surprising for polymers with such low molar masses. For TPA6 it was decided not to use polymer concentrations above 1.5 mg/mL, due to the possibility of aggregation as was noted during the SV study. The "ideal" average M_w values were then determined by plotting the $M_{w,app}$ against concentration (Fig. 5) and extrapolating to zero concentration. These were found to be (3.9 ± 0.8) kDa and (4.2 ± 0.2) kDa for TPA6 and TPA7 respectively.

The SE data was also run through the MultiSig programme, which provides an estimate of the molar mass *distribution*, assuming ideal behaviour[61]. Figure 6a shows the results for TPA6, indicating that it had an M_w range from 1.8 to 14.5 kDa, with a main peak at 4.7 kDa, but a 2nd significant and broad peak from 7 to 14.5 kDa. The results for TPA7 are shown in Fig. 6b, which reveals that the M_w distribution of this polymer system was considerably narrower ranging from 1.9 to 4.4 kDa, with a smaller peak at ~ 7.6 kDa. The results for both polymers appeared to correlate with the ones that were obtained from the SV data, showing that the majority of particles in the polymer systems had a low M_w (and in the targeted range for a consolidant) and with TPA6 being considerably more polydisperse.

Calculation of the intrinsic viscosity $[\eta]$. A rolling ball viscometer was used to measure the viscosity of both polymers in isopropanol. This instrument was specifically chosen since it carries out the measurements in a closed environment, thereby minimising the degree of evaporation of the highly volatile isopropanol. With these measurements, the Solomon–Ciuta equation (Eq. (2)) was then implemented to calculate the final $[\eta]$ value for the polymers. These were (4.88 ± 0.24) and (4.84 ± 0.24) mL/g for TPA6 and TPA7 respectively.

$$[\eta] = \frac{1}{c}\left(2\left(\eta_{sp}\right) - 2\ln(\eta_r)\right)^{\frac{1}{2}} \quad (2)$$

c = concentration of polymer solution; η = solution viscosity; η_0 = viscosity of pure solvent; η_r = relative viscosity $(\frac{\eta}{\eta_0})$; η_{sp} = specific viscosity $(\eta_r - 1)$.

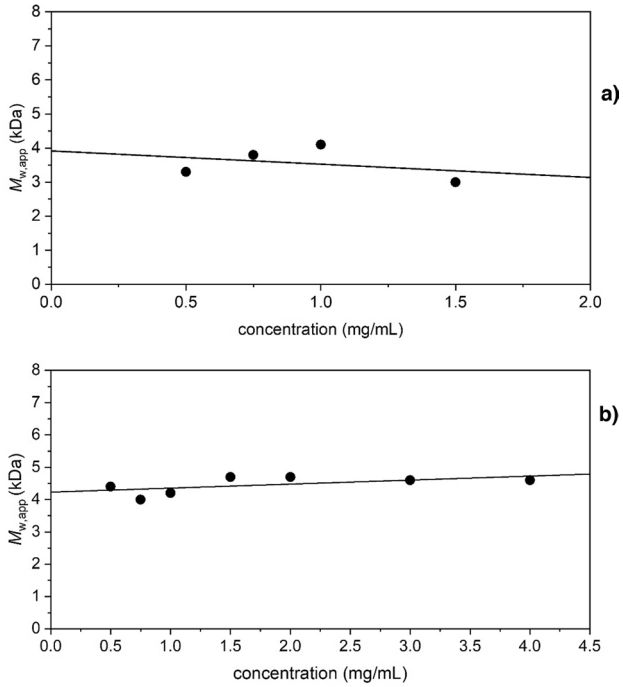

Figure 5. Dependence of apparent $M_{w,app}$ on concentration, with an extrapolation to obtain the thermodynamically ideal $M_{w,app}$. Analysed with SEDFIT-MSTAR using the M^* derived method to obtain the shown $M_{w,app}$ values. Rotor speed = 45,000 rpm. (**a**) TPA6 in isopropanol, $M_w = (3.9 \pm 0.8)$ kDa; (**b**) TPA7 in isopropanol, $M_w = (4.2 \pm 0.2)$ kDa.

Conformation analyses. With the values for the $\overline{\nu}$, M_w, and $[\eta]$ obtained from previous experiments, the conformation of the polymers could then be investigated. This is particularly important as the shape of a polymer in a particular solvent may help us understand its behaviour once it is absorbed by the wood.

The viscosity increment (ν) factor was used to predict the axial ratio of TPA6 and TPA7 with the programme ELLIPS1[62]. ν, described by Eq. (3)[63–66], is a universal shape parameter meaning that it is only affected by the particle's shape and is independent of its size[67].

$$\nu = [\eta]/\nu_s \tag{3}$$

where ν_s is the swollen (through solvent association) specific volume of the polymer (mL/g). ELLIPS1 works by converting the value for a shape function to an estimate of the axial ratio (a/b) for ellipsoids of revolution[62]. Table 3 shows the values for the ν parameter and the corresponding axial ratios for both polymers at different degrees of solvent association, which is the degree of interaction between a polymer in solution and a solvent (defined as $\nu_s/\overline{\nu}$, where ν_s is the swollen specific volume and $\overline{\nu}$ is the partial specific volume). If the polymers did not bind with isopropanol, then the solvent association would be equal to their $\overline{\nu}$. In Table 3, solvent association values of 1.0–1.4 were used for the shape analyses in order to determine whether these would drastically affect the results. Figure 7 shows the visual representation of the shapes (prolate ellipsoid model) of the polymers estimated from these values and indicates that both TPA6 and TPA7 appear to have a long, oval shape. This property may prove to be advantageous for consolidants, as this elongated shape may potentially increase the surface area available for possible interactions between the wood and the polymers.

Conclusion

Two polymers have successfully been synthesised, from α-pinene- and oleic acid-derived monomers. Both monomers can easily undergo FRP and their feedstocks are cheap and highly accessible. Moreover, the other reagents that are utilised in the syntheses are commonly used products which are available commercially. A new protocol for the polymerisation of *trans*-sobrerol acrylate has been described, and a new copolymer composed of *trans*-sobrerol acrylate and acrylated oleic acid has been successfully synthesised. The conditions for the polymerisations appear to be easily reproducible even on scale-up, which would be very beneficial for the eventual testing on wood and for their practical use as conservation materials. Bioinspired polymers such as TPA6 and TPA7 have reduced negative impact on the environment by virtue of being sourced from biomass, however their production cannot be considered to be truly sustainable[7]. Every effort has been made to make the chemical synthesis processes as 'green' as possible, these included using water and mild conditions (the synthesis of *trans*-sobrerol) and making reagent substitutions when appropriate (replacing acryloyl chloride with acrylic acid and T3P®). It should be recognised however that these processes and reagents are still far from being environmentally

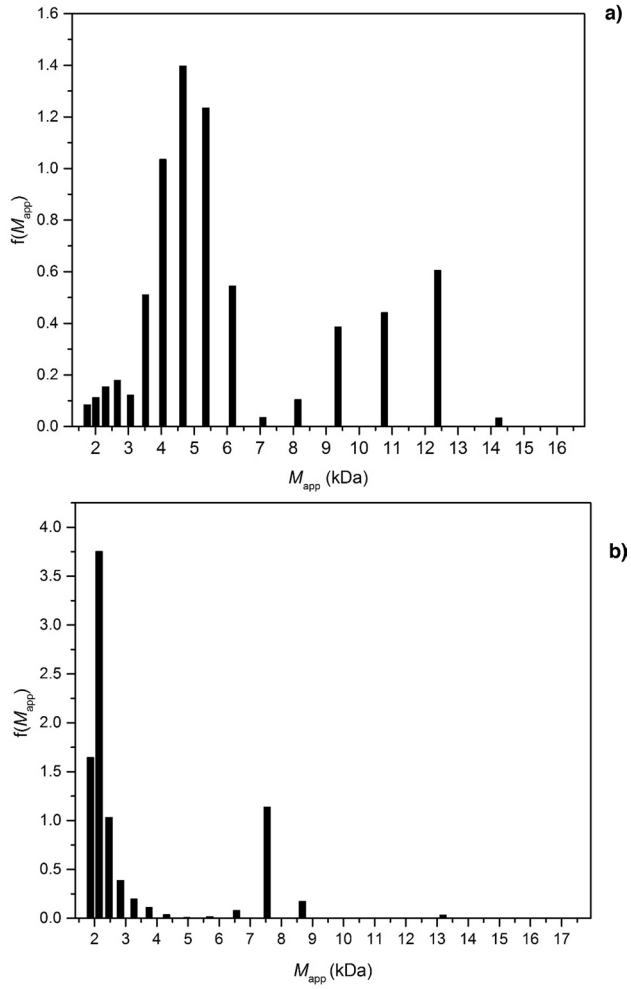

Figure 6. MultiSig analyses of the molar mass distribution f(M) vs M_w of (**a**) TPA6 and (**b**) TPA7 at a loading concentration of 4.0 mg/mL. Rotational speed = 45,000 rpm.

		Degree of solvent association $\nu_s/\overline{\nu}$		
		1	**1.2**	**1.4**
TPA6	Shape factor ν	5.7 ± 0.6	4.8 ± 0.6	4.1 ± 0.6
	Axial ratio (a/b)	5.0	4.1	3.4
TPA7	Shape factor ν	5.7 ± 0.3	4.9 ± 0.3	4.2 ± 0.3
	Axial ratio (a/b)	4.9	4.2	3.6

Table 3. The calculated values for the shape parameter ν and the axial ratios (prolate ellipsoid model) determined by ELLIPS1.

harmless. More optimisation of the monomer and polymer synthesis protocols can therefore be carried out in the future to attempt to make them more sustainable.

The hydrodynamic characterisation analyses indicated that both polymers have good properties for wood consolidation such as a M_w below 5 kDa and an elongated shape but with TPA7 showing greater homogeneity and a lower proportion of aggregation. These are all advantageous properties for a wood consolidant to have, indicating that these two polymers should be investigated further. It should be noted that these studies are still preliminary and that it would be essential for further investigations to be carried out before TPA6 and TPA7 can be considered as official candidates for wood consolidation. This would entail first confirming whether they can penetrate archaeological wood and analysing their consolidative behaviour. Should this prove successful, long-term stability studies will be essential as these would provide information on how these polymers fare in the wood after months or years. In order to be a viable consolidant, more information would also be needed on their toxicity and by-product formation[7,55].

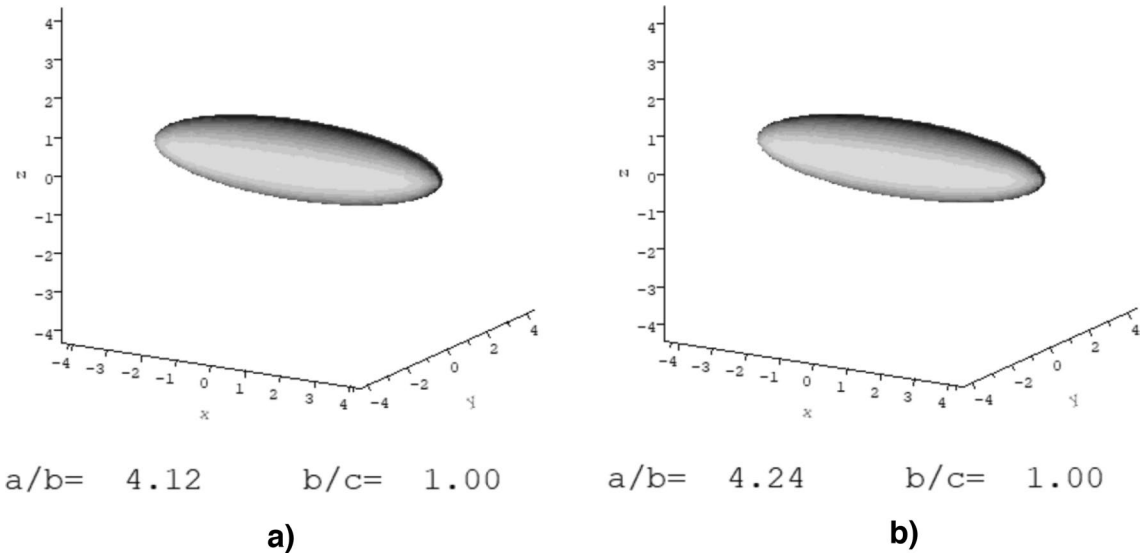

Figure 7. Ellipsoidal representations from the conformation analysis of (**a**) TPA6 and (**b**) TPA7 in isopropanol, using the programme ELLIPS1 with the shape parameter *ν*. The polymers, within experimental error, have identical axial ratios.

As such, the next step for this research will involve testing these polymers on archaeological wood in order to determine whether they can sufficiently penetrate it and to observe the effects that they have on it[55]. This will involve dissolving the polymers in a suitable solvent (such as isopropanol) and then immersing a number of archaeological wood samples in the solutions for an appropriate length of time. After drying, these samples can then be studied to determine the effect of the polymers on the wood. This would involve analysing the samples with infrared spectroscopy and SEM to confirm the penetration of the polymers[55]. Weight change, dimensional change and colour change can also be monitored before and after treatment. The consolidative effect of the polymers can be investigated by testing the hardness of the treated wood, for example with the use of penetrometery which measures resistance to indentation[55]. These studies will give us essential information on the potential of these bioinspired compounds as wood consolidants, and whether they can successfully be used as part of the "polymer treatment toolkit" for the Oseberg artefacts and other archaeological wooden objects under threat in the future.

Materials and methods

Materials. All reagents and solvents were purchased from a chemical supplier (Acros Organics, Alfa Aesar, Merck, Sigma Aldrich and Fischer Scientific UK) and used without further purification. Water was deionised before use. Brine is a saturated aqueous solution of sodium chloride. Rotary evaporators under reduced pressure were used for solvent evaporation.

Nuclear magnetic resonance (NMR). ^{1}H NMR spectra were recorded in deuterated chloroform ($CDCl_3$), deuterated DMSO ($(CD_3)_2SO$) and deuterated methanol (CD_3OD) at ambient temperature using Bruker 400 MHz spectrometers (Bruker Corporation, Germany). ^{13}C NMR spectra were recorded in $CDCl_3$, $(CD_3)_2SO$ and CD_3OD at ambient temperature using 100 MHz spectrometers. Data is expressed as chemical shifts (δ) in ppm relative to solvent signals ($CHCl_3$, ^{1}H NMR 7.26), ($CDCl_3$ ^{13}C NMR 77.16), ($(CH_3)_2SO$, ^{1}H NMR 2.50), ($(CD_3)_2SO$, ^{13}C NMR 39.52), (CH_3OH, ^{1}H NMR 3.31) or (CD_3OD, ^{13}C NMR 49.0) as the internal standard. MestReNova 6.0.2 copyright 2009 (Mestrelab Research S.L.) was used for analysing the spectra. The data is available in the Supplementary Information.

High resolution mass spectrometry (HRMS). A Bruker MicroTOF spectrometer operating in electrospray ionisation (ESI) mode was used (Bruker Corporation, Germany).

Fourier-transform infra-red spectroscopy (FTIR). A Bruker Tensor 27 FT-IR spectrophotometer with an ATR attachment was employed. The measurements were performed in the range of 4000–650 cm^{-1} and spectra were analysed using OPUS software (Bruker Corporation, Germany).

Gel permeation chromatography (GPC). An Agilent 1260 Infinity Series HPLC (Agilent Technologies, USA) fitted with a differential refractive index detector (DRI) was used. THF (HPLC grade, Fisher Scientific) was used as the eluent at room temperature with two Agilent PL-gel mixed-D columns in series at a flow rate of 1 mL/min. A calibration curve was made using poly(methyl methacrylate) standards with ASTRA software (Wyatt Technology, USA) This was used for determination of the relative (compared to the standards) $M_{r,n}$, $M_{r,w}$ and molar mass distribution and dispersity ($Đ = M_{r,w}/M_{r,n}$).

Differential scanning calorimetry (DSC). A TA-Q2000 (TA instruments) calibrated with an indium standard under an N_2 flow was used to measure T_g. A The sample (~ 5 mg) was weighed in a T-zero sample pan (TA instruments), leaving another T-zero pan empty as a reference. Both pans were heated at a rate of 10 °C/min, using a heat/cool/heat method.

Monomer and polymer synthesis. The synthesis of α-pinene oxide (1) and *trans*-sobrerol (2) has been reported in a previous publication[15]. The epoxidised oleic acid (4) and the acrylated oleic acid (5) were synthesised following the protocols described by Neto et al.[39]. The Supplementary Information contains details on these methodologies.

Synthesis of trans-sobrerol acrylate, 3. To a solution of **2** (7.08 g, 41.6 mmol) in MeCN (200 mL) were added Et_3N (17.5 mL, 125.6 mmol), acrylic acid (acid with low H_2O content, 99.5% stab. with ca. 200 ppm methoxyphenol, 3.14 mL, 45.8 mmol) and then T3P® (50 wt% in ethyl acetate, 29.7 mL, 99.8 mmol) was added dropwise. The reaction mixture was stirred for 24 h, after which H_2O (200 mL) was added and the reaction mixture separated. The aqueous layer was separated with diethyl ether (100 mL × 3) and the combined organic layers were washed with HCl (1 M aqueous, 200 mL × 3), $NaHCO_3$ (sat. aq., 200 mL × 3) and brine (100 mL × 2). The reaction mixture was then dried with $MgSO_4$, filtered and concentrated to yield the title compound (**3**) as a brownish orange viscous liquid (6.05 g, 27.0 mmol, 65% yield).

General procedure for the polymerisation of trans-sobrerol acrylate, 3, to yield a terpene-derived acrylated polymer. TPA6. To the monomer (4 g, 17.8 mmol) was added cyclohexanone (24 mL), AIBN (0.5 wt%, 20 mg, 0.1 mmol) and benzyl mercaptan (5 mol%, 112 µL, 1 mmol). The mixture was purged with argon for 1 h 45 min, after which it was stirred for 24 h at 70.0 °C. The mixture was left to cool to room temperature and then purified with excess of hexane (4:1 v/v). The product was dried in a room temperature vacuum oven to yield the title compound (TPA6).

General procedure for the copolymerisation of trans-sobrerol acrylate 3 and acrylated oleic acid 5, to yield a terpene- and oleic acid-derived acrylated copolymer. TPA7. To a mixture of monomer 3 (6.4 g, 28.5 mmol) and monomer 5 (1.6 g, 4.3 mmol) was added cyclohexanone (48 mL), AIBN (1 wt%, 80 mg, 0.5 mmol) and benzyl mercaptan (5 mol%, 223.9 µL, 2 mmol). The mixture was purged with argon for 1 h 45 min, after which it was stirred for 24 h at 70.0 °C. The mixture was left to cool to room temperature and then purified with excess of hexane (4:1 v/v). The product was dried in a room temperature vacuum oven to yield the title compound (TPA7).

Density measurements: calculation of the partial specific volume ($\bar{\nu}$). An Anton Paar DMA 5000 V5.003 was used at 20.0 °C. The partial specific volume is required for the analyses of the sedimentation velocity, sedimentation equilibrium studies and conformational analyses. A 9.0 mg/mL stock solution of each TPA6 and TPA7 in isopropanol were prepared and then diluted to 8.0, 7.0, 6.0, 5.0 and 4.0 mg/mL. These concentrations were thereafter used for the density measurements. The results were evaluated using Eq. (1) and following the procedure of Kratky et al.[56].

Analytical ultracentrifugation (AUC). A Beckman Optima XL-I analytical ultracentrifuge with Rayleigh interference optics was used at 20.0 °C. 12 mm optical path length double sector cells with titanium centrepieces were employed.

Sedimentation velocity. Loading concentrations of 0.5 to 4.0 mg/mL of TPA6 and TPA7 in isopropanol were used. 405 µL of each concentration were injected in the sample solution channel of each AUC cell. Isopropanol was used as the reference solution. A rotational speed of 49,000 rpm was used and the samples centrifuged overnight. The weight average sedimentation coefficient (*s*) and the distributions of sedimentation coefficient *c(s)* vs s were obtained by analysis with the SEDFIT procedure[68]. This analysis was carried out to assess the size distribution and heterogeneity of the polymer systems.

Sedimentation equilibrium. 100 µL of the previous loading concentrations (0.5 to 4.0 mg/mL) of TPA6 and TPA7 in isopropanol were added to each of the AUC cells. Isopropanol was used as the reference solution. The experiment was carried out at a rotational speed of 45,000 rpm over 2 days. The results were analysed with SEDFIT-MSTAR[59] in order to obtain the apparent weight average molar mass ($M_{w,app}$), making use of the M^* extrapolation[60] and the hinge point method. No major concentration dependence was observed for either polymer systems, which suggested that non-ideality was not significant. The data obtained from the highest concentration (4.0 mg/mL) of both polymers was additionally analysed with the MultiSig algorithm[61] to evaluate the extent of any aggregation.

Viscosity measurements: calculation of the intrinsic viscosity [η]. An Anton-Paar AMVn (Graz, Austria) rolling ball viscometer was used at a temperature of 10.0 °C. This low temperature was chosen so as to prevent the solvent (isopropanol) from evaporating due to its high volatility.

The viscosity measurement was carried out using solutions of 6.0 mg/mL concentration of TPA6 and TPA7 in isopropanol. The intrinsic viscosity values were then calculated with the Solomon-Ciuta equation[69,70] (Eq. (2)).

Conformation analyses. The ELLIPS1[62] algorithm was used to estimate macromolecular asymmetry from the viscosity increment (ν) using Eq. (3).

Data availability

Raw data is available in Supplementary Information. Additional information is available from the Corresponding Authors.

Received: 23 June 2022; Accepted: 21 September 2022
Published online: 01 November 2022

References

1. Rosenqvist, A. M. The stabilizing of woodfound in the Viking ship of Oseberg: Part I. *Stud. Conserv.* **4**, 13–22 (1959).
2. Braovac, S. & Kutzke, H. The presence of sulfuric acid in alum-conserved wood—Origin and consequences. *J. Cult. Herit.* **13**, S203–S208 (2012).
3. Braovac, S. *et al.* Chemical analyses of extremely degraded wood using analytical pyrolysis and inductively coupled plasma atomic emission spectroscopy. *Microchem. J.* **124**, 368–379 (2016).
4. Braovac, S. *et al.* Navigating conservation strategies: Linking material research on alum-treated wood from the Oseberg collection to conservation decisions. *Herit. Sci.* **6**, 1–16 (2018).
5. McQueen, C. M. A. *et al.* New insights into the degradation processes and influence of the conservation treatment in alum-treated wood from the Oseberg collection. *Microchem. J.* **132**, 119–129 (2017).
6. Walsh-Korb, Z. & Avérous, L. Recent developments in the conservation of materials properties of historical wood. *Prog. Mater. Sci.* **102**, 167–221 (2019).
7. Walsh-Korb, Z. Sustainability in heritage wood conservation: Challenges and directions for future research. *Forests* **13**, 1–35 (2022).
8. McHale, E. *et al.* Synthesis and characterisation of lignin-like oligomers as a bio-inspired consolidant for waterlogged archaeological wood. *Pure Appl. Chem.* **88**, 969–977. https://doi.org/10.1515/pac-2016-0814 (2016).
9. Christensen, M., Kutzke, H. & Hansen, F. K. New materials used for the consolidation of archaeological wood-past attempts, present struggles, and future requirements. *J. Cult. Herit.* **13S**, S183–S190 (2012).
10. Wakefield, J. M. K., Gillis, R. B., Adams, G. G., McQueen, C. M. A. & Harding, S. E. Controlled depolymerisation assessed by analytical ultracentrifugation of low molecular weight chitosan for use in archaeological conservation. *Eur. Biophys. J.* **47**, 769–775 (2018).
11. Jenssen, V. Conservation of wet organic artefacts excluding wood. In *Conservation of Marine Archaeological Objects* (ed. Pearson, C.) 122–163 (Butterworth-Heinemann, 1987).
12. Christensen, M., Larnøy, E., Kutzke, H. & Hansen, F. K. Treatment of waterlogged archaeological wood using chitosan- and modified chitosan solutions. Part 1: Chemical compatibility and microstructure. *J. Am. Inst. Conserv.* **54**, 3–13 (2015).
13. Jiang, J., Chen, Y., Cao, J. & Mei, C. Improved hydrophobicity and dimensional stability of wood treated with paraffin/acrylate compound emulsion through response surface methodology optimization. *Polymers (Basel)* **12**, 86 (2020).
14. Li, Y., Dong, X., Liu, Y., Li, J. & Wang, F. Improvement of decay resistance of wood via combination treatment on wood cell wall: Swell-bonding with maleic anhydride and graft copolymerization with glycidyl methacrylate and methyl methacrylate. *Int. Biodeterior. Biodegrad.* **65**, 1087–1094 (2011).
15. Cutajar, M. *et al.* Terpene polyacrylate TPA5 shows favorable molecular hydrodynamic properties as a potential bioinspired archaeological wood consolidant. *Sci. Rep.* **11**, 7343 (2021).
16. Sainz, M. F. *et al.* A facile and green route to terpene derived acrylate and methacrylate monomers and simple free radical polymerisation to yield new renewable polymers and coatings. *Polym. Chem.* **7**, 2882–2887 (2016).
17. Winnacker, M. Pinenes: Abundant and renewable building blocks for a variety of sustainable polymers. *Angew. Chem.* **130**, 14560–14569 (2018).
18. Llevot, A. *et al.* Renewability is not enough: Recent advances in the sustainable synthesis of biomass-derived monomers and polymers. *Chem. Eur. J.* **22**, 11510–11521 (2016).
19. Hillmyer, M. A. & Tolman, W. B. Aliphatic polyester block polymers: Renewable, degradable, and sustainable. *Acc. Chem. Res.* **47**, 2390–2396 (2014).
20. Vilela, C. *et al.* The quest for sustainable polyesters-insights into the future. *Polym. Chem.* **5**, 3119–3141 (2014).
21. Lima, M. S., Costa, C. S. M. F., Coelho, J. F. J., Fonseca, A. C. & Serra, A. C. A simple strategy toward the substitution of styrene by sobrerol-based monomers in unsaturated polyester resins. *Green Chem.* **20**, 4880–4890 (2018).
22. Stamm, A. *et al.* Chemo-enzymatic pathways toward pinene-based renewable materials. *Green Chem.* **21**, 2720–2731 (2019).
23. Lligadas, G., Ronda, J. C., Galià, M. & Cádiz, V. Oleic and undecylenic acids as renewable feedstocks in the synthesis of polyols and polyurethanes. *Polymers (Basel)* **2**, 440–453 (2010).
24. Xia, Y. & Larock, R. C. Vegetable oil-based polymeric materials: Synthesis, properties, and applications. *Green Chem.* **12**, 1893–1909 (2010).
25. Seniha Güner, F., Yağci, Y. & Tuncer Erciyes, A. Polymers from triglyceride oils. *Prog. Polym. Sci.* **31**, 633–670 (2006).
26. Sharma, V. & Kundu, P. P. Addition polymers from natural oils—A review. *Prog. Polym. Sci.* **31**, 983–1008 (2006).
27. Meier, M. A. R., Metzger, J. O. & Schubert, U. S. Plant oil renewable resources as green alternatives in polymer science. *Chem. Soc. Rev.* **36**, 1788–1802 (2007).
28. Sharma, V. & Kundu, P. P. Condensation polymers from natural oils. *Prog. Polym. Sci.* **33**, 1199–1215 (2008).
29. Baumann, H. *et al.* Natural fats and oils—Renewable raw materials for the Chemical Industry. *Angew. Chem. Int. Ed. Engl.* **27**, 41–62 (1988).
30. Biermann, U. *et al.* New syntheses with oils and fats as renewable raw materials for the chemical industry. *Biorefin. Ind. Process. Prod. Status Quo Futur. Dir.* **2**, 253–289 (2008).
31. Scott, D., Harding, S. & Rowe, A. *Analytical Ultracentrifugation: Techniques and Methods* (Royal Society of Chemistry, 2005).
32. Harding, S. E. The Svedberg Lecture 2017. From nano to micro: the huge dynamic range of the analytical ultracentrifuge for characterising the sizes, shapes and interactions of molecules and assemblies in Biochemistry and Polymer Science. *Eur. Biophys. J.* **47**, 697–707 (2018).
33. McHale, E., Steindal, C. C., Kutzke, H., Benneche, T. & Harding, S. E. In situ polymerisation of isoeugenol as a green consolidation method for waterlogged archaeological wood. *Sci. Rep.* **7**, 1–9 (2017).
34. Wakefield, J. M. K. *et al.* Aminoethyl substitution enhances the self-assembly properties of an aminocellulose as a potential archaeological wood consolidant. *Eur. Biophys. J.* **49**, 791–798 (2020).
35. Wakefield, J. M. K., Braovac, S., Kutzke, H., Stockman, R. A. & Harding, S. E. Tert-butyldimethylsilyl chitosan synthesis and characterization by analytical ultracentrifugation, for archaeological wood conservation. *Eur. Biophys. J.* **49**, 781–789 (2020).
36. Cutajar, M. *et al.* Comparative hydrodynamic study on non-qqueous soluble archaeological wood consolidants: Butvar B-98 and PDMS-OH Siloxanes. *Molecules* **27**, 2133 (2022).

37. Channell, G. A. *et al.* Use of the Extended Fujita method for representing the molecular weight and molecular weight distributions of native and processed oat beta-glucans. *Sci. Rep.* **8**, 6–13 (2018).
38. Corma Canos, A., Iborra, S. & Velty, A. Chemical routes for the transformation of biomass into chemicals. *Chem. Rev.* **107**, 2411–2502 (2007).
39. Neto, W. S. *et al.* Superparamagnetic nanoparticles stabilized with free-radical polymerizable oleic acid-based coating. *J. Alloys Compd.* **739**, 1025–1036 (2017).
40. Heuts, J. P. A., Muratore, L. M. & Davis, T. P. Preparation and characterization of oligomeric terpolymers of styrene, methyl methacrylate and 2-hydroxyethyl methacrylate: A comparison of conventional and catalytic chain transfer. *Macromol. Chem. Phys.* **201**, 2780–2788 (2000).
41. Henríquez, C., Bueno, C., Lissi, E. A. & Encinas, M. V. Thiols as chain transfer agents in free radical polymerization in aqueous solution. *Polymer (Guildf).* **44**, 5559–5561 (2003).
42. Whitfield, R., Parkatzidis, K., Truong, N. P., Junkers, T. & Anastasaki, A. Tailoring polymer dispersity by RAFT polymerization: A versatile approach. *Chemistry* **6**, 1340–1352 (2020).
43. Schilling, M. R. The glass transition of materials used inconservation. *Stud. Conserv.* **34**, 110–116 (1989).
44. Davis, S. L., Roberts, C. & Poli, A. Paraloid® B-72/B-48N 1:1 as an adhesive for use in hotclimates: Literature review, laboratory testing, and observational field study. *Stud. Conserv.* **67**, 1–9 (2021).
45. Koob, S. P. The use of Paraloid B-72 as an adhesive: Its application for archaeological ceramics and other materials. *Stud. Conserv.* **31**, 7–14 (1986).
46. Yasuda, H. *Plasma Polymerization* (Academic Press Inc., 1985).
47. Sander, M. M., Nicolau, A., Guzatto, R. & Samios, D. Plasticiser effect of oleic acid polyester on polyethylene and polypropylene. *Polym. Test.* **31**, 1077–1082 (2012).
48. Lim, H. & Hoag, S. W. Plasticizer effects on physical-mechanical properties of solvent cast Soluplus® films. *AAPS PharmSciTech* **14**, 903–910 (2013).
49. Hazer, B., Ayyıldız, E., Eren, M., Seçilmiş Canbay, H. & Ashby, R. D. Autoxidized oleic acid bifunctional macro peroxide initiators for free radical and condensation polymerization. Synthesis and characterization of multiblock copolymers. *J. Polym. Environ.* **27**, 2562–2576 (2019).
50. Aharoni, S. M. Increased glass transition temperature in motionally constrained semicrystalline polymers. *Polym. Adv. Technol.* **9**, 169–201 (1998).
51. Schmidt, P. L., Shugar, A. & Ploeger, R. Analytical observations regarding Butvar B-98 and Paraloid B-72 blends as a suitable adhesive in hot climates. *MRS Adv.* **2**, 1927–1941 (2017).
52. Pohoriljakova, I. & Moy, S. A. A re-evaluation of adhesives used for mending ceramics at Kaman-Kalehöyük: A final assessment. *Anatol. Archaeol. Stud.* **9**, 83–92 (2013).
53. Strahan, D., Unruh, J., Strahan, D. & Unruh, J. Conservation of ceramic artifacts on archaeological sites. *F. Notes Pract. Guid. Archaeol. Conserv. Site Preserv.* **12**, 1–6 (2002).
54. Horie, V. *Materials for Conservation: Organic Consolidants, Adhesives and Coatings* 2nd edn. (Elsevier, 2010).
55. Wakefield, J. *Natural Polymers for Consolidation of the Oseberg Artefacts*. PhD Dissertation, University of Nottingham (2020).
56. Kratky, O., Leopold, H. & Stabinger, H. The determination of the partial specific volume of proteins by the mechanical oscillator technique. *Methods Enzymol.* **27**, 98–110 (1973).
57. Andriulo, F. *et al.* Hybrid nanocomposites made of diol-modified silanes and nanostructured calcium hydroxide. Applications to Alum-treated wood. *Pure Appl. Chem.* **89**, 29–39 (2017).
58. Schuck, P. Size-distribution analysis of macromolecules by sedimentation velocity ultracentrifugation and Lamm equation modeling. *Biophys. J.* **78**, 1606–1619 (2000).
59. Schuck, P. *et al.* SEDFIT-MSTAR: Molecular weight and molecular weight distribution analysis of polymers by sedimentation equilibrium in the ultracentrifuge. *Analyst* **139**, 79–92 (2014).
60. Creeth, J. & Harding, S. Some observations on a new type of point average molecular weight. *J. Biochem. Biophys. Methods* **7**, 25–34 (1982).
61. Gillis, R. B. *et al.* MultiSig: A new high-precision approach to the analysis of complex biomolecular systems. *Eur. Biophys. J.* **42**, 777–786 (2013).
62. Harding, S. E., Horton, J. C. & Cölfen, H. The ELLIPS suite of macromolecular conformation algorithms. *Eur. Biophys. J.* **25**, 347–359 (1997).
63. Simha, R. The Influence of Brownian movement on the viscosity of solutions. *J. Phys. Chem.* **44**, 34 (1940).
64. Saito, N. The effect of Brownian motion on the viscosity of solutions of macromolecules, I. Ellipsoid of revolution. *J. Phys. Soc.* **6**, 297–301 (1951).
65. Harding, S. E. & Rowe, A. J. Modeling biological macromolecules in solution. II. The general tri-axial ellipsoid. *Biopolymers* **22**, 1813–1829 (1983).
66. Harding, S. E., Dampier, M. J. & Rowe, A. J. The viscosity increment for ellipsoids of revolution: Some observations on the Simha formula. *Biophys Chem.* **15**, 205–208 (1983).
67. de la Torre, J. G. & Harding, S. E. Hydrodynamic modelling of protein conformation in solution: ELLIPS and HYDRO. *Biophys. Rev.* **5**, 195–206 (2013).
68. Dam, J. & Schuck, P. Calculating sedimentation coefficient distributions by direct modeling of sedimentation velocity concentration profiles. *Methods Enzymol.* **384**, 185–212 (2004).
69. Solomon, O. F. & Ciuta, I. Z. Détermination de la viscosité intrinsèque de solutions de polymères par une simple détermination de la viscosité. *J. Appl. Polym. Sci.* **6**, 683–686 (1962).
70. Harding, S. E. The intrinsic viscosity of biological macromolecules. Progress in measurement, interpretation and application to structure in dilute solution. *Prog. Biophys. Mol. Biol.* **68**, 207–262 (1997).

Acknowledgements

This work was supported by the UK Engineering & Physical Sciences Research Council [grant number EP/L015633/1], the Norwegian Ministry of Education and Research, and the University of Oslo as part of the Saving Oseberg project. M.C. is a UK EPSRC Centre for Doctoral Training in Sustainable Chemistry student. M.C. thanks Vincenzo Taresco (School of Chemistry, University of Nottingham) for contributing to scientific discussions. F.M. thanks the Conselho Nacional de Desenvolvimento Científico e Tecnológico (CNPq, Process no 202176/2020-7) for providing a scholarship to pursue a Post-Doctoral Training at the University of Nottingham.

Author contributions

The synthetic, analytic and characterisation work was carried out by M.C; S.E.H., R.A.S., S.M.H. and S.B. contributed to the planning of the experiments and provided supervision for the research work. F.M. provided expertise on the acrylated oleic acid monomer and contributed to its synthesis and analysis. V.C.C. provided

expertise on the use of benzyl mercaptan and contributed to the design of the polymerisation reactions. The paper was written by M.C. and all authors reviewed and edited the article.

Competing interests
The authors declare no competing interests.

Additional information
Supplementary Information The online version contains supplementary material available at https://doi.org/10.1038/s41598-022-21027-4.

Correspondence and requests for materials should be addressed to M.C. or S.E.H.

Reprints and permissions information is available at www.nature.com/reprints.

Publisher's note Springer Nature remains neutral with regard to jurisdictional claims in published maps and institutional affiliations.

Evaluation of two terpene-derived polymers as consolidants for archaeological wood

Michelle Cutajar[1,2*], Susan Braovac[3], Robert A. Stockman[2], Steven M. Howdle[2] and Stephen E. Harding[1,3*]

1. *National Centre for Macromolecular Hydrodynamics (NCMH), University of Nottingham, School of Biosciences, Sutton Bonington, LE12 5RD, UK*
2. *School of Chemistry, University of Nottingham, University Park, Nottingham, NG7 2RD UK*
3. *Museum of Cultural History, University of Oslo, Kabelgata 34, 0580 Oslo, Norway*

*Corresponding authors: michelle.cutajar@nottingham.ac.uk and steve.harding@nottingham.ac.uk

Abstract

The evaluation of two terpene-derived polymers, termed TPA6 and TPA7, as possible consolidants for archaeological wood was carried out. The overall objective of this work was to expand the non-aqueous treatment toolkit which is available for the conservation of the highly degraded Oseberg collection. The wood artefacts which were found on the Oseberg ship were treated with alum in the early 20th century, leading to the formation of sulfuric acid and to the precarious state that they are in today. Some of these artefacts cannot be treated with conventional aqueous consolidants, like polyethylene glycol, due to their highly degraded and/or reconstructed nature. This study sought to examine the level of penetration of the polymers in archaeological wood and to evaluate their consolidative effect. Both TPA6 and TPA7 were soluble in isopropanol and had a M_w of 3.9 and 4.2 kDa respectively. A number of archaeological wood specimens were immersed in solutions of these polymers. Their penetration and effects were evaluated using weight and dimensional change, colour change, infrared spectroscopy, scanning electron microscopy and hardness tests. Both polymers successfully penetrated the wood specimens, with a higher concentration found on the surface versus the core. Additionally, both polymers appeared to increase the hardness of the specimen surfaces. Increasing the polymer concentration and soaking time in future investigations could potentially facilitate the penetration to the wood cores.

Introduction

Treating wooden artefacts with hot alum solutions was a popular method amongst conservators from the mid-1800s all the way to the 1950s[1]. This was the method that was used on the artefacts found in the Oseberg ship in the early 1900s. Unfortunately, these well-meaning conservators could not predict the damage that this treatment would eventually cause. We now know that heating alum solutions generates sulfuric acid, leading to the degraded state that these artefacts are in today[2].

In Northern Europe archaeological wood is usually found in a waterlogged state and therefore water-based conservation methods are the most effective to conserve it. The most popular conservation method usually involves treatment with polyethylene glycol (PEG) and subsequent freeze-drying[3]. If the Oseberg artefacts are retreated using this method, they would first have to be immersed in water, to remove the alum salts and acid, before adding PEG[4]. Retreating the Oseberg artefacts is not such a simple matter however, due to the large variation of the wood's preservation state. Some of the most highly degraded artefacts cannot withstand this type of aqueous treatment as it may result in the dissolution of the alum inside the wood, leading to total collapse. Additionally, some of the artefacts contain non-wood components which were added in past restorations such as metal rods, glue and plaster[1]. For these objects, there is increased risk of damage if they are immersed in water (see reference 1 and references cited therein). The Saving Oseberg project was established by the University of Oslo to safeguard these artefacts and to investigate appropriate ways with which to treat them. One of the main aims of this endeavour was to develop new treatment materials and strategies in order to have alternatives to existing consolidants (see, e.g. reference 5). The polymers which are commonly used in conservation nowadays are mostly derived from non-sustainable sources[6,7]. Such consolidants include Butvar® B-98, a polyvinyl butyral-based resin[6], and Kauramin® which is a melamine urea formaldehyde resin[7].A particular emphasis was put on the sustainability of the new materials, with the use of bioinspired polymers whenever possible. Examples of materials that have been investigated include lignin[4], isoeugenol[8,9], chitosan[5,10] and aminocellulose[11]. Most recently, we have developed

polymers derived from terpenes with functionalised hydroxylated moieties[12,13]. In this work we wanted to further investigate the potential of two of these polymers, TPA6 and TPA7 (Figure 1), as wood consolidants. TPA6 is a homopolymer made from an α-pinene-derived monomer, with a M_w of 3.9 kDa. TPA7 is a copolymer derived from this same terpene monomer along with an oleic acid-based comonomer and has a M_w of 4.2 kDa. The T_g values for TPA6 and TPA7 were measured to be 31.1 °C and 18.9 °C respectively[13]. Both are yellow solids at room temperature and 50 g of each polymer was available for the wood testing. Since the two polymers have low M_w values, it was envisaged that they would be able to successfully penetrate wood. Moreover, they both possess hydroxyl groups which were anticipated to aid in the hydrogen bonding taking place between the consolidants and the wood. The main aim of this investigation was to determine the extent to which these polymers penetrate wood after immersion in isopropanol and to determine if they provided any consolidative effect. Isopropanol was deemed a good solvent to use in such studies since it has an acceptable safety profile and had been previously used in conservation experiments with degraded alum-treated wood[14]. Moreover, volatile solvents like isopropanol are particularly useful for wood impregnation since they can efficiently transport the consolidant polymers and then evaporate rapidly after treatment[15].

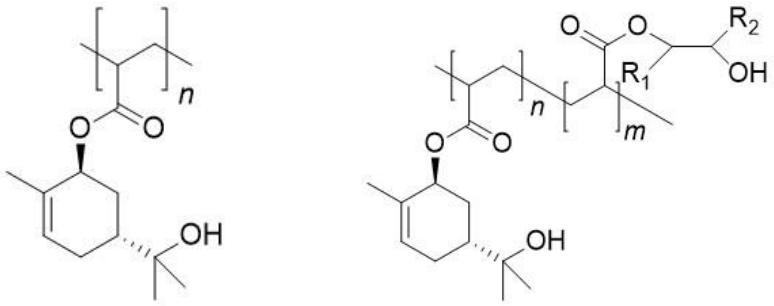

TPA6 **TPA7**

Figure 1. The structures for the two terpene-derived polymers that were evaluated in this study. Their synthesis and characterisation have already been described in a previous paper[13].

Materials and methods

Preparation of wood samples

Cube specimens were made from waterlogged archaeological wood which was the property of the Cultural History Museum. The wood, identified as *Pinus* (pine) with light microscopy, was initially in the form of a branch. The branch (diameter ~ 8 cm) did not contain heartwood, which would have been darker than the surrounding sapwood. The pith was centred in the branch, which indicated there was likely no reaction wood. Furthermore, the branch was evenly degraded, evidenced by lack of difference in resistance of surface and core when poked with a pin during preliminary examinations. Even degradation was also reflected in density measurements (as discussed below), which did not indicate differences between surface and core samples.

The branch was sawn into six slices, with each slice then being cut into 2 x 2 x 2 cm^3 cubes, where sides were aligned with radial and tangential directions (Figure S1). These were freeze-dried and then acclimatised to 20 °C and 50% RH. A total of 30 cubes of archaeological wood were used for these experiments: 20 for immersion tests with the polymer solutions and the remaining 10 for the two control groups. In addition, the leftover pieces of wood that remained after the cutting of the cubes were used for density and maximum moisture content measurements.

Naming system

The wood specimens were named in a way so that one could identify which slice they were cut from, and whether they were a surface or a core sample. Generally, the ID for each specimen was comprised of three characters: the first indicates their slice number (1-6), the second denotes whether they were cut from the surface or core (S = surface; C = core) and the last is a nominal specimen number. For each slice, eight cubes originated from the surface and two cubed from the core (Figure S1, right).

Density and maximum water content measurements

For these studies, 6 wedges from each of the six wood slices were used: 4 sawn from the surface from each slice, and 2 from the core. This was done to be able see whether the wood slices were degraded to different degrees and to observe whether there was any difference between the surface and the core of the wood. The basic density was determined by dividing the oven-dried weight by waterlogged volume (Equation 1), following the notation of Jensen and Gregory[16]:

$$\rho_{so} = (M_{ss}/M_{up} - 1)/(1/\rho_{lpor} - 1/\rho_{ms} + R_{sorp}/\rho_{lpor}) \quad \textbf{(1)}$$

where M_{ss} = mass of waterlogged sample (g); M_{up} = mass of displaced volume of waterlogged sample (g); ρ_{lpor} = mass of water in pores per volume of pore water at 20 °C (0.99823 g/cm^3); ρ_{ms} = mass of cell wall material per volume of cell wall material (g/cm^3); R_{sorp} = correction factor due to sorbed water (0.028).

The waterlogged volume was determined from the weight of water displaced by the waterlogged samples. The ρ_{lpor} was assumed to be equal to the density of free water at 20 °C (0.99823 g/cm^3)[16]. The ρ_{ms} value used in Equation 1 was calculated using Equation 2, again following the notation of Jensen and Gregory[16]:

$$\rho_{ms} = \rho_{lpor}/\{1 + (W_{up} - W_{ss})/(M_{ms} + R_{sorp})\} \quad \textbf{(2)}$$

where ρ_{lpor} = mass of water in pores per volume of pore water at 20 °C (0.99823 g/cm^3); W_{up} = weight of displaced volume of waterlogged sample and surface water (g); W_{ss} = weight of waterlogged sample and surface water (g); M_{ms} = mass of cell wall material (g); R_{sorp} = correction factor due to sorbed water (0.028).

The maximum water content (MWC) percentage was also determined at the same time and is expressed as the weight of water contained in the sample relative to the oven-dried weight (Equation 3)[16]:

$$MWC = \{(M_{swet} - M_{ms})/M_{ms}\} * 100 \quad \textbf{(3)}$$

where MWC (%) = mass of maximum water per mass of cell wall material (g/g); M_{swet} =mass of wood in saturated condition; M_{ms} = mass of wood in anhydrous condition, obtained by placing the sample at 103 °C in an oven for at least 24 hours.

Immersion tests with polymer solutions

The wood cubes were divided into two control groups and two treatment groups (Table 1). The cubes in control group 1 were freeze-dried only and kept at 50% RH throughout the entire study. The control group was used to estimate the error range of the measurement method that was used to determine linear dimensional change (radial and tangential). Those in control group 2 were freeze-dried and then immersed in isopropanol. The specimens in treatment group 1 and 2 were freeze-dried and then immersed in polymer solutions of TPA6 and TPA7 respectively. The specimens were laid on their sides, to promote infusion from the transverse faces during immersion, which are the most easily penetrated. The beakers were then sealed to avoid evaporation using a watch glass and Parafilm. The solution level was monitored by tracing the surface of the impregnation solution after samples were saturated with it (a few hours) on the beaker; the solution level did not change over the 2-week impregnation period.

Table 1. The IDs of the wood specimens in each group used in this study

Control group 1 – freeze-dried only	Control group 2 – isopropanol	Treatment group 1 – TPA6	Treatment group 2 – TPA7
1.S.6	2.S.7	4.S.3	4.S.6
2.S.4	3.S.5	1.S.4	1.C.2
4.C.1	4.C.2	2.S.1	2.S.2
5.S.5	5.S.3	2.C.2	2.S.3
	6.S.6	3.S.1	3.S.2
		3.S.4	3.S.7
		4.S.2	4.S.5
		4.S.4	4.S.1
		5.S.1	5.S.2
		6.S.1	6.S.4

The two polymers were dissolved in isopropanol at a 15% w/w concentration. This concentration was decided upon as a result of preliminary tests which had been carried out in order to determine the best testing concentration. This involved using mixtures of wood powder and different concentrations of polymer/isopropanol solutions to make thin films of wood/polymer. Concentrations of 5% - 15% were tested and the highest concentration appeared to impart the most strength, meaning that the concentration of 15% produced the most robust films. Because of this, it was decided to use this concentration in these immersion tests. Higher concentrations were not tested due to the limited amount of polymer that was available. Both polymers appeared to dissolve completely in this concentration, therefore we assumed full dissolution. These solutions were then used to soak the assigned wood specimens. Control group 2, as well as both treatment groups were left immersed in their respective solutions for two weeks, based on a previous report of wood testing with non-aqueous treatments[4]. The wood cubes were then removed from the solutions and left to slowly air-dry in a fume-hood for one week, after which they were kept in climate chamber at 20 °C and 50% RH.

Change in weight and dimensions

Weight was measured using a four decimal balance. The weight of the cubes was reported before (after freeze-drying and after conditioning to 20 °C and 50% RH) and after treatment (after evaporation of solvent and after conditioning to 20 °C and 50% RH).

Dimensions were measured with digital callipers, using pins inserted into the cross-section of the cubes along radial and tangential directions. Changes in the longitudinal direction are minor in comparison. Both the radial and the tangential directions were measured, referred to as 'linear dimension', of Control Group 1 (freeze-dried only) and of treated specimens before and after treatment. All measurements were taken after freeze-drying and acclimatisation to 20.0 °C and 50% RH, such that it was possible to compare change from the same point of reference. The reason for measuring radial and tangential directions of specimens in Control Group 1 was to estimate the error involved in this measurement technique, since in theory, there should not be differences in the radial and tangential dimensions when stored under constant climatic conditions. The % weight change and % linear dimensional change were calculated for the treated groups using Equations 4 and 5:

$$\%\ \text{weight change} = \frac{(\text{weight after} - \text{weight before})}{\text{weight before}} \times 100\% \quad \textbf{(4)}$$

$$\%\ \text{linear dimensional change} = \frac{(\text{dimension after} - \text{dimension before})}{\text{dimension before}} \times 100\% \quad \textbf{(5)}$$

Colour change

Colour measurements were taken of all treatment groups and control groups. This was carried out with a Konica Minolta CM-700d handheld spectrophotometer, making use of the CIELAB (L*a*b*) colour space. The L* coordinate measures the lightness / darkness of the samples, on a scale from black (-) to white (+). The a* coordinate indicates a colour change from green (-) to red (+) and the b* measures a colour change from blue (-) to yellow (+). The light source used was D65 (daylight), the measurement diameter was 4 mm and the data provided was Specular Component Excluded (SCE). Colour measurements were taken of the longitudinal sides, two random spots were measured on each side. However the specimens' dark sides – if present – were not included. This amounted to six to eight measurements per specimen. Measurements from each control and treatment group were then averaged for each coordinate (L*, a*, b*). The change in colour caused by TPA6 and TPA7 was calculated from the difference of the averaged group measurements (ΔL*, Δa*, Δb*) between each of the two treatment groups and control group 2 (wood treated with just isopropanol). The absolute change, ΔE*, was finally calculated from the coordinate measurements using Equation 6:

$$\Delta E^* = (\Delta L^{*2} + \Delta a^{*2} + \Delta b^{*2})^{\frac{1}{2}} \quad \textbf{(6)}$$

Attenuated total reflection-Fourier transform infrared spectroscopy (ATR-FTIR)

Fourier transform infrared spectroscopy was carried out using an attenuated total reflection mode on a Thermo Fischer FTIR spectrometer (Nicolet iS50), with range 4000 – 400 cm^{-1}. The samples used for this part of the study included those from sound pine, an isopropanol-treated control, the treatment groups, as well as pure polymer samples. A resolution of 4 cm^{-1} was used and each spectrum was derived from 32 scans. Three spectra from each sampling site were taken and averaged. The wood samples were analysed at four points: the surface, the core and between the surface and core both along and across the grain (Figure S2). Thermo Scientific OMNIC FTIR software was used to analyse the data. Spectra were baseline corrected and normalised to 1508 cm^{-1} (wood spectra) or 1725 cm^{-1} (pure polymer spectra).

Scanning electron microscope (SEM) analyses

A FEI Quanta 450 Scanning Electron Microscope with a voltage of 8 kV on low vacuum was used. Spot size was 4.5, chamber pressure was 50-80 Pa with working distances of 7.0 – 10.0 mm. The SEM samples were carefully shaved with a razor in order to get a surface which was flat, enabling better visualisation of the wood cells. It was ensured that not too much material was shaved off from the surface, in order not to compromise the results. No coating was required since a high vacuum was not used.

Resistance to indentation (hardness test)

A fruit penetrometer (Lutron FR-5120) motorised with a TRINAMIC Motion control engine (Model TMCS-40.6.35-10000-AT-01) with 10000 P/R resolution was utilised (Figure S3). The penetrometer was fitted with a 3 mm radius tip which was used to apply a force on the tangential face of the wood specimens. The motor was operated through a hardwired controller. It was ensured that the wood specimens were lying on a flat surface and that the penetrometer's tip touched the wood's testing face perpendicularly. The testing faces of the wood specimens were shaved with a razor in order to ensure that they were flat and parallel. This was not always possible however, as a balance had to be struck between how much material was shaved off and the flatness of the testing faces. A specimen of sound pine was first measured. The wood specimens in the control groups were all measured. Eight specimens were measured from each treatment group. Each wood specimen was measured five times on its tangential surface and the values were then averaged (Figure S3). Additionally, each wood specimen from the treatment groups were split in two and the core was measured once on each half and averaged (Figure S3). Prior to each measurement, a preload was applied by lowering the penetrometer tip on to the testing face of the wood specimen until the force read by the sensor was between 6 – 10 N. For the actual measurement, the tip was lowered down 1 mm and the force in N was recorded. The net force was calculated by subtracting the preload force from the measured force. IBM® SPSS® software was used to analyse the data with a one-way ANOVA test to measure whether the differences in hardness were significant.

Results and Discussion

Density and maximum water content (MWC) measurements

The density and MWC of wood are both important indicators of its degradation. Knowing the density of the wood can give us an idea of the amount of consolidant required to conserve it[16]. The water content of waterlogged wood is referred to as MWC since it is assumed that wood which has been preserved in such conditions would possess the highest possible volume of water in its pores[17]. The MWC increases and the basic density decreases with increasing wood degradation, which results from the loss of mass and volume of cell wall material due to bacterial degradation taking place during burial[18].

From the density and MWC measurements, it appeared that the state of preservation of our wood branch was approximately even throughout, that is, there was no difference between surface and core specimens. The density measurements ranged from 0.132 to 0.179 g/cm^3. Sound pine is reported to have a density of around 0.5 g/cm^3 [19]. The MWC ranged from 492 to 653% indicating a high degree of degradation for pine, since above 250% water content it is considered to be degraded[20]. Based on this, our wood samples seemed to have a high degree of degradation, with the means of the density and MWC being 0.146 g/ cm^3 and 610% respectively. Moreover, the samples taken from the surface and the core of our wood branch appeared to show little difference in both density and MWC, meaning that they had similar preservation states.

Macroscopic observations

After treatment, the specimens treated with both polymers seemed darker, with a yellowish tinge. They felt denser when handled. There did not appear to be any new cracks that developed on the wood after treatment and they kept their original shape. This was ascertained by looking at photos taken before and after treatment (see Figures 3a and 3b as examples).

Weight change

The specimen groups treated with TPA6 and TPA7 were observed to substantially increase in weight (Figure 2a). The control group treated with isopropanol (referred to as IPA in Figure 2a) was expected to decrease in weight due to the dissolution of some pine resin in the solvent. During immersion, the solvent was observed to turn from transparent to a pale yellow, possibly indicating that some resin may have exited the wood. This was not found to be the case however since the specimens actually increased in weight, albeit very slightly. It is possible that these cubes were not conditioned to the same extent before and after isopropanol immersion, thus leading to a slight irregularity in the weight measurements.

Weight gain appeared to be uniform for the specimens treated with TPA6 and TPA7. TPA6 had a % weight change ranging from 40.5 – 45.9% while TPA7 ranged from 39.5 – 50.4%. The specimen with the most weight gain overall (50.4%) was a piece from the core treated with TPA7 (1.C.2). The sample showing the least weight gain (39.5%) was also from the TPA7 group (3.S.2). It is unclear why the polymer deviated in its penetration for these two particular specimens. Since the wood specimens were

conditioned both before and after treatment, then this meant that these differences in penetration were not influenced by temperature or the relative humidity. Taking this into consideration, TPA6's penetration into the wood appeared to be slightly more regular with no extremes. It is uncertain whether this is due to the polymer's properties, or if it is an effect of the wood's inherent variability.

Dimensional change

For all groups, the dimensional change for both radial and tangential faces primarily ranged at ±2%, except for a few outliers (Figure 2b). Both radial and tangential faces seemed to change to the same degree, that is, one face did not predominate over the other. Control group 2 appeared to shrink after isopropanol treatment. The treatment groups had more varied results, showing both shrinkage (negative values) and swelling (positive values). TPA6 seemed to mainly cause shrinkage. TPA7 seemed to have a more variable effect, with swelling slightly predominating over shrinkage.

As mentioned, there were a few outliers in these measurements. The most extreme was 2.S.7 (control group 2), which showed a radial dimensional change of -8.7%. Other outliers include 4.C.2 (control group 2; tangential change of 3.1%), 6.S.1 (treatment group 1; tangential change of -3.2%) and 1.C.2 (treatment group 2; radial change of 4.2%). These measurements may potentially be attributed to the high variability of the wood or they may also be due to experimental error. The 'pin method' of measuring dimensional changes has limitations when it comes to the accuracy of the measurements. This is because the measurement values are highly dependent on the angle of the calliper relative to the pins. Therefore, if this angle is not exactly replicated during the 'before' and 'after' measurements, it will be difficult to get results that truly represent the dimensional change that has taken place.

With regards to control group 1 (freeze-dried only), the specimens were kept in a desiccator at ~ 20.0 °C and 50% RH during the soaking of the other groups. Its measurements were then repeated after the treatment of the other specimens was completed and after they were acclimatized to 50% RH. This means that theoretically the specimens in control group 1 should have exhibited no dimensional changes since they were not subjected to any treatment after freeze-drying. Nevertheless, slight dimensional changes were still recorded (~ ±2%). This demonstrates the inherent inaccuracy of this measuring method. The dimensional changes recorded in control group 2 may therefore be considered as the error range that can be expected for the other measurements (~ ±2%). If we take this into consideration, then this means that most of wood specimens did not exhibit significant dimensional changes after treatment.

(a)

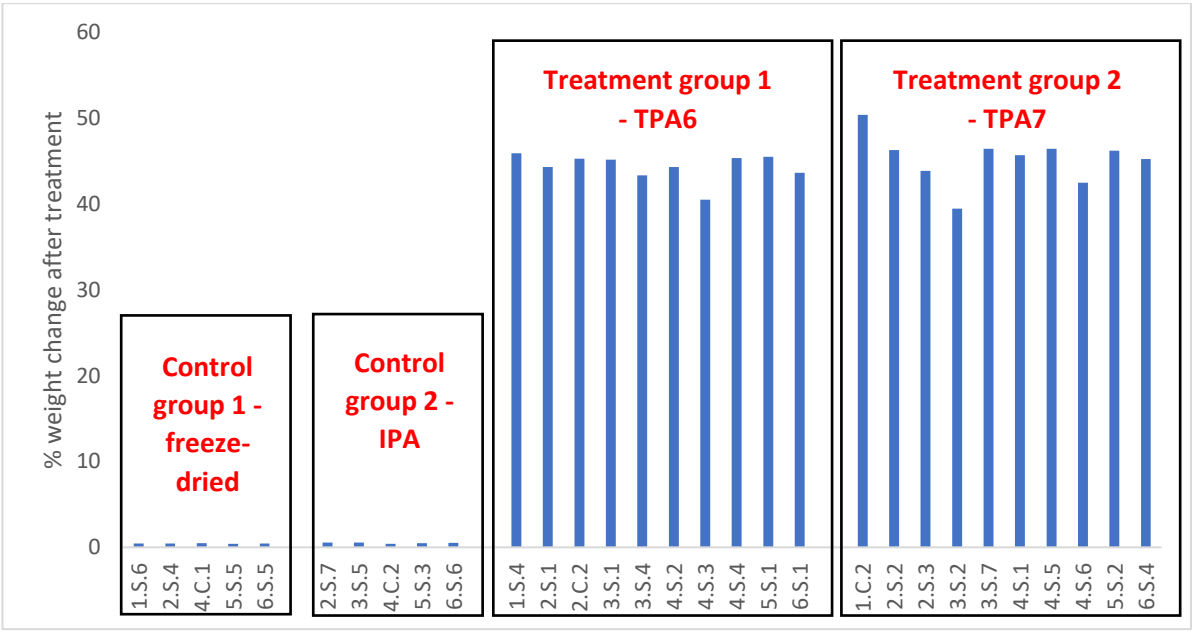

(b)

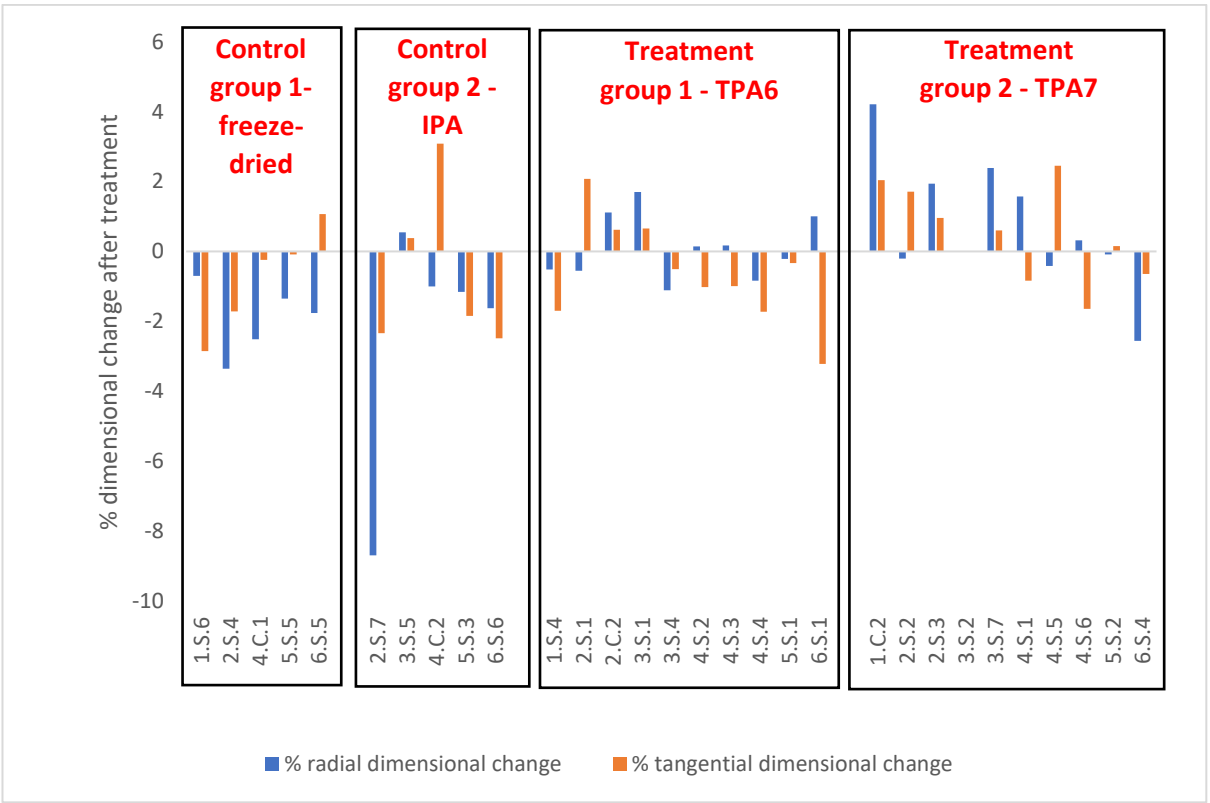

Figure 2. **(a**) The % weight change for all the measured groups. Control group 1 was freeze-dried and kept in a desiccator at ~20 °C and 50% RH during the immersion of control group 2 (isopropanol-immersed) and treatment groups 1 and 2 (TPA6- and TPA7-immersed respectively). **(b)** A comparison of the radial and tangential dimensional % changes for control groups 1 and 2 and treatment groups 1 and 2.

Colour change

Based on visual inspection alone, it was obvious that the polymers had caused a colour change in the wood specimens, mostly darkening them and imparting a yellow tinge (Figure 3). This is possibly a result of the polymers imparting their colour to the wood. The spectrophotometer colour measurements of both treatment groups were compared to those of control group 2, which was treated with isopropanol (Figure 4). Both polymers seemed to change the colour to a similar degree, as was observed visually. The measurements show that TPA7 seemed to cause slightly less colour change than TPA6, although this could not be seen by the naked eye. The largest degree of change was observed in the L* coordinate which decreased after the treatments, meaning that the specimens became darker. There was also a substantial difference in the b* axes, indicating a shift from blue to yellow. The measurements also showed a positive difference in the a* axes (green to red), although at a smaller degree. Figure 5 shows the ΔE values for the treatment groups, in relation to control group 2. Treatment groups 1 (TPA6) and 2 (TPA7) had a ΔE value of 11.55 and 10.55 respectively.

An ΔE above 3 can generally be seen by the human eye[21]. However, the colour change caused by these polymers may possibly not be detected if applied to the alum-treated Oseberg collection, since the artefacts are already dark[4]. As such, such changes would be considered acceptable. The final colour of the re-conserved collection should ideally not differ dramatically from that before re-conservation. Additionally, if different retreatment methods are applied to different parts of the collection (for example, aqueous treatments for those that can withstand water and non-aqueous methods for the remaining alum-treated objects), the resulting changes in colour should be similar. Thus, future work must include application of these polymers to test fragments of original Oseberg material, in order to evaluate colour change.

(a)

(b)

Figure 3 (a) Photographs of treatment group 1 (TPA6) before (top) and after (bottom) treatment. Specimens became noticeably darker, with a yellow tinge. **(b)** Photographs of treatment group 2 (TPA7) before (top) and after (bottom) treatment. Specimens were similar to those treated with TPA6.

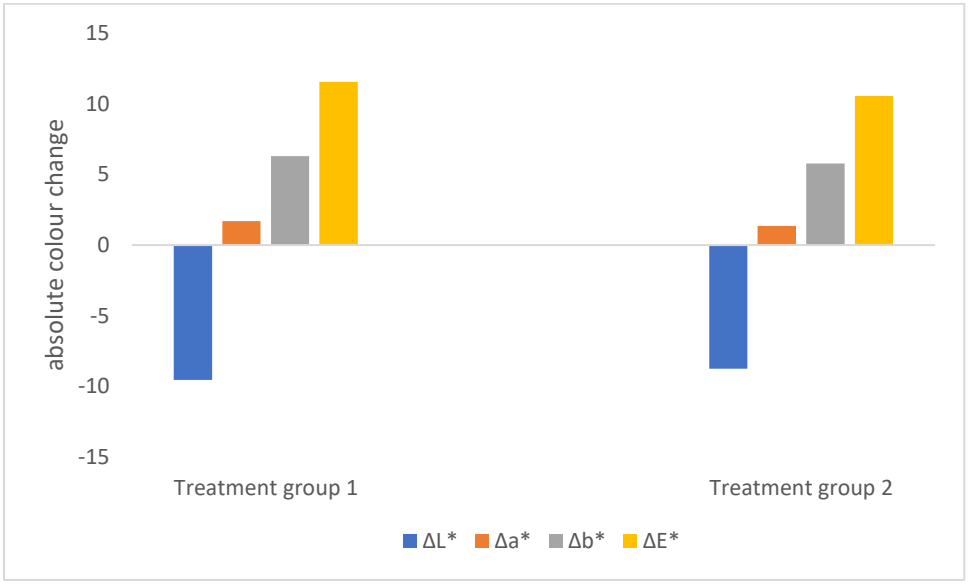

Figure 4. Colour change of treatment group 1 (TPA6) and treatment group 2 (TPA7) relative to control group 2 (isopropanol-immersed). Treatment group 1 ΔE = 11.55; treatment group 2 ΔE = 10.55.

ATR-FTIR analyses

The archaeological wood controls were first compared to sound wood, in order to better understand their state of degradation. Figure 5a shows such a comparison, with the use of a a surface sample 6.S.6 (isopropanol-immersed control) and a core sample 4.C.2 as the archaeological wood. Normalisation was carried out at the lignin peak (1508 cm^{-1}). One could see that the cellulose peaks (1369, 1156 and 895 cm^{-1})[22,23] were muted in the archaeological wood, indicating its state of degradation and signals for the hemicellulose peaks at 1734 and 1239 cm^{-1} were not visible[22]. The lignin signals at 1596, 1264 and 1219 cm^{-1} were prominent in the archaeological wood, mainly due to their amplification as a result of the loss of cellulose and hemicellulose[22]. The band at 1029 cm^{-1} is due to a combination of several wood components (cellulose,

hemicellulose and lignin)[23] and as such, it shows the greatest absorption in both sound and archaeological pine.

Figure S5 shows a comparison of the IR absorbances of pure TPA6 and TPA7, normalised at 1725 cm^{-1} (C=O bond). The spectra of the two polymers were almost identical to one another. This was expected as they are structurally very similar. The major difference between the polymers was at 2856 cm^{-1}, where TPA7 had a more pronounced peak. This could be attributed to a C-H stretching vibration, possibly due to the oleic acid component of the copolymer.

The absorbances of the two pure polymers were then compared to those of a control specimen. The spectra showed that both polymers were easily distinguishable from the wood, although some signals overlapped, such as at the 3500 – 3000 cm^{-1} region (Figure S6). The polymers had identifiable signals at 3000 – 2900 cm^{-1}, as well as at 1716 and 1154 cm^{-1} (assigned as C=O and C-O respectively). Due to these differences, it was expected that the polymers would be easily distinguished from the wood in the treated samples.

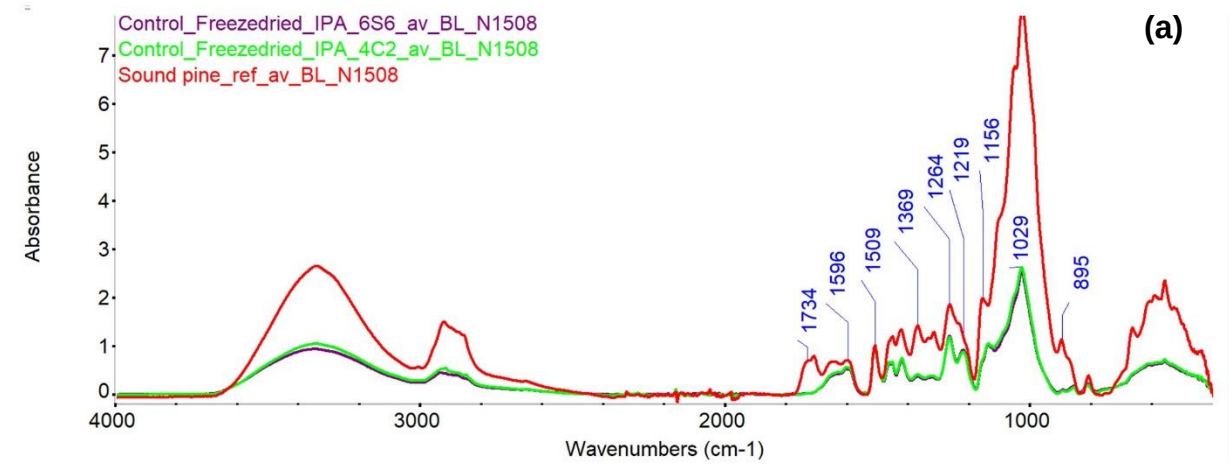

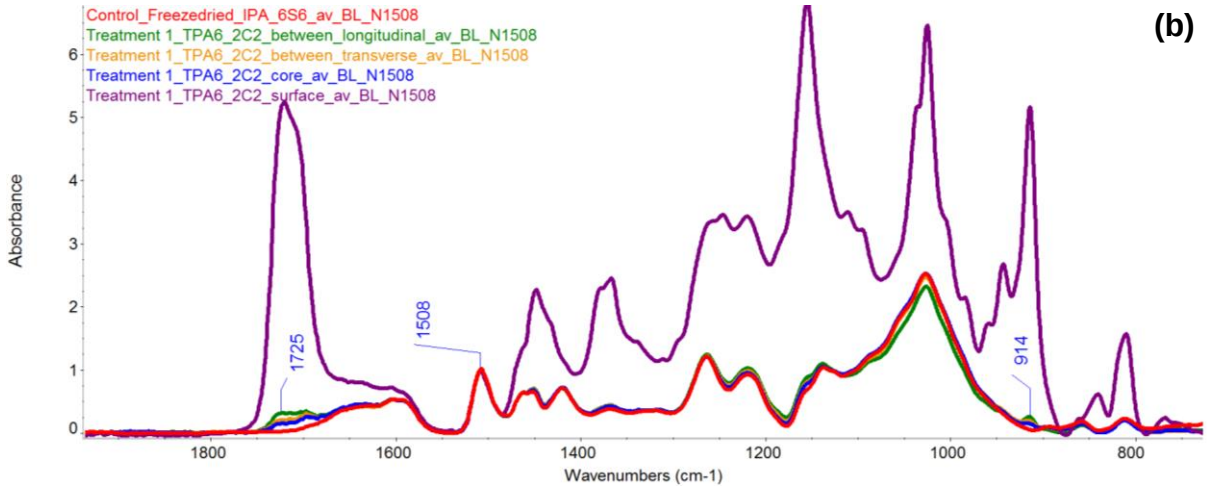

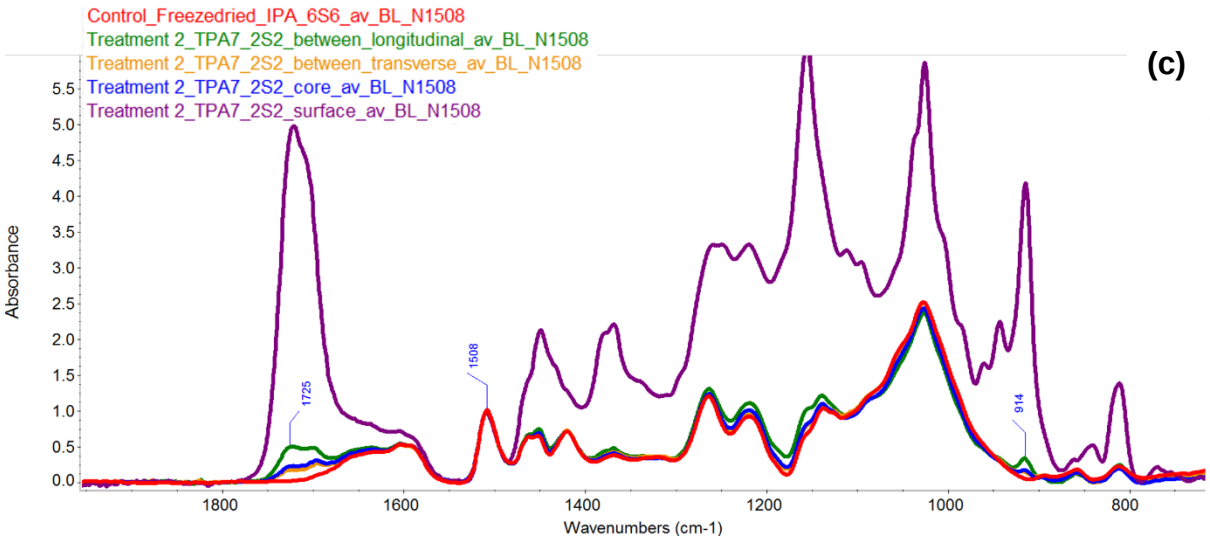

Figure 5 (a). IR spectra of sound pine (red) and archaeological pine (purple; isopropanol immersed surface control 6.S.6 and green; isopropanol immersed core control 4.C.2). The major peaks of sound wood are annotated. The spectra were normalised at 1508 cm^{-1}.**(b)** IR spectra comparison (fingerprint region) between the isopropanol-immersed control (red; 6.S.6) and the samples treated with TPA6 (2.C.2) **(c)** As (b), but showing the TPA7-treated samples (2.S.2). The treated samples were measured at different depths: at the surface (purple), core (blue), between the surface and the core along the grain (green) and between the surface and the core across the grain (yellow). The signals depicting polymer penetration are annotated. Spectra were normalised at 1508 cm^{-1}.

The wood specimens treated with the polymers were analysed at different depth points. This was done to be able to get an indication of the level of distribution of the polymer through the entire specimen. Samples were taken from the surface, core, between the surface and the core along the grain and between the surface and the core across the grain. Their spectra were then compared to those of an untreated, isopropanol-immersed control (Figures 5b and 5c). The spectra were normalised at the lignin peak at 1508 cm^{-1} as this was shared by all the samples.

Figures 5b and 5c show that the specimen surface spectra were very different from all the other signals, clearly showing a high concentration of polymer. The rest of the treated wood specimens were more similar to the control, however they still showed a clear indication of polymer penetration. This was seen at 1725 and 914 cm^{-1} in particular. The spectra taken from the core of the treated specimen had the least absorbance. The sample taken from in between the surface and core absorbed less than the surface but more than the core. The sample taken along the grain had more absorbance than the one across the grain, as can be seen at both 1725 and 914 cm^{-1}. This was somehow expected since it would be easier for the polymer to penetrate along the grain of the wood rather than across it. The decreasing degree of polymer penetration (both TPA6 and TPA7) could therefore be described as follows:

surface > between surface and core (along the grain) > between surface and core (across the grain) > core

SEM analyses

Cross-sections of latewood were primarily looked at, as opposed to earlywood. This is because generally, morphological changes appear more prominently in latewood due to its thicker cell walls. Sound pine was first compared to an archaeological wood control. The sound pine image showed that the cells clearly had a more robust shape, with regular and thick cell walls. In contrast, the archaeological wood had cells which appeared ‘feathery’ and fragile, with very thin cell walls appearing to be mostly dislodged (Figure S7) This may be due to the loss of holocellulose (the term for combined cellulose and hemicellulose) previously depicted by the FTIR analyses.

Samples from wood specimens treated with both TPA6 and TPA7 (Figure 6) were taken. For each specimen, a sample was taken from the surface and the core. It should be noted that generally, it is difficult to identify organic polymers such as TPA6 and TPA7 from other organic materials such as wood with SEM. The specimens treated with both polymers showed similar results. The polymer was clearly visible in the surface samples, in some cases clogging the wood pores or lumina. The polymer was more difficult to discern in the samples taken from the cores. It could be noted however that the treated cores appeared to be less airy than the control, with some cells having slightly thicker cell walls. They also seemed to be less deformed and appeared to be able to withstand the shaving that was carried out on the samples more than the control, possibly indicating an increased resilience. It was however difficult to say for certain whether this was due to the presence of the polymer.

In general, the SEM analyses appeared to correlate with the FTIR results. Both techniques showed that the highest concentration of polymer was on the surface of the wood specimens. FTIR indicated that the polymers managed to penetrate the cores of the specimens, albeit at a much lower concentration. This was difficult to observe with the SEM, but there were possible morphological changes that could perhaps indicate the presence of the polymers.

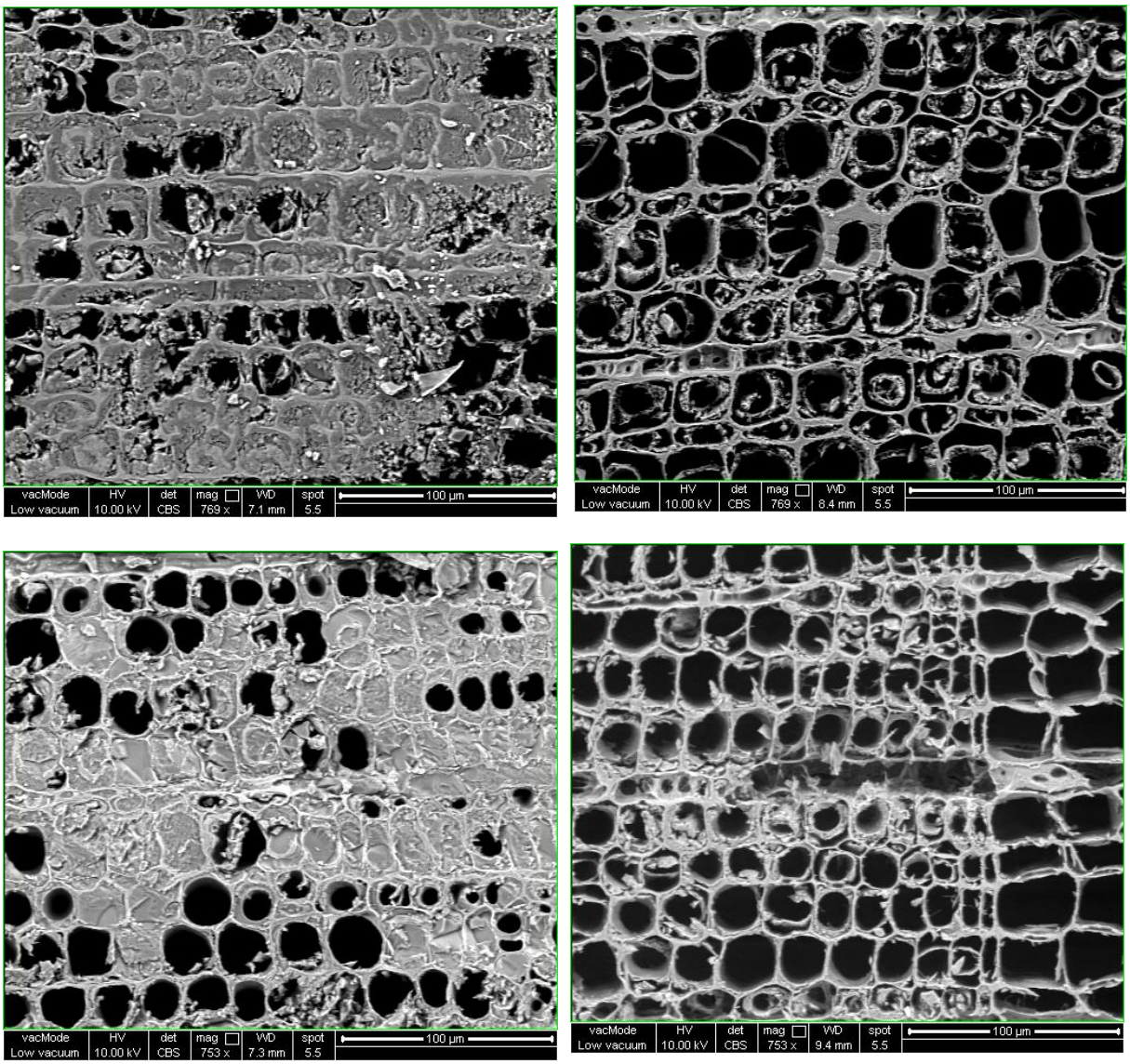

Figure 6. SEM images of samples treated with TPA6 (top), taken from the surface (top left) and core (top right). Bottom figures are the SEM images of samples treated with TPA7, taken from the surface (bottom left) and core (bottom right). The surface images show a high distribution of polymer, which filled many wood cells. The polymers were more difficult to observe in the core images, but the cells appear to be more structurally sound than the untreated sample, indicating polymer presence.

Hardness test

The hardness tests were carried out in order to get an indication of the extent of consolidation that the polymers conferred. The fruit penetrometer measures the wood's resistance to indentation. Specimens from control group 1 (freeze-dried only) and control group 2 (freeze-dried and immersed in isopropanol) were measured five times on the tangential surface. Specimens from both polymer treatment groups were measured five times on the tangential surface. In addition, each of the treated

specimens was split in half and two measurements were taken from the core (one measurement per half piece, totalling two measurements of each core). The multiple measurements taken from every specimen were then averaged (Figure 7).

From the averaged values, one could see that there seemed to be an increase in surface hardness compared to the controls. Conversely, the core hardness did not appear to change in the treated groups. Statistical analysis with the one-way ANOVA was carried out on the surface measurements of the treated groups in order to determine whether the observed change in hardness was significant. This was done using the individual measurements instead of the averaged values.

The control group used for the statistical analysis was made up of both the freeze-dried and isopropanol-treated controls. This was justified since the difference in means between the two groups was not significant (Figure S8). There were 40 values in the control group, 40 values in the TPA6 treatment group and 40 values in the TPA7 treatment group. There were two outliers in the TPA6 treatment group, as assessed by a boxplot. It was decided to not remove these outliers from the dataset. The data was normally distributed except for the TPA7 group, as assessed by the Shapiro-Wilk test ($p > 0.05$). However, the one-way ANOVA is known to be robust to deviations from normality, especially if the sample sizes are equal (as was the case here)[24]. The Levene's Test indicated that homogeneity of variances was violated ($p = 0.025$), therefore the Welch's one-way ANOVA was used for this analysis. The surface hardness score was found to be statistically significantly different for the two groups treated with the different polymers (Welch's $F(2, 1641.693) = 33.258$, $p < 0.001$) (Figure S9). The surface hardness increased from the control (58.7 ± 6.8) to the TPA6 treatment group (69.8 ± 6.4) and the TPA7 treatment group (69.8 ± 8.9). Games-Howell post hoc analysis revealed that the increase from the control to the TPA6 treatment group (11.0875, 95% CI (7.561 to 14.614)) was statistically significant ($p < 0.001$), as well as the increase in surface hardness for the TPA7 treatment group (11.1050, 95% CI (6.855 to 15.355), $p < 0.001$). The difference between the groups treated with the different polymers was not statistically significant (0.0175, 95% CI (0.0 to 4.174), $p = 1.00$).

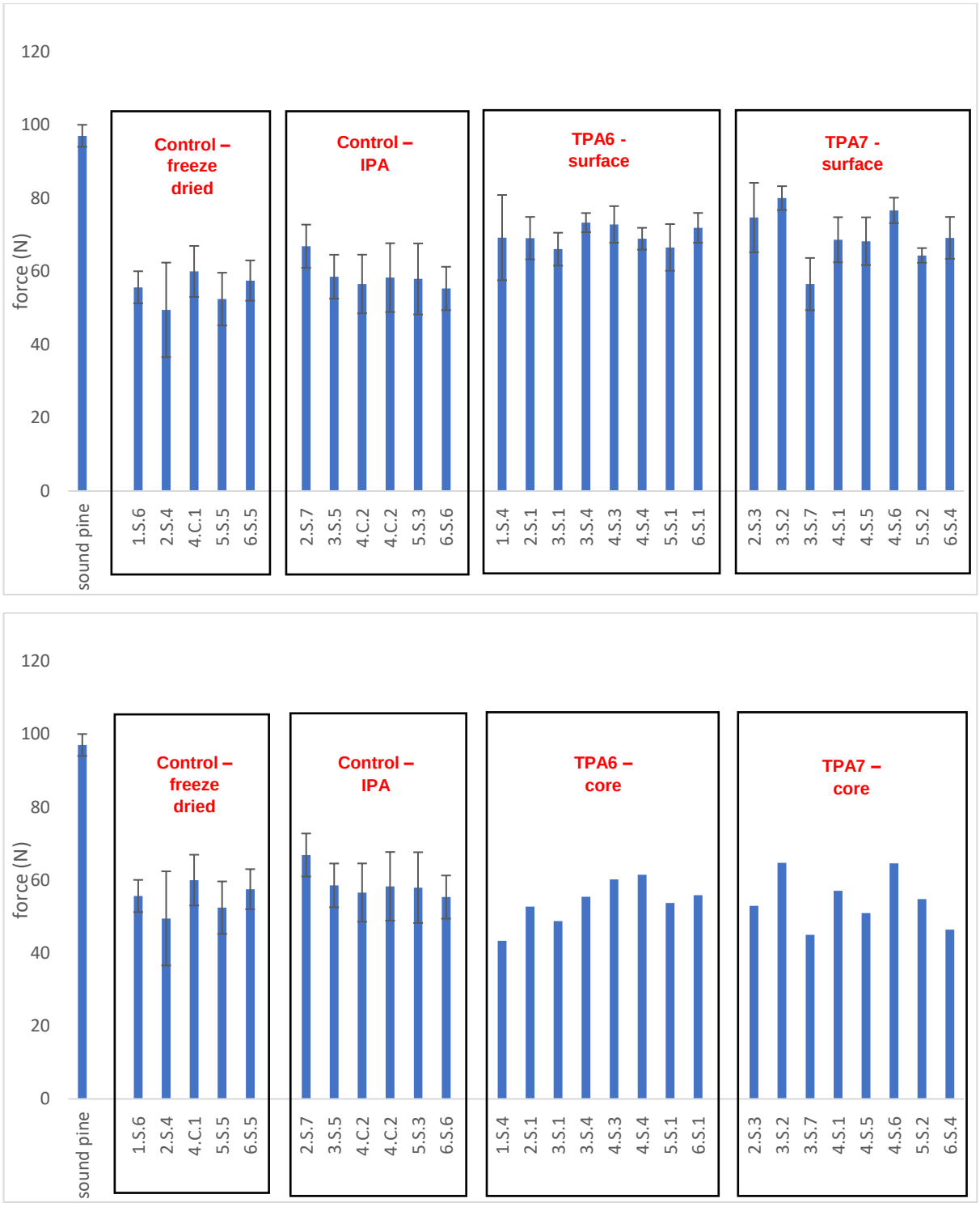

Figure 7. A comparison of the results from the hardness tests. The values for the treatment groups show the surface measurements (top) and the core measurements (bottom). The values for the treated cores do not have error bars since only two measurements were taken per sample.

This analysis indicated that the polymers imparted a clear increase in surface hardness, possibly making the wood more resistant to stresses caused by handling or the environment. Both TPA6 and TPA7 seemed to increase the hardness to the

same extent, as there was no statistical difference between them. Conversely, the cores of the treated samples did not appear to increase in hardness but this was expected, as there was only a small amount of polymer present compared to the surfaces.

TPA6 or TPA7?

This preliminary study aimed to determine the extent of penetration of two terpene-derived polymers, TPA6 and TPA7, in highly degraded archaeological pine. This was carried out by monitoring weight and dimensional change, alongside the use of ATR-FTIR supplemented with SEM. Other tests were carried out to observe the effects that the polymers had on the wood, such as colour change measurements and hardness tests.

TPA6 and TPA7 showed very similar results and they seemed to affect the wood in mostly the same way. Generally, all the treated specimens increased in weight, indicating polymer uptake. Slight dimensional changes were also recorded for all specimens. The colour of the polymer-treated wood was slightly darker, with a yellowish tinge. FTIR showed that the polymers successfully penetrated the wood, with the highest concentration on the surface. This correlated well with the SEM analyses, which showed an abundance of polymer on the surface of the wood specimens. Both polymers also penetrated the core of the wood specimens, although to a lesser extent, making them difficult to pinpoint in the SEM images. Hardness tests proved that the surface of the treated specimens was significantly harder than the controls and therefore more resistant to indentation. Overall, the differences between the two polymer treatment groups were not significant, as was observed for all the tests that were carried out. Because of this, TPA6 should be favoured over TPA7, due to its higher T_g and since its synthesis possesses fewer steps and is therefore less time-consuming.

Concluding Remarks

Compared to other experimental consolidants currently being investigated, TPA6 and TPA7 appear to be very promising. Colour change proved to be not as drastic as reported for other consolidants like soda lignin[4]. Other investigated materials such as isoeugenol[8,9] and aminocellulose[11] have yet to be proven to have a consolidative effect. Conversely, the hardness tests described in this study have shown that TPA6 and TPA7 improve the wood's resistance to indentation. One of the possible limitations of these terpene-derived polymers is the fact that they have been shown to plug the surface wood lumina, as shown by the SEM results. This could possibly hinder any future re-treatment attempts of the wood. Moreover, these polymers did not appear to increase the hardness of the wood cores. This was expected since the IR results did not indicate a large degree of polymer penetration into the cores.

Due to the promising results, the general scope of this study can be expanded in future work. A new, more accurate method of measuring dimensional change should be developed. A possible idea is to make markings on the wood with a pen before treatment, and then measure the dimensional changes with a technical ruler as opposed to callipers. Higher concentrations of polymer can be used to determine whether this would make a difference in the extent of penetration to the wood core. The immersion time can also be prolonged as this may also potentially increase the amount of polymer that manages to penetrate to the core. Other different methods of polymer administration can also be explored, such as injection. Additionally, these

tests should be run using higher sample numbers of archaeological wood in order to increase the robustness of these studies. Long-term studies should also be carried out to determine the degree of stability of the polymers over time and to see whether it interacts with alum and whether it is stable in the presence of the remaining acidity in wood (target pH 4-5) after deacidification. Moreover, the effects of relative humidity, both on these polymers in their pure form and after with wood and alum penetration, should be investigated. This can be done by monitoring weight changes at different RH levels. If the results from these tests prove to be promising then the polymers may pass into the next phase of investigation, where they'll be tested on alum-treated Oseberg samples, using the same methods applied here. Finally, if the polymer has shown promising results, work must focus on optimizing the scaling-up process to obtain larger quantities. Here, we must also focus on ensuring the polymer batches are consistent and predictably synthesised.

Acknowledgements

This work was supported by the UK Engineering & Physical Sciences Research Council [grant number EP/L015633/1], the Norwegian Ministry of Education and Research, and the University of Oslo as part of the Saving Oseberg project. M.C. is supported by a UK EPSRC Centre for Doctoral Training award.

Author Contributions

M.C. synthesised and characterised the polymers TPA6 and TPA7; the wood cubes were cut and prepared by S.B.; the evaluation and analyses of the wood was carried out by M.C. and S.B.; S.B., S.E.H, R.A.S. and S.M.H. provided supervision for the research; the paper was written by M.C. and edited by S.B. and S.H.; all other authors reviewed and agreed to the published article.

Additional Information

All procedures were conducted in accordance with the relevant guidelines. Archaeological *Pinus* wood was supplied by the Museum of Cultural History in Oslo and had been stored in a waterlogged state until use. Collection and use of this wood did not require permission.

The authors declare no competing financial interests.

Data availability

Raw data is available in Supplementary Information and on request from the Corresponding Authors.

References

1. Braovac, S., McQueen, C. M. A., Sahlstedt, M., Kutzke, H., Łucejko, J. J. & Klokkernes, T. Navigating conservation strategies: linking material research on alum-treated wood from the Oseberg collection to conservation decisions. *Herit. Sci.* **6**, 1–16 (2018).

2. Braovac, S. & Kutzke, H. The presence of sulfuric acid in alum-conserved wood

- Origin and consequences. *J. Cult. Herit.* **13**, S203–S208 (2012).

3. Hocker, E., Almkvist, G. & Sahlstedt, M. The Vasa experience with polyethylene glycol: A conservator's perspective. *J. Cult. Herit.* **13S**, S175–S182 (2012).

4. Łucejko, J. J., de Lamotte, A., Andriulo, F., Kutzke, H., Harding, S., Phillips-Jones, M., Modugno, F., Slaghek, T. M., Gosselink, R. J. A. & Braovac, S. Evaluation of soda lignin from wheat straw/sarkanda grass as a potential future consolidant for archaeological wood. *Forests* **12**, 1–28 (2021).

5. Wakefield, J. M. K., Gillis R. B., Adams, G. G., McQueen, C. M. A. & Harding, S. E. Controlled depolymerisation assessed by analytical ultracentrifugation of low molecular weight chitosan for use in archaeological conservation. *Eur. Biophys. J.* **47**, 769–775 (2018).

6. Spirydowicz, K. E., Simpson, E., Blanchette, R. A., Schniewind, A. P., Toutloff, M. K. & Murray, A. Alvar and Butvar: The Use of Polyvinyl Acetal Resins for the Treatment of the Wooden Artifacts from Gordion, Turkey. *J. Am. Inst. Conserv.* **40**, 43–57 (2001).

7. Hoffmann, P. & Wittköpper, M. The Kauramin method for stabilizing waterlogged wood. in *Proceedings of the 7th ICOM Group on Wet Organic Archaeological Materials Conference* (eds. Bonnot-Diconne, C., Hiron, X., Tran, K. & Hoffmann, P.) 163–166 (1999).

8. McHale, E., Braovac, S., Steindal, C. C., Gillis, R. B., Adams, G. G., Harding, S. E., Benneche, T. & Kutzke, H. Synthesis and characterisation of lignin-like oligomers as a bio-inspired consolidant for waterlogged archaeological wood. *Pure Appl. Chem.* 969–977 (2016). doi:10.1515/pac-2016-0814

9. McHale, E., Steindal, C. C., Kutzke, H., Benneche, T. & Harding, S. E. In situ polymerisation of isoeugenol as a green consolidation method for waterlogged archaeological wood. *Sci. Rep.* **7**, 1–9 (2017).

10. Wakefield, J. M. K., Braovac, S., Kutzke, H., Stockman, R. A. & Harding, S. E. Tert-butyldimethylsilyl chitosan synthesis and characterization by analytical ultracentrifugation, for archaeological wood conservation. *Eur. Biophys. J.* **49**, 781–789 (2020).

11. Wakefield, J. M. K., Hampe, R. Gillis, R. B., Sitterli, A., Adams, G. G., Kutzke, H., Heinze, T. & Harding, S. E. Aminoethyl substitution enhances the self-assembly properties of an aminocellulose as a potential archaeological wood consolidant. *Eur. Biophys. J.* **49**, 791–798 (2020).

12. Cutajar, M., Andriulo, F., Thomsett, M. R., Moore, J. C., Couturaud, B., Howdle, S. M., Stockman, R. A. & Harding, S. E. Terpene polyacrylate TPA5 shows favorable molecular hydrodynamic properties as a potential bioinspired archaeological wood consolidant. *Sci. Rep.* **11**, 7343 (2021).

13. Cutajar, M., Machado, F., Cuzzucoli Crucitti, V., Braovac, S., Stockman R. A., Howdle, S. M. & Harding, S. E. Comparative hydrodynamic characterisation of two hydroxylated polymers based on α-pinene- or oleic acid-derived monomers for potential use as archaeological consolidants. *Sci. Rep.* **12**, 18411 (2022).

14. Andriulo, F., Giorgi, R., Steindal, C. C., Kutzke, H., Braovac, S. & Baglioni, P. Hybrid nanocomposites made of diol-modified silanes and nanostructured calcium hydroxide. Applications to Alum-treated wood. *Pure Appl. Chem.* **89**,

29–39 (2017).

15. Cavallaro, G., Lazzara, G., Milioto, S., Parisi, F. & Ruisi, F. Nanocomposites based on esterified colophony and halloysite clay nanotubes as consolidants for waterlogged archaeological woods. *Cellulose* **24**, 3367–3376 (2017).

16. Jensen, P. & Gregory, D. J. Selected physical parameters to characterize the state of preservation of waterlogged archaeological wood: A practical guide for their determination. *J. Archaeol. Sci.* **33**, 551–559 (2006).

17. Macchioni, N., Pecoraro, E. & Pizzo, B. The measurement of maximum water content (MWC) on waterlogged archaeological wood: A comparison between three different methodologies. *J. Cult. Herit.* **30**, 51–56 (2018).

18. Babiński, L., Izdebska-Mucha, D. & Waliszewska, B. Evaluation of the state of preservation of waterlogged archaeological wood based on its physical properties: Basic density vs. wood substance density. *J. Archaeol. Sci.* **46**, 372–383 (2014).

19. Gregory, D., Jensen, P., Matthiesen, H. & Strætkvern, K. The correlation between bulk density and shock resistance of waterlogged archaeological wood using the Pilodyn. *Stud. Conserv.* **52**, 289–298 (2007).

20. McConnachie, G., Eaton, R. & Jones, M. A Re-evaluation of the Use of Maximum Moisture Content Data for Assessing the Condition of Waterlogged Archaeological Wood. *e-Preservation Sci.* **5**, 29–35 (2008).

21. *Wood and Cellulosic Chemistry*. (Marcel Dekker, 2021).

22. Schwanninger, M., Rodrigues, J. C., Pereira, H. & Hinterstoisser, B. Effects of short-time vibratory ball milling on the shape of FT-IR spectra of wood and cellulose. *Vib. Spectrosc.* **36**, 23–40 (2004).

23. Mohebby, B. Attenuated total reflection infrared spectroscopy of white-rot decayed beech wood. *Int. Biodeterior. Biodegrad.* **55**, 247–251 (2005).

24. Lix, L. M., Keselman, J. C. & Keselman, H. . J. Consequences of Assumption Violations Revisited : A Quantitative Review of Alternatives to the One-Way Analysis of Variance 'F' Test Author (s): Lisa M . Lix , Joanne C . Keselman and H . J . Keselman Published by : American Educational Research Assoc. *Rev. Educ. Res.* **66**, 579–619 (1996).

Isotopes for provenancing ancient iron artefacts: a pilot project

Stephen Harding (Uni Nottingham), Chas Jones (Fulford Battlefield Soc), Jane Evans (BGS), Jean Milot (ENS de Lyon & Université de Toulouse), Michelle Cutajar (Uni Nottingham), Liz Bailey (Uni Nottingham), Mark Pearce (Uni Nottingham)

Introduction. Lead isotope analysis (LIA) has shown itself to be the most effective tool for the provenancing of ancient metal artefacts of silver and copper and its alloys[1] but its usefulness for the provenancing of iron artefacts has not been established. Recent research has proposed the use of LIA together with trace element patterns of slag inclusions[2], LIA in combination with Sr isotopes[3], or an alternative combination of Os and Sr isotopes[4]. Moreover, it has recently been proposed that Fe isotopes may be useful for provenancing iron artefacts[5, 6]. The approach taken by previous studies has been to concentrate on analysing material from a single site and the ores which are thought likely to be the source of the iron[2, 3, 4] rather than comparing artefacts from a selection of sites. Iron ores are extremely widespread throughout the British Isles[7] and consequently in many cases it is difficult to identify the likely sources of the iron ore used at specific sites, especially in later periods when iron circulated more widely. After the collapse of Roman Britain, it is thought that iron was initially obtained from bog iron during the Saxon period, with the mining of iron ore restarting in the later part of the period[8]

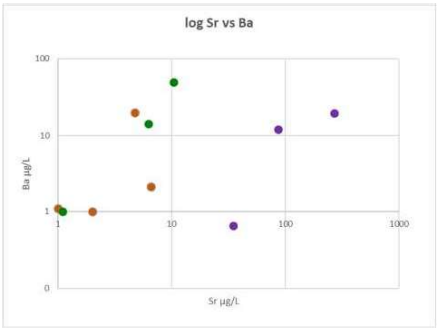

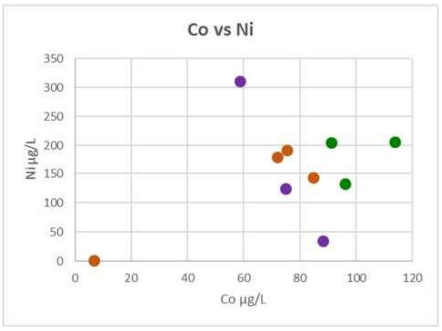

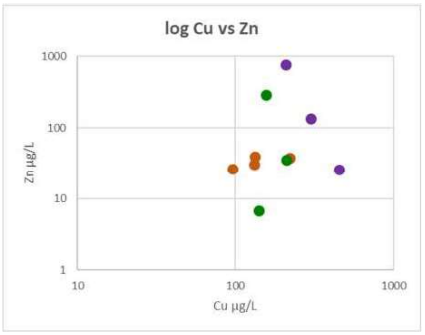

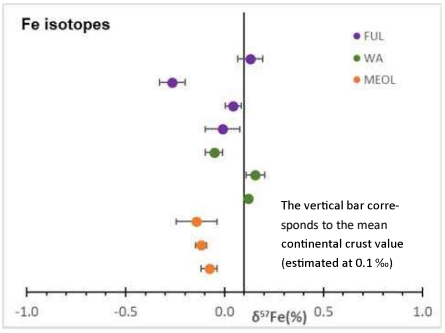

Pilot project. We examined the Pb, Sr and Fe isotopes of 10 Viking Age artefacts from **Fulford** in North Yorkshire[9] (● possible location of the AD 1066 battle, 4 samples), **Bebington Heath on Wirral** (● possible location of the AD 937 Battle of Brunanburh[10], 3 samples) and **Meols** (● a Viking seaport, 3 samples). Artefact compositions were determined by ICP-QMS at the University of Nottingham. Our pilot study showed clear patterns in the data, Meols seems to separate in Sr vs Ba and Cu vs Zn, while Wirral/Bebington Heath seems to separate in Co vs Ni, but the number of samples was much too low to understand their significance, given the lack of isotope studies on iron artefacts. The high range of 87Sr/86Sr values, beyond what would be expected for bog iron (with a cut-off around 7.09), suggests that mined ore was being used, a preliminary conclusion supported by the narrow range of Fe isotope data.

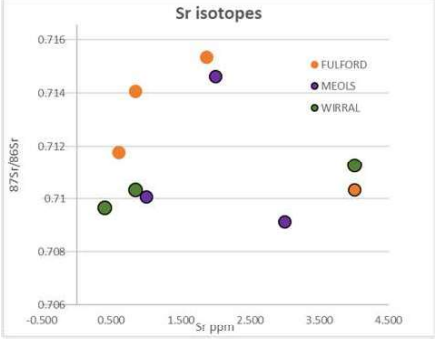

Future plans. We shall test our hypothesis that it is possible to use isotopes to characterize ancient iron artefacts from the Viking Age by studying iron artefacts from 3 early medieval sites in England: the Saxon-Viking battlefield site at **Fulford** (30 samples)[9], the Viking Age site at **Bebington Heath/Wirral** (30 artefacts)[10], and the Viking encampment of **Torksey**, Lincs, in the Trent valley[11] (30 artefacts—in collaboration with Julian Richards and Dawn Hadley, University of York), together with 10 samples of bog iron in slag from the **Foulness valley**, East Yorks (in collaboration with Peter Hakon, University of Hull) using isotopes of Pb, Sr and Fe, in association with trace element patterns (such as phosphorus and manganese). The samples of bog iron from the important and well-documented[12] source in Foulness Valley (East Yorkshire), which is known to have been exploited since the later first millennium BC, are included in the study in order to exemplify the isotope signal of bog iron.

References. 1. Artioli G et al (2020). LIA of prehistoric metals in the central Mediterranean area: a review. *Archaeometry* **62**, suppl. 1: 53-85. 2. Schwab R et al (2006). The provenance of iron artefacts from Manching: a multi-technique approach. *Archaeometry* **48**: 433-452. 3. Degryse P, et al (2007). Tracing the resources of iron working at ancient Sagalassos (south-west Turkey): a combined lead and strontium isotope study on iron artefacts and ores. *Archaeometry* **49**: 75-86. 4. Brauns M et al (2010). Provenance of Iron Age iron in southern Germany: a new approach. *J Arch Sci* **40:** 841-849. 5. Milot J et al (2016). Iron isotopes as a potential tool for ancient iron metals tracing. *J Arch Sci* **76**: 9-20. 6. Milot J et al. (2022) Investigating the provenance of iron bars from Les Saintes-Maries-de-la-Mer Roman shipwrecks (south-east France) with iron isotopes. *Archaeometry* **64.2**: 385-407. 7. Tylecote RF (1962). *Metallurgy in Archaeology*: 175-179. London: Edward Arnold. 8. Hall NS (2017). *An investigation into phosphoric iron production in Eastern England*. PhD thesis, Univ. Nottingham. http://eprints.nottingham.ac.uk/id/eprint/42308. 9. Jones C 2012 The role of storeroom collections in the identification of battle debris. *Arms & Armour* **9**: 54-62. 10 Harding SE (2011) Locations & Legends in (Livingston M ed.) *The Battle of Brunanburh*: Univ Exeter Press pp351-361. 11. Hadley D & Richards J (2016). The winter camp of the Viking Great Army, AD 872–3, Torksey, Lincolnshire. *Antiquaries J* **96**: 23-67. 12. Halkon P (1999). *Valley of the First Iron Masters: Landscape Archaeology in the Foulness Valley, East Yorkshire*. Hull.